Universidade do Minho
Escola de Engenharia

Rui Filipe Ramos da Costa

Nanostructured functional multilayer coatings incorporating biomimetic macromolecules for biomedical applications

setembro 2013

Nanostructured functional multilayer coatings incorporating biomimetic macromolecules for biomedical applications
Rui Filipe Ramos da Costa
UMinho | 2013

Universidade do Minho
Escola de Engenharia

Rui Filipe Ramos da Costa

Nanostructured functional multilayer coatings incorporating biomimetic macromolecules for biomedical applications

Programa Doutoral em Engenharia Biomédica

Trabalho efetuado sob a orientação do
Professor Doutor João Filipe Colardelle da Luz Mano

setembro 2013

DECLARAÇÃO

Nome: Rui Filipe Ramos da Costa

Endereço eletrónico: rui.costa@dep.uminho.pt

Telefone: (+351) 253 510 900

Número de Cartão de Cidadão: 12702894

Título da dissertação: Nanostructured functional multilayer coatings incorporating biomimetic macromolecules for biomedical applications

Orientador: Professor Doutor João Filipe Colardelle da Luz Mano

Ano de conclusão: 2013

Programa Doutoral em Engenharia Biomédica

É AUTORIZADA A REPRODUÇÃO PARCIAL DESTE PROGRAMA DOUTORAL APENAS PARA EFEITOS DE INVESTIGAÇÃO, MEDIANTE DECLARAÇÃO ESCRITA DO INTERESSADO, QUE A TAL SE COMPROMETE

Universidade do Minho, ___/___/_____

Assinatura: _____

"Those who look for the laws of Nature as a support for their new works collaborate with the Creator."

Antoni Gaudí i Cornet

Acknowledgements

After 4 years of arduous work, it is very gratifying to finally reach the end of my PhD. Patience is the Mother of Science. A lot of patience was employed in this thesis, and so it is my wishful thinking that one day this work may be useful for someone – either physician or scholar – in the world.

My greatest acknowledgement goes to my parents. Everything I did was for them. In the beginning of my PhD, they asked several times: "so, what are you working on exactly?" It was quite interesting, actually, especially considering that they still ask me this regularly. After all, what can a weird technology called "layer-by-layer" do to prevent things like high blood pressure, cholesterol, kidney stones, heart diseases, thrombosis, acute muscular pain and blindness, of which they suffer? I can honestly say that such question was the turning point in my research, because it gave me purpose. Now, I try to look for the medical potential of the things I do and hope that this thesis makes them proud.

I want to deliver a word of appreciation and admiration to my supervisor, Prof. João Mano. I believe most of my progress in the scientific world has been possible because of him. He was always very receptive to new ideas – as long as they were good – comprehensive about situations going on out of 3B's and challenged my mind and the minds of all his students with new techniques and workarounds for experimental "headaches". Looking back, I believe I couldn't have asked for a better supervisor! Thank you for your help.

I would like to acknowledge the 3B's Research Group and its director, Prof. Rui Reis, for the possibility of developing my PhD thesis in the facilities at AvePark, providing everything I needed at my disposal. Also, I would like to acknowledge Prof. Nuno Neves who, as a representative of the Doctoral Program in Biomedical Engineering, helped me several times through the whole academic process related to the University of Minho, and very quickly when these things may take weeks.

To my colleagues of 3B's, it is complicated naming people, since we are so many. In 4 years, we all shared happiness and frustration, but all are moments that I cherish. Although I appreciate help from everybody, I would like to thank especially Álvaro, Albino, Ana Catarina, Catarina Custódio, Clara, Diana

Ribeiro, Isabel, João Requicha, Manuel, Mariana, Nuno, Pedro, Praveen, Sara Oliveira, Sílvia Mihaila, Sofia and Yan, for their help in my work and, particularly, during lunches and coffee-breaks! Of course, I couldn't forget my "beloved former students", Joana and Sara Gil, who were introduced to the lab environment for the first time by me. Thank you for your patience, especially Sara. She arrived just before I departed to Spain, and, even when I tried to give her my utmost attention, I'm pretty sure she must have felt abandoned. Sorry!

To my colleagues of Bioforge. These "colorful" researchers at Valladolid sure have a way to receive foreign people in their group: we didn't need 1 week to feel like we had known each other for years. Actually, that was the case for a couple of them but not for most of the new people. Alicia, Ana, Arturo, Chus, Guillermo, Irene, Israel, Ito, Laura, Lucía (allora ragazza!), Luis, Matilde, Mohamed, Rocío and Vanessa, thank you for making me feel at home. But my deepest gratitude goes to the people that accompanied my research since the beginning: Javier, Merche, and, of course, Prof. Carlos – my cosupervisor during my time abroad and a very enjoyable host – and Alessandra. Let me thank you with my best Italian – the little I managed to grasp: "grazie per tuo aiuto"! Next time I go to Valladolid, I'll make sure to bring you the fabled "pão-de-ló" you kept hearing about!

To Cristina: I can't imagine how this period of my life would have been without you! I will never forget all the talks, the laughs, and the moments we spent together. Thank you for all the support, friendship and love, basically for being always there to me, even when I didn't deserve.

Last, but not least, I would like to thank my dear friends "The Seven Dwarves", or six, since I am one of them: Corália, Diana, Emília, Joaquim, Joana, and Vera (no Snow White in the group). I want to thank you for your company and contact during all these years, and the good moments we spent together. It is nice to see, even when separated, how your friendship and your support could make things so much easier.

I acknowledge financial support from Fundação para a Ciência e Tecnologia (FCT, grant SFRH/BD/61126/2009), Fundo Social Europeu (FSE) and Programa Diferencial de Potencial Humano (POPH).

Abstract

The modification of surfaces has been a key aspect in biology and biotechnology, for applications including cell expansion, biomaterials development and preparation of substrates for regenerative medicine. In this thesis, the layer-by-layer (LbL) technique was employed in the modification of surfaces for multiple purposes, namely for films with improved adhesiveness, enhanced cell adhesion, drug delivery capsules, and magnetic spatial positioning. The working hypothesis was that LbL could be used in the modification of surfaces not only planar but also three-dimensional, using solely polymeric materials from a variety of natural origins or obtained by recombinant routes.

Herein, chitosan (CHI), a well-known polycation with marine origins, was used recurrently as an ingredient in various multilayer formulations, driven by intermolecular forces such as electrostatic and hydrophobic interactions. First, multilayer coatings of CHI and an adhesive bacterial exopolysaccharide, levan, were fabricated. As a control, CHI and alginate films – two marine polysaccharides often regarded as good natural adhesives – were assembled in parallel. The adhesive strength of 50 CHI/levan bilayers was determined to be about 3 times higher than the control. The adhesion of L929 cells was also higher in levan-based films.

Next, CHI was used along polyanionic elastin-like recombinamers (ELRs), a recombinant class of elastin-like polymers, exhibiting the cell adhesion motif arginine-glycine-aspartic acid (RGD). Although electrostatic interactions were relied upon to construct LbL coatings, they were not the sole mechanism of buildup between CHI and ELRs. The film construction of CHI and one of nine ELRs differing in amino acid content, length and biofunctionality was followed *in situ* at pH 4.0 and 5.5 using a quartz-crystal microbalance. Their thicknesses were estimated using the Voigt-based model for viscoelastic films, revealing that thicker films were obtained in the presence of hydrophobic interactions between ELRs and partially neutralized chitosan, i.e., when the pH was adjusted to 5.5, near its pK_a. ELR/alginate coatings were also monitored, completing a total of 36 combinations studied. The results agreed with the ones from the CHI-based films: thicker films were obtained for partially neutralized alginate, at a pH value of 4.0.

Bidimensional coatings of CHI and CHI/ELR-RGD were demonstrated to be stimuli-responsive by means of wettability measurements: they exhibited a moderate hydrophobic surface but switched to an extremely hydrophilic one when temperature, pH or ionic strength were raised above 50°C, 11, or

1.25 M, respectively. The presence of RGD enhanced the adhesion of SaOs-2 cells, in comparison to films ending either in CHI or a nonbioactive RDG analogue.

CHI/ELR-RGD coatings were extrapolated to the third dimension as spherical microcapsules assembled around calcium carbonate particles. Aiming at drug administration, two mechanisms were studied: (i) simple diffusion out of the microcapsules, and (ii) cellular uptake. In the first case, release studies at 25 and 37°C with "bovine serum albumin"-loaded microcapsules demonstrated that they provided a sustained release over 14 days, but with reduced capsule permeability at physiological temperature, due to the temperature-induced molecular transition of ELRs. Furthermore, a higher numbers of layers provided an added barrier to the diffusion of the encapsulated protein. The microcapsules were also noncytotoxic towards L929 cells. In the second case, the internalization efficacy and intracellular traffic of RGD- or nonbioactive RDG-functionalized microcapsules by human mesenchymal stem cells (hMSCs) was assessed. The data suggests that microcapsules were internalized mainly through macropinocytosis and that surface functionalization did not play a significant role on this phenomenon, although intracellular processing was faster for RGD-functionalized microcapsules. Both microcapsule types were noncytotoxic toward hMSCs for microcapsule/cell ratios between 5:1 and 100:1.

Finally, inspired by the complex hierarchical and compartmentalized structure of cells, liquefied alginate macroscopic spheres coated with a chitosan/alginate shell were conceived. Within this liquefied environment, rhodamine and multilayer microcapsules were confined, with the latter encapsulating further either rhodamine or magnetic nanoparticles (MNPs). At 25 and 37°C, rhodamine when encapsulated within the inner microcapsules showed a sustained release profile, with the diffusion kinetics being even more reduced at 25°C. The release of rhodamine encapsulated in the outer liquefied alginate compartment did not show significant differences as a function of temperature. Encapsulating MNPs within the microcapsules provided magnetic responsiveness to the whole compartmentalized device and guided mobility capability.

The developed work shows that LbL is a versatile technique that provides the means to develop a wide array of systems useful in biomedical applications, from adhesive and cell seeding planar supports to three dimensional structures for smart drug delivery, guided therapies and customized microreactors as disease models and microtissue production in laboratory.

Resumo

A modificação de superfícies tem sido um aspeto fundamental em biologia e biotecnologia, em aplicações como a expansão de células, desenvolvimento de biomateriais e preparação de substratos para medicina regenerativa. Neste trabalho, a técnica de camada-a-camada foi utilizada na modificação de superfícies para vários fins, como filmes com adesividade e adesão celular melhoradas, cápsulas para administração de drogas, e o posicionamento espacial magnético. A hipótese foi a de que esta técnica poderia ser utilizada na modificação de superfícies planares ou tridimensionais, usando exclusivamente polímeros obtidos de várias origens naturais ou a partir de vias recombinantes.

O quitosano (CHI), um reconhecido policatião com origens marinhas, foi recorrentemente utilizado como ingrediente em várias formulações de multicamadas, impulsionado por forças intermoleculares, tais como interações eletrostáticas e hidrofóbicas. Primeiro, revestimentos de CHI e um exopolissacarídeo bacteriano adesivo, levano, foram construídos. Como controlo, foram comparados com filmes de CHI e alginato – polissacarídeos marinhos considerados bons adesivos naturais. A força adesiva de 50 bicamadas de CHI/levano foi determinada como sendo cerca de 3 vezes mais elevada do que o controlo. A adesão de células L929 foi também maior em filmes contendo levano.

Em seguida, CHI foi utilizado juntamente com recombinâmeros tipo-elastina (ELRs), uma classe de polímeros tipo-elastina, exibindo a sequência de adesão celular "arginina-glicina-ácido aspártico" (RGD). Embora interações eletrostáticas tenham sido invocadas para a construção de multicamadas auto-organizadas, estas não foram o único mecanismo de interação entre CHI e ELRs. A construção de filmes de CHI e um de nove ELRs diferentes em conteúdo aminoacídico, tamanho e biofuncionalidade foi monitorizado *in situ* a pH 4.0 e 5.5 utilizando uma microbalança de cristais de quartzo. As suas espessuras foram estimadas usando o modelo de Voigt para filmes viscoelásticos, revelando que os filmes mais espessos foram obtidos na presença de interações hidrofóbicas entre ELRs e CHI parcialmente neutralizado, isto é, quando o pH foi ajustado para 5.5, próximo do seu pK_a. Filmes de ELR/alginato também foram monitorados, completando um total de 36 combinações estudadas. Os resultados obtidos estiveram em concordância com os dados dos filmes baseados em CHI: filmes mais espessos foram obtidos para alginato parcialmente neutralizado, a um valor de pH de 4.0.

Através de medições de ângulos de contato, demonstrou-se que os revestimentos bidimensionais de CHI e ELR-RGD eram responsivos a estímulos: exibiram uma superfície moderadamente hidrofóbica mas converteram-se em extremamente hidrofílicas quando se aumentou a temperatura, o pH ou força

iónica acima de 50°C, 11, ou 1,25 M, respetivamente. A presença de RGD melhorou a adesão de células SaOs-2, em comparação com filmes terminados ou em CHI ou num análogo não bioativo, RDG. Os revestimentos de CHI/ELR-RGD foram extrapolados para a terceira dimensão sob a forma de microcápsulas esféricas construídas em torno de partículas de carbonato de cálcio. Com a finalidade de administração de drogas, foram estudados dois mecanismos: (i) a difusão simples para o exterior das microcápsulas e (ii) a incorporação celular. No primeiro caso, estudos de libertação a 25 e 37°C com microcápsulas contendo albumina do soro bovino demonstraram uma libertação sustentada ao longo de 14 dias, mas sendo as cápsulas menos permeáveis a uma temperatura fisiológica, devido à transição molecular dos ELRs induzida pela temperatura. Além disso, um número mais elevado de camadas proporcionou uma barreira adicional à difusão da proteína encapsulada. As microcápsulas foram também não citotóxicas para células L929. No segundo caso, a eficácia de internalização e tráfego intracelular de microcápsulas funcionalizadas com RGD ou a sequência não bioativa RDG por células estaminais mesenquimais humanas (hMSCs) foi avaliada. Os dados sugerem que as microcápsulas foram internalizadas principalmente através de macropinocitose, e que a funcionalização da superfície não desempenhou um papel significativo neste fenómeno, embora o processamento intracelular tenha sido mais rápido para microcápsulas funcionalizadas com RGD. Ambos os tipos de microcápsulas foram não citotóxicas para hMSCs para rácios de microcápsula/célula entre 5:1 e 100:1. Finalmente, com inspiração na hierarquia complexa e estrutura compartimentada das células, esferas macroscópicas de alginato liquefeito revestidas com camadas de CHI/alginato foram concebidas. Dentro deste ambiente liquefeito, rodamina e microcápsulas foram confinadas, com estas últimas podendo conter ou mais rodamina ou nanopartículas magnéticas (MNPs). A 25 e 37°C, rodamina quando encapsulada no interior de microcápsulas mostrou um perfil de libertação sustentada, sendo a cinética de difusão ainda mais reduzida a 25°C. A libertação de rodamina encapsulada no compartimento externo de alginato não exibiu diferenças significativas em função da temperatura. MNPs encapsuladas dentro das microcápsulas providenciaram resposta magnética a todo o dispositivo compartimentado e capacidade de mobilidade dirigida.

O trabalho aqui desenvolvido mostra que a técnica de modificação camada-a-camada é uma técnica versátil capaz de fornecer meios para desenvolver uma ampla gama de sistemas úteis em aplicações biomédicas, desde suportes planos adesivos e para adesão celular até estruturas tridimensionais para a administração “inteligente” de drogas, terapias guiadas e microreatores personalizados para o desenvolvimento de modelos de doenças e produção de microtecidos em laboratório.

Table of Contents

Acknowledgements ..... **v**

Abstract ..... **vii**

Resumo ..... **ix**

Table of Contents ..... **xi**

List of Abbreviations and Acronyms ..... **xxiii**

List of Figures ..... **xxix**

List of Tables ..... **xliii**

List of Publications ..... **xlv**

Introduction to the thesis format ..... **li**

SECTION I – GENERAL INTRODUCTION

Chapter 1. Nanostructured devices produced by layer-by-layer self-assembly adsorption for tissue engineering applications **3**

Abstract **3**

1.1 Introduction 5

1.2 Interaction between biomaterials as ingredients for multilayer formulations 6

1.2.1 Buildup mechanisms of synthetic and inorganic materials *7*

1.2.2 Natural-based polymeric materials *9*

1.3 Scalability to three dimensions 12

1.3.1 Membranes *12*

1.3.2 Capsules *13*

1.3.3 Tubes *14*

1.3.4 Three-dimensional scaffolds *15*

1.4 Application of nanostructured multilayer devices in tissue engineering 15

1.4.1 Controlling cell adhesion and proliferation *16*

1.4.2 Controlling cellular metabolism: encapsulation and differentiation ... 17
1.4.3 Biomimetic and "intelligent" and substrates ... 19
1.4.4 Multilayers in controlled drug delivery ... 21
1.4.5 Biomineralized multilayers ... 22
1.5 Conclusion ... 23
1.6 References ... 24
Chapter 2. Polyelectrolyte multilayered assemblies in biomedical technologies ... 37
Abstract ... 37
2.1 Introduction ... 39
2.2 Fundamentals of the layer-by-layer technique ... 41
2.2.1 Layer-by-Layer as a tool for surface modification ... 41
2.2.2 Moving LbL toward faster production ... 42
2.3 Surfaces with specialized properties ... 44
2.3.1 Surfaces containing adhesive constituents ... 44
2.3.2 Mineralization control ... 45
2.3.3 Stimuli-responsive surfaces ... 48
2.4 Coating of implantable devices ... 49
2.4.1 Coating of synthetic implantable devices ... 50
2.4.2 Cells as supports for the assembly of multilayer coatings ... 53
2.5 Engineering biomedical devices ... 54
2.5.1 Construction of films for wound healing ... 54
2.5.1.1 Development of nanostructured substrate-free membranes ... 54
2.5.1.2 Healing of tissue defects *in vivo* ... 56
2.5.2 Multilayer coatings for enhanced cell adhesion on flat surfaces ... 57
2.5.3 Multilayer reservoirs for drug loading and delivery ... 59
2.5.3.1 Films loaded with active agents ... 59
2.5.3.2 Polyelectrolyte capsules with tunable permeability ... 60
2.5.3.3 Capsules for the intracellular delivery of encapsulated agents ... 63
2.5.4 Biosensors ... 65
2.5.5 Implantable structural devices with tubular shape ... 68

2.5.6 Compartmentalized environments 71
2.5.6.1 Confined enzymatic reactions 72
2.5.6.2 Customizable environments with multifunctional components 74
2.6 Engineering tissues *in vitro* 75
2.6.1 Three-dimensional porous structures 75
2.6.2 Cells as components in the LbL construction 78
2.6.3 Production of microtissues in confined environments 80
2.7 Conclusions 82
2.8 References 83

Chapter 3. Elastin-like macromolecules 103

3.1 General introduction 103
3.2 Materials engineering – an overview on synthetic and natural biomaterials 104
3.3 Elastin as a source of inspiration for nature-inspired polymers 104
3.3.1 Genetic coding 105
3.3.2 Characteristics of elastin 106
3.3.3 Elastin disorders 107
3.3.4 Current applications of elastin as biomaterials 108
3.3.4.1 Skin 108
3.3.4.2 Vascular constructs 109
3.4 Nature-inspired biosynthetic elastins 110
3.4.1 General properties of elastin-like recombinamers 110
3.4.2 The principle of genetic engineering – a powerful tool for engineering materials 111
3.4.3 From genetic construction to molecules with tailored bio-functionality 113
3.4.4 Biocompatibility of ELRs 115
3.5 ELRs as advanced materials for biomedical applications 115
3.5.1 Tissue engineering 115
3.5.2 Drug- and gene- delivery 118
3.5.3 Surface engineering 120
3.6 Conclusions 122
3.7 Acknowledgements 123

3.8 References 123

Chapter 4. Stimuli-responsive surfaces for biomedical applications 139

4.1 Introduction 139

4.2 Surface modification methodologies: how to render substrates with stimuli responsiveness 140

4.2.1 Self-assembled monolayers 140

4.2.2 Thin polymer network films 142

4.2.3 Grafting 143

4.2.4 Layer-by-layer 144

4.3 Exploitable stimuli and model smart biomaterials 146

4.3.1 Physical stimuli 146

4.3.1.1 Temperature 146

4.3.1.2 Light 148

4.3.2 Chemical stimuli 149

4.3.2.1 pH 149

4.3.2.2 Ionic strength 150

4.3.3 Biochemical stimuli 150

4.3.3.1 Antigens 150

4.3.3.2 Enzymes 151

4.3.3.3 Glucose 151

4.3.4 Multiple responsive surfaces 151

4.4 Biomedical applications of smart surfaces 152

4.4.1 Smart coatings for tissue engineering, regenerative medicine and drug delivery applications 152

4.4.2 Smart biomineralization 155

4.4.3 Cell sheet engineering 156

4.5 Conclusions 157

4.6 Acknowledgements 157

4.7 References 158

SECTION II – EXPERIMENTAL SECTION

Chapter 5. Materials and methods 173

5.1 Materials 173

5.1.1 Polysaccharides 173

5.1.1.1 Microbial levan production 175

5.1.1.2 Levan phosphonate modification 176

5.1.2 ELR expression and purification 176

5.1.3 Synthesis of magnetic nanoparticles 179

5.2 Characterization of the materials 179

5.2.1 Degree of deacetylation of chitosan 179

5.2.2 Phosphonate-levan modification assessment 180

5.2.3 Elastin-like recombinamers bioproduction assessment 181

5.2.4 Magnetization of MNPs 181

5.2.5 Measurement of charges 182

5.2.6 Temperature responsiveness of the polymers 183

5.3 Assessment of LbL films' growth 184

5.3.1 In situ monitoring 184

5.3.2 Estimation of films' thicknesses 185

5.4 Assembly and characterization of multilayer films 186

5.4.1 In planar substrates 186

5.4.1.1 Adhesiveness of the films 187

5.4.1.2 Contact angle measurements 187

5.4.1.3 Surface topography 189

5.4.2 In three dimensional substrates 189

5.4.2.1 Preparation of spherical microparticle templates 189

5.4.2.2 Construction of the multilayer shells 190

5.4.2.3 Compartmentalized structures 191

5.4.2.4 Encapsulation losses and pre-loading efficiency 193

5.4.2.5 Microscopy evaluation of the structures 193

5.5 In vitro release studies from three-dimensional capsules 194

5.6 Mechanical resistance of compartmental units 195
5.7 Magnetic responsiveness assays 195
5.8 *In vitro* biological studies 196
5.8.1 Cell seeding 196
5.8.2 Staining of cells adhered to bidimensional surfaces 197
5.8.3 Cellular uptake of three dimensional microcapsules 198
5.8.4 Cell metabolism and viability 199
5.8.5 Alkaline phosphatase assays 200
5.9 References 201

SECTION III – OPTIMIZATION OF LAYER-BY-LAYER STRATEGIES FOR BIOMEDICAL APPLICATIONS

Chapter 6. Adhesive nanostructured multilayer films using a bacterial exopolysaccharide for biomedical applications 209

Abstract 209

6.1 Introduction 211
6.2 Experimental section 213
6.2.1 Materials 213
6.2.2 Microbial levan production 213
6.2.3 Phosphonate modification of levan 214
6.2.4 Measurement of charges 214
6.2.5 Construction of hybrid self-assembled films 214
6.2.6 Estimation of the films' thicknesses 215
6.2.7 Preparation of hybrid multilayer films 215
6.2.8 Adhesiveness of the films 215
6.2.9 In vitro cell culture 216
6.2.10 Nuclei-staining fluorescence assay 216
6.3 Results and Discussion 216
6.4 Conclusions 223
6.5 Acknowledgements 224

6.6 References 224

Chapter 7. Layer-by-layer film-growth using polysaccharides and recombinant polypeptides: a combinatorial approach 229

Abstract 229

7.1 Introduction 231

7.2 Experimental section 233

7.2.1 Materials 233

7.2.2 Assessment of the ELR compositions 234

7.2.3 Measurement of the charges 234

7.2.4 Construction of hybrid self-assembled films 234

7.2.5 Estimation of the film thicknesses 234

7.3 Results and discussion 235

7.3.1 Characterization of the polysaccharides and ELRs 235

7.3.2 Effect of the charged state by means of the ζ-potential 237

7.3.3 QCM-D data acquisition 240

7.3.4 Data modeling and thickness analysis 242

7.3.5 Effect of molecular weight 245

7.3.6 General model for hybrid multilayer growth 247

7.4 Conclusions 248

7.5 Supplemental information 248

7.5.1 Neutralization of V84 248

7.5.2 Amino acid composition 249

7.5.3 Molecular weight 251

7.5.4 ζ-potential and molecular weight effect on thickness: 256

7.5.5 QCM-D acquisition graphics and Voigt-based model fitting result 256

7.6 Acknowledgements 266

7.7 References 266

Chapter 7 – Appendix. Nanostructured thin coatings from chitosan and an elastin-like recombinamer with acute stimuli-responsive behavior 271

Abstract.....271

7A.1 Introduction 273

7A.2 Experimental section 273

7A.2.1 ELRs expression and purification 273

7A.2.2 Buildup kinetics monitoring 274

7A.2.3 Contact angle measurements 274

7A.2.4 Topography studies 274

7A.3 Results and discussion 275

7A.3.1 ELRs peptide sequence 275

7A.3.2 Buildup monitoring of the films 275

7A.3.3 Wettability variations of the films 277

7A.3.4 Topography analysis 278

7A.4 Conclusions 279

7A.5 Acknowledgements 280

7A.6 References 280

Chapter 8. Layer-by-layer assembly of chitosan and recombinant biopolymers into biomimetic coatings with multiple stimuli-responsive properties 283

Abstract.....283

8.1 Introduction 285

8.2 Experimental section 287

8.2.1 ELR-RGD expression and purification 287

8.2.2 ELR-RGD characterization 287

8.2.3 Buildup and characterization of the self-assembled coatings 288

8.2.4 Contact-angle measurements 288

8.2.5 Atomic force microscopy measurements 289

8.2.6 Cell culture studies of SaOs-2 osteoblast-like cells 289

8.3 Results and discussion 290

8.3.1 ELR-RGD characterization 290

8.3.1 Analysis of CHI/ELR-RGD film buildup 292

8.3.2 Characterization of the self-assembled coatings 293

8.3.3 Cell culture studies of SaOS-2 osteoblast-like cells 300
8.4 Conclusions 303
8.5 Acknowledgements 303
8.6 References 304

Chapter 9. Nanostructured and thermoresponsive recombinant biopolymer-based microcapsules for the delivery of active molecules 309

Abstract 309

9.1 Introduction 311
9.2 Experimental section 312
9.2.1 Materials for the microcapsule composition 312
9.2.2 ELR aggregate-size measurements 313
9.2.3 Entrapment of BSA in calcium carbonate particles 313
9.2.4 Construction of the multilayer shells and microcapsule formation 313
9.2.5 Determination of pre-loading encapsulation efficiency 314
9.2.6 In vitro biological performance 314
9.2.7 Quantification of FITC-BSA release 315
9.2.8 Microscopy characterization of the $CaCO_3$ microparticles and multilayered microcapsules 315
9.3 Results 316
9.4 Discussion 321
9.5 Conclusion 325
9.6 Supplemental information 325
9.6.1 Schematic structure of the ELR 325
9.6.2 Morphology of the sacrificial $CaCO_3$ templates: 326
9.6.3 Cumulative losses and encapsulation efficiency 326
9.6.4 Release kinetics calculation 327
9.6.4.1 Korsmeyer kinetics 327
9.6.4.2 Zero-order release 328
9.6.4.3 First-order release 329
9.6.4.4 Higuchi release model 330

9.7 Acknowledgements 331
9.8 References 331

Chapter 10. Cellular uptake of multilayered capsules produced with biomimetic and genetically engineered macromolecules 337

Abstract 337

10.1 Introduction 339
10.2 Experimental section 341
10.2.1 Materials 341
10.2.2 Measurement of the charges 342
10.2.3 Synthesis of calcium carbonate sacrificial templates 342
10.2.4 Construction of the multilayer shells and microcapsule formation 342
10.2.5 Characterization of the hybrid microcapsules 343
10.2.6 Cell culture 343
10.2.7 Cell viability assays 344
10.2.8 Statistical analysis 344
10.2.9 Internalization and intracellular processing experiments 344
10.2.10 Cell analysis by flow cytometry 345
10.3 Results and discussion 345
10.4 Conclusion 356
10.5 Acknowledgements 357
10.6 References 358

Chapter 11. Multifunctional compartmentalized capsules with a hierarchical organization from the nano- to the macro-scales 363

Abstract 363

11.1 Introduction 365
11.2 Experimental section 366
11.2.1 Materials 366
11.2.2 Bioproduction of the elastin-like recombinamers 367
11.2.3 Synthesis of magnetic nanoparticles 367

11.2.4 Characterization of the MNPs 367
11.2.5 Temperature-induced aggregate measurements 368
11.2.6 Synthesis of the calcium carbonate sacrificial particles, either empty or entrapping fluorophores/MNPs 368
11.2.7 Construction of the microparticle multilayer coating 368
11.2.8 Construction of multilayer coated external subcompartment-containing beads 369
11.2.9 Characterization of the compartmental units 369
11.2.10 Mechanical resistance of the external compartments 370
11.2.11 Rhodamine release studies 370
11.2.12 Magnetic-based responsiveness 370
11.3 Results and discussion 371
11.4 Conclusion 380
11.5 Supplemental information 381
11.5.1 Deacetylation degree of chitosan. 381
11.5.2 ELR transition temperature 381
11.5.3 Rhodamine encapsulation losses 383
11.5.4 Magnetic responsiveness assay 384
11.6 Acknowledgements 385
11.7 References 385

SECTION IV – CONCLUDING REMARKS

Chapter 12. Major conclusions and future perspectives 393

List of Abbreviations and Acronyms

0-9
2D – two dimensional
3D – three dimensional

A
A – alanine
AA – acrylic acid
AFM – atomic force microscopy
ALG – alginate
ALP – alkaline phosphatase
ANOVA – analysis of variance
ASTM – American Society for Testing Materials

B
β – beta
BG – Bioglass®
BMP – bone morphogenetic protein
BNP – bioactive nanoparticle
BSA – bovine serum albumin

C
χ^2 – chi-square
CA – contact angle
$CaCl_2$ – calcium chloride
CHI – chitosan
CLSM – confocal laser scanning microscopy
cm – centimeter
CO_2 – carbon dioxide
cP – centipoise
CRP – controlled/living radical polymerization
°C - degree Celsius

D
δ – delta
ΔD – variation of dissipation
ΔF – variation of frequency
Δm – variation of adsorbed film mass
D – aspartic acid
D_20 – deuterated water
Da – Dalton
DAPI – 4',6-diamidino-2-phenylindole
DCl – deuterated hydrochloric acid
DD – degree of deacetylation
DHR 123 – dihydrorhodamine 123
DIC – differential interference contrast
DL-1 – delta-like 1 Notch ligands
DLS – dynamic light scattering
DMEM – Dulbecco's modified Eagle's medium
DMPEI – *N,N*- dodecyl methyl polyethylenimine
DNA – deoxyribonucleic acid
DOPA – 3,4-dihydroxy-phenylalanine
DOX – doxorubicin
DPBS - Dulbecco's phosphate-buffered saline
DSC – differential scanning calorimetry

E
η – eta
E – glutamic acid
EC – external compartment
ECM – extracellular matrix
EDAC – 1-ethyl-3-(3-dimethylaminopropyl) carbodiimide

EDS – energy dispersive spectroscopy
EDTA – ethylenediamine tetraacetic acid
EDX – energy dispersive X-ray
EFG – epidermal growth factor
ELP – elastin-like polymers
ELR – elastin-like recombinamer
ePTFE – expanded poly(tetrafluoroethylene)
ES – embryonic stem cell
ESA – electrostatic self-assembly

F
F – phenylalanine
FBS – fetal bovine serum
$FeCl_2 \cdot 4H_2O$ – iron(II) chloride tetrahydrate
$FeCl_3 \cdot 6H_2O$ – iron(III) chloride hexahydrate
FGF – fibroblast growth factor
FITC – fluorescein isothiocyanate
FTIR – Fourier transform infrared

G
γ – gamma
G – glycine
GAG – glucosaminoglycan
GEL – gelatin
GOX – glucose oxidase

H
H – histidine (amino acid)
h – hour (unit)
^{1}H-NMR – hydrogen-1 nuclear magnetic resonance
H_2O – water
HA – hyaluronic acid / hyaluronan
HAP – hydroxyapatite
HCl – hydrochloric acid
HEPES – 4-(2-hydroxyethyl)-1-piperazineethanesulfonic acid
hMSC – human mesenchymal stem cell
HPLC – high-performance liquid chromatography
HRP – horseradish peroxidase
HSA – human serum albumin
HSC – hematopoietic stem cells
HUVECS – human umbilical vein endothelial cells
Hz – hertz

I
I – isoleucine
IC – internal compartment
I_{FS} – forward-scattering intensity
Ig – immunoglobulin
I_{green} – green fluorescence intensity
I_{red} – red fluorescence intensity
I_{SS} – side-scattering intensity
ITT – inverse temperature transition

K
K – lysine
K_2HPO_4 – dipotassium phosphate
kDa – kilodalton
kg – kilogram
KH_2PO_4 – monopotassium phosphate
kOe – kiloOersted
kV – kilovolts

L
λ - lambda
L – leucine (amino acid)
L – liter (unit)
LbL – layer-by-layer
LCST – lower critical solution temperature

M

μ – mu

μm – micrometer

μL – microliter

M – methionine (M)

m – meter (unit)

MALDI-TOF – Matrix-assisted laser desorption/ionization time-of-flight

MAPLE – matrix-assisted pulsed laser evaporation

mg – milligram

$MgSO_4 \cdot 7H_2O$ – magnesium sulfate heptahydrate

MHC – major histocompatibility complex

MHz – megahertz

min – minute

mL – milliliter

mm – millimeter

M_n – polymer molecular weight

MNP – magnetic nanoparticle

MRI – magnetic resonance imaging

MSC – mesenchymal stem cell

MTS – 3-(4,5-dimethylthiazol-2-yl)-5-(3-carboxymethoxyphenyl)-2-(4-sulfophenyl)-2H-tetrazolium

mV – millivolt

N

ν – nu

Na_2CO_3 – sodium carbonate

Na_2HPO_4 – disodium phosphate

NaCl – sodium chloride

NADH – nicotinamide adenine dinucleotide, reduced form

NaH_2PO_4 – monosodium phosphate

NaOH – sodium hydroxide

NdFeB – neodymium

NH_3 – ammonia

NH_4OH – hydroxide solution

$(NH_4)_2SO_4$ – ammonium sulfate

NIR – near-infrared

nm – nanometer

O

ω – omega

P

% (v/v) – percentage of volume/volume

% (w/v) – percentage of mass/volume

P – proline

Pa – Pascal

PAA – poly(acrylic acid)

PAH – poly(allylamine hydrochloride)

PBS – phosphate-buffered saline

PC – personal computer

PCl_3 – phosphorus trichloride

PD-PPO-PD/PAA – poly(*N,N* –dimethyl aminoethyl methacrylate)-poly(propylene oxide)/poly(acrylic acid)

PDAAEMA – poly(*N,N*-dyakylamino ethylmethacrylates

PDADMAC – poly(diallyldimethylammonium) chloride

PDGF – platelet-derived growth factor

PEG – poly(ethylene glycol)

PEI – poly(ethyleneimine)

PEM – polyelectrolyte multilayer

PGA – poly(glutamic acid)
Ph-levan – phosphonate-derivatized levan
pK_a – acid dissociation constant
PLGA – poly(lactic-co-glycolic acid)
PLL – poly(L-lysine)
PLLA – poly(L-lactic acid)
PLLs – poly(L-lysine succinylated)
PMAc – poly-(methacrylic acid)-co-(cholesteryl methacrylate)
PMEMA-b-PDPA – poly[2-(*N*-morpholino) ethyl methacrylate-block-2-(diisopropylamino)ethyl methacrylate]
PMLC – polymeric multilayer capsules
PMMA – poly(methyl methacrylate)
PNIPAAm – poly(*N*-isopropylacrylamide)
pNP – p-nytrophenyl
PS – polystyrene
PSP – poly(sodium phosphate)
PSS – poly(styrene sulfonate)
PTFE – poly(tetrafluoroethylene)
PVA – poly(vinyl alcohol)
PVCL – poly(*N*-vinylcaprolactam)
PVDF – polyvinylidene difluoride
PVS – poly(vinyl sulfate)

Q

QBP – glutamine binding proteins
QCM-D – quartz-crystal microbalance with dissipation monitoring

R

ρ – rho
R – arginine
RDL – recursive directional ligation
rhBMP-2 – recombinant human bone morphogenetic protein-2
Rhod – rhodamine-B isothiocyanate
rISECS – rat liver sinusoidal endothelial cells
RMS – root-mean-square
rpm – rotations per minute
Ru(dpp) – tris(4,7-diphenyl-1,10-phenanthroline)ruthenium(II) dichloride complex

S

S – serine (amino acid)
s – second (unit)
SBF – simulated body fluid
SAM – self-assembled monolayer
SD – standard deviation
SE – standard error
SEM – scanning electron microscopy
SNARF-1 – seminaphtho-rhodafluor-1-dye
STM – scanning tunneling microscopy
SVAS – supravalvular aortic stenosis

T

T – threonine (amino acid)
T – tesla (unit)
TB – terrific broth
TC – thiocoraline
TCP – tricalcium phosphate
TCPS – tissue culture polystyrene
TEM – transmission electron microscopy
TERM – tissue engineering and regenerative medicine
TFE – trifluoroethanol

TGF – tissue growth factor

TRAP – thermodynamically reversible addressing of proteins

TRITC – tetramethylrhodamine B isothiocyanate

T_t – transition temperature

U $U \cdot mL^{-1}$ – units per milliliter

UCST – upper critical solution temperature

UV – ultraviolet

V V – valine

VEGF – vascular endothelial growth factor

Z ζ – zeta

List of Figures

SECTION I – GENERAL INTRODUCTION

Chapter 1. Nanostructured devices produced by layer-by-layer self-assembly adsorption for tissue engineering applications

Figure 1.1. On the left: Individual connections between two paraffin wax particles. On the right: Florescence images showing the multilayered 3D assembly after leaching of the core material. Reprinted (adapted) with permission from [113]. Copyright 2010 Wiley-VCH. 17

Figure 1.2. On the left: Light microscopy image of trypan blue-stained islets after encapsulation with three pairs of polyelectrolyte layers $(PDADMAC/PSS)_3$. On the right: Electron micrographs of PAH/PSS/PAH-coated islets. Reprinted (adapted) with permission from [123]. Copyright 2006 American Chemical Society. 18

Figure 1.3. Physical changes induced in ELR modified surfaces. (a) Wettability variations with different temperatures. Reprinted (adapted) with permission from [131]. Copyright 2009 Wiley-VCH. (b) Topography at distinct pHs. Reprinted (adapted) with permission from [78]. Copyright 2011 Wiley-VCH. 20

Figure 1.4. Effect of incubation time on the formation of calcium phosphate crystals using liposome and liponano–CHI–DNA templates. Each reaction was carried out at pH 7.0 and pH 10.0 for 18 h, using calcium chloride ($CaCl_2$) and disodium phosphate/monosodium phosphate (Na_2HPO_4/NaH_2PO_4) as ion species. Reprinted with permission from [144]. Copyright 2011 American Chemical Society. 23

Chapter 2. Polyelectrolyte multilayered assemblies in biomedical technologies

Figure 2.1. Schematics of layer-by-layer adsorption of polyelectrolytes based on an electrostatic mechanism deposition. The procedure is based on the contact of the substrate with a solution with an oppositely charged polymer. In the depicted example, negatively charged round substrates are submerged in an aqueous solution of a polycation, followed by a solution containing a polyanion. Each adsorption stage is separated by a rinsing step, to remove loosely adsorbed molecules. 41

Figure 2.2. Formation of calcium phosphate over the surface of polysaccharide-coated liposomes. (a) Liposomes encapsulating phosphate ions (PO_4^{3-}) are coated with polysaccharides. Polycations (orange)

and polyanions (green) are adsorbed sequentially over the surface and placed in a medium containing calcium ions (Ca^{2+}), which concentrate around the negatively charged molecules. The counter-diffusion of ions across the wall leads to the formation of a calcium phosphate mineral interface. (b) Field emission TEM image of a liposome coated with CHI and DNA after inducing mineralization at pH 10 for 18 h, exhibiting a thick wall. (c) Energy dispersive X-ray analysis (EDX) exhibiting calcium and phosphate peaks. Adapted with permission from ref. [97] Copyright 2011, American Chemical Society. 47

Figure 2.3. Typical photographs obtained using (heparin/collagen)$_5$-CD34 multilayer-modified stents. In (a) and (b), cross-section optical images of rabbit femoral arteries with (heparin/collagen)$_5$-CD34 multilayer-modified stents. (c) Fluorescence microscopy image of the multilayer on stent, with CD34 tagged with FITC. Inset shows the optical image of the stent. (d) SEM image of the inner wall of the stented rabbit femoral arteries for 48 h, showing the formation of a complete endothelium. Adapted with permission from ref. [121] Copyright 2010, Elsevier. 52

Figure 2.4. Free-standing nanosheets and their various applications. (a) Basic concept of the spin-coating-assisted LbL fabrication method. Upon polyelectrolyte deposition, a PVA layer is cast allowing peeling-off the nanosheet easily, subject to posterior dissolution. (b) CHI/ALG nanosheet securing a repaired visceral pleural defect in beagle dogs when pressurized by over 50cm H_2O pressure 3 h after repair. The region indicated by arrows shows the nanosheet-sealed area. Reprinted with permission from ref. [151] Copyright 2009, Wiley-VCH; (c) Macroscopic images after treating a murine cecal puncture hole with a tetracycline layer sandwiched between CHI/ALG multilayers and poly (vinyl acetate). Reprinted with permission from ref. [153] Copyright 2010, Elsevier; (d) Macroscopic images of murine dorsal skin treated with tetracycline-loaded CHI/ALG nanosheets illuminated under UV light, remaining at the wound site for 7 days. Reprinted with permission from ref. [154] Copyright 2012, Elsevier. 56

Figure 2.5. Temperature-responsiveness of CHI/ELR microcapsules and size/permeability effects. (a) Multilayer coatings were assembled around calcium carbonate sacrificial templates. Confocal laser scanning microscopy images of BSA-loaded (CHI/ELR)$_5$ microcapsules with the final layer tagged with rhodamine at (b) 25 and (c) 37 °C. Cumulative release of BSA from (CHI/ELR)$_1$, (CHI/ELR)$_3$ and (CHI/ELR)$_5$ microcapsules: ■□, ○●, and ▲Δ, respectively, in PBS (pH 7.4), at (d) 25 °C and (e) 37 °C. Adapted with permission from ref. [179] Copyright 2013, Elsevier. 61

Figure 2.6. Enzymatic cleavage of DQ-ovalbumin upon internalization by embryonic NIH/3T3 fibroblasts. Fluorescent cargo was encapsulated either in (a) nondegradable PSS/PAH or (b) degradable dextran sulfate/poly(L-arginine) microcapsules. Images were taken immediately after the addition of the capsules to the culture over-time up to 120 h under confocal microscopy in different channels, green, red, and transmission, where green corresponds to cleaved DQ-ovalbumin and red corresponds to intact cargo. Adapted with permission from ref. [183] Copyright 2009, American Chemical Society. 64

Figure 2.7. Fabrication and response of biosensors based on BSA-functionalized MNPs. (a) Biotin- and avidin-modified HRP layers are assembled on top of bidimensional or three-dimensional surfaces to produce (i) flat mono-enzyme, (ii) spherical mono-enzyme or (iii) spherical bi-enzyme sensors. The substrate accessibility to inner layer enzymes is more favorable when using the spherical templates. (b) Production of multilayer single- and bi-enzyme MNP systems using HRP and GOX. (c) Total HRP activity as a function of the number of HRP layers in HRP-MNP systems, showing a linear activity increase with increasing number of layers. (d) Schematic of the coupled bi-enzymatic reaction in the GOX-HRP-MNP system. (e) Photographs showing the colorimetric detection of glucose with the coupled GOX–$(HRP)_5$–MNP system after 3 h with increasing concentrations of glucose. The discoloration in vial 6 (highest concentration of glucose) is attributed to the protonation of resorufin – which is only absorbing in its deprotonated form – due to the decrease of pH from the formation of gluconic acid. Adapted with permission from ref. [192] Copyright 2011, The Royal Society of Chemistry. 67

Figure 2.8. Hollow CHI/ALG multilayer tubes. (a) PEMs are assembled on paraffin-coated tubes, the latter being leachable using an organic solvent. (b) SEM image of a crosslinked tube. (c) Variations of storage modulus (E') with or without crosslinking obtained by dynamic mechanical analysis in wet conditions and 37°C. (d) L929 fibroblast-like cells seeded on crosslinked tubes at day 7 of culture. Adapted with permission from ref. [201] Copyright 2013, Wiley-VCH. 70

Figure 2.9. (a) General route for the synthesis of shell-in-shell microcapsules. (b) Confocal laser scanning microscopy of the shell-in-shell structure and HAS distribution 5 seconds after core dissolution. The dashed circle indicates the original position of the inner capsule. (c) Formation and diffusion of resorufin in a coupled enzymatic test using GOX and peroxidase. Reprinted with permission from ref. [219] Copyright 2007, Wiley-VCH. 73

Figure 2.10. Biological performance of heparin/CHI multilayer-coated decellularized porcine aortic valves. (a) Fluorescence of the multilayers adsorded onto the valves. The polymers' fluorescence (red

for heparin and green corresponds for CHI) is uniform and non-overlapping. Platelets (b) and leukocytes (c) adhered poorly to the multilayer-coated decellularized valves. (d) The developed devices were repopulated with endothelial progenitor cells exhibiting a contiguous, flat morphology. Reprinted with permission from ref. [229] Copyright 2012, Elsevier. 77

Figure 2.11. Cell-accumulation technique allows assembling three-dimensional cellular constructs. (a) Illustration of the rapid construction of 3D multilayered tissues by cell-accumulation using fibronectin/GEL-coated cells. (b) Schematics of a cellular construct consisting on 4+4 layers of human dermal fibroblast cells, intercalated with a layer of HUVECs. (c) Confocal laser scanning microscopy cross-section image of the construct presented in "b", showing tubular endothelial structures after 1 week of incubation. Green cells correspond to human dermal fibroblast cells and red cells to HUVECs. Adapted with permission from ref. [235], Copyright 2011, Wiley-VCH. 80

Figure 2.12. Production and characterization of multilayer-coated liquefied ALG capsules. (a) Cells are mixed with solutions of either ALG solely ALG-containing PLLA microparticles. Both solutions are extruded separately, originating ALG beads by ionotropic gelation. Upon coating with multilayers of diverse polyelectrolytes (CHI, ALG and PLL), the crosslinked ALG core is liquefied by EDTA, originating liquefied capsules encapsulating cells (ALG capsules), or encapsulating cells and PLLA microparticles (PLLA capsules). Optical microscopy of (b) liquefied capsules encapsulating (c) PLLA microparticles. Adapted with permission from ref. [236] Copyright 2013, American Chemical Society. (d) Fluorescence assay of PLLA capsules at day 7 of culture, showing cells adhered to the surface of the PLLA microparticles. Cell nuclei were stained blue and actin filaments red. Reproduced with permission from ref. [237] Copyright 2013, The Royal Society of Chemistry. 81

Chapter 3. Elastin-like macromolecules

Figure 3.1. The elastogenesis phenomenon, starting by the translation of the elastin gene and proceeding to its alignment by microfibrils. 106

Figure 3.2. The five axioms of elastin-like recombinamers, according to Urry [10]. 112

Figure 3.3. Schematic diagram of increasing complexity of ELRs with different functionality for use in various applications. Recombination techniques allow obtaining several degrees of complex: the schematic represents (a) a simple model of recombinant elastin; (b) the introduction of specific peptide

sequences and blocks with distinct properties; (c) the inclusion of a bioactive motif or; (d) the inclusion of more than one in the same peptidic formulation. 114

Figure 3.4. Microscopy assessment of HUVECs seeded in macroporous ELP hydrogels after 48 h of incubation in: (a) fluorescence microscopy with phalloidin Alexa Fluor488 and 4',6-diamidino-2-phenylindole (DAPI) staining; and (b) SEM magnified view. Reprinted (adapted) with permission from [133]. Copyright 2009 American Chemical Society. 117

Figure 3.5. Physical changes induced in ELR modified surfaces. (a) Wettability variations with different temperatures. Reprinted (adapted) with permission from [172]. Copyright 2009 Wiley-VCH. (b) Topography at distinct pHs. Reprinted (adapted) with permission from [173]. Copyright 2011 Wiley-VCH. 122

Chapter 4. Stimuli-responsive surfaces for biomedical applications

Figure 4.1. Schematic structure of interfaces formed by (a) self-assembled monolayer, (b) thin polymer network films, (c) grafting and (d) layer-by-layer. 141

Figure 4.2. Water drop profiles on ELP-coated substrates at 25 and 50°C. Reprinted (adapted) with permission from [82]. Copyright 2009 Wiley-VCH. 148

Figure 4.3. Transmission electron microscopy (TEM) images of azido- and acetylene-functionalized PNIPAAm microcapsules dried at 25 °C and 50 °C. Scale bar: 2 μm. Reprinted (adapted) with permission from [131]. Copyright 2009 American Chemical Society. 154

Figure 4.4. In-situ detachment of SaOs-2 cell sheets after 10 min (A) and 15 min (B) of incubation at 4°C from $(GRAFT/ALG)_5GRAFT$ films. Reprinted with permission from [70]. Copyright 2011 American Chemical Society. 157

SECTION II – EXPERIMENTAL SECTION

Chapter 5. Materials and methods

Figure 5.1. Molecular structure of (a) chitosan, (b) levan, and (c) alginate. 174

Figure 5.2. Scanning electron microscopy image of a preparation of *Halomonas sp.* strain. Source: http://commtechlab.msu.edu/sites/dlc-me/zoo/zdx0283.html, September 10th 2013. 174

Figure 5.3. The molecular biology steps of RDL. (A) A synthetic monomer gene is inserted into a cloning vector. (B) The gene is designed to contain recognition sites for two different restriction endonucleases, RE1 and RE2, at each of the coding sequence. (C) An insert is prepared by digestion of the vector with both RE1 and RE2 and subsequently ligated into the vector that has been linearized by digestion with only RE1. (D) The product contains two head-to-tail repeats of the original gene, with the RE1 and RE2 sites maintained only at the ends of the gene. (E) Additional rounds of RDL proceed identically, using products from previous rounds as starting materials. Reprinted with permission from [18], Copyright 2002, American Chemical Society. (F) Recombinant bacteria containing the desired gene are submitted to fermentation and purified afterwards to extract the bioproduced polymer. 177

Figure 5.4. Typical structure of the *N*-D-glucosamine monomer in chitosan molecules. Each distinct hydrogen atom is identified from 1 to 6. 180

Figure 5.5. Schematic representation of LbL adsorption on top of gold-coated quartz crystal sensors. 185

Figure 5.6. Experimental setup for the measurement of the lap shear adhesive strength. 187

Figure 5.7. Schematics of contact angle measurements. The dotted surface symbolizes a modified glass substrate. 188

Figure 5.8. Scheme depicting the formation of multilayer hollow microcapsules encapsulating a desired agent. 192

Figure 5.9. Organization of multilayer compartments, with rhodamine molecules and MNPs found at the nanolevel, the smallest scale of the proposed hierarchy. 192

SECTION III – OPTIMIZATION OF LAYER-BY-LAYER STRATEGIES FOR BIOMEDICAL APPLICATIONS

Chapter 6. Adhesive nanostructured multilayer films using a bacterial exopolysaccharide for biomedical applications

Figure 6.1. Reaction scheme of phosphonate modification of levan. 217

Figure 6.2. FTIR spectra of levan samples as-produced (in red) and phosphonate (in black). The Ph-levan spectrum is represented with an offset of +0.04 of absorbance. The bands respective to

phosphonate groups are highlighted with grey background, with the inset showing the augmented spectra between 700 and 1000 cm^{-1}. 218

Figure 6.3. EDS spectrum of a Ph-levan sample. 218

Figure 6.4. Buildup assessment of (CHI/Ph-levan) films. A: QCM-D monitoring of normalized frequency, $\Delta F_v/v$, and dissipation ΔD, obtained from the 5^{th} overtone, for a total of 3 bilayers. Numbers refer to adsorption of CHI (1), adsorption of Ph-levan (3), and rinsing (2 and 4). B: Evolution of thickness of (CHI/Ph-levan) films with the number of layers. An odd layer number represents a film ending in CHI and an even number a film ending in Ph-levan. Data represent mean±standard deviation (SD). 219

Figure 6.5. SEM images of (A) $(CHI/Ph\text{-}levan)_{50}$ and (B) $(CHI/ALG)_{50}$ films assembled onto glass. Inset scale bar: 50 μm. 220

Figure 6.6. Lap shear stress for detachment of $(CHI/Ph\text{-}levan)_{50}$ and $(CHI/ALG)_{50}$ multilayers assembled onto glass slides (A) as a function of extension (representative curves). (B) Lap shear strength for the two multilayer films (mean±SD; n=3; *$p<0.05$). 221

Figure 6.7. A: L929 cell density after 24 h of culture (n=3; $p<0.05$). DAPI staining of adhered cells on (B) $(CHI/Ph\text{-}levan)_{50}$ and (C) $(CHI/ALG)_{50}$ substrates. 223

Chapter 7. Layer-by-layer film-growth using polysaccharides and recombinant polypeptides: a combinatorial approach

Figure 7.1. Range of ζ-potentials for each polysaccharide/ELR combination. CHI40, CHI55, ALG40 and ALG55 represent combinations of CHI or ALG at pH 4.0 or pH 5.5. The division serves to indicate the charge balance between each polymer in terms of positive (red) and negative (blue) proportion of the whole bar length. Bars depicted in light blue and purple represent combinations in which both polymers exhibit potential with the same signal. For example, in the first column, where CHI and 3K-$VRDG^{(-)}V$ were used at pH 4.0, the ζ-potentials were +16.8 mV and -2.7 mV, respectively. In the last column, where ALG and V84 were used at pH 5.5, the ζ-potentials were -15.5 mV and -1 mV, respectively. 240

Figure 7.2. Representative QCM-D acquisition graphics depicting the 5^{th} overtone variations of frequency (A, B) and dissipation (C, D) for hybrid polysaccharide/ELR films at pH 4.0 and 5.5. The case

of H-RGD6 combinations is depicted. Results for CHI40 (□), CHI55 (■), ALG40 (○) and ALG55 (●) are shown. Absolute values of ΔF and ΔD reached values of (A) 24 Hz (□), 200 Hz (■); (B) 223 Hz (○), 81 Hz (●); (C) 6×10^{-6} (□), 21×10^{-6} (■); (D) 32×10^{-6} (○), 5×10^{-6} (●). 241

Figure 7.3. Thickness values for multilayered films containing five bilayers, as estimated using the Voigt-based viscoelastic model, for each polysaccharide/ELR permutation at pH 4.0 and pH 5.5. Deviation bars represent two standard deviations. 243

Figure 7.4. Variations in film thickness with ELR molecular weight sorted by pH and ζ-potential. Results for CHI40 (□), CHI55 (■), ALG40 (○) and ALG55 (●) are shown. The mean thickness of 3K-VRDG$^{(-)}$V and 3K-VRGDV films (M_n=31371 Da) is represented. 246

Figure 7.5. Representative scheme of the hypothetical interactions occurring between polysaccharides and ELRs. 247

Supplemental Figure 7.1. MALDI-TOF spectra of the bioproduced ELRs, with major peaks signaled and experimental molecular weight distribution. Secondary peaks are assigned to doubly charged species. 255

Supplemental Figure 7.2. Evolution of thickness with (A) ζ-potential and (B) molecular weight for the ELRs studied herein. The mean thickness of 3K-VRDG$^{(-)}$V and 3K-VRGDV (M_n=31371 Da) is represented in the latter. 256

Chapter 7 – Appendix. Nanostructured thin coatings from chitosan and an elastin-like recombinamer with acute stimuli-responsive behavior

Appendix Figure 7.1. Representative structure of the featured ELRs and corresponding block peptide sequence. 275

Appendix Figure 7.2. QCM-D monitoring of the frequency (■) and dissipation (Δ) variations for a) CHI/monoblock and b) CHI/triblock. The dashed lines mark the end of the adsorption of one bilayer. 276

Appendix Figure 7.3. Contact angle variations of $(CHI/monoblock)_5$ (■) and $(CHI/triblock)_1$ (Δ) upon temperature changes and evolution with time. 277

Appendix Figure 7.4. AFM imaging for (CHI/monoblock)$_5$ films for 1, 3 and 5 bilayers, at 25 and 50°C. Similar results were obtained for pH 7.4 and pH 14. Scale bar: 200 nm. 278

Chapter 8. Layer-by-layer assembly of chitosan and recombinant biopolymers into biomimetic coatings with multiple stimuli-responsive properties

Figure 8.1. Characterization of the ELR-RGD. a) schematic representation of the featured ELR chemical structure; b) MALDI-TOF of the biopolymer, with major peak signaled at 31229 Da. 291

Figure 8.2. Buildup assessment of CHI/ELR-RGD films. a) QCM-D monitoring of normalized frequency ($\Delta F_\nu/\nu$, ■) and dissipation (ΔD, □) obtained at the 5th overtone. Numbers refer to adsorption of CHI (1), adsorption of ELR-RGD (3) and rinsing (2 and 4). b) Cumulative thickness evolution and thickness increase for the CHI/ELR-RGD film, for 20 layers, estimated using the Voigt model. Odd numbers correspond to films ending in CHI and even numbers to films ending in ELR-RGD. Linear fitting matches well the cumulative thickness variation (r^2=0.99824). 292

Figure 8.3. Evolution of the contact angle of the films obtained with sequential adsorption of CHI and ELR-RGD, up to 10 layers Odd numbers correspond to films ending in CHI and even numbers to films ending in ELR-RGD. Error bars represent two standard deviations (n=9). 294

Figure 8.4. Contact angle measurements as a function of temperature (□), pH (○), and ionic strength (Δ) in a (CHI/ELR-RGD)$_5$ film. Three cycles are represented. Error bars represent two standard deviations (n=9). 295

Figure 8.5. Map of the wettability of (CHI/ELR-RGD)$_5$ films as a function of condition arrays of temperature, pH, and ionic strength stimuli. Open symbols stand for a moderate hydrophobic surface (contact angle of about 67°) and closed ones for a superhydrophilic surface. The blue squares represent measurements performed at 25°C and 37°C and the red circles measurements at 50°C. 297

Figure 8.6. RMS-roughness of 5 pairs of CHI/ELR-RGD layers, ending in CHI (grey) and ELR-RGD (white). Error bars represent two standard deviations (n=3). The insets are AFM images at pH 7.4 and 11, for the 5th pair of layers, ending in ELR-RGD, in a 1×1 μm^2 area. Data are means±standard deviation (SD) (n=3; $p<0.05$, * are samples at the same pH, # are samples at different pH). 299

Figure 8.7. *In vitro* tests on films ending in CHI, ELR-RGD and ELR-RDG$^{(-)}$. a) Cell viability of SaOs-2 cells for 4 h, 24 h and 3 days. Data are means±SD (n=3; *p<0.05). b) ALP assays on the studied films. Data are means±SD (n=3; *p<0.05). 301

Figure 8.8. DAPI (blue) and phalloidin (red) staining of the studied cells cultured for distinct times on the studied multilayer substrates, ending in CHI, ELR-RGD and ELR-RDG$^{(-)}$. Tests performed at 4 h, 24 h, and 3 days. Scale bar: 100 μm. 302

Chapter 9. Nanostructured and thermoresponsive recombinant biopolymer-based microcapsules for the delivery of active molecules

Figure 9.1. Aggregate size profile for a 300 μg·mL^{-1} ELR solution in PBS over the temperature range 25–37°C. Means±standard deviation (SD) are represented. Insets show a transparent solution below 29°C and increased turbidity above it. 316

Figure 9.2. (A) SEM image of a $CaCO_3$ microparticle containing entrapped BSA. (B) CLSM image of a microcapsule containing FITC-BSA after chelation. (C) A graphic showing the stage losses measured during construction of the microcapsules. Data represent mean±SD (n=3; *p<0.05). 317

Figure 9.3. Left: CLSM images of pre-loaded $(CHI/ELR)_5$ microcapsules at (A) 25 and (B) 37°C. The final layer was tagged with rhodamine B. Right: size distribution and fractional frequency (f). The normal distribution approximation, which fits a 95% confidence interval, is depicted. 318

Figure 9.4. (A) Viability of L929 cells after 24 h and 3 and 7 days in the presence of empty and BSA-loaded $(CHI/ELR)_5$ microcapsules. The positive control was L929 cells in the same medium with no microcapsule addition. Data represent mean±SD (n=3; *p<0.05). DAPI (blue) and phalloidin (red) staining in fluorescence microscopy of L929 cells after contact with (B) microcapsule-free medium and (C) BSA-loaded $(CHI/ELR)_5$ microcapsules for 24 hours. Scale bar: 50 μm. 319

Figure 9.5. Cumulative release of BSA from $(CHI/ELR)_1$, $(CHI/ELR)_3$ and $(CHI/ELR)_5$ microcapsules: ■□, ○●, and ▲Δ, respectively, in PBS (pH 7.4), at (A) 25°C and (B) 37°C. 320

Supplemental Figure 9.1. Schematic of the ELR used. The bioactive sequence containing the negatively charged aspartic acids (RGD) is represented in green. 325

Supplemental Figure 9.2. Morphology of the sacrificial $CaCO_3$ templates observed by SEM. (A) Calcium carbonate microparticles with no entrapped BSA (≈2 μm) can be compared to (B) their counterparts containing BSA in their interior (≈5-6 μm). In (B) a rhombohedron can be observed in the background. 326

Supplemental Figure 9.3. Cumulative losses during microcapsule construction (from entrapment to chelation). Means±SD are represented. 326

Supplemental Figure 9.4. Release kinetics of the encapsulated BSA at 25°C. Korsmeyer kinetics (log cumulative percent drug released vs. log time), with correlation values (r^2). 327

Supplemental Figure 9.5. Release kinetics of the encapsulated BSA at 37 °C. Korsmeyer kinetics (log cumulative percent drug released vs. log time), with correlation values (r^2). 328

Supplemental Figure 9.6. Release kinetics of the encapsulated BSA at 25°C. Zero-order kinetics (cumulative percent drug released vs. time), with correlation values (r^2). 328

Supplemental Figure 9.7. Release kinetics of the encapsulated BSA at 37°C. Zero-order kinetics (cumulative percent drug released vs. time), with correlation values (r^2). 329

Supplemental Figure 9.8. Release kinetics of the encapsulated BSA at 25°C. First-order kinetics (log cumulative percent drug remaining vs. time), with correlation values (r^2). 329

Supplemental Figure 9.9. Release kinetics of the encapsulated BSA at 37°C. First-order kinetics (log cumulative percent drug remaining vs. time), with correlation values (r^2). 330

Supplemental Figure 9.10. Release kinetics of the encapsulated BSA at 25°C. Higuchi kinetics (cumulative percent drug released vs. square root of time), with correlation values (r^2). 330

Supplemental Figure 9.11. Release kinetics of the encapsulated BSA at 37°C. Higuchi kinetics (cumulative percent drug released vs. square root of time), with correlation values (r^2). 331

Chapter 10. Cellular uptake of multilayered capsules produced with biomimetic and genetically engineered macromolecules

Figure 10.1. (A) Representative TEM image of a microcapsule showing a detail of the multilayer shell delimited by the dashed lines. (B) CLSM micrograph of several microcapsules with the wall tagged with rhodamine. Micrograph is representative of both $(CHI/ELR\text{-}RGD)_2$ and $(CHI/ELR\text{-}RDG^{(-)})_2$ microcapsules.

(C) Fluorescence intensity plot profile of three individual microcapsules depicted in (B). The peaks coincide with the capsules' walls, while the plateau in between corresponds to the hollow interior. SEM images of (D) (CHI/ELR-RGD)$_2$ and (E) (CHI/ELR-RDG$^{(-)}$)$_2$ microcapsules, with a vertical tilt of 20°. 346

Figure 10.2. Metabolic activity of hMSCs incubated with increasing ratios of (A, B) (CHI/ELR-RGD)$_2$ and (C, D) (CHI/ELR-RDG$^{(-)}$)$_2$ microcapsules for (A, C) 3 h and (B, D) 72 h. Data represent means of four experiments, each performed in quadruplicate, normalized in respect to the positive control. Error bars represent one standard error (mean+SE). No significant statistical differences were found (*p*-value higher than 0.05). 348

Figure 10.3. Estimated metabolic activity of hMSCs incubated with (CHI/ELR-RGD)$_2$ and (CHI/ELR-RDG$^{(-)}$)$_2$ microcapsules for 3 and 72 h. Data represent means of the viability results performed for microcapsule/cell ratios from 5:1 to 100:1, as compared to the positive control (PC, cells cultured without microcapsules). Error bars represent one standard error (mean+SE). No significant statistical differences were found (*p*-value higher than 0.05). 349

Figure 10.4. Representative microphotographs of LIVE/DEAD® assay of hMSCs incubated with (A, B and C) (CHI/ELR-RGD)$_2$ and (D, E and F) (CHI/ELR-RDG$^{(-)}$)$_2$ microcapsules at 0 (A, D) and 72 h (B, E) and 240 h times points. (C, F). 350

Figure 10.5. Confocal microscopy of hMSCs containing (CHI/ELR-RGD)$_2$ microcapsules within their cytoplasm. The nuclei are stained with DAPI (blue) and the microcapsules loaded with DQ-ovalbumin. The schematics represent the relative position of each plane in the cell (A, B and C). The arrows in (A) point to bright green dots, representing fully processed DQ-ovalbumin. (D) Bright field image was merged with the fluorescence-only image in (C). 352

Figure 10.6. Flow cytometry 2D density plots of hMSCs after a 72 h incubation with (A, B) (CHI/ELR-RGD)$_2$ and (C, D) (CHI/ELR-RDG$^{(-)}$)$_2$ microcapsules. The density of the events is color-coded from blue (low frequency) to red (high frequency). (A, C) Side-scattering intensity (I_{SS}) is plotted as a function of forward-scattering intensity (I_{FS}). The area delimited in yellow corresponds to viable cells either empty (low I_{SS}) or with internalized microcapsules (high I_{SS}), and was established based in a control of hMSCs cultured in the absence of microcapsules. (B, D) The events corresponding to viable cells were sorted according to red (I_{red}) and green (I_{green}) fluorescence intensities and events corresponding to empty or cells containing microcapsules were subdivided. (E) Internalization efficiency

of each type of capsule for three independent experiments. Data represent means of three independent experiments. Error bars represent two standard errors (mean±SE). No significant statistical differences were found (*p*-value higher than 0.05). 353

Figure 10.7. The scheme (A) depicts the various degradation stages that DQ-ovalbumin undergoes. Representative microscopy images of $(CHI/ELR\text{-}RGD)_2$ and $(CHI/ELR\text{-}RDG^{(-)})_2$ microcapsules loaded with DQ-ovalbumin incubated with hMSCs after (B, D) 3 or (C, E) 72 h of incubation and DAPI staining (nuclei of the cells stained in blue). A shift from red/orange to green/yellow indicates a transition between fully intact to degraded cargo. Images are of fluorescence and differential interference contrast (DIC) microscopy at 40× magnification. 355

Chapter 11. Multifunctional compartmentalized capsules with a hierarchical organization from the nano- to the macro-scales

Figure 11.1. Hierarchical organization of the multicompartmental capsules. Liquefied alginate beads, delimited by a $(CHI/ALG)_3$ coating, are visible to the naked eye. Multilayer microcapsules of $(CHI/ELR)_3$ and molecular compounds can be suspended within the aqueous polymer phase. The former can further contain other types of molecular compounds and MNPs. 371

Figure 11.2. Scales of hierarchical components. (a) TEM image of MNPs; (b) CLSM image of FITC-containing $(CHI/ELR)_3$ microcapsules; (c) fluorescence microscopy image of the Rhod-containing liquefied ALG bead coated with $(CHI/ALG)_3$. 373

Figure 11.3. Stimuli-responsiveness of the multicompartmental device constituents. (a) aggregate size measurements by DLS of CHI (pH 5.5), ALG and ELR (pH 7.4) at 300 $\mu g \cdot mL^{-1}$ for a temperature cycle of 25–37–25°C; (b) magnetization assay of MNPs. 374

Figure 11.4. Mechanical resistance of $(CHI/ALG)_3$ macrocapsules, ECs, to incremental centrifugal stress, with two standard deviations represented. 375

Figure 11.5. Distribution of the $(CHI/ELR)_3$ ICs within $(CHI/ALG)_3$ ECs by fluorescence microscopy. (a) This image was obtained by loading the former with FITC and the latter with Rhod. Separate green (b) and red (c) filters are shown. 376

Figure 11.6. Kinetics of Rhod release when encapsulated in the internal $(CHI/ELR)_3$ microcapsules (□) and the external $(CHI/ALG)_3$ compartment (○) at (a) 25°C and (b) 37°C for a time, *t*, of 2 h, with

two standard deviations represented. Some standard deviations are too small to be distinguished from the symbol. 377

Figure 11.7. Burst mechanism for Rhod loaded within internal microcompartments. (i) At first, Rhod is physically entrapped within $CaCO_3$ templates. (ii) After chelation, a fraction of Rhod is lost and quantified. The samples are rinsed to remove the lost fraction. However, another fraction remains free within the alginate. (iii) At the start of the release studies, the free Rhod diffuses to the exterior and is readily detected. ICs keep releasing Rhod to the alginate medium at a slower rate, and this Rhod is detected later in the experiment. 378

Figure 11.8. Magnetic characteristics of the multicompartmental system. TEM of a $(CHI/ELR)_3$ microcapsule (a) containing MNPs and (b) empty. Insets scale: 50 nm. (c) Attraction of $(CHI/ALG)_3$ ECs containing MNP-loaded $(CHI/ELR)_3$ ICs by a magnet in a PBS medium. The magnet is placed at a height of 1.4 cm on top of a polystyrene cover. The red color is characteristic of the MNPs within the hierarchical structure. Squares are 1×1 cm^2. 379

Supplemental Figure 11.1. ^{1}H-NMR spectrum of the purified chitosan sample, with 10.00 corresponding to I_c peak and 0.92 to I_e peak. 382

Supplemental Figure 11.2. Aggregate size profile for a 300 $\mu g \cdot mL^{-1}$ ELR solution in PBS over the temperature range, T, of 25–37°C, with two standard deviations represented. 382

Supplemental Figure 11.3. Rhodamine losses during the construction of Rhod-loaded microcapsules (ICs) within macrocapsules (ECs) and empty microcapsules within Rhod-loaded macrocapsules, with two standard deviations represented. 383

Supplemental Figure 11.4. Normalized mean distance, *d* in arbitrary units, traveled by MNP-loaded ICs within ECs as a function of time, *t*, from their starting point to the point of the highest magnetic field value available. 384

List of Tables

SECTION II – EXPERIMENTAL SECTION

Chapter 5. Materials and methods

Table 5.1. List of ELRs and corresponding amino acid sequence used throughout the various subsequent chapters. 178

SECTION III – OPTIMIZATION OF LAYER-BY-LAYER STRATEGIES FOR BIOMEDICAL APPLICATIONS

Chapter 7. Layer-by-layer film-growth using polysaccharides and recombinant polypeptides: a combinatorial approach

Table 7.1. List of ELRs used in this work with their corresponding theoretical molecular weight and proportions of charged and positive/negative amino acids. *Neutralized lysine residues. 236

Table 7.2. ζ-potentials (mV) for CHI, ALG and the ELRs at pH values of 4.0 and 5.5. 237

Supplemental Table 7.1. Theoretical and experimental amino acid compositions of 3K-VRDG$^{(-)}$V, 3K-VRGDV and HAP3. ND = not determined. 249

Supplemental Table 7.2. Theoretical and experimental amino acid compositions of GEG15, H3A20 and IK24. ND = not determined. 250

Supplemental Table 7.3. Theoretical and experimental amino acid compositions of H-RGD6, H3A20H3 and neutralized V84. ND = not determined. *G+H. 250

Chapter 7 – Appendix. Nanostructured thin coatings from chitosan and an elastin-like recombinamer with acute stimuli-responsive behavior

Appendix Table 7.1. Root-mean-square roughness for (CHI/monoblock)$_5$ films for 1, 3 and 5 bilayers, at 25 and 50°C, or pH 7.4 and pH 14, respectively. 279

Chapter 8. Layer-by-layer assembly of chitosan and recombinant biopolymers into biomimetic coatings with multiple stimuli-responsive properties

Table 8.1. Amino acid composition of the bioproduced ELR-RGD. ND = not determined. 291

Chapter 9. Nanostructured and thermoresponsive recombinant biopolymer-based microcapsules for the delivery of active molecules

Table 9.1. Exponents of the Korsmeyer kinetics model (n), correlation factors (r^2) and rate constant (K) for each architecture studied. 321

Supplemental Table 9.1. Calculated encapsulation efficiency, E_e, in %. 327

List of Publications

The work performed under the scope of this PhD thesis resulted in the publications listed below:

Papers in international scientific journals with referees

1. **Costa R. R.**, Custódio C. A., Arias F. J., Rodríguez-Cabello J. C., and Mano J. F., Layer-by-layer assembly of chitosan and recombinant biopolymers into biomimetic coatings with multiple stimuli-responsive properties, Small 2011, 7: 2640-2649, DOI:10.1002/smll.201100875.
2. **Costa R. R.**, Custódio C. A., Arias F. J., Rodríguez-Cabello J. C., and Mano J. F., Nanostructured and thermoresponsive recombinant biopolymer-based microcapsules for the delivery of active molecules, Nanomedicine: Nanotechnology, Biology and Medicine 2013, 9: 895-902, DOI:10.1016/j.nano.2013.01.013.
3. **Costa R. R.**, Neto A. I., Calgeris I., Correia C. R., Pinho A. C. M., Fonseca J., Öner E. T., and Mano J. F., Adhesive nanostructured multilayer films using a bacterial exopolysaccharide for biomedical applications, Journal of Materials Chemistry B 2013, 1: 2367-2374, DOI:10.1039/c3tb20137f.
4. **Costa R. R.**, Testera A. M., Arias F. J., Rodríguez-Cabello J. C., and Mano J. F., Layer-by-layer film-growth using polysaccharides and recombinant polypeptides: a combinatorial approach, The Journal of Physical Chemistry B 2013, 117: 6839-6848, DOI:10.1021/jp4028518.
5. **Costa R. R.**, Castro-Otero E., Arias F. J., Rodríguez-Cabello J. C., and Mano J. F., Multifunctional compartmentalized capsules with a hierarchical organization from the nano to the macro scales, Biomacromolecules 2013, 14: 2403-2410, DOI:10.1021/bm400527y.
6. **Costa R. R.**, Girotti A., Santos M., Arias F. J., Mano J. F., and Rodríguez-Cabello J. C., Cellular uptake of multilayered capsules produced with biomimetic and genetically engineered macromolecules, submitted (2013).
7. **Costa R. R.,** and Mano J. F., Polyelectrolyte multilayered assemblies in biomedical applications, submitted (2013).

Publications resulting from collaborative work

1. Silva J. M., Georgi N., **Costa R. R.**, Praveen S., Reis R. L., van Blitterswijk C. A., Karperien M., and Mano J. F., Nanostructured 3D constructs based on chitosan and chondroitin sulphate

multilayers for cartilage tissue engineering, PLOS ONE 2013, 8(2): e55451 (11 pages), DOI:10.1371/journal.pone.0055451.

Conference papers:

1. **Costa R. R.**, Ribeiro A. J., Rodríguez-Cabello J. C., and Mano J. F., Nanostructured thin coatings from chitosan and an elastin-like recombinamer with acute stimuli-responsive behavior, Materials Science Forum 2013, 730-732: 32-37, DOI:10.4028/www.scientific.net/MSF.730-732.32.

Conference abstracts published in international scientific journals

1. **Costa R. R.**, Custódio C. A., Arias F. J., Rodríguez-Cabello J. C., and Mano J. F., Nanostructured films exhibiting multiple stimuli responsive behavior and improved cell adhesion for tissue engineering, Histology and Histopathology 2011, 26(S1): 228.
2. **Costa R. R.**, Arias F. J., Rodríguez-Cabello J. C., and Mano J. F., Temperature-responsive microcapsules prepared by nanostructured multilayers of chitosan and an elastin-Like recombinamer for the controlled release of therapeutic molecules, The International Journal of Artificial Organs 2011, 34:656-657, DOI:10.5301/IJAO.2011.8701.
3. **Costa R. R.**, Custódio C. A., Arias F. J., Rodríguez-Cabello J. C., and Mano J. F., Self-assembled microcapsules with tunable and sustained release of macromolecules for tissue engineering, Journal of Tissue Engineering and Regenerative Medicine 2012, 6(S1):360, DOI:10.1002/term.1586.
4. **Costa R. R.**, Castro-Otero E., Arias F. J., Rodríguez-Cabello J. C., and Mano J. F., Nanostructured multilayer compartments: towards multifunctionality and 'cell-like' hierarchical complexity, Journal of Tissue Engineering and Regenerative Medicine 2012, 6(S2):25, DOI:10.1002/term.1608.
5. **Costa R. R.**, Castro-Otero E., Testera A. M., Arias F. J., Rodríguez-Cabello J. C., and Mano J. F., Extrapolation of hybrid polysaccharide and recombinant polypeptide multilayer films towards three-dimensional compartmentalization, Journal of Tissue Engineering and Regenerative Medicine, accepted for publication (2013).

6. **Costa R. R.**, Girotti A., Santos M., Arias F. J., Mano J. F., Rodríguez-Cabello J. C., Internalization of biomimetic microcapsules for intracellular delivery of active agents, Journal of Tissue Engineering and Regenerative Medicine, accepted for publication (2013).

Book chapters

1. **Costa R. R.**, Martín L., Mano J. F., and Rodríguez-Cabello J. C., Elastin-like macromolecules, In Mano J. F. (ed.), Biomimetic approaches for biomaterials development, Germany, Wiley-VCH, 2012, DOI:10.1002/9783527652273.ch5.
2. **Costa R. R.**, Alves N. M., Rodríguez-Cabello J. C., and Mano J. F., Stimuli-responsive surfaces for biomedical applications, In Taubert A., Mano J. F., and Rodríguez-Cabello J. C. (eds.), Biomaterials surface science, Germany, Wiley-VCH, 2013, DOI: 10.1002/9783527649600.ch4.
3. **Costa R. R.,** and Mano J. F., Layer-by-layer self-assembly techniques for nanostructured devices in tissue engineering, In Gaharwar A. K., Sant S., Hancock M. J., and Hacking A. (eds.), Nanomaterials in tissue engineering: characterization, fabrication and applications, United Kingdom, Woodhead Publishing Limited, 2013, ISBN: 978-0857095961.

Invited lectures

1. **Costa R. R.**, Rodríguez-Cabello J. C., and Mano J. F., What are elastin-like polymers?, 3B's Short Workshop on Natural-Based Polymers for Biomedical Applications, November 2009, Guimarães (Portugal).
2. **Costa R. R.**, and Mano J. F., Nanostructured multilayers in the production of new devices for biomedical applications, II 3B's Symposium on Biomaterials and Stem Cells in Regenerative Medicine, January 2012, Braga (Portugal).
3. **Costa R. R.**, and Mano J. F., Three-dimensional layer-by-layer strategies for tissue engineering and nanomedicine, II ICVS/3B's - Associate Laboratory Meeting, May 2012, Braga (Portugal).

Oral communications

1. **Costa R. R.**, Ribeiro A. J., Rodríguez-Cabello J. C., and Mano J. F., Nanostructured thin coatings from chitosan and an elastin-like recombinamer with acute stimuli-responsive behavior,

VI International Materials Symposium MATERIAIS 2011 and XV meeting of SPM – Sociedade Portuguesa de Materiais, April 2011, Guimarães (Portugal).

2. **Costa R. R.**, Custódio C. A., Arias F. J., Rodríguez-Cabello J. C., and Mano J. F., Nanostructured Films Exhibiting Multiple Stimuli Responsive Behavior and Improved Cell Adhesion for Tissue Engineering, European Chapter of the Tissue Engineering and Regenerative Medicine International Society (TERMIS-EU), June 2011, Granada (Spain).
3. **Costa R. R.**, Neto A. I., Calgeris I., Correia C. R., Pinho A. C. M., Fonseca J., Öner E. T., and Mano J. F., Layer-by-layer assembly using bacterial levan adhesive polymer, Cost Action TD0906, WG3 & WG4 Scientific Workshop, Biological Adhesives: From Biology to Biomimetics, April 2013, Cluj Napoca (Romania).
4. **Costa R. R.**, and Mano J. F., Revisiting layer-by-layer strategies and three-dimensional expansion, III ICVS/3B's - Associate Laboratory Meeting, June 2013, Braga (Portugal).
5. **Costa R. R.**, Castro-Otero E., Testera A. M., Arias F. J., Rodríguez-Cabello J. C., and Mano J. F., Extrapolation of hybrid polysaccharide and recombinant polypeptide multilayer films towards three-dimensional compartmentalization, Term Stem 2013, October 2013, Porto (Portugal), accepted for presentation.

Conference posters

1. **Costa R. R.**, Ribeiro A. J., Rodríguez-Cabello J. C., and Mano J. F., Development of polysaccharide and elastin-like recombinamers multilayer coatings with tunable surface properties, European Chapter of the Tissue Engineering and Regenerative Medicine International Society (TERMIS-EU), June Galway (Ireland).
2. **Costa R. R.**, Custódio C. A., Arias F. J., Rodríguez-Cabello J. C., and Mano J. F., Buildup of biomimetic and multiple stimuli responsive thin coatings of polysaccharides and recombinant biopolymers, II Meeting of the Institute for Biotechnology and Bioengineering, November 2010, Braga (Portugal).
3. **Costa R. R.**, Arias F. J., Rodríguez-Cabello J. C. and Mano J.F., Nanostructured multilayers for biomedical applications – a combinatorial analysis using biomimetic elastin-like recombinamers and polysaccharides, EUROMAT 2011, September 2011, Montpellier (France).
4. **Costa R. R.**, Arias F. J., Rodríguez-Cabello J. C., and Mano J. F., Temperature-responsive microcapsules prepared by nanostructured multilayers of chitosan and an elastin-like

recombinamer for the controlled release of therapeutic molecules, XXXVIII Annual ESAO & IV Biennial IFAO Congress, October 2011, Porto (Portugal).

5. **Costa R. R.**, Arias F. J., Rodríguez-Cabello J. C., and Mano J. F., Multilayer microcapsules of natural and nature-inspired polymers as drug delivery vessels, School of Engineering Week of the University of Minho, October 2011, Guimarães (Portugal).
6. **Costa R. R.**, Custódio C. A., Arias F. J., Rodríguez-Cabello J. C., and Mano J. F., Self-assembled microcapsules with tunable and sustained release of macromolecules for tissue engineering, III World Congress of the Tissue Engineering and Regenerative Medicine International Society (TERMIS-WC), September 2012, Vienna (Austria).
7. **Costa R. R.**, Castro-Otero E., Arias F. J., Rodríguez-Cabello J. C., and Mano J. F., Nanostructured multilayer compartments: towards multifunctionality and ''cell-like'' hierarchical complexity, Term Stem 2012, October 2012, Guimarães (Portugal).
8. **Costa R. R.**, Neto A. I., Calgeris I., Correia C. R., Pinho A. C. M., Fonseca J., Öner E. T., and Mano J. F., Bacterial levan-derivatives: an alternative adhesive biomaterial for medical and tissue engineering applications, European Chapter of the Tissue Engineering and Regenerative Medicine International Society (TERMIS-EU), June 2013, Istanbul (Turkey).
9. **Costa R. R.**, Castro-Otero E., Arias F. J., Rodríguez-Cabello J. C., and Mano J. F., "Cell-like" compartmentalized vehicles with temperature and magnetic responsiveness, European Chapter of the Tissue Engineering and Regenerative Medicine International Society (TERMIS-EU), June 2013, Istanbul (Turkey).
10. **Costa R. R.**, Castro-Otero E., Arias F. J., Rodríguez-Cabello J. C., and Mano J. F., "Cell-like" compartmentalized vehicles with temperature and magnetic responsiveness, III ICVS/3B's – Associate Laboratory Meeting, June 2013, Braga (Portugal).
11. **Costa R. R.**, Girotti A., Santos M., Arias F. J., Mano J. F., and Rodríguez-Cabello J. C., Internalization of biomimetic microcapsules for intracellular delivery of active agents, Term Stem 2013, October 2013, Porto (Portugal), accepted for presentation.

Awards

1. 1st Prize for "Best Poster Award" of the 2011 School of Engineering Week of University of Minho, with the poster *Multilayer microcapsules of natural and nature-inspired polymers as drug delivery vessels*, October 2011, Guimarães (Portugal).

Nanostructured functional multilayer coatings incorporating biomimetic macromolecules for biomedical applications

Introduction to the thesis format

This thesis is organized in 4 sections that include a total of 12 chapters, plus 1 appendix. The first section provides the general introduction to the thesis. The second section corresponds to the experimental methods and materials used. The third section shows the experimental results obtained in the context of this thesis and their discussion, focusing on the optimization of layer-by-layer (LbL) strategies for biomedical applications. The fourth section finalizes this thesis with concluding remarks.

The body of the thesis chapters is based on a series of peer-reviewed papers and book chapters published or submitted for publication. Each thesis chapter is presented in manuscript form, i.e., abstract, introduction, experimental section, results and discussion (or in two separate sections, results plus discussion), conclusion, and some of them with acknowledgements. A list of relevant references is also provided as a subsection within each chapter. The contents of each part and chapter are described below in more detail.

Section I – General introduction

Chapter 1, Nanostructured devices produced by layer-by-layer self-assembly adsorption for tissue engineering applications: This chapter provides an introduction to the mechanisms behind the construction of LbL films and coatings, a technique based on the self-assembly of materials in the form of nanolayers, which may belong to distinct classes of materials. This technique served as the basis to the whole work described in this thesis.

Chapter 2, Polyelectrolyte multilayered assemblies in biomedical technologies: In the sequence of Chapter 1, which focused primarily on the intermolecular phenomena driving the self-assembly of multilayer films, Chapter 2 reviews the state-of-the-art applications derived from LbL strategies focused on the technologies with interest in biomedicine. A thorough discussion regarding the current applications of LbL is presented, while hypothesizing about the potential of this technique in providing better devices for current medicine and for tissue engineering applications.

Chapter 3, Elastin-like macromolecules: Most of the developed work relied on the use of elastin-like recombinamers (ELRs), a class of genetically-engineered polypeptides with stimuli-responsiveness. The properties and applications of this class of material are described, as well as their origin and resemblance with natural elastin.

Nanostructured functional multilayer coatings incorporating biomimetic macromolecules for biomedical applications

Chapter 4, Stimuli-responsive surfaces for biomedical applications: The use of ELRs allowed developing multilayer devices that exhibited stimuli-responsiveness. In this chapter, the importance of "smart" surfaces for biomedical applications – planar and three-dimensional – obtained by numerous techniques is reviewed.

Section II – Experimental section

Chapter 5, Materials and methods: A list of the materials used and methods applied to obtain the results described further on is provided.

Section III – Optimization of layer-by-layer strategies for biomedical applications

Chapter 6, Adhesive nanostructured multilayer films using a bacterial exopolysaccharide for biomedical applications: This chapter aims to show that LbL coatings can be constructed using natural-occurring materials and retain the original properties of those constituents. Namely, levan, an exopolysaccharide produced by extremophilic bacteria, is known to exhibit adhesive properties. Thus, it was used as an ingredient for multilayer formulations with enhanced adhesiveness.

Chapter 7, Layer-by-layer film-growth using polysaccharides and recombinant polypeptides: a combinatorial approach: In this chapter, the type of interactions that drive the self-assembly of ELRs and polysaccharides into layers – namely chitosan and alginate – was studied. It is based on partial findings from the literature, where there has been evidence that not only electrostatic interactions are at work during the construction of polymer/protein hybrid films but also hydrophobic ones.

Chapter 7 – Appendix, Nanostructured thin coatings from chitosan and an elastin-like recombinamer with acute stimuli-responsive behavior: This appendix complements Chapter 7 and consists in a comparative study between ELR-functionalized films which amino acid sequence is organized either as a single or multiple blocks with distinct properties.

Chapter 8, Layer-by-layer assembly of chitosan and recombinant biopolymers into biomimetic coatings with multiple stimuli-responsive properties: In this chapter, polyanionic elastin-like recombinamers produced by *Escherichia coli* strains were used. ELRs appear as an elegant example of how natural materials inspire the creation of new and tailored materials using biological processes. Their response to external stimuli and genetic nature allows incorporating specific motifs like the cell adhesion motif arginine-glycine-aspartic acid (RGD) while retaining the repeating amino acid structure of natural elastin.

With this polymer, surfaces with stimuli-responsive properties and enhanced cell adhesion were envisaged.

Chapter 9, Nanostructured and thermoresponsive recombinant biopolymer-based microcapsules for the delivery of active molecules: This chapter describes the attempt to extrapolate ELR-polysaccharide hybrid films to the third dimension in the form of spherical microcapsules. The mechanism of diffusion of an encapsulated protein to the exterior of the capsules was studied for the development of drug delivery devices.

Chapter 10. Cellular uptake of multilayered capsules produced with biomimetic and genetically engineered macromolecules: Similarly to Chapter 9, microcapsules are produced for drug delivery. In this case, the mechanism of delivery is focused on the internalization of the microcapsules by cells rather than diffusion to the surrounding medium.

Chapter 11. Multifunctional compartmentalized capsules with a hierarchical organization from the nano- to the macro-scales: The possibility of using LbL to develop structures with higher degrees of complexity is studied in this chapter by assembling compartmentalized spherical structures with hierarchical organization and customized stimuli-responsiveness. It constitutes a fine example of inspiration on natural living structures such as that of natural cells.

Section IV – Concluding remarks

Chapter 12. Major conclusions and future perspectives: To finalize this thesis, the conclusions are summarized, and current limitations and future potential of LbL-based strategies for biomedical applications is reflected upon.

SECTION I – GENERAL INTRODUCTION

Chapter 1. Nanostructured devices produced by layer-by-layer self-assembly adsorption for tissue engineering applications

Chapter 2. Polyelectrolyte multilayered assemblies in biomedical technologies

Chapter 3. Elastin-like macromolecules

Chapter 4. Stimuli-responsive surfaces for biomedical applications

Chapter 1. Nanostructured devices produced by layer-by-layer self-assembly adsorption for tissue engineering applications[1]

Abstract

Devices prepared by bottom-up strategies have been proposed for several biomedical applications. Among various self-assembly techniques, layer-by-layer (LbL) offers ease of preparation, versatility, fine control over the materials structure, and robustness under physiological conditions. Due to its self-assembled nature and use of small masses of material, coatings can be produced using aqueous solutions under mild conditions of temperature, pH, and pressure, with minimal energy requirements and material waste. Herein, we review the multitude of LbL mechanisms for constructing nanostructured devices of relevance to applications such as tunable cell adhesion and metabolism, drug delivery, and biomineralized and smart systems.

[1] This chapter is based on the following publication:

Costa R. R., and Mano J. F., Layer-by-layer self-assembly techniques for nanostructured devices in tissue engineering, In Gaharwar A. K., Sant S., Hancock M. J., and Hacking A. (eds.), Nanomaterials in tissue engineering: characterization, fabrication and applications, United Kingdom, Woodhead Publishing Limited, 2013, ISBN: 978-0857095961.

Chapter 1. Nanostructured devices produced by layer-by-layer self-assembly adsorption for tissue engineering applications

1.1 Introduction

The modification of surfaces has been a key aspect in biology and biotechnology applications, including cell expansion, biomaterials development and preparation of substrates for regenerative medicine [1-3]. In the field of implantable biomaterials and tissue engineered constructs, the bulk material properties are generally considered to determine the overall properties of a biomaterial. Surface properties, however, are of utmost importance as the surface constitutes the first interface between an implant and the organism, and will drive subsequent tissue and cellular events including protein adsorption, cell adhesion and inflammatory response, all of which are necessary for tissue remodeling [4-6]. Thus, surface engineering is highly important for developing devices with improved biological performance.

Many processing techniques have been suggested and employed for the purpose of modifying substrates [7], but in the past two decades alternatives to common surface engineering strategies have emerged. Inspired by Nature, scientists and engineers have developed techniques based on biomimetic concepts. In Nature, evolutionary processes have constantly improved the design and functionality of natural materials. A well-known example is the layered organization of nacre found in the shells of sea animals. This layered and hierarchical structure containing calcium minerals is capable of dissipating high amounts of mechanical energy[8,9]. Mimicking natural layered structures has been attempted in the laboratory. In particular, the alternate adsorption of polyanions and polycations onto solid substrates is a reliable, flexible, and simple approach to modify a substrate while allowing the integration of a wide range of molecules, including those with biological relevance. As a result, multilayered thin films can be constructed with nanometric precision. This technique was first introduced by Decher, Hong and Schmitt and has denominated the layer-by-layer (LbL) field [10].

LbL is a self-assembly-driven surface modification strategy that allows the construction of nanostructured films onto substrates of any geometry, from simple bidimensional surfaces to more complex three-dimensional porous scaffolds. The underlying principle lies in the existence of multiple intermolecular interactions, such as electrostatic contacts, hydrophobic interactions, and hydrogen bonding, where the cooperative effects of multipoint attractions play the most important role. It is a technique that is easy to perform, versatile, offers fine control over the materials structure, and produces materials that are robust in physiological environments [11-13]. Because this technique may be performed using various complementary substances, a vast choice of available materials may be added to a multilayer formulation, such as proteins, nucleic acids, polysaccharides, virus particles,

organic polymers, molecular assemblies, and inorganic substances, allowing construction of LbL assemblies with very specific properties [4]. The buildup can be performed at mild conditions, namely standard laboratory temperatures and pressures, and mild pH, and can be tuned by making small adjustments in such conditions. Moreover, LbL does not involve the use of organic solvents. The mild and non-aggressive processing conditions of LbL make it an appealing technique for tissue engineering applications. Molecules with biological relevance may be embedded in the multilayer materials, with bioactivity preserved, particularly important for drug delivery applications. Biomaterials and ligands with more specific functions, such as cell adhesion enhancers, may be used in order to mimic biological structures and functions, rendering a substrate more instructive for cell behavior [14-16]. Exploiting the advantages of LbL, multilayer systems have already been proposed for various biomedical applications. An example includes biomimetic composite coatings that regulate drug release or manipulate the adhesion, differentiation, proliferation, and even function of attached cells. In the following sections, these applications and associated multilayer formulations will be reviewed.

1.2 Interaction between biomaterials as ingredients for multilayer formulations

One of the key features of LbL adsorption is the ability to use ingredients from distinct classes of materials. Usually the most important requirement is that two distinct materials possess complementarity, that is, the properties of both materials result in attraction. A well-known example most exploited example is the self-assembly driven by electrostatic interactions of oppositely charged components, in which polyanions and polycations interact and assemble [17]. Besides electrostatic self-assembly (ESA), other types of interactions that can drive the construction of multilayers include short-range interactions, such as van der Waals forces and hydrogen bonding [11]. The strength of these interactions may depend on several intrinsic factors, such as the molecular weight of polymers or size of inorganic particles, charge density, polarity, and also external factors, like the temperature, the pH of the solvent, and ionic strength (see following sections). Importantly, it is now acknowledged that the driving force behind multilayer formation is not only mutual interaction, but also by the gain in entropy due to the release of counter-ions [13,18]. The variation of one or more of these parameters can lead to a more favorable interaction and consequent buildup of a nanostructured coating. The result is, however, dependent on the original properties of the materials: for instance, varying the pH of a weak polyelectrolyte will greatly affect its overall charge density. Several biomaterials of synthetic and natural

origins have been used since LbL was first introduced, many of which capable of being used for multilayered constructs while displaying biologically relevant properties.

1.2.1 Buildup mechanisms of synthetic and inorganic materials

Many types of charged molecules and nano-objects are suitable for deposition by ESA. So far, the most popular deposition materials have been synthetic polyelectrolytes. Synthetic materials are usually man-made and can be highly functional [19]. With the availability of thousands of monomers and their seemingly endless combinations, polymer science has developed a wide array of complex but well-defined structures with specific properties, such as molecular weight and charge density. Other materials suitable for deposition using ESA are inorganic (e.g., calcium-containing or clay mineral particles) or metallic materials, usually consisting of a single geometrical charged structure (e.g., spheres or platelet-like objects) with natural or artificial origins [20,21].

Synthetic polymers, though not often similar to biological structures, have been used to define and quantify parameters important for the construction of nanostructured multilayer coatings. The main advantages of synthetic polymers are that they are easily chemically modified and they enable certain buildup parameters to be precisely adjusted. The pioneers of LbL proved its concept by creating ultrathin homogeneous films on solid surfaces [10]. Positively charged aminopropylsilanized fused quartz or silicon single crystal substrates served as supports for the ESA buildup. Poly(styrene sulfonate) (PSS) and poly(vinyl sulfate) (PVS) served as polyanions and poly(allylamine hydrochloride) (PAH) and poly-4-vinylbenzyl-(*N*, *N*-diethyl-*N*-methyl)-ammonium iodide as polycations. Immersing the positive support in an aqueous solution of one of the polyanions resulted in the adhesion of the polymeric molecules and reversal of charge density of the substrate. A rinsing step followed to remove loosely adsorbed molecules. Then the substrate was exposed to a solution of one of the polycations, again reversing the charge. By repeating this process, the stepwise construction of a coating was achieved. With 39 layers, Decher *et al.* were able to produce films as thin as 44 nm.

The striking simplicity of fabricating a wide range of LbL-modified substrates was rapidly recognized by the scientific community. Many studies with different materials collectively identified the key parameters influencing the fabrication of nanostructured multilayer films and determined how to optimize them. The pH of the polyelectrolyte solutions used during buildup has been studied by using poly(acrylic acid) (PAA) and PAH to fabricate polyelectrolyte multilayers (PEMs) [22,23]. Varying the pH of the dipping solutions considerably changes the charge density of a weak polyelectrolyte when operating above or

below the acid dissociation constant (pK_a) of the polymer. When adjusting the pH of PAA and of PAH above and below their pK_a, respectively, a higher degree of ionization could be exploited, favoring ESA-driven adsorption. In the opposite case, when operating near the acidity constant, the charge density is at its lowest. Consequently, fewer charged molecules are available to form a new top layer and more polyelectrolyte molecules are needed to interact with the underlying layer for ESA [16,24,25]. This affects the internal structure of the fi lm in terms of layer conformation since adjusting the pH modifies the charge density of the polyelectrolytes. An additional observation is that increasing the charge density of the adsorbing polymer will favor thinner polyelectrolyte layers, whereas increasing the charge density at the surface will favor thicker adsorbed layers. The latter enables the production of thicker and rougher films, while the former results in thinner and smoother films [23,26].

The addition of salts to the adsorbate solutions has been studied since ions can interfere with the electrostatic balance of molecules and the internal PEM structure. PAH, PSS and poly(diallyldimethylammonium) chloride (PDADMAC) have been used to demonstrate that the addition of salt increases the thickness of the layers due to a screening mechanism of charge–charge repulsions [27,28]. Basically, the electrostatic repulsion among groups with the same charge sign is reduced by the interaction with the salt ions present in solution and allows for a more stable buildup and interaction between layers. The adsorption process can be increased with increasing concentrations of salt, but since this mechanism is somewhat similar to that of pH, high concentration of salt may render the materials uncharged, which may induce desorption or “stripping” rather than adsorption [29,30].

Temperature also affects the buildup mechanism of multilayer films. However, while most studies on temperature focus on its effect on stability and functionality after construction, few study temperature as a buildup variable. A study by Salomäki, Vinokurov and Kankare [31] used films made of PSS and PDADMA to verify that temperature has a remarkable effect on the apparent mass of the resulting films. In aqueous solutions containing sodium bromide, the mass of adsorbed material at 55 °C was approximately 5 times higher than a construction performed at a room temperature of 25 °C, along with a tendency for the mass to increase exponentially. In the same report, similar results were found for PSS and PAH films. The conclusion was that a higher temperature during the deposition increases the mobility of the adsorbed molecules, resulting in deeper layer interpenetration deeper through the PEMs and a greater likelihood of finding more energetically optimal binding sites at the deposition site.

Polyelectrolyte multilayers made using synthetic polymers have been extended to applications other than simple interface tuning. For instance, a dye may be used as a film ingredient or it may be loaded

after film assembly [32]. The latter takes advantage of the swelling properties of multilayer films, in which a dye can be loaded – and reversibly unloaded – into the film by immersion in a saturated solution. Ideally, a dye may be replaced by a therapeutic molecule or growth factor to act as a drug delivery device upon implantation or for use in cell culture. The versatility of LbL is not limited to polymers. Other extended functionalities include the use of inorganic particles, such as bioactive nanoparticles (BNPs), to develop surfaces that could mineralize into calcium phosphate crystals under the presence of a simulated body fluid [33]. Carbon nanotubes have also been used as LbL ingredients along with polyelectrolytes for substrates with improved mechanical properties [34-36]. Work with clay platelets [37], and graphene [38] has also taken advantage of the LbL methodology, although polymers offer more mobility to the internal structure of the film. In summary, LbL can be used as a means to coat surfaces and control the interface in almost any fashion desired, due to the several mechanisms that influence its thickness, roughness and loading capabilities. Such surface property control makes LbL a powerful technique to develop tunable cutting-edge devices whose surfaces influence the fate of cells, important for a range of applications in conventional medicine and tissue engineering.

1.2.2 Natural-based polymeric materials

Natural materials are intricate structures which have risen from hundreds of millions of years of evolution. Comparing to our current technology, natural structures are more multifaceted than man-made materials, forming complex arrays and hierarchical structures with multiples functionalities [39-41]. The advantage of using natural-based polymers for biomedical and tissue engineering applications lies in their similarity with biological macromolecules, thus avoiding triggering chronic or immunological reactions and toxicity [42]. They possess more similarity to the extracellular matrix (ECM) than synthetic materials and are therefore appropriate multifunctional ingredients for constructing multilayer films and coatings with better interface with biological environments. The range of potential LbL ingredients spans the gamut from synthetic to natural materials, including polysaccharides, polypeptides, proteins, nucleic acids, deoxyribonucleic acid (DNA), and even viruses, allowing highly biomimetic surfaces to be engineered [4,12,13,16,27].

One of the natural polymers most exploited to construct multilayer films is hyaluronic acid (HA). Hyaluronic acid, also known as hyaluronan or hyaluronate, is an important glycosaminoglycan component of the connective tissue, synovial fluid and the vitreous humor of the eye [43]. It is a linear polysaccharide composed of numerous repelling anionic groups capable of binding cations and water

molecules. Solutions of HA exhibit clear viscoelastic properties that make them excellent biological absorbers and lubricants. HA may also be obtained through a process of microbial fermentation, avoiding the risk of animal-derived pathogens [44].

Several authors have focused on the use of HA as a polyanion [45-47]. In particular, HA has been combined with poly(L-lysine) (PLL) [48-50]. PLL is a linear polypeptide containing an amino group and has been widely used in biomaterial applications to enhance cell adhesion [51-53]. A thorough investigation of the PLL/HA system provided a better understanding of the exponential growth mechanism of layer thickness, as opposed to the linear growth mechanism introduced by Decher [54-56]. For this system, the exponential growth mechanism relies on the diffusion of at least one of the polymers 'in-and-out' of the molecular chains during each bilayer deposition step. In these studies, it was PLL that diffused through the film.

Polysaccharides of marine origin form another important class of natural materials. Chitosan (CHI) is a polysaccharide exhibiting cationic properties and solubility under acidic conditions. Its precursor, chitin, is the second most important natural polymer in the world and can be extracted from marine crustaceans including shrimp and crabs. CHI possesses several characteristics favorable for promoting dermal regeneration and accelerated wound healing [57]. Alginate (ALG) is another polysaccharide of marine origin, namely from brown algae. Its structure contains carboxyl groups, which makes it negatively charged [58]. Both of these polysaccharides possess adhesive, non-toxic, bacteriostatic, fungistatic, hemostatic, and anti-microbial properties, making them ideal for tissue engineering applications. Because of these unique features, CHI and ALG have been frequently used in biomedical applications including burn dressings, drug delivery, and implants [59-61]. They have been used as LbL ingredients, both together or in conjugation with other materials. PLL/ALG and CHI/HA systems have been shown to possess an internal structure typically produced by the exponential growth mechanism [54,62]. Martins *et al.* [63] demonstrated the loading capability of CHI/ALG films with human serum albumin (HSA) which depended on the availability of amino groups to bind the negatively charged protein. Crosslinking with glutaraldehyde reduced that availability and HSA adsorption in comparison to uncrosslinked films.

The molecular weight of LbL ingredients is an important property influencing the buildup mechanism. However, few studies using natural polymers have systematically investigated the influence of polymer molecular weight on the physical properties of polyelectrolyte multilayers, since it is difficult to obtain monodisperse polymers from natural sources. As such, studies related to molecular weight have mostly

focused on the use of well-characterized synthetic polymers [64-66]. Nevertheless, using CHI and HA films, Kujawa *et al.* [67] found that the thickness increased when the molecular weight of these polysaccharides was higher. They demonstrated that the higher the molecular weight the thicker the film: a longer polymer tends to adsorb in a "loopier" way, while a smaller molecule adsorbs in an extended conformation. Therefore, with longer polymers, there are more anchoring sites available for the next layer to adsorb and potentially higher interpenetrating capabilities than with smaller molecules.

The mechanical properties of multilayer films can affect cell adhesion and differentiation. Increasing the Young's modulus (i.e. stiffness) of multilayer films improves cell adhesion [68-70]. This behavior makes LbL substrates suitable as tunable platforms to control cell adhesion. Moreover, LbL substrates with varying support stiffness could potentially induce stem cell differentiation. Multilayers can also be used as reservoirs for therapeutic molecules (discussed below) and can incorporate naturally occurring smart biomaterials. By fabricating a film containing stimuli-responsive ingredients, interface properties could be changed on demand.

All films constructed by ESA from weak polyelectrolytes – synthetic or natural – are inherently pH-responsive. Properties like Young's modulus, roughness or wettability may be tailored by varying the film assembly conditions, due to the dissociation of the weak acidic and alkaline functional groups on the chains. Wood *et al.* [71] demonstrated the pH controlled degradation of a film, from which therapeutic molecules were release to the bulk medium. Ionic strength may also be used as a stimuli-response mechanism for films made of weak, and, unlike pH, strong polyelectrolytes [27-30]. A screening effect caused by the interaction between free counter-ions and charged polymer groups leads to a reduction of the electrostatic repulsion between charged groups of the same sign. Such mechanisms are potentially useful for drug delivery, because they could provide sustained and controlled release with greater effectiveness, lower toxicity, and improved patient convenience over conventional formulations. However the sharp variations of pH and ionic strength associated with them may be harmful for cells. On the other hand, cells are less sensitive to temperature variations, at least for temperatures near 37°C. Therefore, temperature responsive materials could be a more favorable choice for use with cells. One of the most popular temperature responsive polymers is poly(N-isopropylacrylamide) (PNIPAAm). PNIPAAm has a lower critical solution temperature (LCST) around 32°C enclosing both hydrophobic and hydrophilic domains [72]. Below the LCST, the polymer is soluble in aqueous solution, with an expanded or hydrated coil conformation; above it, the polymer becomes insoluble, preferring a folded globular structure. PNIPAAm is a synthetic material but

combinations with natural polymers are possible. CHI, a weak polycation, has been grafted with PNIPAAm to construct films with dual responsiveness [73]. Elastin-like recombinamers (ELRs) are another class of temperature-responsive materials; a class of the elastin-like polymers (ELPs) family, they are genetically engineered peptide-based macromolecules obtained through the fermentation of modified bacterial strains [74]. ELRs are rooted in the peptide sequence of natural elastin present in tissues that require elasticity as part of their function, such as skin, tendons and muscles. In an aqueous environment they are known to self-assemble and exhibit a transition temperature (T_t): below T_t, the free polymer chains adopt random coil conformations; above it, they fold into an organized structure known as β-spiral. Although ELRs respond primarily to temperature, the effects of other stimuli, such as pH, ionic strength and concentration also affect the transition phenomenon. Their genetically-engineered origin also allows motifs to be integrated that have biological relevance, such as cell adhesion [75] and mineralization enhancers [76]. In LbL, they have already been suggested as suitable ingredients for constructing films with multiple stimuli-responsiveness [77-79]. They are an elegant example of how Nature inspires engineers to develop new multifunctional materials for tissue engineering applications.

1.3 Scalability to three dimensions

LbL was first introduced as a surface engineering technique for planar surfaces. However, this technology can be used to coat surfaces on substrates or templates with a variety of shapes and sizes beyond planar. As a result, devices such as scaffolds that could only be fabricated through conventional methods may now be engineered to exhibit new tunable properties according to the desired application.

1.3.1 Membranes

Most polyelectrolyte multilayers may be assembled with up to dozens of layers to a thickness that may reach tens of micrometers. However, PEMs are assembled and adhere to underlying substrates and cannot be detached without damaging the films. Detached films, usually called “free-standings”, are potentially useful for a range of nanostructured membrane based devices for a range of sensing, detection, and drug delivery applications [80,81].

A typical approach to fabricate free-standings involves a sacrificial layer or substrate that is dissolved after buildup [82,83]. Cellulose acetate, for instance, can be used as a substrate and dissolved with

acetone after buildup [84]. A potential disadvantage of such an approach is that the films may undergo both chemical and physical changes during the post-processing steps to separate the film from the underlying substrate and interfere with the internal structure of the multilayers. More recently, other strategies have been introduced that avoid using chemicals to remove the template. Hydrophobic substrates have been used to assemble free-standing PEMs, exploiting a peeling mechanism of the film from the substrate. Larkin *et al.* [85] used Teflon and polypropylene as planar templates from which CHI and HA films could be easily peeled off without damage. Another method consists of assembling films virtually "on air without templates". Mallwitz and Laschewsky [86] prepared ultrathin freestanding arrays of LbL films in the holes of electron microscopy grids (100 × 100 μm). The precise mechanism was not clear. Apparently, the pores were so small that the multilayer ingredients were suspended across the orifices instead of coating their walls, so that thin polymeric lamellae could remain trapped in the pores. However, the authors did not develop a strategy to extract the free-standings from the grid.

1.3.2 Capsules

LbL has been suggested as a technology to produce capsules as tunable drug carriers for drug delivery applications and cell differentiation [87,88]. Typically, the template for a hollow or loaded capsule is a nano- or micro-particle. Similarly to some free-standings, the template particle is sacrificial. After assembling the multilayers, the core is removed with a solvent. The result is a hollow multilayer shell which may encapsulate molecules of interest such as DNA and proteins [35,89]. The sacrificial cores were organic microparticles (typically 1–10 mm) such as polystyrene or melamine formaldehyde, which were then dissolved by organic solvents or strong acids [90]. The drawback of such an approach is that it employs aggressive solvents that could damage the remaining shell and destroy the functionality and purpose of the structure. Also, organic residues from the aggressive solvents could affect biological environments, making the approach less appealing for tissue engineering. Such drawbacks led to the introduction of other templates that could be dissolved under less aggressive conditions, such as mesoporous silica (with diameters of 500 nm to 5 μm, dissolved in hydrogen fluoride) and porous calcium carbonate (with diameters of 3–5 μm, dissolved in ethylenediamine tetraacetic acid, EDTA) [91,92].

The concept of permeability after the buildup is of great interest for drug delivery and tissue engineering applications: not only must a carrier be able to retain and preserve the drug but also release it when necessary and in a controlled fashion. The most obvious way to control such permeability is to vary the

number of layers assembled around a template: more layers result in higher resistance to molecular [93]. In order to fill the interior of a multilayer capsule with a drug, both pre- and post-loading encapsulation mechanisms have been exploited [94]. In pre-loading, the sacrificial core may already contain the molecule of interest that will remain upon dissolution, or crystals of the molecule of interest that can be used as a template and liquefied after assembly, without removal. In the post-loading approach, prefabricated hollow capsules can be loaded by altering the permeability of the capsule shell [95,96]. Several mechanisms based on the effect of external variables have been exploited to reversibly change the permeability of a multilayer shell. Multilayer capsules are inherently responsive to pH and ionic strength due to their interference with the electrostatic balance between layers. The permeability of such responsive capsules was studied by Shutava *et al.* [97] for capsules based on tannic acid and PAH. The capsules seemed impermeable to fluorescein isothiocyanate (FITC)-dextrans at neutral pH but became permeable at both low and high pH values. Ibarz *et al.* [98] reported that the permeability of hollow PSS/PAH polyelectrolyte capsules sharply improved upon increasing the concentration of salts. Temperature has also been suggested as a mechanism for post-loading. It is believed that a rearrangement occurs with the increase of temperature due to a tendency of shells to reduce the shell/water interface [99]. However it has only been achieved for temperatures as high as 50–70°C, and is thus not suitable for biological applications [100-102]. For drug release, the same mechanisms used to post-encapsulate a molecule of interest could also be used to modulate its release in a controlled fashion.

1.3.3 Tubes

Hollow tubes of micron or submicron diameter and high aspect ratio are interesting for various applications. They possess a large specific surface area, making them appealing for catalysis, sensing, or as tissue scaffolding [103-105]. Hollow tubes could be used for encapsulation purposes and find applications in fields like drug delivery and as transport channels in microfluidics [106]. In biology, tubes of submicron dimensions are commonly found, like protein nanotubes or microtubules, and play an essential role in providing mechanical reinforcement in cells and small blood vessels [34].

Tube-like structures may be fabricated in a similar manner to other shapes templates (cylindrical in this case) are coated and subsequently dissolved under conditions that do not destroy the coating, thus only tube-like objects remain. To date, this morphology has not been extensively used and only a few reports exist of multilayer nanostructured hollow tubes compatible with tissue engineering applications. Tube-

like structures have previously been fabricated by assembling polyelectrolytes onto micrometric glass fibers that were then dissolved by hydrogen fluoride [107]. Another strategy to fabricate tube-like structures is to consists in the coat porous membranes (the templates) with polyelectrolytes, which in turn adsorb to the wall of the pores, after which the membranes are dissolved [35]. He *et al.* [108] pursued an interesting approach by assembling tubes of PSS and PAH using the porous template method and transforming them into capsules by varying temperature. This structural transition from tubular to vesicular or vesicle-like systems is often considered for drug delivery, gene delivery, self-assembled nanoreactors, or biochemical sensors [109].

In the future, multilayer tubular structures may be of significant interest in tissue engineering. For instance, nanostructured artificial blood vessels could be developed as an alternative to the conventional autologous grafting treatment by the incorporation of collagen and elastin to mimic the intima, media and adventitia layers [110,111].

1.3.4 Three-dimensional scaffolds

LbL is not limited to the simple geometries shown so far. The technique may be applied to more complex geometries by using more intricate structures as templates. Porous agglomerates of particles, for instance, can be coated and, similarly to previous structures, the template can be chelated, leaving only the multilayer assembly to serve as supports for cell culture. Miranda *et al.* [112] and Sher, Custódio and Mano [113] have developed nanostructured multilayer structures based on agglomerates of particles of chitosan (not leachable) and paraffin (leachable), respectively. Their works, which will be referred to again, demonstrate that more complex and functional structures may be made using LbL.

1.4 Application of nanostructured multilayer devices in tissue engineering

The numerous possibilities for adjusting the chemical, physical, and mechanical properties of multilayer films have garnered attention from tissue engineers hoping to develop systems to control protein and cell adhesion and release therapeutic molecules and growth/differentiation factors. In addition, researchers wish to tune the surface properties by of such microsystems adding specific ligands or stimuli-responsive biomaterials.

1.4.1 Controlling cell adhesion and proliferation

When a biomedical device enters in contact with a cell-populated biological environment, adhesion is the first event to occur Adhesion is the first cell event that occurs when a cell comes into contact with a material's surface, which will be followed by proliferation and, in the case of stem cell cultures, differentiation.

We have already mentioned that changing the mechanical properties of a multilayer film may affect the cellular adhesion. Schneider *et al.* [69] have studied the cell adhesion of HCS-2/8 human chondrosarcoma cells on PLL/HA films with various degrees of crosslinking. The Young's modulus of the film could be varied over two orders of magnitude simply by varying the concentration of a crosslinker, carbodiimide, from 3 to 400 kPa for the lowest and highest concentrations, respectively. Increasing the film stiffness also increased the roughness and number of attached cells, showing how a simple modification to the mechanical properties to multilayer films can affect their response in a biological environment. Phelps *et al.* [114] also applied this concept to selectively crosslink the outer region of a PLL and poly(glutamic acid) (PGA) film, resulting in a rigid outer skin to promote cell attachment, while leaving the film (and any embedded bioactive species) unaffected. Crosslinked CHI and HA films have also been studied *in vivo* by implantation in a rat oral cavity [115]. Crosslinked films demonstrated up to 60% higher resistance to degradation compared to uncrosslinked samples.

Multilayer films may be engineered with exhibiting anti-fouling properties to control cellular and bacterial adhesion by enhanced resistance to serum proteins. A straightforward way to build "stealth" substrates of any morphology is to use derivatives of poly(ethylene glycol) (PEG), a highly hydrated polymer effective in rendering surfaces non-adsorbent to proteins [116-118]. Another strategy is to add antimicrobial agents. Ettiene *et al.* have added defensin [119] and chromofungin [120] to the films constitution and reported growth inhibition up to 98% for *Escherichia coli* with defensin and 65% for *Candida albicans* with chromofungin. Rendering a surface non-fouling can serve as immuno-''camouflage'' to prevent the immune rejection of implanted biomaterials or to enhance the efficiency of injected drug delivery vehicles.

The application of LbL to more complex structures is highly important for tissue engineering applications such as cell culture platforms, where higher hierarchical organization better resembles native tissues. Besides bidimensional, spherical, and tubular shapes, more complex geometries such as agglomerated shapes can be fabricated and used as scaffolds for cell culture. LbL may be used to agglomerate beads [112] or to coat free-packet leachable templates [113] leading in both cases to

porous structures that may be populated by cells. Recently, Ye *et al.* [121] coated a decellularized porcine aortic valve with CHI and heparin showing anti-thrombotic properties. The device was shown to be hemocompatible by reducing platelet adhesion while allowing the proliferation of endothelial progenitor cells. The work of Sher, Custódio and Mano [113] introduced an interconnected three-dimensional porous scaffold using a new drop-wise perfusion technique over a three-dimensional (3D) template formed by free-form moldable paraffin wax spheres held together only by the LbL coating (Figure 1.1).

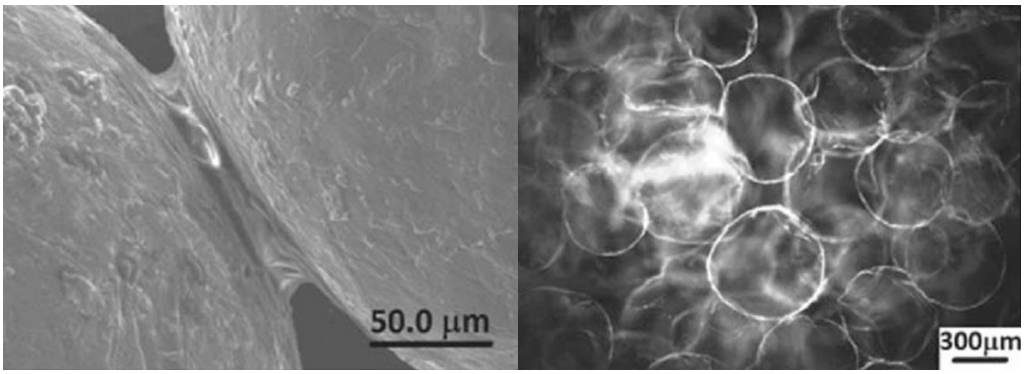


Figure 1.1. On the left: Individual connections between two paraffin wax particles. On the right: Florescence images showing the multilayered 3D assembly after leaching of the core material. Reprinted (adapted) with permission from [113]. Copyright 2010 Wiley-VCH.

The paraffin was dissolved by dichloromethane, leaving only the assembled layers as a scaffold. SaOs-2 human osteoblast-like cells were seeded and showed attachment and proliferation. The authors did not characterize the system for its mechanical properties, however. It is possible that the resulting structure is not adequate for applications involving high loads, such as bone regeneration, but may be more appropriate for regenerating soft tissues, such as cartilage or nerves.

1.4.2 Controlling cellular metabolism: encapsulation and differentiation

Multilayer films may be of use for cell encapsulation since the films can coat various cell types and even be used to build multilayered cell architectures. Developing a device that provides immune protection via microencapsulation as well as enhanced control of both transport and surface physicochemical characteristics is an important and ambitious step in the development of an effective encapsulating barrier. One approach to encapsulate cells is by using coated liquefied capsules. For example, Costa *et*

al. [122] have used liquefied alginate beads coated with CHI and ALG to immobilize SaOs-2 human osteoblast-like cells. Another cell encapsulation approach exploits cell surface charge to assemble polyelectrolytes. Krol *et al.* [123] pursued this surface charge approach with pancreatic islet cells to assemble a multilayer shell that effectively encapsulated them for the treatment of diabetes. By incubating Langerhans cells with alternating solutions of polycationic PAH or PDADMAC and polyanionic PSS, the authors built a barrier that covered and protected the cells. The shell was permeable and the cells were immunologically protected and retained their insulin secretion capability (Figure 1.2). The coating, however, consisted of synthetic materials which could be cytotoxic in the long term.

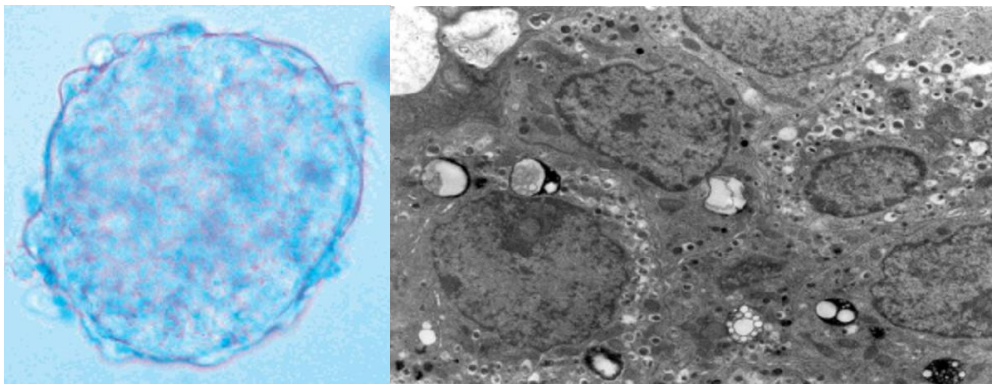


Figure 1.2. On the left: Light microscopy image of trypan blue-stained islets after encapsulation with three pairs of polyelectrolyte layers $(PDADMAC/PSS)_3$. On the right: Electron micrographs of PAH/PSS/PAH-coated islets. Reprinted (adapted) with permission from [123]. Copyright 2006 American Chemical Society.

Veeradabran *et al.* [53] followed a similar approach to encapsulate individual mouse mesenchymal stem cells (MSCs) using PLL and HA. The cells were encapsulated within shells with thicknesses of approximately 6–9 nm. Cell morphology and viability were maintained for up to 1 week. Encapsulation has tremendous potential for the maintenance and differentiation of stem cells. LbL allows the encapsulating shells to be tuned to achieve optimal permeability. Nutrients, waste, and chemical differentiation factors could be exchanged between the cell and its external environment and the differentiation process triggered on demand. Other approaches have been introduced to drive the differentiation of cells by incorporating specific factors in a multilayer formulation. Dierich *et al.* [124] presented a formulation with poly(lactic-co-glycolic acid) (PLGA), PLL and poly(L-lysine succinylated) (PLLs), along with bone morphogenetic proteins (BMPs) and tissue growth factors (TGFs). Using this

system, they were able to drive the differentiation of embryoid bodies into cartilage and bone. Another interesting approach is to embed differentiation factors into spherical shapes, which have a higher surface area and improved accessibility compared to planar substrates. Facca *et al.* [125] created capsules templated in silica particles (1 μm) coated with a similar formulation. The incubation with embryonic stem (ES) cells led to both *in vitro* and *in vivo* bone formation. It is unclear if the delivery of BMP was due to the degradation of the capsules or to their internalization by the cells. The latter option is a possibility: Rivera-Gil *et al.* [126] have recently demonstrated the internalization of multilayer capsules by embryonic NIH/3T3 fibroblasts.

These encapsulation methods have proven to be novel approaches to shield cells from certain external factors and to controllably differentiate stem cells either by taking advantage of the permeable nature of multilayer films or by targeting the intracellular environment directly. Therefore, LbL structures have potential use for tissue engineering applications where cell transplantation or damaged tissue replacement is necessary.

1.4.3 Biomimetic and "intelligent" and substrates

Systems used for biomedical and tissue engineering applications must be biocompatible and not trigger toxic, inflammatory, or rejection responses. The structures and properties found in natural materials have inspired the development of multilayer systems with higher degrees of functionalization. One approach is to incorporate natural materials directly into multilayer systems. For instance, nanostructured films containing CHI retain some of CHI's anti-microbial

properties [127]. Another approach consists of integrating ingredient molecules, such as bioactive ligands, that can drive specific phenomena mimicking their native function. Picart *et al.* [128] incorporated arginine-glycine-(aspartic acid) (RGD) a cell adhesion promoter, with the substrate using PLL and RGD-grafted-PGA in the terminating layer. The proliferation of primary human osteoblast cells was enhanced on for films containing RGD compared to films without. RGD-enhanced proliferation was observed not only for simple adsorbed layers, but also for crosslinked films. To mimic the microenvironments of bone marrow and the thymus, Lee and Kotov [129] incorporated delta-like 1 Notch ligands (DL-1) at the surface of PEM films. The Notch ligands stimulated hematopoietic stem cells (HSCs) to differentiate into T-cell lymphocytes and progressively develop their own ECM.

Adding stimuli-responsive materials to multilayer formulations offers additional functionalization, by controlling surface properties and the conformational rearrangement of molecular chains. Stimuli-

responsive properties have been engineered into several types of systems, such as grafted surfaces and hydrogels [130], and are beginning to be used in multilayer systems for controlling biological events such as cell attachment/detachment. As mentioned before, pH and ionic strength may be useful stimuli response mechanisms for drug delivery applications, but changes of these variables beyond physiological conditions may be too aggressive for cell cultures. Temperature changes, on the other hand, are usually more tolerated by cells for temperatures up to 37°C. Costa *et al.* used an ELR containing RGD to generate bilayer coatings [131] and multiple stimuli-responsive multilayers [78] with enhanced cell adhesion. By varying the pH, ionic strength and temperature of CHI/ELR films, it was possible to switch the wettability of the substrates from a moderately hydrophobic character (contact angle around 70°) to a superhydrophilic (contact angle of 0°) (Figure 1.3).

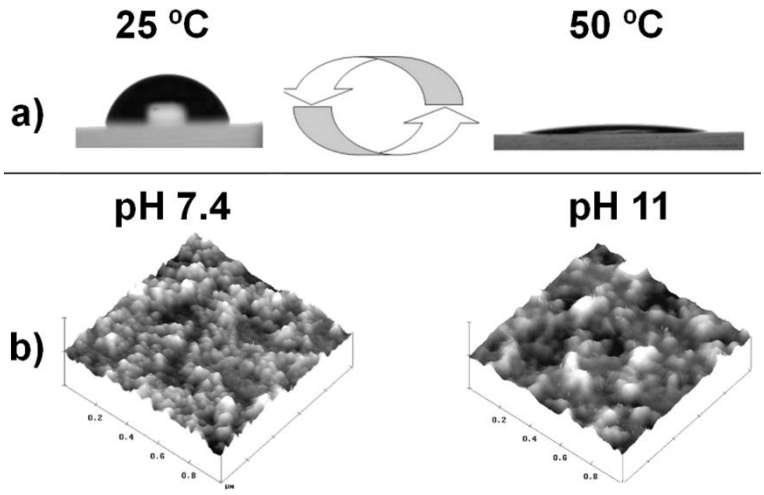


Figure 1.3. Physical changes induced in ELR modified surfaces. (a) Wettability variations with different temperatures. Reprinted (adapted) with permission from [131]. Copyright 2009 Wiley-VCH. (b) Topography at distinct pHs. Reprinted (adapted) with permission from [78]. Copyright 2011 Wiley-VCH.

However, the variation was observed for values not suitable for biological studies: pH 11; ionic strength 0.15 M; and 50 °C. Nevertheless, at physiological conditions, the cellular adhesion of a SaOs-2 osteoblast-like cell line was higher than in films ending in CHI or a scrambled non-functional RDG sequence. Martins *et al.* [73] then described a multilayer system of ALG and PNIPAAm-grafted CHI to reproduce the cell-sheet technology [132]. SaOs-2 human osteoblast-like cells seeded onto coated substrates ending in the modified CHI were allowed to achieve confluence at 37°C. Upon decreasing the temperature to 4°C, the peeling effect enabled cells to be detached from the surface as a thin layer.

Zahn *et al.* [133] demonstrated a similar approach by using the ion-induced detachment of myoblast layers by the eroding effect of ferrocyanide on PLL and HA multilayers. Incorporating biofunctional ingredients and bioinspired concepts into multilayer systems has enhanced the functionality of such systems and is producing promising results for tissue engineering applications.

1.4.4 Multilayers in controlled drug delivery

Current advances in biomedicine have been driven by the need to develop systems that can effectively encapsulate, protect and deliver an active agent with specific kinetics [134]. At the same time, distinct classes of biomolecules are widely available and related to the treatment of several diseases or the development of new biomedical devices. Ideally, a biomolecule carrier should act as a compartment with tunable drug permeability. The multilayered capsule systems described above are ideal for such drug delivery applications, including the associated methods to load and control the release of therapeutic molecules and growth/differentiation factors. The adequate loading efficiency and controlled release of the molecules of interest, such as growth factors, are necessary to ensure the survival of cells in tissue engineering applications. Erel *et al.* [135] fabricated hydrogen-bonded multilayers of micelles of poly[2-(*N*-morpholino)ethyl methacrylate-*block*-2-(diisopropylamino)ethyl methacrylate] (PMEMA-*b*-PDPA), a dicationic block copolymer, encapsulating pyrene onto a surface with tannic acid. The films were dual responsive and released pyrene upon increasing either temperature or pH. Crouzier *et al.* [136] developed crosslinked films of PLL and HA as reservoirs loaded with a recombinant human BMP-2 (rhBMP-2) to control the differentiation of myoblasts into fibroblasts. They demonstrated that the amount of loaded rhBMP-2 could be regulated by film thickness and assembly conditions. Also, the rhBMP-2 loaded in the films retained its bioactivity and was protected for three consecutive cultures.

Another particular area being targeted for multilayer drug delivery systems is cancer treatment, where the uncontrolled systemic administration of chemotherapeutics comes with several drawbacks to the patients. Zhao *et al.* [137] developed CHI/ALG microcapsules loaded with doxorubicin, an effective anticancer drug, and demonstrated that the apoptosis of HepG2 tumor cells could be induced *in vitro* by incubating with loaded microcapsules. A suspension of microcapsules was also injected directly to tumors induced in mice, inducing a higher tumor inhibition compared to free drug administration. De Geest *et al.* [138] demonstrated that polymeric multilayer capsules (PMLCs) increase antigen delivery toward antigen-presenting cells *in vivo*, enforcing antigen presentation and stimulating T-cell proliferation. Poon *et al.* [139] recently addressed the stability and biodistribution of electrostatic self-

assembled nanoparticles for systemic administration and off-body tracing by imaging techniques. They provided evidence of the importance of a larger number of layers and the role of the terminating layer in terms of functional retention. A formulation of PLL and dextran films topped with a final layer of HA assembled onto gold nanoparticles or quantum dots. In mice, these coated particles had a blood elimination half-life of 9 hours and low liver accumulation. These reports represent a step forward the use of LbL systems in *in vivo* applications such as cancer treatment, and augment the mounting evidence that such systems can be designed to have minimal or no negative effects on living organisms.

1.4.5 Biomineralized multilayers

Developing systems with LbL technology to facilitate bone regeneration or to improve the mechanical properties of substrates is an active area of research. Such research is adding versatility to biomineralization processes by developing controlled nanostructured assemblies that tune the kinetics of calcium phosphate, apatite formation, and ultimately bone regeneration [140-142].

Bioactive coatings on orthopedic implants may create an environment compatible with osteogenesis and provide bone-friendly interfaces for forming natural bonding junctions between the implant and host bone [143]. Couto, Alves and Mano [33] developed hybrid films of CHI and bioactive glass nanoparticles that mimicked the brick-and-mortar layered structured of nacre. They showed that the incorporation of BNPs rendered the substrates prone to mineralization upon immersion in simulated body fluid (SBF) solution. The mineralization was also more pronounced with an increasing number of layers. Fukui and Fujimoto [144] described a hybrid nanocapsule templated in phospholipids that encapsulated phosphate ions (Figure 1.4). The phospholipids were coated using CHI, dextran or DNA and then incubated in a solution containing calcium ions. They demonstrated that the chemical surface change could influence the counter-ion diffusion and therefore the mineralization rate.

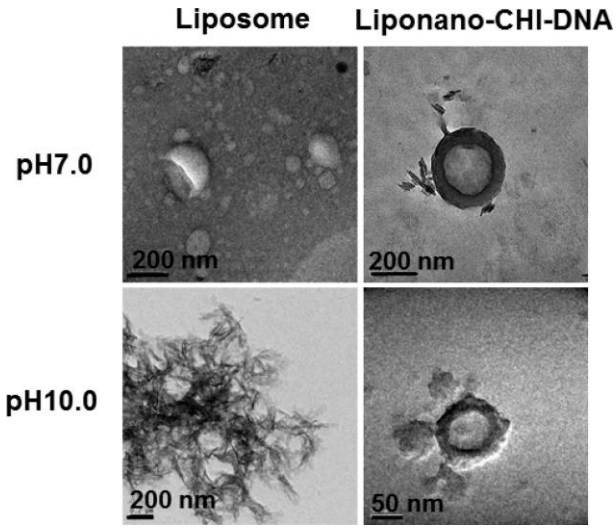


Figure 1.4. Effect of incubation time on the formation of calcium phosphate crystals using liposome and liponano–CHI–DNA templates. Each reaction was carried out at pH 7.0 and pH 10.0 for 18 h, using calcium chloride ($CaCl_2$) and disodium phosphate/monosodium phosphate (Na_2HPO_4/NaH_2PO_4) as ion species. Reprinted with permission from [144]. Copyright 2011 American Chemical Society.

1.5 Conclusion

For the past 20 years, the use of LbL as a processing technique has evolved from traditional surface modification on two-dimensional (2D) planar surfaces to three-dimensional (3D) environments. The procedure can even be performed using mild conditions and in a cell-friendly environment. The most recent results show that LbL may be used to encapsulate cells, control cell adhesion and metabolism, tune the release of encapsulated molecules, render a substrate with smart responsiveness, and enhance mineralization. We believe that the technology will follow two trends in the near future. The first trend will involve using existing nanostructured multilayer devices in more *in vivo* applications that take advantage of the spatial organization and bioactivity, adjustable stiffness and chemistry, or adjustable stiffness and bioactivity, of multilayer devices. The other trend will involve the development of more intricate structures with hierarchical complexity embedded in devices with multiple functionalities, such as controlling the diffusion of gases and nutrients to cultured cells. Higher levels of functionalization should enable the development of systems exhibiting intelligent responses to external stimuli. For example, drug release systems could respond to an external stimulus by releasing encapsulated drugs and therefore influencing cellular metabolism on demand. The inclusion of specific ligands or metallic particles could enable the development of targeted delivery strategies for cell therapies and transplant.

In summary, research on nanostructured multilayer devices will likely result in innovative low-cost technologies to meet critical biomedical needs.

1.6 References

[1] Falconnet D., Csucs G., Michelle Grandin H., and Textor M., Surface engineering approaches to micropattern surfaces for cell-based assays, Biomaterials 2006, 27: 3044-3063.

[2] Hook A. L., Voelcker N. H., and Thissen H., Patterned and switchable surfaces for biomolecular manipulation, Acta Biomaterialia 2009, 5: 2350-2370.

[3] Tirrell M., Kokkoli E., and Biesalski M., The role of surface science in bioengineered materials, Surface Science 2002, 500: 61-83.

[4] Boudou T., Crouzier T., Ren K., Blin G., and Picart C., Multiple Functionalities of Polyelectrolyte Multilayer Films: New Biomedical Applications, Advanced Materials 2010, 22: 441-467.

[5] Hubbell J. A., Bioactive biomaterials, Current Opinion in Biotechnology 1999, 10: 123-129.

[6] Stevens M. M., and George J. H., Exploring and Engineering the Cell Surface Interface, Science 2005, 310: 1135-1138.

[7] Prakash S., Karacor M. B., and Banerjee S., Surface modification in microsystems and nanosystems, Surface Science Reports 2009, 64: 233-254.

[8] Luz G. M., and Mano J. F., Biomimetic design of materials and biomaterials inspired by the structure of nacre, Philosophical Transactions of the Royal Society A: Mathematical, Physical and Engineering Sciences 2009, 367: 1587-1605.

[9] Mayer G., Rigid Biological Systems as Models for Synthetic Composites, Science 2005, 310: 1144-1147.

[10] Decher G., Hong J. D., and Schmitt J., Buildup of ultrathin multilayer films by a self-assembly process: III. Consecutively alternating adsorption of anionic and cationic polyelectrolytes on charged surfaces, Thin Solid Films 1992, 210-211: 831-835.

[11] Clark S. L., and Hammond P. T., The Role of Secondary Interactions in Selective Electrostatic Multilayer Deposition, Langmuir 2000, 16: 10206-10214.

[12] Gribova V., Auzely-Velty R., and Picart C., Polyelectrolyte Multilayer Assemblies on Materials Surfaces: From Cell Adhesion to Tissue Engineering, Chemistry of Materials 2012, 24: 854-869.

[13] Lyklema J., and Deschênes L., The First Step in Layer-by-Layer Deposition: Electrostatics and/or Non-Electrostatics?, Advances in Colloid and Interface Science 2011, 168: 135-148.

[14] Ariga K., Hill J. P., and Ji Q., Biomaterials and biofunctionality in layered macromolecular assemblies, Macromolecular Bioscience 2008, 8: 981-990.

[15] Bertrand P., Jonas A., Laschewsky A., and Legras R., Ultrathin polymer coatings by complexation of polyelectrolytes at interfaces: suitable materials, structure and properties, Macromolecular Rapid Communications 2000, 21: 319-348.

[16] Tang Z., Wang Y., Podsiadlo P., and Kotov N. A., Biomedical Applications of Layer-by-Layer Assembly: From Biomimetics to Tissue Engineering, Advanced Materials 2006, 18: 3203-3224.

[17] Hammond P. T., Form and Function in Multilayer Assembly: New Applications at the Nanoscale, Advanced Materials 2004, 16: 1271-1293.

[18] V. Klitzing R., Internal Structure of Polyelectrolyte Multilayer Assemblies, Physical Chemistry Chemical Physics 2006, 8: 5012-5033.

[19] Fetters L. J., Lohse D. J., Richter D., Witten T. A., and Zirkel A., Connection between polymer molecular-weight, density, chain dimensions, and melt viscoelastic properties, Macromolecules 1994, 27: 4639-4647.

[20] Fendler J. H., Self-assembled nanostructured materials, Chemistry of Materials 1996, 8: 1616-1624.

[21] Zabet-Khosousi A., and Dhirani A.-A., Charge transport in nanoparticle assemblies, Chemical Reviews 2008, 108: 4072-4124.

[22] Shiratori S. S., and Rubner M. F., pH-Dependent Thickness Behavior of Sequentially Adsorbed Layers of Weak Polyelectrolytes, Macromolecules 2000, 33: 4213-4219.

[23] Yoo D., Shiratori S. S., and Rubner M. F., Controlling Bilayer Composition and Surface Wettability of Sequentially Adsorbed Multilayers of Weak Polyelectrolytes, Macromolecules 1998, 31: 4309-4318.

[24] Izumrudov V. A., Chaubet F., Clairbois A.-S., and Jozefonvicz J., Interpolyelectrolyte reactions in solutions of functionalized dextrans with negatively charged groups along the chains, Macromolecular Chemistry and Physics 1999, 200: 1753-1763.

[25] Schlenoff J. B., and Dubas S. T., Mechanism of Polyelectrolyte Multilayer Growth: Charge Overcompensation and Distribution, Macromolecules 2001, 34: 592-598.

[26] Fu J., Ji J., Yuan W., and Shen J., Construction of anti-adhesive and antibacterial multilayer films via layer-by-layer assembly of heparin and chitosan, Biomaterials 2005, 26: 6684-6692.

[27] Chen W., and McCarthy T. J., Layer-by-Layer Deposition: A Tool for Polymer Surface Modification, Macromolecules 1997, 30: 78-86.

[28] Schlenoff J. B., Ly H., and Li M., Charge and Mass Balance in Polyelectrolyte Multilayers, Journal of the American Chemical Society 1998, 120: 7626-7634.

[29] Hoogeveen N. G., Cohen Stuart M. A., and Fleer G. J., Can charged (block co)polymers act as stabilisers and flocculants of oxides?, Colloids and Surfaces A: Physicochemical and Engineering Aspects 1996, 117: 77-88.

[30] Linford M. R., Auch M., and Möhwald H., Nonmonotonic Effect of Ionic Strength on Surface Dye Extraction during Dye–Polyelectrolyte Multilayer Formation, Journal of the American Chemical Society 1998, 120: 178-182.

[31] Salomäki M., Vinokurov I. A., and Kankare J., Effect of Temperature on the Buildup of Polyelectrolyte Multilayers, Langmuir 2005, 21: 11232-11240.

[32] Becker A. L., Johnston A. P. R., and Caruso F., Layer-By-Layer-Assembled Capsules and Films for Therapeutic Delivery, Small 2010, 6: 1836-1852.

[33] Couto D. S., Alves N., M., and Mano J., F., Nanostructured Multilayer Coatings Combining Chitosan with Bioactive Glass Nanoparticles, Journal of Nanoscience and Nanotechnology 2009, 9: 1741-1748.

[34] Komatsu T., Protein-based nanotubes for biomedical applications, Nanoscale 2012, 4: 1910-1918.

[35] Liang Z., Susha A. S., Yu A., and Caruso F., Nanotubes Prepared by Layer-by-Layer Coating of Porous Membrane Templates, Advanced Materials 2003, 15: 1849-1853.

[36] Mamedov A. A., Kotov N. A., Prato M., Guldi D. M., Wicksted J. P., and Hirsch A., Molecular design of strong single-wall carbon nanotube/polyelectrolyte multilayer composites, Nature Materials 2002, 1: 190-194.

[37] Elzbieciak M., Wodka D., Zapotoczny S., Nowak P., and Warszynski P., Characteristics of Model Polyelectrolyte Multilayer Films Containing Laponite Clay Nanoparticles, Langmuir 2010, 26: 277-283.

[38] Kong B.-S., Geng J., and Jung H.-T., Layer-by-layer assembly of graphene and gold nanoparticles by vacuum filtration and spontaneous reduction of gold ions, Chemical Communications 2009: 2174-2176.

[39] Ashby M. F., and Jones D. R. H., Engineering Materials 2: An Introduction to Microstructures, Processing and Design, Oxford, United Kingdom: Elsevier; 2006.

[40] Langer R., and Tirrell D. A., Designing materials for biology and medicine, Nature 2004, 428: 487-492.

[41] Meyers M. A., Chen P.-Y., Lin A. Y.-M., and Seki Y., Biological materials: Structure and mechanical properties, Progress in Materials Science 2008, 53: 1-206.

[42] Mano J. F., Silva G. A., Azevedo H. S., Malafaya P. B., Sousa R. A., Silva S. S., Boesel L. F., Oliveira J. M., Santos T. C., Marques A. P., Neves N. M., and Reis R. L., Natural origin biodegradable systems in tissue engineering and regenerative medicine: present status and some moving trends, Journal of The Royal Society Interface 2007, 4: 999-1030.

[43] Drury J. L., and Mooney D. J., Hydrogels for tissue engineering: scaffold design variables and applications, Biomaterials 2003, 24: 4337-4351.

[44] Sutherland I. W., Novel and established applications of microbial polysaccharides, Trends in Biotechnology 1998, 16: 41-46.

[45] Chua P.-H., Neoh K.-G., Kang E.-T., and Wang W., Surface functionalization of titanium with hyaluronic acid/chitosan polyelectrolyte multilayers and RGD for promoting osteoblast functions and inhibiting bacterial adhesion, Biomaterials 2008, 29: 1412-1421.

[46] Johansson J. Å., Halthur T., Herranen M., Söderberg L., Elofsson U., and Hilborn J., Build-up of Collagen and Hyaluronic Acid Polyelectrolyte Multilayers, Biomacromolecules 2005, 6: 1353-1359.

[47] Picart C., Schneider A., Etienne O., Mutterer J., Schaaf P., Egles C., Jessel N., and Voegel J.-C., Controlled Degradability of Polysaccharide Multilayer Films In Vitro and In Vivo, Advanced Functional Materials 2005, 15: 1771-1780.

[48] Garza J. M., Schaaf P., Muller S., Ball V., Stoltz J.-F., Voegel J.-C., and Lavalle P., Multicompartment Films Made of Alternate Polyelectrolyte Multilayers of Exponential and Linear Growth, Langmuir 2004, 20: 7298-7302.

[49] Khademhosseini A., Suh K. Y., Yang J. M., Eng G., Yeh J., Levenberg S., and Langer R., Layer-by-layer deposition of hyaluronic acid and poly-L-lysine for patterned cell co-cultures, Biomaterials 2004, 25: 3583-3592.

[50] Zhang J., Senger B., Vautier D., Picart C., Schaaf P., Voegel J.-C., and Lavalle P., Natural polyelectrolyte films based on layer-by layer deposition of collagen and hyaluronic acid, Biomaterials 2005, 26: 3353-3361.

[51] Mazia D., Schatten G., and Sale W., Adhesion of cells to surfaces coated with polylysine. Applications to electron microscopy, The Journal of Cell Biology 1975, 66: 198-200.

[52] Richert L., Lavalle P., Vautier D., Senger B., Stoltz J.-F., Schaaf P., Voegel J.-C., and Picart C., Cell Interactions with Polyelectrolyte Multilayer Films, Biomacromolecules 2002, 3: 1170-1178.

[53] Veerabadran N. G., Goli P. L., Stewart-Clark S. S., Lvov Y. M., and Mills D. K., Nanoencapsulation of Stem Cells within Polyelectrolyte Multilayer Shells, Macromolecular Bioscience 2007, 7: 877-882.

[54] Elbert D. L., Herbert C. B., and Hubbell J. A., Thin Polymer Layers Formed by Polyelectrolyte Multilayer Techniques on Biological Surfaces, Langmuir 1999, 15: 5355-5362.

[55] Picart C., Mutterer J., Richert L., Luo Y., Prestwich G. D., Schaaf P., Voegel J.-C., and Lavalle P., Molecular basis for the explanation of the exponential growth of polyelectrolyte multilayers, Proceedings of the National Academy of Sciences of the United States of America 2002, 99: 12531-12535.

[56] Porcel C., Lavalle P., Decher G., Senger B., Voegel J.-C., and Schaaf P., Influence of the Polyelectrolyte Molecular Weight on Exponentially Growing Multilayer Films in the Linear Regime, Langmuir 2007, 23: 1898-1904.

[57] Rinaudo M., Chitin and Chitosan - Properties and Applications, Progress in Polymer Science 2006, 31: 603-632.

[58] Percival E., and McDowell R. H., Algal polysaccharides, In Dey P. M., ed. Methods in plant biochemistry Carbohydrates, London, United Kingdom: Academic Press; 1990.

[59] Berger J., Reist M., Mayer J. M., Felt O., Peppas N. A., and Gurny R., Structure and interactions in covalently and ionically crosslinked chitosan hydrogels for biomedical applications, European Journal of Pharmaceutics and Biopharmaceutics 2004, 57: 19-34.

[60] Boateng J. S., Matthews K. H., Stevens H. N. E., and Eccleston G. M., Wound healing dressings and drug delivery systems: A review, Journal of Pharmaceutical Sciences 2008, 97: 2892-2923.

[61] George M., and Abraham T. E., Polyionic hydrocolloids for the intestinal delivery of protein drugs: Alginate and chitosan — a review, Journal of Controlled Release 2006, 114: 1-14.

[62] Picart C., Lavalle P., Hubert P., Cuisinier F. J. G., Decher G., Schaaf P., and Voegel J.-C., Buildup Mechanism for Poly(l-lysine)/Hyaluronic Acid Films onto a Solid Surface, Langmuir 2001, 17: 7414-7424.

[63] Martins G. V., Merino E. G., Mano J. F., and Alves N. M., Crosslink Effect and Albumin Adsorption onto Chitosan/Alginate Multilayered Systems: An in situ QCM-D Study, Macromolecular Bioscience 2010, 10: 1444-1455.

[64] Ariga K., Lvov Y., and Kunitake T., Assembling Alternate Dye–Polyion Molecular Films by Electrostatic Layer-by-Layer Adsorption, Journal of the American Chemical Society 1997, 119: 2224-2231.

[65] Stockton W. B., and Rubner M. F., Molecular-Level Processing of Conjugated Polymers. 4. Layer-by-Layer Manipulation of Polyaniline via Hydrogen-Bonding Interactions, Macromolecules 1997, 30: 2717-2725.

[66] Sui Z., Salloum D., and Schlenoff J. B., Effect of Molecular Weight on the Construction of Polyelectrolyte Multilayers: Stripping versus Sticking, Langmuir 2003, 19: 2491-2495.

[67] Kujawa P., Moraille P., Sanchez J., Badia A., and Winnik F. M., Effect of Molecular Weight on the Exponential Growth and Morphology of Hyaluronan/Chitosan Multilayers: A Surface Plasmon Resonance Spectroscopy and Atomic Force Microscopy Investigation, Journal of the American Chemical Society 2005, 127: 9224-9234.

[68] Richert L., Lavalle P., Payan E., Shu X. Z., Prestwich G. D., Stoltz J.-F., Schaaf P., Voegel J.-C., and Picart C., Layer by Layer Buildup of Polysaccharide Films: Physical Chemistry and Cellular Adhesion Aspects, Langmuir 2004, 20: 448-458.

[69] Schneider A., Francius G., Obeid R., Schwinté P., Hemmerlé J., Frisch B., Schaaf P., Voegel J.-C., Senger B., and Picart C., Polyelectrolyte Multilayers with a Tunable Young's Modulus: Influence of Film Stiffness on Cell Adhesion, Langmuir 2006, 22: 1193-1200.

[70] Schneider A., Vodouhê C., Richert L., Francius G., Le Guen E., Schaaf P., Voegel J. C., Frisch B., and Picart C., Multifunctional polyelectrolyte multilayer films: Combining mechanical resistance, biodegradability, and bioactivity, Biomacromolecules 2007, 8: 139-145.

[71] Wood K. C., Boedicker J. Q., Lynn D. M., and Hammond P. T., Tunable Drug Release from Hydrolytically Degradable Layer-by-Layer Thin Films, Langmuir 2005, 21: 1603-1609.

[72] Schild H. G., Poly(N-isopropylacrylamide): experiment, theory and application, Progress in Polymer Science 1992, 17: 163-249.

[73] Martins G. V., Mano J. F., and Alves N. M., Dual Responsive Nanostructured Surfaces for Biomedical Applications, Langmuir 2011, 27: 8415-8423.

[74] Rodríguez-Cabello J. C., Martín L., Alonso M., Arias F. J., and Testera A. M., "Recombinamers" as advanced materials for the post-oil age, Polymer 2009, 50: 5159-5169.

[75] Girotti A., Reguera J., Rodríguez-Cabello J. C., Arias F. J., Alonso M., and Testera A. M., Design and bioproduction of a recombinant multi(bio)functional elastin-like protein polymer containing cell

adhesion sequences for tissue engineering purposes, Journal of Materials Science: Materials in Medicine 2004, 15: 479-484.

[76] Prieto S., Shkilnyy A., Rumplasch C., Ribeiro A., Arias F. J., Rodríguez-Cabello J. C., and Taubert A., Biomimetic calcium phosphate mineralization with multifunctional elastin-like recombinamers, Biomacromolecules 2011, 12: 1480-1486.

[77] Barbosa J. S., Costa R. R., Testera A. M., Alonso M., Rodríguez-Cabello J. C., and Mano J. F., Multi-Layered Films Containing a Biomimetic Stimuli-Responsive Recombinant Protein, Nanoscale Research Letters 2009, 4: 1247 - 1253.

[78] Costa R. R., Custódio C. A., Arias F. J., Rodríguez-Cabello J. C., and Mano J. F., Layer-by-Layer Assembly of Chitosan and Recombinant Biopolymers into Biomimetic Coatings with Multiple Stimuli-Responsive Properties, Small 2011, 7: 2640-2649.

[79] Golonka M., Bulwan M., Nowakowska M., Testera A. M., Rodríguez-Cabello J. C., and Zapotoczny S., Thermoresponsive multilayer films based on ionic elastin-like recombinamers, Soft Matter 2011, 7: 9402-9409.

[80] Choi H. J., Brooks E., and Montemagno C. D., Synthesis and characterization of nanoscale biomimetic polymer vesicles and polymer membranes for bioelectronic applications, Nanotechnology 2005, 16: S143-S149.

[81] Jiang C., and Tsukruk V. V., Freestanding Nanostructures via Layer-by-Layer Assembly, Advanced Materials 2006, 18: 829-840.

[82] Lee S., Lee B., Kim B. J., Park J., Yoo M., Bae W. K., Char K., Hawker C. J., Bang J., and Cho J., Free-Standing Nanocomposite Multilayers with Various Length Scales, Adjustable Internal Structures, and Functionalities, Journal of the American Chemical Society 2009, 131: 2579-2587.

[83] Ott P., Trenkenschuh K., Gensel J., Fery A., and Laschewsky A., Free-Standing Membranes via Covalent Cross-Linking of Polyelectrolyte Multilayers with Complementary Reactivity, Langmuir 2010, 26: 18182-18188.

[84] Mamedov A. A., and Kotov N. A., Free-Standing Layer-by-Layer Assembled Films of Magnetite Nanoparticles, Langmuir 2000, 16: 5530-5533.

[85] Larkin A. L., Davis R. M., and Rajagopalan P., Biocompatible, Detachable, and Free-Standing Polyelectrolyte Multilayer Films, Biomacromolecules 2010, 11: 2788-2796.

[86] Mallwitz F., and Laschewsky A., Direct Access to Stable, Freestanding Polymer Membranes by Layer-by-Layer Assembly of Polyelectrolytes, Advanced Materials 2005, 17: 1296-1299.

[87] De Cock L. J., De Koker S., De Geest B. G., Grooten J., Vervaet C., Remon J. P., Sukhorukov G. B., and Antipina M. N., Polymeric multilayer capsules in drug delivery, Angewandte Chemie International Edition 2010, 49: 6954-6973.

[88] Peyratout C. S., and Dähne L., Tailor-Made Polyelectrolyte Microcapsules: From Multilayers to Smart Containers, Angewandte Chemie International Edition 2004, 43: 3762-3783.

[89] Caruso F., Caruso R. A., and Möhwald H., Nanoengineering of inorganic and hybrid hollow spheres by colloidal templating, Science 1998, 282: 1111-1114.

[90] Donath E., Sukhorukov G. B., Caruso F., Davis S. A., and Möhwald H., Novel hollow polymer shells by colloid-templated assembly of polyelectrolytes, Angewandte Chemie International Edition 1998, 37: 2201-2205.

[91] Mauser T., Déjugnat C., Möhwald H., and Sukhorukov G. B., Microcapsules made of weak polyelectrolytes: templating and stimuli-responsive properties, Langmuir 2006, 22: 5888-5893.

[92] Wang Y., and Caruso F., Nanoporous Protein Particles Through Templating Mesoporous Silica Spheres, Advanced Materials 2006, 18: 795-800.

[93] She Z., Antipina M. N., Li J., and Sukhorukov G. B., Mechanism of Protein Release from Polyelectrolyte Multilayer Microcapsules, Biomacromolecules 2010, 11: 1241-1247.

[94] De Geest B. G., Sanders N. N., Sukhorukov G. B., Demeester J., and De Smedt S. C., Release mechanisms for polyelectrolyte capsules, Chemical Society Reviews 2007, 36: 636-649.

[95] Köhler K., and Sukhorukov G. B., Heat Treatment of Polyelectrolyte Multilayer Capsules: A Versatile Method for Encapsulation, Advanced Functional Materials 2007, 17: 2053-2061.

[96] Sukhorukov G. B., Antipov A. A., Voigt A., Donath E., and Möhwald H., pH-Controlled Macromolecule Encapsulation in and Release from Polyelectrolyte Multilayer Nanocapsules, Macromolecular Rapid Communications 2001, 22: 44-46.

[97] Shutava T., Prouty M., Kommireddy D., and Lvov Y., pH Responsive Decomposable Layer-by-Layer Nanofilms and Capsules on the Basis of Tannic Acid, Macromolecules 2005, 38: 2850-2858.

[98] Ibarz G., Dähne L., Donath E., and Möhwald H., Smart Micro- and Nanocontainers for Storage, Transport, and Release, Advanced Materials 2001, 13: 1324-1327.

[99] Köhler K., Möhwald H., and Sukhorukov G. B., Thermal behavior of polyelectrolyte multilayer microcapsules: 2. insight into molecular mechanisms for the PDADMAC/PSS system, The Journal of Physical Chemistry B 2006, 110: 24002-24010.

[100] Bedard M. F., Munoz-Javier A., Mueller R., Del Pino P., Fery A., Parak W. J., Skirtach A. G., and Sukhorukov G. B., On the mechanical stability of polymeric microcontainers functionalized with nanoparticles, Soft Matter 2009, 5: 148-155.

[101] Glinel K., Sukhorukov G. B., Möhwald H., Khrenov V., and Tauer K., Thermosensitive hollow capsules based on thermoresponsive polyelectrolytes, Macromolecular Chemistry and Physics 2003, 204: 1784-1790.

[102] Huang C.-J., and Chang F.-C., Using click chemistry to fabricate ultrathin thermoresponsive microcapsules through direct covalent layer-by-layer assembly, Macromolecules 2009, 42: 5155-5166.

[103] Murugan R., and Ramakrishna S., Nano-featured scaffolds for tissue engineering: a review of spinning methodologies, Tissue Eng 2006, 12: 435-447.

[104] Sanchez-Castillo M. A., Couto C., Kim W. B., and Dumesic J. A., Gold-Nanotube Membranes for the Oxidation of CO at Gas–Water Interfaces, Angewandte Chemie International Edition 2004, 43: 1140-1142.

[105] Wang X., Kim Y.-G., Drew C., Ku B.-C., Kumar J., and Samuelson L. A., Electrostatic Assembly of Conjugated Polymer Thin Layers on Electrospun Nanofibrous Membranes for Biosensors, Nano Letters 2004, 4: 331-334.

[106] Choi S.-W., Zhang Y., and Xia Y., Fabrication of Microbeads with a Controllable Hollow Interior and Porous Wall Using a Capillary Fluidic Device, Advanced Functional Materials 2009, 19: 2943-2949.

[107] Mueller R., Daehne L., and Fery A., Hollow Polyelectrolyte Multilayer Tubes: Mechanical Properties and Shape Changes, The Journal of Physical Chemistry B 2007, 111: 8547-8553.

[108] He Q., Song W., Möhwald H., and Li J., Hydrothermal-Induced Structure Transformation of Polyelectrolyte Multilayers: From Nanotubes to Capsules, Langmuir 2008, 24: 5508-5513.

[109] Vriezema D. M., Aragonès M. C., Elemans J. A. A. W., Cornelissen J. J. L. M., Rowan A. E., and Nolte R. J. M., Self-assembled nanoreactors, Chemical Reviews 2005, 105: 1445-1489.

[110] Koens M. J. W., Faraj K. A., Wismans R. G., van der Vliet J. A., Krasznai A. G., Cuijpers V. M. J. I., Jansen J. A., Daamen W. F., and van Kuppevelt T. H., Controlled fabrication of triple layered and molecularly defined collagen/elastin vascular grafts resembling the native blood vessel, Acta Biomaterialia 2010, 6: 4666-4674.

[111] Patel A., Fine B., Sandig M., and Mequanint K., Elastin biosynthesis: The missing link in tissue-engineered blood vessels, Cardiovascular Research 2006, 71: 40-49.

[112] Miranda E. S., Silva T. H., Reis R. L., and Mano J. F., Nanostructured Natural-Based Polyelectrolyte Multilayers to Agglomerate Chitosan Particles into Scaffolds for Tissue Engineering, Tissue Engineering Part A 2011, 17: 2663-2674.

[113] Sher P., Custódio C. A., and Mano J. F., Layer-By-Layer Technique for Producing Porous Nanostructured 3D Constructs Using Moldable Freeform Assembly of Spherical Templates, Small 2010, 6: 2644-2648.

[114] Phelps J. A., Morisse S., Hindié M., Degat M.-C., Pauthe E., and Van Tassel P. R., Nanofilm Biomaterials: Localized Cross-Linking To Optimize Mechanical Rigidity and Bioactivity, Langmuir 2011, 27: 1123-1130.

[115] Etienne O., Schneider A., Taddei C., Richert L., Schaaf P., Voegel J. C., Egles C., and Picart C., Degradability of polysaccharides multilayer films in the oral environment: an in vitro and in vivo study, Biomacromolecules 2005, 6: 726-733.

[116] Ochs C. J., Such G. K., Städler B., and Caruso F., Low-Fouling, Biofunctionalized, and Biodegradable Click Capsules, Biomacromolecules 2008, 9: 3389-3396.

[117] Wagner V. E., Koberstein J. T., and Bryers J. D., Protein and bacterial fouling characteristics of peptide and antibody decorated surfaces of PEG-poly(acrylic acid) co-polymers, Biomaterials 2004, 25: 2247-2263.

[118] Wattendorf U., Kreft O., Textor M., Sukhorukov G. B., and Merkle H. P., Stable stealth function for hollow polyelectrolyte microcapsules through a poly(ethylene glycol) grafted polyelectrolyte adlayer, Biomacromolecules 2008, 9: 100-108.

[119] Etienne O., Picart C., Taddei C., Haikel Y., Dimarcq J. L., Schaaf P., Voegel J. C., Ogier J. A., and Egles C., Multilayer polyelectrolyte films functionalized by insertion of defensin: A new approach to protection of implants from bacterial colonization, Antimicrobial Agents and Chemotherapy 2004, 48: 3662-3669.

[120] Etienne O., Gasnier C., Taddei C., Voegel J.-C., Aunis D., Schaaf P., Metz-Boutigue M.-H., Bolcato-Bellemin A.-L., and Egles C., Antifungal coating by biofunctionalized polyelectrolyte multilayered films, Biomaterials 2005, 26: 6704-6712.

[121] Ye X. F., Hu X., Wang H. Z., Liu J., and Zhao Q., Polyelectrolyte multilayer film on decellularized porcine aortic valve can reduce the adhesion of blood cells without affecting the growth of human circulating progenitor cells, Acta Biomaterialia 2012, 8: 1057-1067.

[122] Costa N. L., Sher P., and Mano J. F., Liquefied Capsules Coated with Multilayered Polyelectrolyte Films for Cell Immobilization, Advanced Engineering Materials 2011, 13: B218-B224.

[123] Krol S., del Guerra S., Grupillo M., Diaspro A., Gliozzi A., and Marchetti P., Multilayer nanoencapsulation. New approach for immune protection of human pancreatic islets, Nano Letters 2006, 6: 1933-1939.

[124] Dierich A., Le Guen E., Messaddeq N., Stoltz J.-F., Netter P., Schaaf P., Voegel J.-C., and Benkirane-Jessel N., Bone formation mediated by synergy-acting growth factors embedded in a polyelectrolyte multilayer film, Advanced Materials 2007, 19: 693-697.

[125] Facca S., Cortez C., Mendoza-Palomares C., Messadeq N., Dierich A., Johnston A. P. R., Mainard D., Voegel J.-C., Caruso F., and Benkirane-Jessel N., Active multilayered capsules for in vivo bone formation, Proceedings of the National Academy of Sciences of the United States of America 2010, 107: 3406-3411.

[126] Rivera-Gil P., De Koker S., De Geest B. G., and Parak W. J., Intracellular Processing of Proteins Mediated by Biodegradable Polyelectrolyte Capsules, Nano Letters 2009, 9: 4398-4402.

[127] Joshi M., Khanna R., Shekhar R., and Jha K., Chitosan Nanocoating on Cotton Textile Substrate Using Layer-by-Layer Self-Assembly Technique, Journal of Applied Polymer Science 2011, 119: 2793-2799.

[128] Picart C., Elkaim R., Richert L., Audoin T., Arntz Y., Da Silva Cardoso M., Schaaf P., Voegel J.-C., and Frisch B., Primary cell adhesion on RGD-functionalized and covalently crosslinked thin polyelectrolyte multilayer films, Advanced Functional Materials 2005, 15: 83-94.

[129] Lee J., and Kotov N. A., Notch Ligand Presenting Acellular 3D Microenvironments for ex vivo Human Hematopoietic Stem-Cell Culture made by Layer-By-Layer Assembly, Small 2009, 5: 1008-1013.

[130] Mano J. F., Stimuli-Responsive Polymeric Systems for Biomedical Applications, Advanced Engineering Materials 2008, 10: 515-527.

[131] Costa R. R., Custódio C. A., Testera A. M., Arias F. J., Rodríguez-Cabello J. C., Alves N. M., and Mano J. F., Stimuli-Responsive Thin Coatings Using Elastin-Like Polymers for Biomedical Applications, Advanced Functional Materials 2009, 19: 3210-3218.

[132] Okano T., Yamada N., Sakai H., and Sakurai Y., A novel recovery system for cultured cells using plasma-treated polystyrene dishes grafted with poly(N-isopropylacrylamide), Journal of Biomedical Materials Research 1993, 27: 1243-1251.

[133] Zahn R., Thomasson E., Guillaume-Gentil O., Vörös J., and Zambelli T., Ion-induced cell sheet detachment from standard cell culture surfaces coated with polyelectrolytes, Biomaterials 2012, 33: 3421-3427.

[134] Wohl B. M., and Engbersen J. F. J., Responsive layer-by-layer materials for drug delivery, Journal of Controlled Release 2012, 158: 2-14.

[135] Erel I., Karahan H. E., Tuncer C., Bütün V., and Demirel A. L., Hydrogen-bonded multilayers of micelles of a dually responsive dicationic block copolymer, Soft Matter 2012, 8: 827-836.

[136] Crouzier T., Ren K., Nicolas C., Roy C., and Picart C., Layer-By-Layer Films as a Biomimetic Reservoir for rhBMP-2 Delivery: Controlled Differentiation of Myoblasts to Osteoblasts, Small 2009, 5: 598-608.

[137] Zhao Q., Han B., Wang Z., Gao C., Peng C., and Shen J., Hollow chitosan-alginate multilayer microcapsules as drug delivery vehicle: doxorubicin loading and in vitro and in vivo studies, Nanomedicine: Nanotechnology, Biology and Medicine 2007, 3: 63-74.

[138] De Geest B. G., Willart M. A., Hammad H., Lambrecht B. N., Pollard C., Bogaert P., De Filette M., Saelens X., Vervaet C., Remon J. P., Grooten J., and De Koker S., Polymeric Multilayer Capsule-Mediated Vaccination Induces Protective Immunity Against Cancer and Viral Infection, ACS Nano 2012, 6: 2136-2149.

[139] Poon Z., Lee J. B., Morton S. W., and Hammond P. T., Controlling in Vivo Stability and Biodistribution in Electrostatically Assembled Nanoparticles for Systemic Delivery, Nano Letters 2011, 11: 2096-2103.

[140] Kokubo T., Kim H.-M., and Kawashita M., Novel bioactive materials with different mechanical properties, Biomaterials 2003, 24: 2161-2175.

[141] Rezwan K., Chen Q. Z., Blaker J. J., and Boccaccini A. R., Biodegradable and bioactive porous polymer/inorganic composite scaffolds for bone tissue engineering, Biomaterials 2006, 27: 3413-3431.

[142] Suchanek W., and Yoshimura M., Processing and properties of hydroxyapatite-based biomaterials for use as hard tissue replacement implants, Journal of Materials Research 1998, 13: 94-117.

[143] Boccaccini A. R., and Blaker J. J., Bioactive composite materials for tissue engineering scaffolds, Expert Review of Medical Devices 2005, 2: 303-317.

[144] Fukui Y., and Fujimoto K., Control in Mineralization by the Polysaccharide-Coated Liposome via the Counter-Diffusion of Ions, Chemistry of Materials 2011, 23: 4701-4708.

Chapter 2. Polyelectrolyte multilayered assemblies in biomedical technologies[2]

Abstract

Layer-by-layer (LbL) was first introduced as a surface modification technique based on the sequential spontaneous adsorption of at least two distinct materials to planar substrates. In the last two decades, this technique has evolved to the coating of more convoluted geometries with high levels of tailored functionalization or with structural purposes. In this review, the potential uses of LbL films in biomedical engineering based mainly in the assembly of polyelectrolytes are reviewed. Examples of recent developments are provided, from the modification of substrates to improve their biointegration or to add specialized properties, to the three-dimensional extrapolation of this technique as more complex structures for cell seeding, drug delivery devices, biosensors and customizable microreactors. Future strategies and opportunities are compared with current medical and laboratorial methodologies. Through them, it is expected that LbL will contribute greatly to the development of new functional devices with high perspectives of return for the administration of active agents, biosensing and construction of microtissues and disease models in laboratory.

[2] This chapter is based on the following publication:

Costa R. R., and Mano J. F., Polyelectrolyte multilayered assemblies in biomedical technologies, submitted (2013).

2.1 Introduction

Surface modification is a prominent field of engineering of utmost importance for biomedical applications. When having in mind the contact of a medical device with the human body – resulting from surgical or topical implantation – the reaction to this "foreign body" must be considered. The surface of a medical device is the first contact with the biological environment. Upon contact, a series of bio-recognition processes (such as protein/cell adhesion and inflammatory response) occur between the surface of biomaterials and the biological environment [1-5]. It is evident that such interface defines whether the device will be accepted or rejected by the body, and therefore the surface properties play an extremely important role in its success.

Surface engineering has been commonly achieved through techniques such as plasma [6], polymer grafting [7], micro/nanofabrication [8] and Langmuir-Blodgett [9]. Each one of them, different as they may seem, often aim for the same goal: to modify the characteristics of a selected surface while retaining the properties of the bulk materials. Using the example of artificial prosthesis, the surface could be improved for better biointegration through the enhancement of its antimicrobial properties, biocompatibility, degradation resistance and drug loading capability [10-12], while preserving the native mechanical properties.

It is notable how surface modification in biomedical applications has motivated so much interest in the scientific community. Nowadays, modifying a surface is no longer limited to the improvement of an implant's integration. Technological ramifications have allowed producing surfaces that respond to stimuli, tune cell adhesion, mineralize and adjust the permeability of active agents' carriers [13-16]. In particular, surfaces containing nano- or micro-scale features in a well-controlled manner have been shown to influence cellular adhesion and metabolism [17]. In this sense, surface modification has also become a synonym of "control".

Taking Nature as the greatest of inspirations, scientists and engineers have developed many biomimetic concepts based on the constant evolutionary improvement of designs and functionalities of natural occurring materials [18]. One example is the layered organization found in natural materials, such as the case of nacre found in the shells of sea animals. Nacre consists in a hierarchical and layered structure of calcium minerals capable of dissipating high amounts of mechanical energy [19-21]. In an attempt to mimic natural layered structures, a strategy consisting in the alternate adsorption of polyelectrolytes onto solid surfaces – polyanions and polycations – was introduced. In this process, two or more constituents can be added on top of a substrate sequentially with nanometric precision as

many times as desired, until stacks of numerous layers give rise to multilayered thin films. This concept was first introduced by Iller [22] in 1966, who assembled alternate layers of positively and negatively charged colloidal particles (such as silica and alumina) onto solid smooth surfaces. Later, Decher and Hong [23] expanded this concept using anionic and cationic bipolar amphiphiles containing rigid biphenyl cores, and adsorbed them alternately onto a positively charged planar surface. They demonstrated the construction of a film with 35 amphiphile layers accounting for a total thickness of 170 nm. After completion of their follow-up work [24,25] this strategy became known as layer-by-layer (LbL). Since its introduction, it has become one of the most prominent surface engineering strategies in materials science, capable of providing a reliable, easy, versatile and cost-effective way of tuning interfaces. Furthermore, a wide variety of constituents can be selected. The only requirement is that multipoint interactions – such as electrostatic contacts, van der Walls forces, and hydrogen bonding – exist between each of them to enable their sequential adsorption [1,26-30]. It is a simple and versatile technique that allows producing robust coatings, even in substrates with convoluted and three dimensional geometries. Harmful solvents (e.g., crosslinkers, organic solvents) and harsh processing conditions (e.g., high temperatures, extreme pH values) are seldom required, making LbL an attractive technique for biological-based applications. Specialized biomaterials and ligands, such as cell adhesion enhancers, may be used in order to mimic biological structures and functions, rendering a substrate more instructive for cell behavior [27,31]. Multilayered films can also act as drug reservoirs: active agents may be embedded in the multilayer constitution while preserving their bioactivity, especially when the protection of drugs until their delivery is desired [32,33].

Due to the broad scope and fast development of LbL, dozens of review articles have contributed to this topic in the last decade. In 2006, Kotov and coworkers [30] focused on a comprehensive review about the bioactivity of multilayer films for biomedical applications, such as superhydrophobic surfaces, biosensors, drug delivery, protein/cell adhesion, mediation of cellular functions and implantable materials. These authors estimated that LbL could be extrapolated to the third dimension in the following years in order to conceive scaffolds with specific embedded growth factors, receptors, or ligands. Their expectations have been met as several works have showed the production of complex geometrical structures using this technology. Another review by Picart and coworkers [1] in 2010 reminded us of the fundamentals of LbL and how the experimental conditions affect the final properties of a multilayer films. Namely, the mechanism of exponential growth, which describes an alternative non-linear model of thickness growth per layer, was reflected upon. In 2012, Tong, Song and Gao [34] reviewed the construction of spherical containers (namely capsules) for drug delivery, biosensing and

confining chemical reactions, showing how LbL has surpassed the simple idea of improving interfaces and creating functional surfaces.

In this review, we intend to discuss the state-of-the-art developments of LbL-based strategies, especially those with applicability in the biomedical field. Through selected recent examples from the literature, we will discuss how LbL has been established as a conventional surface modification technique in little more than 20 years thanks to this technique's capability to address a wide range of biomedical applications. Simultaneously, it is our intention to open the question of whether LbL, as it stands now, surpasses other existent technologies and what potential is still reserved for the future development of multilayered biomedical devices with value for biomedical applications.

2.2 Fundamentals of the layer-by-layer technique

2.2.1 Layer-by-Layer as a tool for surface modification

LbL adsorption relies in the interaction between two or more distinct materials that possess complementary interactions, i.e. that the properties of both materials result in their mutual attraction. The most exploited buildup mechanism of multilayer films is the assembly driven by electrostatic interactions of oppositely charged components, as depicted in Figure 2.1.

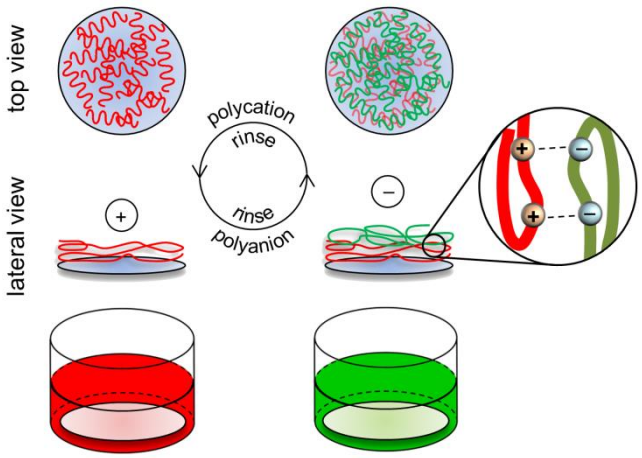


Figure 2.1. Schematics of layer-by-layer adsorption of polyelectrolytes based on an electrostatic mechanism deposition. The procedure is based on the contact of the substrate with a solution with an oppositely charged polymer. In the depicted example, negatively charged round substrates are submerged in an aqueous solution of a polycation, followed by a solution containing a polyanion. Each adsorption stage is separated by a rinsing step, to remove loosely adsorbed molecules.

Besides electrostatic assembly, constructing multilayer films may rely on short-range interactions, such as van der Walls forces and hydrogen bonding [35-37]. Nowadays it is acknowledged that the gain in entropy due to the release of counterions plays a key role in the LbL adsorption process. Its outcome is often the organization of the layers in a more coiled and interdigitated conformation, leading the polyelectrolyte molecules to lose degrees of freedom [38-40].

Many types of charged molecules and nano-objects are suitable for deposition by electrostatic interactions, from nanoparticles [41-43], carbon nanotubes [44,45], clay platelets [46], dendrimers [47,48], polysaccharides [49-51], polypeptides [52-54], nucleic acids [55,56] and viral components [57,58]. Special emphasis has been given to synthetic polyelectrolytes, such as the widely investigated poly(styrene sulfonate)/poly(allylamine hydrochloride) (PSS/PAH) system – considered so far as a model of multilayered thin films [1]. Synthetic materials are usually highly versatile materials with well-defined structures with tailored properties, such as molecular weight and charge density [59]. Thanks to their tailored properties these systems have been used as a means to determine the influence of several construction conditions involved in the LbL buildup. For example, it is known that varying the pH of weak polyelectrolytes also varies the protonation state of their ionizable groups, this way influencing the availability of charged groups; additionally, a moderate ionic strength can help reducing electrostatic repulsion between charged groups and favor electrostatic assembly [60-62]. Another parameter is temperature, which increases the mobility of the adsorbed molecules and the chances of finding more energetically optimal binding sites at the deposition site [63].

Synthetic materials have served their purpose, but for biomedical applications materials that exhibit biological features should be more appropriate. Natural materials are intricate structures which have risen from hundreds of millions of years of evolution. Comparing to our current technology, Nature was able to conceive structures more multifaceted than man-made materials, forming complex arrays, hierarchical structures and multifunctionality [11,64,65]. Natural materials often avoid triggering chronic or immunological reactions and toxicity, and are therefore appropriate multifunctional ingredients for constructing multilayer films and coatings with improved interface with the biological environment [66].

2.2.2 Moving LbL toward faster production

The number of parameters that may influence the buildup of multilayer films is broad: LbL requires complementarity between the multilayer constituents, but the strength of the forces driving the assembly may be influenced by other parameters. Intrinsic properties – such as the molecular weight of

polymers or size of inorganic particles, charge density and polarity – and external properties – such as temperature, pH of the solvent and ionic strength – may facilitate or hinder a constituent's adsorption. The result depends on the original properties of the materials. For instance, varying the pH of a weak polyelectrolyte above or below its acidic constant (pK_a) will greatly impact on its overall charge density and ultimately electrostatic interactions [67,68]. Therefore, the construction of multilayer films based on new and not much used constituents may require a thorough preliminary screening process. Nonetheless, as soon as this temporal hardship is overcome, the optimal conditions will be determined and they can be applied in the mass-production robust nanostructured coatings.

Despite all the presented advantages of LbL, this technique has one fundamental drawback: it is generally a time-consuming process. To construct a multilayer film, the adsorption time to assemble a single layer may vary with the nature of the constituents. A standard time of 10 minutes is usually acceptable, plus a rinsing step that may take an equivalent time scale. Surprisingly, the effect of reducing the processing times (sacrificing some mass deposition) was never properly addressed as a way to accelerate the fabrication of the films. In a scale-up perspective, and when large numbers of layers are required, automated devices have been proposed for the production of multilayer films. The most common devices are dipping machines, which allow parallel construction of several films at once. They function similarly to manual dipping in every aspect but its automated nature permits not only the repetition of multiple adsorption cycles over long construction times but also the parallel assembly of multiple films. This way, thicker multilayer films with several micrometers can be obtained in high quantities [69-71].

One could argue that, although many films can be fabricated in parallel, the fabrication time is still too long. An alternative procedure is a sputtering-based strategy which, rather than dipping, sprays the surface. The fabrication time of the latter has been reported to be greatly shortened due to enhanced adsorption by the spray pressure. Schlenoff, Dubas and Farhat [72] showed the construction of poly(diallyldimethylammonium) chloride/poly(styrenesulfonate) (PDADMAC/PSS) multilayer films by spraying the respective solutions onto silicon wafers. For that purpose, they used a sprayer as simple as a hand-operated "plant mister", making it possible for each layer to be adsorbed in a matter of seconds. Their morphology, uniformity, and chemical composition were similar to coatings made by dipping. Izquierdo *et al.* [70] followed a similar spraying strategy for the assembly of PSS/poly(allylamine) hydrochloride (PAH) multilayers, where they reiterated the findings of the previous authors.

Although the process of LbL started as being an inherently slow processing method that requires a lengthy preliminary screening stage, these drawbacks have been addressed and reduced to a minimum

in the last decade [73]. Furthermore, the use of automated devices, including unconventional sputtering-based approaches, have made it possible to construct multilayers a lot faster (about a factor of 250 in the latter example) and are appropriate for future industrial mass-production with low risk of stock shortage.

2.3 Surfaces with specialized properties

2.3.1 Surfaces containing adhesive constituents

Multilayer films and coatings can exhibit higher forms of specialized properties by selecting functional materials as their components. One such example is the use of polymers that are known to exhibit adhesive properties in nature. Without much effort, a great source of adhesive natural materials can be found in the sea, such as the polysaccharides chitosan (CHI) and alginate (ALG). CHI is derived from chitin, found in the exoskeleton of shellfish or crustaceans, like shrimp and crabs, and ALG is a structural component found in brown algae. These two polysaccharides share a marine origin and exhibit important properties for biomedical applications – biocompatible, adhesive, nontoxic, bacteriostatic, fungistatic, antimicrobial and hemostatic [66,74] – which proved to be useful in drug delivery, implants and wound dressings [75-77]. Another strategy to obtain adhesive materials is to produce synthetic analogues based on natural systems, such as the adhesive proteins rich in 3,4-dihydroxy-phenylalanine (DOPA). DOPA, also a precursor of dopamine, can be found in the threads expressed by mussels, which have been shown to attach to many types of inorganic and organic surfaces thanks to the exhibition of catechol hydroxyl groups [78,79]. Catechol-modified biomimetic polymers can be used to aid in the construction of the multilayer film itself. As demonstrated by Lee *et al.* [80] catechol-functionalized poly(ethylenimine) (PEI) and hyaluronic acid (HA) adsorbed could be adsorbed onto any sort of substrate, namely poly(tetrafluoroethylene) (PTFE), silicon and gold. Karabulut *et al.* [81] exploited the iron(III) (Fe^{3+}) crosslinking mechanism of catechol groups to tune the mechanical properties of films made of carboxymethylated cellulose nanofibrils modified with dopamine. The adhesive forces were measured using a silica probe demonstrating that, in the presence of Fe^{3+}, dopamine-functionalized films are more resistant to deformation than films prepared from unmodified nanofibrils. Wu *et al.* [82] prepared multilayers of PAH and poly(acrylic acid) (PAA), the latter modified with dopamine, and crosslinked the films by an oxidation reaction mediated by sodium periodate for better stability. These coatings could be peeled by a sodium hydroxide solvent, providing undamaged free-standing membranes. Curiously, DOPA and its analogues have been used as a mechanism to

improve the construction of LbL films, rather than increasing adhesiveness to surrounding tissues. It is however expectable that the adhesiveness of such films is indeed augmented, judging by how catechol-modified gels and membranes behave.[83-85]

Adhesive materials can be found in places other than the sea. For instance, Costa *et al.* [86] assembled multilayer films made of CHI and phosphonate-modified levan, a fructan exopolysaccharide produced by the halophilic bacterium *Halomonas smyrnensis* sp. nov. AAD6T. The adhesiveness of this polymer comes from their hydroxyl groups that form strong adhesive bonds with various substrates [87,88]. The adhesiveness of these films was verified by lap shear bonding stress between two overlapped films with 100 bilayers assembled onto glass slides, meaning that no peeling was attempted. In comparison to CHI/ALG films used as controls – two polysaccharides often regarded as good natural adhesives – the detachment force of the levan-functionalized surfaces was about 3 times higher than the control (2.5±0.3 MPa and 0.9±0.1 MPa, respectively). The cell adhesion for 24 h conducted using a fibroblast cell line also showed that cells were sensitive to the incorporation of levan and adhered mostly to these coatings (110 cells·mm^{-2} in comparison to 20 cells·mm^{-2} in the control).

The technology of LbL films using adhesive materials has the potential to address issues related to wound healing, namely in the performance of medical adhesives. Many synthetic adhesives currently approved present limitations, which include poor adhesion in the presence of biological fluids, allergic response and inflammation [89]. Therefore, the use of natural adhesive constituents may help in the development of wound healing dressings and surgical biomaterials with improved adhesiveness to organs and tissues.

2.3.2 Mineralization control

Bone regeneration and integration is probably one of the most researched areas in biomedical engineering and a variety of systems have been proposed for this purpose [90-92]. Using the recurrent example of orthopedic bone implants, coatings that exhibit biomineralization capability may provide a favorable environment for osteogenesis and a bone-friendly interface between the implant and host's bone [93,94].

Biomineralization can be achieved following two strategies: (i) addition of inorganic components (e.g. silicate-based particles), or (ii) incorporation of osteoinductive molecules (e.g. polymers and proteins). An example of (i) are bioactive glasses. These materials have been subject of much research in the last decades because when in contact with physiological or simulated body fluids they form a surface apatite layer. Such apatite layer permits an adjusted bonding of the implant to bone *in vivo*, preventing

the formation of a fibrous capsule and promoting a stronger osseo-integration. Ultimately, this layer can bind to the collagen of connective tissue cells, like osteoblasts [95]. In the case of (ii), bone morphogenetic proteins (BMPs) are well-known growth factors which have been widely used for bone repair and are known to stimulate the proliferation, migration and differentiation of stem cells [96].

One would not expect LbL devices to be used as systems aimed to integrate or regenerate a hard tissue such as bone, since most polymeric multilayer films do not exhibit mechanical properties equivalent to the bone. However, it may be used to engineer an appropriate interface between an implantable device and bone, since LbL allows incorporating distinct classes of materials in their structure. Thus, strategies can be devised to convert a "soft" multilayer to the purpose of triggering biomineralization.

Couto, Alves and Mano [41] constructed multilayer films that contained bioglass nanoparticles as an inorganic ingredient that provided biomineralization capability *in vitro*. The synthesized nanoparticles had a charge of -25 mV, which enabled them to interact with the polycationic CHI via electrostatic interactions. Using a quartz-crystal microbalance (QCM), they demonstrated that films up to 10 bilayers could be successfully assembled. Using a simulated body fluid (SBF), they showed that it was possible to induce the formation of apatite crystalline layers, similar to the ones found in the inorganic component of bone. The mineralization was also more pronounced with increasing number of layers.

Fukui and Fujimoto [97] described the conception of a nanocapsule templated in phospholipids that encapsulated phosphate ions. The phospholipids were coated using CHI, dextran sulfate or DNA and then incubated in a solution containing calcium ions. They demonstrated that changes in the surface chemistry could influence the counterion diffusion and therefore the biomineralization rate (Figure 2.2).

Despite the efforts made so far, biomineralization-inducing multilayers still remain a largely unexplored approach. Most likely the reason lies within the fact that immobilizing particles inside a multilayer structure is not an easy task. While a polymeric film may have only a few nanometers but an interpenetrated structure, a nanoparticle can be very large in comparison. Thus, it is likely that the production of biomineralizing surfaces will be limited to the loading of osteoconductive agents.

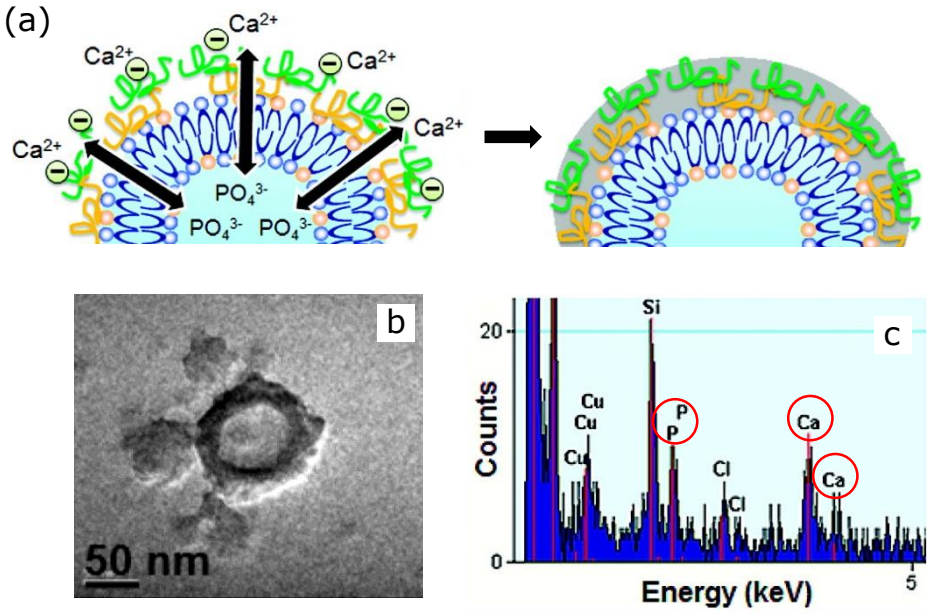


Figure 2.2. Formation of calcium phosphate over the surface of polysaccharide-coated liposomes. (a) Liposomes encapsulating phosphate ions (PO_4^{3-}) are coated with polysaccharides. Polycations (orange) and polyanions (green) are adsorbed sequentially over the surface and placed in a medium containing calcium ions (Ca^{2+}), which concentrate around the negatively charged molecules. The counter-diffusion of ions across the wall leads to the formation of a calcium phosphate mineral interface. (b) Field emission TEM image of a liposome coated with CHI and DNA after inducing mineralization at pH 10 for 18 h, exhibiting a thick wall. (c) Energy dispersive X-ray analysis (EDX) exhibiting calcium and phosphate peaks. Adapted with permission from ref. [97] Copyright 2011, American Chemical Society.

For instance, Hu *et al.* [98] took another approach by adding bone morphogenetic protein-2 (BMP-2) and fibronectin to a CHI/gelatin (GEL) multilayer formulation. Disks and rods of a titanium alloy were first subjected to the adsorption of a layer of GEL conjugated with dopamine – a fine example of how dopamine and its analogues can be used as the starting layer of any substrate, as previously demonstrated by Lee *et al.* [80] Next a combination of CHI, unmodified GEL, recombinant human bone morphogenetic protein-2 (rhBMP-2) and fibronectin was used. The *in vitro* release of rhBMP-2 showed that 30% of the initial adsorbed amount was released within 2 hours and around 50% after 6 days. After 2 weeks, around 20% was still retained at the surface. Mesenchymal stem cells (MSCs) were seeded onto these substrates up to 21 days and showed higher production levels of alkaline phosphatase (ALP), mineralization and expression of osteogenic genes compared to a control of bare titanium substrate. *In vivo* studies using a rabbit femur model were carried out up to 12 weeks and were shown to increase

the density and formation of bone. More examples of multilayered systems containing BMPs will provided later in this review, in the context of drug delivery systems (Section 2.5.3).

2.3.3 Stimuli-responsive surfaces

Higher degrees of functionalization can be achieved by introducing stimuli-responsive constituents. Usually, a surface – modified or not – is perceived as a static interface, that is, no structural changes occur upon switching environmental parameters. However, stimuli-responsive surfaces are dynamic and undergo conformational changes upon variations of specific external factors. An elegant example found in Nature exhibiting such mechanism is skin. Skin is the largest organ of the human body and it can be perceived as the ideal multifunctional membrane that responds to every variation in its environment – heat/cold, humidity, chemical/mechanical stress and even light [99]. Exploiting external stimuli has been extensively researched for several devices, such as grafted surfaces and hydrogels [100], but not as much in multilayer systems for controlling biological events, like cell attachment/detachment mechanisms. Some works described films made of CHI and elastin-like recombinamers (ELRs), a recombinant class of elastin-like polymers (ELPs). ELRs are genetically modified polypeptides that undergo a phase transition when in solution dependent on temperature: below a critical transition temperature, the free polymer chains adopt random coil conformations; above it, they fold into an organized structure known as β-spiral [101]. Using this polysaccharide/polypeptide formulation, both bilayer coatings [102] and multiple responsive multilayers [27] were made. In the latter, variations of pH, ionic strength and temperature triggered a transition of wettability between a moderately hydrophobic character (contact angle around 70°) to a superhydrophilic surface (contact angle of 0°). These variations were observed above pH 11, ionic strength 1.25 M in NaCl, and temperature of 50°C. The genetic nature of ELRs permitted the inclusion of the cell adhesion sequence arginine-glycine-aspartic acid (RGD), the minimal sequence required for recognition by cell membrane integrins [103]. The adhesion of osteoblast-like cells was higher in these films than in films ending in CHI or a scrambled nonfunctional RDG analogue. Although cell adhesion was influenced by the exhibition of specialized bioactive groups, the possibility to use external stimuli to control the attachment or detachment of cells was not explored. The reason lies in the fact that the variation of the surface properties evaluated in terms of wettability variations only occurred at values that are simply not suitable for biological experiments. However, in another report from the same group [104], a multilayer film made of ALG and CHI modified with poly(*N*-isopropylacrylamide) (PNIPAAm) was developed to reproduce the cell-sheet technology developed by Okano and coworkers [105], which allows a thin layer

of cells to be harvested for reculture, transplantation or differentiation. Human osteoblast-like cells were seeded until confluence was achieved at 37°C and the temperature was lowered afterwards to 4°C. Cells started to peel and detached from the surface as a thin layer, which occurs due to the extension of the PNIPAAm chains and increase of hydrophilicity. These cell-sheets could be harvested and seeded again in a different culture support to demonstrate their viability. A similar approach was demonstrated by Zahn *et al.* [106] who used an ion-induced detachment of myoblast cell layers through the eroding effect of ferrocyanide on PLL/HA multilayers.

Temperature, ionic strength, and pH can be easily manipulated to influence the response of "intelligent" materials contained within the LbL formulation. However, sharp variations of the last two may be aggressive to cells as they are not capable of withstanding hypotonic/hypertonic and extreme acid/alkaline conditions. Temperature changes, on the other hand, are usually more tolerated by cells for temperatures up to 37°C, and the example of cell-sheet technology is a fine example of that [107].

Another stimulus that may be exploited is light. The use of light would be a convenient way of controlling a surface's properties since it can be easily emitted or blocked on demand. Moreover, biomedical applications could benefit from its noninvasive character, capability of deep tissue penetration and fine spatial control over its intensity [108]. One example of light-responsive films is the work of Ahmad, Saqib and Barret [109], who developed films containing anionic azobenzene-functionalized polyelectrolytes. The polyelectrolytes were distinct and exhibited different hydrophilicity/hydrophobicity character, which ultimately reflected upon the ultraviolet (UV)-visible absorption spectrum of each film. Azobenzenes linked to hydrophilic groups exhibited higher absorption maxima (423–440 nm) than azobenzenes linked to hydrophobic groups (407–414 nm), in both cases values slightly higher than the maximum UV wavelength of 400 nm. Multilayer systems that respond to light are seldom referred in the literature. This may be related to the fact that most light-sensitive molecules respond mostly to light in the UV spectrum, which is harmful to biological cells. Nevertheless, the presented example shows how the inclusion of light-responsive groups linked to distinct radical groups may help shifting the maximum absorption wavelengths toward the visible spectrum.

2.4 Coating of implantable devices

The modification of implantable medical devices is perhaps the most evident application resulting from LbL strategies in the biomedical field. The versatility of LbL and the possibility of developing surfaces with specialized properties have already been applied as a means to improve the integration and to adjust the biorecognition of implantable devices, such as prosthesis and stents. Currently, most of the

improvements in the performance of an implant are possible thanks to the development of more anatomically-shaped geometries. This is particularly evident in the case of bone implants, which are increasingly easier to attach to the bone and provide more comfort for the patients [110-112]. Besides design, it is known that an efficient integration is determined mainly by the surface characteristics of the implantable device (surface microstructure and chemical/biochemical nature), which influence the subsequent adhesion of proteins and cells. It is common to find metallic implants (e.g. steel or titanium) during surgical interventions [3,10,113]. However, it is difficult to assume that a metal with no resemblance to biological materials provides appropriate integration and recognition by the body. Therefore, LbL constitutes an adequate methodology to modify the surface of implantable devices, as it could be employed regardless of their geometry.

2.4.1 Coating of synthetic implantable devices

Most metallic alloys are negatively charged, like other common materials found outside the medical field (e.g., glass), and thus provide support for the formation of a multilayer coating by adsorbing a primer polycationic layer [30]. Zhankovich *et al.* [114] proposed to coat a titanium alloy using multilayer coatings of either CHI/GEL or CHI/HA to improve osseo-integration. Their study was based on prior conclusions by the same group that had shown showed that while CHI/GEL coatings stimulated the *in vitro* adhesion and proliferation of human osteoblasts, CHI/HA coatings reduced it [115]. So, using a rat tibia model, shear strength analysis did not show any biomechanical difference between the coated implants and a control of uncoated implants after 3 weeks. However, after 8 weeks, compared to the titanium alloy control, shear strength was increased up to 1.84-fold and 1.86-fold for CHI/GEL and CHI/HA, respectively, indicating improved osseo-integration of the implant to the surrounding tissue. Interestingly, these results contradicted their expectation to observe significantly higher integration with GEL-coated implants. The explanation to this similar osseo-integration observed in the rat tibia model could be due to the long-term exposure of the coating to a biological environment. This exposure could have led to the partial dissolution of the outer HA layer and its inhibitory effect decreased. CHI would then come in contact with the biological tissue and promote osteoblast proliferation. Both works demonstrate the potential of LbL modified implants in orthopedic implant surgery, even using very simple biopolymers, where a regulated osteointegration is desirable to avoid early loosening, especially when osteoporotic fractures are involved.

Aiming for the treatment of coronary artery diseases, stents have been coated with polymeric films [116,117]. Stents with no modification can trigger thrombosis and cytokines secretion, leading to

in-stent restenosis – a particular refractory form of neointimal hyperplasia [118]. Schweizer *et al.* [119] coated nitinol stents with a multilayer formulation of CHI and heparin, a well-known glucosaminoglycan with anticoagulant properties. First, tubes made of the stent bulk material were coated and bent in a 37° angle, showing that the LbL coating could be maintained and withstand mechanical loading. Then, they conducted a mineralization study by immersion in a calcium nitrate and ammonium phosphate bath in agitation for one week. The formation of calcium phosphate particles with less than 100 nm was observed in the coated stents, while in the control large microcrystals were formed. Large calcium phosphate crystals may be dangerous if released and transported into the blood stream, but nanocrystals are not expected to trigger high thrombogenicity. Furthermore, they may help to increase the mechanical stability of the assembled multilayers. In the same study, titanium samples were coated and studied simultaneously. Surprisingly, crystals on the order of 10 μm were observed on coated samples, much larger than in the case of coated nitinol ones. This conclusion alerts to the role of the substrate used, since it is likely that synergistic effects occur between not only the coating constituents but also between the assembled coating and the substrate's chemistry. The use of CHI/heparin films may also result in antibacterial activity and suppression of blood clot formation, respectively. In fact, Meng *et al.* [120] had previously shown that stainless steel coronary stents with the same coating has a better hemocompatibility and more efficient re-endotelyzation than bare metallic samples, using a porcine coronary injury model.

Lin *et al.* [121] tested the hypothesis that a stent that promotes the adhesion of endothelial cells – either circulating in the blood or migrating from neighbor tissues – facilitates its integration and reduces risk of stent failure. Stainless steel stents were coated with heparin/collagen multilayers, which could be or not be further functionalized with an anti-CD34 antibody. Both types of samples and a control of uncoated stents were implanted in rabbit femoral arteries. While no significant difference of neointimal hyperplasia was observed between uncoated metal stents and heparin/collagen multilayer modified stents, neointimal hyperplasia on the anti-CD34 antibody-functionalized multilayer coated stents was significantly inhibited and provided an accelerated adhesion of both vascular and endothelial cells (Figure 2.3).

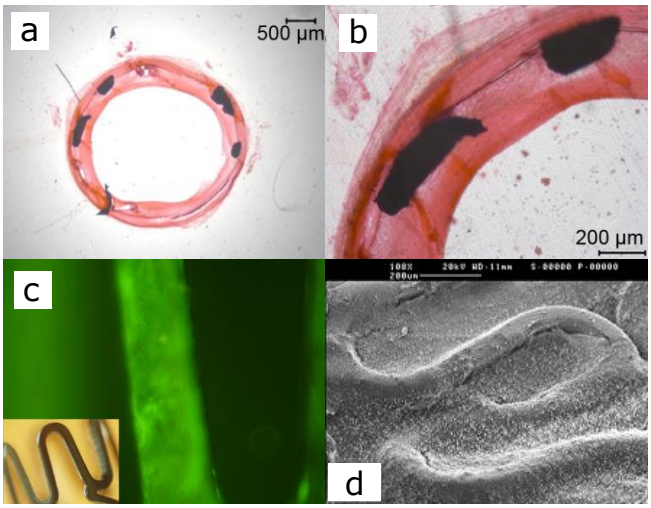


Figure 2.3. Typical photographs obtained using (heparin/collagen)$_5$-CD34 multilayer-modified stents. In (a) and (b), cross-section optical images of rabbit femoral arteries with (heparin/collagen)$_5$-CD34 multilayer-modified stents. (c) Fluorescence microscopy image of the multilayer on stent, with CD34 tagged with FITC. Inset shows the optical image of the stent. (d) SEM image of the inner wall of the stented rabbit femoral arteries for 48 h, showing the formation of a complete endothelium. Adapted with permission from ref. [121] Copyright 2010, Elsevier.

Post-surgical infection due to bacterial contamination constitutes another major issue that leads to implant failure. Bacteria can form biofilms on the surface of implants, therefore compromising the performance of the device [122]. Therefore, it is crucial that initial bacteria adhesion to an implant's surface is prevented. Building multilayer films that exhibit antifouling properties is a possible solution for this problem. Rendering a surface non-fouling can serve as immuno-''camouflage'' to prevent immune rejection of implanted biomaterials or to enhance the efficiency of injected drug delivery vehicles [123-125]. Reisch *et al.* [126] demonstrated that films containing PAH and a PAA containing phosphorylcholine side chains resisted the adsorption of albumin, which served as an estimation of cellular adhesion. Caruso and coworkers [127] demonstrated that PSS/PAH multilayer films with a terminal layer of PSS-b- poly(ethylene glycol) (PEG) were up to five-fold more resistant to bovine serum albumin (BSA) adsorption than PSS-terminated films. Moreover, the binding of coated polystyrene particles to human colorectal cancer cells was reduced 6.5-fold in comparison to native PSS-terminated particles. However, since LbL allows the inclusion of active agents to the formulation of a multilayer coating, the most straightforward strategy to avoid deleterious effects caused by microorganisms is perhaps the addition of antimicrobial agents. For instance, Hammond and coworkers [128] coated

silicon substrates with *N,N*-dodecyl,methyl-poly(ethylenimine) (DMPEI) as a polycation with microbicidal activity and a polyanion, such as PAA. The surfaces proved to be lethal against airborne and waterborne bacteria (*Escherichia coli* and *Staphylococcus aureus*) and viruses (influenza virus, strain H1N1).

2.4.2 Cells as supports for the assembly of multilayer coatings

Cell therapies based on bioencapsulation strategies have recently found utility in the treatment of numerous pathologies, such as for diabetes, bone and cartilage defects, and cancer. Usually, ALG is the most frequently employed biomaterial for the encapsulation of cells due to its abundance, water solubility, mild gelling properties, high biocompatibility, and resemblance to the natural extracellular matrix (ECM). However, the diffusion of essential molecules in hydrogels is usually less efficient than in liquefied environments, which may compromise cell survivability [129,130].

Developing a device that provides immune protection and selective permeability is an important and ambitious step in the development of an effective encapsulating barrier [131-133]. In the field of LbL implantable devices, cells or cell agglomerates can be used as suitable substrates for the buildup of multilayers. Therefore, cell surface engineering offers great potential to improve clinical outcomes associated with this promising class of therapeutic devices.

An application that would benefit greatly of such approach would be the treatment of diabetes. The widespread clinical solution for this disease is that of islet transplantation, but this brings problems such as immune rejection, inflammation, thrombosis, hypoxia and weakened revascularization [134-136], leading ultimately to the destruction of the encapsulated cells. Krol *et al.* [137] demonstrated that Langerhan cells could be effectively coated with the polycations PAH or PDADMAC. Coating pancreatic cells with multilayers is an alternative to the conventional microencapsulation approaches within highly viscous ultrapure alginate droplets [138-140]. By taking advantage of the negative charge provided by the peri-islet capsule, polycations could be adsorbed to the membrane of the cells, followed by the polyanionic PSS. The multilayer coating succeeded in providing immunological protection to the cells. They also retained their insulin secretory function *in vitro* up to 4 days and diffusion was allowed through the coating. Furthermore, insulin release increased when high quantities of glucose were present. This is a very promising approach of LbL for the development of effective cellular therapies, which seemed promising to solve diabetes related problems, and their application *in vivo* was most anticipated.

Recently, Wilson *et al.* [141] presented a polyelectrolyte multilayer (PEM) comprised of ALG and poly(L-lysine) (PLL)-g-PEG to coat the surface of pancreatic islet cells. The surface engineered islets

were introduced through the portal vein and into the liver microvasculature in diabetic mice. Two weeks after transplantation, 47% of the mice receiving the coated islets converted from a diabetic to an euglycemic state, while 25% of mice that received uncoated cells showed improvements.

Given these examples, one can see that LbL-based strategies have the potential to improve the integration of diverse types of implants. It can be easily applied to existing biomedical devices implants and even to biological materials like cells for transplantation purposes. The possibility to introduce functionalized and bioactive materials to a surface may lead ultimately to a good integration in a living system and constitutes an advantage in comparison to other conventional techniques (e.g., temperature and plasma treatments). The possibility to coat biological structures directly is unusual and may have a great impact in the management of cellular viability prior and after implantation. This technology may be extended to develop cellular strategies, for instance in the form of cell infusions that may be injected intravenously for delivery to targeted tissues, such as the heart, or with other therapeutic functions, such as immunoregulation or systemic production of growth factors.

2.5 Engineering biomedical devices

2.5.1 Construction of films for wound healing

With LbL, one can develop films with just a couple of layers or hundreds, with obvious implications in the films' thickness. Thin coatings with several nanometers or membranes that may reach tens of micrometers can be obtained this way. When considering the production of membranes, film casting and hot-melt extrusion are the most recurrent used techniques [142]. However, these techniques are not completely compatible with biological applications: the use of organic solvents in film casting and the addition of plasticizers in hot-melt extrusion may cause adverse reactions when introduced in a biological environment. Since LbL-based strategies disregard the use of such agents, thick multilayer films appropriate for biological applications can be constructed.

2.5.1.1 Development of nanostructured substrate-free membranes

Multilayers adhere strongly to the underlying substrate and usually cannot be harvested without risk of damaging the film. Thus, many strategies were developed to produce films that could be detached, which are usually referred to as free-standing films. These free-standing films resemble membranes but, unlike conventional membranes, they are nanostructured and exhibit nanoscale precision thanks to their organization in layers. Such a device offers all the advantages of multilayered coatings and is

useful for applications such as wound healing and drug delivery, with the added benefit of manual handling [143-145].

A typical approach to fabricate free-standings is through the use of sacrificial layers or substrates that can be dissolved after the buildup [42,146,147]. Ott *et al.* [147] used silicon wafers precoated with PEI to assemble chemically polymerized polyanions bearing aldehyde groups and polycations with 4-methylpyridinium moieties. After crosslinking, the film could be detached easily from the substrate by salty solutions. The salt weakened the PEI interactions with the silicon wafers, after which robust free-standing films could be harvested.

Using salty solutions is preferable to chemical solvents, since the latter may cause both chemical and physical changes to the film during this stage. However, even salt may interfere in the internal structures of the multilayers [68,148,149]. Consequently, other strategies have been introduced as alternatives to the solvent-assisted detachment of multilayer films more recently. Larkin *et al.* [145] used planar substrates of Teflon and polypropylene to assemble polymeric free-standing films. Polymeric constituents and these substrates form weak van der Waals interactions, which make it possible to peel the films safely without risk of damage. The proof-of-concept was demonstrated for 50 bilayers of CHI/HA, crosslinked by glutaraldehyde to increase their stability in aqueous solutions. A unique feature of these detachable free-standing films was their optical transparency. The transmission of light is critical for microscopy observations and makes them suitable to be used as cell culture substrates. Indeed, in that work fibroblasts were seeded and could be observed under light microscopy.

Caridade *et al.* [150] recently developed CHI and ALG free-standing films assembled on distinct low surface energy substrates. In comparison to the work of Larkin *et al.* [145] no crosslinking was made. Instead, 100 bilayers were assembled (around 35 μm). They also exploited the possibility to produce free-standing films exhibiting asymmetrical properties, that is, distinct properties in each face of the membrane. After the assembly was concluded, one side of the membrane was effectively made of ALG and the other of CHI. This property is useful if one envisages having two distinct properties in distinct faces of the same membrane. In this regard, the *in vitro* adhesion of myoblasts showed that cells adhered more to the ALG face (200 cells·mm^{-2}) than to the CHI face (40 cells·mm^{-2}), showing how the simple selection of the starting and ending constituents can significantly influence the biological performance of free-standing films.

2.5.1.2 Healing of tissue defects *in vivo*

Free-standings may also result from hybrid approaches using LbL together with other techniques. Not only that, they can be associated with an additional substrate that helps in the posterior application of the membrane to a wound. In this sense, free-standings may serve as protective coating for wounds, requiring ultimately that a film is harvested and used independently of the substrate.

The group of Takeoka and coworkers has developed a LbL-assisted strategy involving spin-coating and casting for the purpose of healing wounds in animals. One of their first works reported the use of a "spin-coating"-assisted-LbL subsequently followed by casting [151]. Shortly, CHI and ALG were sequentially adsorbed onto spinning silica substrates to obtain a film 75 nm thick. Poly(vinyl alcohol) (PVA) was cast over the bilayered films and left at room temperature during a cure time of 12 hours. Together with this PVA layer, with a thickness around 70 μm, the CHI/ALG film could be easily peeled from the silica substrates, making it easier to carry and place over a tissue defect (Figure 2.4a).

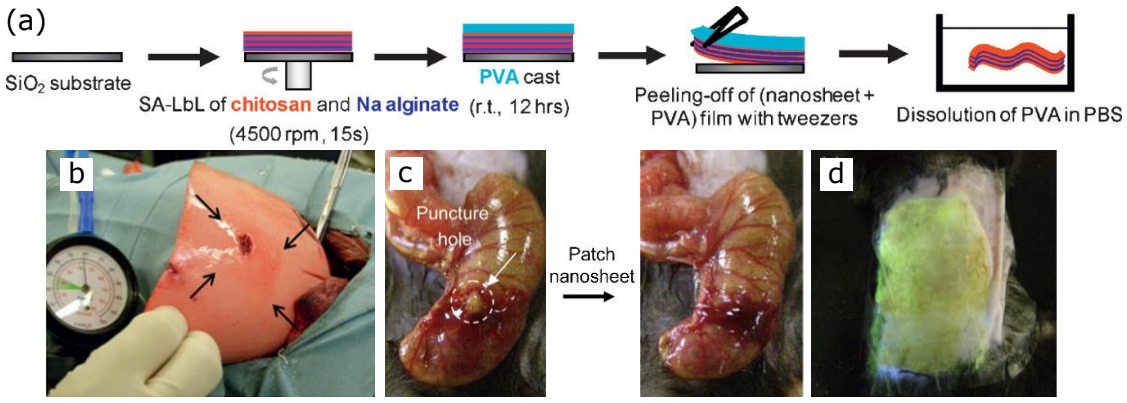


Figure 2.4. Free-standing nanosheets and their various applications. (a) Basic concept of the spin-coating-assisted LbL fabrication method. Upon polyelectrolyte deposition, a PVA layer is cast allowing peeling-off the nanosheet easily, subject to posterior dissolution. (b) CHI/ALG nanosheet securing a repaired visceral pleural defect in beagle dogs when pressurized by over 50cm H_2O pressure 3 h after repair. The region indicated by arrows shows the nanosheet-sealed area. Reprinted with permission from ref. [151] Copyright 2009, Wiley-VCH; (c) Macroscopic images after treating a murine cecal puncture hole with a tetracycline layer sandwiched between CHI/ALG multilayers and poly (vinyl acetate). Reprinted with permission from ref. [153] Copyright 2010, Elsevier; (d) Macroscopic images of murine dorsal skin treated with tetracycline-loaded CHI/ALG nanosheets illuminated under UV light, remaining at the wound site for 7 days. Reprinted with permission from ref. [154] Copyright 2012, Elsevier.

The authors performed a minimally invasive procedure to repair a visceral pleural defect in beagle dogs: the PVA/$(CHI/ALG)_n$ complex was placed in contact with the defect. Next PVA was dissolved using non-aggressive aqueous solvents, such as phosphate-buffered saline (PBS). Over a period of 24 hours after the defect repair, this thin membrane resisted the pressure of respiration and blood circulation, and was able to sustain the stress due to ventilation (Figure 2.4b). Problems such as the reduction in the pulmonary tissue volume due to suture, and pulmonary air leakage could benefit from the use of multilayer thin films as protective membranes and sealants [152]. Later, this hybrid LbL technique and ingredient formulation was used to develop tetracycline-loaded films with antimicrobial effects in a murine cecal punctured model (Figure 2.4c) [153] and nanosheets as a protective membrane for full-thickness burn-wound infection in a murine model (Figure 2.4d) [154]. Their production differed slightly from the first proposed strategy, in the fact that tetracycline was cast in the opposite face to that of the PVA, followed by a spin-coated layer of poly(vinyl acetate) and dissolution of PVA.

These two last examples are particularly important for the translation of such approach to humans. Burn injuries are perhaps one of the most common skin defects. Such an injury creates a large skin area which is susceptible to bacterial colonization, leading ultimately to infections, systemic sepsis, severe septicemia and, if left untreated, death [155,156]. Full-thickness burn wounds may require tissue grafting [157]; thus it is important to have an effective protective barrier that protects the wound until grafting is carried out. The necessity for bacterial protection takes greater proportions when considering gastro-intestinal lesions, where the presence of multiple microorganisms may lead to bacterial peritonitis [158]. The presented examples were able to circumvent such problems and have great potential for future wound treatments in human patients.

Although the technology of LbL membranes has the potential to act as wound healing dressings, there has been little research on LbL coatings *in vivo*. Based on the existing animal tests with hybrid "spin coating-LbL-casting" technology and on the robustness of films made purely with LbL, its broad application may be a matter of time. Additionally, this evolution may benefit from the use of biomimetic approaches and natural sources of adhesive ingredients (as mentioned in Section 2.3.1) for dressings with improved mechanical and biological performances.

2.5.2 Multilayer coatings for enhanced cell adhesion on flat surfaces

The surface of an implant is the first contact with the biological environment, and its modification – if any – will dictate the extent of its integration and long-term stability. Modifying surfaces is not limited to

devices currently used in surgical practice but also to more sophisticated ones for tissue engineering and regenerative medicine.

The versatility of LbL can help achieving better cellular attachment by tuning a variety of factors. One of those is the stiffness of the multilayer film. It was demonstrated by Schneider *et al.* [159] how films of PLL and HA were assembled and crosslinked with increasing concentrations of a water-soluble carbodiimide. Higher concentrations of carbodiimide allowed achieving higher crosslinking degrees and, consequently, higher elastic moduli, as well as higher surface roughness. The cellular adhesion was affected by the stiffness: human chondrosarcoma cells adhered and spread preferentially in stiffer films. Using the same mechanism, Phelps *et al.* [160] assembled films of PLL and polyglycolic acid (PGA) and selectively crosslinked it by exposing only the outermost layers to carbodiimide. This interface was turned into a rigid external skin that promoted the adhesion of pre-osteoblast cells, while leaving the interior of the film unaffected. Although unexplored, this structure could be useful to encapsulate an active agent within. Because the crosslinking is selective and not fully uniform, the deactivation of embedded bioactive species due to crosslinking may be avoided.

Martins *et al.* [161] used CHI/ALG films crosslinked with glutaraldehyde, to study the adhesion and proliferation of osteoblast- and fibroblast-cell lines during 1 week. In the first case, the cells proliferated in a rate similar to cells seeded onto CHI-ending films, but appeared as more elongated and with a higher metabolic activity. In the case of fibroblast-like cells, the proliferation was inhibited in crosslinked films. The results of these authors show that films with higher stiffness are not always clearly beneficial to cells and that different cell types may behave differently when contacting with different substrates. In fact, the authors justified that the reduction of positive charges due to CHI crosslinking affected both the attachment and adhesion of this cell line – L929 human fibroblast-like cells – which are known to favor their adhesion.

The addition of bioactive compounds is another form of tuning the adhesion and metabolism of cells in a surface. Lee and Kotov [162] incorporated delta-like 1 Notch ligands (DL-1) at the surface of PEM films. The Notch ligands stimulated hematopoietic stem cells (HSCs) to differentiate into T-cell lymphocytes and progressively develop their own ECM. Gribova *et al.* [31] developed PLL/PGA films to study the effect of the stiffness and the exhibition of RGD-modified PGA on muscle cell differentiation. It was shown that uncrosslinked films exhibiting RGD were the most appropriate to induce the differentiation of myoblasts, while crosslinked films – with and without RGD – inhibited it and exhibited an excessive cell confluence that led to detachment.

Aiming to use multilayer coatings in living organisms, Picart *et al.* [163] tested the performance of CHI/HA coatings – either crosslinked with a carbodiimide or uncrosslinked – *in vitro* and *in vivo*. By using a QCM and fluorimetry, degradation of the films *in situ* was followed upon their contact with an enzyme solution containing lysozyme, chitosanase and hyaluronidase. The *in vivo* degradation was studied by implanting both types of films in mouse peritoneal cavity for 1 week. In both cases, crosslinked films were more resistant to degradation in comparison to native films, which showed almost complete degradation by the end of the studies.

The use of LbL-based substrates for cell expansion is an ever-evolving field. In contrast to the case of implantable devices, which consist on the improvement of already existing devices, the reviewed works pushed forward toward new ways of improving cell adhesion. Most of the times it involved the development of new types of substrates, such as the example of ligand-functionalized surfaces. It is debatable whether the modification of 2D surfaces using LbL is a solution or an alternative to already existing approaches. For the simple purpose of cell adhesion, conventional techniques such as grafting or plasma can achieve the same result, usually with much faster processing times. As will be debated in Section 2.6.1, the future innovations brought by LbL may lie in the coating of substrates with increasingly complex geometry and the addition of bioactive or smart constituents that may further extend the functionality of 3D multilayer cell substrates.

2.5.3 Multilayer reservoirs for drug loading and delivery

The technological advances in drug delivery have been driven by the need to develop systems that can effectively encapsulate, protect and deliver an active agent with specific kinetics, such as micelles, liposomes, polymersomes, and polymer particles/capsules [164-168]. Such wide availability of delivery systems – not to mention the quantity of drugs available in the market – are proof enough that there is need to develop drug delivery strategies capable of improving the efficacy and bioavailability of bioactive agents.

2.5.3.1 Films loaded with active agents

Picart and coworkers have performed several works consisting on the assembly of PEMs loaded with BMPs. First, PLL/HA films crosslinked with carbodiimide were doped with rhBMP-2 after construction [169]. Myoblast cells were seeded on these films and showed differentiation into osteoblasts, as evidenced by the increasing secretion of ALP. Consecutive *in vitro* cultures showed that rhBMP-2 retained its bioactivity for the length of 3 successive experiments. Recent works using the

same formulation assembled onto tricalcium phosphate/hydroxyapatite (TCP/HAP) macroporous granules [170] and titanium [171] demonstrated the osteoinductive character of the BMP-loaded multilayers in a rat ectopic model. Furthermore, these coatings could be stored up to 1 year without significant loss of bioactivity. By studying the secondary structure of rhBMP-2, Gilde *et al.* [172] showed that this growth factor retained its bioactivity when the films were stored in the hydrated and, to a lesser extent, in the dry state.

Hammond and coworkers also developed a series of multilayer formulations for the loading and release of various growth factors. They constructed a multilayer composition of polycationic poly(β-amino-esters) and noncytotoxic polyanions – heparin sulfate and chondroitin sulfate – intercalated with fibroblast growth factor 2 (FGF-2, negatively charged below pH 9.6) [173]. Assembling more layers equaled to more FGF-2 loaded and also a faster release. The bioactivity of the growth factor was retained, as revealed by *in vitro* biological assays. Using films built with distinct constituents, the released FGF-2 promoted the proliferation of a preosteoblastic cell line up to 12 days in culture. Loading multiple growth factors is a strategy that may help, for instance, to accelerate joint implant integration and reduce recovery time and failure rates by delivering active agents that intervene in the multiple biological events. In another report [174], multiple growth factors – rhBMP2 and a recombinant human vascular endothelial growth factor (rhVEGF) – were loaded by adsorption into multilayers assembled in macroporous polycaprolactone/β-tricalcium phosphate. The release of rhBMP-2 was sustained over a period of 2 weeks, while it took 8 days for rhVEGF to elute from the films. Using a rat ectopic bone model, films loaded with both growth factors were able to potentiate the formation of *de novo* bone, to an extent 33% higher than films loaded solely with rhBMP-2 was introduced.

2.5.3.2 Polyelectrolyte capsules with tunable permeability

From all the 3D shapes that can be coated with LbL, the simplest is the sphere. When coated, spherical multilayer shells surround particles that can often be dissolved to produce hollow capsules. Multilayer capsules present several advantages that are not coupled so often in other conventional fabrication techniques: (i) they can be prepared under mild conditions of pH and temperature, avoiding the denaturation of sensitive species and thus allowing encapsulation in high quantities [175]; (ii) a wide variety of drugs can be encapsulated, regardless of their water solubility [176]; (iii) they allow tuning the release kinetics of an encapsulated agent to the external environment simply by adding a variable number of layers and selecting the shell constituents [177]; and (iv) specialized functions can be attributed by using stimuli-responsive or biofunctional materials with relevant biological interest [178].

Combining distinct ingredients in the coating provide different properties to the shell, such as controlled permeability and, if smart materials are included, stimuli-responsive behavior. Costa *et al.* [179] constructed microcapsules of CHI/ELR bilayers adsorbed onto inorganic calcium carbonate sacrificial microparticles (around 5 μm in diameter) preloaded with BSA (Figure 2.5a).

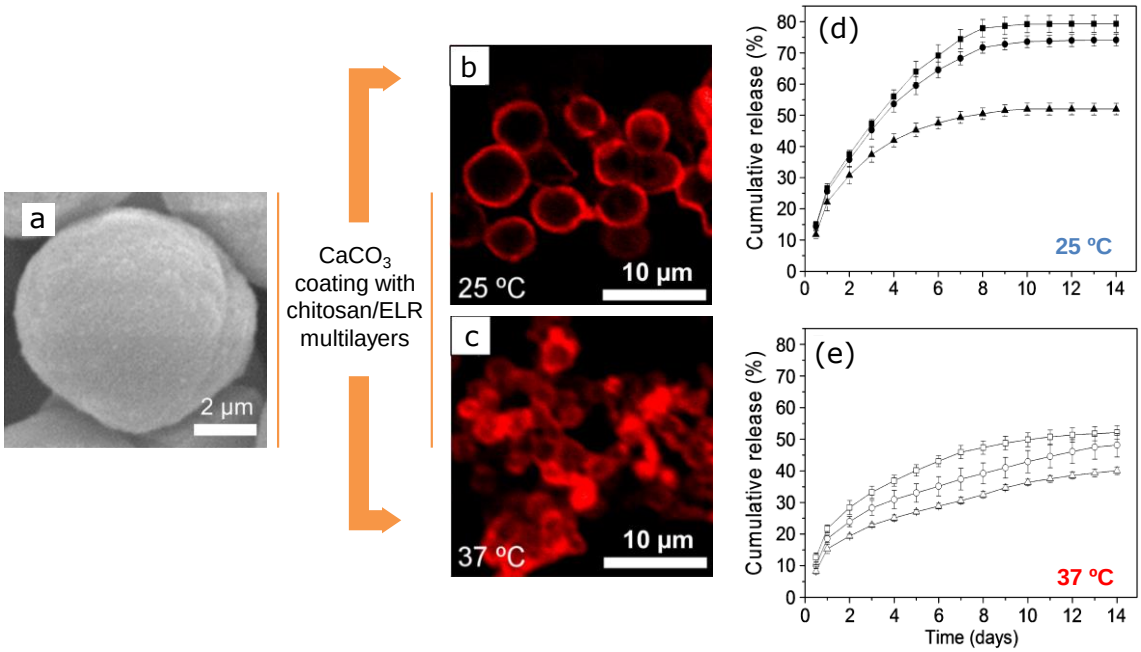


Figure 2.5. Temperature-responsiveness of CHI/ELR microcapsules and size/permeability effects. (a) Multilayer coatings were assembled around calcium carbonate sacrificial templates. Confocal laser scanning microscopy images of BSA-loaded $(CHI/ELR)_5$ microcapsules with the final layer tagged with rhodamine at (b) 25 and (c) 37 °C. Cumulative release of BSA from $(CHI/ELR)_1$, $(CHI/ELR)_3$ and $(CHI/ELR)_5$ microcapsules: ■□, ○●, and ▲Δ, respectively, in PBS (pH 7.4), at (d) 25 °C and (e) 37 °C. Adapted with permission from ref. [179] Copyright 2013, Elsevier.

After the assembly, the template was dissolved by ethylenediamine tetraacetic acid (EDTA), resulting in a hollow multilayer microcapsule encapsulating BSA. The inclusion of such a temperature responsive polypeptide was expected to provide smart-responsiveness, and so, by changing the temperature between 25 and 37°C, the mean diameter of the microcapsules varied between 5.5 and 3.2 μm, respectively (Figure 2.5b and Figure 2.5c). The release of BSA was also affected by temperature: the release of this protein was more sustained in the latter case due to the temperature response of the ELRs, which in the case resulted in a permeability decrease of the multilayer shells. The influence of the number of layers was also studied. As expected, having more layers resulted in an added barrier to the

protein diffusion, that is, a high number of layers reduced the shell permeability (Figure 2.5d and Figure 2.5e).

Kainourgios *et al.* [180] developed PSS/PDADMAC multilayer shells using silica nanoparticles (around 500 nm in diameter) as templates. Following the dissolution of the template by ammonium fluoride and hydrofluoric acid, hollow spheres were obtained. After chelation, two additional layers (PAA and methoxy-polyethylene glycol amine) were deposited on their surface and crosslinked. Daunorubicin was loaded and released at distinct pHs, showing a high quantity release at acidic pH values (pH=4, around 70%) in comparison to pH 7.4 (around 15%). The reduced release at pH 7.4 was attributed to the electrostatic interactions between the sulfonate group of the PSS – which is negatively charged at this pH value – and the amino group of the daunosamine sugar of daunorubicin, which is positively charged. The cytotoxicity of these structures towards breast cancer cells was dose-dependent and higher for increasing daunorubicin content.

Recently, Shen *et al.* [181] fabricated BSA-gel capsules via a two-step procedure. First, calcium carbonate microparticles entrapping BSA were coated with PAH/PSS bilayers, followed by removal of the sacrificial core. Afterwards, a heat treatment at 80°C converted BSA into gel. By exploiting the isoelectric point of BSA (pI=4.8), loading and releasing doxorubicin (DOX) as a model drug could be tuned. At a pH higher than 4.8, the negatively charged BSA allowed a favorable loading of the polycationic DOX and its release upon lowering the pH below 4.8. Thus, rather than exploiting the permeability of the LbL shell to load and release bioactive agents, as described by Kainourgios and coworkers [180], they relied on the jellified interior to retain DOX. Melanoma models were created in the lungs of mice and after injection of DOX-loaded BSA-gel capsules they were more effective in the reduction of the number of melanoma metastatic nodules than injected free DOX.

Ingredients other than polymers can be used to render capsules stimuli-responsive. For instance, Liu *et al.* [182] used an emulsification method to produce magnetic alginate microspheres with around 600 nm in diameter and coated them with PAH/PSS multilayer coatings. After the assembly, the emulsified alginate was liquefied by EDTA but remained entrapped within the coatings, along with the iron oxide nanoparticles. DOX (cationic) was post-loaded by diffusion from concentrated solutions to the interior and was immobilized by electrostatic interaction with alginate (anionic), with an entrapment efficiency of about 56%. Applying a high-frequency magnetic field resulted in an increase of the internal temperature, resulting in an increase in shell permeability and DOX release with higher kinetics. Furthermore, increasing times of exposure to the magnetic field resulted in increased released quantities.

2.5.3.3 Capsules for the intracellular delivery of encapsulated agents

Multilayer microcapsules have been demonstrated to be suitable carriers for drugs and to deliver them either by conventional mechanisms of diffusion to the surrounding environment or by delivering them directly to the intracellular environment. The latter possibility is particularly interesting. In theory, the delivery of an active agent directly to the cells ensures that higher drug quantities will be available at the targeted cell or tissue. Szarpak *et al.* [168] constructed microcapsules using HA and either PAH or PLL. The microcapsules were labeled with fluorescein isothiocyanate (FITC) and co-incubated for 2 hours with mouse macrophages, being both types internalized, deformed, and excreted by lysosomes. Caruso and coworkers [167] reported that the shape of the capsules influences the internalization rate: spherical capsules were more prone to undergo cellular uptake by human cervical cancer cells than cylindrical ones.

Parak and coworkers [183] demonstrated the internalization of degradable dextran sulfate/poly(L-arginine) and non-degradable PSS/PAH by embryonic fibroblasts for a period of 5 days. The intracellular degradability of each capsule type could be followed thanks to the encapsulation of a fluorescent compound, DQ-ovalbumin. Due to a characteristic self-quenching mechanism, this compound exhibits a red fluorescence characterized by the close proximity of the fluorescent dyes, but it shifts to a bright green upon proteolysis. After a culture time of up to 5 days, the biodegradable capsules exhibited a green fluorescence, while the PSS/PAH capsules were in their majority red (Figure 2.6). This results showed that, although both types of microcapsules could be delivered to cells, the availability of DQ-ovalbumin was higher when encapsulated within dextran sulfate/poly(L-arginine) microcapsules.

The results from Parak and coworkers suggest that it is not enough to ensure that a drug is delivered to cells: after delivery, the encapsulated agent needs to be available to the cellular machinery. Moreover, with this strategy the release of the drug is mediated by the degradation of the capsule inside the cell, making external control over this process not possible. In this regard, Palankar *et al.* [184] devised a strategy to release an encapsulated agent on demand upon cellular uptake using infrared light. A peptide ligand of the major histocompatibility complex (MHC) class I molecules was encapsulated within PDADMAC/PSS microcapsules (around 2 μm in diameter) doped with gold nanoparticles.

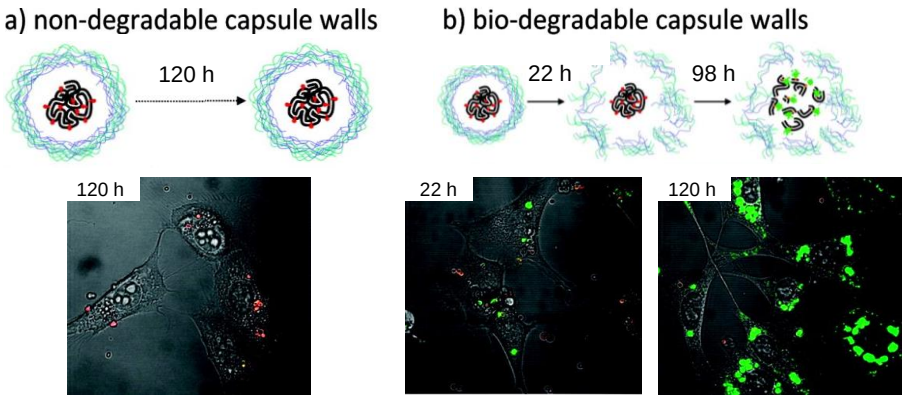


Figure 2.6. Enzymatic cleavage of DQ-ovalbumin upon internalization by embryonic NIH/3T3 fibroblasts. Fluorescent cargo was encapsulated either in (a) nondegradable PSS/PAH or (b) degradable dextran sulfate/poly(L-arginine) microcapsules. Images were taken immediately after the addition of the capsules to the culture over-time up to 120 h under confocal microscopy in different channels, green, red, and transmission, where green corresponds to cleaved DQ-ovalbumin and red corresponds to intact cargo. Adapted with permission from ref. [183] Copyright 2009, American Chemical Society.

Upon internalization by monkey kidney epithelial cells and chinese hamster ovary cells, an infrared laser was irradiated over cells individually. This caused the disruption of the microcapsules' walls due to heating release by the gold nanoparticles and consequently the release of the encapsulated peptide. Moreover, contrary to what occurs with UV light, infrared light did not result in any adverse consequence to the cells. With this strategy, bioactive agents may be encapsulated in nondegradable microcapsules that protect them until their release is desired and triggered on demand.

The stability and biodistribution of electrostatic self-assembled nanoparticles for systemic administration and off-body tracing was recently addressed by Poon *et al.* [185] by imaging techniques. They evidenced the importance of a larger number of layers and the role of the terminating layer in terms of functional retention. A formulation of PLL and dextran films capped with a final layer of HA assembled onto gold nanoparticles or quantum dots showed a blood elimination half-life of 9 hours and low liver accumulation could be observed in mice.

A lot of effort has been done in the context of drug delivery devices made with LbL. This approach has potential for the construction of nano- and micro-carriers that provide tunable release by varying not only the number of layers but also external parameters, such as temperature and pH. It is even possible to exploit mechanisms of delivery directly to the intracellular environment. Judging by the reviewed works, multilayer microcapsules can be inherently uptaken by cells without requiring specific

functionalization wit bioactive materials. However, the intracellular degradation kinetics should be taken into account since capsules made of nondegradable materials may limit the bioavailability of the encapsulated agents. Much research has been carried out using DOX as a model drug. These reports represent a step forward the usage of LbL systems in actual *in vivo* applications, such as in cancer treatments, and their low or even absent negative impact in a living organism. Given the extensive knowledge of such systems using chemotherapeutics to target cancerous cells, it is likely that cancer treatments will be the most studied application using this class of carriers in the short term.

2.5.4 Biosensors

Biosensors are analytical devices that incorporate biological sensing elements. Screening metabolites present in biological fluids and in the human body is of growing importance for medical analysis, rapid disease diagnosis and drug discovery [186-188]. This concept has been transcribed to the LbL technology, mainly in the form of capsules, where metabolite-sensitive fluorophores are immobilized inside a carrier, resulting in a measurable response upon contact with a specific biological agent. Parak and coworkers [189] developed microcapsules delimited by PSS/PAH multilayers and magnetite nanoparticles that encapsulated seminaphtho-rhodafluor-1-dye (SNARF-1)-dextran conjugate as mobile pH sensors. The purpose of using magnetite particles was to enable a magnetic separation of capsules during their construction. SNARF-1 exhibits a pH-responsive fluorophore that emits green fluorescence under acidic conditions and red under alkaline ones. Using this combination, they exploited the mechanism of cellular intracellular uptake by fibroblasts and breast cancer cells. First, due to the alkaline properties of the culture medium, the microcapsules exhibited red fluorescence. After 30 minutes of incubation, capsules internalized by lysosomal/endosomal compartments turned from red to green, due to the acidic pH found inside the intracellular environment. The cells retained their viability and capacity to divide and proliferate. Although two types of cells were used to study this biosensor, there seemed to be no difference in the fluorescence response observed upon cellular uptake. In the future, it could be interesting to have a biosensor of this class capable of measuring physiological parameters in distinct types of cells with clear distinct signals.

This simple formulation is one of the pioneer works of LbL microcapsules that act as biosensors, namely toward physical physiological parameters like pH. However, different approaches may allow identifying other parameters such as biochemical signals. Pan, Zhang and Li [190] presented films made of single-walled carbon nanotubes and CHI-dispersed tin disulfide nanoparticles assembled onto glassy carbon electrodes by electrostatic interactions. While bare electrodes did not provide a clear

distinct electrochemical signal for individual compounds – dopamine hydrochloride and uric acid, in the presence of ascorbic acid – the multilayer coating enabled the identification of clear separate electrochemical voltammetric signals. Thus, the assembly of the coating allowed identifying simultaneously two distinct compounds. This strategy could be useful for the fabrication of tailored electrodes in a rapid and simple way that allow detecting and quantifying multiple specific metabolites present in biological fluids.

Yu *et al.* [191] presented gold substrates coated with multiple dendritic stars of opposite charge finished with an ending layer containing negatively charged carboxyl groups. These groups could be functionalized with by carbodiimide and *N*- hydroxysuccinimide which allowed binding covalently fluorophore-amino-modified single stranded DNA via amidation. Using this strategy, it was possible to distinguish and quantify DNA hybridization behaviors between one mismatch and complementary target DNA molecules, showing that such devices could be interesting DNA biosensor platforms.

Another approach is the use of reservoirs made by LbL that encapsulate sensing molecules. One such example is the encapsulation of enzymes as sensing molecules. Enzymes are versatile biocatalysts which have a wide range of important catalytic and sensing applications [192]. Kazakova *et al.* [186] presented PSS/PAH microcapsules that acted as multilayer biosensors and as reservoirs of (i) glucose oxidase, (ii) lactate oxidase or (iii) both enzymes. PSS was labeled with tris(4,7-diphenyl-1,10-phenanthroline)ruthenium(II) dichloride complex (Ru(dpp)) – a well-known dye used in luminescence-based oxygen sensors – and dihydrorhodamine 123 (DHR123) – a non-fluorescent molecule that yields rhodamine123 which, in the presence of peroxidase, emits green fluorescence upon oxidation by hydrogen peroxide. Oxygen-, glucose- and lactate-dependent spectrofluorimetric assays dependent on concentration were conducted, showing reliable detection at the millimolar range in all cases.

The problem with enzymes is that they lack long-term stability and limited reusability for biosensing purposes [193,194]. We described before how Parak and coworkers [189] introduced magnetite to allow separation and harvesting during microcapsule production, but this concept could be used to retrieve and reuse enzyme-encapsulating devices until the enzymatic content is depleted. Garcia *et al.* [192] presented a thorough study in which they developed BSA-functionalized magnetic nanoparticles (MNPs) coated with biotin- and avidin-modified horseradish peroxidase (HRP) layers (Figure 2.7a and Figure 2.7b). The enzymatic activity of peroxidase adsorbed as a single layer was compared to that of peroxidase in solution, revealing that the enzymatic activity was similar in both cases. However, peroxidase activity increased linearly with the number of layers, exhibiting a four-fold total activity upon the assembly of 5 layers in respect to the solution control (Figure 2.7c).

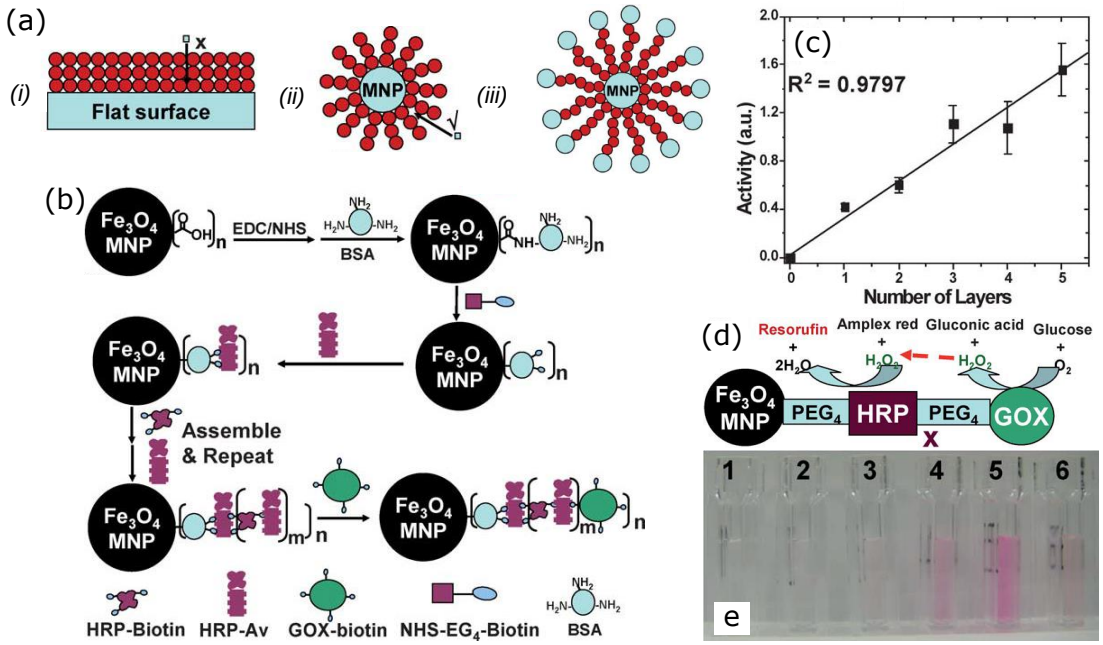


Figure 2.7. Fabrication and response of biosensors based on BSA-functionalized MNPs. (a) Biotin- and avidin-modified HRP layers are assembled on top of bidimensional or three-dimensional surfaces to produce (i) flat mono-enzyme, (ii) spherical mono-enzyme or (iii) spherical bi-enzyme sensors. The substrate accessibility to inner layer enzymes is more favorable when using the spherical templates. (b) Production of multilayer single- and bi-enzyme MNP systems using HRP and GOX. (c) Total HRP activity as a function of the number of HRP layers in HRP-MNP systems, showing a linear activity increase with increasing number of layers. (d) Schematic of the coupled bi-enzymatic reaction in the GOX-HRP-MNP system. (e) Photographs showing the colorimetric detection of glucose with the coupled GOX–$(HRP)_5$–MNP system after 3 h with increasing concentrations of glucose. The discoloration in vial 6 (highest concentration of glucose) is attributed to the protonation of resorufin – which is only absorbing in its deprotonated form – due to the decrease of pH from the formation of gluconic acid. Adapted with permission from ref. [192] Copyright 2011, The Royal Society of Chemistry.

These results suggest that LbL-immobilized enzymatic molecules do not block any active site in the enzyme, since the enzymatic activity increased with the number of layers, and is therefore adequate for biosensing activities. The authors studied this system further. They showed that these biosensors could be retrieved by magnetic-assisted harvesting and reused up to 10 consecutive cycles without loss of enzymatic activity. Then, this system was turned into a bi-enzymatic system by the incorporation of biotin-activated glucose oxidase (GOX) as the ending layer. Two enzymatic reactions could then be exploited for the detection of glucose. Shortly, the degradation of glucose by GOX results in gluconic

acid and hydrogen peroxide, which is a colorless reaction (Figure 2.7d). In the presence of peroxidase, Amplex red reacted with hydrogen peroxide producing resorufin, a pink-colored product observable in the visible spectrum. Increasing concentrations of glucose could be detected and measurable by the increasing absorbance of pink in the retrieved samples (Figure 2.7e). This work presents potential for applications concerning the detection of glucose, namely to diagnose and follow diabetes, which account for approximately 85% of the world market for biosensors [187].

The use of colorimetric biosensors is particularly interesting. A patient could use it for rapid screening purposes conveniently at home without any specific operation training. Colorimetric changes could provide a quick indication of whether a person suffers from a specific disease. In a recent highlight from McShane and Ritter [195] the potential of colorimetric biosensors was discussed. With the advent of portable devices, such as smartphones and tablet PCs, it would be possible to install multiple diagnostic software tools that permitted to identify and rate a response from a biosensor based on colorimetric scales. Smart tattoos – color changing particles intended for a minimally invasive dermal implantation – could react to the metabolites present in the interstitial fluids, resulting in measurable shifts of their optical properties. Then, an external device could read that response, give a diagnostic and even send it directly to a physician. Given the potential of LbL devices for biosensing and the present technological advances, it is likely that this concept will grow, accompanied by a miniaturization of biosensors, commodity and ease of use. LbL will contribute to this evolution since this technique allows achieving higher levels of functionalization, customization and measurement of multiple metabolites at once.

2.5.5 Implantable structural devices with tubular shape

LbL allows coating substrates with distinct geometries to obtain devices from thin coatings to membranes and three-dimensional objects. Those could have adequate anatomic shapes that could be used to replace or regenerate tissues or organs. Particular interesting examples of such devices are tubular structures, which constitute another three-dimensional shape that can be obtained by LbL besides spheres.

One typical approach to construct tubular structures is to coat the interior of cylindrical pores, which usually lead to the fabrication of tubes with low caliber, in the order of nanometers. Liang *et al.* [196] were able to conceive hybrid polyelectrolyte/nanoparticle tubes templated on the pores of

polycarbonate membranes, each pore with around 400 nm in diameter and maximum pore length of 10 μm. The membrane was first functionalized with a PEI solution that acted as the primer layer and as support for the assembly of PAA and PAH layers. The membrane was then dissolved with dichloromethane, leaving intact only the coatings of the inner pores with tubular shape. To give mechanical stability to these structures, the tubes were crosslinking with high temperatures (160°C) or in alternative they could be assembled with gold or cadmium telluride nanoparticles intercalated between bilayers. Their inclusion could play an essential role in providing mechanical reinforcement, affecting the properties of small blood vessels substitutes and the structure of cells. In both cases, hollow tubes could be formed with an outer diameter similar to the size of the pore and wall thickness ranging from about 50 to 80 nm. Yang *et al.* [197] studied the *in vitro* biological properties of CHI/ALG tubes with around 400 nm of diameter and estimated wall thickness of 80 nm (thickness for 16 bilayers), fabricated using polycarbonate porous membranes. Their biodegradability in pancreatin carried out overnight resulted in a diameter reduction to 160 nm, attributed to the CHI degradation due to lipase present in pancreatic fluids. Cellular assays using human cervical cancer cells or breast cancer cells demonstrated their low cytotoxicity. They also carried out cellular uptake experiments with each cell type, showing that after 24 h the tubes could be found inside the cells. Due to the small size of these nanotubes, such tubular structures could be useful as drug carriers for the intracellular delivery of active agents.

Another approach for construction tubular structures is by coating sacrificial templates with cylindrical shape to assemble multilayer coatings. Since this approach relies on the use of physical shapes, it is possible to develop tubes with larger calibers that could be useful as blood vessel substitutes. Mueller, Daehne and Fery [198] used tubular templates for the fabrication of hollow LbL tubes instead of porous membranes. Glass fibers ranging from 5 to 10 μm were coated with PDADMAC and PSS, after which the fibers were dissolved by hydrogen fluoride. However, the authors warned for the possibility of pearling instability, that is, the deterioration of a liquid cylinder into a series of droplets, also known as the Rayleigh instability. This effect results from the tension of the wall surface provoked by a high ionic strength at the time of template dissolution. To solve this issue, they added an additional layer of PAH, which is known to withstand high concentrations of salt. Indeed, the addition of this material eliminated pearling instability, resulting in the formation of stable hollow tubes. The tubes were dried and shown to be resistant, with a Young's modulus of around 200 MPa. Curiously, He *et al.* [199] took advantage of the pearling instability to construct tubes that transform into capsules. They used the polycarbonate porous membrane template to assemble PSS/PAH multilayer tubes. Then, by increasing temperature

up to 138°C, tube segments separated, closed and formed capsules. This interesting tubular-derived capsular formation strategy can be useful for other applications, such as delivery of drugs or genes and for the preparations of reactors or biochemical sensors [200].

In the work of Silva *et al.* [201] CHI/ALG hollow tubes were developed using glass tubes (around 1 mm) as templates. Glass was first coated with a thin sacrificial layer of paraffin, which served as the substrate to adsorb 100 bilayers. Upon assembly, the paraffin was dissolved by dichloromethane, resulting in hollow cylindrical structures with a caliber comparable to the template (Figure 2.8a). Afterwards, some tubes were crosslinked by genipin (Figure 2.8b) which provided structures with storage and Young's moduli about twice the uncrosslinked tubes when immersed in PBS (Figure 2.8c), an important property for implantable devices. *In vitro* biological studies up to 7 days using a fibroblast-like cell line demonstrated that the cells adhered preferentially to crosslinked films, showing a more elongated and spread morphology (Figure 2.8d) in comparison to native films.

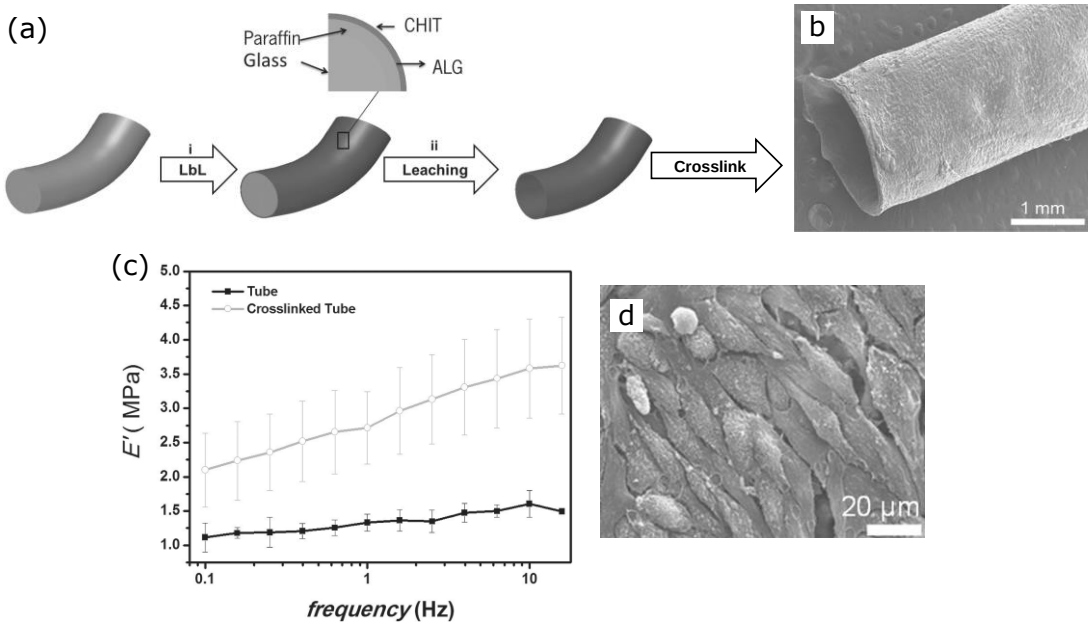


Figure 2.8. Hollow CHI/ALG multilayer tubes. (a) PEMs are assembled on paraffin-coated tubes, the latter being leachable using an organic solvent. (b) SEM image of a crosslinked tube. (c) Variations of storage modulus (E') with or without crosslinking obtained by dynamic mechanical analysis in wet conditions and 37°C. (d) L929 fibroblast-like cells seeded on crosslinked tubes at day 7 of culture. Adapted with permission from ref. [201] Copyright 2013, Wiley-VCH.

The synthesis of hollow tubular structures has the potential to mimic the structure of blood vessels. The tuned permeability of the multilayered walls potentiates the control of gas and nutrient exchanges from and into circulating fluids. They could help in cases of coronary artery and peripheral vascular diseases, which are still a cause of high mortality in western societies. Usually, autologous vessel grafts are the standard treatment when small diameter vessels are involved. However, to many patients this option is limited due to the lack of suitable vessels or because of a previous harvest [202,203]. Moreover, their large surface area makes them appealing for other applications such as catalysis, sensing or tissue growth supports [204-206].

Tubular LbL structures still remain a largely unexplored area. A possible reason for this is the difficulty associated with their fabrication: collapsing of the internal wall and pearling instability, which are phenomena not encountered for simpler structures, such as the 2D films and 3D spheres and scaffolds. Most of these studies also focus on the morphological, mechanical and *in vitro* biological characterization, but, to our knowledge, attempts of cellular colonization of multilayer tubes' interior has yet to be attempted. Indeed, LbL tubular structures may be envisaged as blood vessels, but one must be aware that blood vessels – artery, vein, capillary – have different calibers, with capillaries being suggested to have a mean diameter of 5 μm [207].

The possibility of LbL to control the constituents with each adsorbing layer may be used to mimic the structure of blood vessels, which is organized in three layers: intima, media and adventitia. In each layer, distinct percentages of collagen and elastin are found to supply the arterial wall matrix with strength and elasticity [203,208]. Furthermore, besides the conventional approaches of sacrificial templates coated with PEMs described herein, tubular multilayer structures may be produced with new strategies that disregard the dissolution of templates and may even incorporate natural constituents of blood vessels. In respect to the latter, as we will be discussed in Section 2.6.2, Akashi and coworkers have been exploring hybrid multilayers containing cells and ECM components to fabricate tissue analogues *in vitro*, including analogues of blood vessels.

2.5.6 Compartmentalized environments

With the successful extrapolation of LbL to 3D, multilayer films have started to be perceived not as coatings but as boundaries that delimit and confine an internal environment. One can find such analogy in Nature in the elegant example of cells. Cells are unique for their hierarchical and compartmentalized organization. Delimited by the phospholipidic membrane, the cytoplasm provides a balanced intracellular environment where the organelles are maintained and execute various specialized functions

such as the transport of numerous compounds, synthesis of proteins and regulation of enzymatic reactions. Thus, besides compartmentalization, cells also exhibit multifunctionality thanks to the specialized structures confined within [209-211].

Although cells may seem a complex inspiration to follow, some strategies have already been proposed to mimic their structure using multi-shelled organic and inorganic capsules prepared by template-assisted strategies [212-214]. However, as they are often accompanied by harsh processing conditions, compartmentalized assemblies of polymeric multilayer nano/microcapsules within larger partitions have been achieved by using non-aggressive bottom-up strategies [215], among them LbL [216,217]. In a simplistic structural organization, cells can be transcribed to a compartmental model, where a large compartment confines a liquefied environment in which subcompartments are suspended. Each compartment exhibits a distinct function and is delimited by its own membrane. In any case, multilayered or not, compartmentalization has allowed combining properties and confining reactions that could not be achieved simply with single-component assemblies [218].

2.5.6.1 Confined enzymatic reactions

The concept of multilayered multicompartments was first demonstrated by Sukhorukov and coworkers [219] who developed concentric shell-in-shell nanostructured microcapsules. They used calcium carbonate microparticles produced by co-precipitation of calcium chloride and sodium carbonate, during which fluorescent-tagged human serum albumin (HSA) and magnetite nanoparticles were entrapped. As observed in Figure 2.9a, the microparticles were coated with PSS/PAH multilayers and, instead of dissolving this sacrificial template afterwards, they submitted the coated particles to a second coprecipitation stage. At this stage, HSA tagged with another fluorophore was also present. This way, a second calcium carbonate inorganic layer was assembled around the first one while entrapping HSA separated from the underlying core by the PSS/PAH multilayers. In this formulation, the magnetite was used for magnetic separation and harvesting of ball-in-ball structures. After chelation of both inorganic sections, fluorescence microscopy confirmed the presence of a shell-in-shell structure, each of them containing HSA tagged with the distinct fluorophores (Figure 2.9b). Following the same procedure, the authors used this concept to encapsulate also GOX in the outer compartment and peroxidase in the inner compartment. Upon the addition of glucose to the surrounding medium, the enzymatic reaction could be detected by the Amplex Red fluorescence in the inner compartment due to the formation of resorufin (Figure 2.9c). This is a similar situation to that reported previously by Garcia *et al.* [192] in single-compartment capsules, where an identical enzymatic reaction was identified by the visible optical

properties of Amplex Red, but with the added advantage of confining the whole enzymatic reaction in a confined and controlled environment.

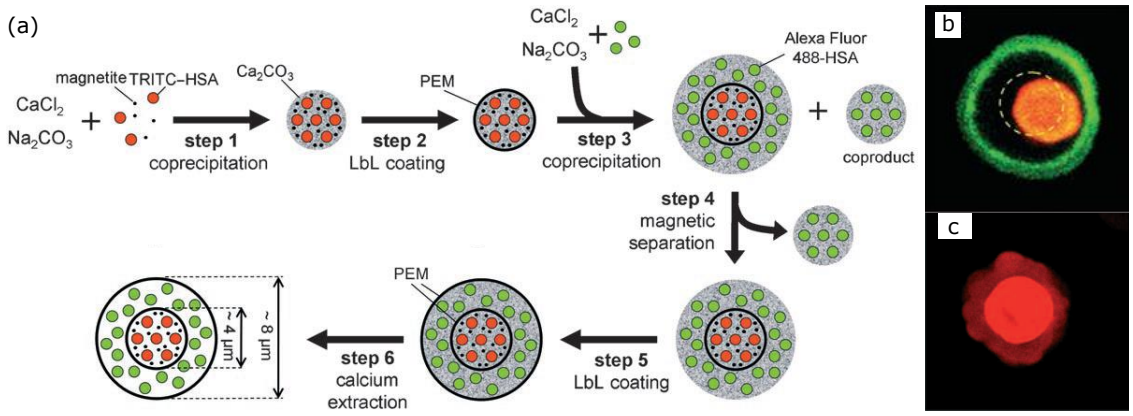


Figure 2.9. (a) General route for the synthesis of shell-in-shell microcapsules. (b) Confocal laser scanning microscopy of the shell-in-shell structure and HAS distribution 5 seconds after core dissolution. The dashed circle indicates the original position of the inner capsule. (c) Formation and diffusion of resorufin in a coupled enzymatic test using GOX and peroxidase. Reprinted with permission from ref. [219] Copyright 2007, Wiley-VCH.

Other complex structures can be obtained through similar approaches. Instead of concentric compartments, Tong *et al.* [220] produced PAH/PSS coatings around calcium carbonate microparticles pre-doped with polystyrene-block-poly(acrylic acid) (PS-b-PAA) micelles. After chelation with EDTA, it was possible to observe the free micelles (around 30 nm) suspended inside the PEM microcapsules (around 3 μm). In contrast to Sukhorukov and coworkers [219], in this work not just one "ball" was encapsulated inside a larger one. Instead, several smaller containers were suspended within the larger multilayer compartment. They also demonstrated the loading capability of water soluble and water insoluble drugs. Namely, the hydrophobic triclosan was encapsulated in the micelles' cores and the water soluble DOX in the microcapsule's interior by association with the negatively charged PAA corona of the micelles. This strategy has clear potential for the simultaneous delivery of hydrophobic and hydrophilic drugs.

Hosta-Rigau *et al.* [221] constructed LbL-based capsosomes – polymer capsules containing liposomal subcompartments – as carriers of therapeutic molecules. Silica microparticles (around 3 μm) were coated with a precursor PLL layer followed by the adsorption of liposomes containing thiocoraline (TC), a hydrophobic antitumoral drug. Two liposome layers were assembled, each separated by a PEM of PLL

and poly-(methacrylic acid)-co-(cholesteryl methacrylate) (PMA_C) and this structure was then protected by adding additional polymer layers to hold the liposomes in place. In comparison to the other described works, this approach was developed to show compartmentalization organization at an interfacial level, rather than in the interior of the microcapsules. Incubation with colon cancer cells showed an increased anti-carcinogenic activity of capsosomes containing TC-loaded liposomes, when compared to capsosomes without TC. In the presence of the former, cells exhibited a reduction of viability as high as 43%.

2.5.6.2 Customizable environments with multifunctional components

Compartmental devices are useful in fields such as catalysis, sensors, multiple drug delivery, disease models, energy storage and microreactors, which often require complex phenomena to occur simultaneously [34,222,223]. In particular, this technology permits adding materials that respond to external stimuli either in the composition of the coatings or in the interior of three dimensional structures. This opportunity opens chances for customization of compartmentalized devices rather than being limited to the confinement of enzymatic reactions and drug encapsulation. Costa *et al.* [224] used a hybrid ionic gelation strategy assisted by LbL to fabricate temperature and magnetic responsive compartmentalized capsules with hierarchical organization from the nano- to the macro scales. First, CHI/ELR multilayers coated calcium carbonate microparticles (3 μm) entrapping superparamagnetic nanoparticles (MNPs, 10 nm). Afterwards, they were encapsulated within ALG beads (2 mm) by ionic gelation, which were further coated with CHI/ALG films. EDTA was then used to chelate the calcium carbonate that served as template for the microcapsules and liquefy the jellified ALG. The result was a multilayer-confined liquefied alginate environment encapsulating smaller microscopic compartments with both temperature and magnetic responsive materials. Each of the capsular compartments was loaded with rhodamine. Release studies at 25 and 37°C showed that the rhodamine release was more sustained at physiological temperature (71%, in comparison to 84% at room temperature), being this behavior in accordance with the previous work of the same group with BSA-loaded microcapsules [179]. MNPs, which were confined within the microcompartments, were shown to attribute magnetic responsiveness towards external magnetic fields to the whole compartmentalized device, allowing their spatial mobilization and immobilization. One could think that a millimetric device delimited with a nanometric coating would be unable to withstand the stress of carrying a cargo. The authors, however, also showed that the millicapsules were capable of withstand centrifugal stress and handling without rupturing the LbL external membrane. This is a useful and convenient property, which makes it easy to

transport and transfer these devices between different containers if necessary (e.g., well-plates, Petri dishes). This class of customizable hierarchical systems can be envisaged to control the release of several biomolecules simultaneously, their spatial immobilization in targeted therapies and the control over a multitude of cellular in controllable reactors. The authors studied the two stimuli in separate and did not explore the mixed influence of temperature and magnetic response in the release of encapsulated molecules. Nonetheless, it may be possible to explore their combined effect for amplified hyperthermia treatments such as those found in cancer treatments [225] and studying its effectiveness in killing cancer cells inside such a millimetric model reactor for drug discovery and screening.

Compartmentalized systems inspired on cells are still in an early infancy but their future potential as drug delivery and enzymatic reactors has already been proved. The potential of such devices may allow for this technology to advance in terms of functionality and customization by coupling functionality that is not found together in Nature. In Section 2.6.3, we will show that mammalian cells may be encapsulated and form microtissues inside such liquefied capsules that could be explored in tissue engineering applications.

2.6 Engineering tissues *in vitro*

Presently, when a patient's organ fails the only treatment available is transplantation. However, organ availability for transplantation is limited and in many cases the waiting leads to the patient's death. As a response, tissue engineering has appeared as a multidisciplinary field that applies principles of biology, chemistry, physics and engineering, culminating in life and health sciences [226]. The ultimate objective of this field is not only to help biological structures to regenerate for themselves but also to produce tissues and organs in lab that could serve as functional substitutes for damaged tissues and organs. For that purpose, it is typical for tissue engineering strategies to combine cells, scaffolds that provide a three-dimensional environment and biochemical signals, such as growth factors.

2.6.1 Three-dimensional porous structures

LbL can be used to coat substrates with complex and convoluted geometries other than simple planar surfaces. Three-dimensional substrates may be coated and eventually provide a porous structure to be populated by cells for the development of alternative cell growth platforms for tissue engineering applications. This feature is particularly important when considering the development of environments resembling the spatial arrangement of cells in native tissues and organs as much as possible.

It is possible to construct convoluted three-dimensional structures made exclusively with LbL constituents with porosity for cell seeding. For example, Sher, Custódio and Mano [227] developed porous scaffolds using leachable PEI-functionalized paraffin wax particles as template. Aggregates of paraffin wax particles were packed together and coated with CHI/ALG films using a perfusion-assisted LbL strategy. Afterwards, the particles were dissolved by dichloromethane, leaving only the PEM structure with porosity and interconnectivity. They served as substrates to seed human osteoblast-like cells, which adhered and proliferated within 7 days. Following an identical approach to produce scaffolds, Silva *et al.* [228] developed 3D structures of CHI and chondroitin sulfate multilayers for bovine chondrocytes and multipotent bone marrow derived stromal cells. Both types of cells were able to proliferate significantly and retain their viability for as long as 35 days. Histology on scaffolds seeded with bovine chondrocytes showed that the number of cells per section increased with the time of culture and started to show a more homogeneous dispersion after 14 days of culture. Lacunae formation was also observed in the matrix surrounding these cells, indicating the maintenance of the chondrogenic phenotype. Similar results were obtained for scaffolds seeded with the stromal cells, accompanied by the deposition of glucosaminoglycans (GAGs), an indicator of chondrogenic differentiation.

Instead of a 3D template, it is possible to modify pre-existing structures with LbL to improve the biological performance upon contact with the cells. Ye *et al.* [229] used a decellularized porcine aortic valve that acted as support for heparin and CHI multilayers (Figure 2.10a). In comparison to uncoated matrices, they exhibited lower platelet adhesion and activation, lower adhesion of leukocytes and significantly higher whole-blood clotting time (Figure 2.10b and Figure 2.10c). Human blood derived endothelial progenitor cells were seeded into the coated matrix for 5 days and showed almost full coverage of the available surface with a well-spread morphology and maintenance of the endothelial phenotype (Figure 2.10d). Therefore, a matrix with anti-thrombotic properties and good repopulation capability by endothelial cells was obtained and it constitutes a viable alternative to current valve transplantation alternatives.

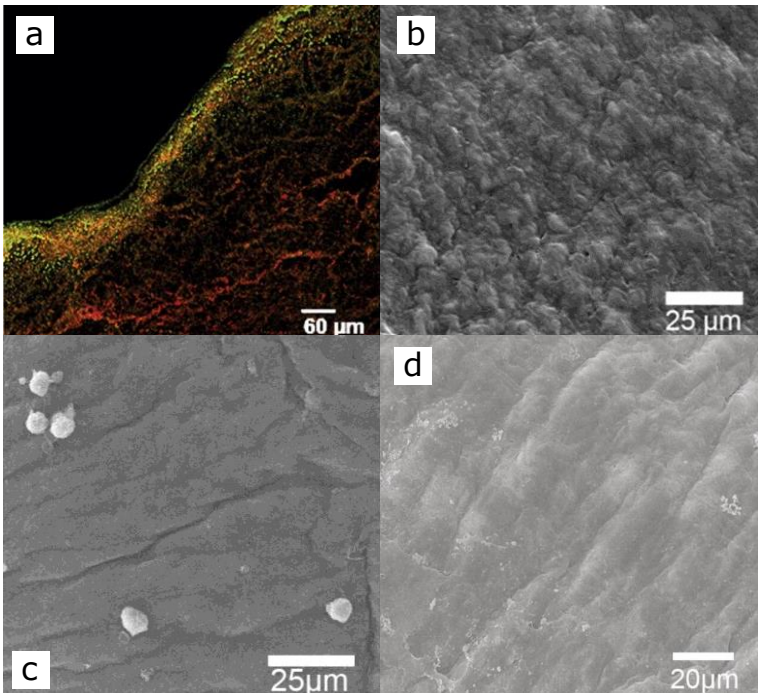


Figure 2.10. Biological performance of heparin/CHI multilayer-coated decellularized porcine aortic valves. (a) Fluorescence of the multilayers adsorded onto the valves. The polymers' fluorescence (red for heparin and green corresponds for CHI) is uniform and non-overlapping. Platelets (b) and leukocytes (c) adhered poorly to the multilayer-coated decellularized valves. (d) The developed devices were repopulated with endothelial progenitor cells exhibiting a contiguous, flat morphology. Reprinted with permission from ref. [229] Copyright 2012, Elsevier.

The internal structure of a porous scaffold can also be modified using LbL to create new hierarchical microstructures. Oliveira *et al.* [230] presented a strategy in which the formation of fibrillar structures is was induced across the pores' walls of diamine-modified poly(ε-caprolactone) scaffolds. Using a custom-made dipping robot, the pores were coated with ALG/CHI multilayers from solutions with different concentrations (0.5–5 $mg{\cdot}mL^{-1}$) and rinsing times (5–40 minutes). After the assembly, the scaffolds were frozen at -80°C, which led to the formation of ice crystals that caused localized compression, shear and stretching on the assembled layers. Consequently, the coating would experience displacement from the walls toward the center of the pores, resulting in fibrillar structures of ALG/CHI multilayers. High rinsing times inhibited the formation of such structures: a lengthy washing step did not allow excess polyelectrolyte solution to remain inside the pores which would lead to the formation of complexes and fibrillar structures. Moreover, the use of the most concentrated solutions led to an increase in the formation fibrillar structures and more uniformly spread than with more diluted

solutions. With these structures, it could be possible to increase the surface available area for cell growth. In fact, using osteoblast-like cells, they demonstrated that cells adhered and proliferated preferentially in scaffolds containing fibrils that resulted from shorter rinsing times and concentrated polyelectrolyte solutions.

2.6.2 Cells as components in the LbL construction

Akashi and coworkers have followed an elegant LbL-based approach to develop hybrid polymeric and cellular constructs capable of providing a three-dimensional environment and simulate the hierarchical organization of tissues. In an early report [231], they started by seeding a monolayer of fibroblasts on a fibronectin-functionalized cover glass, followed by the adsorption of seven fibronectin and GEL bilayers. Fibronectin is a well-known ECM glycoprotein related to the adhesion, migration and differentiation of cells. They are also known to interact with materials of the collagen class, like GEL, which was exploited to drive the LbL assembly between these two materials. The preparation of this multilayer was expected to provide an interface similar to the natural ECM to seed a second layer of cells. Following this pattern, they were able to construct 4 cell layers intercalated by fibronectin/GEL bilayers with controlled thickness (around 6 nm). More recently, using a similar multilayer construct, they intercalated human primary dermal fibroblasts and umbilical vascular endothelial cells to evaluate their stability and function, including after a heat shock of 45°C [232]. They observed that the layered structure provided a protective and biologically suitable environment for the cells in comparison to the ones seeded in culture dishes. Using a similar approach, Kim and Rajagopalan [233] focused on hepatic-related applications by seeding a rat hepatocyte monolayer over a collagen gel-coated substrate, followed by a coating of CHI/HA multilayers. Afterwards, a layer of rat liver sinusoidal endothelial cells (rLSECs) was added. The CHI/HA served as an analogue of the Space of Disse, a separator between the endothelium and the epithelium which helps in the diffusion of nutrients to the hepatocytes. Its role helps maintaining the hepatic functions of the liver cells and their differentiation state. It was expected that such construct would provide hepatocytes with a hepatic three-dimensional adequate environment that would prevent their dedifferentiation. Thus, in comparison to a cultured monolayer of rLSECs, rLSEC-PEM-hepatocyte cultures maintained their differentiated state over 12 days, whereas in the former case, rLSECs lost their phenotype within 3 days.

The use of ECM components and cells opens the way for LbL to be used in the fabrication of tissues *in vitro* by allowing cells to be stratified in a 3D environment. Akashi and coworkers have been very active in the development of devices that could help achieve such a three-dimensional cell organization for

transplantable constructs or angiogenesis models. Recently [234], they presented layered polyelectrolyte/cell structures as blood vessel analogues. To achieve this purpose, hydrogels of γ-PGA containing spatially arranged silica tubes (up to 620 μm in diameter) were used. The tubes were removed afterwards, thereby resulting in a gel containing uniaxial pores with inner diameter of around 700 μm. Fibronectin/GEL films were then assembled by perfusion, followed by a suspension of human umbilical artery smooth muscle cells, another polymeric film, and finally human umbilical vein endothelial cells. With these two types of cells, the typical composition of blood capillaries and the intima and media layers – containing endothelial and smooth muscle cells, respectively – could be mimicked. The permeability of this capillary analog was assessed by following the perfusion of BSA from the capillary lumen to the hydrogel template. The coating of the microchannels was able to act as a barrier to the diffusion of this high molecular weight protein (around 66 kDa) with a diffusion rate constant about 7 times inferior to uncoated microchannels. In contrast with the conventional approach of tubular constructs involving sacrificial templates, this work did not take such an approach. Instead, they demonstrated that LbL can be used to construct blood vessel analogues within three-dimensional porous hydrogel networks. This way, it may be possible to develop a three-dimensional device with enhanced perfusion of nutrients, oxygen and also delivery of bioactive molecules to cells confined within the gel.

Another strategy to construct 3D multilayer structures consists in the rapid cell-accumulation technique. This approach consists in the assembly of ECM components directly at the surface of cells and the consequent cell self-organization into layers. For this purpose, Akashi and coworkers [235] assembled fibronectin and GEL layers (with an estimated total thickness of 6 nm) onto the membrane of various types of cells (Figure 2.11a). Coated mouse fibroblast cells were able to organize themselves into 8 dense and homogeneous layers (around 35 μm), in comparison to a tattered and porous structure obtained using noncoated cells. The authors justified that since fibronectin/GEL films assembled on individual cell surfaces provide an interactive property with the α5β1 integrin receptor of the cell membrane, the cell-cell adhesion of all seeded cells in three-dimensions can be induced at the same time. Their study proceeded with an attempt to produce 3D cell structures with in which endothelial tube networks could be formed. The cell accumulation technique allows “sandwich” structures containing different cell types to be made. A cellular construct consisting of 8 layers of human dermal fibroblast cells divided by 1 intermediate layer of human umbilical vein endothelial cells (HUVECs) was constructed in a controlled manner by adjusting the number of cells that were incubated simultaneously (Figure 2.11b). After 7 days of incubation, a highly-developed capillary networks and a tubular

morphology of the HUVECs were observed, occupying an area of around 63% of the construct (Figure 2.11c).

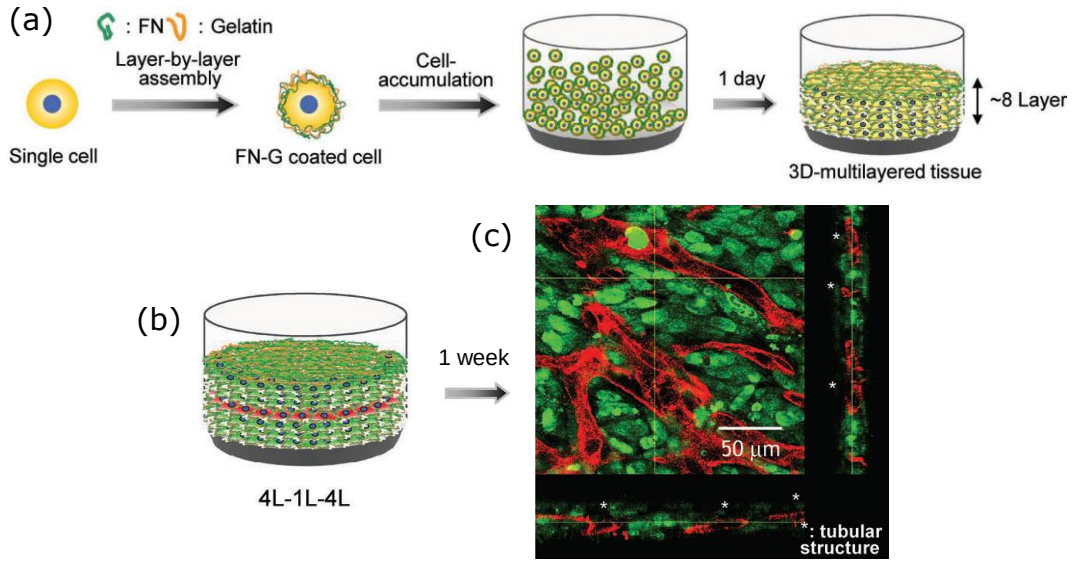


Figure 2.11. Cell-accumulation technique allows assembling three-dimensional cellular constructs. (a) Illustration of the rapid construction of 3D multilayered tissues by cell-accumulation using fibronectin/GEL-coated cells. (b) Schematics of a cellular construct consisting on 4+4 layers of human dermal fibroblast cells, intercalated with a layer of HUVECs. (c) Confocal laser scanning microscopy cross-section image of the construct presented in "b", showing tubular endothelial structures after 1 week of incubation. Green cells correspond to human dermal fibroblast cells and red cells to HUVECs. Adapted with permission from ref. [235], Copyright 2011, Wiley-VCH.

The presented examples show that LbL has made a step toward the engineering of tissues *in vitro* by mimicking the ECM composition and 3D organization of tissues, effectively creating tissue analogues such as blood vessels and liver. This technology may be adapted to produce analogues for other kinds of tissues with interest in tissue engineering, such as the pancreas and heart.

2.6.3 Production of microtissues in confined environments

In tissue engineering, the use of alginate as templates for the fabrication of millimetric capsules permits the incorporation of cells for the formation of microtissues, drug discovery, and to conduct fundamental studies using complex cellular microenvironments. Mano and coworkers used liquefied ALG environments delimited by coatings made of CHI, ALG and PLL for cell encapsulation

purposes.[236,237] The encapsulation of fibroblasts was achieved by suspending them in the ALG solution prior to ionic gelation (Figure 2.12).

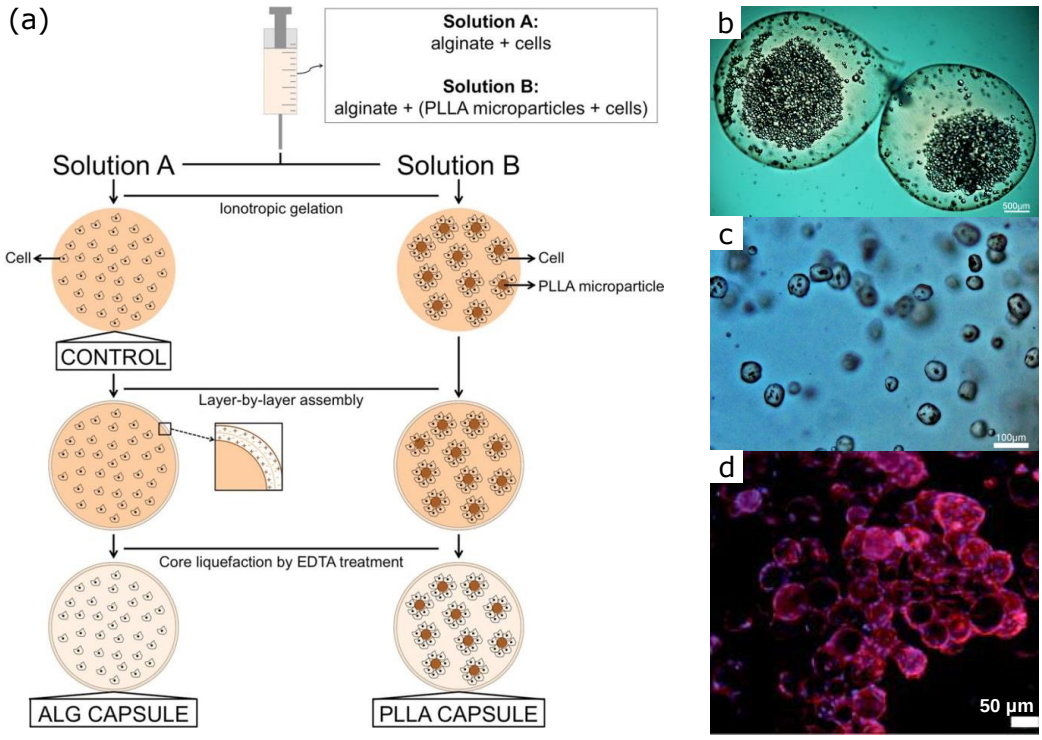


Figure 2.12. Production and characterization of multilayer-coated liquefied ALG capsules. (a) Cells are mixed with solutions of either ALG solely ALG-containing PLLA microparticles. Both solutions are extruded separately, originating ALG beads by ionotropic gelation. Upon coating with multilayers of diverse polyelectrolytes (CHI, ALG and PLL), the crosslinked ALG core is liquefied by EDTA, originating liquefied capsules encapsulating cells (ALG capsules), or encapsulating cells and PLLA microparticles (PLLA capsules). Optical microscopy of (b) liquefied capsules encapsulating (c) PLLA microparticles. Adapted with permission from ref. [236] Copyright 2013, American Chemical Society. (d) Fluorescence assay of PLLA capsules at day 7 of culture, showing cells adhered to the surface of the PLLA microparticles. Cell nuclei were stained blue and actin filaments red. Reproduced with permission from ref. [237] Copyright 2013, The Royal Society of Chemistry.

The subsequent ionic gelation of alginate in calcium chloride solution was not harmful for the cells, making it an appropriate technique for cell encapsulation. However, it is known that often cells require anchorage points that allow them to attach, spread and proliferate, otherwise risking cellular death [238]. To increase available surface area inside the capsules, plasma-functionalized poly(L-lactic

acid) (PLLA) microparticles were co-encapsulated in the ALG medium along with fibroblasts, which ensured that cells survived up to 28 days. In principle, such devices could be adapted to include more complex features such as microparticles, they could be able to deliver bioactive agents inside the capsules or the combination of multiple cellular populations.

2.7 Conclusions

The multitude of multilayer devices developed so far show how LbL-based strategies have surpassed the simple purpose of modifying surfaces. It is clear that LbL permits achieving high degrees of functionalization and complexity, both in bioactivity and geometry, for various biomedical applications. We summarized the factors that influence the construction of PEMs, with pH and ionic strength being the factors most often manipulated to improve the assembly output. Also, we described the efforts made to minimize the lengthy construction times that are necessary to obtain not only thicker films but films in sheer quantity, an important feature when envisaging future mass production of multilayered biomedical devices.

Emphasis was given to discussing an exhaustive list of potential biomedical applications that may benefit from LbL-based approaches. Implantable devices, such as coated prosthesis cells, may have facilitated biointegration in a living organism. Surfaces may be modified to exhibit "special" properties that result in improved mechanical properties, or with stimuli-responsiveness that may help tuning the adhesion of cells or tissues to PEMs. Moreover, being LbL a versatile technique, convoluted three-dimensional PEM arrangements can be obtained throughout all dimensional scales: 0D (nanoparticles and fibers), 1D (nanotubes), 2D (thin coatings and membranes) and 3D (tubes, capsules, scaffolds). Free-standing membranes may act as wound healing dressings, porous scaffolds as novel cell expansion supports for tissue engineering, and tubular structures as analogues for blood vessels. Also, the use of cells as multilayer constituents may allow building hybrid constructs that resemble tissues both in function and structure. From all 3D devices explored, spherical capsules have been by far the most studied. They offer possibilities of drug delivery and biosensing either by diffusion or by targeting cells, while degradation and cargo release/reactivity can be finely controlled by a variety of mechanisms. Finally, structures mimicking natural structures, such as that of biological cells, can be constructed in the form of compartmentalized structures exhibiting organization at distinct size scales. Although generally limited to confining enzymatic reactions, they may be customized and act as multifunctional microreactors to simulate specific events, such as disease models and microtissue production. It is expected that LbL will continue to contribute to technological advancements in the biomedical field.

Both in conventional medicine and in tissue engineering and regenerative medicine, the possibilities opened by LbL will allow developing devices with superior performance when compared to the technology currently in use.

2.8 References

References

[1] Boudou T., Crouzier T., Ren K., Blin G., and Picart C., Multiple Functionalities of Polyelectrolyte Multilayer Films: New Biomedical Applications, Advanced Materials 2010, 22: 441-467.

[2] Elbert D. L., and Hubbell J. A., Surface Treatments of Polymers for Biocompatibility, Annual Review of Materials Science 1996, 26: 365-294.

[3] Liu X., Chu P. K., and Ding C., Surface nano-functionalization of biomaterials, Materials Science and Engineering: R: Reports 2010, 70: 275-302.

[4] Ma Z., Mao Z., and Gao C., Surface modification and property analysis of biomedical polymers used for tissue engineering, Colloids and Surfaces B: Biointerfaces 2007, 60: 137-157.

[5] Prakash S., Karacor M. B., and Banerjee S., Surface modification in microsystems and nanosystems, Surface Science Reports 2009, 64: 233-254.

[6] Chu P. K., Chen J. Y., Wang L. P., and Huang N., Plasma-surface modification of biomaterials, Materials Science and Engineering: R: Reports 2002, 36: 143-206.

[7] Kato K., Uchida E., Kang E.-T., Uyama Y., and Ikada Y., Polymer surface with graft chains, Progress in Polymer Science 2003, 28: 209-259.

[8] Lu Y., and Chen S. C., Micro and nano-fabrication of biodegradable polymers for drug delivery, Advanced Drug Delivery Reviews 2004, 56: 1621-1633.

[9] Zasadzinski J., Viswanathan R., Madsen L., Garnaes J., and Schwartz D., Langmuir-Blodgett films, Science 1994, 263: 1726-1733.

[10] Chu P. K., Surface engineering and modification of biomaterials, Thin Solid Films 2013, 528: 93-105.

[11] Meyers M. A., Chen P.-Y., Lin A. Y.-M., and Seki Y., Biological materials: Structure and mechanical properties, Progress in Materials Science 2008, 53: 1-206.

[12] Tirrell M., Kokkoli E., and Biesalski M., The role of surface science in bioengineered materials, Surface Science 2002, 500: 61-83.

[13] De Koker S., De Cock L. J., Rivera-Gil P., Parak W. J., Auzély Velty R., Vervaet C., Remon J. P., Grooten J., and De Geest B. G., Polymeric multilayer capsules delivering biotherapeutics, Advanced Drug Delivery Reviews 2011, 63: 748-761.

[14] Gribova V., Auzely-Velty R., and Picart C., Polyelectrolyte Multilayer Assemblies on Materials Surfaces: From Cell Adhesion to Tissue Engineering, Chemistry of Materials 2012, 24: 854-869.

[15] Shi J., Alves N. M., and Mano J. F., Thermally Responsive Biomineralization on Biodegradable Substrates, Advanced Functional Materials 2007, 17: 3312-3318.

[16] Alves N. M., Pashkuleva I., Reis R. L., and Mano J. F., Controlling Cell Behavior Through the Design of Polymer Surfaces, Small 2010, 6: 2208-2220.

[17] Desai T. A., Micro- and nanoscale structures for tissue engineering constructs, Medical Engineering and Physics 2000, 22: 595-606.

[18] Mano J. F., Biomimetic Approaches for Biomaterials Development, Weinheim, Germany: Wiley-VCH; 2012.

[19] Finnemore A., Cunha P., Shean T., Vignolini S., Guldin S., Oyen M., and Steiner U., Biomimetic layer-by-layer assembly of artificial nacre, Nature Communications 2012, 3: 966.

[20] Luz G. M., and Mano J. F., Biomimetic design of materials and biomaterials inspired by the structure of nacre, Philosophical Transactions of the Royal Society A: Mathematical, Physical and Engineering Sciences 2009, 367: 1587-1605.

[21] Mayer G., Rigid Biological Systems as Models for Synthetic Composites, Science 2005, 310: 1144-1147.

[22] Iler R. K., Multilayers of colloidal particles, Journal of Colloid and Interface Science 1966, 21: 569-594.

[23] Decher G., and Hong J.-D., Buildup of ultrathin multilayer films by a self-assembly process, 1 consecutive adsorption of anionic and cationic bipolar amphiphiles on charged surfaces, Makromolekulare Chemie Macromolecular Symposia 1991, 46: 321-327.

[24] Decher G., and Hong J. D., Buildup of Ultrathin Multilayer Films by a Self-Assembly Process: II. Consecutive Adsorption of Anionic and Cationic Bipolar Amphiphiles and Polyelectrolytes on Charged Surfaces, Berichte der Bunsengesellschaft für physikalische Chemie 1991, 95: 1430-1434.

[25] Decher G., Hong J. D., and Schmitt J., Buildup of ultrathin multilayer films by a self-assembly process: III. Consecutively alternating adsorption of anionic and cationic polyelectrolytes on charged surfaces, Thin Solid Films 1992, 210–211, Part 2: 831-835.

[26] Bertrand P., Jonas A., Laschewsky A., and Legras R., Ultrathin polymer coatings by complexation of polyelectrolytes at interfaces: suitable materials, structure and properties, Macromolecular Rapid Communications 2000, 21: 319-348.

[27] Costa R. R., Custódio C. A., Arias F. J., Rodríguez-Cabello J. C., and Mano J. F., Layer-by-Layer Assembly of Chitosan and Recombinant Biopolymers into Biomimetic Coatings with Multiple Stimuli-Responsive Properties, Small 2011, 7: 2640-2649.

[28] Decher G., Fuzzy Nanoassemblies: Toward Layered Polymeric Multicomposites, Science 1997, 277: 1232-1237.

[29] Hammond P. T., Engineering materials layer-by-layer: Challenges and opportunities in multilayer assembly, AIChE Journal 2011, 57: 2928-2940.

[30] Tang Z., Wang Y., Podsiadlo P., and Kotov N. A., Biomedical Applications of Layer-by-Layer Assembly: From Biomimetics to Tissue Engineering, Advanced Materials 2006, 18: 3203-3224.

[31] Gribova V., Gauthier-Rouvière C., Albigès-Rizo C., Auzely-Velty R., and Picart C., Effect of RGD functionalization and stiffness modulation of polyelectrolyte multilayer films on muscle cell differentiation, Acta Biomaterialia 2013, 9: 6468-6480.

[32] Becker A. L., Johnston A. P. R., and Caruso F., Layer-By-Layer-Assembled Capsules and Films for Therapeutic Delivery, Small 2010, 6: 1836-1852.

[33] Shukla A., Avadhany S. N., Fang J. C., and Hammond P. T., Tunable Vancomycin Releasing Surfaces for Biomedical Applications, Small 2010, 6: 2392-2404.

[34] Tong W., Song X., and Gao C., Layer-by-layer assembly of microcapsules and their biomedical applications, Chemical Society Reviews 2012, 41: 6103-6124.

[35] Clark S. L., and Hammond P. T., The Role of Secondary Interactions in Selective Electrostatic Multilayer Deposition, Langmuir 2000, 16: 10206-10214.

[36] Costa R. R., Testera A. M., Arias F. J., Rodríguez-Cabello J. C., and Mano J. F., Layer-by-Layer Film Growth Using Polysaccharides and Recombinant Polypeptides: A Combinatorial Approach, The Journal of Physical Chemistry B 2013, 117: 6839-6848.

[37] Kotov N. A., Layer-by-layer self-assembly: The contribution of hydrophobic interactions, Nanostructured Materials 1999, 12: 789-796.

[38] Dubas S. T., and Schlenoff J. B., Factors Controlling the Growth of Polyelectrolyte Multilayers, Macromolecules 1999, 32: 8153-8160.

[39] Lyklema J., and Deschênes L., The First Step in Layer-by-Layer Deposition: Electrostatics and/or Non-Electrostatics?, Advances in Colloid and Interface Science 2011, 168: 135-148.

[40] V. Klitzing R., Internal Structure of Polyelectrolyte Multilayer Assemblies, Physical Chemistry Chemical Physics 2006, 8: 5012-5033.

[41] Couto D. S., Alves N., M., and Mano J., F., Nanostructured Multilayer Coatings Combining Chitosan with Bioactive Glass Nanoparticles, Journal of Nanoscience and Nanotechnology 2009, 9: 1741-1748.

[42] Mamedov A. A., and Kotov N. A., Free-Standing Layer-by-Layer Assembled Films of Magnetite Nanoparticles, Langmuir 2000, 16: 5530-5533.

[43] Srivastava S., and Kotov N. A., Composite Layer-by-Layer (LBL) Assembly with Inorganic Nanoparticles and Nanowires, Accounts of Chemical Research 2008, 41: 1831-1841.

[44] Komatsu T., Protein-based nanotubes for biomedical applications, Nanoscale 2012, 4: 1910-1918.

[45] Mamedov A. A., Kotov N. A., Prato M., Guldi D. M., Wicksted J. P., and Hirsch A., Molecular design of strong single-wall carbon nanotube/polyelectrolyte multilayer composites, Nature Materials 2002, 1: 257-257.

[46] Elzbieciak M., Wodka D., Zapotoczny S., Nowak P., and Warszynski P., Characteristics of Model Polyelectrolyte Multilayer Films Containing Laponite Clay Nanoparticles, Langmuir 2010, 26: 277-283.

[47] Nguyen P. M., Zacharia N. S., Verploegen E., and Hammond P. T., Extended Release Antibacterial Layer-by-Layer Films Incorporating Linear-Dendritic Block Copolymer Micelles, Chemistry of Materials 2007, 19: 5524-5530.

[48] Wang S. H., Shi X., Van Antwerp M., Cao Z., Swanson S. D., Bi X., and Baker J. R., Dendrimer-Functionalized Iron Oxide Nanoparticles for Specific Targeting and Imaging of Cancer Cells, Advanced Functional Materials 2007, 17: 3043-3050.

[49] Boddohi S., Killingsworth C. E., and Kipper M. J., Polyelectrolyte Multilayer Assembly as a Function of pH and Ionic Strength Using the Polysaccharides Chitosan and Heparin, Biomacromolecules 2008, 9: 2021-2028.

[50] Cai K., Rechtenbach A., Hao J., Bossert J., and Jandt K. D., Polysaccharide-protein surface modification of titanium via a layer-by-layer technique: Characterization and cell behaviour aspects, Biomaterials 2005, 26: 5960-5971.

[51] Gao L., Fei J., Zhao J., Cui W., Cui Y., and Li J., pH- and Redox-Responsive Polysaccharide-Based Microcapsules with Autofluorescence for Biomedical Applications, Chemistry – A European Journal 2012, 18: 3185-3192.

[52] Halthur T. J., Claesson P. M., and Elofsson U. M., Stability of Polypeptide Multilayers As Studied by in Situ Ellipsometry: Effects of Drying and Post-Buildup Changes in Temperature and pH, Journal of the American Chemical Society 2004, 126: 17009-17015.

[53] Haynie D. T., Balkundi S., Palath N., Chakravarthula K., and Dave K., Polypeptide Multilayer Films: Role of Molecular Structure and Charge, Langmuir 2004, 20: 4540-4547.

[54] He Q., Tian Y., Cui Y., Mohwald H., and Li J., Layer-by-layer assembly of magnetic polypeptide nanotubes as a DNA carrier, Journal of Materials Chemistry 2008, 18: 748-754.

[55] He P., and Bayachou M., Layer-by-Layer Fabrication and Characterization of DNA-Wrapped Single-Walled Carbon Nanotube Particles, Langmuir 2005, 21: 6086-6092.

[56] Shi X., Sanedrin R. J., and Zhou F., Structural Characterization of Multilayered DNA and Polylysine Composite Films: Influence of Ionic Strength of DNA Solutions on the Extent of DNA Incorporation, The Journal of Physical Chemistry B 2002, 106: 1173-1180.

[57] Liu A., Abbineni G., and Mao C., Nanocomposite Films Assembled from Genetically Engineered Filamentous Viruses and Gold Nanoparticles: Nanoarchitecture- and Humidity-Tunable Surface Plasmon Resonance Spectra, Advanced Materials 2009, 21: 1001-1005.

[58] Suci P. A., Klem M. T., Arce F. T., Douglas T., and Young M., Assembly of Multilayer Films Incorporating a Viral Protein Cage Architecture, Langmuir 2006, 22: 8891-8896.

[59] Fetters L. J., Lohse D. J., Richter D., Witten T. A., and Zirkel A., Connection between Polymer Molecular Weight, Density, Chain Dimensions, and Melt Viscoelastic Properties, Macromolecules 1994, 27: 4639-4647.

[60] Fu J., Ji J., Yuan W., and Shen J., Construction of anti-adhesive and antibacterial multilayer films via layer-by-layer assembly of heparin and chitosan, Biomaterials 2005, 26: 6684-6692.

[61] Shiratori S. S., and Rubner M. F., pH-Dependent Thickness Behavior of Sequentially Adsorbed Layers of Weak Polyelectrolytes, Macromolecules 2000, 33: 4213-4219.

[62] Yoo D., Shiratori S. S., and Rubner M. F., Controlling Bilayer Composition and Surface Wettability of Sequentially Adsorbed Multilayers of Weak Polyelectrolytes, Macromolecules 1998, 31: 4309-4318.

[63] Salomäki M., Vinokurov I. A., and Kankare J., Effect of Temperature on the Buildup of Polyelectrolyte Multilayers, Langmuir 2005, 21: 11232-11240.

[64] Ashby M. F., and Jones D. R. H., Engineering Materials 2: An Introduction to Microstructures, Processing and Design, Oxford, United Kingdom: Elsevier; 2006.

[65] Langer R., and Tirrell D. A., Designing materials for biology and medicine, Nature 2004, 428: 487-492.

[66] Mano J. F., Silva G. A., Azevedo H. S., Malafaya P. B., Sousa R. A., Silva S. S., Boesel L. F., Oliveira J. M., Santos T. C., Marques A. P., Neves N. M., and Reis R. L., Natural origin biodegradable systems in tissue engineering and regenerative medicine: present status and some moving trends, Journal of The Royal Society Interface 2007, 4: 999-1030.

[67] Izumrudov V. A., Chaubet F., Clairbois A.-S., and Jozefonvicz J., Interpolyelectrolyte reactions in solutions of functionalized dextrans with negatively charged groups along the chains, Macromolecular Chemistry and Physics 1999, 200: 1753-1763.

[68] Schlenoff J. B., Ly H., and Li M., Charge and Mass Balance in Polyelectrolyte Multilayers, Journal of the American Chemical Society 1998, 120: 7626-7634.

[69] Fukao N., Kyung K.-H., Fujimoto K., and Shiratori S., Automatic Spray-LBL Machine Based on in-Situ QCM Monitoring, Macromolecules 2011, 44: 2964-2969.

[70] Izquierdo A., Ono S. S., Voegel J. C., Schaaf P., and Decher G., Dipping versus Spraying: Exploring the Deposition Conditions for Speeding Up Layer-by-Layer Assembly, Langmuir 2005, 21: 7558-7567.

[71] Krogman K. C., Zacharia N. S., Schroeder S., and Hammond P. T., Automated Process for Improved Uniformity and Versatility of Layer-by-Layer Deposition, Langmuir 2007, 23: 3137-3141.

[72] Schlenoff J. B., Dubas S. T., and Farhat T., Sprayed Polyelectrolyte Multilayers, Langmuir 2000, 16: 9968-9969.

[73] Li Y., Wang X., and Sun J., Layer-by-layer assembly for rapid fabrication of thick polymeric films, Chemical Society Reviews 2012, 41: 5998-6009.

[74] Silva T. H., Alves A., Ferreira B. M., Oliveira J. M., Reys L. L., Ferreira R. J. F., Sousa R. A., Silva S. S., Mano J. F., and Reis R. L., Materials of marine origin: a review on polymers and ceramics of biomedical interest, International Materials Reviews 2012, 57: 276-306.

[75] Boateng J. S., Matthews K. H., Stevens H. N. E., and Eccleston G. M., Wound healing dressings and drug delivery systems: A review, Journal of Pharmaceutical Sciences 2008, 97: 2892-2923.

[76] George M., and Abraham T. E., Polyionic hydrocolloids for the intestinal delivery of protein drugs: Alginate and chitosan — a review, Journal of Controlled Release 2006, 114: 1-14.

[77] Skaugrud Ø., Hagen A., Borgersen B., and Dornish M., Biomedical and Pharmaceutical Applications of Alginate and Chitosan, Biotechnology and Genetic Engineering Reviews 1999, 16: 23-40.

[78] Lee B. P., Messersmith P. B., Israelachvili J. N., and Waite J. H., Mussel-Inspired Adhesives and Coatings, Annual Review of Materials Research 2011, 41: 99-132.

[79] Lee H., Dellatore S. M., Miller W. M., and Messersmith P. B., Mussel-Inspired Surface Chemistry for Multifunctional Coatings, Science 2007, 318: 426-430.

[80] Lee H., Lee Y., Statz A. R., Rho J., Park T. G., and Messersmith P. B., Substrate-Independent Layer-by-Layer Assembly by Using Mussel-Adhesive-Inspired Polymers, Advanced Materials 2008, 20: 1619-1623.

[81] Karabulut E., Pettersson T., Ankerfors M., and Wågberg L., Adhesive Layer-by-Layer Films of Carboxymethylated Cellulose Nanofibril–Dopamine Covalent Bioconjugates Inspired by Marine Mussel Threads, ACS Nano 2012, 6: 4731-4739.

[82] Wu J., Zhang L., Wang Y., Long Y., Gao H., Zhang X., Zhao N., Cai Y., and Xu J., Mussel-Inspired Chemistry for Robust and Surface-Modifiable Multilayer Films, Langmuir 2011, 27: 13684-13691.

[83] Brubaker C. E., and Messersmith P. B., Enzymatically Degradable Mussel-Inspired Adhesive Hydrogel, Biomacromolecules 2011, 12: 4326-4334.

[84] Guvendiren M., Brass D. A., Messersmith P. B., and Shull K. R., Adhesion of DOPA-Functionalized Model Membranes to Hard and Soft Surfaces, The Journal of Adhesion 2009, 85: 631-645.

[85] Xi Z.-Y., Xu Y.-Y., Zhu L.-P., Wang Y., and Zhu B.-K., A facile method of surface modification for hydrophobic polymer membranes based on the adhesive behavior of poly(DOPA) and poly(dopamine), Journal of Membrane Science 2009, 327: 244-253.

[86] Costa R. R., Neto A. I., Calgeris I., Correia C. R., Pinho A. C. M., Fonseca J., Oner E. T., and Mano J. F., Adhesive nanostructured multilayer films using a bacterial exopolysaccharide for biomedical applications, Journal of Materials Chemistry B 2013, 1: 2367-2374.

[87] Donot F., Fontana A., Baccou J. C., and Schorr-Galindo S., Microbial exopolysaccharides: Main examples of synthesis, excretion, genetics and extraction, Carbohydrate Polymers 2012, 87: 951-962.

[88] Sima F., Mutlu E. C., Eroglu M. S., Sima L. E., Serban N., Ristoscu C., Petrescu S. M., Oner E. T., and Mihailescu I. N., Levan Nanostructured Thin Films by MAPLE Assembling, Biomacromolecules 2011, 12: 2251-2256.

[89] Spotnitz W. D., and Burks S., Hemostats, sealants, and adhesives III: a new update as well as cost and regulatory considerations for components of the surgical toolbox, Transfusion 2012, 52: 2243-2255.

[90] Bose S., and Tarafder S., Calcium phosphate ceramic systems in growth factor and drug delivery for bone tissue engineering: A review, Acta Biomaterialia 2012, 8: 1401-1421.

[91] Hutmacher D. W., Scaffolds in tissue engineering bone and cartilage, Biomaterials 2000, 21: 2529-2543.

[92] Karageorgiou V., and Kaplan D., Porosity of 3D biomaterial scaffolds and osteogenesis, Biomaterials 2005, 26: 5474-5491.

[93] Boccaccini A. R., and Blaker J. J., Bioactive composite materials for tissue engineering scaffolds, Expert Review of Medical Devices 2005, 2: 303-317.

[94] Alves N. M., Leonor I. B., Azevedo H. S., Reis R. L., and Mano J. F., Designing biomaterials based on biomineralization of bone, Journal of Materials Chemistry 2010, 20: 2911-2921.

[95] Neel E. A. A., Pickup D. M., Valappil S. P., Newport R. J., and Knowles J. C., Bioactive functional materials: a perspective on phosphate-based glasses, Journal of Materials Chemistry 2009, 19: 690-701.

[96] Piek E., Sleumer L. S., van Someren E. P., Heuver L., de Haan J. R., de Grijs I., Gilissen C., Hendriks J. M., van Ravestein-van Os R. I., Bauerschmidt S., Dechering K. J., and van Zoelen E. J., Osteo-transcriptomics of human mesenchymal stem cells: Accelerated gene expression and osteoblast differentiation induced by vitamin D reveals c-MYC as an enhancer of BMP2-induced osteogenesis, Bone 2010, 46: 613-627.

[97] Fukui Y., and Fujimoto K., Control in Mineralization by the Polysaccharide-Coated Liposome via the Counter-Diffusion of Ions, Chemistry of Materials 2011, 23: 4701-4708.

[98] Hu Y., Cai K., Luo Z., Zhang Y., Li L., Lai M., Hou Y., Huang Y., Li J., Ding X., Zhang B., and Paul Sung K. L., Regulation of the differentiation of mesenchymal stem cells in vitro and osteogenesis in vivo by microenvironmental modification of titanium alloy surfaces, Biomaterials 2012, 33: 3515-3528.

[99] Tokarev I., and Minko S., Multiresponsive, Hierarchically Structured Membranes: New, Challenging, Biomimetic Materials for Biosensors, Controlled Release, Biochemical Gates, and Nanoreactors, Advanced Materials 2009, 21: 241-247.

[100] Mano J. F., Stimuli-Responsive Polymeric Systems for Biomedical Applications, Advanced Engineering Materials 2008, 10: 515-527.

[101] Rodríguez-Cabello J. C., Martín L., Girotti A., García-Arévalo C., Arias F. J., and Alonso M., Emerging applications of multifunctional elastin-like recombinamers, Nanomedicine 2011, 6: 111-122.

[102] Costa R. R., Custódio C. A., Testera A. M., Arias F. J., Rodríguez-Cabello J. C., Alves N. M., and Mano J. F., Stimuli-Responsive Thin Coatings Using Elastin-Like Polymers for Biomedical Applications, Advanced Functional Materials 2009, 19: 3210-3218.

[103] Hynes R. O., Integrins: Bidirectional, Allosteric Signaling Machines, Cell 2002, 110: 673-687.

[104] Martins G. V., Mano J. o. F., and Alves N. l. M., Dual Responsive Nanostructured Surfaces for Biomedical Applications, Langmuir 2011, 27: 8415-8423.

[105] Okano T., Yamada N., Sakai H., and Sakurai Y., A novel recovery system for cultured cells using plasma-treated polystyrene dishes grafted with poly(N-isopropylacrylamide), Journal of Biomedical Materials Research 1993, 27: 1243-1251.

[106] Zahn R., Thomasson E., Guillaume-Gentil O., Vörös J., and Zambelli T., Ion-induced cell sheet detachment from standard cell culture surfaces coated with polyelectrolytes, Biomaterials 2012, 33: 3421-3427.

[107] Tang Z., Akiyama Y., and Okano T., Temperature-Responsive Polymer Modified Surface for Cell Sheet Engineering, Polymers 2012, 4: 1478-1498.

[108] Volodkin D., Skirtach A., and Möhwald H., Bioapplications of light-sensitive polymer films and capsules assembled using the layer-by-layer technique, Polymer International 2012, 61: 673-679.

[109] Ahmad N. M., Saqib M., and Barrett C. J., Novel Azobenzene-Functionalized Polyelectrolytes of Different Substituted Head Groups 3: Control of Properties of Self-Assembled Multilayer Thin Films, Journal of Macromolecular Science, Part A 2010, 47: 571-579.

[110] Haidukewych G. J., and Ricci W., Locked Plating in Orthopaedic Trauma: A Clinical Update, Journal of the American Academy of Orthopaedic Surgeons 2008, 16: 347-355.

[111] Miller D. L., and Goswami T., A review of locking compression plate biomechanics and their advantages as internal fixators in fracture healing, Clinical Biomechanics 2007, 22: 1049-1062.

[112] Mudgal C. S., and Jupiter J. B., Plate and Screw Design in Fractures of the Hand and Wrist, Clinical Orthopaedics and Related Research 2006, 445: 68-80 10.1097/1001.blo.0000205887.0000204200.0000205821.

[113] Geetha M., Singh A. K., Asokamani R., and Gogia A. K., Ti based biomaterials, the ultimate choice for orthopaedic implants – A review, Progress in Materials Science 2009, 54: 397-425.

[114] Zankovych S., Diefenbeck M., Bossert J., Mückley T., Schrader C., Schmidt J., Schubert H., Bischoff S., Faucon M., Finger U., and Jandt K. D., The effect of polyelectrolyte multilayer coated titanium alloy surfaces on implant anchorage in rats, Acta Biomaterialia 2013, 9: 4926-4934.

[115] Zankovych S., Bossert J., Faucon M., Finger U., and Jandt K. D., Selectively Promoting or Preventing Osteoblast Growth on Titanium Functionalized with Polyelectrolyte Multilayers, Advanced Engineering Materials 2011, 13: B454-B461.

[116] Hossfeld S., Nolte A., Hartmann H., Recke M., Schaller M., Walker T., Kjems J., Schlosshauer B., Stoll D., Wendel H. P., and Krastev R., Bioactive coronary stent coating based on layer-by-layer technology for siRNA release, Acta Biomaterialia 2013, 9: 6741-6752.

[117] Khan W., Farah S., and Domb A. J., Drug eluting stents: Developments and current status, Journal of Controlled Release 2012, 161: 703-712.

[118] Bauters C., and Isner J. M., The biology of restenosis, Progress in Cardiovascular Diseases 1997, 40: 107-116.

[119] Schweizer S., Schuster T., Junginger M., Siekmeyer G., and Taubert A., Surface Modification of Nickel/Titanium Alloy and Titanium Surfaces via a Polyelectrolyte Multilayer/Calcium Phosphate Hybrid Coating, Macromolecular Materials and Engineering 2010, 295: 535-543.

[120] Meng S., Liu Z., Shen L., Guo Z., Chou L. L., Zhong W., Du Q., and Ge J., The effect of a layer-by-layer chitosan–heparin coating on the endothelialization and coagulation properties of a coronary stent system, Biomaterials 2009, 30: 2276-2283.

[121] Lin Q., Ding X., Qiu F., Song X., Fu G., and Ji J., In situ endothelialization of intravascular stents coated with an anti-CD34 antibody functionalized heparin–collagen multilayer, Biomaterials 2010, 31: 4017-4025.

[122] Costerton J. W., Stewart P. S., and Greenberg E. P., Bacterial Biofilms: A Common Cause of Persistent Infections, Science 1999, 284: 1318-1322.

[123] Etienne O., Gasnier C., Taddei C., Voegel J.-C., Aunis D., Schaaf P., Metz-Boutigue M.-H., Bolcato-Bellemin A.-L., and Egles C., Antifungal coating by biofunctionalized polyelectrolyte multilayered films, Biomaterials 2005, 26: 6704-6712.

[124] Ochs C. J., Such G. K., Städler B., and Caruso F., Low-Fouling, Biofunctionalized, and Biodegradable Click Capsules, Biomacromolecules 2008, 9: 3389-3396.

[125] Wattendorf U., Kreft O., Textor M., Sukhorukov G. B., and Merkle H. P., Stable Stealth Function for Hollow Polyelectrolyte Microcapsules through a Poly(ethylene glycol) Grafted Polyelectrolyte Adlayer, Biomacromolecules 2008, 9: 100-108.

[126] Reisch A., Hemmerle J., Voegel J.-C., Gonthier E., Decher G., Benkirane-Jessel N., Chassepot A., Mertz D., Lavalle P., Mesini P., and Schaaf P., Polyelectrolyte multilayer coatings that resist protein adsorption at rest and under stretching, Journal of Materials Chemistry 2008, 18: 4242-4245.

[127] Cortez C., Quinn J. F., Hao X., Gudipati C. S., Stenzel M. H., Davis T. P., and Caruso F., Multilayer Buildup and Biofouling Characteristics of PSS-b-PEG Containing Films, Langmuir 2010, 26: 9720-9727.

[128] Wong S. Y., Li Q., Veselinovic J., Kim B.-S., Klibanov A. M., and Hammond P. T., Bactericidal and virucidal ultrathin films assembled layer by layer from polycationic N-alkylated polyethylenimines and polyanions, Biomaterials 2010, 31: 4079-4087.

[129] Broughton R. L., and Sefton M. V., Effect of capsule permeability on growth of CHO cells in Eudragit EL microcapsules: use of FITC-dextran as a marker of capsule quality, Biomaterials 1989, 10: 462-465.

[130] Chang P. L., Shen N., and Westcott A. J., Delivery of recombinant gene products with microencapsulated cells in vivo, Hum Gene Ther 1993, 4: 433-440.

[131] Nafea E. H., L.A P.-W. A. M., and Martens P. J., Immunoisolating semi-permeable membranes for cell encapsulation: Focus on hydrogels, Journal of Controlled Release 2011, 154: 110-122.

[132] Orive G., Hernandez R. M., Gascon A. R., Calafiore R., Chang T. M. S., Vos P. D., Hortelano G., Hunkeler D., Lacik I., Shapiro A. M. J., and Pedraz J. L., Cell encapsulation: Promise and progress, Nature Medicine 2003, 9: 104-107.

[133] Uludag H., De Vos P., and Tresco P. A., Technology of mammalian cell encapsulation, Advanced Drug Delivery Reviews 2000, 42: 29-64.

[134] Linn T., Schmitz J., Hauck-Schmalenberger I., Lai Y., Bretzel R. G., Brandhorst H., and Brandhorst D., Ischaemia is linked to inflammation and induction of angiogenesis in pancreatic islets, Clinical and Experimental Immunology 2006, 144: 179-187.

[135] Ricordi C., and Strom T. B., Clinical islet transplantation: advances and immunological challenges, Nature Reviews Immunology 2004, 4: 259-268.

[136] Zheng X., Zheng X., Wang X., Ma Z., Gupta Sunkari V., Botusan I., Takeda T., Bjorklund A., Inoue M., Catrina S. B., Brismar K., Poellinger L., and Pereira T. S., Acute hypoxia induces apoptosis of pancreatic [beta]-cell by activation of the unfolded protein response and upregulation of CHOP, Cell Death Dis 2012, 3: e322.

[137] Krol S., del Guerra S., Grupillo M., Diaspro A., Gliozzi A., and Marchetti P., Multilayer Nanoencapsulation. New Approach for Immune Protection of Human Pancreatic Islets, Nano Letters 2006, 6: 1933-1939.

[138] Hunt N., and Grover L., Cell encapsulation using biopolymer gels for regenerative medicine, Biotechnology Letters 2010, 32: 733-742.

[139] Peirone M., Ross C. J. D., Hortelano G., Brash J. L., and Chang P. L., Encapsulation of various recombinant mammalian cell types in different alginate microcapsules, Journal of Biomedical Materials Research 1998, 42: 587-596.

[140] Su J., Hu B.-H., Lowe Jr W. L., Kaufman D. B., and Messersmith P. B., Anti-inflammatory peptide-functionalized hydrogels for insulin-secreting cell encapsulation, Biomaterials 2010, 31: 308-314.

[141] Wilson J. T., Cui W., Kozlovskaya V., Kharlampieva E., Pan D., Qu Z., Krishnamurthy V. R., Mets J., Kumar V., Wen J., Song Y., Tsukruk V. V., and Chaikof E. L., Cell Surface Engineering with Polyelectrolyte Multilayer Thin Films, Journal of the American Chemical Society 2011, 133: 7054-7064.

[142] Morales J. O., and McConville J. T., Manufacture and characterization of mucoadhesive buccal films, European Journal of Pharmaceutics and Biopharmaceutics 2011, 77: 187-199.

[143] Choi H.-J., Brooks E., and Montemagno C. D., Synthesis and characterization of nanoscale biomimetic polymer vesicles and polymer membranes for bioelectronic applications, Nanotechnology 2005, 16: S143.

[144] Jiang C., and Tsukruk V. V., Freestanding Nanostructures via Layer-by-Layer Assembly, Advanced Materials 2006, 18: 829-840.

[145] Larkin A. L., Davis R. M., and Rajagopalan P., Biocompatible, Detachable, and Free-Standing Polyelectrolyte Multilayer Films, Biomacromolecules 2010, 11: 2788-2796.

[146] Lee S., Lee B., Kim B. J., Park J., Yoo M., Bae W. K., Char K., Hawker C. J., Bang J., and Cho J., Free-Standing Nanocomposite Multilayers with Various Length Scales, Adjustable Internal Structures, and Functionalities, Journal of the American Chemical Society 2009, 131: 2579-2587.

[147] Ott P., Trenkenschuh K., Gensel J., Fery A., and Laschewsky A., Free-Standing Membranes via Covalent Cross-Linking of Polyelectrolyte Multilayers with Complementary Reactivity, Langmuir 2010, 26: 18182-18188.

[148] Chen W., and McCarthy T. J., Layer-by-Layer Deposition: A Tool for Polymer Surface Modification, Macromolecules 1997, 30: 78-86.

[149] Linford M. R., Auch M., and Möhwald H., Nonmonotonic Effect of Ionic Strength on Surface Dye Extraction during Dye−Polyelectrolyte Multilayer Formation, Journal of the American Chemical Society 1998, 120: 178-182.

[150] Caridade S. G., Monge C., Gilde F., Boudou T., Mano J. F., and Picart C., Free-Standing Polyelectrolyte Membranes Made of Chitosan and Alginate, Biomacromolecules 2013, 14: 1653-1660.

[151] Fujie T., Matsutani N., Kinoshita M., Okamura Y., Saito A., and Takeoka S., Adhesive, Flexible, and Robust Polysaccharide Nanosheets Integrated for Tissue-Defect Repair, Advanced Functional Materials 2009, 19: 2560-2568.

[152] Porte H. L., Jany T., Akkad R., Conti M., Gillet P. A., Guidat A., and Wurtz A. J., Randomized controlled trial of a synthetic sealant for preventing alveolar air leaks after lobectomy, The Annals of Thoracic Surgery 2001, 71: 1618-1622.

[153] Fujie T., Saito A., Kinoshita M., Miyazaki H., Ohtsubo S., Saitoh D., and Takeoka S., Dual therapeutic action of antibiotic-loaded nanosheets for the treatment of gastrointestinal tissue defects, Biomaterials 2010, 31: 6269-6278.

[154] Saito A., Miyazaki H., Fujie T., Ohtsubo S., Kinoshita M., Saitoh D., and Takeoka S., Therapeutic efficacy of an antibiotic-loaded nanosheet in a murine burn-wound infection model, Acta Biomaterialia 2012, 8: 2932-2940.

[155] MacNeil S., Progress and opportunities for tissue-engineered skin, Nature 2007, 445: 874-880.

[156] Revathi G., Puri J., and Jain B. K., Bacteriology of burns, Burns 1998, 24: 347-349.

[157] Brusselaers N., Pirayesh A., Hoeksema H., Richters C. D., Verbelen J., Beele H., Blot S. I., and Monstrey S., Skin Replacement in Burn Wounds, Journal of Trauma- Injury, Infection, and Critical Care 2010, 68: 490-501 410.1097/TA.1090b1013e3181c1099c1074.

[158] Brook I., Microbiology and Management of Abdominal Infections, Digestive Diseases and Sciences 2008, 53: 2585-2591.

[159] Schneider A., Francius G., Obeid R., Schwinté P., Hemmerlé J., Frisch B., Schaaf P., Voegel J.-C., Senger B., and Picart C., Polyelectrolyte Multilayers with a Tunable Young's Modulus: Influence of Film Stiffness on Cell Adhesion, Langmuir 2006, 22: 1193-1200.

[160] Phelps J. A., Morisse S., Hindié M., Degat M.-C., Pauthe E., and Van Tassel P. R., Nanofilm Biomaterials: Localized Cross-Linking To Optimize Mechanical Rigidity and Bioactivity, Langmuir 2011, 27: 1123-1130.

[161] Martins G. V., Merino E. G., Mano J. F., and Alves N. M., Crosslink Effect and Albumin Adsorption onto Chitosan/Alginate Multilayered Systems: An in situ QCM-D Study, Macromolecular Bioscience 2010, 10: 1444-1455.

[162] Lee J., and Kotov N. A., Notch Ligand Presenting Acellular 3D Microenvironments for ex vivo Human Hematopoietic Stem-Cell Culture made by Layer-By-Layer Assembly, Small 2009, 5: 1008-1013.

[163] Picart C., Schneider A., Etienne O., Mutterer J., Schaaf P., Egles C., Jessel N., and Voegel J. C., Controlled Degradability of Polysaccharide Multilayer Films In Vitro and In Vivo, Advanced Functional Materials 2005, 15: 1771-1780.

[164] Blanazs A., Armes S. P., and Ryan A. J., Self-Assembled Block Copolymer Aggregates: From Micelles to Vesicles and their Biological Applications, Macromolecular Rapid Communications 2009, 30: 267-277.

[165] Malam Y., Loizidou M., and Seifalian A. M., Liposomes and nanoparticles: nanosized vehicles for drug delivery in cancer, Trends in Pharmacological Sciences 2009, 30: 592-599.

[166] Meng F., Zhong Z., and Feijen J., Stimuli-Responsive Polymersomes for Programmed Drug Delivery, Biomacromolecules 2009, 10: 197-209.

[167] Shimoni O., Yan Y., Wang Y., and Caruso F., Shape-Dependent Cellular Processing of Polyelectrolyte Capsules, ACS Nano 2013, 7: 522-530.

[168] Szarpak A., Cui D., Dubreuil F. d. r., De Geest B. G., De Cock L. J., Picart C., and Auzély-Velty R., Designing Hyaluronic Acid-Based Layer-by-Layer Capsules as a Carrier for Intracellular Drug Delivery, Biomacromolecules 2010, 11: 713-720.

[169] Crouzier T., Ren K., Nicolas C., Roy C., and Picart C., Layer-By-Layer Films as a Biomimetic Reservoir for rhBMP-2 Delivery: Controlled Differentiation of Myoblasts to Osteoblasts, Small 2009, 5: 598-608.

[170] Crouzier T., Sailhan F., Becquart P., Guillot R., Logeart-Avramoglou D., and Picart C., The performance of BMP-2 loaded TCP/HAP porous ceramics with a polyelectrolyte multilayer film coating, Biomaterials 2011, 32: 7543-7554.

[171] Guillot R., Gilde F., Becquart P., Sailhan F., Lapeyrere A., Logeart-Avramoglou D., and Picart C., The stability of BMP loaded polyelectrolyte multilayer coatings on titanium, Biomaterials 2013, 34: 5737-5746.

[172] Gilde F., Maniti O., Guillot R., Mano J. F., Logeart-Avramoglou D., Sailhan F., and Picart C., Secondary Structure of rhBMP-2 in a Protective Biopolymeric Carrier Material, Biomacromolecules 2012, 13: 3620-3626.

[173] Macdonald M. L., Rodriguez N. M., Shah N. J., and Hammond P. T., Characterization of Tunable FGF-2 Releasing Polyelectrolyte Multilayers, Biomacromolecules 2010, 11: 2053-2059.

[174] Shah N. J., Macdonald M. L., Beben Y. M., Padera R. F., Samuel R. E., and Hammond P. T., Tunable dual growth factor delivery from polyelectrolyte multilayer films, Biomaterials 2011, 32: 6183-6193.

[175] Volodkin D. V., Larionova N. I., and Sukhorukov G. B., Protein Encapsulation via Porous CaCO3 Microparticles Templating, Biomacromolecules 2004, 5: 1962-1972.

[176] Sivakumar S., Bansal V., Cortez C., Chong S.-F., Zelikin A. N., and Caruso F., Degradable, Surfactant-Free, Monodisperse Polymer-Encapsulated Emulsions as Anticancer Drug Carriers, Advanced Materials 2009, 21: 1820-1824.

[177] She Z., Antipina M. N., Li J., and Sukhorukov G. B., Mechanism of Protein Release from Polyelectrolyte Multilayer Microcapsules, Biomacromolecules 2010, 11: 1241-1247.

[178] Cortez C., Tomaskovic-Crook E., Johnston A. P. R., Radt B., Cody S. H., Scott A. M., Nice E. C., Heath J. K., and Caruso F., Targeting and Uptake of Multilayered Particles to Colorectal Cancer Cells, Advanced Materials 2006, 18: 1998-2003.

[179] Costa R. R., Custódio C. A., Arias F. J., Rodríguez-Cabello J. C., and Mano J. F., Nanostructured and thermoresponsive recombinant biopolymer-based microcapsules for the delivery of active molecules, Nanomedicine: Nanotechnology, Biology and Medicine 2013, 9: 895-902.

[180] Kainourgios P., Efthimiadou E. K., Tziveleka L. A., Pappas G. S., Boukos N., and Kordas G., Comparative study of LbL and crosslinked pH sensitive PEGylated LbL microspheres: Synthesis, characterization and biological evaluation, Colloids and Surfaces B: Biointerfaces 2013, 104: 91-98.

[181] Shen H. J., Shi H., Ma K., Xie M., Tang L. L., Shen S., Li B., Wang X. S., and Jin Y., Polyelectrolyte capsules packaging BSA gels for pH-controlled drug loading and release and their antitumor activity, Acta Biomaterialia 2013, 9: 6123-6133.

[182] Liu J., Zhang Y., Wang C., Xu R., Chen Z., and Gu N., Magnetically Sensitive Alginate-Templated Polyelectrolyte Multilayer Microcapsules for Controlled Release of Doxorubicin, The Journal of Physical Chemistry C 2010, 114: 7673-7679.

[183] Rivera-Gil P., De Koker S., De Geest B. G., and Parak W. J., Intracellular Processing of Proteins Mediated by Biodegradable Polyelectrolyte Capsules, Nano Letters 2009, 9: 4398-4402.

[184] Palankar R., Skirtach A. G., Kreft O., Bédard M., Garstka M., Gould K., Möhwald H., Sukhorukov G. B., Winterhalter M., and Springer S., Controlled Intracellular Release of Peptides from Microcapsules Enhances Antigen Presentation on MHC Class I Molecules, Small 2009, 5: 2168-2176.

[185] Poon Z., Lee J. B., Morton S. W., and Hammond P. T., Controlling in Vivo Stability and Biodistribution in Electrostatically Assembled Nanoparticles for Systemic Delivery, Nano Letters 2011, 11: 2096-2103.

[186] Kazakova L., Shabarchina L., Anastasova S., Pavlov A., Vadgama P., Skirtach A., and Sukhorukov G., Chemosensors and biosensors based on polyelectrolyte microcapsules containing fluorescent dyes and enzymes, Analytical and Bioanalytical Chemistry 2013, 405: 1559-1568.

[187] Turner A. P. F., Biosensors: sense and sensibility, Chemical Society Reviews 2013, 42: 3184-3196.

[188] Wilson G. S., and Gifford R., Biosensors for real-time in vivo measurements, Biosensors and Bioelectronics 2005, 20: 2388-2403.

[189] Kreft O., Javier A. M., Sukhorukov G. B., and Parak W. J., Polymer microcapsules as mobile local pH-sensors, Journal of Materials Chemistry 2007, 17: 4471-4476.

[190] Pan Y., Zhang Y.-Z., and Li Y., Layer-by-layer self-assembled multilayer films of single-walled carbon nanotubes and tin disulfide nanoparticles with chitosan for the fabrication of biosensors, Journal of Applied Polymer Science 2013, 128: 647-652.

[191] Yu Y., Yin M., Mullen K., and Knoll W., LbL-assembled multilayer films of dendritic star polymers: surface morphology and DNA hybridization detection, Journal of Materials Chemistry 2012, 22: 7880-7886.

[192] Garcia J., Zhang Y., Taylor H., Cespedes O., Webb M. E., and Zhou D., Multilayer enzyme-coupled magnetic nanoparticles as efficient, reusable biocatalysts and biosensors, Nanoscale 2011, 3: 3721-3730.

[193] Lee D.-G., Ponvel K. M., Kim M., Hwang S., Ahn I.-S., and Lee C.-H., Immobilization of lipase on hydrophobic nano-sized magnetite particles, Journal of Molecular Catalysis B: Enzymatic 2009, 57: 62-66.

[194] Rossi L. M., Quach A. D., and Rosenzweig Z., Glucose oxidase–magnetite nanoparticle bioconjugate for glucose sensing, Analytical and Bioanalytical Chemistry 2004, 380: 606-613.

[195] McShane M., and Ritter D., Microcapsules as optical biosensors, Journal of Materials Chemistry 2010, 20: 8189-8193.

[196] Liang Z., Susha A. S., Yu A., and Caruso F., Nanotubes Prepared by Layer-by-Layer Coating of Porous Membrane Templates, Advanced Materials 2003, 15: 1849-1853.

[197] Yang Y., He Q., Duan L., Cui Y., and Li J., Assembled alginate/chitosan nanotubes for biological application, Biomaterials 2007, 28: 3083-3090.

[198] Mueller R., Daehne L., and Fery A., Hollow Polyelectrolyte Multilayer Tubes: Mechanical Properties and Shape Changes, The Journal of Physical Chemistry B 2007, 111: 8547-8553.

[199] He Q., Song W., Möhwald H., and Li J., Hydrothermal-Induced Structure Transformation of Polyelectrolyte Multilayers: From Nanotubes to Capsules, Langmuir 2008, 24: 5508-5513.

[200] Vriezema D. M., Aragones M. C., Elemans J., Cornelissen J., Rowan A. E., and Nolte R. J. M., Self-assembled nanoreactors, Chemical Reviews 2005, 105: 1445-1489.

[201] Silva J. M., Duarte A. R. C., Custódio C. A., Sher P., Neto A. I., Pinho A. C. M., Fonseca J., Reis R. L., and Mano J. F., Nanostructured Hollow Tubes Based on Chitosan and Alginate Multilayers, Advanced Healthcare Materials 2013: 10.1002/adhm.201300265.

[202] Gotlieb A. I., Atherosclerosis and acute coronary syndromes, Cardiovascular Pathology 2005, 14: 181-184.

[203] Koens M. J. W., Faraj K. A., Wismans R. G., van der Vliet J. A., Krasznai A. G., Cuijpers V. M. J. I., Jansen J. A., Daamen W. F., and van Kuppevelt T. H., Controlled fabrication of triple layered and molecularly defined collagen/elastin vascular grafts resembling the native blood vessel, Acta Biomaterialia 2010, 6: 4666-4674.

[204] Murugan R., and Ramakrishna S., Nano-featured scaffolds for tissue engineering: a review of spinning methodologies, Tissue Eng 2006, 12: 435-447.

[205] Sanchez-Castillo M. A., Couto C., Kim W. B., and Dumesic J. A., Gold-Nanotube Membranes for the Oxidation of CO at Gas–Water Interfaces, Angewandte Chemie International Edition 2004, 43: 1140-1142.

[206] Wang X., Kim Y.-G., Drew C., Ku B.-C., Kumar J., and Samuelson L. A., Electrostatic Assembly of Conjugated Polymer Thin Layers on Electrospun Nanofibrous Membranes for Biosensors, Nano Letters 2004, 4: 331-334.

[207] Furlani D., Ugurlucan M., Ong L., Bieback K., Pittermann E., Westien I., Wang W., Yerebakan C., Li W., Gaebel R., Li R.-k., Vollmar B., Steinhoff G., and Ma N., Is the intravascular administration of mesenchymal stem cells safe?: Mesenchymal stem cells and intravital microscopy, Microvascular Research 2009, 77: 370-376.

[208] Patel A., Fine B., Sandig M., and Mequanint K., Elastin biosynthesis: The missing link in tissue-engineered blood vessels, Cardiovascular Research 2006, 71: 40-49.

[209] Demaurex N., pH Homeostasis of Cellular Organelles, Physiology 2002, 17: 1-5.

[210] Gray M. W., Burger G., and Lang B. F., Mitochondrial evolution, Science 1999, 283: 1476-1481.

[211] Yates Iii J. R., Gilchrist A., Howell K. E., and Bergeron J. J. M., Proteomics of organelles and large cellular structures, Nature Reviews Molecular Cell Biology 2005, 6: 702-714.

[212] Huang C.-C., Huang W., and Yeh C.-S., Shell-by-shell synthesis of multi-shelled mesoporous silica nanospheres for optical imaging and drug delivery, Biomaterials 2011, 32: 556-564.

[213] Li G., Shi Q., Yuan S. J., Neoh K. G., Kang E. T., and Yang X., Alternating Silica/Polymer Multilayer Hybrid Microspheres Templates for Double-shelled Polymer and Inorganic Hollow Microstructures, Chemistry of Materials 2010, 22: 1309-1317.

[214] Xu H., and Wang W., Template Synthesis of Multishelled Cu2O Hollow Spheres with a Single-Crystalline Shell Wall, Angewandte Chemie 2007, 119: 1511-1514.

[215] Marguet M., Sandre O., and Lecommandoux S., Polymersomes in "Gelly" Polymersomes: Toward Structural Cell Mimicry, Langmuir 2012, 28: 2035-2043.

[216] De Geest B. G., McShane M. J., Demeester J., De Smedt S. C., and Hennink W. E., Microcapsules Ejecting Nanosized Species into the Environment, Journal of the American Chemical Society 2008, 130: 14480-14482.

[217] Delcea M., Yashchenok A., Videnova K., Kreft O., Möhwald H., and Skirtach A. G., Multicompartmental Micro- and Nanocapsules: Hierarchy and Applications in Biosciences, Macromolecular Bioscience 2010, 10: 465-474.

[218] Chandrawati R., van Koeverden M. P., Lomas H., and Caruso F., Multicompartment Particle Assemblies for Bioinspired Encapsulated Reactions, The Journal of Physical Chemistry Letters 2011, 2: 2639-2649.

[219] Kreft O., Prevot M., Möhwald H., and Sukhorukov G. B., Shell-in-Shell Microcapsules: A Novel Tool for Integrated, Spatially Confined Enzymatic Reactions, Angewandte Chemie International Edition 2007, 46: 5605-5608.

[220] Tong W., Zhu Y., Wang Z., Gao C., and Möhwald H., Micelles-Encapsulated Microcapsules for Sequential Loading of Hydrophobic and Water-Soluble Drugs, Macromolecular Rapid Communications 2010, 31: 1015-1019.

[221] Hosta-Rigau L., Städler B., Yan Y., Nice E. C., Heath J. K., Albericio F., and Caruso F., Capsosomes with Multilayered Subcompartments: Assembly and Loading with Hydrophobic Cargo, Advanced Functional Materials 2010, 20: 59-66.

[222] Marguet M., Bonduelle C., and Lecommandoux S., Multicompartmentalized polymeric systems: towards biomimetic cellular structure and function, Chemical Society Reviews 2013, 42: 512-529.

[223] Zhang Y., Ruder W. C., and LeDuc P. R., Artificial cells: building bioinspired systems using small-scale biology, Trends in Biotechnology 2008, 26: 14-20.

[224] Costa R. R., Castro E., Arias F. J., Rodríguez-Cabello J. C., and Mano J. F., Multifunctional Compartmentalized Capsules with a Hierarchical Organization from the Nano to the Macro Scales, Biomacromolecules 2013, 14: 2403-2410.

[225] Wust P., Hildebrandt B., Sreenivasa G., Rau B., Gellermann J., Riess H., Felix R., and Schlag P. M., Hyperthermia in combined treatment of cancer, The Lancet Oncology 2002, 3: 487-497.

[226] Langer R., and Vacanti J., Tissue engineering, Science 1993, 260: 920-926.

[227] Sher P., Custódio C. A., and Mano J. F., Layer-By-Layer Technique for Producing Porous Nanostructured 3D Constructs Using Moldable Freeform Assembly of Spherical Templates, Small 2010, 6: 2644-2648.

[228] Silva J. M., Georgi N., Costa R., Sher P., Reis R. L., Van Blitterswijk C. A., Karperien M., and Mano J. F., Nanostructured 3D Constructs Based on Chitosan and Chondroitin Sulphate Multilayers for Cartilage Tissue Engineering, PLoS ONE 2013, 8: e55451.

[229] Ye X., Hu X., Wang H., Liu J., and Zhao Q., Polyelectrolyte multilayer film on decellularized porcine aortic valve can reduce the adhesion of blood cells without affecting the growth of human circulating progenitor cells, Acta Biomaterialia 2012, 8: 1057-1067.

[230] Oliveira S. M., Silva T. H., Reis R. L., and Mano J. F., Hierarchical Fibrillar Scaffolds Obtained by Non-conventional Layer-By-Layer Electrostatic Self-Assembly, Advanced Healthcare Materials 2013, 2: 422-427.

[231] Matsusaki M., Kadowaki K., Nakahara Y., and Akashi M., Fabrication of Cellular Multilayers with Nanometer-Sized Extracellular Matrix Films, Angewandte Chemie International Edition 2007, 46: 4689-4692.

[232] Kadowaki K., Matsusaki M., and Akashi M., Three-dimensional constructs induce high cellular activity: Structural stability and the specific production of proteins and cytokines, Biochemical and Biophysical Research Communications 2010, 402: 153-157.

[233] Kim Y., and Rajagopalan P., 3D Hepatic Cultures Simultaneously Maintain Primary Hepatocyte and Liver Sinusoidal Endothelial Cell Phenotypes, PLoS ONE 2010, 5: e15456.

[234] Yoshida H., Matsusaki M., and Akashi M., Multilayered Blood Capillary Analogs in Biodegradable Hydrogels for In Vitro Drug Permeability Assays, Advanced Functional Materials 2013, 23: 1736-1742.

[235] Nishiguchi A., Yoshida H., Matsusaki M., and Akashi M., Rapid Construction of Three-Dimensional Multilayered Tissues with Endothelial Tube Networks by the Cell-Accumulation Technique, Advanced Materials 2011, 23: 3506-3510.

[236] Correia C. R., Reis R. L., and Mano J. F., Multilayered Hierarchical Capsules Providing Cell Adhesion Sites, Biomacromolecules 2013, 14: 743-751.

[237] Correia C. R., Sher P., Reis R. L., and Mano J. F., Liquified chitosan-alginate multilayer capsules incorporating poly(l-lactic acid) microparticles as cell carriers, Soft Matter 2013, 9: 2125-2130.

[238] Brun-Graeppi A. K. A. S., Richard C., Bessodes M., Scherman D., and Merten O.-W., Cell microcarriers and microcapsules of stimuli-responsive polymers, Journal of Controlled Release 2011, 149: 209-224.

Chapter 3. Elastin-like macromolecules[3]

3.1 General introduction

Scientists have long discovered that macromolecules are the best option for obtaining highly functional and complex materials. Hierarchical organization, self-assembly, or "intelligence" are common to many natural macromolecules and desirable for several applications in biology and biotechnology. Proteins, nucleic acids, and polysaccharides are fine examples of structures that have been employed in many biomimetic concepts displaying such properties.

In biomedicine, several advances have been made in the last decades regarding the design and conception of new state-of-the-art devices with great potential for future in-depth studies and, ultimately, use in human healthcare services. Some of them emerged from the increasing use of elastin-derived materials, consisting in viable and functional protein-based molecules as alternatives to the conventional polymers used in biomedical applications, including in tissue engineering and regenerative medicine (TERM).

Elastin-like macromolecules are genetically engineered materials rooted in the repeating sequence of natural elastin, a vital protein component of the extracellular matrix (ECM) found in various mammalian tissues [1]. As biomaterials, they became popular for exhibiting excellent mechanical properties [2-6] and biocompatibility [7-10]. They have also shown potential to self-assemble and respond to changes of the environment or under physiological conditions [11-14].

Because of their genetic-engineered origin, they are often called elastin-like polymers or, more recently, elastin-like recombinamers [15]. This class of materials can be modified to virtually include any desired peptide sequence, especially functional sequences with relevant biological role [16-18], and has already been studied extensively for applications in drug delivery [19-21], and cell and tissue engineering [22-24]. In the following sections, a comprehensive discussion of the importance of elastin-like macromolecules in the conception of TERM devices will be presented. Here, not only their properties will be presented but also their origin and natural inspiration.

---

[3] This chapter is based on the following publication:

Costa R. R., Martín L., Mano J. F., and Rodríguez-Cabello J. C., Elastin-like macromolecules, In Mano J. F. (ed.), Biomimetic approaches for biomaterials development, Germany, Wiley-VCH, 2012, DOI:10.1002/9783527652273.ch5.

3.2 Materials engineering – an overview on synthetic and natural biomaterials

Biomaterials have been applied in Medicine since the early 1950's and expanded in four traditional directions: metals, polymers, ceramics, and combinations thereof – composites [25,26]. More recently, biological or natural materials, found in animals and plants, were added as a fifth direction. Natural materials are intricate structures which have risen from hundreds of millions of years of evolution. Comparing to our current technology, Nature was able to conceive structures more complex than man-made materials, forming complex arrays, hierarchical structures and multi-functionality [26,27]. According to Wegst and Ashby [28], natural materials can be categorized into four groups: (i) ceramics and ceramic composites – shells, bones or any material where the mineral component is prevalent; (ii) polymer and polymer composites – e.g. ligaments and silk; (iii) elastomers – elastic soft tissues in the body which undergo large stretches or strains; and (iv) cellular materials – typically light-weight materials prevalent for example in feathers, wood and cancellous bone.

Upon implantation, natural-based biomaterials can be recognized by the body and process it through established metabolic pathways [29,30]. The metabolic products end up being simple sugars, amino acids or minerals. This eliminates the possibility of cytotoxic and inflammatory response from the host, a situation occurring with wear particles of long-term orthopedic joint prostheses made of metal or synthetic polymers [31]. In this regard, inspiration was found in Nature to develop new materials and new methods of processing. In particular, the scientific community has been exploiting biological systems to produce tailored materials. Such synergy between the idealized material and its final construction is the basis of Biomimetism [32,33]. This principle has already started to be applied through genetic engineering, through the construction of specific deoxyribonucleic acid (DNA) sequences in order to obtain a desired peptide [34]. Elastin-like macromolecules are one successful example of this methodology, mimicking natural elastin, which will be discussed in the following sections.

3.3 Elastin as a source of inspiration for nature-inspired polymers

Elastin is a vital biopolymer with elastic properties. It can be found in the structures that require elasticity as part of their function, stretching and relaxing more than a billion times during life [1]. For instance, the content of elastin in skin is 5–10%, in ligaments is 10–15% and in the aorta it is as high as 40–50% [35].

3.3.1 Genetic coding

The elastin gene is a single copy gene found in chromosome 7 in humans [36]. Tropoelastin is the product of this gene and the precursor of human elastin. It is a 72 kDa soluble precursor with 760 residues [37,38], and is expressed by various cell types during the pre- and neonatal stages of development, including smooth muscle [39] and endothelial cells [40], fibroblasts [41] and chondrocytes [42]. Currently, the full amino acid composition of tropoelastin is known for several species besides humans, like rats and bovines. Although some variations exist, there is still a similarity of 70% among the different tropoelastin species [36,43-46].

The elastin gene possesses 36 exons, encoding two major alternating domains: hydrophobic (responsible for elasticity) and hydrophilic crosslinking domains. The composition of the hydrophobic domains is a combination of glycine (G), valine (V), proline (P), alanine (A), leucine (L) and isoleucine (I) residues – being the first two the most abundant – often repeated in sequences of (GVGVP), (GVPGV) and (GVGVAP). The hydrophilic domains contain several lysine (K) and A residues, which show an important role in the crosslinking of tropoelastin.[1,36,47]

In order to synthesize the mature elastin, the precursor must undergo a process called elastogenesis (Figure 3.1), a highly complex phenomenon comprising all the events that lead to the synthesis of a fully functional elastic fiber [48]. The process starts with the synthesis of tropoelastin itself, in the rough endoplasmic reticulum. As soon as they are formed, a galactolectin – an elastin-binding protein – acts as a chaperone that prevents premature intracellular aggregation [48]. This association lasts until the complex is excreted into the extracellular medium. The binding protein has a higher affinity for galactosugars of the microfibrilar component of the extracellular medium. Outside the cells, the microfibrils act as scaffolds for the deposition and alignment of tropoelastin molecules, which end up cross-linked to each other in K-containing sites [49,50]. Crosslinking is the culmination of elastogenesis, resulting in mature elastin, which is insoluble but extremely stable. In fact, it is one of the most stable proteins known and has a half-life of from 40 to 70 years [51,52].

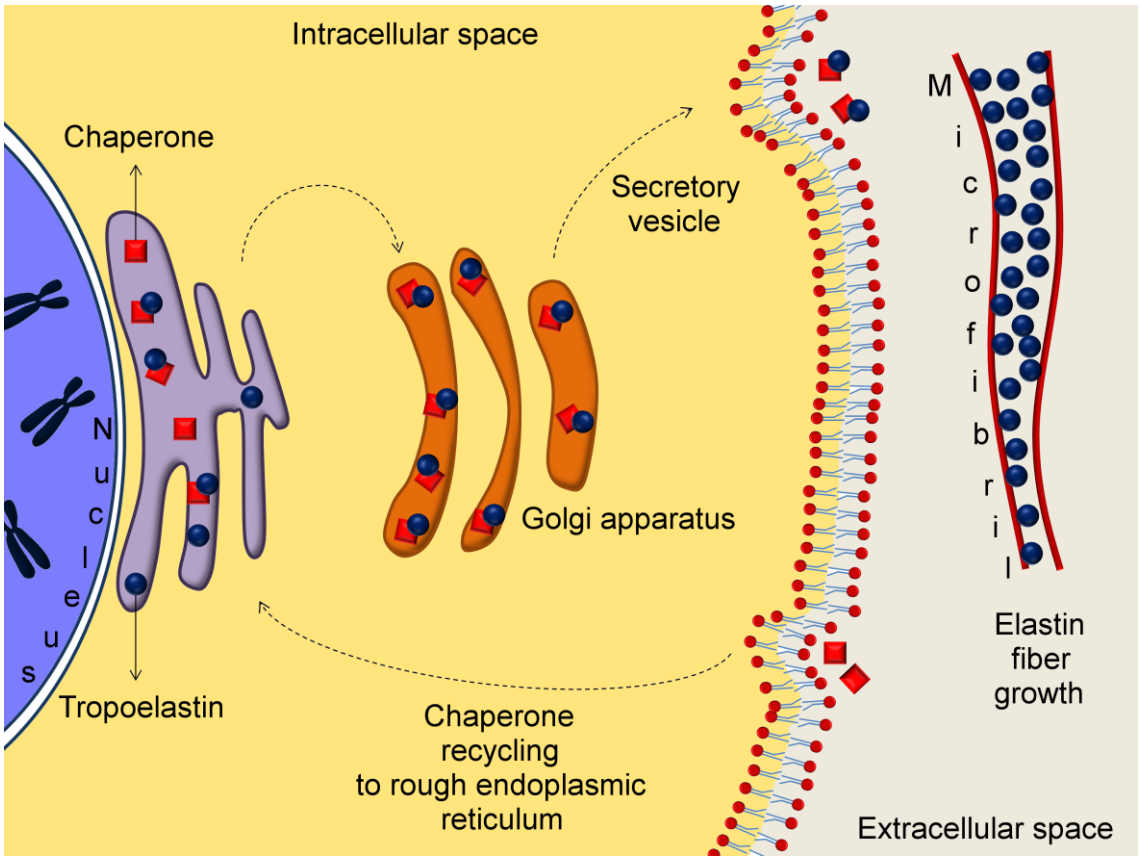


Figure 3.1. The elastogenesis phenomenon, starting by the translation of the elastin gene and proceeding to its alignment by microfibrils.

3.3.2 Characteristics of elastin

Mature elastin is an insoluble polymer composed by several or more tropoelastin molecules covalently bound to each other by crosslinks. Despite its essential hydrophobic nature, elastin can be highly hydrated by water molecules from both hydration and solvent water. In between the very rigid crosslinking domains, the hydrophobic segments exhibit a considerable mobility [36,53].

Despite several decades of research, elastin's own nature has hindered the study of its properties and structure, mostly due to the insolubility in water and backbone mobility. Nevertheless, scientists were able to obtain important knowledge regarding this polymer. For example, calorimetric studies have shown that entropy is the primary source of its remarkable elasticity and swelling capability *in vivo* [54-56].

There are two main models that attempt to explain elastin's behavior: the single-phase model (also known as random-chain model) and the two-phase model. The latter can be further divided into the liquid-drop and the oiled-coil models. The single-phase model considers elastin to be like a typical rubber with randomly distributed polymeric chains in any solvent system [55,57]. The two-phase

models state that water-swollen elastin is composed of hydrophobic domains between cross-linked proteins and the aqueous solvent is driven to the spaces between its domains. Specifcally, the liquid-drop model [58] assumes that the peptide segments between the crosslinks are globular domains. The oiled-coil model [59] is similar to the liquid-drop model, but assumes that the so called "oiled-coils" are broader in comparison and composed of a series of β-turns between the crosslinking domains.

Unfortunately, none of the models described provide sufficient insight regarding the molecular basis for its elastomeric properties at atomic level. The groups of Urry and Tamburro carried out a variety of physical-chemical studies using synthetic elastin-based pentapeptides to investigate the relationship between its structure and function [4,56,60,61]. Their studies led to the conception of yet another two-phase perspective: the β-spiral or fibrillar model, stating that there is one type II β-turn per pentameric unit, stabilized by intra-spiral, inter-turn, and inter-spiral hydrophobic contacts. The repetition of this conformational unit results in an organized helical arrangement called the β-spiral, hence the name of the model.

3.3.3 Elastin disorders

Mutations involving elastic fibers are important for understanding the function of elastin and the process of elastogenesis and associated disorders. Congenital supravalvular aortic stenosis (SVAS) is a pathological condition associated with a mutation in the elastin gene. The symptom is the obstruction of the outflow from the left ventricle narrowing of the arterial lumen, due to a failure to regulate cellular proliferation and matrix deposition of elastin [62-64]. At the molecular level, the cause is a lack of some crosslinking domains or deficient coacervation of tropoelastin molecules [62,65]. SVAS can be inherited as an autosomal dominant trait or as part of the Williams' syndrome, a developmental disorder involving the central nervous system and the connective tissues [66]. Another pathology linked to the elastin gene is cutis laxa, a rare autosomal dominant disease caused by abnormally branched and fragmented elastic fibers with reduced tropoelastin deposition in the elastic fibers and few microfibrills in the dermis. The symptoms are inelastic loose-hanging skin, hernias, and emphysema [67,68]. Changes in other molecules found in elastic fibers may also result in deficient elastogenesis or abnormal structures. Marfan's syndrome, for example, is an autosomal dominant disorder associated with mutations in the gene encoding fibrillin-1, characterized by pleiotropic manifestations in the ocular, skeletal, and cardiovascular systems [69].

3.3.4 Current applications of elastin as biomaterials

Elastin can be used as a biomaterial in different forms. It can be found in its insoluble form in purified elastin preparations, or it can be hydrolyzed to obtain soluble elastin ones. One problem associated with elastin use in biomedical devices is calcification because it serves as a nucleation site for mineralization, a problem to be considered especially in cardiovascular implants. Fortunately, it can be controlled by using molecules that prevent calcification, like ethanol/ ethylenediamine tetraacetic acid (EDTA) treatments or the addition of glycosaminoglycans or basic fibroblast growth factor [70-72].

Naturally, elastin can be found also in autografts, allografts, xenografts and decellularized ECM's. Well-known examples are split-skin autografts for burn wounds, autologous saphenous veins and umbilical vein allografts for coronary artery bypass graft surgery, and aortic heart valve xenografts. Incorporation of elastin in biomaterials is especially significant when its elasticity or biological effects can be exploited.

3.3.4.1 Skin

Skin is the largest organ of the human body. It is composed by two layers: epidermis and the dermis, which lay on subcutaneous fat. The epidermis consists mainly of layers of keratinocytes scattered with other cell types, among them melanocytes and Langerhans cells. It is separated from the dermis by the basement membrane. The dermis is comprised of papillary and reticular compartments which contain an ECM made of collagen, reticulum fibers, elastin, and glycosaminoglycans. The cellular constituents are mainly fibroblasts [73,74].

Skin substitutes are usually applied to treat either burn or chronic wounds. There are several commercial solutions currently available, like Apligraf®, among others [75]. Apligraf® is a type I collagen gel cultured with human neonatal foreskin dermal fibroblasts and keratinocytes, and has been used for the treatment of venous leg [76] and diabetic foot ulcers [77]. Like others, it contains little elastin, so autologous skin grafting is still the gold standard for skin substitutes. Other solutions have still been investigated. Hafemann *et al.* [78] developed a membrane of collagen and elastin of porcine origin to serve as a matrix for neo-dermis growth with acceptable morphology and function. Using rats as animal models, these membranes showed complete vascularization and colonization with fibroblasts and cells from the immune systems within three weeks.

More recently, Nillesen *et al.* [79] designed an acellular double-layered skin construct, both cross-linked, to improve wound regeneration. The epidermal layer was essentially made of collagen containing heparin and a fibroblast growth factor (FGF) 7 to stimulate the proliferation of keratinocytes. The dermal

layer was porous and consisted of type I collagen fibrils, solubilized elastin from equine ligamentum nuchae, dermatan sulfate, heparin, FGF-2 and vascular endothelial growth factor (VEGF). Using a rat model, and in comparison to another commercial skin substitute, Integra®DRT, the double-layered construct showed more cell influx, significantly less contraction and increased blood vessel formation at early time points. As late as 112 days, it also contained the most elastic fibers and hair follicle- and sebaceous gland-like structures could be identified. This work addressed a current problem of wound closure, which requires minimal contraction, vascularization, and elastogenesis in the early stages.

3.3.4.2 Vascular constructs

Type I collagen and elastin are the main components present in the arterial wall matrix supplying the artery with strength and elasticity, respectively. Blood vessels are structured in three layers: intima, media and adventitia. In the typical three-layered architecture, elastin is found in the intimal and medial layers. Collagen is also found in the media and adventitia sites [80,81].

Coronary artery and peripheral vascular diseases cause high mortality in western societies. The conventional treatment is surgery to restore blood flow using autologous vessels or valves [80,82]. Although autologous vessels remain the standard for small diameter grafts, many patients do not have a vessel suitable for grafting because of vascular disease, amputation, or previous harvest. Artificial grafts made from expanded poly(tetrafluoroethylene) (ePTFE) or Invista Dacron® are an alternative option [83,84], but for smaller vessels (diameter less than 5 mm) the possible formation of clots from thrombotic events may rapidly close them. In the past two decades, tissue-engineered solutions have emerged, using elastin as a crucial ingredient. Stitzel *et al.* [85] have developed vascular graft scaffolds fabricated by electrospinning using polymer blends of type I collagen from calf skin, elastin from bovine neck ligament, and poly (D,L-lactide-*co* -glycolide) (PLGA). The scaffolds were tested both *in vitro* and *in vivo*, using a mice model, and showed an absence of elicit local and systemic toxic effects. They also possessed a tissue composition and mechanical properties similar to that of native vessels. Koens *et al.* [80] developed a triple layered construct consisting of an inner layer of elastin fibers, a middle (porous) film layer of collagen fibrils and an outer scaffold layer, also made of collagen. The substitute did not evoke platelet aggregation *in vitro*. The structure could also be sutured and was considered adequate for *in vivo* application.

3.4 Nature-inspired biosynthetic elastins

Typically, aggressive methods of extraction are used to isolate elastin from tissues. Those can comprise the use of 0.1 M sodium hydroxide (NaOH) at 98°C, or autoclaving [86,87]. More recent approaches follow stepwise protocols under mild conditions by peptide-bond cleavage [88]. However, the yield of these approaches is usually low. Based on the exploitation of biological systems, one was developed that helps addressing this problem by the production of tailored molecules mimicking natural elastin through genetic engineering. The pentapeptide poly(VPGVG) was the first to be extensively studied, for being the most abundant sequence in natural elastin, but variations of this model soon followed. It was possible to produce recombinant peptides with precision over the primary amino acid content, being able to introduce relevant functional sequences, for example to improve cell adhesion, trigger biomineralization and vascularization. Due to their characteristics and peptide sequence, these molecules are known as elastin-like recombinamers (ELRs), a recombinant class of elastin-like polymers (ELPs) [15].

3.4.1 General properties of elastin-like recombinamers

ELRs are a promising class of biocompatible protein-based polymers inspired in the mammalian elastin protein sequences, or modifications thereof [4,34,89]. In aqueous solution and below a certain transition temperature (T_t), the free polymer chains are disordered, consisting in fully hydrated random coils, mainly by hydrophobic hydration. This kind of hydration is characterized by ordered clathrate-like water structures surrounding the nonpolar moieties of the polymer with a structure somewhat similar to that described for crystalline gas hydrates, although a more heterogeneous one that varies in terms of perfection and stability [4,13]. When the temperature is increased above T_t, the structure loses the water molecules from hydrophobic hydration and the chains fold and assemble. A phase-separated state is formed, consisting of 63% water and 37% polymer, in weight. In this self-assembled separated state, the chains adopt a regular non-random structure known as β-spiral conformation [60,61,90].

Urry studied this phenomenon and stated that a polypeptide with a correct balance of polar and nonpolar amino acids can be soluble in water at low temperatures, yet undergoing a phase separation from the aqueous medium upon raising temperature [91]. In the latter case, the structures assemble into anisotropic fibers due to hydrophobic associations between the β-spirals. This folding is completely reversible if the temperature of the sample is decreased again below T_t [4,34]. This transition phenomenon is called inverse temperature transition (ITT) and has become the key issue in the

development of new peptide-based polymers as molecular machines and materials [92]. Although the phenomenology of ELRs is similar to that of amphiphilic polymers with a lower critical solution temperature (LCST), the presence of an ordered state above the T_t led to the usage of the term "inverse temperature transition" as a descriptive term for these polymers' behavior [92,93].

The self-assembly of ELRs is also dependent on others factors and external stimuli besides temperature. There is a strong dependence of the T_t on concentration in the range of 0.01 to 5–10 $mg.mL^{-1}$, showing a decrease in T_t with increasing macromolecule concentration, due to the facilitated aggregation of molecules in higher number [13,34]. Above this range, the T_t does not show further significant changes with increasing concentrations up to 150–200 $mg.mL^{-1}$ [13,94]. Increasing the ionic strength of an ELR solution also influences the T_t and is particularly useful to trigger the ITT phenomenon when its concentration is low. Reguera *et al.* [95] suggested that an increase in the salt concentration increases the polarity of the solvent. This creates a higher difference in polarity with respect to the hydrophobic moieties of the polymer, recruiting more and more ordered water molecules to surround the polymer chains. Increasing the molecular weight of the ELR has also been demonstrated to decrease the T_t [96,97]. ELRs can be modified in order to exhibit smart behavior towards other stimuli. By modifying the composition of the polymer it is possible to conceive materials that react to stimuli like pH, redox reactions and even light [90,98,99].

Some ELR systems have been developed, being successful in maintaining some of the main characteristics of natural elastin. For example, the cross-linked matrices of these polymers retain most of the mechanical properties of elastin [100,101], which becomes important when this behavior is accompanied by other interesting properties, such as biocompatibility, stimuli-responsive behavior, and the ability to self-assemble.

3.4.2 The principle of genetic engineering – a powerful tool for engineering materials

In the last decade protein biosynthesis showed the ability to directly produce high molecular weight polypeptides of exact amino acid sequence with high fidelity. Its usefulness to biosynthesize ELRs proceeds with near-absolute control of their macromolecular architecture in size, composition, sequence, topology, and stereochemistry [102,103]. There are a few limitations, however, in respect to the sequence and its final properties. In the general model (VPGXG), X does not support proline.[15,104] Substitution of amino acids in other positions is also limited. For example,

poly(APGVG) becomes an irreversible granular precipitate instead of a reversible viscoelastic coacervate upon increasing the temperature [105].

Recombinant DNA technology and bacterial protein expression have been employed for the biosynthesis of repetitive polypeptides based on the 20 naturally occurring amino acids with no direct parallels in Nature [91,102,106]. It is a technology that clearly opens infinite possibilities, with far more potential than most common synthetic ways of production, limited only by the living molecular machinery itself. Urry has presented five essential axioms to conceive protein-based macromolecules capable of undergoing hydrophobic folding and assembly due to inverse temperature transitions, presented in Figure 3.2. Shortly, the axioms describe that the ITT depends on an ELR aminoacid composition and that external factors can also influence its conformation and T_t.

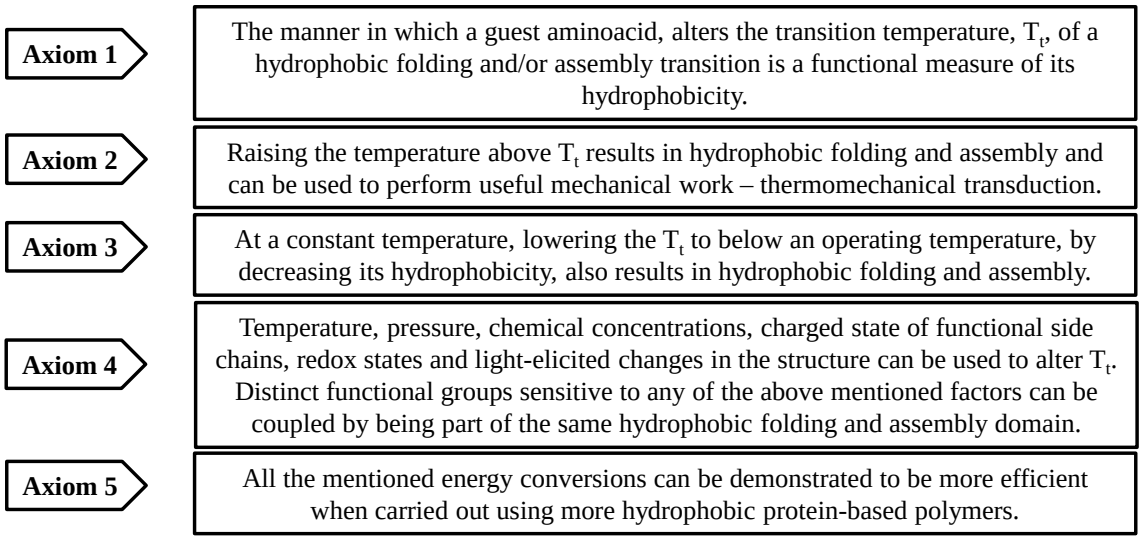


Figure 3.2. The five axioms of elastin-like recombinamers, according to Urry [10].

Typically, ELRs are produced by *Escherichia coli* strains through bacteria fermentation, accounting for nearly 80% of the cell's volume by the end of the process within cytoplasmatic inclusion bodies. It can achieve low production costs by producing an elastin sequence via the machinery of living cells, independently of its complexity. The production cost of those materials is not related to their complexity since the most costly task in terms of both time and money is the gene construction. However, once the plasmid is inserted in the microorganism genetic information, the fast and cheap production of the polymer rapidly compensates for the costs associated with the molecular biology steps. This intrinsic advantage also has environmental benefits, since recombinant protein-based materials are obtained by

an easily scalable technology fermentation that uses only moderate amounts of energy and temperatures, with water as the only solvent [15,91,107,108].

3.4.3 From genetic construction to molecules with tailored bio-functionality

The design of an appropriate strategy at the gene level is critical for the efficient synthesis of the protein encoding sequence and to produce a uniform protein product with an optimal quality and yield. The biosynthesis of any artificial protein generally includes: (i) design and construction of a coding synthetic gene for the protein of interest in a plasmid with close transcription control; (ii) the cloning of a recombinant gene with the necessary transcriptional regulatory elements into competent host cells; (iii) the screening of plasmids containing the desired clones and verification of their DNA sequence; (iv) transformation of the chosen plasmids into expression-competent host cells; (v) the growth of appropriate volumes of host cells and induction of protein expression; and (vi) purification of the protein of interest from cell lysates [109].

Molecular biology techniques are typically employed to self-ligate monomer DNA fragments in an oligomerization process that relies on restriction-enzyme-based approaches when designing genes that encode repetitive recombinamers. In this case, the monomeric fragments must be oligomerized in a "head-to-tail" orientation and can either be seamless in sequence or contain intervening linkers between the desired repeats. Approaches to oligomerization can be classified as: (i) iterative, where a DNA segment is oligomerized in a series of single, uniform steps. Each step extends the oligomer by one unit of length of the monomer gene; (ii) random method or "concatemerization", where an uncontrolled number of monomer DNA segments are oligomerized in a single step to create a population of oligomerized clones with different lengths. This method creates a library of genes of different lengths that encode oligomeric polypeptides with the same repeat sequences but sacrifices the precision of the oligomerization process; finally, (iii) recursive directional ligation (RDL), an alternative method in which DNA segments with two different restriction sites flanking the insert are joined in sequential steps, with the length of the ligated segments growing geometrically in each step. This approach is suitable for the synthesis of repetitive polypeptides with a specific and predetermined chain length as it seamlessly joins the two monomeric inserts and also eliminates the restriction sites placed at either end of the dimerized gene [110].

An obvious disadvantage of oligomerization would seem to be the incapability to generate biopolymers with unnatural aminoacids, such as those not encoded by conventional codons or ones containing

chemical modifications, cyclic aminoacids, aromatic amino acids or β-amino acids, amongst others. Fortunately, this problem can be resolved by native chemical ligation [111,112]. Recently, Liu *et al.* [113] have developed a new approach that allows incorporating unnatural amino acids to be genetically encoded in mammalian cells.

One of the main goals in the materials field is to develop materials with an increasing and programmable degree of complexity which is closely related with the application. More complex materials are capable to perform more complex and tailored functions (Figure 3.3).

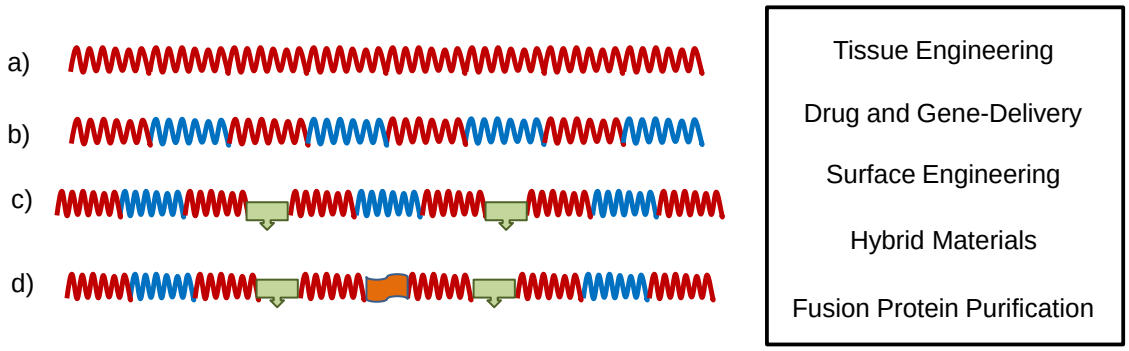


Figure 3.3. Schematic diagram of increasing complexity of ELRs with different functionality for use in various applications. Recombination techniques allow obtaining several degrees of complex: the schematic represents (a) a simple model of recombinant elastin; (b) the introduction of specific peptide sequences and blocks with distinct properties; (c) the inclusion of a bioactive motif or; (d) the inclusion of more than one in the same peptidic formulation.

The primary sequence of ELRs is responsible for the formation of well-defined secondary structures, such as α-helices, β-sheets or β-turns, assembling into supramolecular structures. Furthermore, they can be switched by several factors, such as temperature, pH and light in aqueous solution and can include crosslinking or self-assembling domains and diverse bio-functionalities along the polypeptide chain. Those may include targeting ligands, cell adhesion or specific biodegradation sequences, fluorescent or contrast agents. Combined with their good expected biocompatibility and favorable degradation rate and products, they constitute promising materials for multiple applications, with particular emphasis in biomedical and nanotechnological applications [114,115].

3.4.4 Biocompatibility of ELRs

The biocompatibility feature of ELRs, which is relevant for their use in advanced biomedical applications, was evaluated by the complete series of the American Society for Testing Materials (ASTM) generic biological tests for materials and devices in contact with tissues, tissue fluids and blood [101,116,117]. Regarding these biopolymers, it has not been possible to obtain monoclonal antibodies against them; it would seem that the immune system cannot distinguish them from the natural elastin. In a more detailed interpretation of this effect, Urry *et al.* [118] have suggested that the β-spiral strongly contributes to prevent the identification of these foreign materials by the immune system. Additionally, the secondary products of its biodegradation are just simple and natural amino acids that can be metabolized by the body to produce non-toxic degradation products. More detailed examples of their biocompatibility and multifunctional possibilities will be discussed in the next section.

3.5 ELRs as advanced materials for biomedical applications

ELRs have found widespread use due to their good biocompatibility and non-immunogenicity in the fields of drug delivery and tissue engineering. As they can be genetically synthesized, the precisely-defined molecular weight is ideal for drug delivery, because the molecular weight is a key parameter in the route of clearance from the body and *in vivo* half-life of the polymer [104]. The ability to display stimuli-driven variations in their structure as consequence of their self-assembling behavior in aqueous solution has been exploited into useful functional structures and devices combining these properties, with an adequate arrangement of specific building blocks and physicochemical and mechanical properties.

3.5.1 Tissue engineering

New classes of materials with additional tissue-specific properties or ones which could be tailored to several tissue systems are required for TERM. The ECM is an important model for the design of biomaterials. The goal of mimicking the ECM structure and biological functions requires the design of artificial scaffolds that reproduce one or, preferably, more properties and functionalities of the natural tissue [119,120]. The scaffold must be biocompatible and biodegradable and it should own properties that support tissue morphogenesis. This generally requires a multifunctional artificial ECM that can supply temporary mechanical support until the engineered tissue has sufficient mechanical integrity to

support itself. Future advances in tissue engineering will depend on the development of biomimetic materials that actively participate in the formation of new functional tissues [27].

Recombinant DNA technologies allow designing and expressing artificial genes to prepare artificial analogues of ECM proteins with controlled mechanical properties that incorporate domains to modulate cell behavior. Crosslinked ELRs of poly(VPGVG) resulted in a matrix showing a mechanical response similar to the natural elastin [116], which is an important factor to provide a structural basis that properly transmits the forces from the environment to the growing tissue. However, these cross-linked matrices showed anti-fouling properties limiting cell adhesion. Although lacking bio-functionality that would promote unspecific cell adhesion, the poly(VPGVG) concept matrix was used as starting material with good mechanical and biocompatible properties, and short peptides having specific bioactivities were inserted into the polymer chain, even though by chemical synthesis. Once genetic engineering techniques became the production method of choice, the molecular design started to increase in complexity. To increase the complexity of ELRs, a simple substitution of the amino acid X in the elastin repeated unit (VPGXG) results in the addition of cross-linking domains to obtain more stable substrates, which are usually based on lysine residues [2,121-123].

Several modular ELRs have been designed to include bioactive peptides into the polymer chain such as the well-known, general purpose cell-adhesion sequence RGD [124], found in several ECM proteins [18,125-127], and arginine-(glutamic acid)-(aspartic acid)-valine (REDV) [128], included in the CS5 domain of fibronectin and specific for endothelial cells [17,129]. An extra feature – namely degradation responsiveness – has been included into more advanced versions of ELRs for tissue repair to allow the renovation and replacement of natural ECM by living tissue [17,130]. In this regard, ELR-hydrogels have been obtained by different cross-linking methods such as photo-initiation [131], irradiation [132], or enzymatic cross-linking [121]. The physical properties can be tuned by the cross-linking conditions and degree, while retaining the stimuli-responsive behavior. This way, appropriate bioactive substrates can be obtained for a wide range of applications. Highly porous hydrogels have been conceived by chemical cross-linking of ELRs containing REDV sequence: a salt leaching/gas foaming was performed to obtain suitable 3D scaffolds promoting infiltration of human umbilical vein endothelial cells (HUVECs) inside the porous network (Figure 3.4) [133].

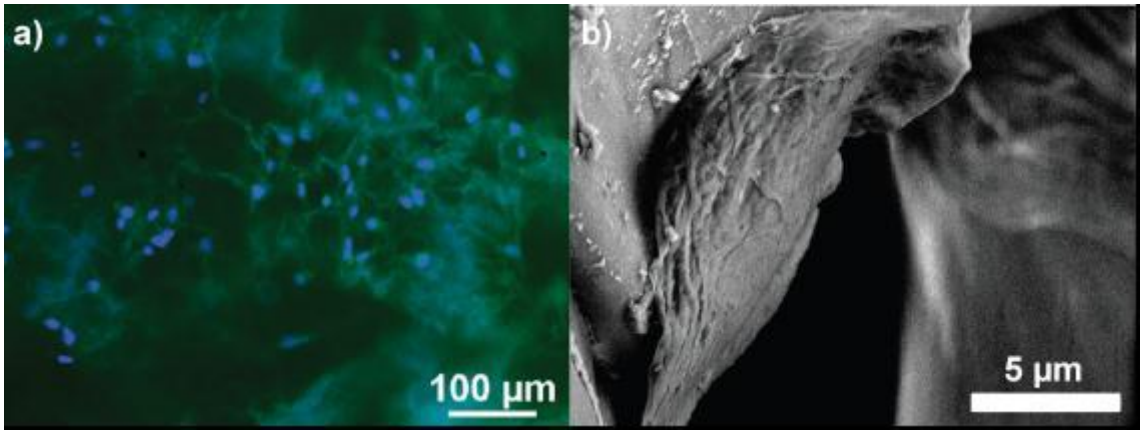


Figure 3.4. Microscopy assessment of HUVECs seeded in macroporous ELP hydrogels after 48 h of incubation in: (a) fluorescence microscopy with phalloidin Alexa Fluor488 and 4',6-diamidino-2-phenylindole (DAPI) staining; and (b) SEM magnified view. Reprinted (adapted) with permission from [133]. Copyright 2009 American Chemical Society.

Another potential application of these bioactive ELRs is the preparation of films to be used for ocular surface tissue engineering [134,135]. Recently, Srivastava *et al.* [135] have successfully investigated the use of ELRs as a substrate to maintain the growth, phenotype, and functional characteristics of retinal pigment epithelial cells *in vitro* to obtain a suitable carrier for transplantation in the treatment of age-related macular degeneration.

Hybrid scaffolds composed of collagen and different proportions of this ELR-REDV have been obtained by enzymatic cross-linking by tissue transglutaminase, affecting physical properties such as porosity, thermal behavior and mechanical strength. Such approach led to a differential colonization of the scaffolds with diverse cell lines, which is very useful for vascular-tissue and skin-wound healing [121]. Other complex hybrid scaffolds were created to obtain an acellular arterial substitute as artificial vessel-like platforms: they were produced by the combination of several layers of an ELR matrix reinforced with collagen microfibers, resulting in constructs with appropriate mechanical properties, such as compliance or suture retention strength [136]. Other types of smart bilayer scaffolds of an ELR containing RGD and collagen have also been investigated – foams, fibers and foam-fiber bilayer scaffolds [137]. The study of the structural and mechanical properties indicated that the incorporation of ELRs into the scaffold improved the uniformity of the pore network and decreased the fiber diameter. The culture of human fibroblasts and epithelial cells in these scaffolds showed the positive contribution of the bioactive ELR on the proliferation of both cell types, compared to a collagen foam. These results were promising for the reconstruction of full-thickness skin and oral mucosa equivalents.

Other strategies consist in the incorporation of ELR coatings onto different materials to improve cell attachment or stimuli-responsiveness. Barbosa *et al.* [138] developed chemically cross-linked chitosan hydrogels with an ELR coating containing an osteoconductive sequence inducing precipitation of calcium phosphate when the gels were soaked in simulated body fluid. More recently, an ELR incorporating octaglutamic acid with well-defined charged backbone has been used to design multifunctional bone cements resulting in materials with hydroxyapatite binding ability and improved mechanical strength [139]. Prieto *et al.* [140] have designed a set of ELRs containing the SN_A15 statherin analog domain. *In vitro* mineralization showed interesting results in the effect of the ELR composition as a key parameter to control the calcium phosphate nucleation. These studies show the high potential of ELRs for biomedical hybrid materials development.

Another attractive alternative is based in the thermal behavior of modular amphiphilic ELRs to form *in situ* stable gels under physiological conditions [141,142]. They constitute low viscosity solutions below their T_t and form physically cross-linked hydrogels by self-assembling that are suitable for fixing materials and biological elements in specific sites in the body through minimally invasive procedures. When greater mechanical integrity is desired, the mechanical properties can be enhanced by including additional chemical crosslinking domains in the ELR chain [117,143]. Sallach *et al.* [144] have also highlighted the good biocompatibility of these ELR physical gels showing a minimal inflammatory response and robust *in vivo* stability for periods exceeding 1 year. These self-gelating materials offer the possibility to obtain multifunctional bioactive versions, which can be also used as carriers for controlled drug release or as biocompatible surface coatings. Oliveira *et al.* [145] used an ELR containing the RGD cell adhesion domain to fabricate cell-induced microparticle aggregates as scaffolds for TERM. Using a SaOs-2 osteoblast-like cell line and microparticles with varying degrees of crosslinking, they have shown that for higher degrees of crosslinking the cell proliferation was more favorable and formed cell-induced aggregation scaffold.

3.5.2 Drug- and gene- delivery

Drug delivery carriers have several advantages over free drug delivery systems such as specific site targeting, sustained release, minimized systemic exposure and reduced toxicity. In order to be effective, systemic drug delivery carriers must be biocompatible and have controllable composition and molecular weight. Although a wide range of materials have been employed for controlled and targeted drug release, the most common carriers are polymeric-based systems [146,147].

ELRs exhibit several properties that can be useful for drug delivery purposes, such as precise control over molecular weight and composition, self-assembly and stimuli-responsive behavior, as well as biocompatibility, non-toxic properties and efficient pharmacokinetics. In addition, their genetic nature allows incorporating targeting ligands, cell membrane fusion sequences or reactive sites for drugs conjugation [21,148,149]. Their self-assembly can also be designed in response to an extrinsic temperature stimulus, such as the local application of heat, ultrasound or light, or intrinsic to the site environment, such as low extracellular pH or up-regulated protease expression for cancer drug delivery [150].

The ability of ELRs to form stable micro- and nano-particles that are able to trap active substances has facilitated the development of smart systems for therapeutic release. Poly(VPAVG) was shown to form stable particles in water solution with a size below 3 μm above its T_t. They exhibited hysteresis behavior and were capable of encapsulating significant amounts dexamethasone phosphate with a sustained release profile for about 30 days.[151] Later, two bone morphogenetic proteins (BMP-2 and BMP-14) were encapsulated for combined release in a sustained way for 14 days, promising for bone tissue engineering [19]. Electrospraying has been used by Wu *et al.* [152] to generate stimuli-responsive ELR nanoparticles (300–400 nm in diameter) that can encapsulate drugs. The molecular weight and solution concentration of the ELRs were found to have a significant influence on the morphology and size distribution of the nanoparticles. Doxorubicin, a cancer chemotherapeutic agent, was released by the ITT-driven solubility of the particles at 37°C. In other recent report, Dash *et al.* [153] have fabricated tunable monodispersed cross-linked ELR hollow spheres ranging from 100 nm to 1000 nm by using a template-based method. Plasmid DNA and polyplexes were efficiently loaded inside hollow spheres by diffusion and charge interactions. These polyplex-loaded spheres displayed controlled release and transfection ability in their use as gene transfection agents, with the possibility to include future functionalities to the spheres for targeted gene delivery applications.

Some of the recent studies are more focused on controlling the size and monodispersity of ELR particles, since these are two key factors in improving therapeutic efficacy. Genetic engineering of protein-based block copolymers is a suitable way to program defined polypeptide block sequences to study the influence of macromolecular architecture in the hierarchical structural organization and morphology. ELR-based amphiphilic block copolymers undergo ordered nanoscale self-assembly forming protein-like micellar systems with controlled structure and function. Strategies that describe stable monodispersed ELR particles include those of Chilkoti and co-workers [150,154,155] who fabricated sub-100 nm sized micelles conjugated to diverse hydrophobic molecules and

chemotherapeutics. The goal of these studies was to investigate the design rules for tuning the self-assembly of different ELRs forming multivalent spherical micelles within the clinically relevant hyperthermic temperature range 37 to 42°C and target cancer cells. Similarly, Kim *et al.* [156] improved the stability of micelles from ELR-diblock copolymers incorporating cysteine residues at the core-shell interface, which undergo covalent cross-linking through disulfide bond formation. Most of these studies involve diblocks, although there are some examples based on triblocks, such as one that relies upon a reversible switch of secondary structures [157]. The triblock-ELR copolymer can form monodispersed temperature-responsive micelles in dilute solutions below its T_t and an abrupt increase in the micelle compacticity with a reduction in particle size occurs upon raising the temperature.

3.5.3 Surface engineering

In the field of biomaterials science the control and modification of surfaces and interfaces has opened novel frontiers for developing advanced materials and devices with distinct and specific features for biomedical applications [158,159]. Surfaces can be functionalized by multiple approaches involving physical or chemical modifications, such as coatings and grafts. They allow introducing small biological ligands, like peptides or proteins with fouling/anti-fouling features, specific groups for cell-material interactions, smart behavior (stimuli responsive or environmentally sensitive), or micro- and nano-patterns [160-162].

Surfaces modified with stimuli-responsive polymers, called “smart surfaces”, undergo physical and chemical changes in response to external variations [163-165]. In this regard, ELRs exhibit some additional advantages that make them excellent candidates for the development of smart surfaces: their stimuli-responsive behavior can depend on other factors such as pH, light, or ionic strength, amongst others. Genetic engineering also allows for a precise control of the reactive sites on the polypeptide chain for use in surface grafting, leading to an extensive potential of the self-assembly exhibited by these polymers. Biosensing surfaces displaying topologically modified self-assembly with ELRs have been developed by Chilkoti’s group. The “thermodynamically reversible addressing of proteins” (TRAP) technology obtained by covalent micro-patterning of ELRs onto glass surfaces against an inert background allows a reversible, spatio-temporal modulation of ligand-binding triggered by the phase transition of the ELR at a solid-liquid interface. Such technology can be applied in different systems for bio-analytical sensors in order to detect single biomolecules [159,164]. Fluorophore-labeled glutamine binding proteins (QBPs) and derivatives - which can be coupled to a designed hydrophobic polypeptide - can be constructed and adhered onto solid surfaces [166]. Another novel fusion protein for controlling

cellular functions combines the RGD sequence, epidermal growth factor (EFG), and a hydrophobic sequence into a single molecule: it was shown to exhibit both cell-adhesive and growth-factor activity. In addition, the hydrophobic sequence contributed to self-assembly of the RGD, retaining its activity on a solid-phase surface and proving its use for wound healing [167].

For tissue engineering, novel temperature-responsive culture surfaces coated with ELR has been developed for cell harvesting. By reducing the temperature using a polyvinylidene difluoride (PVDF) membrane, the cell sheet was detached from the coated surface and subsequently transferred to new surfaces, suggesting its potential for the fabrication of multilayer cell sheets for transplantation.[24] For bone tissue engineering, an ELR-RGD has been adsorbed onto micro-patterned poly(*N* -isopropyl acrylamide) films displaying a positive maintaining of the cell attachment in the scaffolds under dynamic culture conditions [168]. Na *et al.* [169] have also developed a lysine-containing ELR conjugated onto aldehyde-glass surface by micro-patterning. The sharp and controllable phase transition of ELR enabled reversible cell adhesion on the surface by changing the temperature or salt concentration, demonstrating potential applications for cell-based micro-devices.

Other techniques using ELRs include the alternating adsorption of polyelectrolytes. This is a simple technique for generating bioactive surfaces, driven by complementary forces occurring between two distinct materials [170]. These ultra-thin nanoscale coatings promote cell adhesion and proliferation and the results show that the thickness and mechanical integrity of the multilayer assembly modulates the cell response. Swierczewska *et al.* [170] have reported the use of ELRs – modified either with poly(ethyleneimine) (PEI) or poly(acrylic acid) (PAA) to provide positive or negative charge, respectively – to conceive films in a sequential fashion. Another similar work described a similar approach but with ELRs containing negatively charged residues [171]. Costa *et al.* also reported the construction of thin coatings [172] and nanostructured multilayers [173] made of chitosan and RGD-containing ELRs with smart properties towards temperature and pH (Figure 3.5) and also improved cell adhesion. These examples opened up a field where polymeric coatings include specific biofunctional responses.

Progress in the last few years combining surface chemistry with microfabrication techniques has provided new tools to study cell-material interactions with their environment. Using lithography and patterning techniques, peptides and proteins can be deposited with absolute spatial control on specific regions of a surface [174,175].

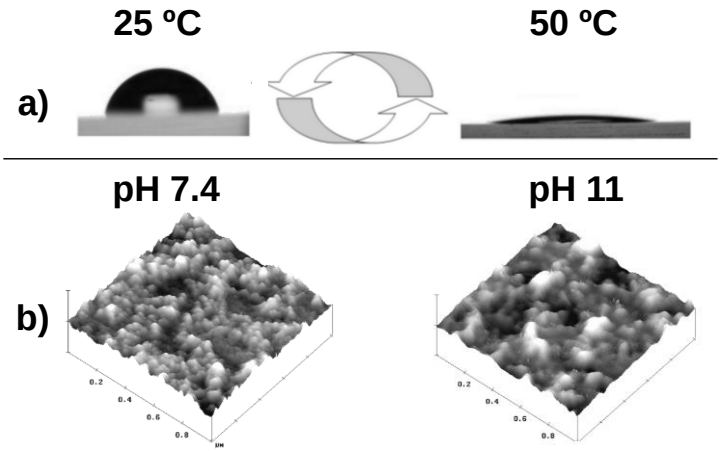


Figure 3.5. Physical changes induced in ELR modified surfaces. (a) Wettability variations with different temperatures. Reprinted (adapted) with permission from [172]. Copyright 2009 Wiley-VCH. (b) Topography at distinct pHs. Reprinted (adapted) with permission from [173]. Copyright 2011 Wiley-VCH.

The ability to obtain nano- and micro-structured surfaces of patterned biomacromolecules is of great importance for several applications, including biological assays, miniaturized biosensors, and biomedical diagnostics. In this regard, ELRs have been employed in the design and development of biosensors and microfluidic bioanalytical devices, as reported by Nath and Chilkoti [176]. Nanostructured surfaces taking advantage of the self-assembly properties of ELRs have been obtained for capturing and releasing proteins by combining ELRs and dip-pen nanolithography.

Recently, the replica molding method has been adapted to obtain 3D micro-structured thermo-responsive ELR hydrogels by Martín *et al.* [123]. In this study, the thermally responsive behavior of macroscopic and micro-patterned features with different dimensions and spacing was studied, showing dimensional changes with no alteration of the topography. This feature could be used during cell culture adjusting the T_t in the correct range to study cell behavior by changing the dimensions of the micro-pattern and subsequent mechanical properties.

3.6 Conclusions

Elastin is the root of inspiration for a class of versatile materials with physical and biological properties of great interest for TERM applications. The cumulative studies of elastin and elastin-like macromolecules now provide the required background for understanding in more detail structure-related aspects of such biomaterials from a functional point of view.

Taking advantage of genetic recombination approaches, one can easily "engineer" a peptide-based macromolecule exhibiting characteristics that can be tuned for specific fields: skin substitutes, vascular constructs, drug delivery devices and functional interfaces. Their functionality can be further expanded by adding sequences with biological relevance to the common elastin structure, like cell adhesion-, tissue-specific- and degradation-motifs. Complex, well-defined and tailored polymers can be obtained with a wide range of properties and possibilities for new devices. One could say that such degree of complexity is only limited by the imagination of the scientist: it still needs to be faithful to the original properties of elastin-like macromolecules, though, since an unfavorable modification can lead to a non-functional polypeptide.

The study and use of elastin-like macromolecules is leading to the design of new cutting-edge and more complex ones emerging as promising candidates for future treatments. Their smart behavior and self-assembly properties may be exploited for further tuning and ultimate control of the performance of an elastin-based system, like how a specific cell phenotype will bind to a substrate, or how an active agent will be released under stimuli variations and biological conditions.

3.7 Acknowledgements

We acknowledge financial support from the Portuguese Fundação para a Ciência e Tecnologia – FCT (grant SFRH/BD/61126/2009), Fundo Social Europeu – FSE, Programa Diferencial de Potencial Humano/POPH, the European Commission through the 7th Framework Programme (projects HEALTH-F4-2011-278557 and NMP3-LA-2011-263363), from the Spanish Minister of Economy and Competitiveness – MEC (projects MAT2009-14195-C03-03, MAT-2010-15982, MAT2010-15310, IT2009-0089, ACI2009-0890 and PRI-PIBAR-2011-1403), the Junta de Castilla y León -JCyL (projects VA034A09 and VA0049A11-2), the CIBER-BBN (project CB06-01-1038), and the JCyL and the Instituto de Salud Carlos III under the "Network Center of Regenerative Medicine and Cellular Therapy of Castilla and León".

3.8 References

[1] Almine J. F., Bax D. V., Mithieux S. M., Nivison-Smith L., Rnjak J., Waterhouse A., Wise S. G., and Weiss A. S., Elastin-based materials, Chemical Society Reviews 2010, 39: 3371-3379.

[2] Nowatzki P. J., and Tirrell D. A., Physical properties of artificial extracellular matrix protein films prepared by isocyanate crosslinking, Biomaterials 2004, 25: 1261-1267.

[3] Trabbic-Carlson K., Setton L. A., and Chilkoti A., Swelling and Mechanical Behaviors of Chemically Cross-Linked Hydrogels of Elastin-like Polypeptides, Biomacromolecules 2003, 4: 572-580.

[4] Urry D. W., Molecular machines: how motion and other functions of living organisms can result from reversible chemical changes, Angewandte Chemie International Edition in English 1993, 32: 819-841.

[5] Urry D. W., and Parker T. M., Section: Extracellular matrix proteins; Mechanics of elastin: molecular mechanism of biological elasticity and its relationship to contraction, Journal of Muscle Research and Cell Motility 2002, 23: 543-559.

[6] Welsh E. R., and Tirrell D. A., Engineering the Extracellular Matrix: A Novel Approach to Polymeric Biomaterials. I. Control of the Physical Properties of Artificial Protein Matrices Designed to Support Adhesion of Vascular Endothelial Cells, Biomacromolecules 2000, 1: 23-30.

[7] Gigante A., Chillemi C., Bevilacqua C., Greco F., Bisaccia F., and Tamburro A. M., Effects of elastin-derived peptide on Achilles' tendon healing: An experimental study, Journal of Materials Science: Materials in Medicine 2003, 14: 717-720.

[8] Ito S., Ishimaru S., and Wilson S. E., Effect of Coacervated α-Elastin on Proliferation of Vascular Smooth Muscle and Endothelial Cells, Angiology 1998, 49: 289-297.

[9] Leach J. B., Wolinsky J. B., Stone P. J., and Wong J. Y., Crosslinked α-elastin biomaterials: towards a processable elastin mimetic scaffold, Acta Biomaterialia 2005, 1: 155-164.

[10] Urry D. W., Asima P., Xu J., Woods T. C., McPherson D. T., and Partker T. M., Elastic protein-based polymers in soft tissue augmentation and generation, Journal of Biomaterials Science, Polymer Edition 1998, 9: 1015-1048.

[11] Meyer D. E., and Chilkoti A., Quantification of the Effects of Chain Length and Concentration on the Thermal Behavior of Elastin-like Polypeptides, Biomacromolecules 2004, 5: 846-851.

[12] Mithieux S. M., Rasko J. E. J., and Weiss A. S. A. S., Synthetic elastin hydrogels derived from massive elastic assemblies of self-organized human protein monomers, Biomaterials 2004, 25: 4921-4927.

[13] Rodríguez-Cabello J. C., Alonso M., Pérez T., and Herguedas M. M., Differential scanning calorimetry study of the hydrophobic hydration of the elastin-based polypentapeptide, poly(VPGVG), from deficiency to excess of water, Biopolymers 2000, 54: 282-288.

[14] Sciortino F., Urry D. W., Palma M. U., and Prasad K. U., Self-assembly of a bioelastomeric structure: Solution dynamics and the spinodal and coacervation lines, Biopolymers 1990, 29: 1401-1407.

[15] Rodríguez-Cabello J. C., Martín L., Alonso M., Arias F. J., and Testera A. M., "Recombinamers" as advanced materials for the post-oil age, Polymer 2009, 50: 5159-5169.

[16] Arias F., Reboto V., Martín S., López I., and Rodríguez-Cabello J., Tailored recombinant elastin-like polymers for advanced biomedical and nano(bio)technological applications, Biotechnology Letters 2006, 28: 687-695.

[17] Girotti A., Reguera J., Rodríguez-Cabello J., Arias F., Alonso M., and Testera A., Design and bioproduction of a recombinant multi(bio)functional elastin-like protein polymer containing cell adhesion sequences for tissue engineering purposes, Journal of Materials Science: Materials in Medicine 2004, 15: 479-484.

[18] Nicol A., Channe Gowda D., and Urry D. W., Cell adhesion and growth on synthetic elastomeric matrices containing ARG-GLY–ASP–SER–3, Journal of Biomedical Materials Research 1992, 26: 393-413.

[19] Bessa P. C., Machado R., Nürnberger S., Dopler D., Banerjee A., Cunha A. M., Rodríguez-Cabello J. C., Redl H., van Griensven M., Reis R. L., and Casal M., Thermoresponsive self-assembled elastin-based nanoparticles for delivery of BMPs, Journal of Controlled Release 2010, 142: 312-318.

[20] Dreher M. R., Raucher D., Balu N., Michael Colvin O., Ludeman S. M., and Chilkoti A., Evaluation of an elastin-like polypeptide-doxorubicin conjugate for cancer therapy, Journal of Controlled Release 2003, 91: 31-43.

[21] Furgeson D. Y., Dreher M. R., and Chilkoti A., Structural optimization of a "smart" doxorubicin-polypeptide conjugate for thermally targeted delivery to solid tumors, Journal of Controlled Release 2006, 110: 362-369.

[22] Betre H., Setton L. A., Meyer D. E., and Chilkoti A., Characterization of a Genetically Engineered Elastin-like Polypeptide for Cartilaginous Tissue Repair, Biomacromolecules 2002, 3: 910-916.

[23] McHale M. K., Setton L. A., and Chilkoti A., Synthesis and in Vitro Evaluation of Enzymatically Cross-Linked Elastin-Like Polypeptide Gels for Cartilaginous Tissue Repair, Tissue Engineering 2005, 11: 1768-1779.

[24] Zhang H., Iwama M., Akaike T., Urry D. W., Pattanaik A., Parker T. M., Konishi I., and Nikaido T., Human Amniotic Cell Sheet Harvest Using a Novel Temperature-Responsive Culture Surface Coated with Protein-Based Polymer, Tissue Engineering 2006, 12: 391-401.

[25] Ashby M. F., and Jones D. R. H., Engineering Materials 2: An Introduction to Microstructures, Processing and Design, Oxford, United Kingdom: Elsevier; 2006.

[26] Meyers M. A., Chen P.-Y., Lin A. Y.-M., and Seki Y., Biological materials: Structure and mechanical properties, Progress in Materials Science 2008, 53: 1-206.

[27] Langer R., and Tirrell D. A., Designing materials for biology and medicine, Nature 2004, 428: 487-492.

[28] Wegst U. G. K., and Ashby M. F., The mechanical efficiency of natural materials, Philosophical Magazine 2004, 84: 2167-2186.

[29] Mano J. F., Silva G. A., Azevedo H. S., Malafaya P. B., Sousa R. A., Silva S. S., Boesel L. F., Oliveira J. M., Santos T. C., Marques A. P., Neves N. M., and Reis R. L., Natural origin biodegradable systems in tissue engineering and regenerative medicine: present status and some moving trends, Journal of The Royal Society Interface 2007, 4: 999-1030.

[30] Nair L. S., and Laurencin C. T., Biodegradable polymers as biomaterials, Progress in Polymer Science 2007, 32: 762-798.

[31] Anderson J. M., Biological Responses to Materials, Annual Review of Materials Research 2001, 31: 81-110.

[32] Hubbell J. A., Biomaterials in Tissue Engineering, Nature Biotechnology 1995, 13: 565-576.

[33] Sanchez C., Arribart H., and Giraud Guille M. M., Biomimetism and bioinspiration as tools for the design of innovative materials and systems, Nature Materials 2005, 4: 277-288.

[34] Rodríguez-Cabello J., Reguera J., Girotti A., Arias F., and Alonso M., Genetic Engineering of Protein-Based Polymers: The Example of Elastinlike Polymers, In Vancso G. J., Reiter G., eds. Ordered Polymeric Nanostructures at Surfaces, Berlin, Germany: Springer; 2006.

[35] Holzapfel G. A., Biomechanics of Soft Tissue, In Lemaitre J., ed. Handbook of Materials Behavior Models, New York NY, USA: Academic Press; 2001.

[36] Debelle L., and Tamburro A. M., Elastin: molecular description and function, The International Journal of Biochemistry & Cell Biology 1999, 31: 261-272.

[37] Bashir M. M., Indik Z., Yeh H., Ornstein-Goldstein N., Rosenbloom J. C., Abrams W., Fazio M., Uitto J., and Rosenbloom J., Characterization of the complete human elastin gene. Delineation of unusual features in the 5'-flanking region, Journal of Biological Chemistry 1989, 264: 8887-8891.

[38] Indik Z., Yeh H., Ornstein-Goldstein N., Sheppard P., Anderson N., Rosenbloom J. C., Peltonen L., and Rosenbloom J., Alternative splicing of human elastin mRNA indicated by sequence analysis of cloned genomic and complementary DNA, Proceedings of the National Academy of Sciences 1987, 84: 5680-5684.

[39] Jones P. A., Scott-Burden T., and Gevers W., Glycoprotein, elastin, and collagen secretion by rat smooth muscle cells, Proceedings of the National Academy of Sciences 1979, 76: 353-357.

[40] Mecham R. P., Madaras J., McDonald J. A., and Ryan U., Elastin production by cultured calf pulmonary artery endothelial cells, Journal of Cellular Physiology 1983, 116: 282-288.

[41] Sephel G. C., and Davidson J. M., Elastin Production in Human Skin Fibroblast Cultures and Its Decline with Age, Journal of Investigative Dermatology 1986, 86: 279-285.

[42] Moskalewski S., Elastic fiber formation in monolayer and organ cultures of chondrocytes isolated from auricular cartilage, American Journal of Anatomy 1976, 146: 443-448.

[43] Hsiao H., Stone P. J., Toselli P., Rosenbloom J., Franzblau C., and Schreiber B. M., The Role of the Carboxy Terminus of Tropoelastin in its Assembly into the Elastic Fiber, Connective Tissue Research 1999, 40: 83-95.

[44] Mauch J. C., Sandberg L. B., Roos P. J., Jimenez F., Christiano A. M., Deak S. B., and Boyd C. D., Extensive alternate exon usage at the 5' end of the sheep tropoelastin gene, Matrix Biology 1995, 14: 635-641.

[45] Pierce R. A., Deak S. B., Stolle C. A., and Boyd C. D., Heterogeneity of rat tropoelastin mRNA revealed by cDNA cloning, Biochemistry 1990, 29: 9677-9683.

[46] Raju K., and Anwar R. A., Primary structures of bovine elastin a, b, and c deduced from the sequences of cDNA clones, Journal of Biological Chemistry 1987, 262: 5755-5762.

[47] Daamen W. F., Veerkamp J. H., van Hest J. C. M., and van Kuppevelt T. H., Elastin as a biomaterial for tissue engineering, Biomaterials 2007, 28: 4378-4398.

[48] Hinek A., and Rabinovitch M., 67-kD elastin-binding protein is a protective "companion" of extracellular insoluble elastin and intracellular tropoelastin, The Journal of Cell Biology 1994, 126: 563-574.

[49] Brown-Augsburger P., Broekelmann T., Rosenbloom J., and Mecham R. P., Functional domains on elastin and microfibril-associated glycoprotein involved in elastic fibre assembly, Biochem J 1996, 318: 149-155.

[50] Rosenbloom J., Abrams W., and Mecham R., Extracellular matrix 4: the elastic fiber, The FASEB Journal 1993, 7: 1208-1218.

[51] Martyn C. N., and Greenwald S. E., Impaired synthesis of elastin in walls of aorta and large conduit arteries during early development as an initiating event in pathogenesis of systemic hypertension, The Lancet 1997, 350: 953-955.

[52] Powell J. T., Vine N., and Crossman M., On the accumulation of D-aspartate in elastin and other proteins of the ageing aorta, Atherosclerosis 1992, 97: 201-208.

[53] Tirrell M., Kokkoli E., and Biesalski M., The role of surface science in bioengineered materials, Surface Science 2002, 500: 61-83.

[54] Andrady A. L., and Mark J. E., Thermoelasticity of swollen elastin networks at constant composition, Biopolymers 1980, 19: 849-855.

[55] Hoeve C. A. J., and Flory P. J., The Elastic Properties of Elastin, Journal of the American Chemical Society 1958, 80: 6523-6526.

[56] Tamburro A. M., Guantieri V., Daga-Gordini D., and Abatangelo G., Concentration-dependent conformational transition of alpha-elastin in aqueous solution, Journal of Biological Chemistry 1978, 253: 2893-2894.

[57] Dorrington K. L., and McCrum N. G., Elastin as a rubber, Biopolymers 1977, 16: 1201-1222.

[58] Weis-Fogh T., and Andersen S. O., New Molecular Model for the Long-range Elasticity of Elastin, Nature 1970, 227: 718-721.

[59] Gray W. R., Sandberg L. B., and Foster J. A., Molecular Model for Elastin Structure and Function, Nature 1973, 246: 461-466.

[60] Tamburro A. M., Guantieri V., and Daga Gordini D., Synthesis and structural studies of a pentapeptide sequence of elastin. Poly (Val-Gly-Gly-Leu-Gly), Journal of Biomolecular Structure and Dynamics 1992, 10: 441-454.

[61] Urry D. W., Shaw R. G., and Prasad K. U., Polypentapeptide of elastin: Temperature dependence of ellipticity and correlation with elastomeric force, Biochemical and Biophysical Research Communications 1985, 130: 50-57.

[62] Ewart A. K., Jin W., Atkinson D., Morris C. A., and Keating M. T., Supravalvular aortic stenosis associated with a deletion disrupting the elastin gene, The Journal of Clinical Investigation 1994, 93: 1071-1077.

[63] Kumar A., Olson T. M., Thibodeau S. N., Michels V. V., Schaid D. J., and Wallace M. R., Conformation of Linkage of Supravalvular Aortic Stenosis to the Elastin Gene on Chromosome 7q, American Journal of Cardiology 1994, 74: 1281-1283.

[64] Li D. Y., Toland A. E., Boak B. B., Atkinson D. L., Ensing G. J., Morris C. A., and Keating M. T., Elastin Point Mutations Cause an Obstructive Vascular Disease, Supravalvular Aortic Stenosis, Human Molecular Genetics 1997, 6: 1021-1028.

[65] Wu W. J., and Weiss A. S., Deficient coacervation of two forms of human tropoelastin associated with supravalvular aortic stenosis, European Journal of Biochemistry 1999, 266: 308-314.

[66] Ewart A. K., Morris C. A., Atkinson D., Jin W., Sternes K., Spallone P., Stock A. D., Leppert M., and Keating M. T., Hemizygosity at the elastin locus in a developmental disorder, Williams syndrome, Nature Genetics 1993, 5: 11-16.

[67] Rodriguez-Revenga L., Iranzo P., Badenas C., Puig S., Carrio A., and Mila M., A Novel Elastin Gene Mutation Resulting in an Autosomal Dominant Form of Cutis Laxa, Archives of Dermatological Research 2004, 140: 1135-1139.

[68] Zhang M.-C., He L., Giro M., Yong S. L., Tiller G. E., and Davidson J. M., Cutis Laxa Arising from Frameshift Mutations in Exon 30 of the Elastin Gene (ELN), Journal of Biological Chemistry 1999, 274: 981-986.

[69] Robinson P. N., and Godfrey M., The molecular genetics of Marfan syndrome and related microfibrillopathies, Journal of Medical Genetics 2000, 37: 9-25.

[70] Kurane A., Simionescu D. T., and Vyavahare N. R., In vivo cellular repopulation of tubular elastin scaffolds mediated by basic fibroblast growth factor, Biomaterials 2007, 28: 2830-2838.

[71] Schinke T., and Karsenty G., Vascular calcification—a passive process in need of inhibitors, Nephrology Dialysis Transplantation 2000, 15: 1272-1274.

[72] Singla A., and Lee C. H., Inhibition of CEM calcification by the sequential pretreatment with ethanol and EDTA, Journal of Biomedical Materials Research Part A 2003, 64A: 706-713.

[73] Phillips T. J., and Gilchrest B. A., Clinical Applications of Cultured Epithelium, Epithelial Cell Biology 1992, 1.

[74] Pomahač B., Svensjö T., Yao F., Brown H., and Eriksson E., Tissue Engineering of Skin, Critical Reviews in Oral Biology & Medicine 1998, 9: 333-344.

[75] Ehrenreich M., and Ruszczak Z., Update on Tissue-Engineered Biological Dressings, Tissue Engineering 2006, 12: 2407-2424.

[76] Falanga V., and Sabolinski M., A bilayered living skin construct (APLIGRAF®) accelerates complete closure of hard-to-heal venous ulcers, Wound Repair and Regeneration 1999, 7: 201-207.

[77] Ramsey S. D., Newton K., Blough D., McCulloch D. K., Sandhu N., Reiber G. E., and Wagner E. H., Incidence, outcomes, and cost of foot ulcers in patients with diabetes, Diabetes Care 1999, 22: 382-387.

[78] Hafemann B., Ensslen S., Erdmann C., Niedballa R., Zuhlke A., Ghofrani K., and Kirkpatrick C. J., Use of a collagen/elastin-membrane for the tissue engineering of dermis, Burns 1999, 25: 373-384.

[79] Nillesen S. T. M., Lammers G., Wismans R. G., Ulrich M. M., Middelkoop E., Spauwen P. H., Faraj K. A., Schalkwijk J., Daamen W. F., and van Kuppevelt T. H., Design and in vivo evaluation of a molecularly defined acellular skin construct: Reduction of early contraction and increase in early blood vessel formation, Acta Biomaterialia 2011, 7: 1063-1071.

[80] Koens M. J. W., Faraj K. A., Wismans R. G., van der Vliet J. A., Krasznai A. G., Cuijpers V. M. J. I., Jansen J. A., Daamen W. F., and van Kuppevelt T. H., Controlled fabrication of triple layered and molecularly defined collagen/elastin vascular grafts resembling the native blood vessel, Acta Biomaterialia 2010, 6: 4666-4674.

[81] Patel A., Fine B., Sandig M., and Mequanint K., Elastin biosynthesis: The missing link in tissue-engineered blood vessels, Cardiovascular Research 2006, 71: 40-49.

[82] Gotlieb A. I., Atherosclerosis and acute coronary syndromes, Cardiovascular Pathology 2005, 14: 181-184.

[83] Isenberg B. C., Williams C., and Tranquillo R. T., Small-Diameter Artificial Arteries Engineered In Vitro, Circulation Research 2006, 98: 25-35.

[84] Nerem R. M., and Seliktar D., Vascular Tissue Engineering, Annual Review of Biomedical Engineering 2001, 3: 225-243.

[85] Stitzel J., Liu J., Lee S. J., Komura M., Berry J., Soker S., Lim G., Van Dyke M., Czerw R., Yoo J. J., and Atala A., Controlled fabrication of a biological vascular substitute, Biomaterials 2006, 27: 1088-1094.

[86] Neuman R. E., and Logan M. A., The Determination of Collagen and Elastin in Tissues, Journal of Biological Chemistry 1950, 186: 549-556.

[87] Rasmussen B. L., Bruenger E., and Sandberg L. B., A new method for purification of mature elastin, Analytical Biochemistry 1975, 64: 255-259.

[88] Daamen W. F., Hafmans T., Veerkamp J. H., and Kuppevelt T. H. V., Isolation of Intact Elastin Fibers Devoid of Microfibrils, Tissue Engineering 2005, 11: 1168-1176.

[89] Tamburro A. M., Pepe A., Bochicchio B., Quaglino D., and Ronchetti I. P., Supramolecular Amyloid-like Assembly of the Polypeptide Sequence Coded by Exon 30 of Human Tropoelastin, Journal of Biological Chemistry 2005, 280: 2682-2690.

[90] Rodríguez-Cabello J. C., Reguera J., Alonso M., Parker T. M., McPherson D. T., and Urry D. W., Endothermic and exothermic components of an inverse temperature transition for hydrophobic association by TMDSC, Chemical Physics Letters 2004, 388: 127-131.

[91] Urry D. W., Elastic molecular machines in metabolism and soft-tissue restoration, Trends in Biotechnology 1999, 17: 249-257.

[92] Lee J., MacOsko C. W., and Urry D. W., Phase transition and elasticity of protein-based hydrogels, Journal of Biomaterials Science, Polymer Edition 2001, 12: 229-242.

[93] Urry D. W., Physical Chemistry of Biological Free Energy Transduction As Demonstrated by Elastic Protein-Based Polymers†, The Journal of Physical Chemistry B 1997, 101: 11007-11028.

[94] Rodríguez-Cabello J. C., Reguera J., Girotti A., Alonso M., and Testera A. M., Developing functionality in elastin-like polymers by increasing their molecular complexity: the power of the genetic engineering approach, Progress in Polymer Science 2005, 30: 1119-1145.

[95] Reguera J., Urry D. W., Parker T. M., McPherson D. T., and Rodríguez-Cabello J. C., Effect of NaCl on the Exothermic and Endothermic Components of the Inverse Temperature Transition of a Model Elastin-like Polymer, Biomacromolecules 2007, 8: 354-358.

[96] Meyer D. E., and Chilkoti A., Genetically Encoded Synthesis of Protein-Based Polymers with Precisely Specified Molecular Weight and Sequence by Recursive Directional Ligation: Examples from the Elastin-like Polypeptide System, Biomacromolecules 2002, 3: 357-367.

[97] Urry D. W., Hayes L. C., Gowda D. C., Harris C. M., and Harris R. D., Reduction-driven polypeptide folding by the [Delta]Tt mechanism, Biochemical and Biophysical Research Communications 1992, 188: 611-617.

[98] Strzegowski L. A., Martinez M. B., Gowda D. C., Urry D. W., and Tirrell D. A., Photomodulation of the inverse temperature transition of a modified elastin poly(pentapeptide), Journal of the American Chemical Society 1994, 116: 813-814.

[99] Urry D. W., Hayes L. C., Channe Gowda D., and Parker T. M., Pressure effect on inverse temperature transitions: biological implications, Chemical Physics Letters 1991, 182: 101-106.

[100] Di Zio K., and Tirrell D. A., Mechanical Properties of Artificial Protein Matrices Engineered for Control of Cell and Tissue Behavior, Macromolecules 2003, 36: 1553-1558.

[101] Urry D. W., Parker T. M., Reid M. C., and Gowda D. C., Biocompatibility of the Bioelastic Materials, Poly(GVGVP) and Its γ-Irradiation Cross-Linked Matrix: Summary of Generic Biological Test Results, Journal of Bioactive and Compatible Polymers 1991, 6: 263-282.

[102] McMillan R. A., Lee T. A. T., and Conticello V. P., Rapid Assembly of Synthetic Genes Encoding Protein Polymers, Macromolecules 1999, 32: 3643-3648.

[103] Padgett K. A., and Sorge J. A., Creating seamless junctions independent of restriction sites in PCR cloning, Gene 1996, 168: 31-35.

[104] Simnick A. J., Lim D. W., Chow D., and Chilkoti A., Biomedical and Biotechnological Applications of Elastin-Like Polypeptides, Polymer Reviews 2007, 47: 121 - 154.

[105] Urry D. W., Luan C. H., Parker T. M., Gowda D. C., Prasad K. U., Reid M. C., and Safavy A., Temperature of polypeptide inverse temperature transition depends on mean residue hydrophobicity, Journal of the American Chemical Society 1991, 113: 4346-4348.

[106] McPherson D. T., Xu J., and Urry D. W., Product Purification by Reversible Phase Transition FollowingEscherichia coliExpression of Genes Encoding up to 251 Repeats of the Elastomeric Pentapeptide GVGVP, Protein Expression and Purification 1996, 7: 51-57.

[107] Fothergill-Gilmore L. A., Peptide Sequence Determination, In Franks F., ed. Protein Biotechnology: Isolation, Characterization, and Stabilization, Totowa NJ, USA: Humana Press; 1993.

[108] Guda C., Zhang X., McPherson D. T., Xu J., Cherry J. H., Urry D. W., and Daniell H., Hyper expression of an environmentally friendly synthetic polymer gene, Biotechnology Letters 1995, 17: 745-750.

[109] Mi L. X., Molecular cloning of protein-based polymers, Biomacromolecules 2006, 7: 2099-2107.

[110] Chilkoti A., Dreher M. R., and Meyer D. E., Design of thermally responsive, recombinant polypeptide carriers for targeted drug delivery, Advanced Drug Delivery Reviews 2002, 54: 1093-1111.

[111] Dawson P. E., Muir T. W., Clarklewis I., and Kent S. B. H., SYNTHESIS OF PROTEINS BY NATIVE CHEMICAL LIGATION, Science 1994, 266: 776-779.

[112] Paramonov S. E., Gauba V., and Hartgerink J. D., Synthesis of collagen-like peptide polymers by native chemical ligation, Macromolecules 2005, 38: 7555-7561.

[113] Liu W. S., Brock A., Chen S., Chen S. B., and Schultz P. G., Genetic incorporation of unnatural amino acids into proteins in mammalian cells, Nature Methods 2007, 4: 239-244.

[114] Rabotyagova O. S., Cebe P., and Kaplan D. L., Protein-Based Block Copolymers, Biomacromolecules 2011, 12: 269-289.

[115] Rodriguez-Cabello J. C., Martin L., Girotti A., Garcia-Arevalo C., Arias F. J., and Alonso M., Emerging applications of multifunctional elastin-like recombinamers, Nanomedicine 2011, 6: 111-122.

[116] Li B., Alonso D. O. V., Bennion B. J., and Daggett V., Hydrophobic hydration is an important source of elasticity in elastin-based biopolymers, Journal of the American Chemical Society 2001, 123: 11991-11998.

[117] Sallach R. E., Cui W., Wen J., Martinez A., Conticello V. P., and Chaikof E. L., Elastin-mimetic protein polymers capable of physical and chemical crosslinking, Biomaterials 2009, 30: 409-422.

[118] Urry D. W., What sustains life? Consilient mechanisms for protein-based machines and materials, New York NY, USA: Springer-Verlag; 2006.

[119] Badylak S. F., Freytes D. O., and Gilbert T. W., Extracellular matrix as a biological scaffold material: Structure and function, Acta Biomaterialia 2009, 5: 1-13.

[120] Furth M. E., Atala A., and Van Dyke M. E., Smart biomaterials design for tissue engineering and regenerative medicine, Biomaterials 2007, 28: 5068-5073.

[121] Garcia Y., Hemantkumar N., Collighan R., Griffin M., Rodriguez-Cabello J. C., and Pandit A., In Vitro Characterization of a Collagen Scaffold Enzymatically Cross-Linked with a Tailored Elastin-like Polymer, Tissue Engineering Part A 2009, 15: 887-899.

[122] Lim D. W., Nettles D. L., Setton L. A., and Chilkoti A., Rapid cross-linking of elastin-like polypeptides with (hydroxymethyl)phosphines in aqueous solution, Biomacromolecules 2007, 8: 1463-1470.

[123] Martín L., Alonso M., Moller M., Rodríguez-Cabello J. C., and Mela P., 3D microstructuring of smart bioactive hydrogels based on recombinant elastin-like polymers, Soft Matter 2009, 5: 1591-1593.

[124] Hersel U., Dahmen C., and Kessler H., RGD modified polymers: biomaterials for stimulated cell adhesion and beyond, Biomaterials 2003, 24: 4385-4415.

[125] Liu J. C., Heilshorn S. C., and Tirrell D. A., Comparative cell response to artificial extracellular matrix proteins containing the RGD and CS5 cell-binding domains, Biomacromolecules 2004, 5: 497-504.

[126] Panitch A., Yamaoka T., Fournier M. J., Mason T. L., and Tirrell D. A., Design and biosynthesis of elastin-like artificial extracellular matrix proteins containing periodically spaced fibronectin CS5 domains, Macromolecules 1999, 32: 1701-1703.

[127] Straley K. S., and Heilshorn S. C., Design and adsorption of modular engineered proteins to prepare customized, neuron-compatible coatings, Frontiers in Neuroengineering 2009, 2.

[128] Heilshorn S. C., DiZio K. A., Welsh E. R., and Tirrell D. A., Endothelial cell adhesion to the fibronectin CS5 domain in artificial extracellular matrix proteins, Biomaterials 2003, 24: 4245-4252.

[129] Plouffe B. D., Njoka D. N., Harris J., Liao J., Horick N. K., Radisic M., and Murthy S. K., Peptide-mediated selective adhesion of smooth muscle and endothelial cells in microfluidic shear flow, Langmuir 2007, 23: 5050-5055.

[130] Straley K. S., and Heilshorn S. C., Independent tuning of multiple biomaterial properties using protein engineering, Soft Matter 2009, 5: 114-124.

[131] Nagapudi K., Brinkman W. T., Leisen J. E., Huang L., McMillan R. A., Apkarian R. P., Conticello V. P., and Chaikof E. L., Photomediated solid-state cross-linking of an elastin-mimetic recombinant protein polymer, Macromolecules 2002, 35: 1730-1737.

[132] Lee J., Macosko C. W., and Urry D. W., Swelling behavior of gamma-irradiation cross-linked elastomeric polypentapeptide-based hydrogels, Macromolecules 2001, 34: 4114-4123.

[133] Martín L., Alonso M., Girotti A., Arias F. J., and Rodríguez-Cabello J. C., Synthesis and Characterization of Macroporous Thermosensitive Hydrogels from Recombinant Elastin-Like Polymers, Biomacromolecules 2009, 10: 3015-3022.

[134] Martínez-Osorio H., Juárez-Campo M., Diebold Y., Girotti A., Alonso M., Arias F. J., Rodríguez-Cabello J. C., García-Vázquez C., and Calonge M., Genetically Engineered Elastin-Like Polymer as a Substratum to Culture Cells from the Ocular Surface, Current Eye Research 2009, 34: 48-56.

[135] Srivastava G. K., Martín L., Singh A. K., Fernandez-Bueno I., Gayoso M. J., Garcia-Gutierrez M. T., Girotti A., Alonso M., Rodríguez-Cabello J. C., and Pastor J. C., Elastin-like recombinamers as substrates for retinal pigment epithelial cell growth, Journal of Biomedical Materials Research Part A 2011, 97A: 243-250.

[136] Caves J. M., Kumar V. A., Martinez A. W., Kim J., Ripberger C. M., Haller C. A., and Chaikof E. L., The use of microfiber composites of elastin-like protein matrix reinforced with synthetic collagen in the design of vascular grafts, Biomaterials 2010, 31: 7175-7182.

[137] Kinikoglu B., Rodríguez-Cabello J., Damour O., and Hasirci V., A smart bilayer scaffold of elastin-like recombinamer and collagen for soft tissue engineering, Journal of Materials Science: Materials in Medicine 2011: 1-14.

[138] Barbosa J. S., Ribeiro A., Testera A. M., Alonso M., Arias F. J., Rodriguez-Cabello J. C., and Mano J. F., Development of Biomimetic Chitosan-Based Hydrogels Using an Elastin-Like Polymer, Advanced Engineering Materials 2010, 12: B37-B44.

[139] Wang E. D., Lee S. H., and Lee S. W., Elastin-Like Polypeptide Based Hydroxyapatite Bionanocomposites, Biomacromolecules 2011, 12: 672-680.

[140] Prieto S., Shkilnyy A., Rumplasch C., Ribeiro A., Arias F. J., Rodríguez-Cabello J. C., and Taubert A., Biomimetic Calcium Phosphate Mineralization with Multifunctional Elastin-Like Recombinamers, Biomacromolecules 2011: null-null.

[141] Wu X., Sallach R. E., Caves J. M., Conticello V. P., and Chaikof E. L., Deformation responses of a physically cross-linked high molecular weight elastin-like protein polymer, Biomacromolecules 2008, 9: 1787-1794.

[142] Martín L., Arias F. J., Alonso M., García-Arévalo C., and Rodríguez-Cabello J. C., Rapid micropatterning by temperature-triggered reversible gelation of a recombinant smart elastin-like tetrablock-copolymer, Soft Matter 2010, 6: 1121-1124.

[143] Wu X. Y., Sallach R., Haller C. A., Caves J. A., Nagapudi K., Conticello V. P., Levenston M. E., and Chaikof E. L., Alterations in physical cross-linking modulate mechanical properties of two-phase protein polymer networks, Biomacromolecules 2005, 6: 3037-3044.

[144] Sallach R. E., Cui W. X., Balderrama F., Martinez A. W., Wen J., Haller C. A., Taylor J. V., Wright E. R., Long R. C., and Chaiko E. L., Long-term biostability of self-assembling protein polymers in the absence of covalent crosslinking, Biomaterials 2010, 31: 779-791.

[145] Oliveira M. B., Song W., Martin L., Oliveira S. M., Caridade S. G., Alonso M., Rodriguez-Cabello J. C., and Mano J. F., Development of an injectable system based on elastin-like recombinamer particles for tissue engineering applications, Soft Matter 2011, 7: 6426-6434.

[146] Chilkoti A., Dreher M. R., Meyer D. E., and Raucher D., Targeted drug delivery by thermally responsive polymers, Advanced Drug Delivery Reviews 2002, 54: 613-630.

[147] Kost J., and Langer R., Responsive Polymeric Delivery Systems, Advanced Drug Delivery Reviews 1991, 6: 19-50.

[148] Bidwell G. L., Davis A. N., and Raucher D., Targeting a c-Myc inhibitory polypeptide to specific intracellular compartments using cell penetrating peptides, Journal of Controlled Release 2009, 135: 2-10.

[149] Massodi I., Bidwell G. L., and Raucher D., Evaluation of cell penetrating peptides fused to elastin-like polypeptide for drug delivery, Journal of Controlled Release 2005, 108: 396-408.

[150] MacEwan S. R., Callahan D. J., and Chilkoti A., Stimulus-responsive macromolecules and nanoparticles for cancer drug delivery, Nanomedicine 2010, 5: 793-806.

[151] Herrero-Vanrell R., Rincón A. C., Alonso M., Reboto V., Molina-Martínez I. T., and Rodríguez-Cabello J. C., Self-assembled particles of an elastin-like polymer as vehicles for controlled drug release, Journal of Controlled Release 2005, 102: 113-122.

[152] Wu Y. Q., MacKay J. A., McDaniel J. R., Chilkoti A., and Clark R. L., Fabrication of Elastin-Like polypeptide Nanoparticles for Drug Delivery by Electrospraying, Biomacromolecules 2009, 10: 19-24.

[153] Dash B. C., Mahor S., Carroll O., Mathew A., Wang W., Woodhouse K. A., and Pandit A., Tunable elastin-like polypeptide hollow sphere as a high payload and controlled delivery gene depot, Journal of Controlled Release 2011, 152: 382-392.

[154] Dreher M. R., Simnick A. J., Fischer K., Smith R. J., Patel A., Schmidt M., and Chilkoti A., Temperature triggered self-assembly of polypeptides into multivalent spherical micelles, Journal of the American Chemical Society 2008, 130: 687-694.

[155] MacKay J. A., Chen M. N., McDaniel J. R., Liu W. G., Simnick A. J., and Chilkoti A., Self-assembling chimeric polypeptide-doxorubicin conjugate nanoparticles that abolish tumours after a single injection, Nature Materials 2009, 8: 993-999.

[156] Kim W., Thevenot J., Ibarboure E., Lecommandoux S., and Chaikof E. L., Self-Assembly of Thermally Responsive Amphiphilic Diblock Copolypeptides into Spherical Micellar Nanoparticles, Angewandte Chemie-International Edition 2010, 49: 4257-4260.

[157] Sallach R. E., Wei M., Biswas N., Conticello V. P., Lecommandoux S., Dluhy R. A., and Chaikof E. L., Micelle density regulated by a reversible switch of protein secondary structure, Journal of the American Chemical Society 2006, 128: 12014-12019.

[158] Akiyama Y., Kikuchi A., Yamato M., and Okano T., Ultrathin poly(N-isopropylacrylamide) grafted layer on polystyrene surfaces for cell adhesion/detachment control, Langmuir 2004, 20: 5506-5511.

[159] Nath N., Hyun J., Ma H., and Chilkoti A., Surface engineering strategies for control of protein and cell interactions, Surface Science 2004, 570: 98-110.

[160] Hyun J., Lee W. K., Nath N., Chilkoti A., and Zauscher S., Capture and release of proteins on the nanoscale by stimuli-responsive elastin-like polypeptide "switches", Journal of the American Chemical Society 2004, 126: 7330-7335.

[161] Kato R., Kaga C., Kunimatsu M., Kobayashi T., and Honda H., Peptide array-based interaction assay of solid-bound peptides and anchorage-dependant cells and its effectiveness in cell-adhesive peptide design, Journal of Bioscience and Bioengineering 2006, 101: 485-495.

[162] Luzinov I., Minko S., and Tsukruk V. V., Adaptive and responsive surfaces through controlled reorganization of interfacial polymer layers, Progress in Polymer Science 2004, 29: 635-698.

[163] Idota N., Tsukahara T., Sato K., Okano T., and Kitamori T., The use of electron beam lithographic graft-polymerization on thermoresponsive polymers for regulating the directionality of cell attachment and detachment, Biomaterials 2009, 30: 2095-2101.

[164] Nath N., and Chilkoti A., Creating "Smart" surfaces using stimuli responsive polymers, Advanced Materials 2002, 14: 1243-1247.

[165] Shi J., Alves N. M., and Mano J. F., Thermally Responsive Biomineralization on Biodegradable Substrates, Advanced Functional Materials 2007, 17: 3312-3318.

[166] Wada A., Mie M., Aizawa M., Lahoud P., Cass A. E. G., and Kobatake E., Design and construction of glutamine binding proteins with a self-adhering capability to unmodified hydrophobic surfaces as reagentless fluorescence sensing devices, Journal of the American Chemical Society 2003, 125: 16228-16234.

[167] Elloumi I., Kobayashi R., Funabashi H., Mie M., and Kobatake E., Construction of epidermal growth factor fusion protein with cell adhesive activity, Biomaterials 2006, 27: 3451-3458.

[168] Ozturk N., Girotti A., Kose G. T., Rodríguez-Cabello J. C., and Hasirci V., Dynamic cell culturing and its application to micropatterned, elastin-like protein-modified poly(N-isopropylacrylamide) scaffolds, Biomaterials 2009, 30: 5417-5426.

[169] Na K., Jung J., Kim O., Lee J., Lee T. G., Park Y. H., and Hyun J., "Smart" Biopolymer for a Reversible Stimuli-Responsive Platform in Cell-Based Biochips, Langmuir 2008, 24: 4917-4923.

[170] Swierczewska M., Hajicharalambous C. S., Janorkar A. V., Megeed Z., Yarmush M. L., and Rajagopalan P., Cellular response to nanoscale elastin-like polypeptide polyelectrolyte multilayers, Acta Biomaterialia 2008, 4: 827-837.

[171] Barbosa J., Costa R., Testera A., Alonso M., Rodríguez-Cabello J., and Mano J., Multi-layered films containing a biomimetic stimuli-responsive recombinant protein, Nanoscale Research Letters 2009, 4: 1247-1253.

[172] Costa R. R., Custódio C. A., Testera A. M., Arias F. J., Rodríguez-Cabello J. C., Alves N. M., and Mano J. F., Stimuli-Responsive Thin Coatings Using Elastin-Like Polymers for Biomedical Applications, Advanced Functional Materials 2009, 19: 3210-3218.

[173] Costa R. R., Custódio C. A., Arias F. J., Rodríguez-Cabello J. C., and Mano J. F., Layer-by-Layer Assembly of Chitosan and Recombinant Biopolymers into Biomimetic Coatings with Multiple Stimuli-Responsive Properties, Small 2011, 7: 2640-2649.

[174] Bernard A., Renault J. P., Michel B., Bosshard H. R., and Delamarche E., Microcontact printing of proteins, Advanced Materials 2000, 12: 1067-1070.

[175] Offenhausser A., Bocker-Meffert S., Decker T., Helpenstein R., Gasteier P., Groll J., Moller M., Reska A., Schafer S., Schulte P., and Vogt-Eisele A., Microcontact printing of proteins for neuronal cell guidance, Soft Matter 2007, 3: 290-298.

[176] Nath N., and Chilkoti A., Fabrication of a reversible protein array directly from cell lysate using a stimuli-responsive polypeptide, Analytical Chemistry 2003, 75: 709-715.

Chapter 4. Stimuli-responsive surfaces for biomedical applications[4]

4.1 Introduction

Surface engineering is a field of expertise dealing with the modification and improvement of interfaces. In conventional medicine, the surface properties of an implantable device are regarded with the utmost importance since the first contact with the organism is mediated by the interface with the organism. This interaction is what drives the subsequent tissue and cellular events, including protein adsorption, cell adhesion, and inflammatory response [1-3].

A device which surface is modified is often perceived as a static product that gives rise to an improved interface while retaining the mechanical bulk properties. However, specific applications may require that such interface is dynamic. In these cases, a surface should be able to respond towards external factors and considered as a step forward when developing systems with increasing complexity in healthcare, biomedicine and tissue engineering applications. An example of such a dynamic system is our own skin. Skin can be perceived as a multifunctional membrane that responds to its environment. Its reaction is different when exposed to distinct conditions – heat/cold, humidity, chemical/mechanical stress and light – and constitutes an elegant example of a sensorial stimuli-responsive structure found in Nature [4]. Such mechanism can be found in many other living processes: they can use macromolecules as construction elements or parts of cell machinery, including proteins/enzymes, polysaccharides and nucleic acids that typically exhibit a clear non-linear and reversible behavior. Some are stable along wide ranges of some external variables and undergo drastic conformational changes upon narrow variations around given critical points [5-7].

Inspired by natural examples, stimuli-responsive surfaces have been developed in the past two decades, often recurring to materials that exhibit reversible property switchability. These surfaces are capable of reversibly changing their properties depending on the environmental conditions, such as temperature, pH, ionic strength, light, electrical fields and biomolecules [8-10]. Thanks to their properties, stimuli-responsive materials have been used to develop “smart” surfaces with significant potential in the fields

[4] This chapter is based on the following publication:

Costa R. R., Alves N. M., Rodríguez-Cabello J. C., and Mano J. F., Stimuli-responsive surfaces for biomedical applications, In Taubert A., Mano J. F., and Rodríguez-Cabello J. C. (eds.), Biomaterials surface science, Germany, Wiley-VCH, 2012, DOI: 10.1002/9783527649600.ch4.

of material science and biotechnology for the spatial and temporal control of the attachment of cells, microorganisms or biomolecules, biosensor or diagnosis, or to control de diffusion of encapsulated molecules for drug delivery and bioseparation [4,11-14].

4.2 Surface modification methodologies: how to render substrates with stimuli responsiveness

Many processing techniques have been suggested and employed for the purpose of modifying substrates. Most of them often rely on the use of physical or chemical methods, such as plasma and ion-beam sputtering [15]. However, in most cases, they are not suitable to produce stimuli-responsiveness. Meanwhile, other techniques were introduced with capability of rendering a substrate with smart properties and will discussed in the following sections.

4.2.1 Self-assembled monolayers

Self-assembled monolayers (SAMs) are ordered molecular assemblies formed by the self-assembly of an active surfactant onto a solid surface. In these two-dimensional systems, order is achieved by a spontaneous chemical synthesis at the interface [16]. The self-assembling molecules consist generally of three groups: (i) a head group, (ii) an alkyl chain and (ii) a terminal end group. The head group is responsible for the anchoring of the molecules onto the substrate (see Figure 4.1a). The alkyl chain, or spacer group, provides the stability of the monolayer, through van der Waals interactions. The terminal end group introduces chemical functionality into the monolayer system and is important for the overall properties of surfaces [17].

Surface chemistry represents an important tool for the preparation of a large variety of differently functionalized SAMs bearing a diversity of functional groups. There are three main approaches one can follow to obtain a suitable functional surface: (i) nucleophilic substitution, (ii) click chemistry and (iii) supramolecular modification. The first is a process through which a nucleophile (such as hydroxide, cyanide and ammonia) attacks an atom with a positive or partially positive charge connected to a negative or neutral leaving group [18]. Click chemistry generates substances by joining small units together with heteroatom links. Kolb, Finn and Sharpless [19] first introduced click chemistry as a technique that uses C–C bonds as a “currency”. Finally, the supramolecular modification is achieved by the functionalization of surfaces with tailor-made supramolecular binding motifs through specific interactions with the surface [20].

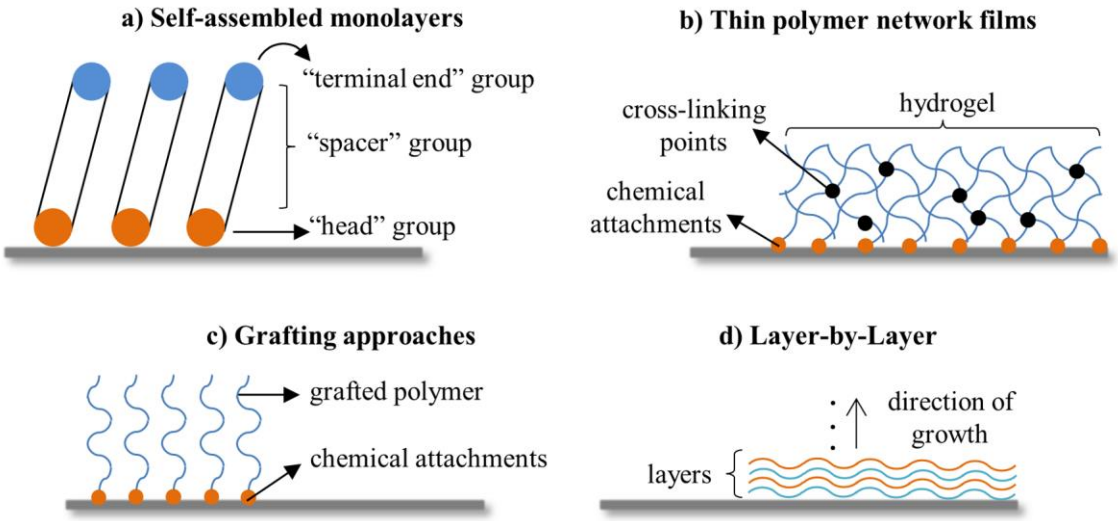


Figure 4.1. Schematic structure of interfaces formed by (a) self-assembled monolayer, (b) thin polymer network films, (c) grafting and (d) layer-by-layer.

SAMs can be assembled by adsorption of a variety of functional organic molecules onto suitable solid substrates. For instance, long-chain alkanethiols bearing a terminal functional group spontaneously assemble onto gold to form densely packed and ordered monolayers [21]. They are the most commonly used materials for SAMs and – besides gold – can be assembled onto noble metals, such as silver and platinum [22,23]. Other combinations of adsorbates and substrates include silane compounds onto silicon oxide and titanium [24,25], and phosphonic acids onto titanium [26].

Unfortunately, the specificity of SAMS is a shortcoming: they can only be fabricated upon the adsorption of *specific* molecules onto *specific* surfaces. Furthermore, the resulting monolayers show generally a limited stability under ambient and physiological conditions, leading to facile exchange and "stripping" of the adsorbates [27]. Nonetheless, SAMs have thrived because they are easy to prepare as they do not require any specialized equipment for their preparation and can be constructed on objects of different size and shape such as thin films, nano-particles/wires/cages in colloids, with clear impact in nanoscience and nanotechnology. In particular, SAM-modified surfaces have been constructed to exhibit smart properties towards external stimuli such as electrical fields (due to the desorption of alkanethiolates) [28], light (by the inclusion of azobenzenes or spiropyrans) [29], redox reactions (by the inclusion of supramolecular rotaxanes) [30] to obtain surfaces for protein separation, diagnostic and with switchable wettability.

4.2.2 Thin polymer network films

Nanostructured thin network films are structures in which surface confinement brings a range of opportunities for engineering stimuli-responsive properties. These are polymeric networks – in many cases very thin hydrogel films prepared from water-soluble polymers chemically linked to a surface, resulting in a soft surface with well-defined mechanical, physical and biochemical properties (see Figure 4.1b) [31]. This kind of polymer network provides a soft three-dimensional scaffold similar to that of macroscopic hydrogels, capable of hosting a wide-array of functionalities, ranging from proteins to inorganic nanoparticles, but typically produced at the nano- and micro- scales. They can undergo substantial swelling and contraction in response to external stimuli, making them excellent candidates for "smart" surfaces with sensing and actuating characteristics [13].

The advantage towards their macroscopic counterparts is that gel thin films exhibit a fast swelling and shrinkage kinetics. In fact, this behavior was predicted by the Tanaka and Fillmore's model which states that the characteristic time of the swelling transition is directly proportional to the square of the linear size of the gel [32]. A critical issue for understanding and predicting the properties of surface-attached polymer networks is the impact of confinement on their swelling behavior. Chemical linkage of the thin gel to a surface prevents swelling in the parallel direction to that of the substrate, effectively confining the volume change to one dimension. Such an effect has an impact in properties such as the structure, mechanical properties, dynamics, and permeability of the network [33]. Additionally, the swelling behavior of the polymer network is also influenced by the crosslinking degree of the film, as well as the nature of the polymer, e.g. if it is stimuli-responsive.

An interesting property of thin gel polymer networks is that they are not limited to surfaces: they can also be processed in the form of freestanding films if neither adhesion or covalent bonding to the surface is triggered [4]. Therefore, it is possible to synthesize thin responsive membranes that can be used in the selective separation of molecules and particles. While traditional membranes can perform this function based on parameters like size and charge, responsive membranes can demonstrate a gating function controlled by external stimuli. For instance, pores in the membrane can be switched between an "open" or "closed" state and allow the passage of specific solution components at a specific time in function of one or more stimuli [34,35].

Summarizing, thin polymer networks have a fast swelling/shrinking response and can accommodate in their bulk various chemicals, biomolecules and nanoparticles. These properties make of thin gel polymer networks attractive systems in microtechnology, namely as selective membranes, intelligent drug delivery devices and biosensors [36-38].

4.2.3 Grafting

Grafting is a technique by which a polymer is attached to a substrate, usually solid [39]. The bound polymer chains are often called "grafts" or "brushes" and lend their properties to the substrate (see Figure 4.1c). There are two major approaches of grafting that can be applied: "grafting-to" and "grafting-from" [40-42].

The "grafting-to" method refers to a chemical reaction between an end-functionalized polymer and a suitable surface containing complementary functional groups, and requires that the polymer is modified beforehand. Reactive end-functionalized polymers can be obtained through techniques such as controlled/living radical polymerization (CRP), group transfer and ring opening metathesis polymerizations [43-45]. A drawback of the "grafting-to" approach is the low density yield of the grafted chains: steric repulsions between polymer chains hamper the formation of dense polymer brushes [46]. Another drawback is that with increasing molecular weight of the polymer's the reaction between the polymer end-group and the complementary group on the substrate becomes less efficient [47]. Nevertheless, "grafting-to" is simple to perform and, thanks to the covalent bond formed between surface and polymer, the brushes are robust and capable of withstanding both chemical and physical efforts.

The "grafting-from" method refers to the preparation of polymer brushes in which the polymerization is triggered by initiator-functionalized surfaces. The immobilization of initiators on the surface can be achieved by treating the substrate with plasma or glow discharge in the presence of a gas or forming initiator-containing SAMs on the substrates. It can produce tethered layers of higher grafting densities than the "grafting-to" approach since the active centers (radicals, ions, and ion pairs) of the growing chains at the surface are easily accessible for monomer molecules in the swollen brush during the course of polymerization [48,49].

Regardless of the method – "to" or "from" – the principles are common to both: (i) the grafting techniques imply chemical attachment of polymers to the surface; (ii) the reaction occurs under appropriate reactive conditions, which are usually specific for the kind of materials and substrates involved; (iii) the polymers can be grafted to distinct types of surfaces, e.g. metals, glasses and silica, and not limited to planar substrates but also applied to spherical ones; and (iv) the substrates often assume the properties of the grafted polymer, with stimuli-responsive grafts rendering a smart-responsive surface.

A grafted polymer brush can be composed of chains from a single homopolymer – single-component homopolymer brushes – two or more different homopolymers – mixed brushes – or block-copolymers – block-copolymer brushes. In the first case, when dealing with smart surfaces, the responsive behavior originates from the inherent properties of the grafted polymer chains, their grafting densities, or by changes in the balance between polymer–polymer and polymer-solvent interactions [50]. In mixed polymer brushes, response comes from phase segregation, which causes the switching of the spatial distribution of the functional groups that are exhibited by the brush exterior. Consequently the materials' properties can be switched between among the ones of the constituent polymers [51]. The responsive behavior of block copolymer brushes (as in mixed brushes) is based on the phase segregation of the different blocks. The combination of different polymeric blocks in the responsive film broadens the range of properties upon switching, so that the surface changes from the property of one polymer to the property of the second polymer, or is locked in some intermediate state [52]. Graft-modified surfaces with stimuli-responsive behavior have been extensively used in biology and nanotechnology. The cell-sheet technology achieved through the attachment of poly(*N* -isopropyl acrylamide) (PNIPAAm), a thermoresponsive polymer, is one of the most representative examples of the grafting approach in tissue engineering [50]. Other applications based on other and stimuli (e.g. pH and ionic strength) have also been addressed, such as the switchable wettability of substrates, controlled release of drug delivery devices and sensors.

4.2.4 Layer-by-layer

Layer-by-layer (LbL) is a self-assembly-driven surface modification strategy that allows the construction of nanostructured films onto distinct geometries, from simple bidimensional surfaces to more complex three-dimensional porous structures. The principle behind it lies in the existence of multiple intermolecular interactions where the cooperative effects of multipoint attractions play the most important role (see Figure 4.1d) [11,53,54]. Constructing a multilayer film usually has two requirements: (i) a reactive surface as the assembly support and (ii) a combination of two or more ingredients for the constitution of the film that can interact with each other. The buildup process is initiated by dipping the substrate in a solution of one ingredient that shows complementary interactions with the surface, forming therefore the first layer. Then another ingredient follows, interacting with the preformed layer, assembling a second one. Between each dip, a rinsing step is performed to remove excess of non-adhered material from the interface. In comparison with SAMs and polymer brushes, usually neither the surface nor the ingredients require modification prior to the LbL construction since

assembling the layers rely on the intrinsic properties of each counterpart and their spontaneous assembly.

Usually the most important requirement is that two distinct materials possess complementarity, i.e. that the properties of both materials result in attraction. In other words, LbL is a generic surface modification technique with which (in theory) any material and surface can be used for this end, in opposition to the methods described in the previous sections. The most representative buildup mechanism relies on electrostatic interactions among surface/ingredient and ingredient/ingredient. For instance, a polycation can be adsorbed to a negatively charged surface to form a layer. A polyanion can then adsorb to the now positively charged interface, rendering it with a negative charge [55]. This process can be repeated as many times as necessary under aqueous conditions to construct films with thickness at the order of a few nanometers to tens of micrometers. Although electrostatic self-assembly (ESA) is the most exploited mechanism, other interactions can be present, such as hydrophobic interactions and hydrogen bonding [53,56].

LbL offers ease of preparation at mild conditions of temperature, pressure and pH, versatility, fine control over the materials structure and robustness under physiological conditions. Additionally, the mild and non-aggressive processing conditions of LbL make of it an appealing technique for tissue engineering applications. There is a vast choice of available materials that one can add to a multilayer formulation, such as proteins, nucleic acids, polysaccharides, and virus particles, as well as various organic polymers, molecular assemblies [57-59]. and inorganic substances (e.g. clay platelets [60], grapheme [61] and glass nanoparticles [62]). Furthermore, although LbL has been first introduced as a surface engineering technique of planar surfaces [63], the concept has been extrapolated to 3D. The sequential mechanism of layer adsorption can be extrapolated to construct thick membrane-like films with tens of micrometers assembled on non-adhesive substrates (e.g. through van der Waals interactions with polypropylene) to produce freestanding films [64]. Other types of complex geometries with distinct shapes and sizes and as a result, devices such as porous scaffolds and drug delivery capsules can now exhibit new properties with the option of further tuning by varying the nature of the LbL ingredients and number of layers [65,66].

LbL films and shells can contain stimuli-responsive ingredients in order to render a system with a smart response. Exploiting the advantages of LbL and intelligent multilayer systems have already been proposed for different biomedical applications, including for biomimetic composite-like coatings, to control the release of drugs, or to manipulate the adhesion of attached cells. In particular, systems assembled using weak polyelectrolytes (e.g. chitosan and alginate) are inherently responsive towards

ionic strength and pH responsive, since they interfere with the electrostatic balance within the internal structure of the film [58,67,68]. In similarity with polymer brushes, multilayer films with temperature responsive properties have also been fabricated to control the cell attachment/detachment to a surface for cell sheet technology, and to fabricate surfaces with acute wettability transitions [69,70].

4.3 Exploitable stimuli and model smart biomaterials

4.3.1 Physical stimuli

4.3.1.1 Temperature

Among the stimuli used to control the response, temperature has been extensively studied in the biomedical field as certain diseases manifest temperature changes and this factor can be easily controlled and applicable both *in vitro* and *in vivo* conditions. Thermo-responsive systems have a critical solution temperature at which the phase of the polymer and solution is discontinuously changed according to their composition.[8] PNIPAAm is the thermo-responsive polymer most used for conferring thermo-responsiveness to surfaces. It exhibits a lower critical solution temperature (LCST) at about 32°C in aqueous solution, changing sharply from a hydrophilic to a hydrophobic state upon heating [71]. It is believed that this transition involves the breakage of intermolecular hydrogen bonds between the water molecules and the amide groups in the polymeric chains, which are replaced, above the LCST, by intramolecular hydrogen bonds amongst the dehydrated amine groups. PNIPAAm has been copolymerised with hydrophilic or hydrophobic monomers in order to control the kinetics of the response [72,73].

Typically, above the LCST of PNIPAAm based surface-grafted polymers, surface wettability decreases and the thickness of the grafted layer decreases (deswelling). The work of Shi and co-workers [74] illustrates this behavior for bioactive composites of poly(L-lactic acid) (PLLA) reinforced with Bioglass® (BG) and grafted with PNIPAAm through the use of plasma activation. The water contact angle for the PNIPAAm modified PLLA+10% BG composite was 51.9±2.4°, at 25°C and at 37°C it changed to 58.8±2.4°, being consistent with the increase in the surface hydrophobicity above the LCST. The range of wettability can be further amplified to the super- hydrophobic/hydrophilic regimen by using substrates with increasing roughness [75], which is also predicted in the Wenzel model [76].

Besides the grafting of PNIPAAm-based polymers on distinct substrates, LbL assembling has also been used to confer temperature-responsiveness to surfaces. Serpe *et al.* [77] were the first to apply the LbL

technique to produce temperature-responsive PNIPAAM/-co-acrylic acid (AA)/polyallylamine coatings. Since then, LbL surfaces containing PNIPAAm have already been suggested for cell sheet engineering [70].

Other thermo-responsive polymers may be used instead of PNIPAAm. Poly(N-vinylcaprolactam) (PVCL) is another thermo-sensitive polymer that can be deposited onto surfaces, which possesses very interesting properties for biomedical applications such as solubility in water, biocompatibility, a transition temperature around 31°C and its cytoxicity has been referred as being much lower than the one of PNIPAAm.[78,79] Thermo-sensitive films based on triblock copolymers have also been prepared [80].

Nature also houses inspiration for the development of new polymers. Elastin-like recombinamers (ELRs) – a recombinant class of elastin-like polymers (ELPs) – are genetically engineered peptide-based materials that mimic the structure of natural elastin [81]. By exploiting microorganism systems, tailored recombinant elastins based on the pentapeptide poly(VPGVG) can be produced and, thanks to their recombinant nature, recombinant peptides with precision over the primary aminoacid content is possible, being able to introduce relevant functional sequences, for example to improve cell adhesion, trigger biomineralization and vascularization [82-84].

In aqueous solution, and below a certain transition temperature (T_t), the free polymer chains are disordered, consisting in fully hydrated random coils. When the temperature is increased above T_t, the structure loses the water molecules from hydrophobic hydration and the chains fold and assemble into a β-spiral conformation [85-87]. Although often associated with temperature-responsive polymers, the fact is that such transition phenomenon can occur due to other stimuli, such as pH, ionic strength, redox reactions and in specific modifications even due to light. In this perspective, ELRs could be classified as a multiple-responsive material, and surfaces modified with this kind of macromolecules have already been demonstrated to respond towards temperature, pH and ionic strength at the same time [69].

Biosensing surfaces displaying topologically modified self-assembly with ELRs have been developed by Chilkoti's group. The "thermodynamically reversible addressing of proteins" (TRAP) technology obtained by covalent micropatterning of ELRs onto glass surfaces against an inert background allows a reversible, spatio-temporal modulation of ligand-binding triggered by the phase transition of the ELR at a solid-liquid interface. Such technology can be applied in different systems for bio-analytical sensors in order to detect single biomolecules [88,89].

Smart thin coatings using an ELR containing RGD sequences are also a new and interesting example of thermo-responsive surfaces. These coatings can be fabricated through simple deposition of the ELR dissolved in aqueous-based solutions onto chitosan membranes [82]. It was shown that the conformational changes suffered by the ELR at its inverse temperature transition modified the topography at the nanoscale and the wettability of the polymeric substrate, which could be potentially used to control cell adhesion and protein adsorption (see Figure 4.2).



Figure 4.2. Water drop profiles on ELP-coated substrates at 25 and 50°C. Reprinted (adapted) with permission from [82]. Copyright 2009 Wiley-VCH.

4.3.1.2 Light

Light could be an interesting stimulus in the context of stimuli-responsive surfaces, as it is widely used in Nature as a source of energy. Photo-responsive polymers change their properties when irradiated with light, due to light-induced structural transformations of specific functional groups (e.g. chromophores) along the polymer backbone or side chains [90-92]. An important aspect of photo-sensitive polymer systems is that using irradiation as a stimulus is a relatively straightforward, non-invasive mechanism to induce a responsive behavior. The most well studied examples of photo-responsive polymers are those that contain azobenzene groups. Azobenzene is a well-known chromophore with an irradiation-induced *cis* -to-*trans* isomerization that is accompanied by a fast and complete change in electronic structure, geometric shape, and polarity. By incorporating azobenzene derivatives into polymer structures, materials with variable shape, polarity, and self-assembly behavior can be obtained [91]. Azochromophores have been incorporated into a variety of polymeric systems [10,91]. Other chromophores, namely spiropyran and its derivatives have been incorporated terminally or pendantly to confer light sensitivity [93,94]. Spiropyran groups are relatively non-polar, but irradiation with the appropriate wavelength of light leads to the zwitterionic merocyanine isomer that has a larger dipole moment.

Illustrative works where photo-responsive LbL films were prepared can be found elsewhere [91,95]. The studies related with photo-responsive LbL systems have shown that the photoresponsive *cis –trans* -isomerization rates in the layers are highly dependent on the functional groups attached to the

chromophores [91]. Most of the works regarding photo-responsive polymers require isomerization induced by ultraviolet (UV) radiation or visible light. Recent years have also seen a growing interest in employing near-infrared (NIR) radiation as a trigger to activate delivery of encapsulated material from LbL systems [96]. The use of NIR light is particularly attractive in biomedical applications because of the weak absorption of NIR radiation by most tissues.

Photo-isomerizable monolayers applied to surfaces can also be used to control surface properties, such as wettability [97]. In this case, the water contact angle was found to be lower for the spiropyran-modified surfaces after irradiation with UV light, when compared with the contact angle found for visible light. This was ascribed to the changes in the surface energy of the surfaces correlated to the switching of the surface-bound spiropyran molecules between polar, zwitterionic and nonpolar forms.

4.3.2 Chemical stimuli

4.3.2.1 pH

"pH" has also been extensively studied in the biomedical field because this factor can be easily controlled and applicable both *in vitro* and *in vivo* conditions. It is well-known that there is a pH change along the gastrointestinal tract from the stomach (pH=1–3) to the intestine (pH=5–8) and chronic wounds and tumor tissue are also slightly acidic. So, for example, pH-responsive systems can be used for releasing drugs in the intestine in order to avoid their degradation in the environment of the stomach [8]. They have also been investigated for gene delivery and gene therapy. "pH"-responsive polymers contain ionizable groups that can accept and donate protons in response to a pH change. Examples of pH-responsive polymers are chitosan, alginate, hyaluronic acid, PAA, poly(ethyleneimine) (PEI), poly(*N,N*-dyakylamino ethylmethacrylates (PDAAEMA) and poly-lysine [98]. Grafting of pH-responsive polymers has been used to confer pH-responsiveness to a surface. For example, chitosan was grafted onto the surface of PLLA/BG composites [99]. In an acidic medium, chitosan becomes positively charged due to the protonation of the free amine groups. The pH-responsive behavior of the PLLA/BG composites modified with chitosan was confirmed by contact angle measurements. After modification, the contact angle changed from 88.9±4.05° at pH 7.4 to 67.6±2.3° at pH 5.4. The unmodified PLLA/BG composites revealed a hydrophobic character, presenting a contact angle of 82°, independently of the pH.

In LbL, the growth of polyelectrolyte-based coatings is dependent on pH [100,101]. For instance, for chitosan/alginate films, a value of 56 nm was obtained for the final thickness of the films built at a pH

of 7.0 and 34 nm for the multilayers assembled at a pH of 5.5 [101]. When the charge density of the adsorbing species decreases (i.e., chitosan at a pH of 7.0), more polyelectrolyte chains are needed to overcompensate and invert the surface charge, explaining the higher thickness associated with the deposition of polymers at pH 7.0. Also, LbL coatings of polyelectrolytes respond intrinsically to pH. Multilayer films conceived with chitosan and ELRs were demonstrated to be pH-responsive [69]. At high pH values, the roughness of the substrates increased due to the triggering of the ELR self-assembly mechanism into aggregates, besides the variation of the internal electrostatic interactions.
Micro- and nano-scale porosity can be introduced in LbL films by pH variations, thus allowing to control film permeability [102,103].

4.3.2.2 Ionic strength

Polymers that contain ionizable groups are typically sensitive to ionic strength. In fact, due to the attractive Coulombic interactions between oppositely charged species, such polymers may be insoluble in deionized water but soluble in the presence of a determined oncentration of added electrolytes where the attractive charge/charge interactions are shielded, as higher ionic strength solutions reduce the range of electrostatic interactions [104]. So, changes in the ionic strength can lead to changes in the polymer solubility and, therefore, in the length of the deposited polymer chains. Ionic strength is also an important parameter that allows controlling film swelling. In the case poly-lysine/hyaluronic acid LbL films prepared at an ionic strength of 0.15 M in NaCl, reversible swelling and deswelling occurs when the ionic strength is cycled between 0.15 and 0.225 M [105]. Ionic strength has also been used to control the permeability of LbL films as ionic variations can introduce porosity [106].

4.3.3 Biochemical stimuli

4.3.3.1 Antigens

Antigen-antibody interactions have been also explored under the scope of stimuli-responsive surfaces. Such interactions are quite specific and associated with the complex immune responses that help recognize and neutralize foreign infection-causing objects in the body.
Ai and co-workers [107] showed that platelets coated with anti-“immunoglobulin G” (IgG) multilayers could be targeted to IgG-coated surfaces. An antigen responsive membrane based on dextran grafted with both a fluorescent fluorescein isothiocyanate (FITC) antigen and anti-FITC IgC antibody was proposed by Zhang and co-workers [108]. When free sodium fluorescein was added to the membrane,

antibody-antigen crosslinks were broken by competitive binding of the free antigen. The disruption of the crosslinks caused the reversible swelling of the membrane. So, such membranes could be used as gates for selective diffusion controlled by the presence of an antigen.

4.3.3.2 Enzymes

Bacteria located mainly in the colon produce reductive enzymes (e.g. azoreductase) or hydrolytic enzymes (e.g. glycosidases) capable of degrading various types of polysaccharides, such as pectin, chitosan, amylase/amylopectin, cyclodextrin and dextrin [109-111]. For example, polymer systems based on alginate/chitosan are responsive to chitosanase and azoaromatic bonds are sensitive to azoreductase [112,113]. Enzyme responsive polymers present the advantage of not requiring an external trigger for decomposing, exhibit high selectivity and work under mild conditions, although is not straightforward to determine the beginning of degradation. An interesting example regarding enzyme-responsive surfaces are the ones developed by Todd and co-workers, which present cell adhesive arginine-glycine-aspartic acid (RGD) sequences on-demand, that is, by enzymatic hydrolysis of inactive RGD containing precursors that carry cleavable steric blocking groups [114].

4.3.3.3 Glucose

Glucose-responsive polymers can be specifically used in the controlled relase of insulin and for glucose sensing. Typically, glucose oxidase (GOX) is conjugated to a pH-sensitive polymer [115]. GOX oxidizes glucose to gluconic acid, inducing a pH change and the corresponding release of the insulin encapsulated in the pH-system. For example Imanashi and co-workers [116] grafted GOX-conjugated PAA onto a cellulose film. At neutral and high pH the PAA chains were extended due to the negative charged of the carboxylate groups, occluding the pores of the cellulose membrane. The gluconic acid that resulted from the addition of glucose led to a local pH decrease, protonation and subsequent collapse of the PAA chains, leading to the insulin release.

4.3.4 Multiple responsive surfaces

Smart surfaces that respond simultaneously to more than one stimulus could be particularly interesting regarding biomedical applications and could be used, for instance, to control in a more effective way drug release or cell response. Some representative works where this type of surfaces was developed will now be given. For example, dual responsive coatings of chitosan-graft-NIPAAm and alginate were

built [70]. AFM analysis confirmed that PNIPAAm is able to reconform upon temperature swaps even when combined with other layers in a polyelectrolyte multilayer, demonstrating that the nano-assemblies are thermo-responsive. In another work, a smart and stable polymer brush interface based on PNIPAAm, PAA and poly(NIPAAm-co-AA) was able to reversibly respond to temperature, ionic strength and pH, independently or simultaneously [117].

Thermo- and pH- sensitive films of poly(*N,N*-dimethyl aminoethyl methacrylate)-poly(propylene oxide)-poly(*N,N*-dimethyl aminoethyl methacrylate)/PAA ((PD-PPO-PD)/PAA) were prepared by Tan and co-workers [80]. These films present a thickness of 2150 nm at 6°C and of 941 nm at 20°C, when they were deposited from distilled water at pH 7. This volumetric transition does not occur any more when the same films were prepared from water at pH 4 because PPO already forms hydrogen bonds with PAA (mostly in the protonated, neutral form) which are not available any more for water molecules.

Other interesting example of multi-responsive coatings are the PNIPAAm-co-AA copolymers sensitive to pH and temperature that were prepared by Xia and co-workers [75]. The combination of this dual stimuli-responsive coating combined with surface micro and nanostructure enabled the water contact angle (CA) of the surface to be controlled over a range of 150°. On a flat surface, however, the CA change was only 13° and 9.6° for a temperature range of 21–45°C and a pH range of 2–11, respectively.

4.4 Biomedical applications of smart surfaces

4.4.1 Smart coatings for tissue engineering, regenerative medicine and drug delivery applications

Smart coatings can be used to control the properties of the surface of a substrate, such as an implant, by changing the surface chemistry, topography and/or hydrophobicity, and therefore modifying protein adsorption and cell adhesion. These coatings can be simultaneously used to release a drug or bioactive compound in a controlled way. Some representative examples of smart biomaterial coatings will now be presented.

Protein adsorption on PNIPAAm coatings has been investigated by distinct authors, showing that adsorption is typically unfavorable below the LCST, being stronger above the LCST [118-120]. For some proteins and some conditions, protein adsorption might become irreversible, inhibiting repeated switching. It was found that protein adsorption reversibility on PNIPAAm coatings depends whether the

phase transition back to the hydrated protein resistant state is energetically more favorable than the interactions formed between chains and the protein in the collapsed state [119].

Several studies have focused on the influence of the LbL film composition on protein adsorption [121,122]. For instance, the adsorption of human serum albumin (HSA) onto chitosan/alginate multilayer assemblies was assessed *in situ* using QCM-D [123]. It was found that the behavior of human serum albumin (HAS) on biomaterials surface can be tuned by adjusting parameters of the polyelectrolyte system such as pH, layer number, crosslinker and polymer terminal layer. The key role of electrostatic interactions during HSA adsorption was evidenced in that work, since oppositely charged surfaces were more effective in promoting protein adhesion. Also, novel protein-based systems have been developed by self-assembly, introducing the possibility to prepare, in a controllable way, thin reservoirs of proteins [124] and, by embedding biologically active proteins, film functionalization can be achieved [125]. The LbL approach has enabled protein encapsulation to release active proteins in a way that is applicable to objects of any desired geometry and size scale [126]. Moreover, microcapsules with a hierarchical shell-within-shell structure of different proteins entrapped in polymeric layers have been developed [127].

In the field of active molecule release, it is also very interesting to develop LbL films in which one of the components hydrolyses above a critical pH value leading to film erosion and release of the active molecule. This concept has been used for the pH triggered release of anionic polysaccharides and of deoxyribonucleic acid (DNA) from poly-(β-amino ester)-DNA films [67,128]. The decomposition or release of active compounds can also occur through enzymatic hydrolysis [129]. For example, DNA and non-activated DNAase were co-encapsulated in hollow polyelectrolyte capsules. The enzyme can be activated by a chemical trigger which diffuses through the polyelectrolyte membrane, activating the enzyme, the subsequent hydrolysis of DNA and the diffusion of small oligonucleotides through the capsule wall [130]. LbL can also be used to coat inorganic microspheres to conceive smart microreservoirs. Huang and Chang [131] developed multilayer microcapsules made of azido- and acetylene-functionalized PNIPAAm that shrunk upon increasing the temperature from 25 to 50°C (Figure 4.3). These microcapsules were also permeable to low-molecular weight substances, such as dextran.

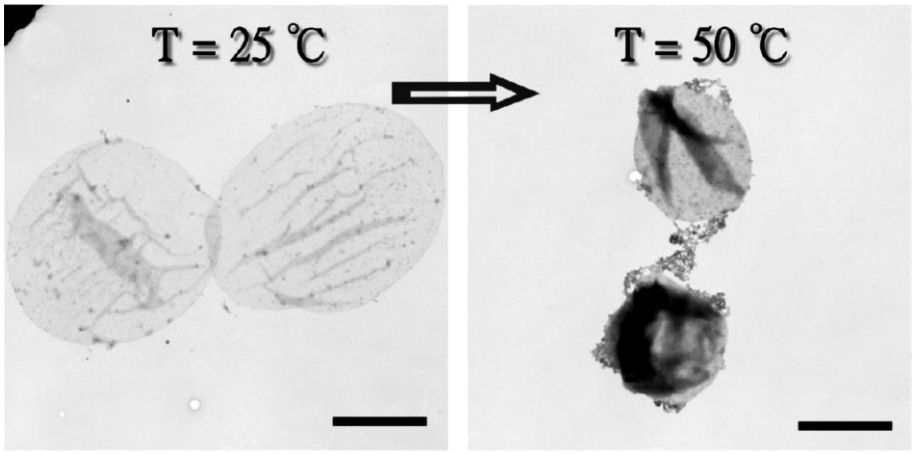


Figure 4.3. Transmission electron microscopy (TEM) images of azido- and acetylene-functionalized PNIPAAm microcapsules dried at 25°C and 50°C. Scale bar: 2 μm. Reprinted (adapted) with permission from [131]. Copyright 2009 American Chemical Society.

There are many other interesting examples related with the field of active molecule release. For instance, pH-responsive polymers may be used to deliver fragile biomolecules such as peptides or oligonucleotides to the cytoplasm of macrophages, as the work of Murthy and co-workers evidenced [132]. They used pH cleavable acetal linkages to remove poly(ethylene glycol) (PEG) grafts that mask the delivery vehicle and disrupt the endosome causing the delivery of biomolecules into the cytoplasm before they are degraded in the lysosomes. PNIPAAm/-co-AA microgels/polyallylamine coatings retained their thermo-responsiveness within the multilayer and allowed their use for thermally triggered release of insulin [133]. An antimicrobial coating that can simultaneously discourage bacteria attachment to the implant surface and release, in a tuneable dosage and rate, antibiotics into the surrounding tissues has also been developed [134].

Regarding the use of smart surfaces to control cell response, several works can also be found in literature. For example, Picart *et al.* [135] investigated the effect of grafting an RGD peptide onto distinct LbL films on the adhesion of primary cells, and observed an enhanced cell proliferation for the functionalized films. Boura *et al.* [136] evaluated the adhesion properties of endothelial cell on two types of polyelectrolyte films ending either by polylysine, or poly(allylamine hydrochloride) (PAH), and compared them to data obtained on polylysine or PAH monolayers, glass and fibronectin-coated glass. They found that the cells seeded on the LbL films showed a good morphology and resisted to physiological shear stress better, when compared to the cell seeded on glass or fibronectin.

Photo-responsive layers composed of made of PNIPAAm and spiropyrans have been used to tailor cell adhesion by switching light on or off [95]. Cell adhesion has also been photo-chemically controlled

using RGD-functionalized azobenzene poly(methyl methacrylate) (PMMA) surfaces [137]. It was found that azobenzenes enhanced cell adhesion but, upon UV-irradiation-induced *trans -cis* isomerization, which shortened the distance of the RGD-containing peptides from the surface, cell adhesion decreased. Nakanishi *et al.* [138] built self-assembled monolayers having photo-cleavable 2-nitrobenzyl groups that could be used to template cell adhesion. Bovine serum albumin (BSA), inert to cell adhesion, was adsorbed over this monolayer. Upon exposing defined regions with UV light, BSA was released from such regions. Finally, fibronectin, a protein promoting cell adhesion, was then incubated and covered the irradiated regions. This method allowed producing patterned regions for cell adhesions and by subsequent illumination it could be also possible to induce cell migration and proliferation.

4.4.2 Smart biomineralization

In medical devices for orthopaedic applications, either under traditional replacement concepts or regeneration strategies, such as tissue engineering, it is important to promote the production of bonelike apatite onto the biomaterial's surface. It has been shown that surface biomimetic mineralization may be triggered by either temperature or pH [74,99]. For PNIPAAm modified composite PLLA film with 10% BG, it was found that the conformational changes occurring at the surface affect the mineral formation below and above the LCST [74]. No mineral phase could be observed at 25°C after 2 weeks in simulated body fluid (SBF). However, at 37°C the treated film could form dense precipitates with the typical cauliflower morphology, containing needle-like nanometric structures, characteristic of biomimetic-formed apatite. Moreover, by exposing some regions of the surface to the plasma treatment, a patterning could be made to combine stimuli and spatial control of biomimetic apatite [74]. This allowed the insertion of PNIPAAm in specific chosen areas. Again, no apatite formation was observed for these modified films at 25°C. On the other hand, apatite aggregates were formed at 37°C, with a circular shape and randomly distributed over the composite surface, being consistent with the PNIPAAm patterning generated during the plasma activation step. These apatite patterned surfaces could be used in fundamental studies on differentiation, adhesion, proliferation and cell-cell signaling of bone-related cells. These surfaces could also be used in fundamental co-culture studies involving bone cells and other cell types [139,140].

For chitosan-modified PLLA/BG composites no apatite formation was found at pH 5.4 [99]. On the other hand, a dense apatite layer of a carbonated apatite mineral similar to the major mineral component of vertebrate bone tissue was formed at pH 7.4. For the unmodified substrates an apatite

layer was formed at both pH. Temperature and pH were chosen in the above mentioned works, but this concept of smart apatite formation can be extended for other source of responsiveness and for other type of mineral deposition.

4.4.3 Cell sheet engineering

The use of smart surfaces, specifically thermo-responsive surfaces, has been applied to the so-called "cell sheet engineering". This technology has been proposed to construct ideal transplantable tissues composed exclusively of cells [141]. Initially, Okano and co-workers proposed temperature-responsive cell culture polystyrene substrates prepared by the grafting of PNIPAAm onto these surfaces, which allow the culture of confluent cell monolayers at 37°C and their recovery as single cell sheets when the temperature is below the LCST of PNIPAAm. Afterwards, they have combined these smart surfaces with patterning, with the aim of producing complicated three-dimensional tissues [142-145]. For instance, micropatterned dual thermo-responsive surfaces that enable the culture and recovery of patterned heterotopic cell sheets were proposed [142,143].

Okano and co-workers have shown that it is possible to obtain cell sheet constructs with five layers, where the viability of the transferred cells and the adequate organization of the functional cell-cell junctions were demonstrated [144]. Direct transplantations of cell sheets have been already successfully applied to corneal epithelia, mucosal epithelia, periodontal ligament cells, bladder epithelia and esophageal epithelia [141]. Cell sheets have also been layered in order to successfully recreate thicker tissue-like constructs such as cardiac and more recently bone [146].

The LbL approach has also been explored as a potential alternative to the traditional grafting techniques employed for cell sheet engineering. It was shown that (chitosan-graft-NIPAAm)/alginate LbL films enabled the attachment and proliferation until confluence of cells at 37°C and the spontaneous detachment of cell sheets along with their deposited extracellular matrix by simple temperature modulation (Figure 4.4) [70]. Thus, these multilayered thermo-responsive surfaces could potentially be used in cell sheet engineering. The mild conditions and the absence of harmful solvents, the simplicity of the method and the ability to modulate cellular adhesiveness by controlling the "nanometric" thickness of the coatings are some of the advantages of this novel strategy. A completely new strategy for cell culture focusing on the design of three-dimensional smart surfaces by supercritical fluid technology has also been recently proposed based on supercritical carbon dioxide [147]. This approach might overcome the limitations on cell expansion and harvesting of currently existing techniques.

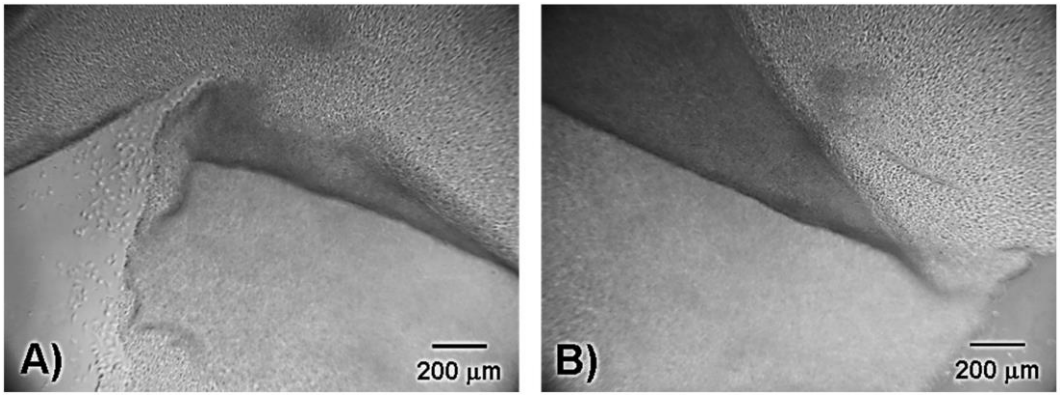


Figure 4.4. In-situ detachment of SaOs-2 cell sheets after 10 min (A) and 15 min (B) of incubation at 4°C from $(GRAFT/ALG)_5GRAFT$ films. Reprinted with permission from [70]. Copyright 2011 American Chemical Society.

4.5 Conclusions

The latest advancements in healthcare have emphasized the need to develop dynamic devices that can adjust themselves to a specific situation. Although many of these concepts are still under development in the lab bench, substrates modified with stimuli-responsive properties have already been proposed for controlling the adhesion of cells or proteins, microfluidics and biosensors.

From the literature, it is clear that such advances are owed to the variety of methods that one can use to modify an interface and to the wide array of materials that can be used to build it. Thus substrates that respond to distinct physical, chemical and biochemical stimuli can be made with potential for new cutting-edge applications in biology and biotechnology. In the next decade, we expect to assist to the rise of dynamic smart systems with new designs and complexity moving further into the third dimension. Switchable surfaces exhibiting alternating biological active signals will be used to develop new cell culture protocols. Substrates with dynamic molecular conformation upon the contact with a specific biochemical agent will be used as biosensors for rapid diagnostic. Stimuli-responsive interfaces built onto drug reservoirs will be further optimized to tune and control better the release of encapsulated therapeutic molecules. With such nature, smart surfaces offer opportunities for a wide array of applications in medicine and tissue engineering where an interface with switchable properties is needed.

4.6 Acknowledgements

We acknowledge financial support from the Portuguese "Fundação para a Ciência e Tecnologia" – FCT (grant SFRH/BD/61126/2009), "Fundo Social Europeu" – FSE, "Programa Diferencial de Potencial

Humano'' – POPH, the European Commission through the 7th Framework Programme (projects HEALTH-F4-2011-278557 and NMP3-LA-2011-263363), from the Spanish Minister of Economy and Competitiveness – MEC (projects MAT2009-14195-C03-03, MAT-2010-15982, MAT2010-15310, IT2009-0089, ACI2009-0890 and PRI-PIBAR-2011-1403), the Junta de Castilla y León -JCyL (projects VA034A09 and VA0049A11-2), the CIBER-BBN (project CB06-01-1038), and the JCyL and the Instituto de Salud Carlos III under the "Network Center of Regenerative Medicine and Cellular Therapy of Castilla and León".

4.7 References

[1] Cole M. A., Voelcker N. H., Thissen H., and Griesser H. J., Stimuli-responsive interfaces and systems for the control of protein–surface and cell–surface interactions, Biomaterials 2009, 30: 1827-1850.

[2] Lahann J., and Langer R., Smart Materials with Dynamically Controllable Surfaces, MRS Bulletin 2005, 30: 185-188.

[3] Stevens M. M., and George J. H., Exploring and Engineering the Cell Surface Interface, Science 2005, 310: 1135-1138.

[4] Tokarev I., and Minko S., Multiresponsive, Hierarchically Structured Membranes: New, Challenging, Biomimetic Materials for Biosensors, Controlled Release, Biochemical Gates, and Nanoreactors, Advanced Materials 2009, 21: 241-247.

[5] Hubbell J. A., Bioactive biomaterials, Current Opinion in Biotechnology 1999, 10: 123-129.

[6] Langer R., and Tirrell D. A., Designing materials for biology and medicine, Nature 2004, 428: 487-492.

[7] Mitragotri S., and Lahann J., Physical approaches to biomaterial design, Nat Mater 2009, 8: 15-23.

[8] Gil E. S., and Hudson S. M., Stimuli-reponsive polymers and their bioconjugates, Progress in Polymer Science 2004, 29: 1173-1222.

[9] Mano J. F., Stimuli-responsive polymeric systems for biomedical applications, Advanced Engineering Materials 2008, 10: 515-527.

[10] Roy D., Cambre J. N., and Sumerlin B. S., Future perspectives and recent advances in stimuli-responsive materials, Progress in Polymer Science 2010, 35: 278-301.

[11] Boudou T., Crouzier T., Ren K., Blin G., and Picart C., Multiple Functionalities of Polyelectrolyte Multilayer Films: New Biomedical Applications, Advanced Materials 2010, 22: 441-467.

[12] Mendes P. M., Stimuli-responsive surfaces for bio-applications, Chemical Society Reviews 2008, 37: 2512-2529.

[13] Stuart M. A. C., Huck W. T. S., Genzer J., Muller M., Ober C., Stamm M., Sukhorukov G. B., Szleifer I., Tsukruk V. V., Urban M., Winnik F., Zauscher S., Luzinov I., and Minko S., Emerging applications of stimuli-responsive polymer materials, Nat Mater 2010, 9: 101-113.

[14] Zhou F., and Huck W. T. S., Surface grafted polymer brushes as ideal building blocks for "smart" surfaces, Physical Chemistry Chemical Physics 2006, 8: 3815-3823.

[15] Prakash S., Karacor M. B., and Banerjee S., Surface modification in microsystems and nanosystems, Surface Science Reports 2009, 64: 233-254.

[16] Ulman A., Formation and Structure of Self-Assembled Monolayers, Chemical Reviews 1996, 96: 1533-1554.

[17] Haensch C., Hoeppener S., and Schubert U. S., Chemical modification of self-assembled silane based monolayers by surface reactions, Chemical Society Reviews 2010, 39: 2323-2334.

[18] Fryxell G. E., Rieke P. C., Wood L. L., Engelhard M. H., Williford R. E., Graff G. L., Campbell A. A., Wiacek R. J., Lee L., and Halverson A., Nucleophilic Displacements in Mixed Self-Assembled Monolayers, Langmuir 1996, 12: 5064-5075.

[19] Kolb H. C., Finn M. G., and Sharpless K. B., Click Chemistry: Diverse Chemical Function from a Few Good Reactions, Angewandte Chemie International Edition 2001, 40: 2004-2021.

[20] Onclin S., Mulder A., Huskens J., Ravoo B. J., and Reinhoudt D. N., Molecular Printboards: Monolayers of β-Cyclodextrins on Silicon Oxide Surfaces, Langmuir 2004, 20: 5460-5466.

[21] Poirier G. E., and Pylant E. D., The Self-Assembly Mechanism of Alkanethiols on Au(111), Science 1996, 272: 1145-1148.

[22] Laiho T., Lukkari J., Meretoja M., Laajalehto K., Kankare J., and Leiro J. A., Chemisorption of alkyl thiols and S-alkyl thiosulfates on Pt(111) and polycrystalline platinum surfaces, Surface Science 2005, 584: 83-89.

[23] Mrksich M., Dike L. E., Tien J., Ingber D. E., and Whitesides G. M., Using Microcontact Printing to Pattern the Attachment of Mammalian Cells to Self-Assembled Monolayers of Alkanethiolates on Transparent Films of Gold and Silver, Experimental Cell Research 1997, 235: 305-313.

[24] Appelhans D., Ferse D., Adler H. J. P., Plieth W., Fikus A., Grundke K., Schmitt F. J., Bayer T., and Adolphi B., Self-assembled monolayers prepared from ω-thiophene-functionalized n-

alkyltrichlorosilane on silicon substrates, Colloids and Surfaces A: Physicochemical and Engineering Aspects 2000, 161: 203-212.

[25] Raynor J. E., Petrie T. A., García A. J., and Collard D. M., Controlling Cell Adhesion to Titanium: Functionalization of Poly[oligo(ethylene glycol)methacrylate] Brushes with Cell-Adhesive Peptides, Advanced Materials 2007, 19: 1724-1728.

[26] Gnauck M., Jaehne E., Blaettler T., Tosatti S., Textor M., and Adler H.-J. P., Carboxy-Terminated Oligo(ethylene glycol)−Alkane Phosphate: Synthesis and Self-Assembly on Titanium Oxide Surfaces, Langmuir 2006, 23: 377-381.

[27] Raynor J., Capadona J., Collard D., Petrie T., and García A., Polymer brushes and self-assembled monolayers: Versatile platforms to control cell adhesion to biomaterials (Review), Biointerphases 2009, 4: FA3-FA16.

[28] Abbott N. L., Gorman C. B., and Whitesides G. M., Active Control of Wetting Using Applied Electrical Potentials and Self- Assembled Monolayers, Langmuir 1995, 11: 16-18.

[29] Katsonis N., Lubomska M., Pollard M. M., Feringa B. L., and Rudolf P., Synthetic light-activated molecular switches and motors on surfaces, Progress in Surface Science 2007, 82: 407-434.

[30] Bayly S. R., Gray T. M., Chmielewski M. J., Davis J. J., and Beer P. D., Anion templated surface assembly of a redox-active sensory rotaxane, Chemical Communications 2007: 2234-2236.

[31] Toomey R., Freidank D., and Rühe J., Swelling Behavior of Thin, Surface-Attached Polymer Networks, Macromolecules 2004, 37: 882-887.

[32] Tanaka T., and Fillmore D. J., Kinetics of swelling of gels, Journal of Chemical Physics 1979, 70: 1214-1218.

[33] Onuki A., Theory of phase transition in polymer gels, In Dušek K., ed. Responsive Gels: Volume Transitions I, Berlin/Heidelberg, Germany: Springer Verlag; 1993.

[34] Gabai R., Sallacan N., Chegel V., Bourenko T., Katz E., and Willner I., Characterization of the Swelling of Acrylamidophenylboronic Acid−Acrylamide Hydrogels upon Interaction with Glucose by Faradaic Impedance Spectroscopy, Chronopotentiometry, Quartz-Crystal Microbalance (QCM), and Surface Plasmon Resonance (SPR) Experiments, The Journal of Physical Chemistry B 2001, 105: 8196-8202.

[35] Matsukuma D., Yamamoto K., and Aoyagi T., Stimuli-Responsive Properties of N-Isopropylacrylamide-Based Ultrathin Hydrogel Films Prepared by Photo-Cross-Linking, Langmuir 2006, 22: 5911-5915.

[36] Beebe D. J., Moore J. S., Bauer J. M., Yu Q., Liu R. H., Devadoss C., and Jo B.-H., Functional hydrogel structures for autonomous flow control inside microfluidic channels, Nature 2000, 404: 588-590.

[37] Tokarev I., Orlov M., and Minko S., Responsive Polyelectrolyte Gel Membranes, Advanced Materials 2006, 18: 2458-2460.

[38] Zhao B., and Moore J. S., Fast pH- and Ionic Strength-Responsive Hydrogels in Microchannels, Langmuir 2001, 17: 4758-4763.

[39] Milner S. T., Polymer Brushes, Science 1991, 251: 905-914.

[40] Barbey R., Lavanant L., Paripovic D., Schüwer N., Sugnaux C., Tugulu S., and Klok H.-A., Polymer Brushes via Surface-Initiated Controlled Radical Polymerization: Synthesis, Characterization, Properties, and Applications, Chemical Reviews 2009, 109: 5437-5527.

[41] Zhao B., and Brittain W. J., Polymer brushes: surface-immobilized macromolecules, Progress in Polymer Science 2000, 25: 677-710.

[42] Fan X., Lin L., Dalsin J. L., and Messersmith P. B., Biomimetic Anchor for Surface-Initiated Polymerization from Metal Substrates, Journal of the American Chemical Society 2005, 127: 15843-15847.

[43] Gao H., and Matyjaszewski K., Synthesis of Molecular Brushes by "Grafting onto" Method: Combination of ATRP and Click Reactions, Journal of the American Chemical Society 2007, 129: 6633-6639.

[44] Heroguez V., Gnanou Y., and Fontanille M., Novel Amphiphilic Architectures by Ring-Opening Metathesis Polymerization of Macromonomers, Macromolecules 1997, 30: 4791-4798.

[45] Gerle M., Fischer K., Roos S., Müller A. H. E., Schmidt M., Sheiko S. S., Prokhorova S., and Möller M., Main Chain Conformation and Anomalous Elution Behavior of Cylindrical Brushes As Revealed by GPC/MALLS, Light Scattering, and SFM, Macromolecules 1999, 32: 2629-2637.

[46] Balazs A. C., Singh C., Zhulina E., Chern S.-S., Lyatskaya Y., and Pickett G., Theory of polymer chains tethered at interfaces, Progress in Surface Science 1997, 55: 181-269.

[47] Motornov M., Roiter Y., Tokarev I., and Minko S., Stimuli-responsive nanoparticles, nanogels and capsules for integrated multifunctional intelligent systems, Progress in Polymer Science 2010, 35: 174-211.

[48] Brittain W. J., and Minko S., A structural definition of polymer brushes, Journal of Polymer Science Part A: Polymer Chemistry 2007, 45: 3505-3512.

[49] Luzinov I., Voronov A., Minko S., Kraus R., Wilke W., and Zhuk A., Encapsulation of fillers with grafted polymers for model composites, Journal of Applied Polymer Science 1996, 61: 1101-1109.

[50] Okano T., Yamada N., Sakai H., and Sakurai Y., A novel recovery system for cultured cells using plasma-treated polystyrene dishes grafted with poly(N-isopropylacrylamide), Journal of Biomedical Materials Research 1993, 27: 1243-1251.

[51] Draper J., Luzinov I., Minko S., Tokarev I., and Stamm M., Mixed Polymer Brushes by Sequential Polymer Addition: Anchoring Layer Effect, Langmuir 2004, 20: 4064-4075.

[52] Xu C., Wu T., Drain C. M., Batteas J. D., Fasolka M. J., and Beers K. L., Effect of Block Length on Solvent Response of Block Copolymer Brushes: Combinatorial Study with Block Copolymer Brush Gradients, Macromolecules 2006, 39: 3359-3364.

[53] Clark S. L., and Hammond P. T., The Role of Secondary Interactions in Selective Electrostatic Multilayer Deposition, Langmuir 2000, 16: 10206-10214.

[54] Tang Z., Wang Y., Podsiadlo P., and Kotov N. A., Biomedical Applications of Layer-by-Layer Assembly: From Biomimetics to Tissue Engineering, Advanced Materials 2006, 18: 3203-3224.

[55] Hammond P. T., Form and Function in Multilayer Assembly: New Applications at the Nanoscale, Advanced Materials 2004, 16: 1271-1293.

[56] Wang X., Kim Y.-G., Drew C., Ku B.-C., Kumar J., and Samuelson L. A., Electrostatic Assembly of Conjugated Polymer Thin Layers on Electrospun Nanofibrous Membranes for Biosensors, Nano Letters 2004, 4: 331-334.

[57] Ariga K., Hill J. P., and Ji Q., Biomaterials and biofunctionality in layered macromolecular assemblies, Macromolecular Bioscience 2008, 8: 981-990.

[58] Bertrand P., Jonas A., Laschewsky A., and Legras R., Ultrathin polymer coatings by complexation of polyelectrolytes at interfaces: suitable materials, structure and properties, Macromolecular Rapid Communications 2000, 21: 319-348.

[59] Gribova V., Auzely-Velty R., and Picart C., Polyelectrolyte multilayer assemblies on materials surfaces: from cell adhesion to tissue engineering, Chemistry of Materials 2011, 24: 854-869.

[60] Elzbieciak M., Wodka D., Zapotoczny S., Nowak P., and Warszynski P., Characteristics of Model Polyelectrolyte Multilayer Films Containing Laponite Clay Nanoparticles, Langmuir 2009, 26: 277-283.

[61] Kong B.-S., Geng J., and Jung H.-T., Layer-by-layer assembly of graphene and gold nanoparticles by vacuum filtration and spontaneous reduction of gold ions, Chemical Communications 2009, 16: 2174-2176.

[62] Couto D. S., Alves N., M., and Mano J., F., Nanostructured Multilayer Coatings Combining Chitosan with Bioactive Glass Nanoparticles, Journal of Nanoscience and Nanotechnology 2009, 9: 1741-1748.

[63] Decher G., Hong J. D., and Schmitt J., Buildup of ultrathin multilayer films by a self-assembly process: III. Consecutively alternating adsorption of anionic and cationic polyelectrolytes on charged surfaces, Thin Solid Films 1992, 210-211: 831-835.

[64] Larkin A. L., Davis R. M., and Rajagopalan P., Biocompatible, Detachable, and Free-Standing Polyelectrolyte Multilayer Films, Biomacromolecules 2010, 11: 2788-2796.

[65] She Z., Antipina M. N., Li J., and Sukhorukov G. B., Mechanism of Protein Release from Polyelectrolyte Multilayer Microcapsules, Biomacromolecules 2010, 11: 1241-1247.

[66] Sher P., Custódio C. A., and Mano J. F., Layer-By-Layer Technique for Producing Porous Nanostructured 3D Constructs Using Moldable Freeform Assembly of Spherical Templates, Small 2010, 6: 2644-2648.

[67] Wood K. C., Boedicker J. Q., Lynn D. M., and Hammond P. T., Tunable Drug Release from Hydrolytically Degradable Layer-by-Layer Thin Films, Langmuir 2005, 21: 1603-1609.

[68] Linford M. R., Auch M., and Möhwald H., Nonmonotonic Effect of Ionic Strength on Surface Dye Extraction during Dye–Polyelectrolyte Multilayer Formation, Journal of the American Chemical Society 1998, 120: 178-182.

[69] Costa R. R., Custódio C. A., Arias F. J., Rodríguez-Cabello J. C., and Mano J. F., Layer-by-Layer Assembly of Chitosan and Recombinant Biopolymers into Biomimetic Coatings with Multiple Stimuli-Responsive Properties, Small 2011, 7: 2640-2649.

[70] Martins G. V., Mano J. F., and Alves N. M., Dual Responsive Nanostructured Surfaces for Biomedical Applications, Langmuir 2011, 27: 8415-8423.

[71] Schild H. G., Poly(N-isopropylacrylamide): experiment, theory and application, Progress in Polymer Science 1992, 17: 163-249.

[72] Liu S.-Q., Yang Y.-Y., Liu X.-M., and Tong Y.-W., Preparation and Characterization of Temperature-Sensitive Poly(N-isopropylacrylamide)-b-poly(d,l-lactide) Microspheres for Protein Delivery, Biomacromolecules 2003, 4: 1784-1793.

[73] Shibayama M., and Tanaka T., Volume phase transition and related phenomena of polymer gels, In Dušek K., ed. Responsive Gels: Volume Transitions I, Berlin/Heidelberg, Germany: Springer Verlag; 1993.

[74] Shi J., Alves N. M., and Mano J. F., Thermally responsive biomineralization on biodegradable substrates, Advanced Functional Materials 2007, 17: 3312–3318.

[75] Xia F., Feng L., Wang S., Sun T., Song W., Jiang W., and Jiang L., Dual-Responsive Surfaces That Switch between Superhydrophilicity and Superhydrophobicity, Advanced Materials 2006, 18: 432-436.

[76] Wenzel R. N., Resistance of solid surfaces to wetting by water, Industrial & Engineering Chemistry 1936, 28: 988-994.

[77] Serpe M. J., Jones C. D., and Lyon L. A., Layer-by-Layer Deposition of Thermoresponsive Microgel Thin Films, Langmuir 2003, 19: 8759-8764.

[78] Galaev I. Y., Warrol C., and Mattiasson B., Temperature-induced displacement of proteins from dye-affinity columns using an immobilized polymeric displacer, Journal of Chromatography A 1994, 684: 37-43.

[79] Vihola H., Laukkanen A., Valtola L., Tenhu H., and Hirvonen J., Cytotoxicity of thermosensitive polymers poly(N-isopropylacrylamide), poly(N-vinylcaprolactam) and amphiphilically modified poly(N-vinylcaprolactam), Biomaterials 2005, 26: 3055-3064.

[80] Tan W. S., Cohen R. E., Rubner M. F., and Sukhishvili S. A., Temperature-Induced, Reversible Swelling Transitions in Multilayers of a Cationic Triblock Copolymer and a Polyacid, Macromolecules 2010, 43: 1950-1957.

[81] Rodríguez-Cabello J. C., Martín L., Alonso M., Arias F. J., and Testera A. M., "Recombinamers" as advanced materials for the post-oil age, Polymer 2009, 50: 5159-5169.

[82] Costa R. R., Custódio C. A., Testera A. M., Arias F. J., Rodríguez-Cabello J. C., Alves N. M., and Mano J. F., Stimuli-Responsive Thin Coatings Using Elastin-Like Polymers for Biomedical Applications, Advanced Functional Materials 2009, 19: 3210-3218.

[83] Girotti A., Reguera J., Rodríguez-Cabello J., Arias F., Alonso M., and Testera A., Design and bioproduction of a recombinant multi(bio)functional elastin-like protein polymer containing cell adhesion sequences for tissue engineering purposes, Journal of Materials Science: Materials in Medicine 2004, 15: 479-484.

[84] Prieto S., Shkilnyy A., Rumplasch C., Ribeiro A., Arias F. J., Rodríguez-Cabello J. C., and Taubert A., Biomimetic Calcium Phosphate Mineralization with Multifunctional Elastin-Like Recombinamers, Biomacromolecules 2011: null-null.

[85] Rodríguez-Cabello J. C., Reguera J., Alonso M., Parker T. M., McPherson D. T., and Urry D. W., Endothermic and exothermic components of an inverse temperature transition for hydrophobic association by TMDSC, Chemical Physics Letters 2004, 388: 127-131.

[86] Tamburro A. M., Guantieri V., and Daga Gordini D., Synthesis and structural studies of a pentapeptide sequence of elastin. Poly (Val-Gly-Gly-Leu-Gly), Journal of Biomolecular Structure and Dynamics 1992, 10: 441-454.

[87] Urry D. W., Shaw R. G., and Prasad K. U., Polypentapeptide of elastin: Temperature dependence of ellipticity and correlation with elastomeric force, Biochemical and Biophysical Research Communications 1985, 130: 50-57.

[88] Nath N., and Chilkoti A., Creating "Smart" surfaces using stimuli responsive polymers, Advanced Materials 2002, 14: 1243-1247.

[89] Nath N., Hyun J., Ma H., and Chilkoti A., Surface engineering strategies for control of protein and cell interactions, Surface Science 2004, 570: 98-110.

[90] Bédard M. F., De Geest B. G., Skirtach A. G., Möhwald H., and Sukhorukov G. B., Polymeric microcapsules with light responsive properties for encapsulation and release, Advances in Colloid and Interface Science 2010, 158: 2-14.

[91] El Halabieh R. H., Mermut O., and Barrett C. J., Using light to control physical properties of polymers and surfaces with azobenzene chromophores, Pure and Applied Chemistry 2004, 76: 1445-1465.

[92] Schumers J. M., Fustin C. A., and Gohy J. F., Light-responsive block copolymers., Macromolecular Rapid Communications 2010, 31: 1588-1607.

[93] Ogawa M., Ishii T., Miyamoto N., and Kuroda K., Photocontrol of the Basal Spacing of Azobenzene–Magadiite Intercalation Compound, Advanced Materials 2001, 13: 1107-1109.

[94] Ziegler A., Stumpe J., Toutianoush A., and Tieke B., Photoorientation of azobenzene moieties in self-assembled polyelectrolyte multilayers, Colloids and Surfaces A: Physicochemical and Engineering Aspects 2002, 198–200: 777-784.

[95] Garcia A., Marquez M., Cai T., Rosario R., Hu Z., Gust D., Hayes M., Vail S. A., and Park C.-D., Photo-, Thermally, and pH-Responsive Microgels, Langmuir 2007, 23: 224-229.

[96] Angelatos A. S., Radt B., and Caruso F., Light-Responsive Polyelectrolyte/Gold Nanoparticle Microcapsules, The Journal of Physical Chemistry B 2005, 109: 3071-3076.

[97] Rosario R., Gust D., Hayes M., Jahnke F., Springer J., and Garcia A. A., Photon-Modulated Wettability Changes on Spiropyran-Coated Surfaces, Langmuir 2002, 18: 8062-8069.

[98] Cabane E., Zhang X., Langowska K., Palivan C., and Meier W., Stimuli-Responsive Polymers and Their Applications in Nanomedicine, Biointerphases 2012, 7: 1-27.

[99] Dias C. I., Mano J. F., and Alves N. M., pH-Responsive biomineralization onto chitosan grafted biodegradable substrates, Journal of Materials Chemistry 2008, 18: 2493-2499.

[100] Alves N. M., Picart C., and Mano J. F., Self Assembling and Crosslinking of Polyelectrolyte Multilayer Films of Chitosan and Alginate Studied by QCM and IR Spectroscopy, Macromolecular Bioscience 2009, 9: 776-785.

[101] Martins G. V., Mano J. F., and Alves N. M., Nanostructured self-assembled films containing chitosan fabricated at neutral pH, Carbohydrate Polymers 2010, 80: 570-573.

[102] Déjugnat C., and Sukhorukov G. B., pH-Responsive Properties of Hollow Polyelectrolyte Microcapsules Templated on Various Cores, Langmuir 2004, 20: 7265-7269.

[103] Hiller J. A., Mendelsohn J. D., and Rubner M. F., Reversibly erasable nanoporous anti-reflection coatings from polyelectrolyte multilayers, Nat Mater 2002, 1: 59-63.

[104] Kathmann E. E. L., White L. A., and McCormick C. L., Water-Soluble Polymers. 73. Electrolyte- and pH-Responsive Zwitterionic Copolymers of 4-[(2-Acrylamido-2-methylpropyl)-dimethylammonio]butanoate with 3-[(2-Acrylamido-2-methyl- propyl)dimethylammonio]propanesulfonate, Macromolecules 1997, 30: 5297-5304.

[105] Mjahed H., Voegel J.-C., Senger B., Chassepot A., Rameau A., Ball V., Schaaf P., and Boulmedais F., Hole formation induced by ionic strength increase in exponentially growing multilayer films, Soft Matter 2009, 5: 2269-2276.

[106] Fery A., Schöler B., Cassagneau T., and Caruso F., Nanoporous Thin Films Formed by Salt-Induced Structural Changes in Multilayers of Poly(acrylic acid) and Poly(allylamine), Langmuir 2001, 17: 3779-3783.

[107] Ai H., Fang M., Jones S. A., and Lvov Y. M., Electrostatic Layer-by-Layer Nanoassembly on Biological Microtemplates: Platelets, Biomacromolecules 2002, 3: 560-564.

[108] Zhang R., Bowyer A., Eisenthal R., and Hubble J., A smart membrane based on an antigen-responsive hydrogel, Biotechnology and Bioengineering 2007, 97: 976-984.

[109] Chambin O., Dupuis G., Champion D., Voilley A., and Pourcelot Y., Colon-specific drug delivery: Influence of solution reticulation properties upon pectin beads performance, International Journal of Pharmaceutics 2006, 321: 86-93.

[110] Sinha V. R., and Kumria R., Polysaccharides in colon-specific drug delivery, International Journal of Pharmaceutics 2001, 224: 19-38.

[111] Vandamme T. F., Lenourry A., Charrueau C., and Chaumeil J. C., The use of polysaccharides to target drugs to the colon, Carbohydrate Polymers 2002, 48: 219-231.

[112] Akala E. O., Kopečková P., and Kopeček J., Novel pH-sensitive hydrogels with adjustable swelling kinetics, Biomaterials 1998, 19: 1037-1047.

[113] Itoh Y., Matsusaki M., Kida T., and Akashi M., Enzyme-Responsive Release of Encapsulated Proteins from Biodegradable Hollow Capsules, Biomacromolecules 2006, 7: 2715-2718.

[114] Todd S. J., Scurr D. J., Gough J. E., Alexander M. R., and Ulijn R. V., Enzyme-Activated RGD Ligands on Functionalized Poly(ethylene glycol) Monolayers: Surface Analysis and Cellular Response, Langmuir 2009, 25: 7533-7539.

[115] Qiu Y., and Park K., Environment-sensitive hydrogels for drug delivery, Advanced Drug Delivery Reviews 2001, 53: 321-339.

[116] Ito Y., Casolaro M., Kono K., and Imanishi Y., An insulin-releasing system that is responsive to glucose, Journal of Controlled Release 1989, 10: 195-203.

[117] Zhou J., Wang G., Hu J., Lu X., and Li J., Temperature, ionic strength and pH induced electrochemical switching of smart polymer interfaces, Chemical Communications 2006: 4820-4822.

[118] Cheng X., Canavan H. E., Stein M. J., Hull J. R., Kweskin S. J., Wagner M. S., Somorjai G. A., Castner D. G., and Ratner B. D., Surface Chemical and Mechanical Properties of Plasma-Polymerized N-Isopropylacrylamide, Langmuir 2005, 21: 7833-7841.

[119] Cho E. C., Kim Y. D., and Cho K., Temperature-dependent intermolecular force measurement of poly(N-isopropylacrylamide) grafted surface with protein, Journal of Colloid and Interface Science 2005, 286: 479-486.

[120] Cho E. C., Kim Y. D., and Cho K., Thermally responsive poly(N-isopropylacrylamide) monolayer on gold: synthesis, surface characterization, and protein interaction/adsorption studies, Polymer 2004, 45: 3195-3204.

[121] Gergely C., Bahi S., Szalontai B., Flores H., Schaaf P., Voegel J.-C., and Cuisinier F. J. G., Human Serum Albumin Self-Assembly on Weak Polyelectrolyte Multilayer Films Structurally Modified by pH Changes, Langmuir 2004, 20: 5575-5582.

[122] Müller M., Rieser T., Lunkwitz K., Berwald S., Meier-Haack J., and Jehnichen D., An in-situ ATR-FTIR study on polyelectrolyte multilayer assemblies on solid surfaces and their susceptibility to fouling, Macromolecular Rapid Communications 1998, 19: 333-336.

[123] Martins G. V., Merino E. G., Mano J. F., and Alves N. M., Crosslink Effect and Albumin Adsorption onto Chitosan/Alginate Multilayered Systems: An in situ QCM-D Study, Macromolecular Bioscience 2010, 10: 1444-1455.

[124] Watanabe J., Shen H., and Akashi M., Polyelectrolyte droplets facilitate versatile layer-by-layer coating for protein loading interface, Acta Biomaterialia 2008, 4: 1255-1262.

[125] Jessel N., Atalar F., Lavalle P., Mutterer J., Decher G., Schaaf P., Voegel J. C., and Ogier J., Bioactive Coatings Based on a Polyelectrolyte Multilayer Architecture Functionalized by Embedded Proteins, Advanced Materials 2003, 15: 692-695.

[126] Macdonald M., Rodriguez N. M., Smith R., and Hammond P. T., Release of a model protein from biodegradable self assembled films for surface delivery applications, Journal of Controlled Release 2008, 131: 228-234.

[127] Picart C., and Discher D. E., Materials science: Embedded shells decalcified, Nature 2007, 448: 879-880.

[128] Fredin N. J., Zhang J., and Lynn D. M., Surface Analysis of Erodible Multilayered Polyelectrolyte Films: Nanometer-Scale Structure and Erosion Profiles, Langmuir 2005, 21: 5803-5811.

[129] Serizawa T., Yamaguchi M., Matsuyama T., and Akashi M., Alternating Bioactivity of Polymeric Layer-by-Layer Assemblies: Anti- vs Procoagulation of Human Blood on Chitosan and Dextran Sulfate Layers, Biomacromolecules 2000, 1: 306-309.

[130] Price A. D., Zelikin A. N., Wang Y., and Caruso F., Triggered enzymatic degradation of DNA within selectively permeable polymer capsule microreactors, Angewandte Chemie International Edition 2009, 48: 329-332.

[131] Huang C.-J., and Chang F.-C., Using click chemistry to fabricate ultrathin thermoresponsive microcapsules through direct covalent layer-by-layer assembly, Macromolecules 2009, 42: 5155-5166.

[132] Murthy N., Campbell J., Fausto N., Hoffman A. S., and Stayton P. S., Bioinspired pH-Responsive Polymers for the Intracellular Delivery of Biomolecular Drugs, Bioconjugate Chemistry 2003, 14: 412-419.

[133] Nolan C. M., Serpe M. J., and Lyon L. A., Thermally Modulated Insulin Release from Microgel Thin Films, Biomacromolecules 2004, 5: 1940-1946.

[134] Chuang H. F., Smith R. C., and Hammond P. T., Polyelectrolyte Multilayers for Tunable Release of Antibiotics, Biomacromolecules 2008, 9: 1660-1668.

[135] Picart C., Elkaim R., Richert L., Audoin F., Arntz Y., Da Silva Cardoso M., Schaaf P., Voegel J. C., and Frisch B., Primary Cell Adhesion on RGD-Functionalized and Covalently Crosslinked Thin Polyelectrolyte Multilayer Films, Advanced Functional Materials 2005, 15: 83-94.

[136] Boura C., Muller S., Vautier D., Dumas D., Schaaf P., Claude Voegel J., François Stoltz J., and Menu P., Endothelial cell—interactions with polyelectrolyte multilayer films, Biomaterials 2005, 26: 4568-4575.

[137] Auernheimer J., Dahmen C., Hersel U., Bausch A., and Kessler H., Photoswitched Cell Adhesion on Surfaces with RGD Peptides, Journal of the American Chemical Society 2005, 127: 16107-16110.

[138] Nakanishi J., Kikuchi Y., Takarada T., Nakayama H., Yamaguchi K., and Maeda M., Spatiotemporal control of cell adhesion on a self-assembled monolayer having a photocleavable protecting group, Analytica Chimica Acta 2006, 578: 100-104.

[139] Chou Y.-F., Huang W., Dunn J. C. Y., Miller T. A., and Wu B. M., The effect of biomimetic apatite structure on osteoblast viability, proliferation, and gene expression, Biomaterials 2005, 26: 285-295.

[140] Richard D., Dumelié N., Benhayoune H., Bouthors S., Guillaume C., Lalun N., Balossier G., and Laurent-Maquin D., Behavior of human osteoblast-like cells in contact with electrodeposited calcium phosphate coatings, Journal of Biomedical Materials Research Part B: Applied Biomaterials 2006, 79B: 108-115.

[141] Matsuda N., Shimizu T., Yamato M., and Okano T., Tissue Engineering Based on Cell Sheet Technology, Advanced Materials 2007, 19: 3089-3099.

[142] Tsuda Y., Kikuchi A., Yamato M., Chen G., and Okano T., Heterotypic cell interactions on a dually patterned surface, Biochemical and Biophysical Research Communications 2006, 348: 937-944.

[143] Tsuda Y., Kikuchi A., Yamato M., Nakao A., Sakurai Y., Umezu M., and Okano T., The use of patterned dual thermoresponsive surfaces for the collective recovery as co-cultured cell sheets, Biomaterials 2005, 26: 1885-1893.

[144] Tsuda Y., Shimizu T., Yamato M., Kikuchi A., Sasagawa T., Sekiya S., Kobayashi J., Chen G., and Okano T., Cellular control of tissue architectures using a three-dimensional tissue fabrication technique, Biomaterials 2007, 28: 4939-4946.

[145] Tsuda Y., Yamato M., Kikuchi A., Watanabe M., Chen G., Takahashi Y., and Okano T., Thermoresponsive Microtextured Culture Surfaces Facilitate Fabrication of Capillary Networks, Advanced Materials 2007, 19: 3633-3636.

[146] Pirraco R. P., Obokata H., Iwata T., Marques A. P., Tsuneda S., Yamato M., Reis R. L., and Okano T., Development of Osteogenic Cell Sheets for Bone Tissue Engineering Applications, Tissue Engineering Part A 2011, 17: 1507.

[147] Duarte A. R. C., Mano J. F., and Reis R. L., Thermosensitive polymeric matrices for three-dimensional cell culture strategies, Acta Biomaterialia 2011, 7: 526-529.

SECTION II – EXPERIMENTAL SECTION

Chapter 5.

Materials and methods

Chapter 5. Materials and methods

Many of the materials used in this thesis – both polymeric constituents and reactives – were either purchased or obtained by biological processes. The detailed specifications of the suppliers can be found in the experimental subsections of each chapter of Section III. Likewise, equipment suppliers are also discriminated in those subsections.

5.1 Materials

5.1.1 Polysaccharides

Several polysaccharides were used for the conception of multiple layer-by-layer (LbL) constructs. Namely, chitosan (CHI) was used in every experimental work, throughout chapters 6 to 11. CHI is a biodegradable linear polysaccharide composed of randomly distributed *N*-D-glucosamine and *N*-acetyl-D-glucosamine, linked by β-(1-4) glycosidic bonds (Figure 5.1a). It is obtained by partial deacetylation of chitin – which is found in the exoskeleton of shellfish, like shrimp and crabs – in the solid state under strong alkaline conditions or by enzymatic hydrolysis in the presence of a chitin deacetylase. In this process, named *N*-deacetylation, the acetyl functional groups of chitin are removed. Conventionally, the compound is called "chitosan" when the degree of deacetylation of chitin reaches about 50%. CHI undergoes a conformational transition in solution around a pH value of 6. Its amine groups, as is characteristic of polybases, are protonated at pH below the pK_a and deprotonated at higher pH values [1-3].

Levan is a linear β-(2-6)-linked fructose polymer (fructan) exhibiting hydroxyl groups that form strong adhesive bonds with various substrates (Figure 5.1b). This polymer – which was used along CHI in Chapter 6 – can be produced by almost every fructan synthesizers: one particular example is levan produced by extremophilic and halophilic bacteria *Halomonas smyrnensis* (Figure 5.2). They are found in highly saline environments to provide adhesion and protection. The fact that superior bioadhesiveness can be achieved under such harsh conditions points to the excellent adhesive properties that levan and its derivatives can provide. In comparison to petrochemically-derived adhesives, levan is biodegradable, biocompatible, nonallergic, nontoxic and water-soluble, useful properties for high-value biomedical applications [4-6].

Occasionally, alginate (ALG) was also used as a multilayer constituent, in Chapters 6, 7 and 11. ALG is a linear anionic copolymer composed of two monomers: β-D-mannuronic acid, α-L-guluronic acid (Figure 5.1c). It can be obtained from the cellular wall, accounting for up to 45% of the dry weight of these seaweeds. ALG has stimuli-responsiveness toward pH. The carboxylic acid groups from the guluronate and mannuronate monomers can be deprotonated above pH values of 3.2 and 4, respectively. Thus, alginate behaves as polyacid and exhibits polyanionic behavior above these pK_a values [7-10]. ALG and also CHI, which share a marine origin, both show biocompatibility, adhesiveness, nontoxicity, as well as bacteriostatic, fungistatic, antimicrobial and hemostatic activities [10-12]. These properties make of these polysaccharides suitable constituents for multilayer formulations that resort to natural materials.

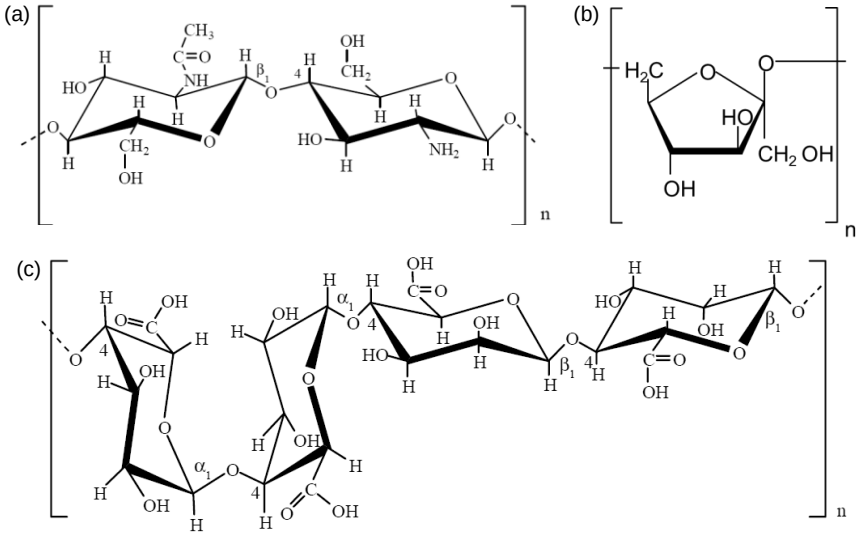


Figure 5.1. Molecular structure of (a) chitosan, (b) levan, and (c) alginate.

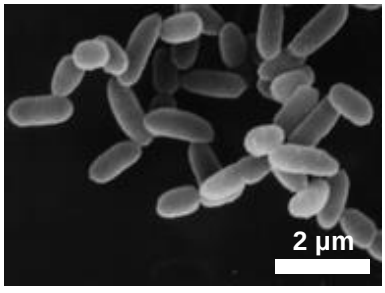


Figure 5.2. Scanning electron microscopy image of a preparation of *Halomonas sp.* strain. Source: http://commtechlab.msu.edu/sites/dlc-me/zoo/zdx0283.html, September 10th 2013.

All materials used in the present thesis were bought from specialized commercial distributors. Among the purchased materials were CHI and ALG: medium molecular weight chitosan (Brookshield viscosity 200-800 cP, molecular weight 190-310 kDa) and alginic acid sodium salt from brown algae (molecular weight 100-200 kDa). The sodium salt group enabled ALG to solubilize in water more easily, in comparison to its unmodified form. Levan was obtained by biological processes, as described below.

Chitosan as-received often contains impurities and debris resulting from the deacetylation process of chitin and requires a purification procedure. Purification of CHI exploits the fact that it undergoes a conformational transition in solution around a pH value around 6, making it soluble below this value and precipitate above it. For purification a method described by Signini and Filho [13] was adapted. A CHI solution at 1% (w/v) using acetic acid at 1% (v/v) as solvent was prepared. The solution was vacuum-filtered twice through filter papers with 20–25 μm of pore size, to remove impurities. The filtered solution was neutralized using sodium hydroxide (NaOH) at a molar concentration of 1 M and was added drop-wise until pH was 8. The precipitated chitosan was then repeatedly rinsed in distilled water until the pH of the residual waters meets the same value of distilled water (around pH 7). CHI was rinsed with ethanol, vacuum-filtered and stored at -80 °C before being lyophilized.

5.1.1.1 Microbial levan production

For Chapter 6, levan was produced by halophilic Halomonas smyrnensis AAD6T batch cultures using pretreated sugar beet molasses as substrate. For this, molasses subjected to tricalcium phosphate, sulphuric acid and activated carbon pre-treatment was added to sterile production medium (7 $g{\cdot}L^{-1}$ dipotassium phosphate (K_2HPO_4); 2 $g{\cdot}L^{-1}$ monopotassium phosphate (KH_2PO_4); 0.1 $g.L^{-1}$ magnesium sulfate heptahydrate ($MgSO_4{\cdot}7H_2O$); 1 $g.L^{-1}$ ammonium sulfate ($(NH_4)_2SO_4$); 0.5 $g{\cdot}L^{-1}$ peptone; 137.2 $g{\cdot}L^{-1}$ sodium chloride (NaCl) to 30 $g{\cdot}L^{-1}$ final carbohydrate concentration and after inoculation, cells were incubated in an orbital shaker set at 37°C and 180 rotations per minute (rpm) agitation rate. Afterwards, cells from the stationary phase cultures were harvested by centrifugation at 11000g for 20 minutes and the supernatant phases were treated with an equal volume of ethanol, held at -18°C overnight, and then centrifuged at 16000g and 4°C for 30 min using a refrigerated centrifuge. The pellets were dissolved in hot distilled water, dialyzed against several runs of distilled water for 3 days and lyophilized. The typical results of this procedure is a levan polymer with a molar mass of at least 1000 kDa [14].

5.1.1.2 Levan phosphonate modification

Levan as-produced does not possess groups exhibiting electrostatic charge. For the purpose of producing multilayer films with CHI driven by electrostatic interactions, phosphonate groups were introduced in the structure of levan. This way, it was expected that the introduced groups provided negative charge for interaction with the polycationic CHI. For the production of phosphonated levan (Ph-levan), 4 g of levan was dissolved in 100 mL of pyridine by vigorously mixing on a magnetic stirrer for 48 hours at ambient conditions and then the solution was cooled down to 0°C. In an ice bath, 4 mL of phosphorus trichloride (PCl_3) was added slowly in a drop-wise manner to the well-stirred solution. After stirring for 30 min under ambient conditions, 100 mL of saturated sodium carbonate (Na_2CO_3) was added. The aqueous phase containing the modified polymer was separated and freed from pyridine, and then subjected to dialysis against distilled water for at least 4 consecutive days with frequent exchanges of the solvent (3–5 times per day). The polymer was freeze-dried and an overall recovery yield of about 50% was achieved.

5.1.2 ELR expression and purification

Elastin-like recombinamers are genetically-engineered polypeptides that can exhibit precise amino acid length and sequence, and stimuli-responsiveness toward external stimuli, such as temperature, pH, ionic strength, and some toward light. An exhaustive description of elastin-like macromolecules has already been provided in Section I, as Chapter 3.

From Chapter 7 to Chapter 11, ELRs were used as one of the constituents of the multilayer films and coatings. Expression conditions and purification protocols were adapted from Meyer and Chilkoti [15] and Girotti *et al.* [16]. ELRs were obtained by the induced gene expression from a stock of recombinant *Escherichia coli* strains containing the desired expressing gene. This stock of recombinant bacteria had been previously obtained. The artificial nature of ELRs means that it is necessary to design and synthesize their genes de novo in order to obtain them. It is impossible to obtain a complete synthetic gene, through an approach involving genetic engineering. The repetitive structure of recombinamers implies that a monomer deoxyribonucleic acid (DNA) segment or "monomeric gene" encoding a specific polypeptide sequence can be created and subsequently seamlessly joined independently of the presence of restriction sites in the target DNA to generate multimerized genes that express the whole recombinamer. Three strategies can be employed to obtain the polymeric genes. One is concatemerization method, a random, directional concatenation of the monomeric gene. This method

allows multimeric genes with a defined distribution and discrete lengths to be obtained in a single cloning cycle. The other is the iterative-recursive method, which allows complete control of the size and distribution of the individual blocks that play central roles in formation of the supramolecular structures. Finally, recursive directional ligation (RDL), an alternative method in which DNA segments with two different restriction sites flanking the insert are joined in sequential steps, with the length of the ligated segments growing geometrically in each step (Figure 5.3) [17].

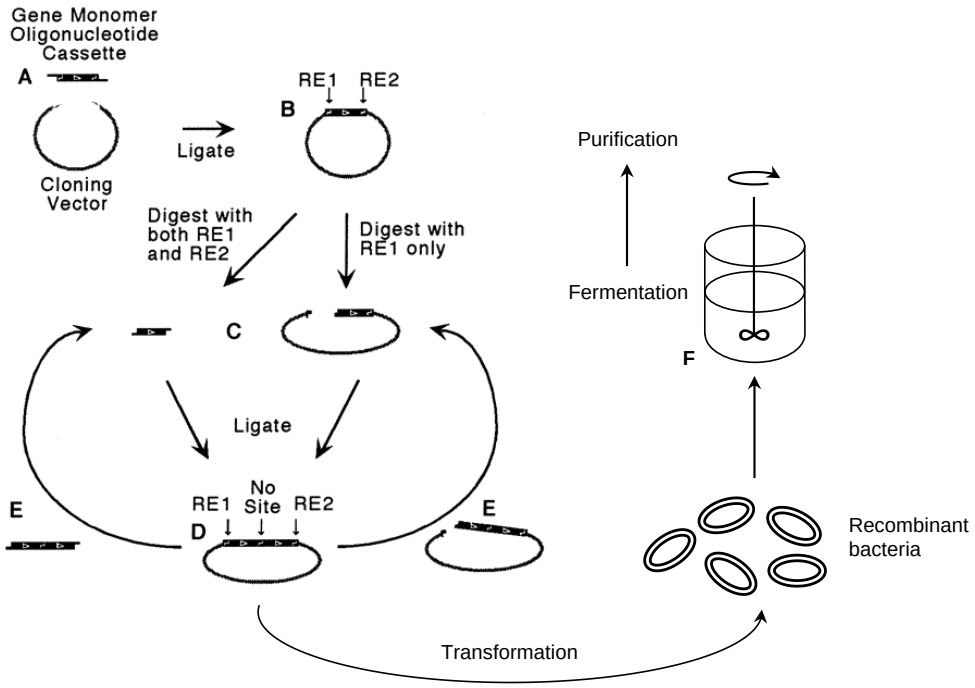


Figure 5.3. The molecular biology steps of RDL. (A) A synthetic monomer gene is inserted into a cloning vector. (B) The gene is designed to contain recognition sites for two different restriction endonucleases, RE1 and RE2, at each of the coding sequence. (C) An insert is prepared by digestion of the vector with both RE1 and RE2 and subsequently ligated into the vector that has been linearized by digestion with only RE1. (D) The product contains two head-to-tail repeats of the original gene, with the RE1 and RE2 sites maintained only at the ends of the gene. (E) Additional rounds of RDL proceed identically, using products from previous rounds as starting materials. Reprinted with permission from [18], Copyright 2002, American Chemical Society. (F) Recombinant bacteria containing the desired gene are submitted to fermentation and purified afterwards to extract the bioproduced polymer.

Nine distinct ELRs were produced, differing in their amino acid sequence, length and, in most cases, bioactivity. Table 5.1 lists the desired ELR sequences produced throughout this thesis. The acronyms were given in accordance to their specific amino acid sequence. Gene expression was induced in 12 L

of terrific broth medium (TB) with 0.1% of carbenicilin and 0.1% of glucose, under controlled conditions of temperature (37°C) and pH (7.00). The fermentation was stopped after registering an optical density variation at 600 nm inferior to 0.25, within 1 h. Subsequent to fermentation, the culture was harvested by centrifugation, resuspended and lysed by ultrasonic disruption. Insoluble debris was removed by centrifugation and the cleared lysate was subjected to several cycles of cold and warm centrifugations, of 4 and 40°C, respectively. All the purification steps were carried out in a sodium chloride (NaCl) solution at 0.5 M. The polymer in solution was then frozen at -24°C and freeze-dried.

Table 5.1. List of ELRs and corresponding amino acid sequence used throughout the various subsequent chapters.

ELR acronym	Sequence
3K-VRDG$^{(-)}$V	MGKKKP-$(VPGVG)_{14}[(VPGIG)_{10}$AVTGRD GSPASS$(VPGIG)_{10}]_2(VPGVG)_{14}$-V
3K-VRGDV	MGKKKP$(VPGVG)_{14}[(VPGIG)_{10}$AVTGRGDSPASS$(VPGIG)_{10}]_2$ $(VPGVG)_{14}$-V
HAP3	MESLLP$[[(VPGIG)_2(VPGKG)(VPGIG)_2]_2$ DDDEEKFLRRIGRFG$[(VPGIG)_2$ $(VPGKG)(VPGIG)_2]_2]_3$-V
GEG15	MD$[(VPGVG)_2(VPGEG)$ $(VPGVG)_2]_{15}$IGSG
H3A20	MESLLP$[[(VPGIG)_2$VPGKG$(VPGIG)_2]_2$DDDEEKFLRRIGRFG$[(VPGIG)_2$VPGKG $(VPGIG)_2]]_3$-$(VPAVG)_{20}$-V
IK24	MESLLP$[(VPGIG)_2(VPGKG)(VPGIG)_2]_{24}$-V
H-RGD6	MGSSHHHHHHSSGLVPRGSHMESLLP$[[(VPGIG)_2(VPGKG)(VPGIG)_2]_2$ AVTGRGDSPASS$[(VPGIG)_2(VPGKG)$ $(VPGIG)_2]_2]_6$-V
H3A20H3	MESLLP$[[(VPGIG)_2(VPGKG)(VPGIG)_2]_2$DDDEEKFLRRIGRFG$[(VPGIG)_2(VPGKG)$ $(VPGIG)_2]_2]_3(VPAVG)_{20}[[(VPGIG)_2(VPGKG)(VPGIG)_2]_2$DDDEEKFLRRIGRFG $[(VPGIG)_2(VPGKG)(VPGIG)_2]_2]_3$-V
V84	MGKKKP-$(VPGVG)_{84}$-V

All ELRs exhibited groups that could undergo protonation and exhibit electrostatic charge, except for V84. This polypeptide was submitted further to a chemical modification to neutralize its three lysines (K), in order to use a neutral ELR in LbL formulations. For that, V84 was modified by amidation of the γ-amine group of the biopolymer with pentynoic anhydride as an acylating agent. The reaction was performed in trifluoroethanol (TFE) with 10 equivalents of pentynoic anhydride per γ-amine group and

1-ethyl-3-(3-dimethylaminopropyl) carbodiimide (EDAC; 5 equivalents) as catalyst. Pentynoic anhydride was synthesized previously from pentynoic acid in a 1:1 (v/v) mixture of dichloromethane and diethyl ether in the presence of dicyclohexylcarbodiimide. The reaction mixture was stirred for 3 days at room temperature. After this time, the functionalized polymer was precipitated into increasing fractions of diethyl ether and dried in a vacuum oven at room temperature for 24 h. Once dry, the modified V84 was solubilized in cold water and the crude product purified by exhaustive dialysis against water, then frozen and finally freeze-dried.

5.1.3 Synthesis of magnetic nanoparticles

For the purpose of constructing LbL-based systems with magnetic response in Chapter 11, magnetic nanoparticles (MNPs) were first synthesized. MNPs are structures susceptible to magnetic fields, often used to enhance medical imaging diagnosis of soft tissues (e.g., magnetic resonance imaging, MRI) and temperature-mediated treatments such as hyperthermia and tissue ablation [19-21]. Their magnetic responsiveness also allows spatial mobilization/immobilization dependent on the application of a magnetic field on demand. In a typical synthesis of spherical iron oxide MNPs, 10 mL of a solution containing 1.2 g of iron(III) chloride hexahydrate ($FeCl_3 \cdot 6H_2O$) and 0.6 g of iron(II) chloride tetrahydrate ($FeCl_2 \cdot 4H_2O$) was added drop-wise to 25 mL of ammonium hydroxide solution (NH_4OH, made of 33% ammonia, NH_3, in H_2O) over 4 h under an inert nitrogen atmosphere. The products of the reaction were collected by magnetic separation and washed three times with ethanol and water. The last washing step was made with ethanol, after which the products were left to dry at room temperature.

5.2 Characterization of the materials

Many characterization techniques were specific for each of the materials used: CHI, Ph-levan, ELRs and MNPs.

5.2.1 Degree of deacetylation of chitosan

After the purification of CHI – which was recurrently used in every experimental work – it was necessary to determine the precise degree of deacetylation (DD) of the obtained stock. For that purpose, hydrogen-1 nuclear magnetic resonance (^{1}H-NMR) spectra were recorded for a sample of purified CHI. NMR is a common technique used to determine the structure of unknown organic structures, by applying a nuclear magnetic resonance with respect to hydrogen-1 nuclei within the molecules of a

substance. Among other things, it allows determining the number of protons in a molecule, different types of hydrogen atoms (e.g., protons bonded to carbon atoms that are attached to different functional groups), and the number of "neighbor" hydrogen atoms a proton has [22]. Thus, 10 mg of chitosan was dissolved in 1 mL of deuterated water (D_2O) and 20 µL of deuterated hydrochloric acid (DCl) to form a viscous solution. An aliquot of this solution was placed in a 5 mm NMR tube and the spectrum recorded at 60°C. The calculation of the DD, in percentage (%), was based on the report of Hirai, Odani and Nakajima [23] and is presented in equation 5.1:

$$DD(\%) = \left[1 - \left(\frac{\frac{1}{3}I_e}{\frac{1}{6}I_c}\right)\right] \times 100 \qquad (5.1)$$

where I_e represents the integral intensity of the CH_3 resonance band and I_c the integral intensity of the H2 to H6 resonance bands (Figure 5.4).

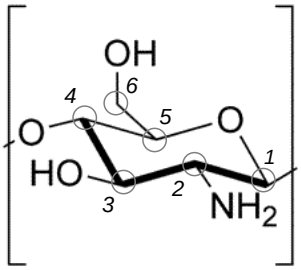


Figure 5.4. Typical structure of the *N*-D-glucosamine monomer in chitosan molecules. Each distinct hydrogen atom is identified from 1 to 6.

5.2.2 Phosphonate-levan modification assessment

To assess if the modification of levan into Ph-levan was successful in Chapter 6, two techniques were used: energy dispersive spectroscopy (EDS) analysis, for the elemental analysis of phosphorous, and Fourier transform infrared (FTIR) spectra, by comparing both modified and unmodified levan samples within wavelength values of 400–4000 cm^{-1}. EDS is performed using a scanning electron microscope (SEM) which, besides the morphology and surface of a sample, allows determining its elemental composition. When the electron beam bombards a sample, X-rays are produced as a result of the ionization of an atom by high-energy radiation. Consequently, an inner shell electron is removed. To return an ionized atom to its ground state, an electron from a higher energy outer shell fills the vacant inner shell and, in the process, releases an amount of energy equal to the potential energy difference

between the two shells. The excess energy is unique for every atomic transition and allows determining the atomic element in analysis [24]. In FTIR, infrared radiation passes through a sample: some of this radiation is absorbed by the sample some of it is transmitted through. The detected infrared spectrum is the result of transitions between vibrational energy states, which can range from simple coupled motion of two atoms in a diatomic molecule to a more complex atomic motion in a large polyfunctional molecule. Thus, it is possible to detect functional groups, for instance, in a modified polymer by measuring characteristic absorption spectra, in respect to an unmodified sample [25].

5.2.3 Elastin-like recombinamers bioproduction assessment

ELRs used throughout Chapters 7 to 11 were characterized following a multitude of techniques. To assess that the desired ELR was appropriately synthesized and produced, amino acid composition analysis and matrix-assisted laser desorption/ionization time-of-flight (MALDI-TOF) mass spectroscopy were used. The amino acid composition was determined according to the AccQTag Waters method and the derivatized amino acids analyzed by high-performance liquid chromatography (HPLC). In general, an ideal derivatizing reagent must consist of an appropriate reactive group and a strong fluorophore. Typically, the protocol of the manufacturer requires the use of 6-aminoquinolyl-*N*-hydroxysuccinimidyl carbamate to react with primary and secondary amines to produce unsymmetrical urea derivatives that are highly fluorescent. Such conjugates can be separated in chromatographic columns and be detected sensitively using ultraviolet fluorescence detectors [26,27]. MALDI-TOF mass spectroscopy was used to determine the molecular weight of the produced ELRs. In MALDI-TOF, proteins are liberated in an ionized form from a target surface by firing a laser pulse at crystallized proteins. The ionized proteins are accelerated through a vacuum tube by an electrical field and reach a detector. Smaller proteins are accelerated to higher velocities than heavier proteins, and the "time-of-flight" is proportional to "m/z". The charge "z" of ionized proteins is often 1, making the m/z value equal to the mass value [28].

5.2.4 Magnetization of MNPs

Magnetic particles can be classified as ferromagnetic and paramagnetic/superparamagnetic. Whereas the former exhibit a permanent magnetic dipole moment, with a paramagnetic particle a magnetic dipole moment is induced only when an external magnetic field is applied [29-32]. The magnetization of the MNPs was therefore measured as a function of an applied external magnetic field. Typically, a vibrating sample magnetometer is used, which is capable of generating a magnetic field and detect the magnetization exhibited by a tested material.

The shape and morphology of the magnetite nanoparticles were determined using high resolution transmission electronic microscope (TEM). TEM is a microscopy technique that detects a beam of electrons transmitted through a specimen. A microscope of this class is capable of imaging at a significantly higher resolution than conventional light microscopes, thus it was appropriate to observe such nanometric structures [33]. The samples were prepared by dropping a dilute aqueous solution (1 $mg \cdot mL^{-1}$) of the nanoparticles onto a 200-mesh copper grid and allowing the solvent to evaporate.

5.2.5 Measurement of charges

The charge exhibited by each polymer in aqueous solution was determined by the measurement of zeta (ζ)-potentials using laser Doppler electrophoresis. When a solid surface is in contact with an aqueous solution, the formation of an interfacial charge causes a rearrangement of the local free ions in the solution to produce a thin region of nonzero net charge density near the interface. The arrangement of the charges at the solid-liquid interface and the balancing counter-ions in the liquid is usually referred to as the electrical double layer. This region consists in a thin layer of counter-ions immediately next to the charged solid surface, called the compact layer, or Stern layer. The counter-ions in the compact layer are immobile due to the strong electrostatic attraction, while counter-ions outside the compact layer are mobile. This last part of the electrical double layer is called the diffuse layer. The ζ-potential is the electrostatic potential at the boundary dividing the compact layer and the diffuse layer [34]. This potential may depend on the polymer concentration, pH and ionic strength. Thus, solutions of each polymeric material were prepared considering one of two situations: (i) the conditions that would be used afterwards for the construction of the LbL films and coatings, in an attempt to relate both charge and successful or unsuccessful multilayer construction, or (ii) the conditions in which the developed coatings are placed after their construction, to determine their behavior at, e.g., physiological conditions. Aqueous solutions of each ingredient were tested all the times at 25°C, 0.15 M of sodium chloride (NaCl), with varying concentrations and pH values. Regarding (i) they were: 1 $mg \cdot mL^{-1}$, pH 5.5 for Ph-levan and CHI (Chapter 6); 100 $\mu g \cdot mL^{-1}$, pH 5.5 for ELR-RGD (herein corresponding to 3K-VRGDV) and CHI (Chapter 8); 100 $\mu g \cdot mL^{-1}$, pH 4.0 or 5.5 for all 9 ELRs, CHI and ALG (Chapter 7). Regarding (ii), they were: 300 $\mu g \cdot mL^{-1}$, pH 7.4 for ELR-RGD and ELR-$RDG^{(-)}$ (herein corresponding to 3K-VRGDV and 3K-$VRDG^{(-)}V$, respectively).

5.2.6 Temperature responsiveness of the polymers

Differential scanning microscopy (DSC) and dynamic laser scattering (DLS) were used to evaluate the stimuli-responsiveness. DSC was used in Chapter 8 to determine the transition temperature of a sample of 3K-VRGDV. This technique measures the change of the difference in the heat flow rate to a sample and to a reference sample while they are subjected to a controlled temperature program. It provides direct, model-independent determinations of the transition properties, such as enthalpy, entropy, and transition temperature, and is an appropriate technique to study the inverse temperature transition of ELRs [35,36]. Experiments were performed with water solutions of 3K-VRGDV at 50 $mg \cdot mL^{-1}$ were prepared at pH 7.4. In a typical DSC run, 20 μL of the solution were placed inside a standard 40 μL aluminum pan hermetically sealed. The same volume of water was placed in the reference pan. All samples were equilibrated for 5 minutes at 5°C inside the sample chamber just before the beginning of each experiment. A heating rate of $5°C \cdot min^{-1}$ was used.

Dynamic laser scattering (DLS) consists in the emission of a laser light over particles, emulsions or molecules dispersed or dissolved in a liquid. The interaction of this laser with the particles causes the light to be scattered at different intensities. The light intensity measured at the other end of the detectors in then interpreted and provides an estimation of the size of the samples dissolved or dispersed in solution [37]. It was used to determine the formation of polymeric aggregates in various solutions at various temperatures. In Chapter 9, 3K-VRGDV aggregate sizes were measured in the temperature range 25–37°C after stabilization for 5 minutes, to determine the transition temperature of the polypeptide. Samples were prepared at 300 $\mu g \cdot mL^{-1}$ in phosphate-buffered solution (PBS, pH 7.4). A total of 20 runs were performed for each sample to obtain a final average value at constant temperature. In Chapter 11, the reversibility of the temperature-induced phase transition of the same ELR-RGD was evaluated. For solutions prepared under the same conditions, measurements were performed first at 25°C, then 37 °C and finally back at 25°C. A total of 20 runs were performed for each sample to obtain an average value at stabilized temperature. In the same chapter, ALG and CHI were also submitted to the same measurements, although CHI – due to this polybase's pK_a – had to be tested at pH 5.5. Nonetheless, it was not expected that temperature influenced significantly the response of CHI, regardless of the pH value.

5.3 Assessment of LbL films' growth

5.3.1 *In situ* monitoring

In order to determine if a set of ingredients can be used to construct multilayer films and coatings, a quartz-crystal microbalance with dissipation monitoring (QCM-D) was used in Chapters 6, 7 and 8, a technique that is able to detect adsorbed surface density changes in the order of ng.cm^{-2} and measure the viscoelastic properties of the resulting surface in real time. In this technique, a sensor is composed of a thin AT-cut quartz disk sandwiched between a pair of electrodes. Quartz allows exploiting the piezoelectric which makes it possible to convert an electric AC voltage across its electrodes into mechanical motion, exciting the quartz to oscillation at a fundamental frequency of 5 MHz. Therefore, the use of quartz sensors for QCM requires the use of "chips" that are coated by the electrode material, which can be one of a number of metals but being gold the one mostly used. An AT-cut quartz crystal can be excited at its fundamental frequency (5 MHz) and at several overtones: 1, 3, 5, 7, 9, 11 and 13, corresponding respectively to 5, 15, 25, 35, 45, 55 and 65 MHz, although different overtones can be monitored, depending on the equipment's supplier. When a thin film is deposited onto the sensor crystal the frequency decreases. If the film is thin and rigid, the decrease in frequency (ΔF) is proportional to the mass of the film. However, when using polymers, the adsorbed film is not rigid and this relation is not valid. At the same time, monitoring of ΔD gives an indirect indication of the film's viscoelastic properties. An increase in ΔD represents a shift towards a film with a higher viscous component and damping properties typical of "soft" polymeric LbL films. The dissipation values for a soft film are higher due to increased energy loss from the crystal, whereas smaller dissipation values are obtained for a rigid film. It is this dampening to the crystal's oscillation that is registered as dissipation, ΔD [38-42].

The adsorption of polymeric layers was studied onto gold-coated quartz crystals *in situ*, cleaned with acetone, absolute ethanol and 2-propanol prior to the experiments. The quartz crystals were excited at multiple overtones: 1, 3, 5, 7, 9, 11 and 13. For all monitoring experiments, adsorption took place at 25°C, using solutions at 0.15 M NaCl. Each multilayer constituent was flushed sequentially to the inside of the chamber where the sensor was immobilized at a constant flow rate of 50 mL·min^{-1}, being each adsorption step separated by a 10-minute intermediate rinsing step with 0.15 M NaCl, as depicted in Figure 5.5.

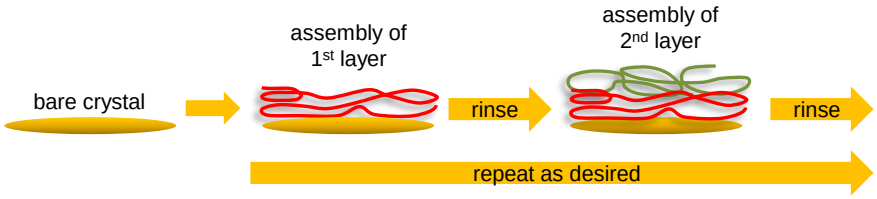


Figure 5.5. Schematic representation of LbL adsorption on top of gold-coated quartz crystal sensors.

The adsorption time and polymer concentration varied for each experiment performed: 10 min, 1 mg·mL^{-1} for CHI (starting layer) and Ph-levan films (Chapter 6); 10 min, 100 μg·mL^{-1} for CHI (starting layer) and 3K-VRGDV films (Chapter 8); 15 min, 100 μg·mL^{-1} for CHI/ELR and ELR/ALG films (Chapter 7), being CHI and ALG always adsorbed first and second, respectively. Except for the latter chapter, the frequency of each overtone was normalized to the fundamental resonant frequency of the quartz crystal, by dividing it by ν (where ν is the number of the overtone). In the specific case of Chapter 7 – Appendix, CHI/monoblock and CHI/triblock films (herein designated as HAP3 and H3A20H3, respectively) were assembled at a pH value of 4.5, with the rest of the solution parameters being similar to the ones in the main chapter.

5.3.2 Estimation of films' thicknesses

The Voigt-based viscoelastic model was used to estimate the thickness of the films from the QCM-D monitoring data. The obtained frequency and dissipation values were converted to their estimated thickness using the Voigt-based viscoelastic model [43], which is integrated into the QTools software from Q-Sense (supplier of the equipment), based on equations 5.2 and 5.3:

$$\Delta F \approx -\frac{1}{2\pi\rho_0 h_0}\left\{\frac{\eta_3}{\delta_3}+\sum_{j=k}\left[h_j\rho_j\omega-2h_j\left(\frac{\eta_3}{\delta_3}\right)^2\frac{\eta_j\omega^2}{\mu_j{}^2+\omega^2\eta_j{}^2}\right]\right\} \qquad (5.2)$$

$$\Delta D \approx \frac{1}{2\pi f\rho_0 h_0}\left\{\frac{\eta_3}{\delta_3}+\sum_{j=k}2h_j\left(\frac{\eta_3}{\delta_3}\right)^2\frac{\mu_j\omega}{\mu_j{}^2+\omega^2\eta_j{}^2}\right\} \qquad (5.3)$$

where, considering a total of *k* thin viscoelastic layers, ρ_0 and h_0 are the density and thickness of the quartz crystal, η_3 is the viscosity of the bulk liquid, δ_3 is the viscous penetration depth of the shear wave in the bulk liquid, ρ_3 is the density of liquid, μ is the elastic shear modulus of an overlayer and ω is the angular frequency of the oscillation.

Iterations of the model were performed using at least three overtones. The model requires three parameters, namely solvent density, solvent viscosity and film density, to be fixed. The solvent viscosity

was therefore fixed at 0.001 Pa·s (same as water) and the film density at 1200 kg.m^{-3} (often assumed to return the lowest calculation error) [44-46]. The solvent density was varied by trial and error until the total error, χ^2, was minimized. The solvent density values that allowed obtaining the minimum error was determined to be within 1000–1015 kg·m^{-3} for levan-based films (Chapter 6) and 1000–1060 kg·m^{-3} for ELR-based films (Chapters 7 and 8). The area density, a rough approximation of the mass adsorbed on top of a gold-coated quartz sensor was calculated by multiplying the thickness by the films density (1200 kg.m^{-3}).

5.4 Assembly and characterization of multilayer films

5.4.1 In planar substrates

After determining if a set of constituents provided a favorable multilayer construction, they were reproduced outside of the QCM-D. Hybrid multilayer films based on the diverse polymeric materials used herein were constructed by dipping alternately glass substrates into the polyelectrolyte solutions for 10 min, with an intermediate rinsing step of 5 (Chapter 6) or 10 min (Chapter 7 - Appendix and Chapter 8) in NaCl 0.15 M. In similarity to most metallic alloys, glass is negatively charged, and thus provided support for the formation of a multilayer coating by adsorbing CHI as a polycation primer layer [47].

In Chapter 6, fresh CHI and Ph-levan polyelectrolyte solutions were prepared (1 mg·mL^{-1}, 0.15 M NaCl, pH 5.5). Commercial glass from a local store were acquired and cut into 100×20 mm^2 slides and cleaned thoroughly by immersion in a sequence of absolute ethanol, 2-propanol and chromosulfuric acid for 24 h. The construction was assisted by an in-house developed dipping robot that allowed the automated assembly of each layer in a programmed manner. The construction proceeded until 100 layers (50 bilayers) were adsorbed. Films consisting of CHI and ALG were produced in parallel under the same experimental conditions for control purposes. In Chapter 7 – Appendix, films of CHI and either HAP3 or H3A20H3 were assembled onto glass pieces (1 cm^2). The number of CHI/HAP3 and CHI/ H3A20H3 bilayers assembled was defined based on the results from the QCM-D screening stage. In Chapter 8, five pairs of CHI and ELR-RGD were prepared by manual dipping at the surface of regular glass microscopy slides cut into 1 cm^2 pieces after undergoing a cleaning stage with acetone, absolute ethanol and 2-propanol.

5.4.1.1 Adhesiveness of the films

In Chapter 6, the adhesiveness of "Ph-levan"-based films was studied by measuring the lap shear adhesive strength between two individual films. This technique determines the force that causes an adhesive to slide on a surface in the direction parallel to the plan of contact [48], as depicted in Figure 5.6.

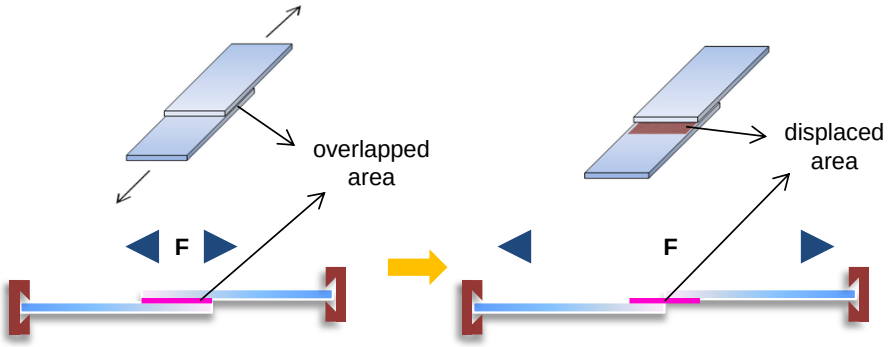


Figure 5.6. Experimental setup for the measurement of the lap shear adhesive strength.

As soon as the construction of the films was concluded, two coated glass slides were put in contact face-to-face with an overlapping area of 20×10 mm^2. To promote better adhesion, a weight of 6 kg was applied perpendicularly to the joint area and after a curing time of 24 h, the weight was removed. The bonded glass slides were placed in a universal mechanical testing machine according to the ASTM D1002-05 standard method and fixed by one binder grip in each extremity. A crosshead speed of 5 $mm \cdot min^{-1}$ was employed and the samples were stressed until enough force was applied to trigger their detachment and pull them apart. The same setup was used to evaluate the adhesiveness of CHI/ALG films for the purpose of comparison. The lap shear bonding strength was then determined from the maximum of the force-deformation curve obtained. The average and standard deviations were determined using the results from five bonded substrates. Values reported reflect means±standard deviation (SD) of three independent experiments, and analyzed using t-student test. All results were considered to be statistically significant at p-value less than 0.05.

5.4.1.2 Contact angle measurements

The wettability of a surface can be quantified by the measurement of contact angles. The contact angle of a liquid drop on a solid surface is the angle at which a liquid/vapor interface meets a solid surface. It is defined by the mechanical equilibrium of the drop under the action of three interfacial tensions and

allows quantifying the wettability of a solid surface by a liquid via the Young equation. Surfaces with high energy typically exhibit a low contact angle, whereas hydrophobic surfaces exhibit low surface energy [49].

In Chapter 7 – Appendix, PBS-contact angles were measured for coatings of CHI/HAP3 and CHI/H3A20H3 at 4 and 50°C. The number of layers was defined based on the results from the QCM-D. The coatings were immersed in PBS placed under each temperature condition. After periods of 10 min of immersion in each temperature condition, the samples were withdrawn and contact angles were measured. If wettability did not change significantly, the samples were placed in immersion for an additional period of 10 min at the same temperature.

In Chapter 8, coatings up to 10 layers – 5 pairs of CHI and 3K-VRGDV – were characterized for their wettability for each layer assembled using the sessile drop method, at 37°C and pH 7.4. These measurement conditions were chosen to simulate the behavior of the films under physiological conditions of temperature and pH for each assembled pH. An approach described by Park *et al.* [50] was used to measure contact angles dependent on several temperature, pH and ionic strength conditions: the samples were immersed in a beaker of PBS placed under each condition. After 1 hour, the samples were withdrawn and contact angles were measured (Figure 5.7). The time of 1 h was determined to be enough to have a stable surface. Therefore, measurements were performed for a pH range from 4 to 12, ionic strength from 0 to 1.5 M of NaCl, and three relevant temperatures: 25, 37 and 50°C. Upon determining the wettability transition parameters, three cycles were performed by changing the transition values above and below each transition value.

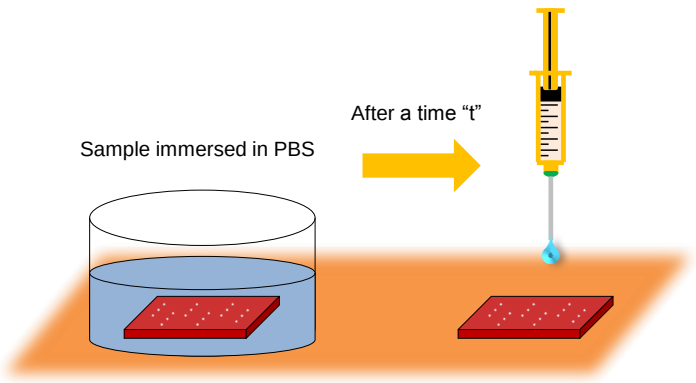


Figure 5.7. Schematics of contact angle measurements. The dotted surface symbolizes a modified glass substrate.

5.4.1.3 Surface topography

Atomic force microscopy (AFM) measurements were performed in LbL-coated glass slides cut into pieces of 1×1 cm^2, in Chapter 7 – Appendix and Chapter 8, following a similar protocol to that of contact angle measurements, in both cases scanning an area of 1×1 μm^2. This technique is a synthesis of the mechanical profilometer, using mechanical springs to sense forces, and the scanning tunneling microscopy (STM), using piezoelectric transducers for scanning. In force microscopy, a probing tip is attached to a cantilever-type spring. In response to the force between tip and sample, the cantilever is deflected. This deflection is then translated into a visual image [51].

In Chapter 8, 5 pairs of CHI/3K-VRGDV were immersed in PBS for 30 min. To assess the influence of pH in the coatings, the samples were immersed in PBS at two pH values: 7.4 and 11. To avoid the formation of crystals during the acquisition, the samples were immersed shortly in ultrapure water for removing excess of saline solution. The samples were then retrieved and introduced in the device. Values reported reflect means±standard deviation (SD) of three independent experiments, and analyzed using t-student test. All results were considered to be statistically significant at p-value less than 0.05.

In Chapter 7 – Appendix, CHI/monoblock and CHI/triblock samples were immersed in PBS at room temperature and 50°C and then retrieved and introduced in the device. "pH" was also analyzed, for values of 7.4 and 12.

When a multilayer film is rough, viscous and/or thick, AFM may not be appropriate technique to scan its topography. In these cases, scanning electron microscopy (SEM) – a technique that allows observing the surface of an object by bombarding it with an electron beam – presents itself as a viable alternative. SEM was used in Chapter 6 to evaluate the topography of CHI/Ph-levan and CHI/ALG films. The surfaces to be observed were left to dry overnight at room temperature and sputtered with gold prior to SEM observations.

5.4.2 In three dimensional substrates

5.4.2.1 Preparation of spherical microparticle templates

Multilayer combinations made of CHI and 3K-VRGDV were extrapolated to the third dimension in the form of capsules. For this purpose, microparticles of calcium carbonate ($CaCO_3$) served as spherical templates, which are easily obtained and provide a very simple three-dimensional structure to perform LbL. Microcapsules made of these constituents were constructed in Chapters 9, 10 and 11. Prior to the shell assembly, the template microparticles were produced. Typically, aqueous solutions of sodium

carbonate (Na_2CO_3) and calcium chloride ($CaCl_2$) were prepared at 1 M. Co-precipitation of both solutions was performed by adding a volume "V" of Na_2CO_3 followed by a volume "V" of $CaCl_2$ to a variable volume of a precipitation medium/bath under rapid stirring for 30 seconds. The volume of the precipitation medium was of "2V" (Chapters 9 and 11) or "4V" (Chapter 10). Stirring was then stopped and the suspension of newly synthesized $CaCO_3$ microparticles left to react and precipitate for 15 min. The supernatant was then removed and the particles washed twice or three times with ultrapure water to remove residual salts.

The co-precipitation could occur in a precipitation medium that, besides water, contains an agent for encapsulation. The encapsulation is achieved due to the physical entrapment of such agent in the newly formed solid microparticles. In Chapter 9, a the entrapment of a "fluorescein isothiocyanate"-tagged bovine serum albumin (FITC-BSA) entrapment was achieved following the method described by She *et al.* [52], by preparing a precipitation medium with a FITC-BSA concentration of 5 $mg \cdot mL^{-1}$. In this work, SEM was used to evaluate the morphology of the sacrificial templates. Specimens were pre-coated with a conductive layer of sputtered gold and micrographs recorded at 10 kV. In Chapter 10, DQ-ovalbumin was entrapped from a medium at 160 $\mu g \cdot mL^{-1}$. DQ-ovalbumin is a protein chemically saturated with BODIPY dyes. The close proximity of the dye molecules causes a self-quenching mechanism characterized by the exhibition of red fluorescence. However, upon enzymatic degradation, their proximity is revoked and dye-labeled peptide fragments are released, exhibiting a fluorescence shift from red to green [53]. It is therefore an excellent agent that can be used to follow cellular uptake and intracellular traffic by monitoring the changes in the fluorescence emitted. Finally, in Chapter 11, a precipitation medium containing either rhodamine-B isothiocyanate or MNPs was prepared at 500 $\mu g \cdot mL^{-1}$ using the same method.

5.4.2.2 Construction of the multilayer shells

The templates – either doped or empty – were immersed alternately in CHI and 3K-VRGDV solutions (300 $\mu g \cdot mL^{-1}$, pH 5.5, 0.15 M of NaCl) for 10 min each, then washed with 0.15 M NaCl (pH 5.5). Centrifugation was avoided to avoid damage and aggregation of the particles each time the samples were to be retrieved from solution; simple precipitation of the suspension was used instead (3 to 5 min). In Chapter 10, where the internalization by cells was to be studied, each adsorption step was followed by three washing steps with 0.15 M NaCl, pH 5.5, with the first being accompanied by 4 sequential ultra-sound pulses of 3 seconds each to disaggregate the substrates. This extra step was performed in order to ensure a more thorough washing, microcapsule separation and therefore avoiding major

biological shock due to undesired residues and aggregation. This construction process was repeated to increase the number of bilayers until the desired coating had been obtained. In Chapter 9, the effect of the number of layers in the multilayer shell permeability was object of study, thus samples with 1, 3 and 5 bilayers were constructed. In Chapters 10 and 11, the coatings were constructed with 2 and 3 bilayers, respectively. After construction, three approaches were followed: (i) in Chapter 9, the $CaCO_3$ core was immediately dissolved with ethylenediamine tetraacetic acid (EDTA, 0.2 M, pH 5.5), which is a known chelating agent of metal ions, like calcium ions, and washed twice PBS; (ii) in Chapter 10, the microcapsules followed a washing procedure with EDTA (0.2 M, pH 7.4) and four with ultrapure water, with centrifugation at 1000 rpm for 25 min in between and ultrasound pulses timed as described above. Although centrifugation should ideally be avoided, the extra washing steps to which the microcapsules were submitted could lead to increased losses in microcapsules' number. In the case of microcapsules intended for cellular contact rather than microscopic observations, Dulbecco's modified Eagle medium (DMEM) was used for the washings instead of water. The result is a batch of hollow multilayer shells entrapping a desired agent inside. A schematic of this procedure can be found in Figure 5.8; (iii) in Chapter 11, the coated particles were left intact for the time being to be employed further in the construction of compartmentalized devices.

5.4.2.3 Compartmentalized structures

Following point (iii) of the previous paragraph, in Chapter 11 a 1% (w/v) solution of ALG was prepared. In a typical experiment, the $(CHI/3K\text{-}VRGDV)_3$-coated microparticles were suspended in 1 mL of ALG solution and the resulting suspension extruded through a 25G needle, at a rate of 0.33 $mL \cdot min^{-1}$, into a 0.75% (w/v) solution of $CaCl_2$ under mild stirring. ALG beads containing coated microparticles were formed by calcium-mediated ionic gelation of alginate (Figure 5.9). The beads were coated with a Chi/ALG multilayer shell. They were immersed alternately in CHI and ALG solutions (300 $\mu g \cdot mL^{-1}$, pH 5.5, 0.15 M NaCl) for 10 min each, then washed with 0.15 M NaCl (pH 5.5 at 0.15 M) and this process was repeated until three bilayers were assembled, $(CHI/ALG)_3$. After the coating was assembled, the beads were immersed in EDTA. At this point, the $CaCO_3$ sacrificial templates were chelated simultaneously with the liquefied alginate bead.

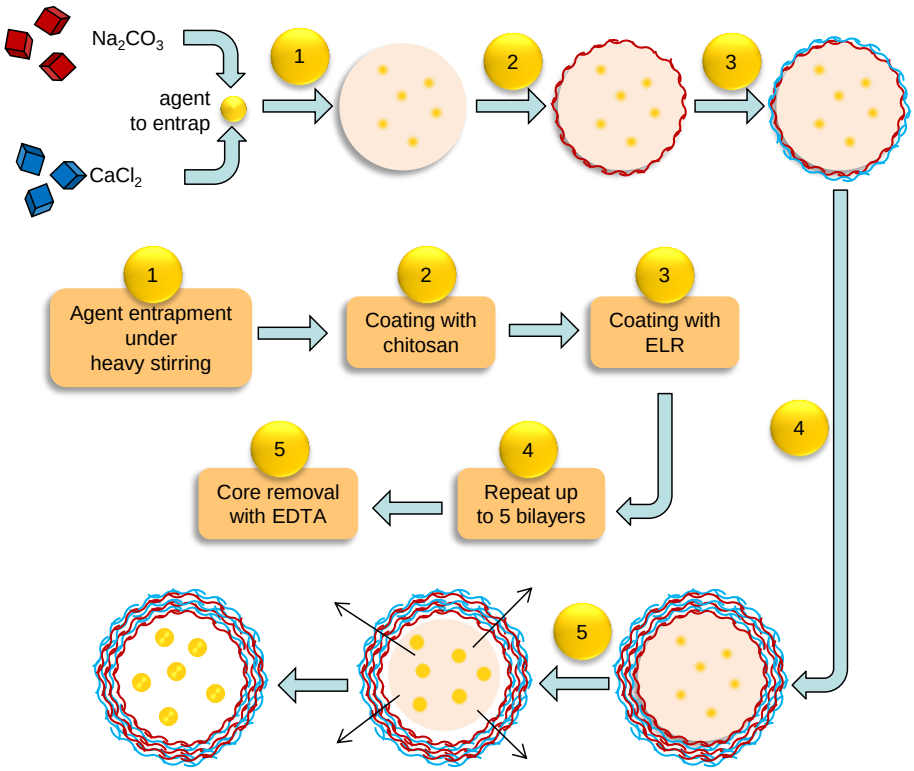


Figure 5.8. Scheme depicting the formation of multilayer hollow microcapsules encapsulating a desired agent.

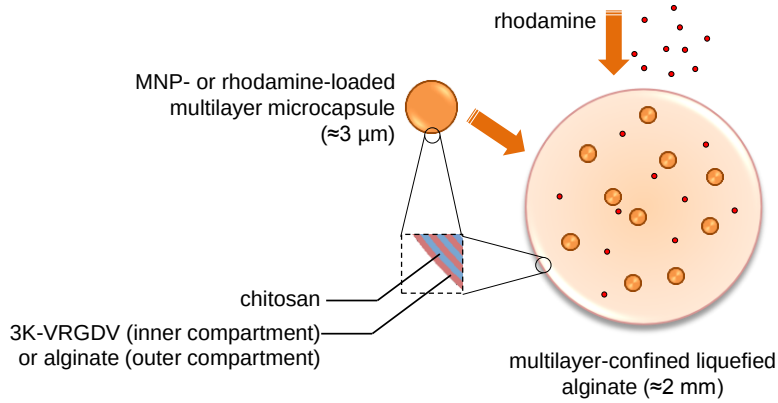


Figure 5.9. Organization of multilayer compartments, with rhodamine molecules and MNPs found at the nanolevel, the smallest scale of the proposed hierarchy.

Liquefied alginate beads coated with $(CHI/ALG)_3$ multilayers loaded with not only empty microcapsules and rhodamine in the ALG medium were also constructed. Rhodamine was suspended alongside microcapsules without any content and encapsulated in the ALG bead compartment instead of in the inner microcapsules. The mass of encapsulated rhodamine at this stage was determined by first

calculating the construction losses resulting from the rhodamine-loaded microcapsules within the external alginate macrocapsule.

5.4.2.4 Encapsulation losses and pre-loading efficiency

It should be noted that for drug delivery studies in Chapters 9 and 11, described below, all supernatants were collected during the diverse construction stages of the multilayer microcapsules, from the synthesis of the sacrificial templates to the chelation stage. This was necessary in order to calculate the BSA or rhodamine losses during each construction stage and determine the pre-loading efficiency. 150 μL of sample was pipetted into a white, opaque 96-well plate in triplicate. Distilled water was used as blank. The excitation (λ_{exc}) and emission (λ_{em}) wavelengths used for the calibration curve and FITC-BSA mass calculations were 485 and 528 nm, respectively. All supernatants collected during entrapment, construction and chelation were measured and quantified. The percentage of FITC-BSA mass lost was plotted both for each stage and cumulatively. The encapsulation efficiency was calculated by subtracting the cumulative losses of each architecture (i.e., microcapsules with distinct number of layers) from the initial FITC-BSA mass. A similar approach was followed for rhodamine, for which the excitation (λ_{exc}) and emission (λ_{em}) wavelengths were 530 and 590 nm, respectively.

5.4.2.5 Microscopy evaluation of the structures

Confocal laser scanning microscopy (CLSM) was used to evaluate the structure of the produced capsular microstructures. This is a technique that allows observing optical and fluorescence images with depth sensitivity, i.e., a sample can be scanned plane-by-plane in the z-axis. CHI/3K-VRGDV shells with 5 layers capped with a final layer of rhodamine B (assembled from a solution at 10^{-6} M) and encapsulating FITC-BSA (Chapter 9) or 3 layers encapsulating FITC (Chapter 11) were produced. In the first case, in the intent of evaluating morphological changes dependent on temperature, all samples were stabilized at either 25 or 37°C and observed under hydrated conditions. In the second case, samples were observed only at 25°C.

The morphology of the produced microcapsules in Chapter 10 consisting in 2 bilayers of CHI/3K-VRGDV or CHI/3K-VRDG$^{(-)}$V was determined using an environmental scanning electron microscopy (ESEM). With this technique, it is possible to observe a sample without a coating of sputtered gold. A number of 2.2×10^4 microcapsules suspended in 200 μL of H_2O was placed on top of a silicon wafer (1 cm^2) and dried overnight at 37°C before the analysis. The samples were placed

inside the equipment in a platform with a 20° tilt. Transmission electron microscopy (TEM) was used to obtain images of the multilayer coating. Prior to the observation, a number of 10^4 microcapsules suspended in 60 μL of H_2O was pipetted onto a TEM grid and left to dry overnight at room temperature. TEM was also used in Chapter 11 to determine the distribution of MNPs within the microcapsules. Prior to the observation, a volume of 60 μL of microcapsule suspension was pipetted onto a TEM grid and left to evaporate overnight. Both MNP-loaded and empty microcapsules were observed. Fluorescence microscopy was used to evaluate the morphology of the coated liquefied ALG beads. In contrast to CLSM, this technique scans the fluorescence exhibited by the surface. If translucid, the interior can also be observed. Based on this consideration, $(CHI/ALG)_3$-coated liquefied beads were observed using transmitted light and fluorescence microscopy for rhodamine-loaded external compartments. The latter also containing FITC-loaded microcapsules were observed to assess the distribution of the subcompartments within the macrocapsules.

5.5 In vitro release studies from three-dimensional capsules

The microcapsules in Chapter 9 were resuspended in PBS at either 25 or 37°C. The upper limit of five bilayers for the microcapsule architecture was chosen to study the effect of temperature along with small changes in the number of different layers. This study was conducted over 14 days, removing the surrounding PBS from each container every 24 h. An additional sample was taken after 12 h from the start of the study. PBS was fully refreshed at each time point, and 100% FITC-BSA was considered to be the total mass remaining in the microcapsules after their construction. The release experiments were performed under mild agitation to improve the diffusion of FITC-BSA through the incubating medium. All experiments were performed in triplicate (n=3), with each sample containing the number of capsules resulting from the attempted encapsulation of 1 mg of BSA. To determine the type of release profile for each condition, the release kinetics were determined using the Korsmeyer kinetic model (equation 5.4):

$$M_t/M_\infty = Kt^n \qquad (5.4)$$

where M_t/M_∞ is the fraction of protein released at time t, K is the rate constant for the Korsmeyer model, and n is the exponent that characterizes the release mechanism [54]. The Korsmeyer model is used when the release mechanism from a swellable polymeric device is not well-known or when more than one type of release phenomenon could be involved. The latter was a possibility since the phase transition of these ELRs is a complex phenomenon, allied to a similarly complex hybrid and three-dimensional shell. The fitting was performed for all architectures and for each temperature. As a means

of comparison, fitting with other models was also made: zero-order (equation 5.5), first-order (equation 5.6) and Higuchi (equation 5.7):

$$Q_t = Q_0 + K_0 t \qquad (5.5)$$

where Q_t is the cumulative amount of protein released at time t, Q_0 is the initial amount of protein and K_0 is the rate constant for the zero-order model;

$$Log(Q_t) = Log(Q_0) + Kt / 2.303 \qquad (5.6)$$

where Q_t is the cumulative amount of protein released at time t, Q_0 is the initial amount of protein and K is the rate constant for the first-order model;

$$Q = K_H t^{1/2} \qquad (5.7)$$

where Q is the cumulative amount of protein released at time t and K_H is the rate constant for the Higuchi model.

The compartmentalized systems from Chapter 11 were suspended in PBS at either 25 or 37°C, with rhodamine being encapsulated in one of two hierarchical locations: the internal (CHI/3K-VRGDV)$_3$ microcapsules (with rhodamine added during the co-precipitation stage) or the external liquefied alginate (CHI/ALG)$_3$-coated macrocapsules (with rhodamine added to the initial alginate solution). The study was conducted for 2 h to assess the early release profile in 3 mL of PBS, with 600 μL of surrounding PBS being removed every 10 min and the container being refilled with the same volume of PBS pre-stabilized at the corresponding temperature. 100% of Rhod was considered to be the total mass remaining in the compartmental systems after taking construction losses into account. The studies were performed three times (n=3).

5.6 Mechanical resistance of compartmental units

A centrifugal rotation test was performed with the samples suspended in PBS to measure the mechanical resistance of the (CHI/ALG)$_3$ macrocapsules (Chapter 11). 100 samples were placed in centrifuge tubes and rotated at a starting centrifugal load of 500g. After 5 min, the number of intact beads was counted. Those that remained intact were submitted to incremental centrifugal loads (500g incremental steps) up to a maximum of 5000g. This experiment was performed three times.

5.7 Magnetic responsiveness assays

Macrocapsules containing MNP-loaded microcapsules were suspended in a PBS-filled square polystyrene Petri dish placed upon a 1×1 cm^2 grid (Chapter 11). A 1.3 T permanent neodymium

(NdFeB) bar magnet (diameter: 4 mm; length: 2.5 cm) was used to apply the external magnetic field. Ten samples were placed 3 cm away from the magnet, with the latter placed at a height of 1.4 cm from the PBS surface. The movement was recorded on video and the mean normalized distance traversed by the samples plotted as a function of time.

5.8 *In vitro* biological studies

5.8.1 Cell seeding

The biological response of cells to biomaterials *in vitro* is critical to estimate if a harmful reaction is triggered upon contact of a newly developed system with a living organism, common when biomedical applications are envisaged. Herein, cells were either seeded onto a substrate modified with multilayers, or seeded first onto a cell culture support and incubated in the presence of microcapsules in suspension in the culture medium.

In Chapter 6, L929 cells – a murine fibroblast cell line – were routinely cultured with DMEM supplemented with 3.7 $g \cdot L^{-1}$ sodium bicarbonate, 10% fetal bovine serum (FBS) and 1% penicillin-streptomycin at pH 7.4. Cells were grown in 75 cm^2 tissue culture flasks and incubated at 37°C in a humidified air atmosphere of 5% carbon dioxide (CO_2). Every 3–4 days fresh medium was added. At 90% of confluence, L929 cells were washed with PBS and subsequently detached by trypsin-EDTA at 37°C. To inactivate the trypsin effect, cell culture medium was added. Cells were then centrifuged at 300g for 5 minutes and the medium was decanted. A 50 μL cell suspension with 2×10^4 cells was added to glass slides with 1×1 cm^2 modified with 50 (CHI/Ph-levan) or 50 (CHI/ALG) bilayers (in triplicate), previously sterilized by ultraviolet (UV)-radiation for 30 min. Surfaces were then incubated at 37°C in a humidified air atmosphere of 5% CO_2 and after 4 h culture medium was added. The experiment was maintained for 24 h, after which the cellular adhesion was quantified.

In Chapter 8, cell adhesion was studied using SaOs-2 cells – a human osteosarcoma cell line – envisaging the use of these coatings in orthopedic applications in order to improve host integration. Cell studies were performed onto coatings of 5 pairs of layers, ending in 3K-VRGDV, CHI or 3K-VRGD$^{(-)}$V (negative control), assembled at the surface of glass coverslips with 1 cm in diameter. Tissue culture polystyrene (TCPS) was used as a positive control. Cell adhesion was studied using the SaOs-2 osteoblast-like osteosarcoma cell line. Cells were seeded on the surfaces (5×10^4 cell$\cdot mL^{-1}$) and incubated in serum free Dulbecco's modified Eagle's medium (DMEM), loaded with 1% antibiotics/antimicotics at 37°C, 5% CO_2. The substrates were analyzed at different time points: 4 h, 24

h and 3 days. At each time point, cells on the coated surfaces were washed with PBS twice and fixed in formalin (3.7%).

In Chapter 9, L929 cells were used for the biological assays. They were cultured in DMEM with phenol red supplemented with 10% of FBS and 1% antibiotic/antimicotic in a humidified atmosphere with 5% CO_2 at 37°C. For the cell viability test, 2×10^3 cells were seeded on 48-well plates and incubated at 37°C, 5% CO_2. After 24 hours, microcapsules were added to the culture medium in a ratio of 40 microcapsules per cell. The incubation was maintained for 24 h, 3 days, and 7 days.

In Chapter 10, human mesenchymal stem cells (hMSCs) were used for the purpose of evaluation the cellular uptake of CHI/ELR microcapsules. Mesenchymal stem cells are hypoimmunogenic and pluripotent able to differentiate in *in vitro*, *ex vivo* and *in vivo*, into multiple cells types such as osteocytes, adipocytes, chondrocytes, neurocytes, hepatocytes, myocytes, and hematopoietic-supporting stroma. The option to use hMSCs in this work a model of internalization of CHI/ELR microcapsules have the potential to be applied in transplantation, local implantation, gene therapy, drug delivery and stem cell differentiation [55,56]. "hMSCs" were cultured in DMEM supplemented with 10% FBS and 100 $U\cdot mL^{-1}$ penicillin, 0.1 $mg\cdot mL^{-1}$ streptomycin replaced every two days and maintained at 37°C in a 5% CO_2 humidified environmental chamber. Near-confluence cells (passages 2–6) were harvested after enzymatically treatment with trypsin/EDTA or Accutase™ and suspended in culture medium. Cell counts were evaluated using a standard Trypan Blue exclusion assay and seeded at $3\times10^3 cell\cdot cm^{-2}$ on numerous circular cover glasses (diameter: 10 mm) and then incubated during 24 hours in standard conditions. Afterwards, the culture medium was refreshed by serum-free medium containing CHI/ELR microcapsules, either functionalized with 3K-VRGDV or 3K-VRDG$^{(-)}$V. After 3 h of CHI/ELR microcapsules co-incubation, the cultures were maintained for longer times (3 days and 10 days), by supplementing the microcapsule suspension with additional fresh medium to reach the final serum concentration of 2% FBS.

5.8.2 Staining of cells adhered to bidimensional surfaces

In Chapters 6, 8 and 9, the cells adhered to the respective films were prepared for 4',6 diamidino-2-phenylindol (DAPI) staining. DAPI stains preferentially double-stranded deoxyribonucleic acid (DNA). DNA-DAPI complexes emit strong blue fluorescence when excited by ultraviolet light so that even very small amounts of DNA [57]. After each cell culture time-point, the films seeded with L929 cells were prepared for DAPI fluorescence assay. Briefly, samples were washed with PBS and formalin (3.7–10% concentration range) was added to each well. After 15–30 min at 4°C, formalin was removed and

samples were washed with PBS. Then, a solution of PBS containing DAPI (1:1000) was added to each well and let to react for 5 min at room temperature and protected from light. Ultimately, samples were washed with PBS and visualized in the dark by fluorescence microscopy. For the specific case of Chapter 6, the nuclei were counted to quantify L929 cells adhered to CHI/Ph-levan and CHI/ALG films: adhered cells were assessed by analyzing fluorescence pictures in triplicate using the software ImageJ (provided by NIH). Values reported reflect means±standard deviation (SD) of three independent experiments, and analyzed using t-student test. All results were considered to be statistically significant at p-value less than 0.05.

Additionally, SaOs-2 (Chapter 8) and L929 (Chapter 9) cells were also stained with (tetramethylrhodamine B isothiocyanate)-phalloidin (TRITC-phalloidin). Phalloidin binds tightly to polymerized actin filaments and, when conjugated with a fluorophore (like rhodamine), they can be observed under fluorescence microscopy [58]. After fixation, cells were incubated with TRITC-phalloidin (10 $\mu g \cdot mL^{-1}$) for 45 min and washed three times with PBS. Cells were observed under fluorescence microscopy.

5.8.3 Cellular uptake of three dimensional microcapsules

For the assays regarding the internalization of microcapsules in Chapter 10, hMSCs were seeded onto deposited in a 48-well plate and incubated during 24 h in standard conditions. $(CHI/3K\text{-}VRGDV)_2$ and $(CHI/3K\text{-}VRDG^{(-)}V)_2$ microcapsules pre-loaded with DQ-ovalbumin were added to the culture. After 3 or 72 h of incubation, samples were washed with Dulbecco's phosphate-buffered saline (DPBS) three times. Samples for microscopy analysis – confocal, phase-contrast, epifluorescence, and differential interference contrast (DIC) microscopy – were fixed in 4% paraformaldehyde for 10 min, permeabilized with 0.2% Triton X-100, and stained with DAPI following a similar protocol as described above. A confocal microscope was used for analyzing microcapsules inside the cells. Z-series were performed with a Z-step of 1 μm. The images of each fluorophore and phase contrast were overlaid to obtain a multilayer image using ImageJ software. Bright field and fluorescence microscopy were performed using blue, green and red fluorescence filters in order to determine the distribution and intracellular degradation of each multilayer microcapsule type.

To quantify microcapsule internalization, 1.5×10^5 hMSCs were seeded in a 25 cm^2 flasks and cultured as described above. $(CHI/ELR\text{-}RGD)_2$ and $(CHI/ELR\text{-}RDG^{(-)})_2$ microcapsules were added at a microcapsule-to-cell ratio of 10:1 and incubated during 72 h. The cell cultures dissociated by Accutase™ treatment – specially developed for gentle and effective cell dissociation – were washed,

counted, suspended in DPBS, 25 mM 4-(2-hydroxyethyl)-1-piperazineethanesulfonic acid (HEPES), 5% FBS and analyzed in a flow cytometer. Flow cytometry is a technique for making rapid measurements on particles or cells as they flow in a fluid stream through a sensing point one by one. It is routinely employed in cell counting, cell sorting, biomarker detection and protein engineering [59]. The assay was repeated three times. Values reported reflect means±standard error (SE) of three independent experiments. The influence of microcapsules/cell ratio on cell viability was analyzed using one-way analysis of variance (ANOVA) and the post test of Bonferroni, considered to be statistically significant at p-value less than 0.05. All data was analyzed using GraphPad Prism.

5.8.4 Cell metabolism and viability

In Chapter 8, to access cell viability, (3-(4,5-dimethylthiazol-2-yl)-5-(3-carboxymethoxyphenyl)-2-(4-sulfophenyl)-2H-tetrazolium) (MTS) assay was performed. MTS and other tetrazolium dyes are bioreduced in cells by nicotinamide adenine dinucleotide, in its reduced form (NADH), in the cytosolic compartment. This reduced product can be detected for by measuring the absorbance at 490 nm, and is therefore directly proportional to the number of living cells in the substrates [60]. After each culturing period, samples were washed twice with PBS. A 250 μL aliquot of FBS-free culture medium and 50 μL of MTS reagent were added to each well. A cell-free well was used as control. Plates were incubated for 3 h at 37°C, 5% CO_2, protected from light. After incubation, 100 μL of this solution was transferred to a 96-well plate and the plate read using a microplate reader in 490 nm absorbance mode. In Chapter 9, for the cell viability test, 2×10^3 L929 cells were seeded on 48-well plates and incubated at 37°C, 5% CO_2. After 24 h, microcapsules were added to the culture medium in a ratio of 40 microcapsules per cell. After each culturing period, the MTS method was performed as described above. In both chapters, values reported reflect means±standard deviation (SD) of three independent experiments, and analyzed using t-student test. All results were considered to be statistically significant at p-value less than 0.05.

In Chapter 10, metabolic activity was evaluated by Alamar Blue® and cell viability by LIVE/DEAD® assays. Similarly to the MTS assay, Alamar Blue® is reduced in living cells, after which it yields not only a colorimetric product but also a very strong fluorescent one, which can be more than ten times as sensitive as the colorimetric assay [61]. The relative number of hMSCs metabolically active within each experimental condition was evaluated by the Alamar Blue® assay according to the manufacturer guidelines. 24 hours after cells seeding, cells culture was washed and then $(CHI/ELR\text{-}RGD)_2$ and $(CHI/ELR\text{-}RDG^{(-)})_2$ microcapsules in serum-free culture medium were added in incremental ratios of 5 to 100 microcapsules per cell. After 3 and 72 h of microcapsules co-incubation, the fluorimetric

reduction of 10% Alamar Blue® reagent in culture medium was measured with a microtiter plate reader. Non-treated cells were employed as positive control and their fluorescence was considered as the 100% of cells viability. Values reported reflect means±standard error (SE) of four samples of four independent cell culture viability experiments at 3 or 72 hours of incubation. The influence of microcapsules/cell ratio on cell viability was analyzed using one-way analysis of variance (ANOVA) and the post test of Bonferroni. All treatment-related effects were considered to be statistically significant at p-value less than 0.05. All data was analyzed using GraphPad Prism.

The viability of cells co-incubated with CHI/ELR was also examined by a LIVE/DEAD® assays. Ten microcapsules per cell of both CHI/ELR microcapsule types were added to the cell culture. The ratio of microcapsules per cell was selected after obtaining the results of the cell viability assays. In this assay, the co-incubation with calcein AM and ethidium homodimer-1 allows distinguishing the cytoplasm of live cells (with esterase cleavage of calcein accompanied by green fluorescence), and dead cells (which compromised membranes enable to stain nucleic acids with red fluorescence) [62]. LIVE/DEAD® assays was carried out at different time points (0, 72 and 240 h) according to the manufacturing specifications.

5.8.5 Alkaline phosphatase assays

The activity of alkaline phosphatase (ALP) is evaluated using a p-nitrophenol assay. Paranitrophenyl phosphate, which is colorless, is hydrolysed by alkaline phosphatase at pH 10.5 and 37°C to form free paranitrophenol, which is colored yellow. The expression of the enzyme ALP by osteoblasts, whether in a membrane form or in secretory form, is a characteristic of these cells and therefore its expression can be a strong indicator of these cells in culture [63]. For alkaline phosphatase (ALP) assays, samples collected on each time point were washed with PBS and immersed in 1 mL of ultra-pure water to lyse the cells. To each well of a 96-well plate were added 20 μL of sample plus 60 μL of substrate solution (0.2% (w/v) p-nytrophenyl (pNP) phosphate/1 M diethanolamine hydrochloric acid (HCl), at pH 9.8). The plate was then incubated in the dark for 45 min at 37°C. After the incubation period, 80 μl of a stop solution (2 M sodium hydroxide (NaOH)/0.2 mM ethylenediaminetetraacetic acid (EDTA)), was added to each well. The absorbance was then measured at 405 nm using p-nitrophenol as standard. For each experiment, a standard curve was constructed from reference suspensions at known cell concentrations. Values reported reflect means±standard deviation (SD) of three independent experiments, and analyzed using t-student test. All results were considered to be statistically significant at p-value less than 0.05.

5.9 References

[1] Chen G., and Hoffman A. S., Graft copolymers that exhibit temperature-induced phase transitions over a wide range of pH, Nature 1995, 373: 49-52.

[2] Hu Y., Jiang X., Ding Y., Ge H., Yuan Y., and Yang C., Synthesis and characterization of chitosan–poly(acrylic acid) nanoparticles, Biomaterials 2002, 23: 3193-3201.

[3] Rinaudo M., Chitin and chitosan: Properties and applications, Progress in Polymer Science 2006, 31: 603-632.

[4] Donot F., Fontana A., Baccou J. C., and Schorr-Galindo S., Microbial exopolysaccharides: Main examples of synthesis, excretion, genetics and extraction, Carbohydrate Polymers 2012, 87: 951-962.

[5] Freitas F., Alves V. D., and Reis M. A. M., Advances in bacterial exopolysaccharides: from production to biotechnological applications, Trends in Biotechnology 2011, 29: 388-398.

[6] Sima F., Mutlu E. C., Eroglu M. S., Sima L. E., Serban N., Ristoscu C., Petrescu S. M., Oner E. T., and Mihailescu I. N., Levan Nanostructured Thin Films by MAPLE Assembling, Biomacromolecules 2011, 12: 2251-2256.

[7] Ju H. K., Kim S. Y., and Lee Y. M., pH/temperature-responsive behaviors of semi-IPN and comb-type graft hydrogels composed of alginate and poly(N-isopropylacrylamide), Polymer 2001, 42: 6851-6857.

[8] Percival E., The polysaccharides of green, red and brown seaweeds: Their basic structure, biosynthesis and function, British Phycological Journal 1979, 14: 103-117.

[9] Rinaudo M., Main properties and current applications of some polysaccharides as biomaterials, Polymer International 2008, 57: 397-430.

[10] Silva T. H., Alves A., Ferreira B. M., Oliveira J. M., Reys L. L., Ferreira R. J. F., Sousa R. A., Silva S. S., Mano J. F., and Reis R. L., Materials of marine origin: a review on polymers and ceramics of biomedical interest, International Materials Reviews 2012, 57: 276-306.

[11] Boateng J. S., Matthews K. H., Stevens H. N. E., and Eccleston G. M., Wound healing dressings and drug delivery systems: A review, Journal of Pharmaceutical Sciences 2008, 97: 2892-2923.

[12] George M., and Abraham T. E., Polyionic hydrocolloids for the intestinal delivery of protein drugs: Alginate and chitosan — a review, Journal of Controlled Release 2006, 114: 1-14.

[13] Signini R., and Campana Filho S. P., On the preparation and characterization of chitosan hydrochloride, Polymer Bulletin 1999, 42: 159-166.

[14] Poli A., Kazak H., Gürleyendağ B., Tommonaro G., Pieretti G., Öner E. T., and Nicolaus B., High level synthesis of levan by a novel Halomonas species growing on defined media, Carbohydrate Polymers 2009, 78: 651-657.

[15] Meyer D. E., and Chilkoti A., Purification of recombinant proteins by fusion with thermally-responsive polypeptides, Nat Biotech 1999, 17: 1112-1115.

[16] Girotti A., Reguera J., Arias F. J., Alonso M., Testera A. M., and Rodríguez-Cabello J. C., Influence of the Molecular Weight on the Inverse Temperature Transition of a Model Genetically Engineered Elastin-like pH-Responsive Polymer, Macromolecules 2004, 37: 3396-3400.

[17] Rodríguez-Cabello J. C., Girotti A., Ribeiro A., and Arias F. J., Synthesis of Genetically Engineered Protein Polymers (Recombinamers) as an Example of Advanced Self-Assembled Smart Materials, In Navarro M., Planell J. A., eds. Nanotechnology in Regenerative Medicine: Humana Press; 2012.

[18] Meyer D. E., and Chilkoti A., Genetically Encoded Synthesis of Protein-Based Polymers with Precisely Specified Molecular Weight and Sequence by Recursive Directional Ligation: Examples from the Elastin-like Polypeptide System, Biomacromolecules 2002, 3: 357-367.

[19] Mailänder V., and Landfester K., Interaction of Nanoparticles with Cells, Biomacromolecules 2009, 10: 2379-2400.

[20] Neuberger T., Schöpf B., Hofmann H., Hofmann M., and von Rechenberg B., Superparamagnetic nanoparticles for biomedical applications: Possibilities and limitations of a new drug delivery system, Journal of Magnetism and Magnetic Materials 2005, 293: 483-496.

[21] Oh J. K., and Park J. M., Iron oxide-based superparamagnetic polymeric nanomaterials: Design, preparation, and biomedical application, Progress in Polymer Science 2011, 36: 168-189.

[22] Balci M., The Transmission Electron Microscope, The Netherlands: Elsevier; 2005.

[23] Hirai A., Odani H., and Nakajima A., Determination of degree of deacetylation of chitosan by 1H NMR spectroscopy, Polymer Bulletin 1991, 26: 87-94.

[24] Brundle C. R., Evans C. A., and Wilson S., Encyclopedia of Materials Characterization: Surfaces, Interfaces, Thin Films, United States of Americ: Manning Publications Co; 1992.

[25] Griffiths P. R., Fourier Transform Infrared Spectrometry, United States of America: John Wiley and Sons; 2007.

[26] Cohen S. A., and Michaud D. P., Synthesis of a Fluorescent Derivatizing Reagent, 6-Aminoquinolyl-N-Hydroxysuccinimidyl Carbamate, and Its Application for the Analysis of Hydrolysate

Amino Acids via High-Performance Liquid Chromatography, Analytical Biochemistry 1993, 211: 279-287.

[27] Hong J. L., Determination of amino acids by precolumn derivatization with 6-aminoquinolyl-N-hydroxysuccinimidyl carbamate and high performance liquid chromatography with ultraviolet detection, Journal of Chromatography A 1994, 670: 59-66.

[28] Albrethsen J., Reproducibility in Protein Profiling by MALDI-TOF Mass Spectrometry, Clinical Chemistry 2007, 53: 852-858.

[29] Gennes P. G., and Pincus P. A., Pair correlations in a ferromagnetic colloid, Physik der kondensierten Materie 1970, 11: 189-198.

[30] Mizuki T., Watanabe N., Nagaoka Y., Fukushima T., Morimoto H., Usami R., and Maekawa T., Activity of an enzyme immobilized on superparamagnetic particles in a rotational magnetic field, Biochemical and Biophysical Research Communications 2010, 393: 779-782.

[31] Promislow J. H. E., Gast A. P., and Fermigier M., Aggregation kinetics of paramagnetic colloidal particles, The Journal of Chemical Physics 1995, 102: 5492-5498.

[32] Yang C., Wu J., and Hou Y., Fe3O4 nanostructures: synthesis, growth mechanism, properties and applications, Chemical Communications 2011, 47: 5130-5141.

[33] Williams D. B., and Carter C. B., The Transmission Electron Microscope, United States of America: Springer; 1996.

[34] Sze A., Erickson D., Ren L., and Li D., Zeta-potential measurement using the Smoluchowski equation and the slope of the current–time relationship in electroosmotic flow, Journal of Colloid and Interface Science 2003, 261: 402-410.

[35] Höhne G. W. H., Hemminger W. F., and Flammersheim H.-J., Differential Scanning Calorimetry, Germany: Springer-Verlag; 2003.

[36] Rodríguez-Cabello J. C., Alonso M., Pérez T., and Herguedas M. M., Differential scanning calorimetry study of the hydrophobic hydration of the elastin-based polypentapeptide, poly(VPGVG), from deficiency to excess of water, Biopolymers 2000, 54: 282-288.

[37] Berne B. J., and Pecora R., Dynamic Light Scattering: With Applications to Chemistry, Biology, and Physics, United States of America: Dover Publications; 2000.

[38] Hook F., Kasemo B., Nylander T., Fant C., Sott K., and Elwing H., Variations in Coupled Water, Viscoelastic Properties, and Film Thickness of a Mefp-1 Protein Film during Adsorption and Cross-Linking: A Quartz Crystal Microbalance with Dissipation Monitoring, Ellipsometry, and Surface Plasmon Resonance Study, Analytical Chemistry 2001, 73: 5796-5804.

[39] Marx K. A., Quartz Crystal Microbalance: A Useful Tool for Studying Thin Polymer Films and Complex Biomolecular Systems at the Solution-Surface Interface, Biomacromolecules 2003, 4: 1099-1120.

[40] Notley S. M., Eriksson M., and Wågberg L., Visco-elastic and adhesive properties of adsorbed polyelectrolyte multilayers determined in situ with QCM-D and AFM measurements, Journal of Colloid and Interface Science 2005, 292: 29-37.

[41] Cho N.-J., Kanazawa K. K., Glenn J. S., and Frank C. W., Employing Two Different Quartz Crystal Microbalance Models To Study Changes in Viscoelastic Behavior upon Transformation of Lipid Vesicles to a Bilayer on a Gold Surface, Analytical Chemistry 2007, 79: 7027-7035.

[42] Höök F., Kasemo B., Nylander T., Fant C., Sott K., and Elwing H., Variations in Coupled Water, Viscoelastic Properties, and Film Thickness of a Mefp-1 Protein Film during Adsorption and Cross-Linking: A Quartz Crystal Microbalance with Dissipation Monitoring, Ellipsometry, and Surface Plasmon Resonance Study, Analytical Chemistry 2001, 73: 5796-5804.

[43] Voinova M. V., Rodahl M., Jonson M., and Kasemo B., Viscoelastic Acoustic Response of Layered Polymer Films at Fluid-Solid Interfaces: Continuum Mechanics Approach, Physica Scripta 1999, 59: 391.

[44] Costa R. R., Custódio C. A., Arias F. J., Rodríguez-Cabello J. C., and Mano J. F., Layer-by-Layer Assembly of Chitosan and Recombinant Biopolymers into Biomimetic Coatings with Multiple Stimuli-Responsive Properties, Small 2011, 7: 2640-2649.

[45] Dutta A. K., and Belfort G., Adsorbed Gels versus Brushes: Viscoelastic Differences, Langmuir 2007, 23: 3088-3094.

[46] Weber N., Pesnell A., Bolikal D., Zeltinger J., and Kohn J., Viscoelastic Properties of Fibrinogen Adsorbed to the Surface of Biomaterials Used in Blood-Contacting Medical Devices, Langmuir 2007, 23: 3298-3304.

[47] Tang Z., Wang Y., Podsiadlo P., and Kotov N. A., Biomedical Applications of Layer-by-Layer Assembly: From Biomimetics to Tissue Engineering, Advanced Materials 2006, 18: 3203-3224.

[48] Thirawong N., Nunthanid J., Puttipipatkhachorn S., and Sriamornsak P., Mucoadhesive properties of various pectins on gastrointestinal mucosa: An in vitro evaluation using texture analyzer, European Journal of Pharmaceutics and Biopharmaceutics 2007, 67: 132-140.

[49] Kwok D. Y., and Neumann A. W., Contact angle measurement and contact angle interpretation, Advances in Colloid and Interface Science 1999, 81: 167-249.

[50] Park E. J., Draper D. D., and Flynn N. T., Adsorption and Thermoresponsive Behavior of Poly(N-isopropylacrylamide-co-N,N'-cystaminebisacrylamide) Thin Films on Gold, Langmuir 2007, 23: 7083-7089.

[51] Meyer E., Atomic force microscopy, Progress in Surface Science 1992, 41: 3-49.

[52] She Z., Antipina M. N., Li J., and Sukhorukov G. B., Mechanism of Protein Release from Polyelectrolyte Multilayer Microcapsules, Biomacromolecules 2010, 11: 1241-1247.

[53] Rivera-Gil P., De Koker S., De Geest B. G., and Parak W. J., Intracellular Processing of Proteins Mediated by Biodegradable Polyelectrolyte Capsules, Nano Letters 2009, 9: 4398-4402.

[54] Ritger P. L., and Peppas N. A., A simple equation for description of solute release I. Fickian and non-fickian release from non-swellable devices in the form of slabs, spheres, cylinders or discs, Journal of Controlled Release 1987, 5: 23-36.

[55] Pittenger M. F., Mackay A. M., Beck S. C., Jaiswal R. K., Douglas R., Mosca J. D., Moorman M. A., Simonetti D. W., Craig S., and Marshak D. R., Multilineage potential of adult human mesenchymal stem cells, Science 1999, 284: 143-147.

[56] Uccelli A., Moretta L., and Pistoia V., Mesenchymal stem cells in health and disease, Nature Reviews Immunology 2008, 8: 726-736.

[57] Hamada S., and Fujita S., DAPI staining improved for quantitative cytofluorometry, Histochemistry 1983, 79: 219-226.

[58] De La Cruz E. M., and Pollard T. D., Transient kinetic analysis of rhodamine phalloidin binding to actin filaments, Biochemistry 1994, 33: 14387-14392.

[59] Carter N. P., and Ormerod M. G., Introduction to the principles of flow cytometry, In Ormerod M. G., ed. Flow Cytometry: A Practical Approach, United States of America: Oxford University Press; 2000.

[60] Berridge M. V., Herst P. M., and Tan A. S., Tetrazolium dyes as tools in cell biology: New insights into their cellular reduction, In El-Gewely M. R., ed. Biotechnology Annual Review: Elsevier; 2005.

[61] Page B., Page M., and Noel C., A new fluorometric assay for cytotoxicity measurements in-vitro, International Journal of Oncolology 1993, 3: 473-476.

[62] Kaneshiro E. S., Wyder M. A., Wu Y.-P., and Cushion M. T., Reliability of calcein acetoxy methyl ester and ethidium homodimer or propidium iodide for viability assessment of microbes, Journal of Microbiological Methods 1993, 17: 1-16.

[63] Magnusson P., Larsson L., Magnusson M., Davie M. W. J., and Sharp C. A., Isoforms of Bone Alkaline Phosphatase: Characterization and Origin in Human Trabecular and Cortical Bone, Journal of Bone and Mineral Research 1999, 14: 1926-1933.

SECTION III – OPTIMIZATION OF LAYER-BY-LAYER STRATEGIES FOR BIOMEDICAL APPLICATIONS

Chapter 6. Adhesive nanostructured multilayer films using a bacterial exopolysaccharide for biomedical applications

Chapter 7. Layer-by-layer film-growth using polysaccharides and recombinant polypeptides: a combinatorial approach

Chapter 7 – Appendix. Nanostructured thin coatings from chitosan and an elastin-like recombinamers with acute stimuli-responsive behavior

Chapter 8. Layer-by-layer assembly of chitosan and recombinant biopolymers into biomimetic coatings with multiple stimuli-responsive properties

Chapter 9. Nanostructured and thermoresponsive recombinant biopolymer-based microcapsules for the delivery of active molecules

Chapter 10. Cellular uptake of multilayered capsules produced with biomimetic and genetically engineered macromolecules

Chapter 11. Multifunctional compartmentalized capsules with a hierarchical organization from the nano- to the macro-scales

Chapter 6. Adhesive nanostructured multilayer films using a bacterial exopolysaccharide for biomedical applications[5]

Abstract

Medical adhesives and sealants often require that long-term adhesiveness is achieved. In this work, nanostructured coatings consisting of chitosan and the adhesive bacterial exopolysaccharide levan are fabricated using layer-by-layer (LbL) assembly. Taking advantage of the electrostatic self-assembly mechanism of LbL, the charges of both chitosan and a phosphonate-derivatized levan (Ph-levan) are measured and the feasibility to construct hybrid films is monitored and confirmed using a quartz crystal microbalance with dissipation monitoring (QCM-D). The adhesive properties between two identical bonded films with a total of 100 layers are compared to control films in which Ph-levan is replaced by alginate, revealing that the detachment force of the former is about 3 times higher than the control. Scanning electron microscopy of the films surface shows that the surface of Ph-levan films is smooth and homogeneous. Cell adhesion tests were conducted using a L929 cell line. Early cell adhesion is significantly higher in chitosan/Ph-levan films when compared to chitosan/alginate controls. These findings establish levan derivatives as bioinspired ingredients for conceiving medical adhesive devices that allow achieving enhanced mechanical and biological performance.

[5] This chapter is based on the following publication:

Costa R. R., Neto A. I., Calgeris I., Correia C. R., Pinho A. C. M., Fonseca J., Öner E. T., and Mano J. F., Adhesive nanostructured multilayer films using a bacterial exopolysaccharide for biomedical applications, Journal of Materials Chemistry B 2013, 1: 2367-2374, DOI:10.1039/c3tb20137f.

Chapter 6. Adhesive nanostructured multilayer films using a bacterial exopolysaccharide for biomedical applications

6.1 Introduction

Wound healing, robust adhesion and protection towards external physical and pathological harm are essential characteristics of medical adhesives and sealants, especially when long-term performance of such devices is required [1-3]. However, many synthetic adhesives currently approved present limitations, which include poor adhesion in the presence of biological fluids, allergic response and inflammation [4]. Overcoming these shortcomings requires the use of materials that can provide sufficient cohesive strength and trigger adequate biological response to cells and tissues.

Nature gives us a wealth of resources that can be exploited in biomedicine and tissue engineering applications. In contrast with synthetic materials, natural-based polymers are similar to biological macromolecules, avoiding triggering chronic or immunological reactions and toxicity [5]. Macromolecular compounds such as collagen, cellulose, and fibrin are used as ingredients for adhesives and sealants [4,6-8]. Namely, chitosan (CHI) and alginate (ALG) have been widely used in biomedical applications including burn dressings, drug delivery and implantation [9-11]. These two polysaccharides share a marine origin derived from materials existing in shells of crustaceans and in algae, respectively, and show biocompatibility, adhesiveness, non-toxicity, as well as bacteriostatic, fungistatic, antimicrobial and hemostatic activities [5,11].

While the sea is a good source of natural bioadhesive materials, it is possible to find interesting materials in other less conventional sources such as extremophilic environments. An elegant example is levan, a linear β(2-6)-linked fructose polymer (fructan) exhibiting hydroxyl groups that form strong adhesive bonds with various substrates [12-14]. It has many advantages over petrochemically derived adhesives, including that it is biodegradable, biocompatible, non-allergic, non-toxic and water-soluble. Levan is also a bioactive polymer mainly associated with high-value biomedical applications [15,16] and has been credited together with xanthan, curdlan and pullulan as the most promising microbial exopolysaccharides for various industrial sectors [12]. Though microbial levan is produced extracellularly from sucrose-based substrates by various microorganisms, of special interest is the halophilic bacterium *Halomonas smyrnensis sp. nov.* AAD6T which was reported as the first extremophilic producer of levan [17,18]. Excreting high molecular weight levan by this halophile to a highly saline environment for adhesion and protection points to the superior bioadhesive properties of levan that were retained under such unusual conditions. Besides its potential use as a bioflocculating agent [19] and in drug nanocarrier systems [20], levan produced by *Halomonas smyrnensis*, as well as

its aldehyde-activated derivative, were successfully deposited by matrix-assisted pulsed laser evaporation (MAPLE) resulting in uniform, homogeneous, nanostructured, biocompatible, thin films [14]. In light of the properties of levan, we intend to demonstrate that this exopolysaccharide can be used as a promising ingredient to conceive new adhesive devices for biomedical applications.

Film casting and hot-melt extrusion are common techniques for manufacturing adhesive membranes, with the former being undoubtedly the most widely used [21]. However, the use of organic solvents in film casting and the addition of plasticizers in hot-melt extrusion are common concerns when considering the use of such membranes in biological environments. The layer-by-layer (LbL) sequential assembly of macromolecules is an approach with the potential to address these issues. LbL techniques are perhaps the most versatile and easy-to-apply of the numerous surface modification tools currently available as they are based on the spontaneous adsorption of ingredients – generally a polymer, biomolecule or inorganic particle – onto a substrate. For instance, the adsorption of charged macromolecules (polyelectrolytes) is driven by electrostatic self-assembly (ESA) between two ingredients and allows the sequential formation of a multilayer film [22-26]. Furthermore, this technique allows robust nanostructured coatings to be produced on substrates with complex geometries and, as it does away with the need for harmful organic solvents, it is of great interest in tissue engineering applications, such as biomimetic composite-like coatings, controlled drug release or manipulation of adhesion, differentiation, proliferation and even function of attached cells [25,27-29]. Because this technique is so versatile, it is possible to synthesize adhesive films by proper selection of its ingredients.

The objective of this work is to demonstrate that a phosphonate-modified levan – henceforth referred to as Ph-levan – can be used in electrostatic LbL adsorption to construct nanostructured films with adhesive properties. For the proof-of-concept, Ph-levan and chitosan were sequentially assembled onto glass using an in-house developed dipping robot and their adhesiveness was studied by measuring the shear strength necessary for two adhered films to detach. Their cell adhesion properties were evaluated *in vitro*, as well as the surface morphology. We hypothesized that these nanostructured hybrid films could have superior adhesive properties when compared to similar films made of the commonly regarded adhesive polysaccharides CHI and ALG.

6.2 Experimental section

6.2.1 Materials

Medium molecular weight chitosan was purchased from Sigma-Aldrich (ref. 448877, Brookshield viscosity 200-800 cP, molecular weight 190-310 kDa) and purified by a series of filtering steps and precipitation in water and ethanol, followed by freeze-drying. Alginate – alginic acic sodium salt from brown algae – was purchased from Fluka (ref. 71238, molecular weight 100-200 kDa). Phosphate-buffered saline (PBS), low glucose Dulbecco's Modified Eagle's Medium (DMEM), sodium bicarbonate and 4',6-diaminidino-2-phenylindole-dilactate (DAPI, 20 $mg \cdot mL^{-1}$) were purchased from Sigma-Aldrich. Fetal bovine serum (FBS), penicillin-streptomycin and trypsin- ethylenediamine tetraacetic acid (EDTA) solution were purchased from Invitrogen. The immortalized mouse lung fibroblast cell line (L929) was purchased from the European Collection of Cell Cultures.

6.2.2 Microbial levan production

Microbial levan production was performed with the halophilic *Halomonas smyrnensis* AAD6^T batch cultures [18,30] using pretreated sugar beet molasses as substrate [31]. For this, molasses subjected to tricalcium phosphate, sulphuric acid and activated carbon pre-treatment was added to sterile production medium (7 $g \cdot L^{-1}$ dipotassium phosphate (K_2HPO_4); 2 $g \cdot L^{-1}$ monopotassium phosphate (KH_2PO_4); 0.1 $g.L^{-1}$ magnesium sulfate heptahydrate ($MgSO_4 \cdot 7H_2O$); 1 $g.L^{-1}$ ammonium sulfate ($(NH_4)_2SO_4$); 0.5 $g \cdot L^{-1}$ peptone; 137.2 $g \cdot L^{-1}$ sodium chloride (NaCl)) to 30 $g \cdot L^{-1}$ final carbohydrate concentration and after inoculation, cells were incubated in a Certomat BS-1 orbital shaker (B. Braun, Germany) set at 37°C and 180 rotations per minute (rpm) agitation rate. For the purification of levan, cells from the stationary phase cultures were harvested by centrifugation at 11000g for 20 minutes and the supernatant phases were treated with an equal volume of ethanol, held at -18°C overnight, and then centrifuged at 16000g and 4°C for 30 min using a refrigerated centrifuge. The pellets were dissolved in hot distilled water, dialyzed against several runs of distilled water for 3 days and lyophilized. The resultant high molecular weight polymer has a molar mass of at least 1000 kDa [17].

6.2.3 Phosphonate modification of levan

For the production of phosphonated levan, 4 g of levan was dissolved in 100 mL of pyridine by vigorously mixing on a magnetic stirrer for 48 hours at ambient conditions and then the solution was cooled down to 0°C. In an ice bath, 4 mL of phosphorus trichloride (PCl_3) was added slowly in a drop wise manner to the well-stirred solution. After stirring for 30 min under ambient conditions, 100 mL of saturated sodium carbonate (Na_2CO_3) was added. The aqueous phase containing the modified polymer was separated and freed from pyridine and then subjected to dialysis against distilled water for at least four consecutive days with frequent exchanges of the solvent (3–5 times per day). The polymer was freeze-dried and an overall recovery yield of about 50% was achieved. Fourier transform infrared (FTIR) spectra of levan samples were obtained with Nicolet 6700 Spectrometer within (400–4000) cm^{-1}. Elemental analysis of phosphorous was estimated by energy dispersive spectroscopy (EDS) analysis performed on the JEOL JSM-5910 LV electron microscope.

6.2.4 Measurement of charges

The ζ-potentials of the polysaccharides were determined using a Nano-ZS from Malvern (United Kingdom), at 25°C. Aqueous solutions of each ingredient were used, at 1 $mg{\cdot}mL^{-1}$, 0.15 M NaCl and pH value of 5.5.

6.2.5 Construction of hybrid self-assembled films

A Q-Sense E4 quartz-crystal microbalance (Q-Sense AB, Sweden) with dissipation monitoring system was used to monitor the adsorption of chitosan and phosphonated levan onto gold-coated quartz crystals *in situ*. The quartz-crystal was excited at multiple overtones: 1, 3, 5, 7, 9, 11 and 13, corresponding respectively to 5, 15, 25, 35, 45, 55 and 65 MHz. Adsorption took place at 25°C, using solutions at 1 $mg{\cdot}mL^{-1}$, 0.15 M NaCl and at a constant flow rate of 50 $mL{\cdot}min^{-1}$, with an adsorption time of 10 min (starting with chitosan) and an intermediate rinsing step of 10 min. The frequency of each overtone was normalized to the fundamental resonant frequency of the quartz crystal, by dividing it by ν (where ν is the number of the overtone).

6.2.6 Estimation of the films' thicknesses

The Voigt model contained in the software QTools from Q-Sense (version 3.0.15.553) was used to estimate the thickness of the films from the QCM-D monitoring data. Iterations of the model were performed using at least 5^{th}, 7^{th} and 9^{th} overtones. The model requires three parameters, namely solvent density, solvent viscosity and film density, to be fixed. The solvent viscosity was therefore fixed at 0.001 Pa·s (same as water) and film density at 1200 $kg \cdot m^{-3}$. The solvent density was varied by trial and error between 1000 and 1015 $kg \cdot m^{-3}$ until the total error, χ^2, was minimized.

6.2.7 Preparation of hybrid multilayer films

Fresh polyelectrolyte solutions were prepared by dissolution of chitosan and phosphonated levan in the same conditions as the ones prepared for the QCM-D. Commercial glass from a local store were acquired and cut into 100×20 mm^2 slides. The slides were cleaned thoroughly by immersion in a sequence of absolute ethanol, 2-propanol and chromosulfuric acid for 24 h. Hybrid multilayer films of the two polysaccharides were constructed by dipping alternately the glass substrate into the polyelectrolyte solutions for 10 min, with an intermediate rinsing step of 5 min in NaCl 0.15 M. The construction was assisted by an in-house developed dipping robot that allowed the automated assembly of each layer in a programmed manner. The construction proceeded until 100 layers (50 bilayers) were adsorbed. Films consisting of chitosan and alginate were produced in parallel under the same experimental conditions for the purpose of comparison.

6.2.8 Adhesiveness of the films

As soon as the construction of the films was concluded, two glass slides were put in contact face-to-face with an overlapping area of 20×10 mm^2. To promote better adhesion, a weight of 6 kg was applied perpendicularly to the joint area and after a curing time of 24 h, the weight was removed. The bonded glass slides were placed in a universal mechanical testing machine (Instron model 5540, USA) according to the ASTM D1002-05 standard method and fixed by one binder grip in each extremity. A crosshead speed of 5 $mm \cdot min^{-1}$ was employed and the samples were stressed until enough force was applied to trigger their detachment and pull them apart. The lap shear bonding strength was then determined from the maximum of the force-deformation curve obtained. The average and standard deviations were determined using the results from five bonded substrates.

6.2.9 In vitro cell culture

L929 cells were routinely cultured with DMEM supplemented with 3.7 $g \cdot L^{-1}$ sodium bicarbonate, 10% FBS and 1% penicillin-streptomycin at pH 7.4. Cells were grown in 75 cm^2 tissue culture flasks and incubated at 37°C in a humidified air atmosphere of 5% carbon dioxide (CO_2). Every 3–4 days fresh medium was added. At 90% of confluence, L929 cells were washed with PBS and subsequently detached by trypsin-EDTA at 37°C. To inactivate the trypsin effect, cell culture medium was added. Cells were then centrifuged at 300g for 5 minutes and the medium was decanted. Prior to cell seeding, the surfaces were sterilized by ultraviolet (UV)-radiation for 30 minutes. A 50 μL cell suspension with 2×10^4 cells was added to glass slides with 1×1 cm^2 modified with 50 (CHI/Ph-levan) or 50 (CHI/ALG) bilayers (in triplicate). Surfaces were then incubated at 37°C in a humidified air atmosphere of 5% CO_2 and after 4 h culture medium was added.

6.2.10 Nuclei-staining fluorescence assay

After 24 h of incubation, the film samples seeded with L929 cells were prepared for DAPI fluorescence assay. Briefly, samples were washed with PBS and 10% formalin was added to each well. After 30 min at 4°C, formalin was removed and samples were washed with PBS. Then, a solution of PBS containing DAPI (1:1000) was added to each well and let to react for 5 min at room temperature and protected from light. Ultimately, samples were washed with PBS and visualized in the dark by fluorescence microscopy. DAPI stains preferentially double-stranded deoxyribonucleic acid (DNA) by delineating cells nuclei in blue. Adhered cells were assessed by analyzing fluorescence pictures in triplicate using the software ImageJ (NIH, version 1.46r).

6.3 Results and Discussion

Phosphorylation is a feasible method for modifying the dissolution properties and bioactivities of polysaccharides. Phosphorylated polysaccharides have found use in various applications as flame retardant additive, cation exchanger, thickener and binder for biomolecules [32-34]. As such, a wide range of potential applications were also proposed for phosphorylated derivatives of the levan polysaccharide [16]. Considering these facts and the limited literature on levan derivatives, Ph-levan has been chosen as a promising biopolymer and its suitability for the fabrication of adhesive multilayer

coatings has been investigated within the scope of this study. The protocol used to modify levan followed the reaction scheme is shown in Figure 6.1.

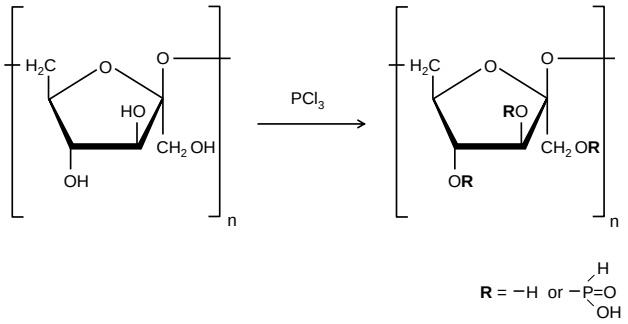


Figure 6.1. Reaction scheme of phosphonate modification of levan.

The obtained Ph-levan was then characterized by FTIR and EDS. In the FTIR spectrum (Figure 6.2), several stretching vibration bands were detected: the hydroxyl (OH) stretching vibration bands around 3200 cm^{-1}, two bands around 2900 cm^{-1}/2930 cm^{-1} corresponding to carbon-hydrogen (C-H) stretching vibration of fructose residues, bands in the region of 1430 cm^{-1} that were assigned to C-H plan deformation vibration combined with aromatic skeletal vibrations, bands at 1120 cm^{-1} and 1000 cm^{-1} that were dominated by the stretching vibrations of the glycosidic linkage contributions of C-O-C and C-O-H, as well as the 920 cm^{-1} band resulting from the stretching vibration of pyran ring. These bands are all characteristic of levan polysaccharides reported earlier [31]. By comparison, in the FTIR spectrum of Ph-levan, more bands could be identified: a band at 2360 cm^{-1} corresponding to the P–H bond, another one at 1200 cm^{-1} corresponding to the P=O bond, a shoulder at 1045 cm^{-1} attributable to the P–OH bond and bands around 875 cm^{-1} corresponding to the P–O–C bonds [32-34].

EDS was performed to further evaluate the efficiency of the modification. From the spectrum in Figure 6.3, a peak of phosphorus was detected and the EDS analysis resulted in an atomic ratio of C:O:P=44:51:3. Thus, both FTIR and EDS pointed towards the production of a Ph-levan stock to be used in the construction of the intended multilayer films.

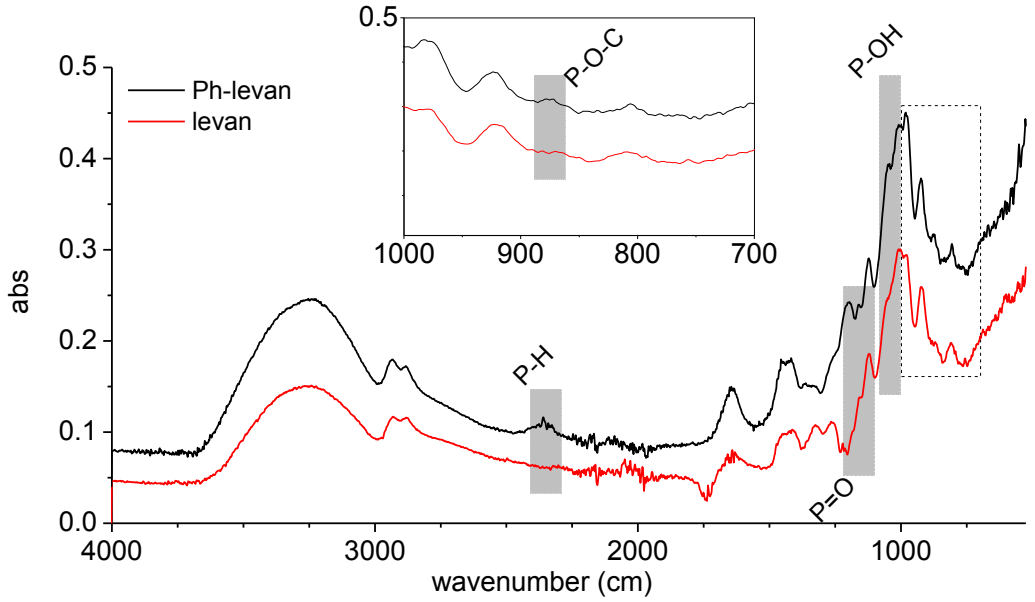


Figure 6.2. FTIR spectra of levan samples as-produced (in red) and phosphonate (in black). The Ph-levan spectrum is represented with an offset of +0.04 of absorbance. The bands respective to phosphonate groups are highlighted with grey background, with the inset showing the augmented spectra between 700 and 1000 cm^{-1}.

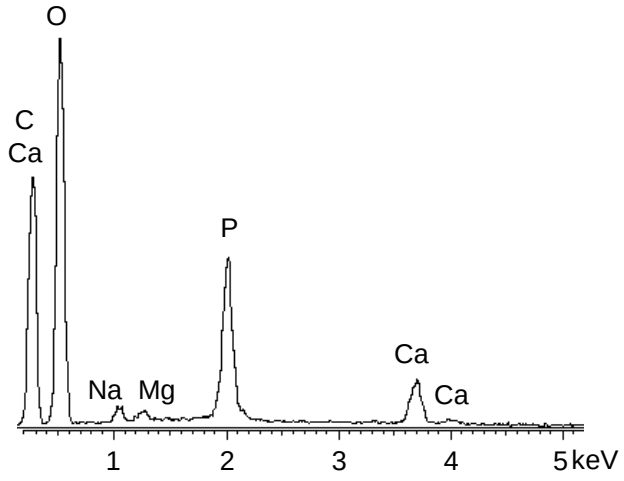


Figure 6.3. EDS spectrum of a Ph-levan sample.

Prior to the QCM-D study, the ζ-potential of CHI and Ph-levan was measured, showing values of +16.8±0.8 mV and -13.1±0.3 mV, respectively. CHI is a well-known polycation due to the protonated state of amine groups in acidic conditions [3]. The negative charge of Ph-levan is possible thanks to the introduction of phosphonate groups to a macromolecule that is otherwise uncharged in nature. This

modification allows the reaction with CHI via electrostatic interactions. The ability of CHI and Ph-levan to adsorb in a sequential fashion by relying on ESA was monitored by QCM-D. This technique is able to detect mass changes in the order of nanograms per square centimeter and measure the viscoelastic properties of the resulting surface [35]. Figure 6.4A shows the normalized frequency, $\Delta F_\nu/\nu$ (where ν is the overtone) and dissipation (ΔD) variations for the 5th overtone (25 MHz) after the construction up to 6 layers onto gold-coated quartz sensors. During QCM-D, a favorable and successful construction is usually identified by a decrease in ΔF caused by mass adsorption at the top of the sensor. The $\Delta F_\nu/\nu$ decreased upon flushing the substrate with the sequence of polyelectrolytes, due to the deposition of polymer on the surface of the crystal, to an approximate absolute value of 38 Hz. At the same time, monitoring of ΔD gives an indirect indication of the film's viscoelastic properties. For instance, an increase in ΔD represents a shift towards a film with a higher viscous component and damping properties that characterize a "softer" film. As observed in Figure 6.4A, the ΔD increased to around 17×10^{-6}. Therefore, the assembled multilayer film is not rigid and exhibits the typical viscoelastic behavior, a typical situation when using macromolecular systems.

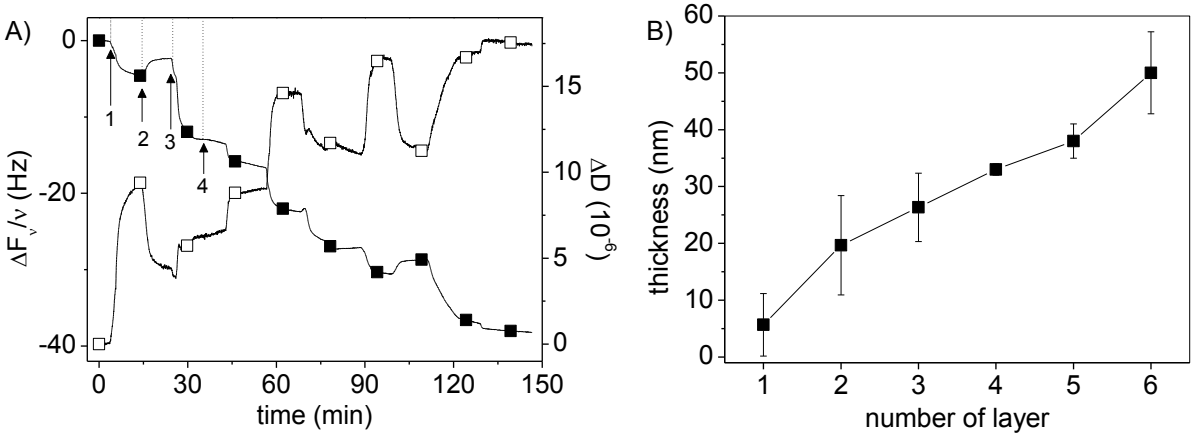


Figure 6.4. Buildup assessment of (CHI/Ph-levan) films. A: QCM-D monitoring of normalized frequency, $\Delta F_\nu/\nu$, and dissipation ΔD, obtained from the 5th overtone, for a total of 3 bilayers. Numbers refer to adsorption of CHI (1), adsorption of Ph-levan (3), and rinsing (2 and 4). B: Evolution of thickness of (CHI/Ph-levan) films with the number of layers. An odd layer number represents a film ending in CHI and an even number a film ending in Ph-levan. Data represent mean±standard deviation (SD).

The QCM-D data was used to estimate the thickness variations of the film with each adsorption cycle. Figure 6.4B shows how the thickness varied with each deposition cycle calculated using the Voigt model [36]. After the deposition of 6 layers, the film had a mean thickness of 50±7 nm, corresponding to an approximate total area density of 6.0±0.9 $\mu g.cm^{-2}$ (obtained by multiplying the thickness by the layer density, 1200 $kg \cdot m^{-3}$). The results obtained through QCM-D measurements demonstrate that Ph-levan can be used successfully with CHI to conceive a viscoelastic polymeric thin coating using the LbL approach.

Afterwards, films of 50 bilayers were assembled onto glass slides – henceforth referred to as $(CHI/Ph\text{-}levan)_{50}$ – for the characterization of their surface and adhesive properties. For the sake of comparison, multilayer films consisting of 50 bilayers of CHI and ALG, $(CHI/ALG)_{50}$, were also constructed and tested under the same experimental conditions. The formulation of this control film consists of well-known adhesive materials which properties were compared with those of $(CHI/Ph\text{-}levan)_{50}$ films. Additionally, it was seen before that this multilayer film can be easily assembled using the experimental parameters utilized in this work.[37,38]

The surface of $(CHI/Ph\text{-}levan)_{50}$ and $(CHI/ALG)_{50}$ films was evaluated by scanning electron microscopy (SEM). Figure 6.5 demonstrates that the former presented a flat surface with few morphological features (Figure 6.5A) in comparison to the $(CHI/ALG)_{50}$ control (Figure 6.5B). In both cases it is clear that the multilayer films completely coated the surface of the substrates.

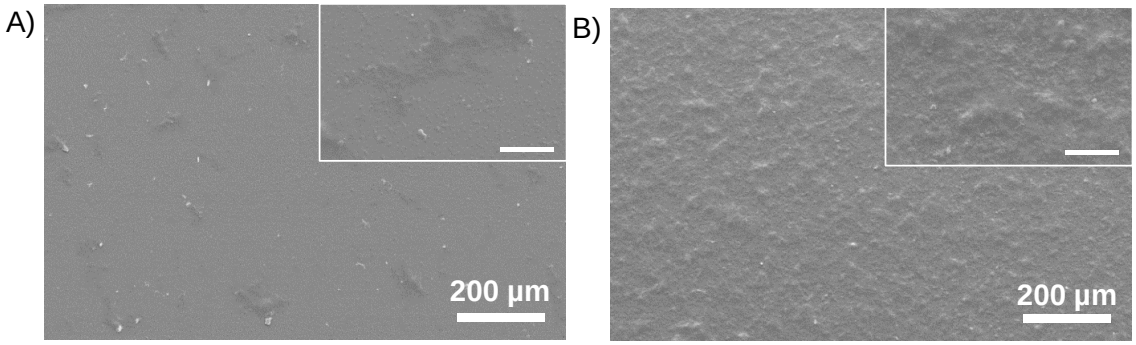


Figure 6.5. SEM images of (A) $(CHI/Ph\text{-}levan)_{50}$ and (B) $(CHI/ALG)_{50}$ films assembled onto glass. Inset scale bar: 50 µm.

It is noteworthy that the more flat surfaces are the ones exhibiting the best adhesive properties. For solid/viscoelastic contacts, it has been reported that if a surface – either the adhesive or the substrate – is rough, the contact between the two surfaces may be incomplete (i.e., the real contact area is lower

than the apparent contact area) and evolve with contact time, leading to surfaces to unbind [39,40]. For elastic surfaces, surface roughness is also known to decrease adhesion [41]. The current work is a case of contact between viscoelastic surfaces, a known property of polymer-based multilayer films [35]. Fitting only partially on the described roughness/adhesiveness models, the roughness observed in Figure 6.5 may have little influence in the adhesion mechanism of these films which, due to their viscous nature, will depend mainly on the strong adhesive bonds formed by the hydroxyl groups.

Most *in vitro* methods for screening the adhesiveness rely on the measurement of either tensile or shear strengths. The first usually tests the perpendicular force necessary to separate two surfaces, while the second determines the force that causes an adhesive to slide on a surface in the direction parallel to the plan of contact [42]. Although the first is the most commonly used, an adhesive or sealant in contact with a biological tissue is more prone to undergo shear stress than tensile, due to inherent muscular movements. In light of this, two glass slides bearing either $(CHI/Ph\text{-}levan)_{50}$ or $(CHI/ALG)_{50}$ hybrid films were overlapped as soon as the adsorption of the layers was concluded. After a cure of 24 h, the lap shear adhesive strength was tested. Figure 6.6 shows that the lap shear strength necessary to separate two $(CHI/Ph\text{-}levan)_{50}$ films was 2.5±0.3 MPa. $(CHI/ALG)_{50}$ films required a lap shear strength of 0.9±0.1 MPa until detachment was observed.

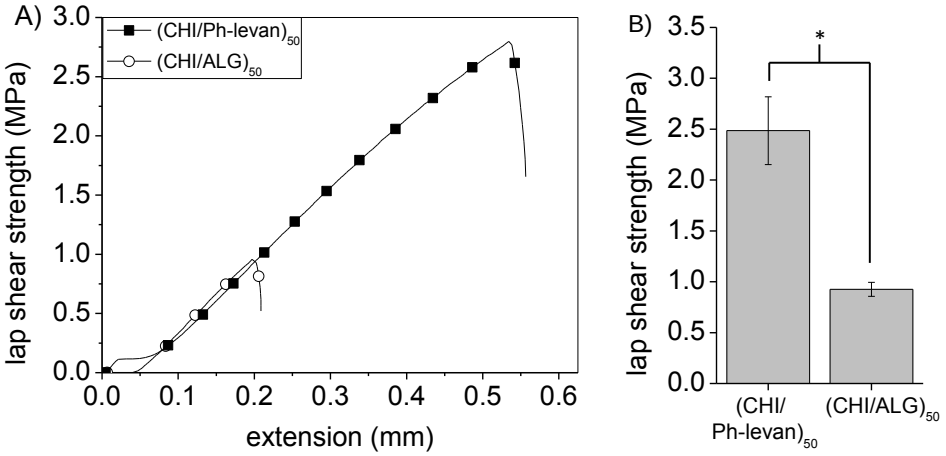


Figure 6.6. Lap shear stress for detachment of $(CHI/Ph\text{-}levan)_{50}$ and $(CHI/ALG)_{50}$ multilayers assembled onto glass slides (A) as a function of extension (representative curves). (B) Lap shear strength for the two multilayer films (mean±SD; n=3; *$p<0.05$).

In comparison, $(CHI/Ph\text{-}levan)_{50}$ films exhibited a value about 3 times superior to that of the control. Also, notice that the shear modulus (estimated from the slope of the graphics in Figure 6.6A) of both

multilayer films is similar, but the final displacement of $(CHI/Ph\text{-}levan)_{50}$ is higher, giving rise to a higher adhesive strength compared with the control, $(CHI/ALG)_{50}$. For clinical procedures, cyanoacrylates have been shown to provide a strong adhesiveness, appropriate for wound closure (around 68 kPa). Fibrin-based materials are weaker (around 13 kPa) are applied as sealants combined with suturing. Hydrogels and other polymer-based devices are also considered weak (ranging from 4 to 17 kPa) and often used as topical wound dressings or as sealants when mechanical properties are of less concern [43]. Independent studies on adhesive and sealant products available in the market have been made. For instance, Tisseel™ – a fibrin-based sealant – and Dermabond™ – a cyanoacrylate-based glue – showed shear adhesive strengths around 20 kPa [44] and 180 kPa [45], respectively. However, the authors used actual bovine tissues and not glass substrates, although other works describe experimental conditions similar to the presented herein. Yamada *et al.* [46] showed that the shear stress between two glass slides overlapped together with dopamine-modified chitosan was over 400 kPa, while unmodified chitosan conferred no adhesive strength. Ishihara *et al.* [47] also developed a photocrosslinkable chitosan hydrogel with a shear adhesive strength around 3 kPa. (Ph-levan)-containing multilayer coatings adhesives surpass these examples. In comparison with the product exhibiting the highest adhesive properties (dopamine-modified chitosan, 400 kPa) the lap shear strength is about 6 times higher. Thus, levan derivatives provide an enhanced adhesive character to these multilayer films that could be useful in applications where strong adhesiveness to a substrate is necessary.

In order to understand how cells interact with films containing Ph-levan, the biological performance was evaluated *in vitro* using L929 cells. In biological applications, an adhesive film could be useful to readily provide fixation to a tissue either externally as a wound healing bandage or internally as a surgical sealant for tissues and organs. In order to study the early cell adhesion on $(CHI/Ph\text{-}levan)_{50}$, we investigated the density of cells adhered onto the films after 24 h of culture and compared it to the $(CHI/ALG)_{50}$ case. A noticeable difference could be observed: cells adhered mostly to $(CHI/Ph\text{-}levan)_{50}$ than to $(CHI/ALG)_{50}$ (Figure 6.7).

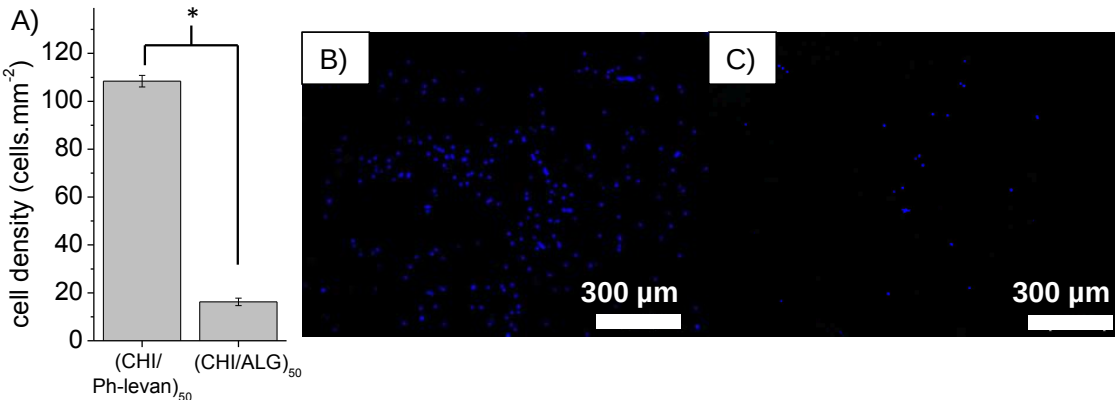


Figure 6.7. A: L929 cell density after 24 h of culture (n=3; $p<0.05$). DAPI staining of adhered cells on (B) $(CHI/Ph\text{-}levan)_{50}$ and (C) $(CHI/ALG)_{50}$ substrates.

Quantitatively, the mean cell area on the former was around 110 cells·mm^{-2}, a high value when compared to the latter, with only around 20 cells·mm^{-2}. The results demonstrated that the biological process of L929 cells adhesion was sensitive to the incorporation of Ph-levan into the LbL surfaces. In order to optimize biomaterials/cellular interactions this effect is of great importance, since those interactions are based on cell surface receptor/substrate ligand binding, which influence different cellular responses. We believe that levan surfaces will lead to new findings in cell/materials interactions, contributing to promote and control specific cellular responses.

6.4 Conclusions

In this work, the feasibility to construct nanostructured multilayer films containing an exopolysaccharide from an unconventional source, namely from extremophile microorganisms, was demonstrated. Relying on electrostatic interactions, hybrid films containing this fructan along with chitosan were compared with a formulation of chitosan and alginate, two natural ingredients widely regarded as good adhesives: the incorporation Ph-levan led to the conception of films that required higher strength for detachment to occur due to shear stress. Furthermore, cells were sensitive to this polysaccharide and adhered in higher number. In the context of biomedical and tissue engineering, these films could provide enhanced adhesiveness and protection to a new generation of wound healing bandages or to surgical sealants and also surfaces with optimized cell/substrate interactions, fabricated by a versatile and cost-effective multilayer technology.

6.5 Acknowledgements

This work was carried out under the scope of Fundação para a Ciência e Tecnologia" – FCT (grants SFRH/BD/61126/2009, SFRH/BD/73119/2010 and SFRH/BD/69529/2010), "Fundo Social Europeu" – FSE, "Programa Diferencial de Potencial Humano" – POPH, COST Action TD0906, and the financial support provided by TUBITAK through Project No: 111M232.

6.6 References

[1] Dash M., Chiellini F., Ottenbrite R. M., and Chiellini E., Chitosan—A versatile semi-synthetic polymer in biomedical applications, Progress in Polymer Science 2011, 36: 981-1014.

[2] Lee K. Y., and Mooney D. J., Alginate: Properties and biomedical applications, Progress in Polymer Science 2012, 37: 106-126.

[3] Rinaudo M., Chitin and chitosan: Properties and applications, Progress in Polymer Science 2006, 31: 603-632.

[4] Spotnitz W. D., and Burks S., Hemostats, sealants, and adhesives III: a new update as well as cost and regulatory considerations for components of the surgical toolbox, Transfusion 2012, 52: 2243-2255.

[5] Mano J. F., Silva G. A., Azevedo H. S., Malafaya P. B., Sousa R. A., Silva S. S., Boesel L. F., Oliveira J. M., Santos T. C., Marques A. P., Neves N. M., and Reis R. L., Natural origin biodegradable systems in tissue engineering and regenerative medicine: present status and some moving trends, Journal of The Royal Society Interface 2007, 4: 999-1030.

[6] Brubaker C. E., Kissler H., Wang L.-J., Kaufman D. B., and Messersmith P. B., Biological performance of mussel-inspired adhesive in extrahepatic islet transplantation, Biomaterials 2010, 31: 420-427.

[7] Chen P.-Y., McKittrick J., and Meyers M. A., Biological materials: Functional adaptations and bioinspired designs, Progress in Materials Science 2012, 57: 1492-1704.

[8] Cheneler D., and Bowen J., Degradation of polymer films, Soft Matter 2013, 9: 344-358.

[9] Boateng J. S., Matthews K. H., Stevens H. N. E., and Eccleston G. M., Wound healing dressings and drug delivery systems: A review, Journal of Pharmaceutical Sciences 2008, 97: 2892-2923.

[10] George M., and Abraham T. E., Polyionic hydrocolloids for the intestinal delivery of protein drugs: Alginate and chitosan — a review, Journal of Controlled Release 2006, 114: 1-14.

[11] Silva T. H., Alves A., Ferreira B. M., Oliveira J. M., Reys L. L., Ferreira R. J. F., Sousa R. A., Silva S. S., Mano J. F., and Reis R. L., Materials of marine origin: a review on polymers and ceramics of biomedical interest, International Materials Reviews 2012, 57: 276-306.

[12] Donot F., Fontana A., Baccou J. C., and Schorr-Galindo S., Microbial exopolysaccharides: Main examples of synthesis, excretion, genetics and extraction, Carbohydrate Polymers 2012, 87: 951-962.

[13] Kazak H., Oner E. T., and Dekker R. F. H., Extremophiles as sources of exopolysaccharides, In Ito R., Matsuo Y., eds. Handbook of carbohydrate polymers: development, properties and applications, New York, U. S. A.: Nova Science Publishers; 2009.

[14] Sima F., Mutlu E. C., Eroglu M. S., Sima L. E., Serban N., Ristoscu C., Petrescu S. M., Oner E. T., and Mihailescu I. N., Levan Nanostructured Thin Films by MAPLE Assembling, Biomacromolecules 2011, 12: 2251-2256.

[15] Freitas F., Alves V. D., and Reis M. A. M., Advances in bacterial exopolysaccharides: from production to biotechnological applications, Trends in biotechnology 2011, 29: 388-398.

[16] Kang S. A., Jang K. H., Seo J. W., Kim K. H., Kim Y. H., Rairakhwada D., Seo M., Lee J. O., Ha S. D., Kim C. H., and Rhee S. K., Levan: applications and perspectives, In Rehm B. H. A., ed. Microbial production of biopolymers and polymer precursors, Norfolk, England: Caister Academic Press; 2009.

[17] Poli A., Kazak H., Gürleyendağ B., Tommonaro G., Pieretti G., Öner E. T., and Nicolaus B., High level synthesis of levan by a novel Halomonas species growing on defined media, Carbohydrate Polymers 2009, 78: 651-657.

[18] Poli A., Nicolaus B., Denizci A. A., Yavuzturk B., and Kazan D., Halomonas smyrnensis sp. nov., a moderately halophilic, exopolysaccharide-producing bacterium, International Journal of Systematic and Evolutionary Microbiology 2013, 63: 10-18.

[19] Sam S., Kucukasik F., Yenigun O., Nicolaus B., Oner E. T., and Yukselen M. A., Flocculating performances of exopolysaccharides produced by a halophilic bacterial strain cultivated on agro-industrial waste, Bioresource Technology 2011, 102: 1788-1794.

[20] Sezer A. D., Kazak H., Öner E. T., and Akbuğa J., Levan-based nanocarrier system for peptide and protein drug delivery: Optimization and influence of experimental parameters on the nanoparticle characteristics, Carbohydrate Polymers 2011, 84: 358-363.

[21] Morales J. O., and McConville J. T., Manufacture and characterization of mucoadhesive buccal films, European Journal of Pharmaceutics and Biopharmaceutics 2011, 77: 187-199.

[22] Ai H., Jones S. A., and Lvov Y. M., Biomedical applications of electrostatic layer-by-layer nano-assembly of polymers, enzymes, and nanoparticles, Cell Biochemistry and Biophysics 2003, 39: 23-43.

[23] Costa R. R., Custódio C. A., Arias F. J., Rodríguez-Cabello J. C., and Mano J. F., Layer-by-Layer Assembly of Chitosan and Recombinant Biopolymers into Biomimetic Coatings with Multiple Stimuli-Responsive Properties, Small 2011, 7: 2640-2649.

[24] Decher G., Hong J. D., and Schmitt J., Buildup of ultrathin multilayer films by a self-assembly process: III. Consecutively alternating adsorption of anionic and cationic polyelectrolytes on charged surfaces, Thin Solid Films 1992, 210-211: 831-835.

[25] Gribova V., Auzely-Velty R., and Picart C., Polyelectrolyte multilayer assemblies on materials surfaces: from cell adhesion to tissue engineering, Chemistry of Materials 2011, 24: 854-869.

[26] Volodkin D. V., Schaaf P., Mohwald H., Voegel J.-C., and Ball V., Effective embedding of liposomes into polyelectrolyte multilayered films: the relative importance of lipid-polyelectrolyte and interpolyelectrolyte interactions, Soft Matter 2009, 5: 1394-1405.

[27] Mjahed H., Porcel C., Senger B., Chassepot A., Netter P., Gillet P., Decher G., Voegel J.-C., Schaaf P., Benkirane-Jessel N., and Boulmedais F., Micro-stratified architectures based on successive stacking of alginate gel layers and poly(l-lysine)-hyaluronic acid multilayer films aimed at tissue engineering, Soft Matter 2008, 4: 1422-1429.

[28] Shukla A., Avadhany S. N., Fang J. C., and Hammond P. T., Tunable Vancomycin Releasing Surfaces for Biomedical Applications, Small 2010, 6: 2392-2404.

[29] Tang Z., Wang Y., Podsiadlo P., and Kotov N. A., Biomedical Applications of Layer-by-Layer Assembly: From Biomimetics to Tissue Engineering, Advanced Materials 2006, 18: 3203-3224.

[30] Sogutcu E., Emrence Z., Arikan M., Cakiris A., Abaci N., Öner E. T., Üstek D., and Arga K. Y., Draft Genome Sequence of Halomonas smyrnensis AAD6T, Journal of Bacteriology 2012, 194: 5690-5691.

[31] Küçükaşik F., Kazak H., Güney D., Finore I., Poli A., Yenigün O., Nicolaus B., and Öner E., Molasses as fermentation substrate for levan production by Halomonas sp, Applied Microbiology and Biotechnology 2011, 89: 1729-1740.

[32] Huang Q., and Zhang L., Preparation, chain conformation and anti-tumor activities of water-soluble phosphated (1 → 3)-α-d-glucan from Poria cocos mycelia, Carbohydrate Polymers 2011, 83: 1363-1369.

[33] Suflet D. M., Chitanu G. C., and Popa V. I., Phosphorylation of polysaccharides: New results on synthesis and characterisation of phosphorylated cellulose, Reactive and Functional Polymers 2006, 66: 1240-1249.

[34] Suflet D. M., Chitanu G. C., and Desbrières J., Phosphorylated polysaccharides. 2. Synthesis and properties of phosphorylated dextran, Carbohydrate Polymers 2010, 82: 1271-1277.

[35] Marx K. A., Quartz Crystal Microbalance: A Useful Tool for Studying Thin Polymer Films and Complex Biomolecular Systems at the Solution–Surface Interface, Biomacromolecules 2003, 4: 1099-1120.

[36] Voinova M. V., Rodahl M., Jonson M., and Kasemo B., Viscoelastic Acoustic Response of Layered Polymer Films at Fluid-Solid Interfaces: Continuum Mechanics Approach, Physica Scripta 1999, 59: 391.

[37] Alves N. M., Picart C., and Mano J. F., Self Assembling and Crosslinking of Polyelectrolyte Multilayer Films of Chitosan and Alginate Studied by QCM and IR Spectroscopy, Macromolecular Bioscience 2009, 9: 776-785.

[38] Martins G. V., Mano J. F., and Alves N. M., Nanostructured self-assembled films containing chitosan fabricated at neutral pH, Carbohydrate Polymers 2010, 80: 570-573.

[39] Creton C., and Leibler L., How does tack depend on time of contact and contact pressure?, Journal of Polymer Science Part B: Polymer Physics 1996, 34: 545-554.

[40] Hui C. Y., Lin Y. Y., and Baney J. M., The mechanics of tack: Viscoelastic contact on a rough surface, Journal of Polymer Science Part B: Polymer Physics 2000, 38: 1485-1495.

[41] Haiat G., and Barthel E., An Approximate Model for the Adhesive Contact of Rough Viscoelastic Surfaces, Langmuir 2007, 23: 11643-11650.

[42] Thirawong N., Nunthanid J., Puttipipatkhachorn S., and Sriamornsak P., Mucoadhesive properties of various pectins on gastrointestinal mucosa: An in vitro evaluation using texture analyzer, European Journal of Pharmaceutics and Biopharmaceutics 2007, 67: 132-140.

[43] Lauto A., Mawad D., and Foster L. J. R., Adhesive biomaterials for tissue reconstruction, Journal of Chemical Technology & Biotechnology 2008, 83: 464-472.

[44] Elvin C. M., Vuocolo T., Brownlee A. G., Sando L., Huson M. G., Liyou N. E., Stockwell P. R., Lyons R. E., Kim M., Edwards G. A., Johnson G., McFarland G. A., Ramshaw J. A. M., and Werkmeister J. A., A highly elastic tissue sealant based on photopolymerised gelatin, Biomaterials 2010, 31: 8323-8331.

[45] Murphy J. L., Vollenweider L., Xu F., and Lee B. P., Adhesive Performance of Biomimetic Adhesive-Coated Biologic Scaffolds, Biomacromolecules 2010, 11: 2976-2984.

[46] Yamada K., Chen T., Kumar G., Vesnovsky O., Topoleski L. D. T., and Payne G. F., Chitosan Based Water-Resistant Adhesive. Analogy to Mussel Glue, Biomacromolecules 2000, 1: 252-258.

[47] Ishihara M., Nakanishi K., Ono K., Sato M., Kikuchi M., Saito Y., Yura H., Matsui T., Hattori H., Uenoyama M., and Kurita A., Photocrosslinkable chitosan as a dressing for wound occlusion and accelerator in healing process, Biomaterials 2002, 23: 833-840.

Chapter 7. Layer-by-layer film-growth using polysaccharides and recombinant polypeptides: a combinatorial approach[6]

Abstract

Nanostructured films consisting of polysaccharides and elastin-like recombinamers (ELRs) are fabricated in a layer-by-layer manner. A quartz-crystal microbalance with dissipation monitoring (QCM-D) is used to follow the buildup of hybrid films containing one polysaccharide (chitosan or alginate) and one of several ELRs that differ in terms of amino acid content, length and biofunctionality *in situ* at pH 4.0 and pH 5.5. The charge density of the ingredients at each pH is determined by measuring their ζ-potential, and the thickness of a total of 36 different films containing five bilayers is estimated using the Voigt-based viscoelastic model. A comparison of the values obtained reveals that thicker films can be obtained when working at a pH close to the acidity constant of the polysaccharide used (near-pK_a conditions), suggesting that the construction of such films is more favorable when based on the presence of hydrophobic interactions between ELRs and partially neutralized polysaccharides. Further analysis shows that the molecular weight of the ELRs plays only a minor role in defining the growth tendency. When taken together, these results point to the most favorable conditions for constructing nanostructured films from natural and distinct recombinant polypeptides that can be tuned to exhibit specialized biofunctionality for tissue-engineering, drug-delivery, and biotechnological applications.

[6] This chapter is based on the following publication:

Costa R. R., Testera A. M., Arias F. J., Rodríguez-Cabello J. C., and Mano J. F., Layer-by-layer film-growth using polysaccharides and recombinant polypeptides: a combinatorial approach, The Journal of Physical Chemistry B 2013, 17: 6839-6848, DOI:10.1021/jp4028518.

7.1 Introduction

Surface engineering is a field of expertise concerned with the modification and improvement of interfaces [1-3]. In the past decades, this technique has been widely applied in the field of biomedical and tissue engineering, where the properties of substrate surfaces need to be tuned to promote cell expansion, improve the interface between an implantable device and its biological environment, and add stimuli-responsiveness for on-demand surface property switching [4-7]. Layer-by-layer (LbL) techniques are perhaps the most versatile and easy-to-apply of the numerous surface-modification tools currently available as they are based on the spontaneous adsorption of ingredients onto a substrate, generally a polymer, biomolecule or inorganic particle, and allow the sequential formation of a nanostructured film. This technique allows robust coatings to be produced on substrates with complex geometries and, as it does away with the need for harmful organic solvents, it is of great interest in tissue-engineering applications [5,8-10]. As such, LbL methods have already been employed in cell-sheet technology [11,12], for drug delivery [13-15] and for the creation of three-dimensional scaffolds for cell culture [16].

Exploiting strong, long-range electrostatic interactions (e.g., attraction between oppositely charged polyelectrolytes) [17] is by far the most widely used LbL construction mechanism, often referred to as electrostatic self-assembly (ESA). LbL synthesis is not restricted to this mechanism: this technique relies on the existence of multiple complementary intermolecular interactions that allow the LbL concept to be widened to include hydrogen bonding and hydrophobic interactions (often referred to as secondary or nonelectrostatic interactions) [18-20]. Nowadays, it is assumed that the gain in entropy is also a key phenomenon for LbL construction which results from the release of counter-ions. The outcome of such a mechanism is often the organization of the layers in a more coiled and interdigitated conformation and loss of degrees of freedom from the polyelectrolyte molecules [19-21].

Herein we intend to demonstrate the feasibility of LbL synthesis using natural marine-based polysaccharides [chitosan (CHI) and alginate (ALG)] and nature-inspired polypeptides, in this case elastin-like recombinamers (ELRs), which are the recombinant analogs of elastin-like polymers (ELPs). The polycationic chitosan and polyanionic alginate are well-known polysaccharides derived from marine crustaceans and brown algae, respectively [22]. Both polymers are non-toxic and exhibit adhesive, bacteriostatic, fungistatic, hemostatic and antimicrobial effects that make them suitable for use in wound dressings and drug-delivery systems [23-25]. ELRs are genetically modified biocompatible and

stimuli-responsive polypeptides that mimic natural elastin, the extracellular elastic protein found in higher classes of animals [26-28]. These polypeptides exhibit a transition temperature (T_t) in aqueous solution above which free polymer chains adopt random coil conformations and separate from the solvent. ELRs follow the standard repeating structure of elastin, namely valine-proline-glycine-valine-glycine (VPGVG), a sequence with no electrostatic charge. Besides their smart nature, the most attractive property of ELRs is their ability to be engineered to contain amino acid sequences with charge and even bioactivity. Indeed, it has proven possible to construct ELRs containing sequences that enhance cell adhesion [29,30] or biomineralization [31]. One could thus consider that such materials may be able to act as versatile and fine-tuned models for protein systems, including nanostructured coatings for highly specific tissue-engineering applications.

A great deal of time and effort has been dedicated to the widely investigated poly(styrene sulfonate)/poly(allylamine hydrochloride) (PSS/PAH) system, which is currently considered to be a model of how multilayered thin films are built, over the past 20 years [5]. The fact that most studies in this field have been based on the application of ESA interactions to synthetic materials with controllable properties has hindered a more in-depth understanding of the secondary construction mechanism. As a consequence, extrapolation to new tailored materials that are more suitable for tissue-engineering applications, as is the case for ELRs or proteins in general, has been limited. In this regard, classical ESA has been unable to explain fully the formation of multilayer thin films and the role of secondary interactions has been brought into question. A report from Cini and co-workers [32] – to which also contributed Decher, one of the pioneers of LbL – have also proposed that the construction of poly(allylamine hydrochloride) (PAH) and poly(sodium phosphate) (PSP) "violates almost all the rules" of LbL, thereby suggesting a possible contribution from hydrophobic interactions. Our group has also considered that the formation of an ELR-containing multilayer film is almost certainly driven, at least in part, by hydrophobic interactions [29]. However, to the best of our knowledge, studies that could systematically and extensively confirm the role of such interactions in the construction of multilayered films have yet not been reported.

In this work we intended to study the conditions needed to successfully obtain a hybrid, biomimetic LbL film that combines the properties of natural and genetically modified polymers. We resorted to a quartz-crystal microbalance with dissipation monitoring (QCM-D), a technique that is able to detect adsorbed surface density changes in the order of $ng \cdot cm^{-2}$ and measure the viscoelastic properties of the resulting surface in real time. Based on the piezoelectric effect, QCM has proven to be a powerful technique for

evaluating the growth of multilayer films as well as for monitoring the effect of factors such as concentration, molecular weight and pH during or after their assembly [33-37]. Thus, our objectives were (i) to study the influence of ESA and secondary interactions in the buildup mechanism of the proposed hybrid films by means of charge variations dependent on pH, (ii) study the influence of distinct ELR molecular weights (M_n), (iii) compare the feasibility of the construction when using two distinct polysaccharides, CHI and ALG, and (iv) extend the knowledge of LbL mechanisms to the class of ELRs.

7.2 Experimental section

7.2.1 Materials

Medium molecular weight chitosan was purchased from Sigma-Aldrich (reference 448877, Brookshield viscosity 200-800 cP, molecular weight 190-310 kDa) and purified by a series of filtering steps and precipitation from water and ethanol, followed by freeze-drying. To determine the degree of deacetylation (DD) of chitosan, hydrogen-1 nuclear magnetic resonance (^{1}H-NMR) was performed using a Varian MR-400 spectrometer. 10 mg of chitosan was dissolved in 1 mL of deuterated water (D_2O) and 20 μL of deuterated hydrochloric acid (DCl). An aliquot of this solution was placed in a 5 mm NMR tube and the spectrum recorded at 60°C. The calculation method of DD was described elsewhere [38] and was determined to be 82%. Alginate (alginic acid sodium salt from brown algae) was purchased from Fluka (reference 71238, molecular weight 100-200 kDa). ELRs were obtained by the induced gene expression of recombinant *Escherichia coli* strains containing the expressing gene. Each ELR was induced in a 12 L Applikon fermenter, in terrific broth medium (TB) supplemented with carbenicillin (0.1% v/v) and glucose (0.1% v/v), under controlled conditions of temperature (37 °C) and pH (7.00). Fermentation was stopped after registering an optical density variation at 600 nm of less than 0.25, in a time-frame of 1 hour. The culture was then harvested by centrifugation, resuspended and lysed by ultrasonic disruption. Insoluble debris was removed by centrifugation and the cleared lysate was subjected to several cycles of cold and warm centrifugations (4 and 40°C, respectively). All purification steps were carried out in sodium chloride solution (0.5 M). The polymer in solution was dialyzed against ultrapure water, frozen at -24°C and freeze-dried.

7.2.2 Assessment of the ELR compositions

The molecular weight and amino acid composition of the samples obtained were determined by matrix-assisted laser desorption/ionization time-of-flight mass spectroscopy (MALDI-TOF) and amino acid content analysis, respectively. These methods, and their results, are described in more detail in the Supporting Information. The percentage of residues subject to ionization and the proportion of positive and negative charges were also calculated.

7.2.3 Measurement of the charges

The ζ-potentials of the polysaccharides and ELRs were determined using a Nano-ZS from Malvern (United Kingdom), at 25°C. Aqueous solutions of each ingredient were used, at 100 $\mu g \cdot mL^{-1}$, 0.15 M NaCl and pH values of 4.0 or 5.5.

7.2.4 Construction of hybrid self-assembled films

A Q-Sense E4 quartz-crystal microbalance (Q-Sense AB, Sweden) with dissipation monitoring system was used to monitor the adsorption of polysaccharides and ELRs onto gold-coated quartz crystals *in situ* (Q-Sense, reference QSX301). The assembled films consisted of a series of polysaccharide/ELR combinations at pH values of either 4.0 or 5.5, thus resulting in a total of 36 different conditions. Combinations containing chitosan had this polycation as the first layer, whereas those containing alginate had this polyanion as the second layer. The quartz-crystal was excited at multiple overtones (1, 3, 5, 7, 9, 11 and 13, corresponding to 5, 15, 25, 35, 45, 55 and 65 MHz respectively). Adsorption took place at 25°C, using solutions at 100 $\mu g \cdot mL^{-1}$, 0.15 M NaCl and at a constant flow rate of 50 $mL \cdot min^{-1}$, with an adsorption time of 15 minutes and an intermediate rinsing step of 10 minutes.

7.2.5 Estimation of the film thicknesses

The Voigt-based viscoelastic model contained in the QTools software from Q-Sense (version 3.0.15.553) was used to estimate the thickness of the films from the QCM-D monitoring data. Iterations of the model were performed using at least three overtones. The model requires three parameters, namely solvent density, solvent viscosity and film density, to be fixed. The solvent viscosity was therefore fixed at 0.001 Pa·s (same as water) and the film density at 1200 $kg.m^{-3}$ (often assumed to return the lowest

calculation error) [29,37,39]. The solvent density was varied by trial and error between 1000 and 1060 $kg \cdot m^{-3}$ until the total error, χ^2, was minimized.

7.3 Results and discussion

7.3.1 Characterization of the polysaccharides and ELRs

We selected nine ELRs for this study as the genetically engineered origin of these compounds allows a class of materials that can differ in terms of sequence, length and bioactivity without significantly altering the original elastin backbone to be studied. The properties of each ELR are summarized in Table 7.1 according to their molecular weight, M_n, amino acid sequence and proportions of charged/uncharged and positive/negative residues. The acronyms were assigned on the basis of their distinct sequence, function and variations on the repeating (VPGVG) sequence. The experimental amino acid composition and MALDI-TOF values can be found in Supplemental Information (Supplemental Table 7.1, Supplemental Table 7.2, Supplemental Table 7.3, Supplemental Figure 7.1) showing that the experimental M_n and number of amino acids agree well with the theoretical values of Table 7.1. Arginine (R), histidine (H) and lysine (K) are positively charged when protonated and aspartic acid (D) and glutamic acid (E) are negatively charged when deprotonated. The properties of these residues were taken into account when calculating the charged and amino acid proportions. A closer look at each ELR sequence shows that they are all distinct and that some even exhibit motifs with biological relevance that could make them useful for current therapies and applications: 3K-VRGDV and H-RGD6, for example, contain the RGD sequence, which promotes cell adhesion. 3K-VRDG$^{(-)}$V is the negative control of the former as it contains the same sequence but with a scrambled, non-functional RDG motif. Similarly, HAP3, H3A20 and H3A20H3 exhibit sequences that promote biomineralization, organized as single, double and triple blocks, respectively, with the alanine-block (A20 portion) being highly hydrophobic. GEG15 and IK24 contain E and K residues, which confer anionic and cationic behavior, respectively. Finally, the neutralized V84 lacks ionizable residues and is therefore uncharged.

Although the original sequence of V84 contains three K-residues, which in theory should confer a positive charge on this ELR, it was neutralized in order to use it as a neutral control (see Supplemental Information, “neutralization of V84”). This sequence was used to analyze the buildup of a neutral ELR hybrid film in comparison with ELRs that are susceptible to ionization.

Table 7.1. List of ELRs used in this work with their corresponding theoretical molecular weight and proportions of charged and positive/negative amino acids. *Neutralized lysine residues.

ELR acronym	Sequence	M_n (Da)	Charged proportion (%)	Positive/negative amino acid proportion (%)
3K-VRDG$^{(-)}$V	MGKKKP-$(VPGVG)_{14}$[$(VPGIG)_{10}$AVTGRDGSPASS$(VPGIG)_{10}]_2(VPGVG)_{14}$-V	31371	1.9	71.4/28.6
3K-VRGDV	MGKKKP$(VPGVG)_{14}$[$(VPGIG)_{10}$AVTGRGDSPASS$(VPGIG)_{10}]_2$ $(VPGVG)_{14}$-V	31371	1.9	71.4/28.6
HAP3	MESLLP[[$(VPGIG)_2(VPGKG)(VPGIG)_2]_2$DDDEEKFLRRIGRFG[$(VPGIG)_2$ $(VPGKG)(VPGIG)_2]_2]_3$-V	31877	11.4	60/40
GEG15	MD[$(VPGVG)_2(VPGEG)$ $(VPGVG)_2]_{15}$IGSG	31948	3.9	4/96
H3A20	MESLLP[[$(VPGIG)_2$VPGKG$(VPGIG)_2]_2$DDDEEKFLRRIGRFG[$(VPGIG)_2$VPGKG $(VPGIG)_2]]_3$-$(VPAVG)_{20}$-V	40361	8.8	60/40
IK24	MESLLP[$(VPGIG)_2(VPGKG)$ $(VPGIG)_2]_{24}$-V	51970	4.0	100/0
H-RGD6	MGSSHHHHHHSSGLVPRGSHMESLLP[[$(VPGIG)_2(VPGKG)(VPGIG)_2]_2$AVTGRGDSPASS[$(VPGIG)_2$(VPGKG) $(VPGIG)_2]_2]_6$-V	60661	6.4	84.4/15.6
H3A20H3	MESLLP[[$(VPGIG)_2(VPGKG)(VPGIG)_2]_2$DDDEEKFLRRIGRFG[$(VPGIG)_2(VPGKG)$ $(VPGIG)_2]_2]_3(VPAVG)_{20}$[[$(VPGIG)_2$ $(VPGKG)(VPGIG)_2]_2$DDDEEKFLRRIGRFG[$(VPGIG)_2(VPGKG)(VPGIG)_2]_2]_3$-V	71462	9.9	60.8/39.2
Neutralized V84	MGK*K*K*P-$(VPGVG)_{84}$-V	35191	0	0/0

Like most proteins, the ionizable residues in the backbone of these ELRs represent only a small fraction of the whole sequence (maximum of 11.4% in the case of HAP3). Therefore, although ELRs can be modified to include specific peptide sequences, they still retain the basic properties of this class of polymers. This is a relevant property for the present study, considering that the nonionizable residues may interact by hydrophobic interactions. Despite the fact that these interactions are weaker and have a shorter range than their electrostatic counterparts, they nevertheless have been shown to play an important role in stabilizing the internal structure of multilayers containing uncharged groups, such as most proteins, which contain large numbers of hydrophobic groups [40-42].

Using a group of ELRs with such distinct properties, we expected to be able to identify the properties that are essential for the construction of this kind of hybrid nanostructured film, especially films containing complex ELRs with bioactivity and practical relevance.

7.3.2 Effect of the charged state by means of the ζ-potential

One of the parameters to be studied was the influence of electrostatic interactions – or lack of them – during the growth process. To this end, we measured the charge of each ELR and polysaccharide prior to the QCM-D experiments by determining their ζ-potentials at pH 4.0 and 5.5. The results are shown in Table 7.2.

Table 7.2. ζ-potentials (mV) for CHI, ALG and the ELRs at pH values of 4.0 and 5.5.

	pH 4.0	pH 5.5
3K-VRDG(ϕ)V	-2.7±0.6	-9.3±1.5
3K-VRGDV	-2.1±0.2	-8.4±0.3
HAP3	-0.4±0.8	-6.8±0.7
GEG15	-2.9±0.6	-4.4±0.4
H3A20	-13.3±1.7	-10.7±2.8
IK24	3.5±0.4	1.6±0.1
H-RGD6	1.8±0.1	-5.1±1.0
H3A20H3	-17.7±2.1	-15.0±2.6
Neutralized V84	1.1±0.8	-1.0±0.1
CHI	16.8±0.8	13.1±0.3
ALG	-8.3±1.0	-17.5±1.5

In the case of the polysaccharides, CHI exhibited a positive and ALG a negative charge as expected and, since both contain ionizable groups, their charge varied with the pH, with their potential decreasing at the pH value closest to their respective pK_a as their charges were progressively neutralized [close to the pK_a of ALG (≈3.2–4) [43] and CHI (≈6) [25], respectively]. As for the ELRs, it is interesting to note that, irrespective of the pH, in general they are all negatively charged despite the fact that all ELRs, except GEG15, have a higher proportion of residues that are susceptible of exhibiting a positive charge, with the highest being H-RGD6 (84.4%) and IK24 (96%), in comparison to the number of negative ones.

One would expect that some ELRs should exhibit positive values, especially at pH 4.0, where the availability of uncharged protonated –COOH groups would be higher. The complexity of the ELR polypeptide family may explain why this did not occur: characteristics such as chain conformation and residue exhibition/inhibition may vary among different peptide sequences. Indeed, previous studies have shown that the pK_a of ionizable side-chains may change significantly, for example with small changes in the amino acid sequence [44,45]. However, such a characterization was not in the scope of this work since only the effective charge of each polymer in solution was considered when reaching the conclusions presented below. The IK24 and H-RGD6 ELRs are indeed positively charged at pH 4.0. In the case of the former, although it has an E-residue that can be ionized with a negative charge, the fact that the K-residues are in excess does not allow for a charge sign inversion below pH 5.5. A similar situation was found for neutralized V84, which contains no ionizable residues, although in this case the small charge fluctuation is due to the effect of pH on the N– and C–termini. In contrast, the block-ELRs (H3A20 and H3A20H3) are more negative at pH 4.0 than at pH 5.5. Again, it is likely that a different conformation arises as a result of organization of the ELR into blocks and their amphiphilic nature.

Currently, two models are accepted to explain LbL growth driven by electrostatic interactions. One states that the LbL ingredients should have a minimum charge density with opposite signs, whereas the other states that, rather than having a minimum charge density, it is the charge balance that favors the buildup, i.e., that two ingredients are equally and symmetrically charged. Also, the gain of entropy can be hypothesized. For instance, it is known that, when using weak polyelectrolytes, polymers with a higher number of charged and polar groups tend to be adsorbed as a thin layer with a flat chain conformation whereas more neutral ones tend to be adsorbed as a thicker layer and to form loop-type structures [46-48]. Since the ELRs used herein are modified versions of the basic repeating block of elastin (some with charged amino acids) they would appear to be the ingredient with the most hydrophobic backbone rather than the polysaccharides, and thus have a higher contribute to the

entropy mechanism due to the formation of loopier and interdigitated layers. Moreover, changing the pH of weak polyelectrolytes, namely the polysaccharides used, will also vary their ionizable state, making them more charged or less charged. However, unlike the presence or absence of electrostatic charges, the real weight of the entropic gain in the LbL mechanism cannot be directly measured, and thus was left out of the discussion presented below. In light of the above, we defined 36 test conditions. Each condition is a combination of a polysaccharide (CHI or ALG) with one of the nine ELRs. Each one of these combinations was then studied at two pH values: 4.0 and 5.5, close to the pK_a of ALG and CHI, respectively. This allowed combinations containing fully charged/ionized or partially charged (near-pK_a conditions) forms of polysaccharides with ELRs to be compared. For convenience, each permutation combining ELRs and either ALG or CHI at pH 4.0 or 5.5 will henceforth be referred to as ALG40 or CHI40 and ALG55 or CHI55, respectively.

Our first step was to represent graphically the ζ-potentials of the polysaccharides and ELRs at each pH in Figure 7.1, in order to estimate the influence of the above-mentioned models. In this graphic, each end of the column represents the charge of each ingredient used in each of the 36 combinations. Lighter colors are used when the ingredients possess the same charge sign. First, identifying the potential combinations meeting the first ESA theory mentioned above is simple, since the only requirement is that the ingredients possess charge with opposite sign. Most CHI permutations meet the criteria, with only a few ALG ones. Second, we analyzed the charge balance under each condition. For CHI combinations, in general the ζ-potential of the highly charged chitosan is not matched by the weakly charged ELRs under CHI40 conditions. This situation can be seen graphically by the different lengths of the bars on the positive and negative sides, or by bars represented in only one charge side.

However, at pH 5.5, CHI becomes less charged (+13.1±0.3 mV, in comparison to +16.8±0.8 mV) and at the same time the charge of the ELRs shifts to a more negatively charged state (notice that the charge of CHI and the block polypeptides H3A20 and H3A20H3 are balanced in either condition), thus leading to a more effective net charge balance. A similar trend is observed for ALG combinations. ALG at pH 4.0 is partially neutralized and the ζ-potentials of the ELRs shift toward more positive values. This way, a more favorable electrostatic situation between ALG and ELRs is achieved but in a different manner than when using CHI: whereas with CHI55 balance is achieved by a decrease of its positive charge and an increase in the negative charge of the ELRs, with ALG40 a reduction in the electrostatic repulsion arising from a lower ionization state of ALG and the ELRs is observed, thereby representing a shift toward a situation where uncharged group interaction is maximized.

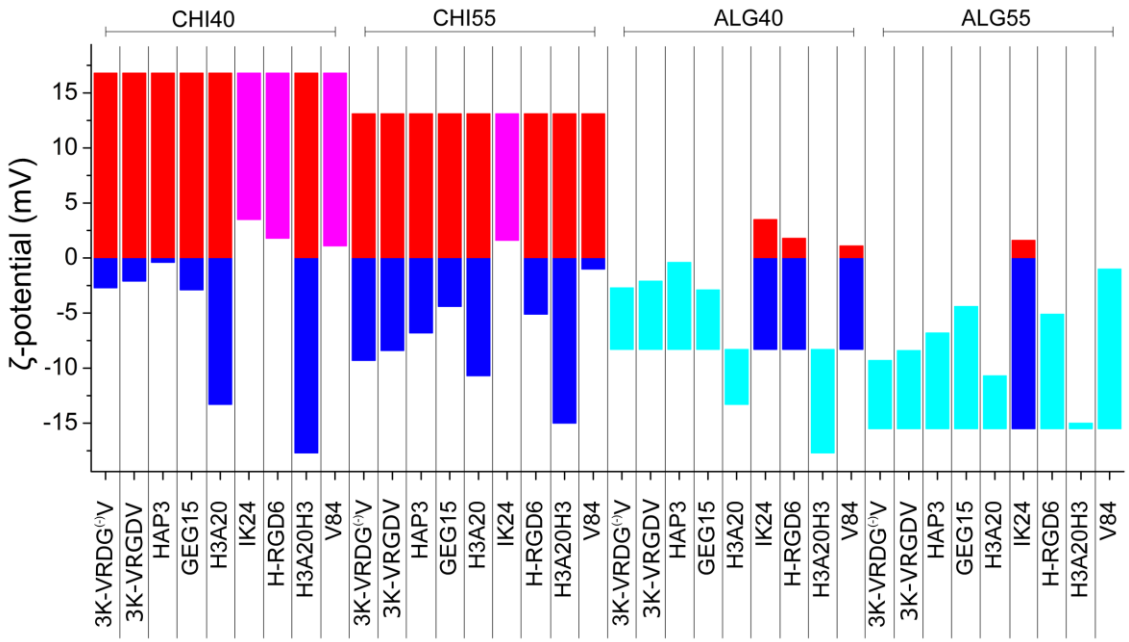


Figure 7.1. Range of ζ-potentials for each polysaccharide/ELR combination. CHI40, CHI55, ALG40 and ALG55 represent combinations of CHI or ALG at pH 4.0 or pH 5.5. The division serves to indicate the charge balance between each polymer in terms of positive (red) and negative (blue) proportion of the whole bar length. Bars depicted in light blue and purple represent combinations in which both polymers exhibit potential with the same signal. For example, in the first column, where CHI and 3K-VRDG$^{(-)}$V were used at pH 4.0, the ζ-potentials were +16.8 mV and -2.7 mV, respectively. In the last column, where ALG and V84 were used at pH 5.5, the ζ-potentials were -15.5 mV and -1 mV, respectively.

Given the potential mechanisms at work under the different polysaccharide/ELR/pH permutations, we have resorted to the QCM-D in order to determine the type of mechanism in which the construction of hybrid polysaccharide/ELR films majorly depends.

7.3.3 QCM-D data acquisition

Each experiment was conducted using a QCM-D to monitor the sequential adsorption of a single polysaccharide and an ELR. In each experiment, the pH of the solutions used (polymeric and rinsing) was adjusted to either 4.0 or 5.5. Also, in order to avoid the induction of conformational changes and data acquisition noise from the layers that had assembled previously, the pH values of the solutions used in each experiment were adjusted to the same value. Typical graphs of frequency (ΔF) and

dissipation (ΔD) variations are depicted for five bilayers of CHI/ELR (Figure 7.2A and Figure 7.2C, respectively) and ELR/ALG (Figure 7.2B and Figure 7.2D, respectively) at different pH values. The example presented (the combinations using H-RGD6) shows the data obtained for the fifth overtone, which corresponds to an excitation frequency of 25 MHz, and is representative of all 36 polysaccharide/ELR/pH conditions. The graphics obtained for each combination studied can be found in Supplemental Figure 7.3.

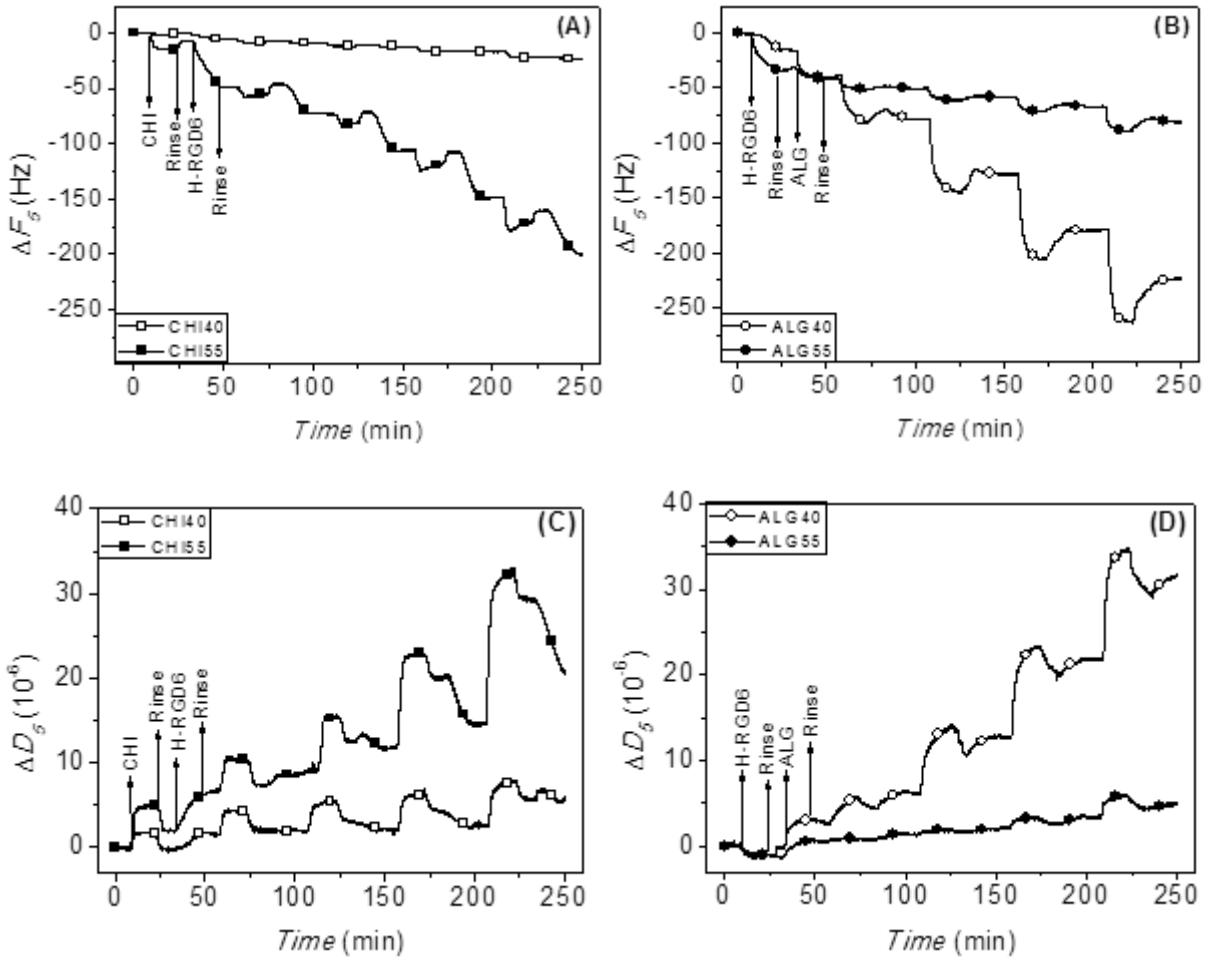


Figure 7.2. Representative QCM-D acquisition graphics depicting the 5th overtone variations of frequency (A, B) and dissipation (C, D) for hybrid polysaccharide/ELR films at pH 4.0 and 5.5. The case of H-RGD6 combinations is depicted. Results for CHI40 (□), CHI55 (■), ALG40 (○) and ALG55 (●) are shown. Absolute values of ΔF and ΔD reached values of (A) 24 Hz (□), 200 Hz (■); (B) 223 Hz (○), 81 Hz (●); (C) 6×10^{-6} (□), 21×10^{-6} (■); (D) 32×10^{-6} (○), 5×10^{-6} (●).

During QCM-D acquisition, a favorable and successful construction is usually identified by a decrease in ΔF caused by mass adsorption at the surface of the gold-coated quartz sensor. At the same time, monitoring of ΔD gives an indirect indication of the film's viscoelastic properties. For instance, an increase in ΔD represents a shift towards a film with a higher viscous component and damping properties that becomes "softer", which is typical of polymeric LbL films. The dissipation values for a soft film are higher due to increased energy loss from the crystal, whereas smaller dissipation values are obtained for a rigid film. It is this dampening to the crystal's oscillation that is registered as dissipation, ΔD [49,50]. A closer look at Figure 7.2 allows the most favorable conditions for LbL construction of these hybrid films to be identified, namely pH values close to the pK_a of the polysaccharide used, i.e. conditions ALG40 and CHI55, with absolute ΔF_5 values of around 225 and 200 Hz, respectively. Under these conditions, the amplitude of ΔF is greater than for the others. A similar trend is observed for ΔD.

7.3.4 Data modeling and thickness analysis

The data acquired allowed the thickness of the films obtained under each of the 36 conditions to be estimated. When constructing rigid films, the frequency values are related to the adsorbed film mass (Δm) and that mass is directly related to ΔF, a relation that is given by the well-known Sauerbrey equation (equation 8.1):

$$\Delta m = -\frac{C \times \Delta F}{n} \qquad (8.1)$$

where C is the mass sensitivity constant and n is the overtone number. However, this relation cannot be used for soft films that exhibit viscoelastic properties since the water content and swelling behavior are also reflected in ΔF and must be taken into account. Therefore, in order to compare every combination in this study, the obtained frequency and dissipation values were converted to their estimated thickness using the Voigt-based viscoelastic model [51], which is integrated into the QTools software from Q-Sense, based on equations 8.2 and 8.3:

$$\Delta F \approx -\frac{1}{2\pi\rho_0 h_0}\left\{\frac{\eta_3}{\delta_3} + \sum_{j=k}\left[h_j\rho_j\omega - 2h_j\left(\frac{\eta_3}{\delta_3}\right)^2 \frac{\eta_j\omega^2}{\mu_j{}^2 + \omega^2\eta_j{}^2}\right]\right\} \qquad (8.2)$$

$$\Delta D \approx \frac{1}{2\pi f\rho_0 h_0}\left\{\frac{\eta_3}{\delta_3} + \sum_{j=k} 2h_j\left(\frac{\eta_3}{\delta_3}\right)^2 \frac{\mu_j\omega}{\mu_j{}^2 + \omega^2\eta_j{}^2}\right\} \qquad (8.3)$$

where, considering a total of *k* thin viscoelastic layers, ρ_0 and h_0 are the density and thickness of the quartz crystal, η_3 is the viscosity of the bulk liquid, δ_3 is the viscous penetration depth of the shear wave in the bulk liquid, ρ_3 is the density of liquid, μ is the elastic shear modulus of an overlayer and ω is the angular frequency of the oscillation. Together with the integrated Voigt-based viscoelastic model, QCM-D constitutes a technique that is both precise and simple to use, allowing one to obtaining a film's properties quickly when comparing to other techniques, such as ellipsometry and surface plasmon spectroscopy. The thickness results can be found in Figure 7.3. Also, the numerical thickness and χ^2 values associated with the model fitting can be found in Supplemental Figure 7.3. The results for CHI and ALG combinations were subsequently analyzed separately in order to avoid an analysis of construction mechanisms that cannot be solely explained by the thickness and potential but are also influenced by the specific nature of the polymer itself.

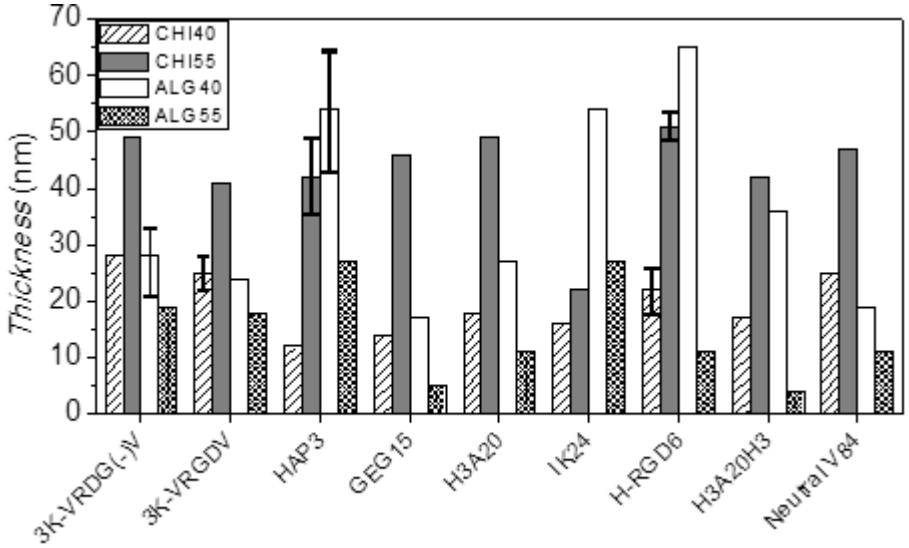


Figure 7.3. Thickness values for multilayered films containing five bilayers, as estimated using the Voigt-based viscoelastic model, for each polysaccharide/ELR permutation at pH 4.0 and pH 5.5. Deviation bars represent two standard deviations.

In LbL growth, different materials tend to adsorb with distinct kinetics and conformations, thus meaning that although both CHI and ALG are polysaccharides, they will react differently with ELRs in a multilayer hybrid film. The series plotted in Figure 7.3 represent the results obtained when using ALG at pH 4.0 or pH 5.5 and CHI at the same pH values. Some combinations were performed in triplicate, leading to an estimated maximum standard error of 12% (estimated from HAP3 at ALG40).

First it can be seen that the overall thickness values are higher for combinations containing CHI as the polysaccharide: the sum of all thickness values for CHI is 566 nm, while that for ALG is 456 nm. If we consider solely the role of ESA interactions, the overall construction of the films is more favorable with CHI than when using ALG since the former is a polycation and most ELRs are negatively charged. For films made of H-RGD6, IK24 and HAP3, ALG40 conditions are actually more favorable than CHI55, but this observation can be explained by their exhibited charge, with the first two being positive at pH 4.0 (1.8 and 3.5 mV, respectively) whereas the third is nearly neutral (-0.4 mV). The overall construction phenomenon looks dependent on the charge sign among the ingredients. However, it should be noted that the analysis resulting from Figure 7.1 shows that most ALG/pH permutations do not meet the criteria to follow a construction based on a minimum charge density, i.e., the ingredients do not possess opposite charge sign and the ingredients are all negatively charged. Despite this fact, LbL was still possible when using ALG and thus the mechanism of construction must depend on additional factors. A more specific look at each polysaccharide combination will allow further data to be obtained regarding the growth mechanism at work.

When analyzing the CHI and ALG combinations separately, another trend was identified. For each polysaccharide/ELR condition, the thickness is higher when the polysaccharides were only partially charged, i.e., at near-pK_a conditions. Following again the example of H-RGD6, for instance, the thickness of films at CHI40 and CHI55 conditions were 22 and 51 nm, whereas at ALG40 and ALG 55 they were 65 and 11 nm, respectively. In the case of CHI/ELR films, the model of charge balance and symmetry alone could explain the construction mechanism, but for ALG permutations such model is not valid, as denoted above. At pH 4.0, there is less electrostatic repulsion between ALG and ELRs are electrostatically more balanced than at pH 5.5. The fact that the majority of permutations involve ingredients with the same charge sign means there is no charge symmetry, and thus also conflict with the charge balance model. This result suggests that the proposed hybrid multilayer construction depends on a lower charge density of the polysaccharides, regardless of charge sign, by increasing the availability of neutral binding sites, and therefore materials with a low charge density are a key factor for the construction of polysaccharide/ELR films. In this case, we hypothesize that secondary hydrophobic interactions are a key force driving LbL growth. The block-ELRs H3A20 and H3A20H3 are a good example of this mechanism. As observed in Figure 7.1, these polymers are electrostatically well-balanced with CHI at both pH values (CHI40/H3A20: +16.8/-13.3 mV; CHI55/H3A20: +13.1/-10.7 mV; CHI40/H3A20H3: +16.8/-17.7 mV; CHI55/H3A20H3: +13.1/-15.0 mV). Although their ζ-

potentials would favor ESA balance in both cases, thicknesses are higher at CHI55 than at CHI40, where the availability of charged groups is lower in comparison. To further consolidate this observation, we have also studied the growth mechanism with the neutralized V84, which has no ionizable groups. It is noteworthy that favorable LbL growth under near-pK_a conditions is also observed for this ELR. Therefore, whereas ESA interactions are present in all other ELRs, the successful construction of polysaccharide/(neutralized V84) films relies solely on the density of hydrophobic groups under ALG40 and CHI55 conditions.

7.3.5 Effect of molecular weight

Due to the complexity of the ELR samples tested, several parameters, namely molecular weight, pH, zeta-potential, charge density and charge balance between each film component, must be considered to determine their contribution to film growth. In this regard, we have tested the obtained data against these parameters assuming that hydrophobic forces play an important role in the self-assembly process. First of all, we plotted thickness as a function of the ζ-potential and M_n of the ELRs for each set of polysaccharide/pH combinations. The variations of thickness with ζ-potential (Supplemental Figure 7.2A) and M_n (Supplemental Figure 7.2B) are represented, which shows no clear trend in either case.

At this point, it was assumed that ELRs with a similar M_n exhibit different potentials, and vice-versa. For instance, 3K-VRGDV (M_n=31371 Da) has a charge of -8.4±0.3 mV at pH 5.5, whereas another ELR with very similar M_n like neutralized V84 (M_n=35191 Da) has a charge of only -1.0±0.1 mV. The ELRs were therefore grouped according to their mean charge and their thickness plotted as a function of M_n for each defined charge range (see Figure 7.4).

In general, one would expect that a higher M_n would lead to a thicker film. Thus, whereas a small molecule adsorbs in an extended conformation, a lengthier polymer tends to adsorb in a more “loopier” manner, thereby providing more anchoring sites for the next layer to adsorb and, potentially, higher interpenetration capabilities than smaller ones [52]. For each ζ-potential range selected, the use of fully charged polysaccharides (ALG55 and CHI40) leads to a thickness decrease with increasing M_n. Under near-pK_a conditions of ALG, the overall thickness of the films increases with M_n.

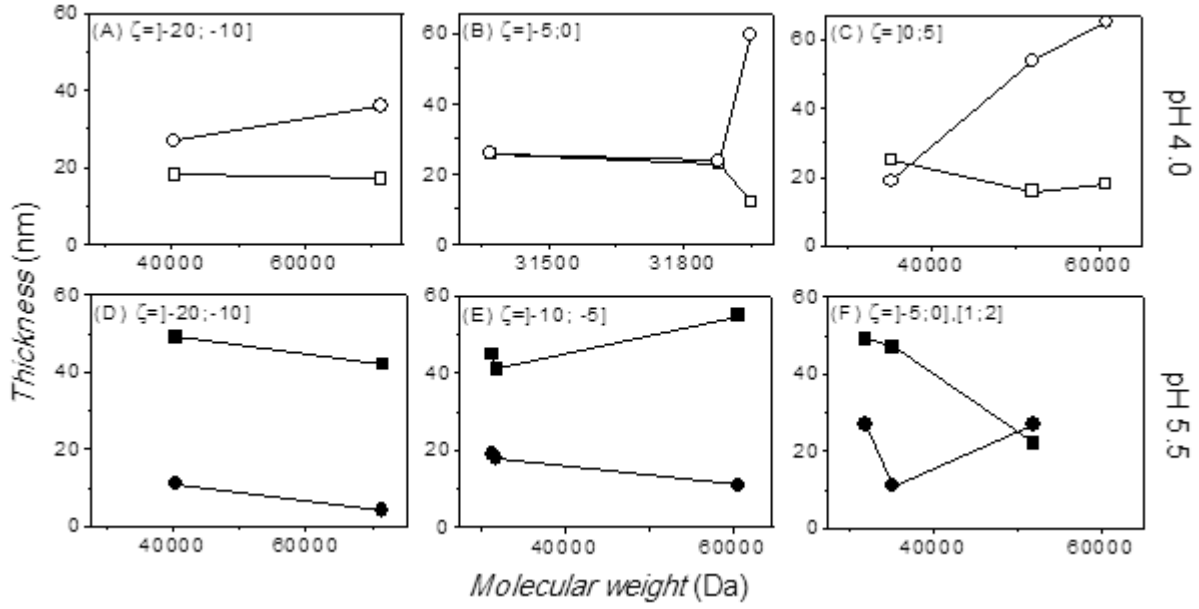


Figure 7.4. Variations in film thickness with ELR molecular weight sorted by pH and ζ-potential. Results for CHI40 (□), CHI55 (■), ALG40 (○) and ALG55 (●) are shown. The mean thickness of 3K-VRDG$^{(-)}$V and 3K-VRGDV films (M_n=31371 Da) is represented.

However, this observation was valid for all ALG40 combinations but not all CHI55 ones, with three of the 36 conditions tested being atypical. It can be seen from Figure 7.4D that the thickness under CHI55 conditions decreases from 49 to 42 nm. The ELR in question is H3A20H3 (M_n=71462 Da), which is organized into two charged blocks separated by another non-polar block of alanine residues (A). We therefore hypothesize that, during LbL growth, the charged blocks are the first to contact with the underlying surface whereas the highly neutral and nonpolar block containing a high number of A-residues (hydropathy index of 1.8) [53] is much less likely to interact with the hydrated film. Although it is true that all ELRs possess hydrophobic residues in their backbone, block-ELRs are spatially organized with one block completely charge-free, thus limiting its interaction with aqueous solvents.

The other two anomalous situations can be seen in Figure 7.4F. The first, at CHI55 for IK24 (M_n=51970 Da), shows a thickness decrease to 22 nm. IK24 exhibits the highest percentage of positively ionizable residues. As such, even when CHI is only partially deprotonated, it is plausible to assume that the positive charges of both ingredients (which are stronger and longer in range) repel, thereby minimizing the interaction between shorter range hydrophobic groups. The second, at ALG55 for the same ELR, shows a thickness increase to 27 nm. Under these conditions, the positively charged IK24 may interact well with ALG as a result of ESA interactions. Note that these M_n-dependent

exceptions do not conflict with the fact that, for each polysaccharide/ELR combination, adsorption is more favorable under near-pK_a conditions: ALG55 is still a less favorable condition than ALG40, even for the polycationic IK24.

It is unclear why the trend in this behavior does not completely match the molecular weight model for LbL assembly and is distinct among many of the studied conditions. Therefore, in light of the uncertain influence of M_n on multilayer construction, the fact that it is only favorable in specific cases leads to the conclusion that it is not a primary influence on the growth mechanism.

7.3.6 General model for hybrid multilayer growth

We have shown that a shift toward near-pK_a conditions for both polysaccharides, although of different nature, favors the construction of hybrid nanostructured polysaccharide/ELR films. The same arguments rule out the theory of minimum charge density, since LbL growth is observed even when charges of the same sign are present. Based on this extensive analysis, the LbL growth of hybrid polysaccharide and ELR films cannot be explained by ESA interactions alone, thus meaning that secondary hydrophobic interactions must be taken into account. The arguments presented herein are also valid for the control ELR (neutralized V84). As this ELR exhibits no ionizable groups, the construction of films with neutralized V84 was also more favorable under near-pK_a conditions, thus further clarifying the role of nonelectrostatic forces. A schematic depiction of our findings is provided in Figure 7.5.

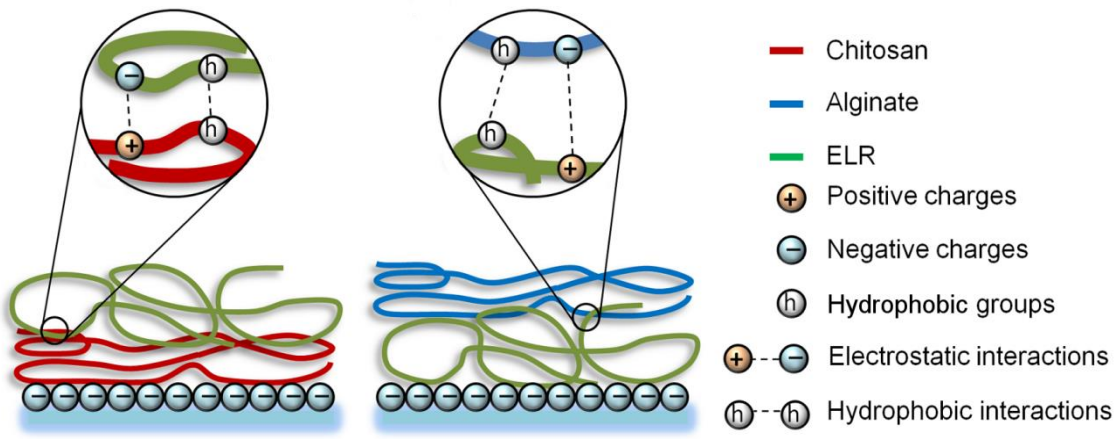


Figure 7.5. Representative scheme of the hypothetical interactions occurring between polysaccharides and ELRs.

7.4 Conclusions

The contributions of the molecular weight and electrostatic and hydrophobic interactions to LbL film growth have been extensively studied using a QCM-D method. Thus, a comparison of the thickness of 36 films formed under different conditions (polysaccharide and ELR combinations and the charges of each intervening ingredient) has shown that the growth of such hybrid nanostructured films is more favorable when the polysaccharide used is partially neutral, i.e., near its pK_a. Under these conditions, hydrophobic groups prevail over charged ones, thus highlighting the greater importance of short-range hydrophobic interactions when compared with ESA interactions. The molecular weight appears to have little effect on LbL growth. Future studies that focus on other parameters, such as ionic strength and temperature, should be considered in order to determine whether additional factors affect this combination model. These conclusions are important in order to correctly predict the most favorable parameters for constructing nanostructured films from natural and nature-inspired materials, especially since the use of genetically engineered polypeptides could lead to films with tailored properties and biologically relevant functions for applications in tissue engineering, drug delivery and biotechnology that require precise and improved specificity.

7.5 Supplemental information

7.5.1 Neutralization of V84

The ELR V84 was chemically modified by amidation of the γ-amine group of the biopolymer with pentynoic anhydride as acylating agent. The reaction was performed in trifluoroethanol (TFE) with 10 equivalents of pentynoic anhydride per γ-amine group and 1-ethyl-3-(3-dimethylaminopropyl) carbodiimide (EDAC; 5 equivalents) as catalyst. Pentynoic anhydride was synthesized previously from pentynoic acid in a 1:1 (v/v) mixture of dichloromethane and diethyl ether in the presence of dicyclohexylcarbodiimide.

The reaction mixture was stirred for 3 days at room temperature. After this time, the functionalized polymer was precipitated into increasing fractions of diethyl ether and dried in a vacuum oven at room temperature for 24 h. Once dry, the modified V84 was solubilized in cold water and the crude product purified by exhaustive dialysis against water, then frozen and finally freeze-dried.

7.5.2 Amino acid composition

The amino acid composition was determined according to the AccQTag Waters method and the derivatized amino acids analyzed by high-performance liquid chromatography (HPLC) using a Waters 600 gradient system and a Waters 2487 detector (Waters, USA).

Supplemental Table 7.1. Theoretical and experimental amino acid compositions of 3K-VRDG$^{(-)}$V, 3K-VRGDV and HAP3. ND = not determined.

	3K-VRDG$^{(-)}$V - 31371 Da		3K-VRGDV - 31371 Da		HAP3 - 31889 Da	
	Theoretical	Experimental	Theoretical	Experimental	Theoretical	Experimental
D	2	2.62	2	2.27	9	9.69
T	2	2.18	2	1.81	0	0
S	6	5.63	6	4.7	1	0.87
E	0	0	0	0	7	7
P	71	74.18	71	70.7	61	59.58
G	141	139.76	141	141.48	126	132
A	4	4.8	4	4.31	0	0
V	99	95.77	99	98.65	61	58.49
M	1	ND	1	ND	1	0.53
I	40	41.19	40	39.6	51	47.12
L	0	0	0	0	5	5.65
F	0	0	0	0	6	5.94
H	0	0	0	0	0	0
K	3	3.29	3	3.13	15	14.76
R	2	2.41	2	2.18	9	9.5

Supplemental Table 7.2. Theoretical and experimental amino acid compositions of GEG15, H3A20 and IK24. ND = not determined.

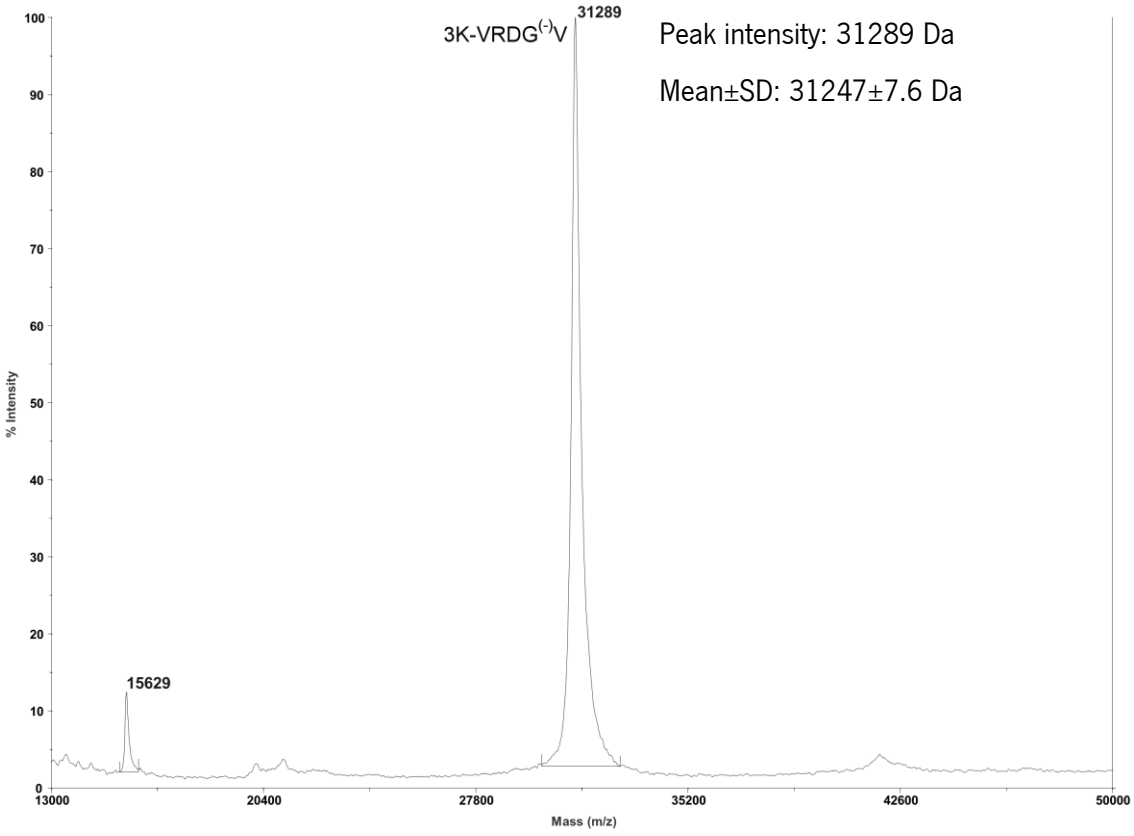
	GEG15 - 31948 Da		H3A20 - 40361 Da		IK24 - 51980 Da	
	Theoretical	Experimental	Theoretical	Experimental	Theoretical	Experimental
D	1	1.53	9	8.92	0	0
T	0	0	0	0.94	0	0
S	1	0.85	1	0.77	1	1.29
E	15	15.28	7	6.64	1	0.65
P	75	76.61	81	82.11	121	118.59
G	152	152.76	146	144.08	240	255.41
A	0	0	20	22.09	0	0
V	135	132.98	101	102.95	121	116.81
M	1	ND	1	ND	1	0.72
I	1	0.43	51	48.64	96	87.34
L	0	0	5	4.44	2	3.51
F	0	0	6	5.55	0	0
H	0	0	0	0	0	0
K	0	0	15	14.7	24	23.23
R	0	0	9	9.89	0	0

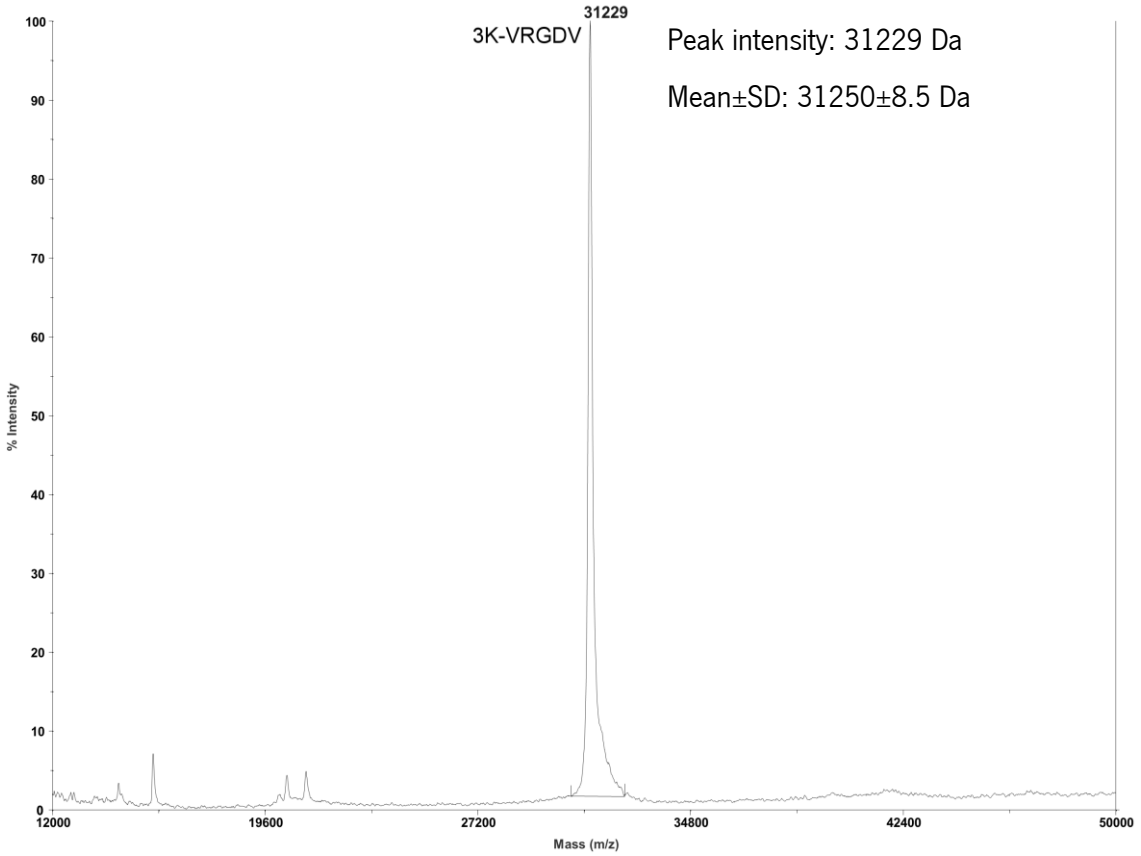
Supplemental Table 7.3. Theoretical and experimental amino acid compositions of H-RGD6, H3A20H3 and neutralized V84. ND = not determined. *G+H.

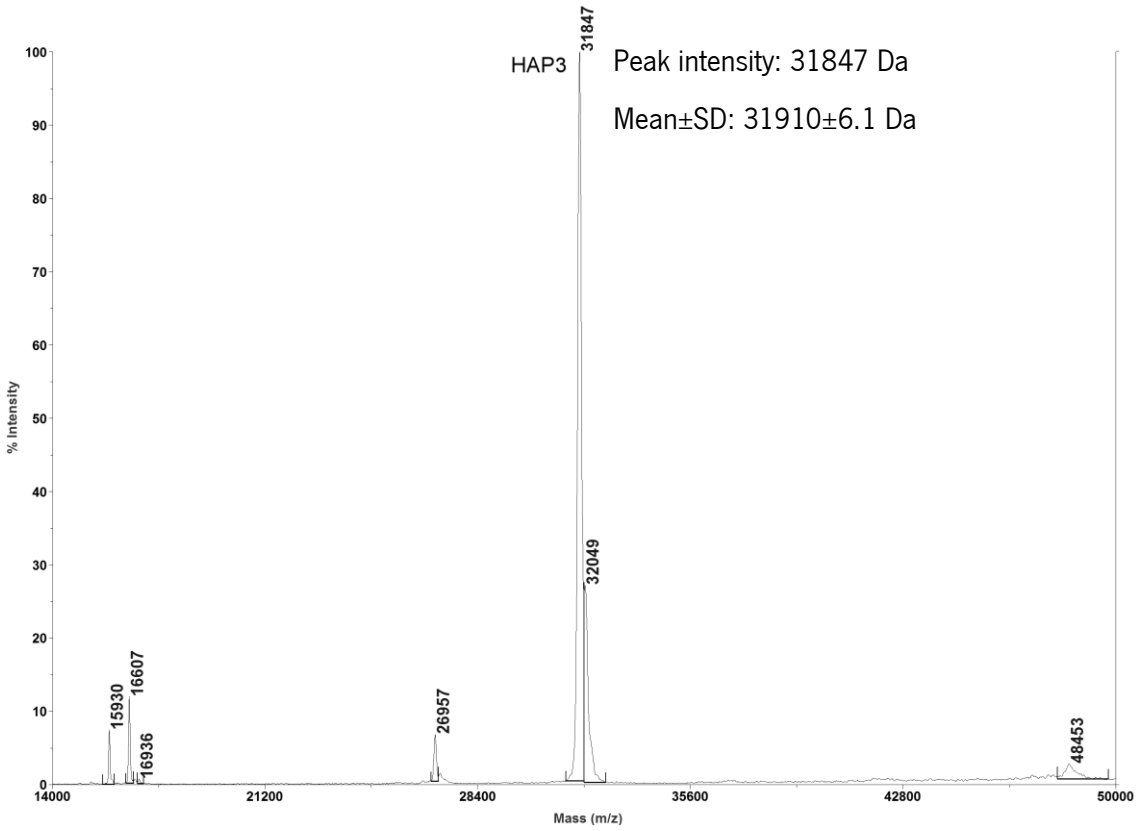
	H-RGD6 - 60661 Da		H3A20H3 - 71462 Da		Neutralized V84 - 35191 Da	
	Theoretical	Experimental	Theoretical	Experimental	Theoretical	Experimental
D	6	6.42	18	18.79	0	0
T	6	5.51	0	1.1	0	0
S	24	18.23	1	1.32	0	0
E	1	1.28	13	13.00	0	0
P	128	124.95	141	143.68	84	97.84
G	255	274.43*	272	268.85	169	169.39
A	12	12.1	20	22.52	0	0
V	128	122.63	161	165.34	169	154.78
M	2	ND	1	ND	1	N.D.
I	96	91.45	102	97.3	0	0
L	3	3.37	8	7.76	0	0
F	0	0	12	11.02	0	0
H	7	*	0	0	0	0
K	24	22.79	30	29.61	0	0
R	7	6.9	18	19.64	0	0

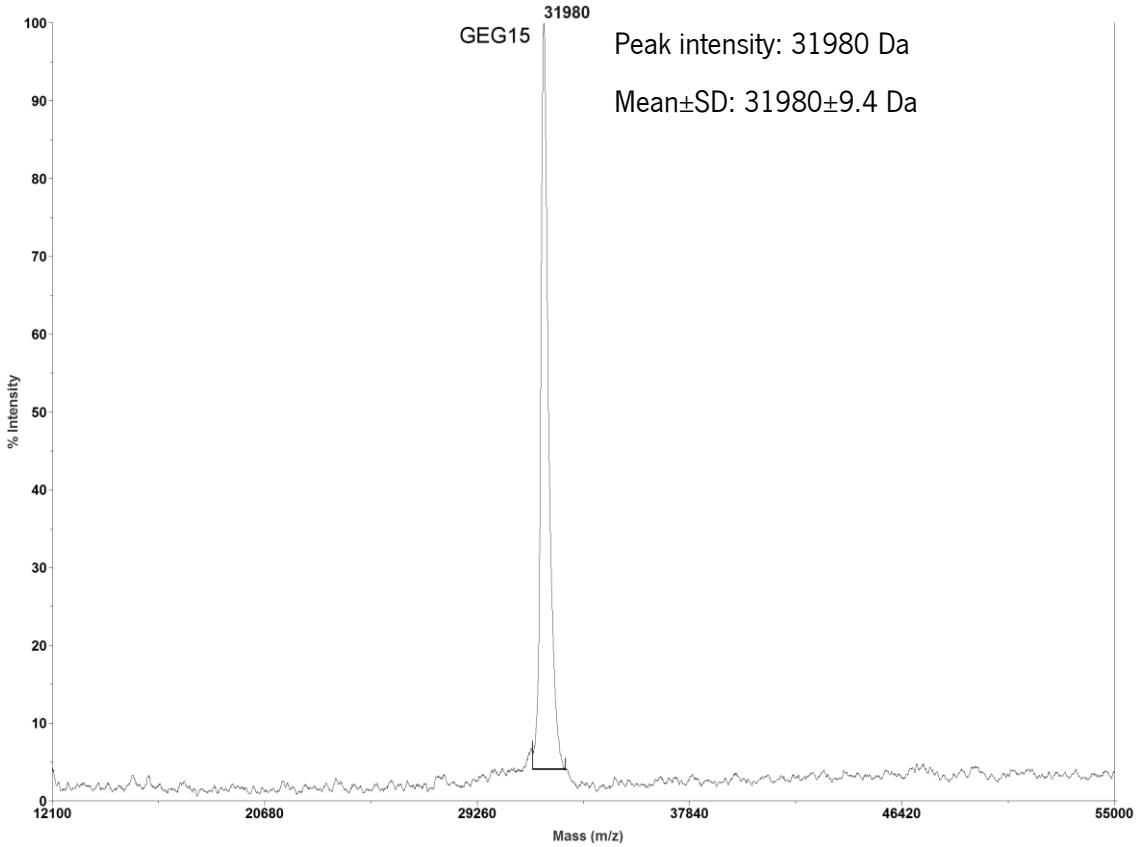
7.5.3 Molecular weight

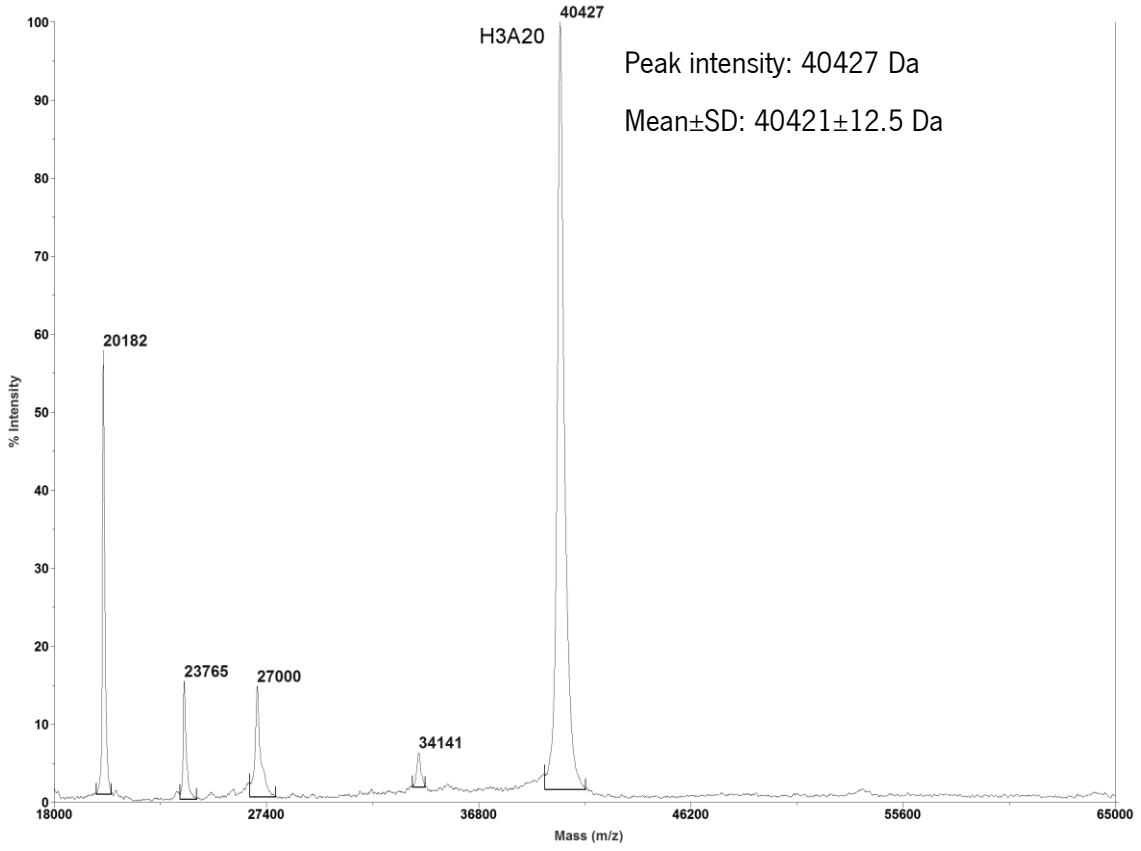
To assess the biopolymer molecular weight, MALDI-TOF mass spectroscopy was performed using a Voyager STR instrument from Applied Biosystems (USA), in linear mode, with external calibration using bovine serum albumin (BSA). The spectra for each ELR can be found below and are referred as a single Figure, namely Supplemental Figure 7.1.

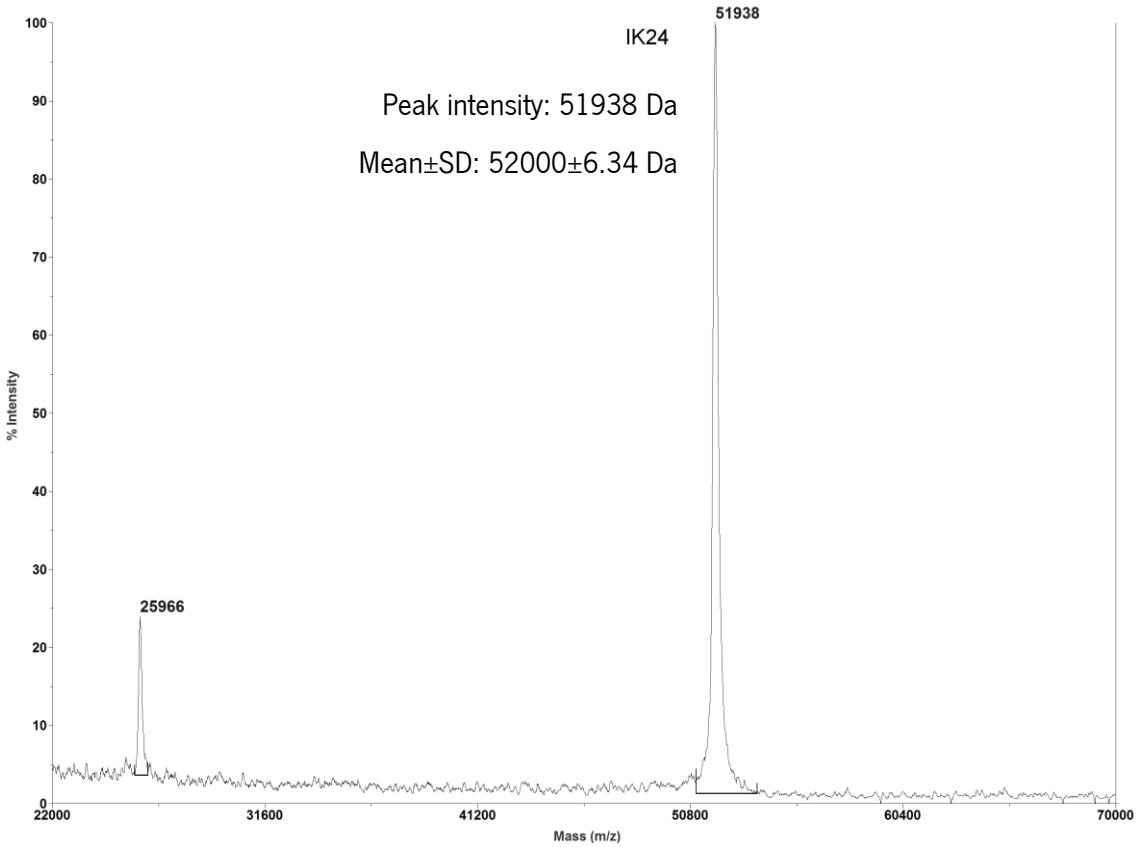


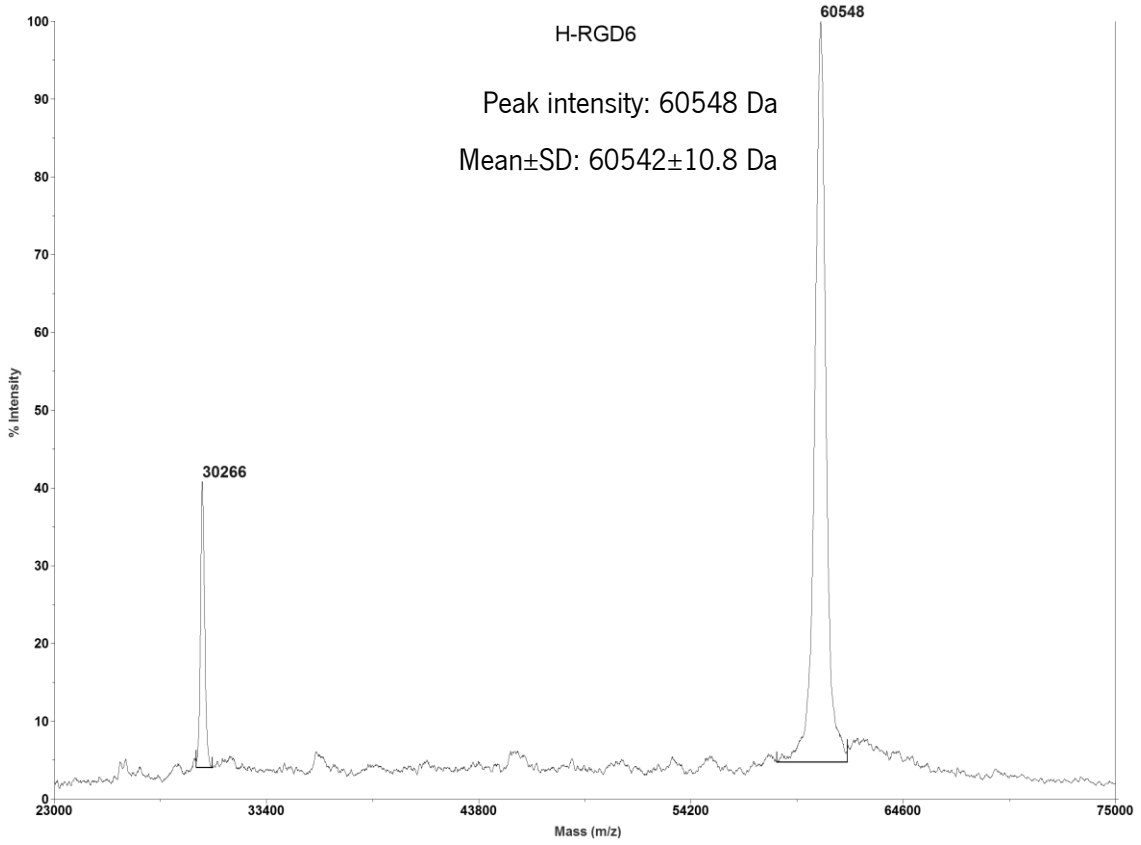

31229
3K-VRGDV
Peak intensity: 31229 Da
Mean±SD: 31250±8.5 Da
% Intensity
Mass (m/z)
100
90
80
70
60
50
40
30
20
10
0
12000
19600
27200
34800
42400
50000

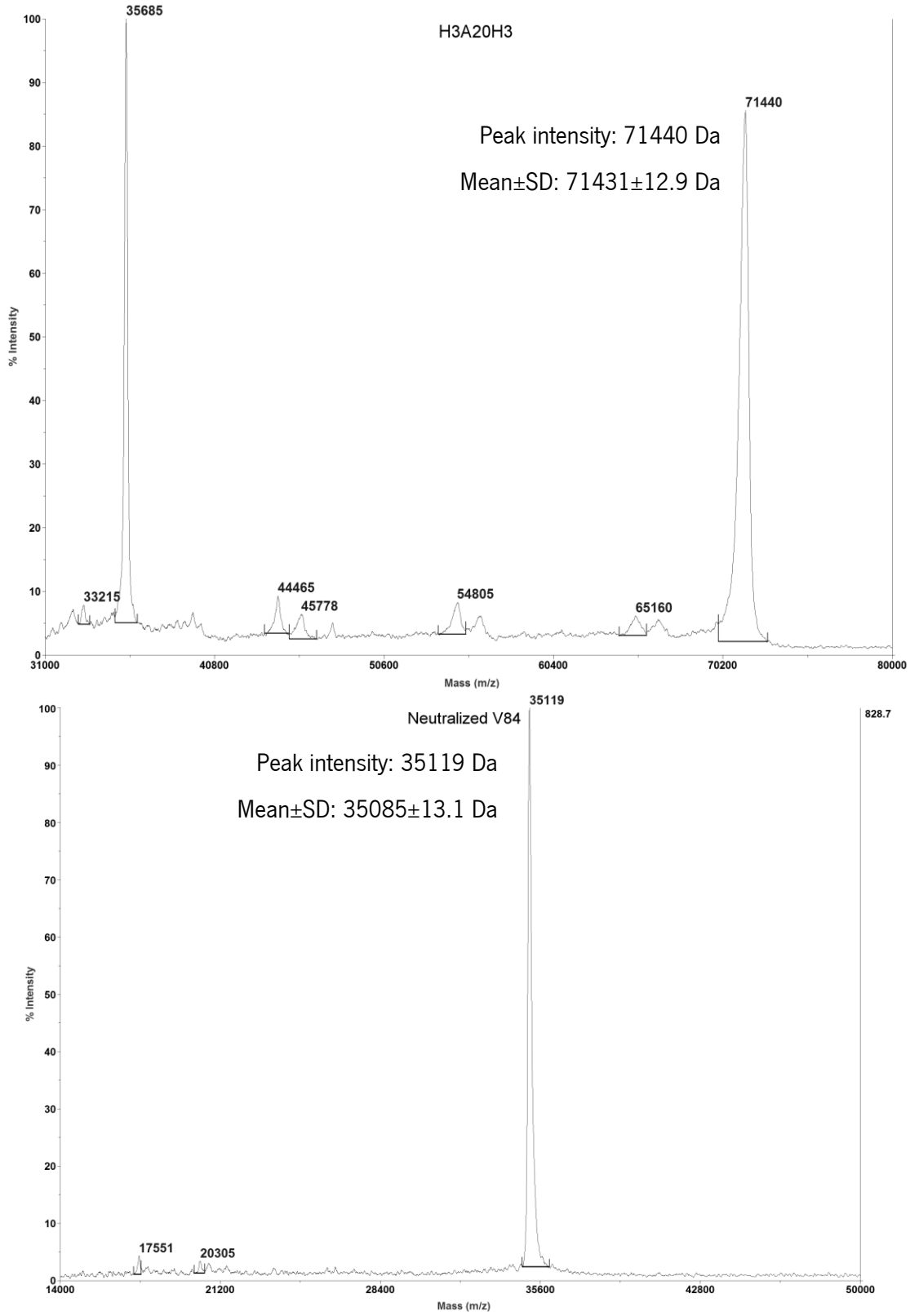

31847
HAP3
Peak intensity: 31847 Da
Mean±SD: 31910±6.1 Da
32049
15930
16607
16936
26957
48453
% Intensity
Mass (m/z)
100
90
80
70
60
50
40
30
20
10
0
14000
21200
28400
35600
42800
50000


GEG15
31980
Peak intensity: 31980 Da
Mean±SD: 31980±9.4 Da
% Intensity
Mass (m/z)
12100
20680
29260
37840
46420
55000


H3A20
40427
Peak intensity: 40427 Da
Mean±SD: 40421±12.5 Da
20182
23765
27000
34141
% Intensity
Mass (m/z)
18000
27400
36800
46200
55600
65000

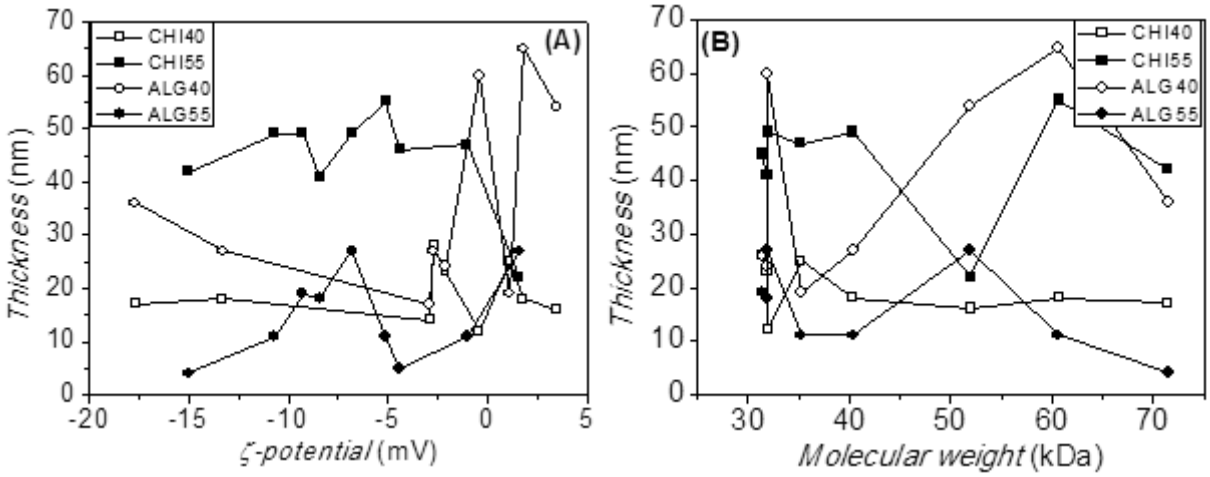

IK24
Peak intensity: 51938 Da
Mean±SD: 52000±6.34 Da
51938
25966
% Intensity
Mass (m/z)
22000
31600
41200
50800
60400
70000


H-RGD6
Peak intensity: 60548 Da
Mean±SD: 60542±10.8 Da
60548
30266
% Intensity
Mass (m/z)
23000
33400
43800
54200
64600
75000



Supplemental Figure 7.1. MALDI-TOF spectra of the bioproduced ELRs, with major peaks signaled and experimental molecular weight distribution. Secondary peaks are assigned to doubly charged species.

7.5.4 ζ-potential and molecular weight effect on thickness:

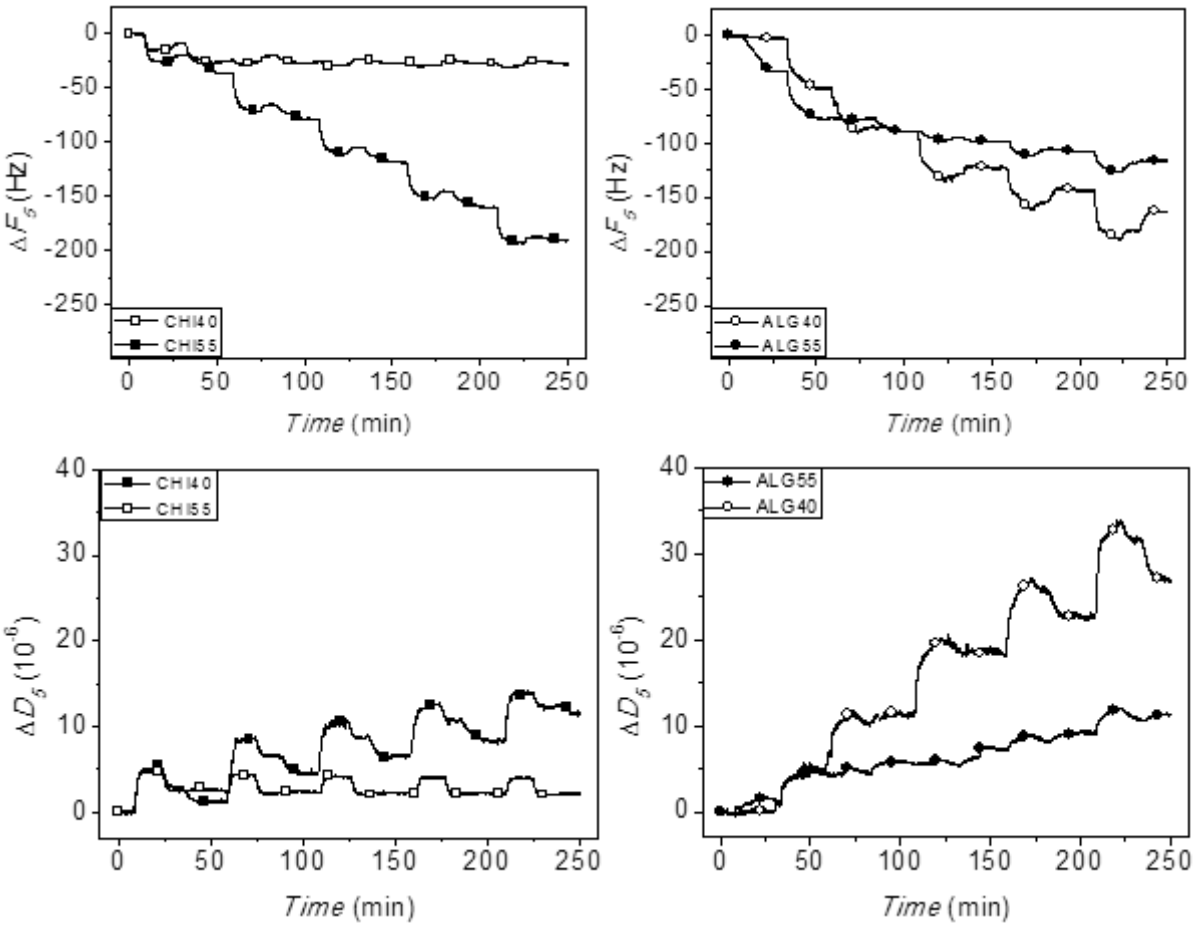


Supplemental Figure 7.2. Evolution of thickness with (A) ζ-potential and (B) molecular weight for the ELRs studied herein. The mean thickness of 3K-VRDG$^{(-)}$V and 3K-VRGDV (M_n=31371 Da) is represented in the latter.

7.5.5 QCM-D acquisition graphics and Voigt-based model fitting result

Herein are presented the acquisition graphics from the QCM-D experiments for every permutation studied. Images are treated as a single figure, namely Supplemental Figure 7.3.

3K-VRDG$^{(-)}$V



Voigt-based model fitting of the thickness:

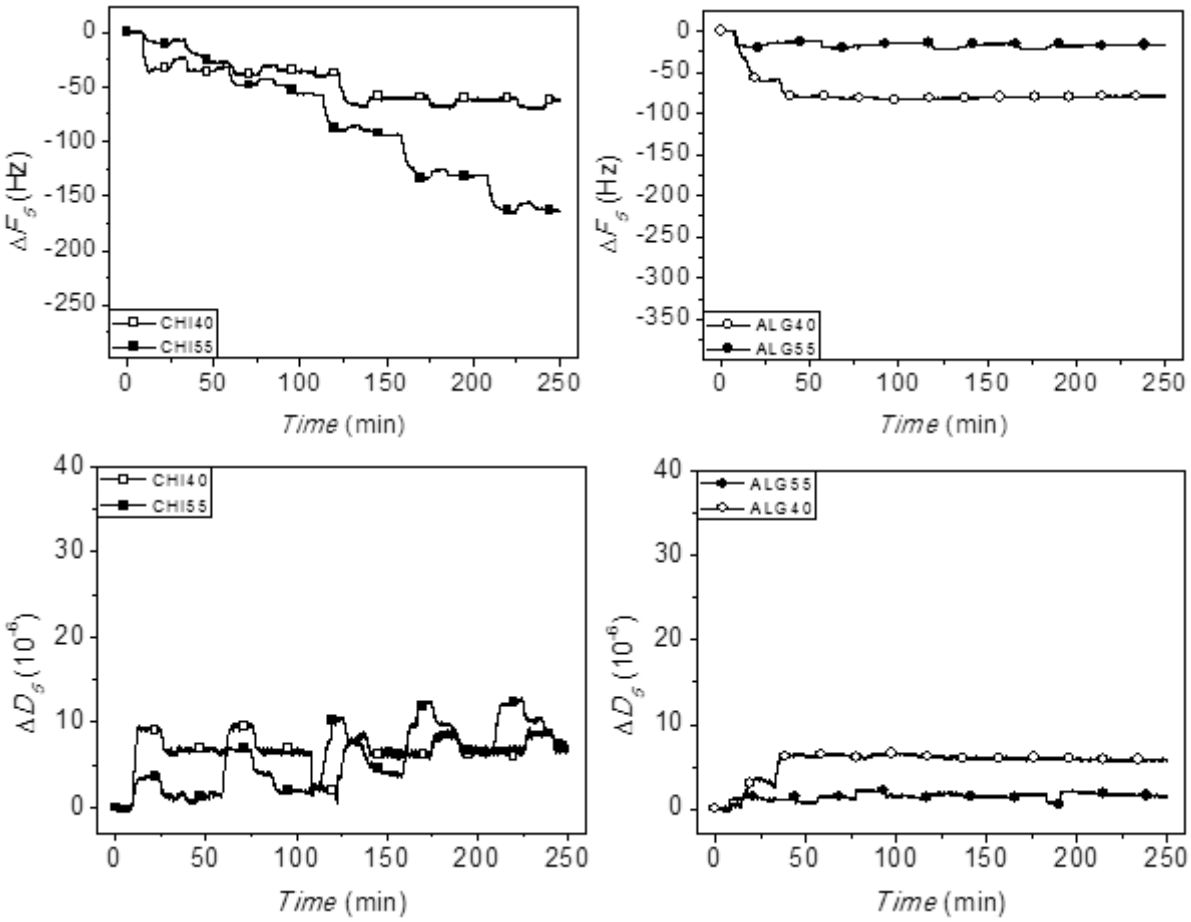
CHI40: 28 nm; χ^2 = 300250

CHI55: 49 nm; χ^2 = 30557

ALG40: 29 nm (mean of three independent experiments: 28±7 nm); χ^2 = 72751

ALG55: 19 nm; χ^2 = 161730

3K-VRGDV



Voigt-based model fitting of the thickness:

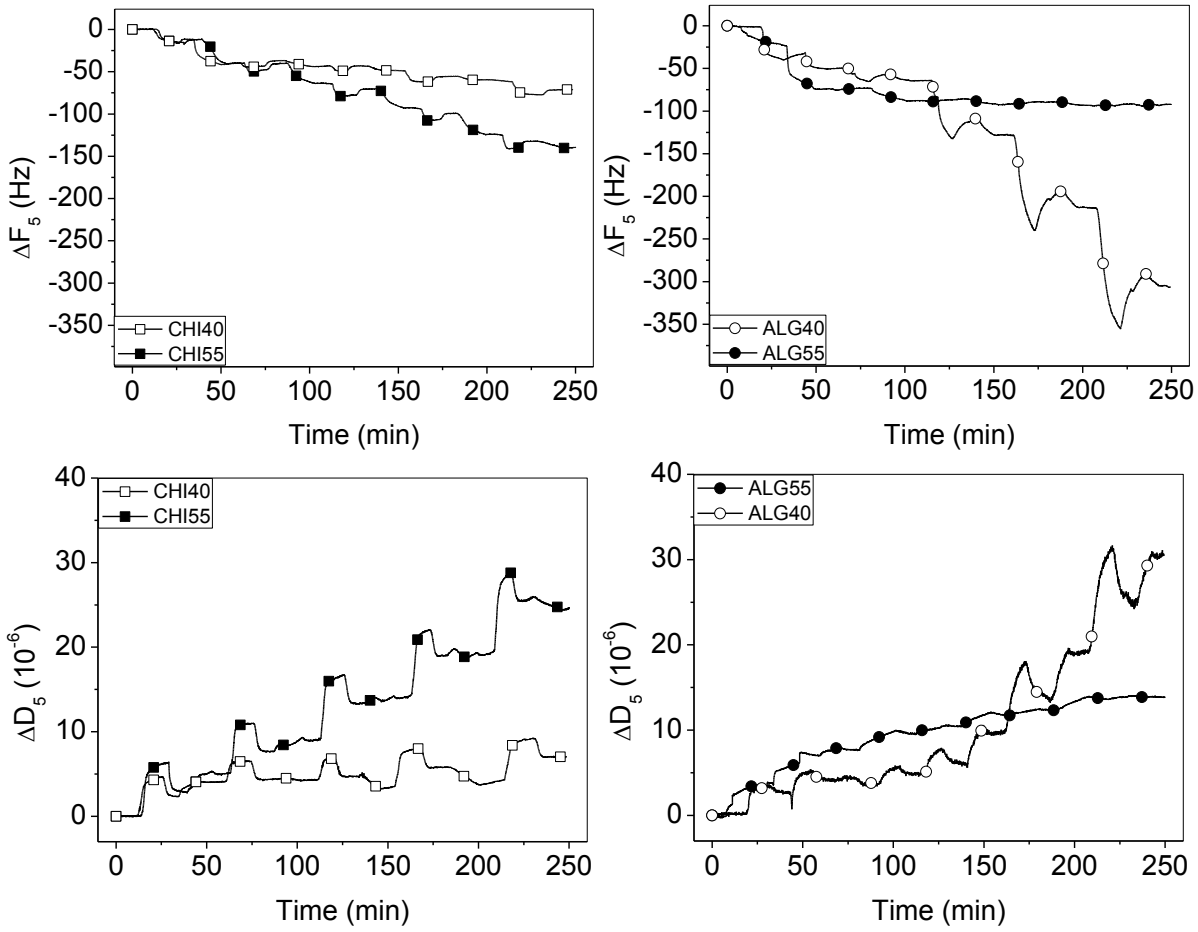
CHI40: 23 nm (mean of three independent experiments: 25±3 nm); χ^2 = 462440

CHI55: 41 nm; χ^2 = 6017

ALG40: 24 nm; χ^2 = 1784

ALG55: 18 nm; χ^2 = 47101

HAP3



Voigt-based model fitting of the thickness:

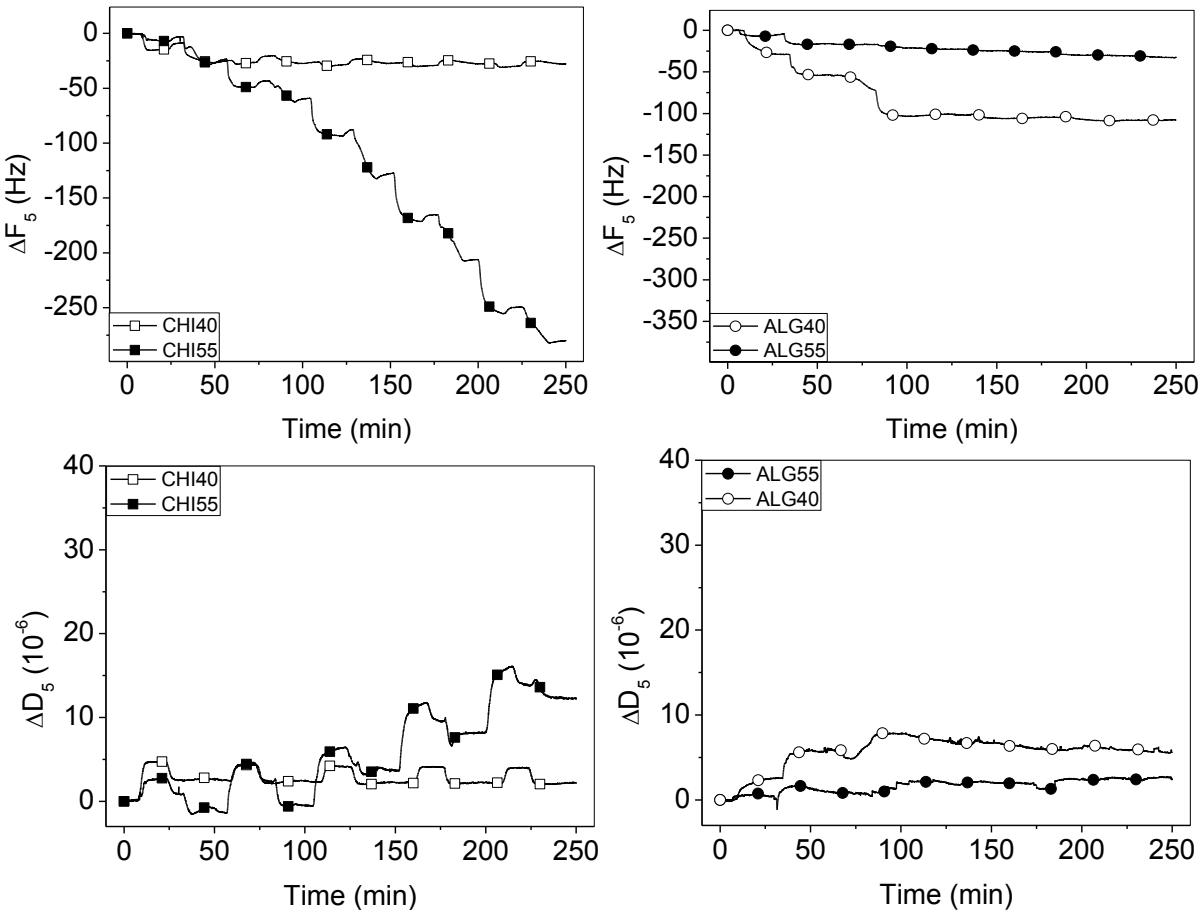
CHI40: 12 nm; χ^2 = 49833

CHI55: 49 nm (mean of three independent experiments: 42±7 nm); χ^2 = 12888

ALG40: 60 nm (mean of three independent experiments: 54±11 nm); χ^2 = 47805

ALG55: 27 nm; χ^2 = 47951

GEG15



Voigt-based model fitting of the thickness:

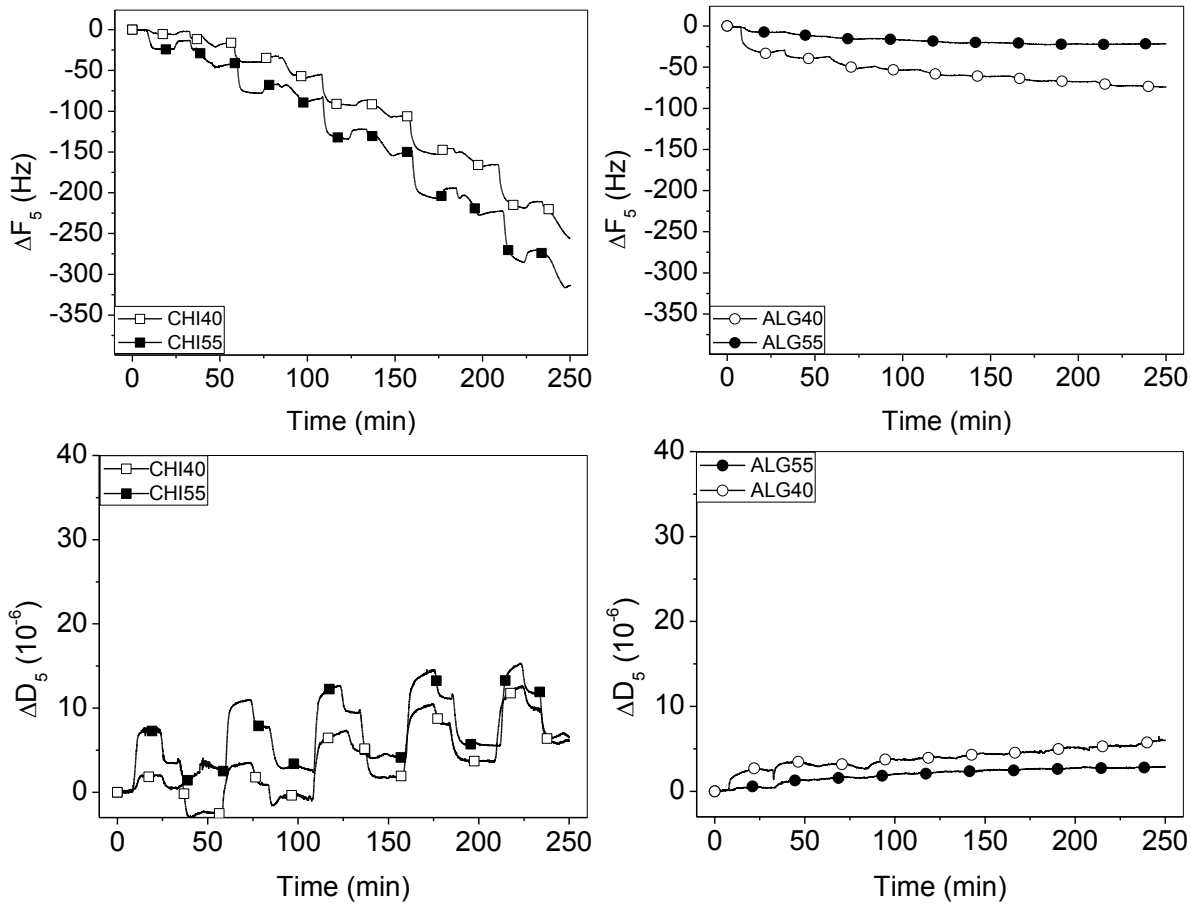
CHI40: 14 nm; χ^2 = 50777

CHI55: 46 nm; χ^2 = 128210

ALG40: 17 nm; χ^2 = 95184

ALG55: 5 nm; χ^2 = 185290

H3A20



Voigt-based model fitting of the thickness:

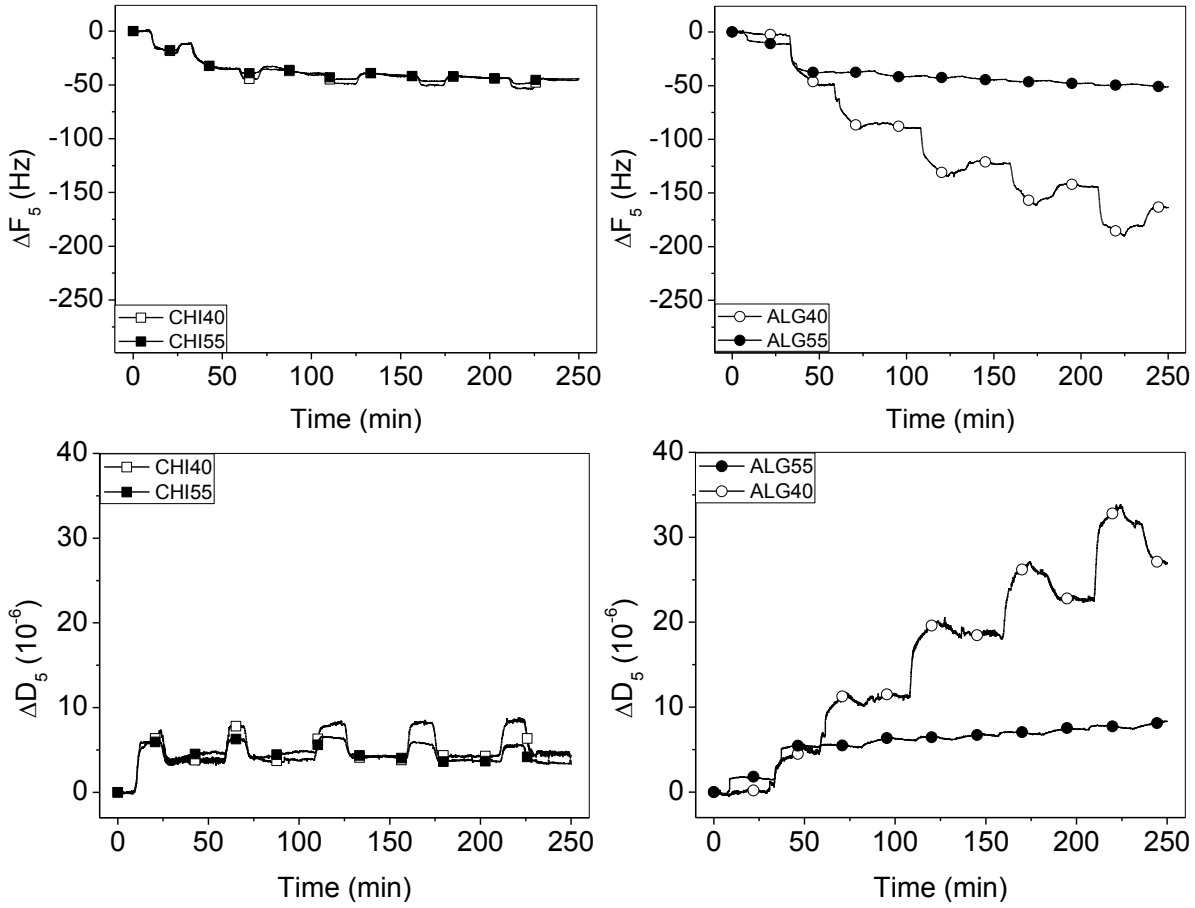
CHI40: 18 nm; χ^2 = 519260

CHI55: 49 nm; χ^2 = 35556

ALG40: 27 nm; χ^2 = 86154

ALG55: 11 nm; χ^2 = 478450

IK24



Voigt-based model fitting of the thickness:

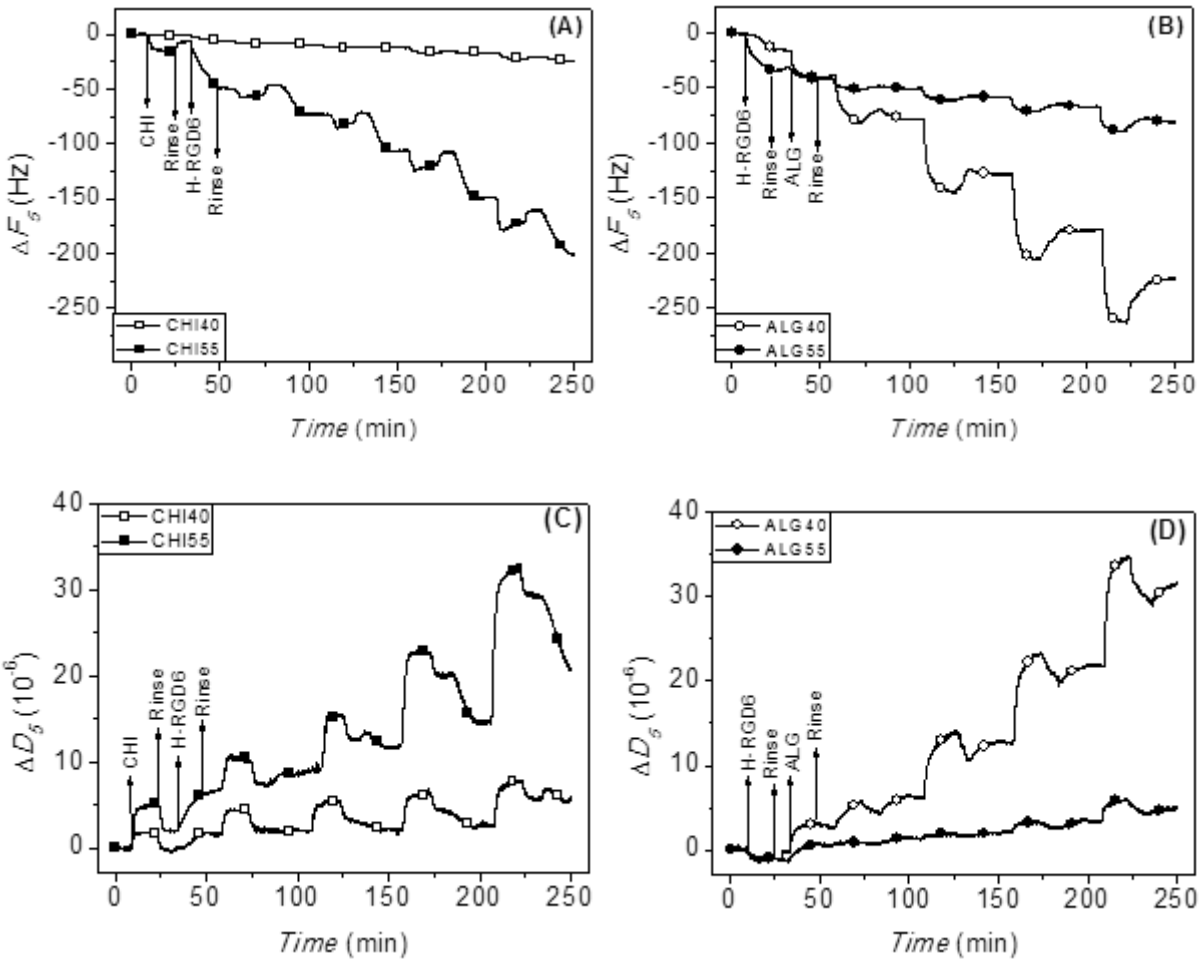
CHI40: 16 nm; χ^2 = 138110

CHI55: 22 nm; χ^2 = 142890

ALG40: 54 nm; χ^2 = 46537

ALG55: 27 nm; χ^2 = 82036

H-RGD6 (equivalent to Figure 7.2)



Voigt-based model fitting of the thickness:

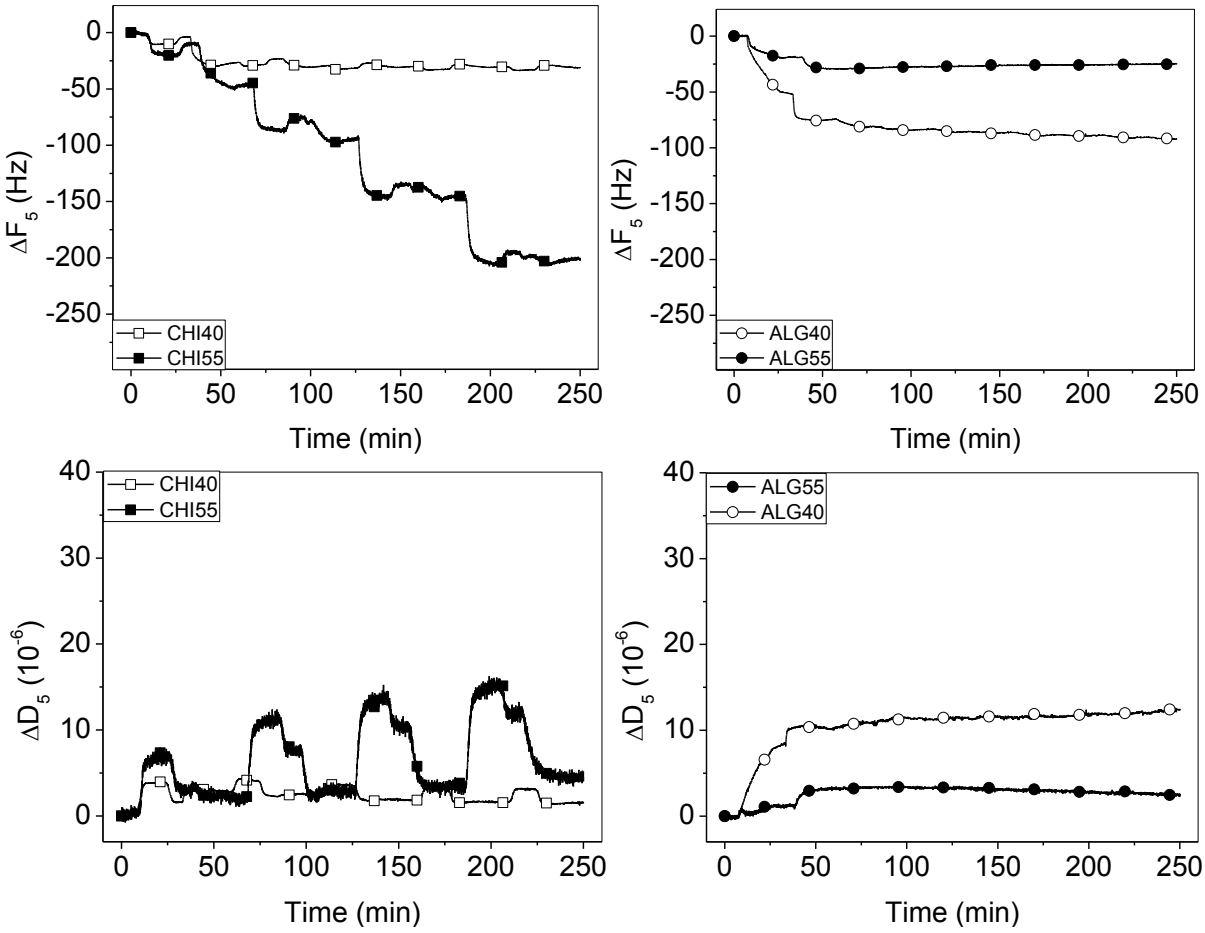
CHI40: 18 nm (mean of three independent experiments: 22±5 nm); χ^2 = 39636

CHI55: 55 nm (mean of three independent experiments: 51±3 nm); χ^2 = 16630

ALG40: 65 nm; χ^2 = 121670

ALG55: 11 nm; χ^2 = 257690

H3A20H3



Voigt-based model fitting of the thickness:

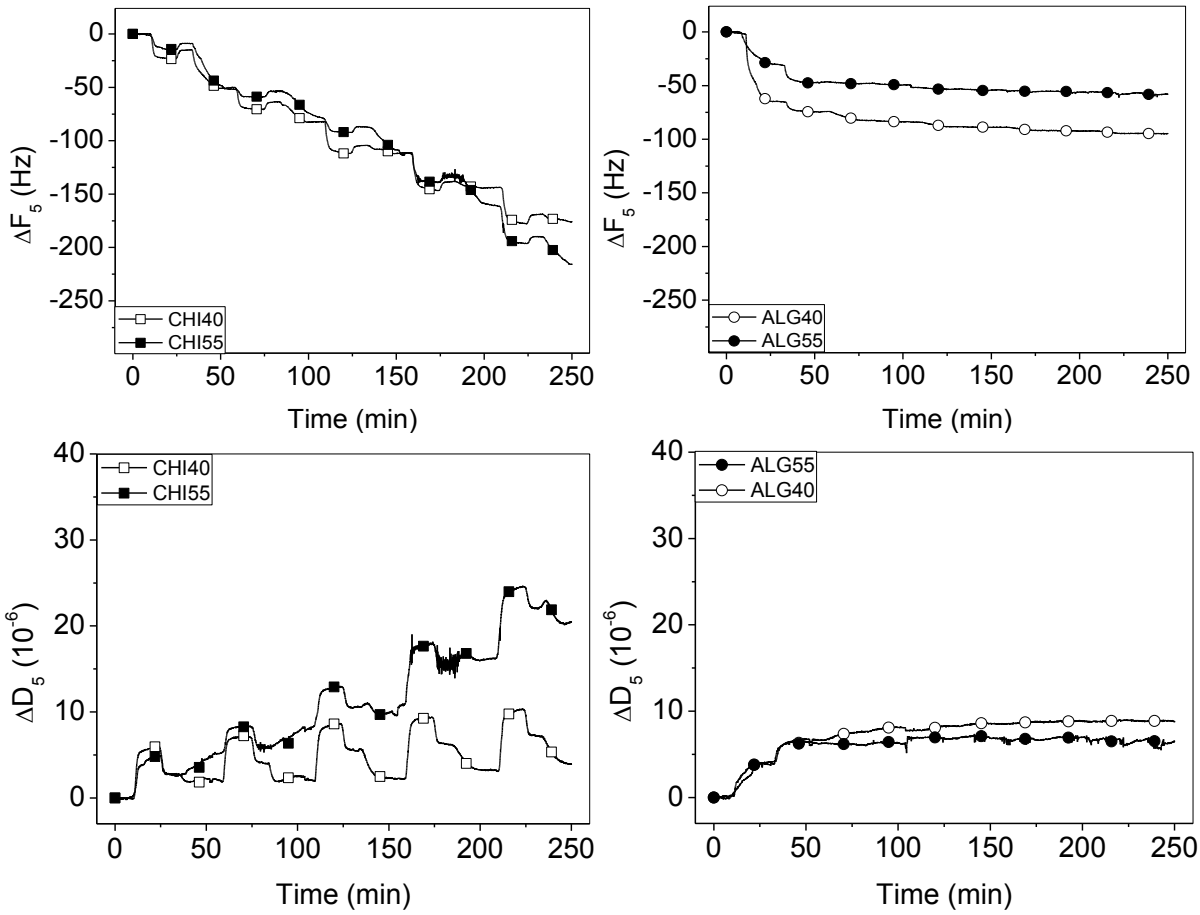
CHI40: 17 nm; χ^2 = 66528

CHI55: 42 nm; χ^2 = 76254

ALG40: 36 nm; χ^2 = 18522

ALG55: 4 nm; χ^2 = 233630

Neutralized V84



Voigt-based model fitting of the thickness:

CHI40: 25 nm; χ^2 = 155950

CHI55: 47 nm; χ^2 = 21258

ALG40: 19 nm; χ^2 = 148370

ALG55: 11 nm; χ^2 = 78622

Supplemental Figure 7.3. QCM-D acquisition graphics depicting the 5th overtone variations of frequency and dissipation of polysaccharide/ELR hybrid films at pH 4.0 and 5.5. Voigt-based viscoelastic model results for thicknesses are shown along the respective χ^2. Experiments that were performed in triplicate are highlighted in bold. Thickness and χ^2 error are shown for the representative experiment only.

7.6 Acknowledgements

This work was carried out under the scope of Fundação para a Ciência e Tecnologia" – FCT (grant SFRH/BD/61126/2009), "Fundo Social Europeu" – FSE, "Programa Diferencial de Potencial Humano" – POPH, EU 7th Framework Programme (nº REGPOT-CT2012-316331-POLARIS), the MICINN (MAT 2009 14195-C03 03, ACI2009-0890, MAT2010-15310, MAT2010-15982 and PRI-PIBAR-2011-1403), the JCyL (VA049A11, VA152A12 and VA155A12), the CIBER-BBN and the E.C.

7.7 References

[1] Hook A. L., Voelcker N. H., and Thissen H., Patterned and switchable surfaces for biomolecular manipulation, Acta Biomaterialia 2009, 5: 2350-2370.

[2] Prakash S., Karacor M. B., and Banerjee S., Surface modification in microsystems and nanosystems, Surface Science Reports 2009, 64: 233-254.

[3] Tirrell M., Kokkoli E., and Biesalski M., The role of surface science in bioengineered materials, Surface Science 2002, 500: 61-83.

[4] Alves N. M., Pashkuleva I., Reis R. L., and Mano J. F., Controlling Cell Behavior Through the Design of Polymer Surfaces, Small 2010, 6: 2208-2220.

[5] Boudou T., Crouzier T., Ren K., Blin G., and Picart C., Multiple Functionalities of Polyelectrolyte Multilayer Films: New Biomedical Applications, Advanced Materials 2010, 22: 441-467.

[6] Stuart M. A. C., Huck W. T. S., Genzer J., Muller M., Ober C., Stamm M., Sukhorukov G. B., Szleifer I., Tsukruk V. V., Urban M., Winnik F., Zauscher S., Luzinov I., and Minko S., Emerging applications of stimuli-responsive polymer materials, Nat Mater 2010, 9: 101-113.

[7] Wong J. E., Müller C. B., Laschewsky A., and Richtering W., Direct Evidence of Layer-by-Layer Assembly of Polyelectrolyte Multilayers on Soft and Porous Temperature-Sensitive PNiPAM Microgel Using Fluorescence Correlation Spectroscopy, The Journal of Physical Chemistry B 2007, 111: 8527-8531.

[8] Gribova V., Auzely-Velty R., and Picart C., Polyelectrolyte multilayer assemblies on materials surfaces: from cell adhesion to tissue engineering, Chemistry of Materials 2011, 24: 854-869.

[9] Silva H. S., and Miranda P. B., Molecular Ordering of Layer-by-Layer Polyelectrolyte Films Studied by Sum-Frequency Vibrational Spectroscopy, The Journal of Physical Chemistry B 2009, 113: 10068-10071.

[10] Tang Z., Wang Y., Podsiadlo P., and Kotov N. A., Biomedical Applications of Layer-by-Layer Assembly: From Biomimetics to Tissue Engineering, Advanced Materials 2006, 18: 3203-3224.

[11] Martins G. V., Mano J. F., and Alves N. M., Dual Responsive Nanostructured Surfaces for Biomedical Applications, Langmuir 2011, 27: 8415-8423.

[12] Zahn R., Thomasson E., Guillaume-Gentil O., Vörös J., and Zambelli T., Ion-induced cell sheet detachment from standard cell culture surfaces coated with polyelectrolytes, Biomaterials 2012, 33: 3421-3427.

[13] Manna U., and Patil S., Borax Mediated Layer-by-Layer Self-Assembly of Neutral Poly(vinyl alcohol) and Chitosan, The Journal of Physical Chemistry B 2009, 113: 9137-9142.

[14] Rivera-Gil P., De Koker S., De Geest B. G., and Parak W. J., Intracellular Processing of Proteins Mediated by Biodegradable Polyelectrolyte Capsules, Nano Letters 2009, 9: 4398-4402.

[15] Volodkin D. V., Madaboosi N., Blacklock J., Skirtach A. G., and Mőhwald H., Surface-Supported Multilayers Decorated with Bio-active Material Aimed at Light-Triggered Drug Delivery, Langmuir 2009, 25: 14037-14043.

[16] Sher P., Custódio C. A., and Mano J. F., Layer-By-Layer Technique for Producing Porous Nanostructured 3D Constructs Using Moldable Freeform Assembly of Spherical Templates, Small 2010, 6: 2644-2648.

[17] Decher G., Hong J. D., and Schmitt J., Buildup of ultrathin multilayer films by a self-assembly process: III. Consecutively alternating adsorption of anionic and cationic polyelectrolytes on charged surfaces, Thin Solid Films 1992, 210-211: 831-835.

[18] Hammond P. T., Form and Function in Multilayer Assembly: New Applications at the Nanoscale, Advanced Materials 2004, 16: 1271-1293.

[19] Lyklema J., and Deschênes L., The First Step in Layer-by-Layer Deposition: Electrostatics and/or Non-Electrostatics?, Advances in Colloid and Interface Science 2011, 168: 135-148.

[20] V. Klitzing R., Internal Structure of Polyelectrolyte Multilayer Assemblies, Physical Chemistry Chemical Physics 2006, 8: 5012-5033.

[21] Dubas S. T., and Schlenoff J. B., Factors Controlling the Growth of Polyelectrolyte Multilayers, Macromolecules 1999, 32: 8153-8160.

[22] Mano J. F., Silva G. A., Azevedo H. S., Malafaya P. B., Sousa R. A., Silva S. S., Boesel L. F., Oliveira J. M., Santos T. C., Marques A. P., Neves N. M., and Reis R. L., Natural origin biodegradable

systems in tissue engineering and regenerative medicine: present status and some moving trends, Journal of The Royal Society Interface 2007, 4: 999-1030.

[23] Boateng J. S., Matthews K. H., Stevens H. N. E., and Eccleston G. M., Wound healing dressings and drug delivery systems: A review, Journal of Pharmaceutical Sciences 2008, 97: 2892-2923.

[24] George M., and Abraham T. E., Polyionic hydrocolloids for the intestinal delivery of protein drugs: Alginate and chitosan — a review, Journal of Controlled Release 2006, 114: 1-14.

[25] Rinaudo M., Chitin and Chitosan - Properties and Applications, Progress in Polymer Science 2006, 31: 603-632.

[26] Almine J. F., Bax D. V., Mithieux S. M., Nivison-Smith L., Rnjak J., Waterhouse A., Wise S. G., and Weiss A. S., Elastin-based materials, Chemical Society Reviews 2010, 39: 3371-3379.

[27] Rodríguez-Cabello J. C., Martín L., Alonso M., Arias F. J., and Testera A. M., "Recombinamers" as advanced materials for the post-oil age, Polymer 2009, 50: 5159-5169.

[28] Urry D. W., Molecular machines: how motion and other functions of living organisms can result from reversible chemical changes, Angewandte Chemie International Edition in English 1993, 32: 819-841.

[29] Costa R. R., Custódio C. A., Arias F. J., Rodríguez-Cabello J. C., and Mano J. F., Layer-by-Layer Assembly of Chitosan and Recombinant Biopolymers into Biomimetic Coatings with Multiple Stimuli-Responsive Properties, Small 2011, 7: 2640-2649.

[30] Nettles D. L., Chilkoti A., and Setton L. A., Applications of elastin-like polypeptides in tissue engineering, Advanced Drug Delivery Reviews 2010, 62: 1479-1485.

[31] Prieto S., Shkilnyy A., Rumplasch C., Ribeiro A., Arias F. J., Rodríguez-Cabello J. C., and Taubert A., Biomimetic calcium phosphate mineralization with multifunctional elastin-like recombinamers, Biomacromolecules 2011, 12: 1480-1486.

[32] Cini N., Tulun T., Decher G., and Ball V., Step-by-Step Assembly of Self-Patterning Polyelectrolyte Films Violating (Almost) All Rules of Layer-by-Layer Deposition, Journal of the American Chemical Society 2010, 132: 8264-8265.

[33] Garg A., Heflin J. R., Gibson H. W., and Davis R. M., Study of Film Structure and Adsorption Kinetics of Polyelectrolyte Multilayer Films: Effect of pH and Polymer Concentration, Langmuir 2008, 24: 10887-10894.

[34] Liu H., and Hu N., Interaction between Myoglobin and Hyaluronic Acid in Their Layer-by-Layer Assembly: Quartz Crystal Microbalance and Cyclic Voltammetry Studies, The Journal of Physical Chemistry B 2006, 110: 14494-14502.

[35] Marx K. A., Quartz Crystal Microbalance: A Useful Tool for Studying Thin Polymer Films and Complex Biomolecular Systems at the Solution–Surface Interface, Biomacromolecules 2003, 4: 1099-1120.

[36] Molino P. J., Higgins M. J., Innis P. C., Kapsa R. M. I., and Wallace G. G., Fibronectin and Bovine Serum Albumin Adsorption and Conformational Dynamics on Inherently Conducting Polymers: A QCM-D Study, Langmuir 2012, 28: 8433-8445.

[37] Weber N., Pesnell A., Bolikal D., Zeltinger J., and Kohn J., Viscoelastic Properties of Fibrinogen Adsorbed to the Surface of Biomaterials Used in Blood-Contacting Medical Devices, Langmuir 2007, 23: 3298-3304.

[38] Hirai A., Odani H., and Nakajima A., Determination of Degree of Deacetylation of Chitosan by 1H NMR Spectroscopy, Polymer Bulletin 1991, 26: 87-94.

[39] Dutta A. K., and Belfort G., Adsorbed Gels versus Brushes: Viscoelastic Differences, Langmuir 2007, 23: 3088-3094.

[40] Caruso F., Niikura K., Furlong D. N., and Okahata Y., 2. Assembly of Alternating Polyelectrolyte and Protein Multilayer Films for Immunosensing, Langmuir 1997, 13: 3427-3433.

[41] Gergely C., Bahi S., Szalontai B., Flores H., Schaaf P., Voegel J.-C., and Cuisinier F. J. G., Human Serum Albumin Self-Assembly on Weak Polyelectrolyte Multilayer Films Structurally Modified by pH Changes, Langmuir 2004, 20: 5575-5582.

[42] Houska M., and Brynda E., Interactions of Proteins with Polyelectrolytes at Solid/Liquid Interfaces: Sequential Adsorption of Albumin and Heparin, Journal of Colloid and Interface Science 1997, 188: 243-250.

[43] Ju H. K., Kim S. Y., and Lee Y. M., pH/Temperature-Responsive Behaviors of Semi-IPN and Comb-Type Graft Hydrogels Composed of Alginate and Poly(N-Isopropylacrylamide), Polymer 2001, 42: 6851-6857.

[44] Urry D. W., Peng S., Gowda D. C., Parker T. M., and Harris R. D., Comparison of Electrostatic- and Hydrophobic-Induced pKa Shifts in Polypentapeptides. The Lysine Residue, Chemical Physics Letters 1994, 225: 97-103.

[45] Urry D. W., Hayes L. C., Gowda D. C., Peng S. Q., and Jing N. J., Electrochemical Transduction in Elastic Protein-Based Polymers: A Model for an Energy Conversion Step of Oxidative Phosphorylation, Biochemical and Biophysical Research Communications 1995, 210: 1031-1039.

[46] Burke S. E., and Barrett C. J., pH-Responsive Properties of Multilayered Poly(L-Lysine)/Hyaluronic Acid Surfaces, Biomacromolecules 2003, 4: 1773-1783.

[47] Fu J., Ji J., Yuan W., and Shen J., Construction of anti-adhesive and antibacterial multilayer films via layer-by-layer assembly of heparin and chitosan, Biomaterials 2005, 26: 6684-6692.

[48] Yoo D., Shiratori S. S., and Rubner M. F., Controlling Bilayer Composition and Surface Wettability of Sequentially Adsorbed Multilayers of Weak Polyelectrolytes, Macromolecules 1998, 31: 4309-4318.

[49] Cho N.-J., Kanazawa K. K., Glenn J. S., and Frank C. W., Employing Two Different Quartz Crystal Microbalance Models To Study Changes in Viscoelastic Behavior upon Transformation of Lipid Vesicles to a Bilayer on a Gold Surface, Analytical Chemistry 2007, 79: 7027-7035.

[50] Höök F., Kasemo B., Nylander T., Fant C., Sott K., and Elwing H., Variations in Coupled Water, Viscoelastic Properties, and Film Thickness of a Mefp-1 Protein Film during Adsorption and Cross-Linking: A Quartz Crystal Microbalance with Dissipation Monitoring, Ellipsometry, and Surface Plasmon Resonance Study, Analytical Chemistry 2001, 73: 5796-5804.

[51] Voinova M. V., Rodahl M., Jonson M., and Kasemo B., Viscoelastic Acoustic Response of Layered Polymer Films at Fluid-Solid Interfaces: Continuum Mechanics Approach, Physica Scripta 1999, 59: 391.

[52] Kujawa P., Moraille P., Sanchez J., Badia A., and Winnik F. M., Effect of Molecular Weight on the Exponential Growth and Morphology of Hyaluronan/Chitosan Multilayers: A Surface Plasmon Resonance Spectroscopy and Atomic Force Microscopy Investigation, Journal of the American Chemical Society 2005, 127: 9224-9234.

[53] Kyte J., and Doolittle R. F., A Simple Method for Displaying the Hydropathic Character of a Protein, Journal of Molecular Biology 1982, 157: 105-132.

Chapter 7 – Appendix. Nanostructured thin coatings from chitosan and an elastin-like recombinamer with acute stimuli-responsive behavior[7]

Abstract

In the present work, chitosan (CHI) and elastin-like recombinamers (ELRs) were used to conceive nanostructured thin films driven by sequential electrostatic layer-by-layer (LbL), a simple and versatile technique that discards the use of harmful reagents. Two similar ELRs were engineered to contain negatively charged amino acids and organized and a single monoblock or a triblock. The buildup of the films was monitored in real time using a quartz-crystal microbalance with dissipation monitoring (QCM-D). Wettability transitions were observed from a moderate hydrophobic surface to an extremely wettable upon increasing the temperature to 50°C, accompanied by topography changes at the nanoscale as assessed by atomic force microscopy (AFM). Furthermore, the dependence on time for the surface molecular rearrangement was studied for the films with each ELR. The potential of this technology may stimulate the development of devices and biomaterials for biomedical applications in the near future, such as surfaces with tunable and patterned cell adhesion, while the use of ELRs will allow developing polypeptides with biological significance.

[7] This appendix is based on the following publication:

Costa R. R., Ribeiro A. J., Rodríguez-Cabello J. C., and Mano J. F., Nanostructured thin coatings from chitosan and an elastin-like recombinamer with acute stimuli-responsive behavior, Materials Science Forum 2013, 730-732: 32-37, DOI:10.4028/www.scientific.net/MSF.730-732.32.

Chapter 7 – Appendix. Nanostructured thin coatings from chitosan and an elastin-like recombinamer with acute stimuli-responsive behavior

7A.1 Introduction

The modification of surfaces has been a key aspect in biology and biotechnology, including cell expansion, development of biomaterials and preparation of substrates for regenerative medicine [1-3]. The surface is the first contact with the organism and dictates the subsequent biological events, namely the cellular events and biointegration. This is an approach with potential impact not only on the properties of current healthcare systems but also in more cutting-edge ones in tissue engineering.

Although several techniques may be used to modify a surface, the last decade has emphasized non-harmful and versatile techniques to modify polymeric substrates: the sequential adsorption of proteins and polysaccharides is one of the most promising today. This approach is known as layer-by-layer and is driven by a multitude of intermolecular interactions – such as electrostatic contacts, hydrophobic interactions, and hydrogen bonding – that may occur between two distinct materials [4-6].

Much work has been done in multilayered systems using poly(styrene sulfonate)/poly(allylamine hydrochloride) and CHI/hyaluronan [7]. However, the knowledge obtained from such systems is not always easily extrapolated to other materials and that limits the use of potentially more relevant combinations for LbL in biomedical applications. In this work, we aimed to apply the concept of LbL to CHI used along with ELRs to conceive multilayered substrates driven by electrostatic interactions. While chitosan is a well-known biocompatible polycation of natural origin [8,9], ELRs are genetically engineered polypeptides mimicking the sequence of natural elastin, showing smart behavior towards external stimuli, among them temperature and pH [10]. We hypothesized that different ELRs, although similar in nature and sequence, would display distinct adsorption kinetics. Therefore, we biosynthesized a negatively charged ELR organized as a single block, and an ELR organized into three blocks – two containing the negative residues and one nonpolar – henceforth designated monoblock and triblock, respectively. Furthermore, we studied the stimuli-responsive properties of the assembled coatings in terms of wettability and topography variations.

7A.2 Experimental section

7A.2.1 ELRs expression and purification

Gene expression of recombinant *Escherichia coli* strains were induced in a 12 L Applikon fermenter under 37°C and controlled pH (7.00). Subsequent to fermentation, the culture was harvested and lysed

by ultrasonic disruption. Insoluble remains were removed by centrifugation and the cleared lysate was subjected to purification based on temperature cycles. The polymer in solution was then freeze-dried.

7A.2.2 Buildup kinetics monitoring

An E4 QCM-D, from Q-Sense (Sweeden) was used to monitor the adsorption of CHI and the ELRs. Aqueous solutions of each polymer were prepared at concentrations of 100 $\mu g.mL^{-1}$, pH 4.5 and in 0.15 M NaCl. The combinations of CHI/monoblock and CHI/triblock and their depositions were studied in parallel at the surface of gold-coated sensors, at 25°C. The adsorption time was 10 minutes.

7A.2.3 Contact angle measurements

Contact angles were measured in a DataPhysics OCA15 system using a phosphate-buffered saline (PBS) solution for sessile drop experiments. Coatings of CHI/monoblock and CHI/triblock assembled onto glass (1 cm^2) were tested for their wettability at 4 and 50°C. The number of layers was defined based on the results from the QCM-D. The coatings were immersed in PBS placed under each temperature condition. After periods of 10 minutes of immersion in each temperature condition, the samples were withdrawn and contact angles were measured. If wettability did not change significantly, the samples were placed in immersion for an additional period of 10 minutes at the same temperature.

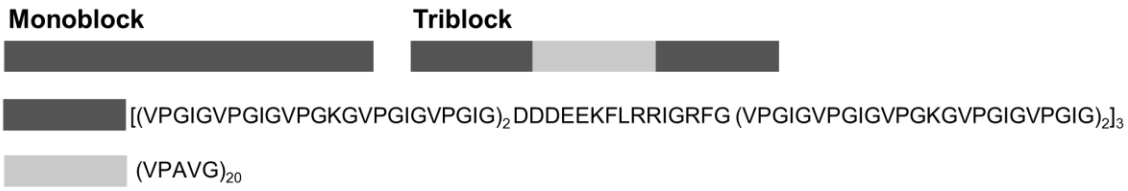
7A.2.4 Topography studies

AFM tests were conducted in a MultiMode STM microscope controlled by a NanoScope III from Digital Instruments system, operating in tapping mode at a frequency of 1Hz. A similar protocol to that of contact angle measurements was adopted. To assess the influence of pH in the coatings, a similar protocol to the contact angle measurements was followed. The samples were immersed in PBS at room temperature and 50°C and then retrieved and introduced in the device. “pH” was also analyzed, for values of 7.4 and 12. The analyzed area was 1 μm^2.

7A.3 Results and discussion

7A.3.1 ELRs peptide sequence

Under the scope of electrostatic LbL, we developed two ELRs containing negative amino acids – namely aspartic acids (D) and glutamic acids (E) – in order to bond with the protonated amine groups of CHI, positively charged under acidic conditions. Other amino acids are present, however, like lysines (K), although in lower number. Their final sequence is justified by the fact that these recombinamers include motifs with potential for biomineralization, which may prove to be useful for future bone regeneration applications. The representative structures of the monoblock and triblock are shown in Appendix Figure 7.1, along with the corresponding amino acidic sequence.



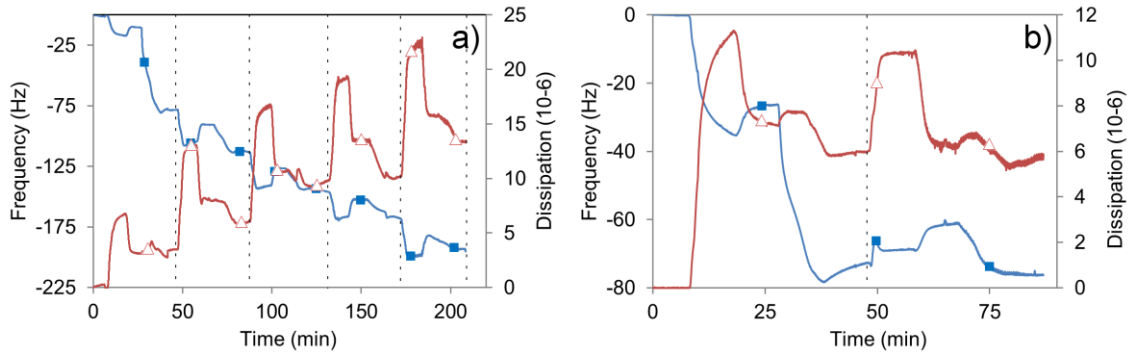
Appendix Figure 7.1. Representative structure of the featured ELRs and corresponding block peptide sequence.

The genetic nature of ELRs ultimately allows constructing macromolecules that are more appropriate for coatings of medical devices, allowing even to include sequences of biological relevance. However, their use for such purpose falls short of expectation and few works exist that use ELRs as ingredients for thin films [11-13]. Comparing both recombinamers, the triblock is different from the monoblock as it contains a polypeptide based on the pentapeptide VPAVG in the middle of the structure. This variation was introduced to evaluate if the buildup kinetics changes from the use of one ELR to another along with CHI for LbL, although their peptide sequence is similar, and to predict if other types of modifications would have the potential to be more favorable for multilayered buildup.

7A.3.2 Buildup monitoring of the films

The ability of CHI and each ELR to adsorb in a sequential fashion was first monitored by QCM-D. This technique is able to detect the adsorption of molecules in the order of ng.cm^{-2} manifested by the decrease of the oscillation frequency of the sensor. It can also measure the viscoelastic properties of

the resulting surface [14]. Appendix Figure 7.2 shows the frequency and dissipation variations (5th overtone, 25 MHz) for CHI/monoblock and CHI/triblock combinations.



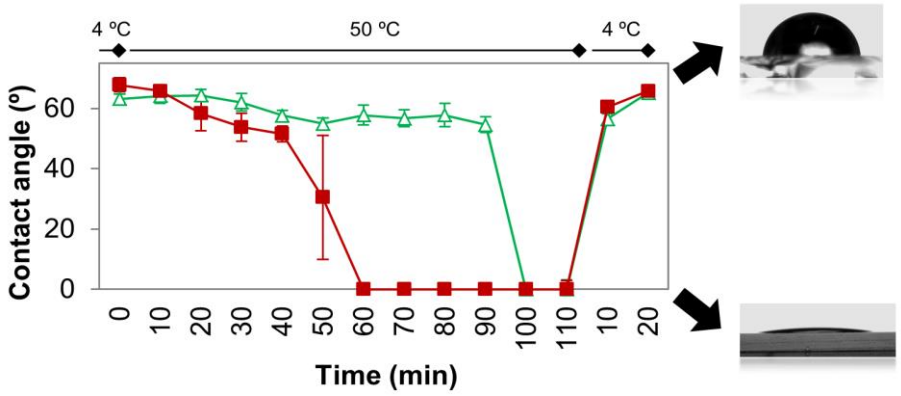
Appendix Figure 7.2. QCM-D monitoring of the frequency (■) and dissipation (Δ) variations for a) CHI/monoblock and b) CHI/triblock. The dashed lines mark the end of the adsorption of one bilayer.

The first case, depicted in Appendix Figure 7.2a, shows a progressive decrease of frequency, ΔF, to an approximate value of 200 Hz, upon flushing the sensors with the sequence of CHI and the monoblock, up to 5 bilayers. Simultaneously, the overall dissipation, ΔD, increases, showing that the film exhibits viscoelastic behavior, typical of macromolecular systems [14,15]. It is worth mentioning that the dissipation decreases during the adsorption steps of the monoblock, corresponding to an increase of rigidity of the film. This characteristic may be usefull for the conception of coatings where a more rigid film is advantageous, like for bone regeneration devices.

Appendix Figure 7.2b, the monitoring of the CHI/triblock buildup is shown. As observed, only 1 bilayer of these polyelectrolytes was successfully adsorbed, up to a ΔF of aroud 80 Hz. The ΔF after the attempt to deposit a second bilayer displays approximately the same value, therefore the following CHI and triblock molecules did not adsorb to the interface. This behavior can be explaned by the organization of the ELR: since the negatively charged blocks bond with the polycationic CHI, the nonpolar one does not intervene in the electrostatic-driven buildup. Therefore it faces outwards the interface of the film, rendering it uncharged, limiting the buildup to a single bilayer. When the adsorption of CHI is attempted, it does not adsorb because of the absence of negative aminoacids from the ELR. The results from the QCM-D show that, although the selected ELRs are similar in nature and peptide sequence, the buildup kinetics along with CHI is different, as previously theorized.

7A.3.3 Wettability variations of the films

ELRs have an intrinsic smart response towards temperature in aqueous solutions. Therefore we expected to observe some variation of the wettability of each film with the temperature. The study of the buildup kinetics of CHI along with a monoblocked or triblocked ELR was shown in the previous section. Based on the QCM-D data, we tested coatings made of 5 bilayers of CHI and the monoblock – $(CHI/monoblock)_5$ – and 1 bilayer of CHI and the triblock – $(CHI/triblock)_1$. Contact angle measurements are easy and quick to perform and may give useful insight about the molecular arrangement of a polymer at a planar surface. It is particularly convenient when the wettability between two arrays of conditions is significantly different. Appendix Figure 7.3 shows the contact angle variations caused by cyclic changes of the temperature – from 4°C to 50°C and vice-versa – and their evolution with time.



Appendix Figure 7.3. Contact angle variations of $(CHI/monoblock)_5$ (■) and $(CHI/triblock)_1$ (Δ) upon temperature changes and evolution with time.

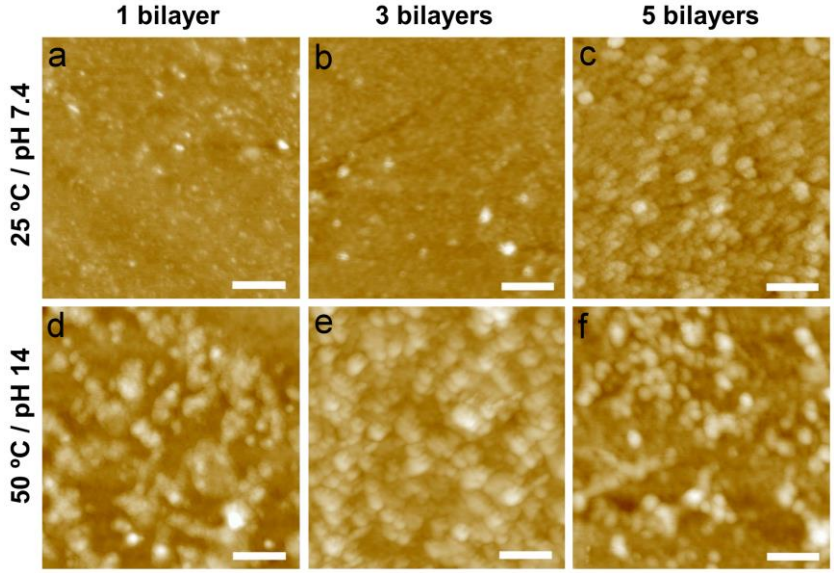
At start, the samples were at equilibrium at 4°C and displayed a moderately hydrophobic feature, around 65°. Upon increasing the temperature to 50°C, a transition was detected to a completely wettable surface in both cases. We have previously demonstrated that this observation is the result of the ELR transition at the surface due to the triggering of its self-assemble [12]. As a result of such phenomenon, there is a molecular rearrangement that favors the exposure of charged residues to the aqueous surroundings, while burying the hydrophobic amino acids underneath.

The transition time was different for each sample, though. While in the case of $(CHI/monoblock)_5$ the superhydrophilic regimen was observed after 60 min, for the $(CHI/triblock)_1$ it took 100 min. This longer time can be explained by the exposure of the nonpolar alanines at the interface: the molecular

rearrangement is more delayed, since at first the free charged amino acids are present below the nonpolar block of the ELR, hindering the rearrangement. The transition is only later fully achieved. This does not happen with the monoblock, since its structure does not contain the highly hydrophobic portion (see Appendix Figure 7.1). Upon decreasing the temperature to 4°C, both films recovered the moderately hydrophobic feature within 20 min. This result reflects the stimuli-responsive behavior of the films due to the properties of ELRs in aqueous solutions. Such behavior is retained and is cyclic when in the form of bidimensional substrates.

7A.3.4 Topography analysis

We determined that the monoblocked ELR is appropriate for constructing multilayered films. Having in mind that we intend to use ELRs using a multilayer approach along with polysaccharides, we studied the topography of CHI/monoblock films with different number of layers. The wettability variations found in the previous section should be accompanied by topography changes. Appendix Figure 7.4 shows the images obtained by AFM for 1, 3 and 5 bilayers. The variations of the topography with temperature were also studied, for 25 and for 50°C. Appendix Table 7.1 shows the root-mean-square roughness (RMS) values for each case. As observed, independently of the temperature, the roughness increases with increasing number of layers due to the increase of mass at the surface, a typical observation of several LbL systems [5].



Appendix Figure 7.4. AFM imaging for $(CHI/monoblock)_5$ films for 1, 3 and 5 bilayers, at 25 and 50°C. Similar results were obtained for pH 7.4 and pH 14. Scale bar: 200 nm.

Appendix Table 7.1. Root-mean-square roughness for (CHI/monoblock)$_5$ films for 1, 3 and 5 bilayers, at 25 and 50°C, or pH 7.4 and pH 14, respectively.

	Roughness, RMS (nm)		
Temperature (°C) or pH	1 bilayer	3 bilayers	5 bilayers
25 or 7.4	0.874	0.905	1.482
50 or 14	2.652	2.833	3.679

In Appendix Figure 7.4a to Appendix Figure 7.4c the topographies at room temperature show no apparent organization for any of the number of layers. Upon increasing the temperature to 50°C, the formation of nanostructures was detected, caused by the triggering of the ELR self-assembly and consequent formation of larger and organized structures. The roughness values also increased in accordance. These results relate well with the contact angle measurements: the detected nanostructures result from the molecular rearrangement of the ELR, where their cores are mainly composed of nonpolar amino acids, while exposing the charged residues to the outer regions. Therefore, these are micelle-like structures which organization favors the affinity of the films to water. It is also worth mentioning that similar topography and roughness results were obtained for the variation of pH, which is also known to trigger the transition of ELRs containing lysines (pk_a ranging 9.4–10.6 [16]). Such organization at the nanoscale may be used in the future development of patterned substrates for tunable cell adhesion.

7A.4 Conclusions

The presented work shows that polysaccharides and ELRS can be successfully combined following a multilayer approach to conceive nanostructured films. Both ELRs are similar in nature and peptide sequence; however the buildup kinetics is different, being limited to only 1 bilayer in the case of the triblock. Acute wettability variations were observed as a function of temperature for coatings of (CHI/monoblock)$_5$ and (CHI/triblock)$_1$, caused by a molecular rearrangement of the ELRs at the surface. Topography changes were detected at the nanoscale, where micelle-like structures were formed due to the increase of temperature or pH. The properties of the films may be exploited in the future for substrates with patterned and tunable cell adhesion. Furthermore, the recombinant nature of such elastin-like macromolecules may enable tuning their sequence to favor LbL constructs and even adding biological relevant motifs.

7A.5 Acknowledgements

The authors acknowledge the financial support through Fundação para a Ciência e Tecnologia (FCT, PhD grant SFRH/BD/61126/2009, ''Junta de Castilla y Leon'' (VA034A09), the MICINN (MAT 2009-14195-C03-03, ACI2009-0890, IT2009-0089, MAT2010-15310, and MAT2010-15982), the CIBER-BBN and the ''Network Center of Regenerative Medicine and Cellular Therapy of Castilla y León''.

7A.6 References

[1] Falconnet D., Csucs G., Grandin H. M., and Textor M., Surface engineering approaches to micropattern surfaces for cell-based assays, Biomaterials 2006, 27: 3044-3063.

[2] Hook A. L., Voelcker N. H., and Thissen H., Patterned and switchable surfaces for biomolecular manipulation, Acta Biomaterialia 2009, 5: 2350-2370.

[3] Tirrell M., Kokkoli E., and Biesalski M., The role of surface science in bioengineered materials, Surface Science 2002, 500: 61-83.

[4] Alves N. M., Pashkuleva I., Reis R. L., and Mano J. F., Controlling cell behavior through the design of polymer surfaces, Small 2010, 6: 2208-2220.

[5] Bertrand P., Jonas A., Laschewsky A., and Legras R., Ultrathin polymer coatings by complexation of polyelectrolytes at interfaces: suitable materials, structure and properties, Macromolecular Rapid Communications 2000, 21: 319-348.

[6] Decher G., Fuzzy nanoassemblies: toward layered polymeric multicomposites, Science 1997, 277: 1232-1237.

[7] Boudou T., Crouzier T., Ren K., Blin G., and Picart C., Multiple functionalities of polyelectrolyte multilayer films: new biomedical applications, Advanced Materials 2010, 22: 441-467.

[8] Alves N. M., and Mano J. F., Chitosan derivatives obtained by chemical modifications for biomedical and environmental applications, International Journal of Biological Macromolecules 2008, 43: 401-414.

[9] Ravi Kumar M. N. V., A review of chitin and chitosan applications, Reactive and Functional Polymers 2000, 46: 1-27.

[10] Rodríguez-Cabello J. C., Martín L., Alonso M., Arias F.J., and Testera A. M., "Recombinamers" as advanced materials for the post-oil age, Polymer 2009, 50: 5159-5169.

[11] Barbosa J. S., Costa R. R., Testera A. M., Alonso M., Rodríguez-Cabello J. C., and Mano J. F., Multi-layered films containing a biomimetic stimuli-responsive recombinant protein, Nanoscale Research Letters 2009, 4: 1247-1253.

[12] Costa R. R., Custódio C. A., Testera A. M., Arias F. J., Rodríguez-Cabello J. C., Alves N. M., and Mano J. F., Stimuli-responsive thin coatings using elastin-like polymers for biomedical applications, Advanced Functional Materials 2009, 19: 3210-3218.

[13] Swierczewska M., Hajicharalambous C. S., Janorkar A. V., Megeed Z., Yarmush M. L., and Rajagopalan P., Cellular response to nanoscale elastin-like polypeptide polyelectrolyte multilayers, Acta Biomaterialia 2008, 4: 827-837.

[14] Marx K. A., Quartz crystal microbalance: a useful tool for studying thin polymer films and complex biomolecular systems at the solution-surface interface, Biomacromolecules 2003, 4: 1099-1120.

[15] Picart C., Lavalle P., Hubert P., Cuisinier F. J. G., Decher G., Schaaf P., and Voegel J.-C., Buildup mechanism for poly(L-lysine)/hyaluronic acid films onto a solid surface, Langmuir 2001, 17: 7414-7424.

[16] Fothergill-Gilmore L. A., Peptide sequence determination, in: Franks F. (ed.), Protein biotechnology: isolation, characterization, and stabilization, United Stated of America, Humana Press, 1993.

Chapter 8. Layer-by-layer assembly of chitosan and recombinant biopolymers into biomimetic coatings with multiple stimuli-responsive properties[8]

Abstract

In this work, biomimetic smart thin coatings using chitosan and a recombinant elastin-like recombinamer containing the cell attachment sequence arginine-glycine-aspartic acid (RGD) are fabricated through layer-by-layer. The synthetic polymer is characterized for its molecular mass and composition using mass spectroscopy and peptide sequencing. The adsorption of each polymeric layer is followed *in situ* at room temperature and pH 5.5 using a quartz-crystal microbalance with dissipation monitoring, showing that both polymers can be successfully combined to conceive nanostructured multilayered coatings. The smart properties of the coatings are tested for their wettability by contact angle (CA) measurements as a function of external stimuli, namely temperature, pH and ionic strength. Wettability transitions are observed from a moderate hydrophobic surface (CAs approximately from 62º to 71º) to an extremely wettable one (CA considered as 0º) as the temperature, pH and ionic strength are raised above 50 ºC, 11, and 1.25 M, respectively. Atomic force microscopy is performed at pH 7.4 and pH 11 to assess the coating topography. In the latter, the results reveal the formation of large and compact structures upon the aggregation of ELRs at the surface, which increase water affinity. Cell adhesion tests are conducted using a SaOs-2 cell line. Enhanced cell adhesion is observed in the coatings, as compared to a coating with a chitosan-ending film and a scrambled RDG biopolymer. The results suggest that such films could be used in the future as smart biomimetic coatings of biomaterials for different biomedical applications, including in tissue engineering or in controlled delivery systems.

[8] This chapter is based on the following publication:

Costa R. R., Custódio C. A., Arias F. J., Rodríguez-Cabello J. C., and Mano J. F., Layer-by-layer assembly of chitosan and recombinant biopolymers into biomimetic coatings with multiple stimuli-responsive properties, Small 2011, 7: 2640-2649, DOI:10.1002/smll.201100875.

Chapter 8. Layer-by-layer assembly of chitosan and recombinant biopolymers into biomimetic coatings with multiple stimuli-responsive properties

8.1 Introduction

The modification of surfaces has been a key aspect in biology and biotechnology, including cell expansion, biomaterials development and preparation of substrates for regenerative medicine) [1-3]. In the field of implantable devices, the surface is the first contact with the organism and dictates the subsequent biological events, namely the cellular behavior and biointegration. Thus, surface engineering is of the utmost significance to lead to the conception of devices with an improved biological performance [4-6].

Surface modification has been also implemented to produce stimuli-responsive surfaces for a variety of applications, including in biomineralization control [7], cell sheet engineering [8,9], surfaces with extreme wettabililty transitions [10], and microfluidics [11], mostly based on variations of the hydration state of polymeric films deposited at the surfaces. Usually, the modification is performed by grafting stimuli-responsive polymers onto a substrate, which are typically synthetic and nonbiodegradable, such as poly(*N*-isopropylacrylamide) (PNIPAAm) [12]. A good example of the latter is the work developed by Okano *et al.* [9] regarding cell-sheet engineering.

In more recent years, emphasis has been given to non-harmful and versatile techniques to modify polymeric substrates: the sequential adsorption of proteins and polysaccharides, known as layer-by-layer (LbL) adsorption, is one of the most promising today. The principle behind LbL adsorption lies in the existence of multiple intermolecular interactions, such as electrostatic contacts, hydrophobic interactions, and hydrogen bonding, where the cooperative effects of multipoint attractions play the most important role. It is a simple and versatile technique which allows producing robust coatings, even in substrates with complex geometries; because it discards the need of organic and harmful solvents, it is an attractive technique for tissue engineering applications [13-15]. Multilayer systems have already been proposed for different biomedical applications, including for biomimetic composite-like coatings, to control the release of drugs, or to manipulate the adhesion, differentiation, proliferation and even function of attached cells [16-19].

In this work, we plan to conceive coatings using natural and nature-inspired macromolecules in a multilayered fashion using the LbL approach at mild processing conditions. Natural materials are intricate and multifunctional structures that often inspire scientists to design novel classes of materials [20]. It is the case of elastin-like recombinamers (ELRs), also designated as elastin-like polymers (ELPs). This family of peptide-based polymers was developed by Urry, relying in genetic

engineering techniques, and have their basic structure rooted in elastin, the extracellular elastic protein of higher animals [21-23]. In aqueous environment they are known to have self-assembly behavior and exhibit a transition temperature (T_t): below T_t, the free polymer chains adopt random coil conformations; above it, they fold into an organized structure known as β-spiral. Although ELRs respond primarily to temperature, the effects of other stimuli, such as pH, ionic strength and concentration, also affect the transition phenomenon [24]. Their recombinant nature is one of their attractive properties because it allows tuning their physicochemical properties and introducing sequences to extend their functionality, including biologically relevant domains [25,26]. The work of Girotti *et al.* [27], who were able to biosynthesize an extracellular matrix analogue enclosing the cell attachment sequence arginine-(glutamic acid)-(aspartic acid)-valine (REDV), is an example of such versatility. Thus, ELRs are an attractive option over the most commonly used formulations in LbL adsorption.

Swierczewska *et al.* [28] have previously reported the use of ELRs for LbL thin films. However, the peptides were modified and conjugated with either poly(ethyleneimine) (PEI) or poly(acrylic acid) (PAA) to provide positive or negative charge, respectively. Our groups have also shown that ELRs can be successfully combined with polysaccharides to conceive coatings and some may even be applied using a multilayer approach [29,30]. In order to explore the potential of ELR properties and the advantages of LbL, we intend to conceive nanostructured thin coatings made from the sequential adsorption of a polysaccharide and an ELR modified with the arginine-glycine-(aspartic acid) (RGD) cell adhesion motif, labeled ELR-RGD. RGD is expected to increase the cell adhesion *in vitro* and prove useful in the design of devices with tunable cell attachment or even improved host integration. We selected chitosan (CHI) because, besides being a well-known biocompatible material, it is one of the few polysaccharides exhibiting positive charge (at acidic conditions), is abundant, and its production is environmentally safe [31,32].

The proposed system will also allow expanding the concept of multilayered films to a new attractive class of peptide-based polymers, making them more robust than simple monolayers, and could bring new possibilities in the development of nanostructured coatings of materials in tissue engineering. The buildup of the multilayers will be monitored in real time using a quartz-crystal microbalance with dissipation monitoring (QCM-D). Distinct techniques, such as contact angle measurements, atomic force microscopy (AFM), and cell adhesion tests will be used to characterize it. We hypothesize that coatings containing this ELR may exhibit changes both in topography and wettability, depending on

several stimuli, namely temperature, pH and ionic strength, and improved biological *in vitro* performance.

8.2 Experimental section

8.2.1 ELR-RGD expression and purification

The featured ELR monomers of RGD were designated as ELR-RGD. Expression conditions and purification protocols were adapted from Meyer and Chilkoti [33] and Girotti *et al.* [34]. Gene expression of a recombinant Escherichia coli strain BLR(DE3) containing the expressing gene of ELR-RGD was induced in a 12 L Applikon fermenter, in terrific broth medium (TB) with 0.1% of carbenicilin and 0.1% of glucose, under controlled conditions of temperature (37°C) and pH (7.00). The fermentation was stopped after registering an optical density variation at 600 nm inferior to 0.25, in a time-frame of 1 h. Subsequent to fermentation, the culture was harvested by centrifugation, resuspended and lysed by ultrasonic disruption. Insoluble debris was removed by centrifugation and the cleared lysate was subjected to several cycles of cold and warm centrifugations, of 4 and 40°C, respectively. All the purification steps were carried out in a sodium chloride (NaCl) solution at 0.5 M. The polymer in solution was then frozen at -24°C and freeze-dried.

8.2.2 ELR-RGD characterization

Differential Scanning Calorimetry (DSC) experiments were performed on a Mettler Toledo 822e (United States) with a liquid nitrogen cooler accessory. Both temperature and enthalpy were calibrated with an indium standard at the same experimental conditions used for the studied materials. Water solutions of ELR-RGD at 50 $mg \cdot mL^{-1}$ were prepared at pH 7.4. In a typical DSC run, 20 μL of the solution were placed inside a standard 40 μL aluminum pan hermetically sealed. The same volume of water was placed in the reference pan. All samples were equilibrated for 5 minutes at 5°C inside the sample chamber just before the beginning of each experiment. A heating rate of $5°C \cdot min^{-1}$ was used. To assess the biopolymer molecular weight, matrix-assisted laser desorption/ionization time-of-flight (MALDI-TOF) mass spectroscopy was performed in a Voyager STR, from Applied Biosystems, in linear mode and with an external calibration using bovine serum albumin (BSA). Amino acid composition determination was previously used to assess the composition of ELRs [27].

8.2.3 Buildup and characterization of the self-assembled coatings

Medium molecular weight grade CHI was purchased from Sigma and purified. Solutions of purified CHI and ELR-RGD were prepared at 0.1 $mg \cdot mL^{-1}$ in 0.15 M NaCl. The pH of the solutions was adjusted to 5.5. ζ-potential of each solution was determined using a Nano-ZS from Malvern (United Kingdom), at 25°C. A Q-Sense E4 quartz-crystal microbalance (Q-Sense AB, Sweden) with dissipation monitoring system was used for monitoring in situ the deposition of CHI/ELR-RGD multilayers at the surface of gold-coated crystals. This technique has previously been extensively described [35-37]. Very briefly, an AT cut quartz crystal can be excited at its fundamental frequency (5 MHz) and at several overtones: 25, 35, and 45 MHz (fifth, seventh, and ninth overtones, respectively). When a thin film is deposited onto the sensor crystal the frequency decreases. If the film is thin and rigid the decrease in frequency (ΔF) is proportional to the mass of the film. However, when using polymers, the adsorbed film is not rigid and this relation is not valid: the film begins dissipating energy and exhibiting the typical viscoelastic behavior, which is evident by the change in the dissipation (ΔD). The crystals were first cleaned in an ultrasound bath at 30°C, and immersed successively in acetone, ethanol, and isopropanol. Adsorption took place at 25°C and pH 5.5 and at a constant flow rate of 50 $mL \cdot min^{-1}$. Starting with the CHI solution, each one was pumped into the system for 10 minutes. Each deposition cycle was followed by a rinsing step with 0.15 M NaCl, at pH 5.5, for 10 min, and ΔF_ν and ΔD were monitored in real time. The frequency of each overtone was normalized to the fundamental resonant frequency of the quartz crystal, by diving it by ν (where ν=5; 7; 9). The thickness of the films was estimated using the Voigt model through the Q-Tools software, from Q-Sense [38]. The area density was calculated by multiplying the thickness by the layer density (1200 $kg.m^{-3}$ led to obtaining calculations with the best fitting).

8.2.4 Contact-angle measurements

Phosphate-buffered saline (PBS) contact angles were measured in a DataPhysics OCA15 system. The coatings were prepared at the surface of regular glass microscopy slides, from Marienfeld (Germany). The glass was cleaned using the same protocol to which QCM-D crystals were submitted. Coatings up to 10 layers – 5 pairs of CHI and ELR-RGD – were characterized for their wettability for each layer assembled, at 37°C and pH 7.4. An approach described by Park *et al.* [39] was used to measure contact angles dependent on several temperature, pH and ionic strength conditions. The measurements were performed for a pH range from 4 to 12, ionic strength from 0 to 1.5 M of NaCl,

and three relevant temperatures: 25, 37 and 50°C. The samples were immersed in a beaker of PBS placed under each condition. After 1 hour, the samples were withdrawn and contact angles were measured. The time of 1 h was determined to be enough to have a stable surface. Upon determining the wettability transition parameters, three cycles were performed by changing the transition values above and below each transition value.

8.2.5 Atomic force microscopy measurements

AFM measurements were performed in a MultiMode STM microscope controlled by the NanoScope III from Digital Instruments system, operating in tapping mode at a frequency of 1 Hz. Glass slides were cut into pieces of 1×1 cm^2 and used as substrates for multilayer adsorption. Surfaces coated with 5 pairs of CHI/ELR-RGD were immersed in PBS for 30 min. To assess the influence of pH in the coatings, a similar protocol to the contact angle measurements was followed. The samples were immersed in PBS at two pH values: 7.4 and 11. To avoid the formation of crystals during the acquisition, the samples were immersed shortly in ultrapure water for removing excess of saline solution. The samples were then retrieved and introduced in the device. The analyzed area was 1×1 μm^2.

8.2.6 Cell culture studies of SaOs-2 osteoblast-like cells

Cell studies were performed onto coatings of 5 pairs of layers, ending in ELR-RGD, CHI or ELR-$RDG^{(-)}$ (negative control), assembled at the surface of glass coverslips with 1 cm of diameter. Tissue culture polystyrene (TCPS) was used as a positive control. Cell adhesion was studied using the SaOs-2 osteoblast-like osteosarcoma cell line. Cells were seeded on the surfaces (5×10^4 cell·mL^{-1}) and incubated in serum free Dulbecco's Modified Eagle's medium (DMEM), loaded with 1% antibiotics/antimicotics at 37°C, 5% carbon dioxide (CO_2). The substrates were analyzed at different time points: 4 h, 24 h and 3 days. At each time point, cells on the coated surfaces were washed with PBS twice, fixed in formalin (3.7%) and nuclei of the cells stained with 4',6 diamidino-2-phenylindol (DAPI), and the actin was stained with phalloidin.

For alkaline phosphatase (ALP) assays, samples collected on each time point were washed with PBS and immersed in 1 mL of ultra-pure water to lyse the cells. To each well of a 96-well plate were added 20 µL of sample plus 60 µL of substrate solution (0.2% (w/v) p-nytrophenyl (pNP) phosphate/1 M diethanolamine hydrochloric acid (HCl), at pH 9.8). The plate was then incubated in the dark for 45 min

at 37°C. After the incubation period, 80 µl of a stop solution (2 M sodium hydroxide (NaOH)/0.2 mM ethylenediaminetetraacetic acid (EDTA)), was added to each well. The absorbance was then measured at 405 nm using p-nitrophenol as standard. For each experiment, a standard curve was constructed from reference suspensions at known cell concentrations. To access cell viability, (3-(4,5-dimethylthiazol-2-yl)-5-(3-carboxymethoxyphenyl)-2-(4-sulfophenyl)-2H-tetrazolium) (MTS) assay was performed. MTS is bioreduced by cells. The values for absorbance of this reduced product at 490 nm are directly proportional to the number of living cells in the substrates.

8.3 Results and discussion

8.3.1 ELR-RGD characterization

For the past two decades, much work has been done on the widely investigated poly(styrene sulfonate)/poly(allylamine hydrochloride) (PSS/PAH) system – considered so far as a model of multilayered thin films – and CHI/hyaluronan [16]. However, the buildup mechanism is not always straightforward to every material and distinct or several forces may influence the construction [40,41]. Furthermore, coatings for tissue engineering applications should ideally contain other materials with more relevant features, including biological activity. It is the case of the biopolymer used in this work, which contains the RGD cell adhesion motif, depicted in Figure 8.1a.

The ELR-RGD, with 371 aminoacids and theoretical molecular weight of 31371 Da, contains 2 monomers of RGD, 2 aspartic acids, and 3 lysines isolated at the amino-terminal and exhibits a T_t of around 23°C in solution at physiological pH (data not shown). In contrast to our previous work [30], this ELR-RGD was engineered to facilitate electrostatic interactions during the multilayer buildup. In Figure 8.1b, MALDI-TOF spectrum shows a high intensity peak at 31229 Da, which is approximate to the theoretical value for this biopolymer.

In order to confirm if the produced ELR matched the theoretical amino acidic composition, peptide sequencing tests were performed. In Table 8.1, it can be confirmed that the produced biopolymer composition matches well the predicted amino acid composition. These results point to the bioproduction of a stock of ELR-RGD retaining the desired amino acid sequence.

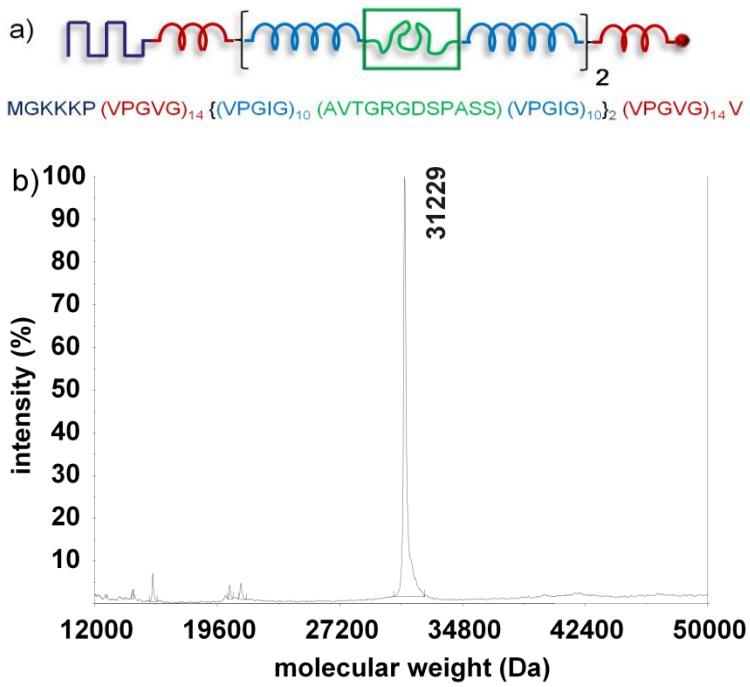


Figure 8.1. Characterization of the ELR-RGD. a) schematic representation of the featured ELR chemical structure; b) MALDI-TOF of the biopolymer, with major peak signaled at 31229 Da.

Table 8.1. Amino acid composition of the bioproduced ELR-RGD. ND = not determined.

Amino acid	Predicted	Experimental
Asp (D)	2	2.27
Thr (T)	2	1.81
Ser (S)	6	4.7
Pro (P)	71	70.7
Gly (G)	141	141.48
Ala (A)	4	4.31
Val (V)	99	98.65
Ile (I)	40	39.6
Lys (K)	3	3
Arg (R)	2	2.18
Met (M)	1	ND

8.3.1 Analysis of CHI/ELR-RGD film buildup

The ability of CHI and ELR-RGD to adsorb in a sequential fashion was first monitored by QCM-D. This technique is able to detect mass changes in the order of ng.cm^{-2} and measure the viscoelastic properties of the resulting surface [35-37]. Due to the recombinant nature of ELRs, it is possible to tune their structure to appropriately fit a multilayer approach and design coatings for tissue engineering substrates. Figure 8.2a shows the normalized frequency ($\Delta F_\nu/\nu$, where ν is the overtone) and dissipation (ΔD) variations for the 5th overtone (25 MHz) after the construction of 20 layers onto gold-coated sensors. The $\Delta F_\nu/\nu$ decreased with time upon flushing the substrate with the sequence of polyelectrolytes, to an approximate value of 40 Hz. On the other hand, the ΔD increased, revealing that the film is not rigid and exhibits the typical viscoelastic behavior, a common situation when using macromolecular systems [36,42].

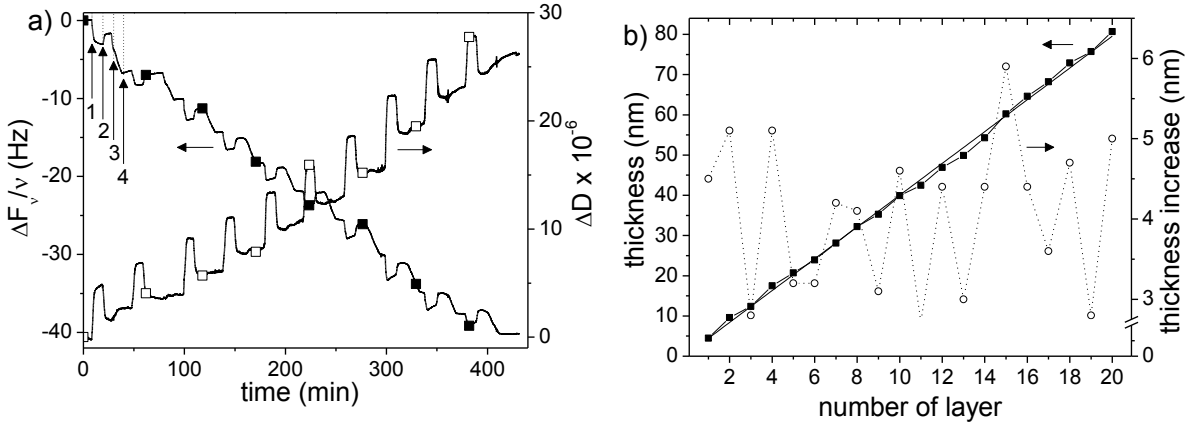


Figure 8.2. Buildup assessment of CHI/ELR-RGD films. a) QCM-D monitoring of normalized frequency ($\Delta F_\nu/\nu$, ■) and dissipation (ΔD, □) obtained at the 5th overtone. Numbers refer to adsorption of CHI (1), adsorption of ELR-RGD (3) and rinsing (2 and 4). b) Cumulative thickness evolution and thickness increase for the CHI/ELR-RGD film, for 20 layers, estimated using the Voigt model. Odd numbers correspond to films ending in CHI and even numbers to films ending in ELR-RGD. Linear fitting matches well the cumulative thickness variation (r^2=0.99824).

At the working pH of 5.5, we relied on the protonation state of the ELR-RGD aspartic acids: under such conditions, these residues are deprotonated and negatively charged (pK_a ranging from 3.0–4.7) [43]. This would allow them to interact by electrostatic self-assembly (ESA) with the positively charged amine

groups of CHI. Prior to the monitoring, the ζ-potential of CHI and ELR-RGD solutions was measured at working conditions (pH=5.5 and ionic strength at 0.15 M), showing a charge of +17.0±0.6 and -8.4±0.33 mV, respectively. ELRs are essentially hydrophobic by nature but can be modified to include specific charged residues. CHI is also insoluble in water and can only be dissolved at acidic conditions, below its pK_a (approximately 6) [44]. It has been reported that electrostatic deposition demands appropriate matching of the charge density of the used polyelectrolyte pair, rather than a minimum charge density [13,45], but in this case the ζ-potential showed no charge balance (i.e. equal absolute values). Although ESA was a driving force of construction, other forces, like hydrophobic interactions, are likely to participate on the assembling phenomenon. In fact, Figure 8.2a shows the successful combination of the used pair, at the assembly pH of 5.5, near the pK_a of CHI. We can assume that a fraction of already deprotonated amine groups interacts with the hydrophobic residues of the ELR-RGD structure and allow the construction of the coating.

The QCM-D data was used to estimate the thickness variations of the film along with the adsorption cycles. Figure 8.2b shows the results calculated using the Voigt model implemented in the Q-Tools software from Q-Sense [38]. It can be observed that the thickness increased linearly during the buildup, in accordance with the evolution of ΔF_ν and ΔD variations. After the deposition of 20 layers, the film had a thickness of 81 nm, corresponding to an approximate total area density of 9.6 $\mu g.cm^{-2}$ (multiplication of thickness by the layer density. 1200 $kg.m^{-3}$ allowed for the best fitting). Figure 8.2b also shows the thickness of each layer ("thickness increase" in the graphic). Overall, the increase of thickness is higher for the adsorption steps of ELR-RGD. This is the result of the lower charged exhibited by the recombinamer, which requires that more material is needed to overcompensate the charges of the underlying CHI ones. The results obtained through QCM-D measurements demonstrate that ELR-RGD can be used successfully with CHI to conceive a viscoelastic polymeric coating using the LbL approach.

8.3.2 Characterization of the self-assembled coatings

When a material adheres to a substrate, it is expected that such phenomenon will result in physicochemical changes at the surface [46,47]. The measurement of contact angles is an easy method that allows a quick assessment of the modification of a surface in terms of wettability, and its usefulness is even higher when such wettability is significantly different for each layer. Figure 8.3 shows the contact angle variation of the CHI/ELR-RGD film with the buildup, up to 10 layers.

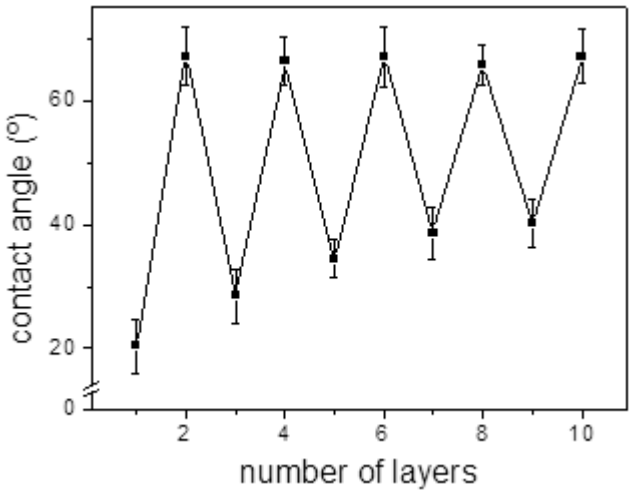


Figure 8.3. Evolution of the contact angle of the films obtained with sequential adsorption of CHI and ELR-RGD, up to 10 layers Odd numbers correspond to films ending in CHI and even numbers to films ending in ELR-RGD. Error bars represent two standard deviations (n=9).

The films were adsorbed onto glass (contact angle of 28.6±2.9°). Each measurement was performed after 1 hour of immersion in PBS at 37 °C. While films ending in ELR-RGD retained their moderate hydrophobic behavior (approximately between 62° and 71°), the ones ending in CHI increased gradually, from 20.4±4.4° in the first layer to 40.1±3.9° in the fifth (layer 9). The increasing values of contact angles obtained for CHI-ending films can be explained by the influence of the underlying adsorbed layers on the coating interface. When using weak polyelectrolytes, the most charged polymer tends to be adsorbed as a thin layer with flat chain conformations, while the less charged polymer tends to be adsorbed as a thicker layer, forming loopier-type structures [48,49]. Since ELR-RGD is a modified version of the basic repeating block of elastin with charged amino acids, CHI appears as the most charged polymer, as already presented by the ζ-potential measurements. Furthermore, the thickness increase of each layer displayed in Figure Figure 8.2b helps to demonstrate that the ELR-RGD layers are overall thicker than the ones of CHI. Thus, the surface properties of the CHI layer may reflect the effect of the underlying ELR one, even in terms of wettability, while the opposite does not occur.

The featured films were conceived using a recombinant ELR, a biomaterial exhibiting stimuli-responsive properties in solution. It would be interesting to observe how the wettability of the films behaves when they are exposed to several stimuli. To achieve this goal, we have measured the contact angles of 5 pairs of layers ending in ELR-RGD, labeled $(CHI/ELR\text{-}RGD)_5$, assembled in glass substrates, at different

values of temperature, pH, and ionic strength (using NaCl as the ionic component). After the assembly, the coatings were placed at different conditions of each studied stimulus (taking 25 °C, pH 7.4, and ionic strength of 0.15 M as starting values), in order to determine if their variation triggers a transition that could be detected by differences in wettability. Figure 8.4 shows the contact angle values measured upon cyclic variations of temperature (25°C to 50°C), pH (7.4 to 11) and ionic strength (0.15 M to 1.25 M).

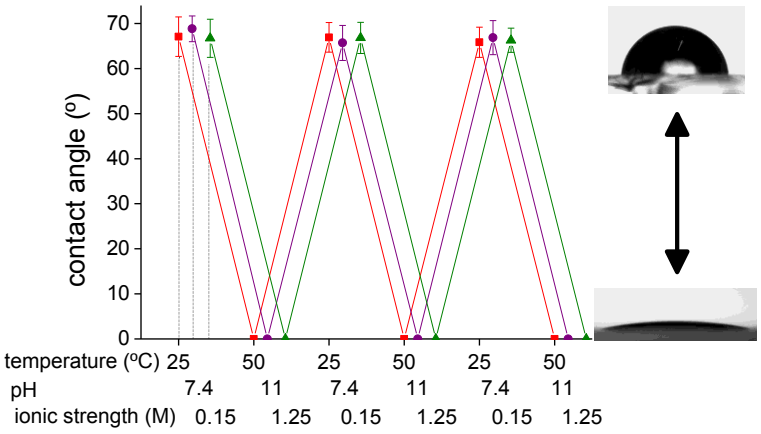


Figure 8.4. Contact angle measurements as a function of temperature (□), pH (○), and ionic strength (Δ) in a $(CHI/ELR\text{-}RGD)_5$ film. Three cycles are represented. Error bars represent two standard deviations (n=9).

Taking the case of the temperature, at 25°C an initial wettability exhibiting values of 67.1±4.7° was measured, corresponding to a moderate hydrophobic surface. However, upon increasing the temperature to 50°C, the contact angle values decreased to those of a superhydrophilic surface, corresponding to a totally wettable surface. ELRs show a phase transition in solution above T_t, similar to the transition of other temperature-sensitive polymers with lower critical solution temperature (LCST). However, the hydrophobicity of such a surface did not increase with the switch to high temperatures. In fact, while the hydrophobicity of surfaces modified with LCST polymers increases [9], the behavior of ELRs when adsorbed onto a surface is opposite to the expected, more in accordance to the case of polymers with an upper critical solution temperature (UCST), which become more hydrophilic [50]. Such atypical wettability behavior of ELR-RGD temperature-responsive coatings has been previously observed in a thin ELR monolayer adsorbed onto CHI substrates [30]. We have shown that upon the transition, the collapsed biopolymer aggregates into micelle-like structures, as suggested by topography

measurements. They assume a conformation where the hydrophobic chains are directed to the inside and the charged residues to the outside of such organizations. Additionally, while the properties of such surfaces change at 50°C, the polymer in solution shows a transition at 23°C, where the association is much more facilitated than at the surface, to which the polymer is tightly connected.

Similar results to that of temperature response were obtained for pH and ionic strength, and even exhibiting similar contact angle values. In the case of pH, ELR-RGD has lysines in its structure, which amine groups are protonated below the pK_a values ranging 9.4–10.6 [43]. Above the pK_a, the amine groups are deprotonated and the hydrophobicity of ELR-RGD increases. It is known that the more hydrophobic the ELR the lower the T_t in solution is [34]. Thus, with the increase of pH, the mean hydrophobicity of ELR-RGD also increases, up to a pH of 11. At this value, the transition to a superhydrophilic regimen was detected, as depicted in Figure 8.4. In the case of ionic strength, Reguera *et al.* [51] suggested that an increase in the salt concentration increases the polarity of the solvent. This creates a higher difference in polarity with respect to the hydrophobic moieties of the polymer, causing more and more ordered structures surrounding the polymer chains. As observed, a transition was detected upon the increase of ionic strength to 1.25 M, which is in accordance to the behavior of this family of polymers. These results show that the wettability of $(CHI/ELR\text{-}RGD)_5$ films are strongly dependent not only on temperature but also on pH and ionic strength, which influence the T_t of ELRs in aqueous solutions as well. Furthermore, the films were submitted to three cycles of variations and still retained full reversibility and similar contact angle values, showing that the films are robust and capable of withstanding sharp changes of the environment, while retaining functionality.

The results presented so far reflect the nature of the studied ELR, and characterize the conceived film as a stimuli-sensitive coating that could prove to be useful in the development of controlled release systems and in surfaces capable to control cell behavior. In order to have full understanding of this behavior, the wettability was further studied for several arrays of conditions, consisting in the combination of pH and ionic strength, at three relevant temperatures: 25°C (room temperature), 37°C (temperature of the body), and 50°C (determined to be the temperature of transition of ELR-RGD at the surface). The diagram of Figure 8.5 is the graphical representation of the measurements performed in $(CHI/ELR\text{-}RGD)_5$, in an attempt to characterize the coating wettability.

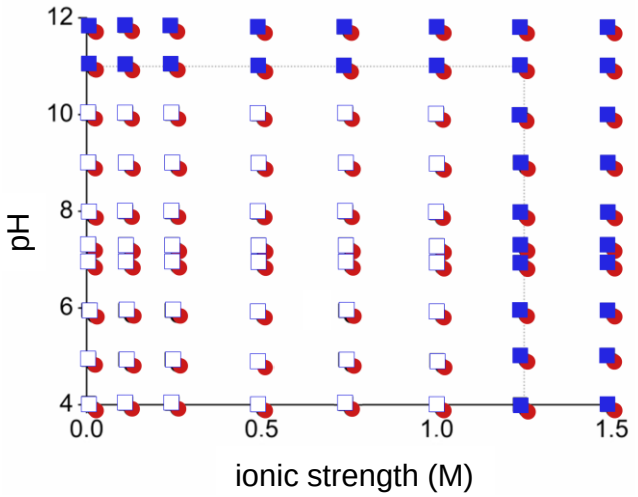


Figure 8.5. Map of the wettability of $(CHI/ELR\text{-}RGD)_5$ films as a function of condition arrays of temperature, pH, and ionic strength stimuli. Open symbols stand for a moderate hydrophobic surface (contact angle of about 67°) and closed ones for a superhydrophilic surface. The blue squares represent measurements performed at 25°C and 37°C and the red circles measurements at 50°C.

To our knowledge, this is the first time that ELR-adsorbed surfaces are extensively characterized for their responsive character towards external stimuli. There are two areas represented, or phases: (i) one represented by open squares and full circles and (ii) the other represented by full squares and full circles. Blue squares and red circles stand for 25°C/37°C and 50°C, and open/full symbols stand for a moderate hydrophobic (characteristic CA of 66.8±3.5°) or a completely wettable surface, respectively. The measurements performed have revealed the conditions of wettability transition for temperature, pH, and ionic strength: 50°C, 11, and 1.25 M, respectively. The transition was also revealed to be rapid and independent of the contribution of the other stimuli: an "all-or-nothing" response towards external stimuli. In other words, the wettability of these systems shifts from a moderate hydrophobic regimen to superhydrophilic only when a stimulus equals or exceeds the above mentioned values, and there is no evidence of cross-dependencies between the three variables. Therefore, observing Figure 8.5, one can easily identify the parameters of transition at room temperature and 50°C. In the former, the wettability shifts at pH 11 or ionic strength 1.25 M, as previously stated; in the latter, 50°C is already the temperature at which the wettability shifts, therefore any combination of the other two stimuli can be disregarded.

The measurements performed at 37°C are of particular interest for biomedical applications, since ultimately these coatings are intended to be used in a biological environment. In the graphic, the wettability of the surfaces at 37°C is similar to the case at room temperature, showing transitions dependent on pH and ionic strength at 11 and 1.25 M, respectively. However, our measurements showed that in the range of pH 10–11 and of ionic strength 1–1.25 M, intermediate values could be observed (CAs of 30.5 ±20.6°). Such behavior is an interesting one: upon heating an ELR in solution above the T_t, aggregation occurs and the solution becomes cloudy; given a few hours, or further increasing the temperature, the aggregates gradually settle and the result is a clean phase separation of solvent and polymer [52]. At the studied surfaces, the equivalent to this "cloudy point" could only be observed for this small range of values and the wettability shift is only fully achieved – and quickly, not gradually as in solution – for pH 11 and ionic strength 1.25 M, as is the case at room temperature. Thus, the diagram summarizes the response of the films ending in ELR-RGD as a function of three distinct variables, showing an independent and immediate effect of three of the parameters influencing the conformation of ELRs.

The molecular organization of a surface may give valuable information about the physical properties of a substrate. Figure 8.6 shows the surface roughness for the 5^{th} pair of layers assembled in glass, ending in either CHI (layer 9) or ELR-RGD (layer 10), and AFM images of $(CHI/ELR\text{-}RGD)_5$ films at physiological and transition pH values. An approach similar to that of contact angle measurement was followed: the samples were placed at room temperature in PBS buffered at two distinct pHs – 7.4 and 11 – and withdrawn for immediate topography image acquisition. We expected that with increasing pH the surface roughness would increase as well, due to the triggering mechanism of CHI and ELR-RGD transitions above each pK_a. The AFM images in Figure 8.6 show the topography changes of $(CHI/ELR\text{-}RGD)_5$ and reveal the formation of large and compact structures upon the aggregation of ELRs at the surface – "micelle-like" structures which increases the water affinity at the interface by the exposure of hydrophilic groups. In fact, such organization is predicted even by the earliest theories of the natural elastin conformation [53].

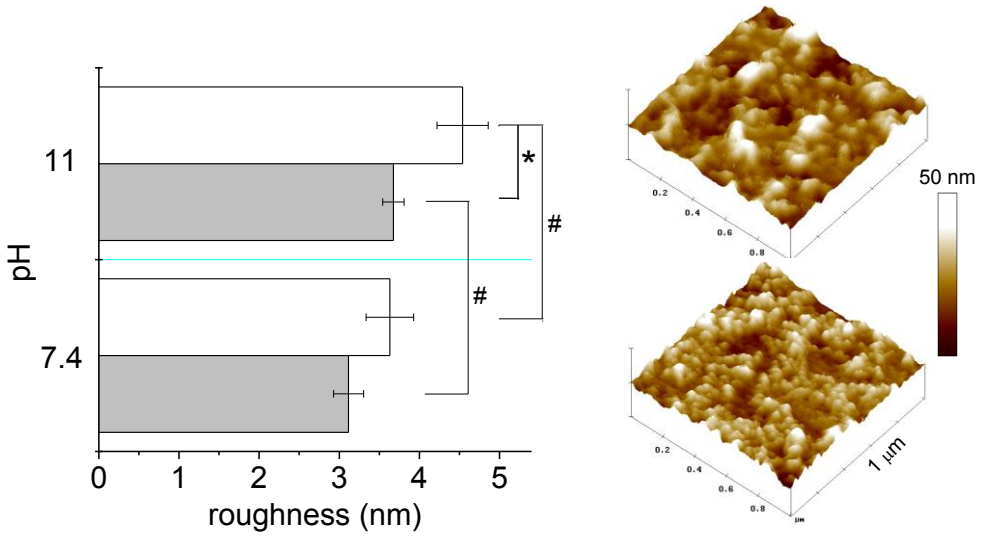


Figure 8.6. RMS-roughness of 5 pairs of CHI/ELR-RGD layers, ending in CHI (grey) and ELR-RGD (white). Error bars represent two standard deviations (n=3). The insets are AFM images at pH 7.4 and 11, for the 5th pair of layers, ending in ELR-RGD, in a 1×1 µm^2 area. Data are means±standard deviation (SD) (n=3; $p<0.05$, * are samples at the same pH, # are samples at different pH).

The analysis of the roughness showed that it increased with pH, from 3.6±0.3 nm to 4.9±0.3 nm ((root-mean-square roughness, RMS), showing that the topography of the films responded to pH changes, regardless of the last adsorbed layer. As a side note, the corresponding contact angle of the (CHI/ELR-RGD)$_4$CHI films displayed a value of 64.3±3.6° upon increasing the pH, higher than the value obtained for layer 9 due to the deprotonation of CHI. Such result reinforces the fact that the properties of a modified surface reflect mainly those of the material present at the interface, as is often expected upon after such approach. The effect of pH on roughness was greater when the last layer was composed of ELR-RGD, as evidenced by the higher values displayed at each condition. Such structural changes were more visible when the ELR-RGD is deposited as the last layer, since the macromolecular segments exhibit more degrees of freedom for conformational rearrangements. "pH" and ionic strength may influence the electrostatic interactions between each layer but similar results were obtained for temperature changes. We suggest that such similar results evidence that the aggregation of the ELR is the factor that contributes the most to the increase of roughness. Similar results were also obtained in previous studies [30].

The rough character of the surface also contributes to the atypical extreme hydrophilic nature of the substrate, based on a simple lotus effect. In fact, the Wenzel model predicts that the change from a

hydrophobic surface towards a more hydrophilic one is amplified in substrates exhibiting nano/micro scale roughness [54].

8.3.3 Cell culture studies of SaOS-2 osteoblast-like cells

Smart surfaces have been used in different fields in situations where it is relevant to control the adhesion of cells or microorganisms, protein adsorption or transport properties for the release of bioactive agents. In many cases, it is desirable that the substrate interacts favorably with cells. It has been reported that the RGD sequence is the minimal sequence required for recognition by cell membrane integrins, such as $\alpha5\beta1$ and $\alpha V\beta3$ integrins [55-57]. The affinity of cells for materials should be improved with the incorporation of a peptide having this sequence.

So far, we have been able to expand the concept of LbL to a class of materials that is not commonly used in literature. We also presented results showing that the films display distinct properties for different conditions of temperature, pH and ionic strength. This feature could be exploited to modulate protein and cell adhesion by playing with one of the mentioned stimuli. Unfortunately, the presented transition values are simply not suitable for most biological applications. We expect to take advantage on the recombinant nature of ELRs in the near future to produce films that could be triggered at lower values. Nonetheless, the biological performance of the current films was analyzed in order to determine if this kind of multilayer film is suitable for future tissue engineering devices with good response from cells, without any hazardous reaction.

In vitro studies were performed using SaOs-2 osteoblast-like cells. Although other possibilities could be explored, one of the uses we envisaged for these coatings is in orthopedic applications in order to improve host integration. To prove that the superior cell attachment was due to a specific interaction with RGD, the cell behavior was compared to surfaces with a negative control of ELR containing a scrambled RDG sequence, labeled $RDG^{(-)}$, in the form of 5 bilayers with CHI, $(CHI/ELR\text{-}RDG^{(-)})_5$. The scrambled RDG sequence has been previously shown to have significantly less cellular adhesion [58] and is similar to ELR-RGD in all aspects, except for the position of the G and D aminoacids.

The SaOs-2 cell viability on ELR-RGD and CHI ending films – $(CHI/ELR\text{-}RGD)_5$ and $(CHI/ELR\text{-}RGD)_4/CHI$ respectively – was assessed at different time points. Independently of the wettability changes of the coatings, cell culture was performed at 37°C, at which the surface is moderately hydrophobic (see Figure 8.5), under serum-free conditions. Cell viability and activity was assessed through MTS and ALP

assays. A qualitative evaluation of the cell number attached to the surfaces was performed using optic microscopy and with DAPI and phalloidin staining of cells.

Figure 8.7a shows the MTS assay in the different surfaces after 4 h, 24 h and 3 days (note: contact angles showed that the films still retain their properties during the studied time-frame).

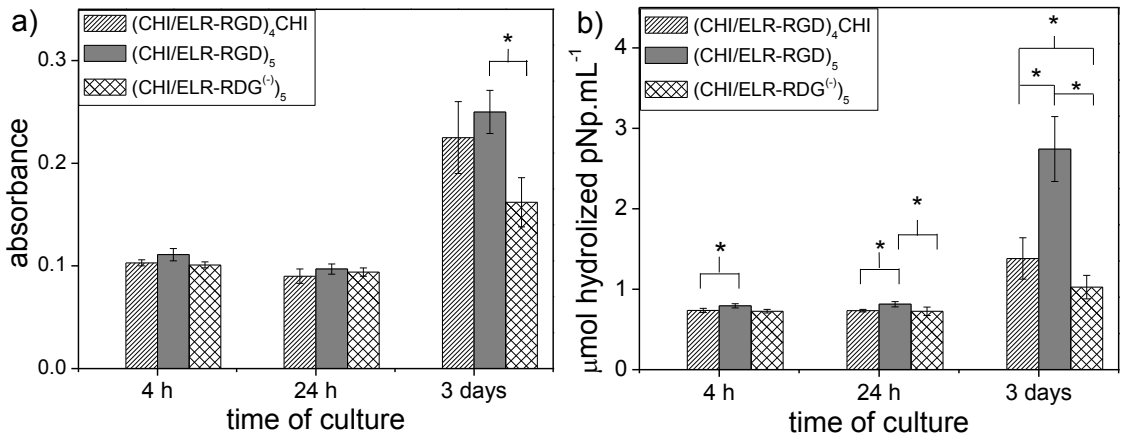


Figure 8.7. *In vitro* tests on films ending in CHI, ELR-RGD and ELR-RDG$^{(-)}$. a) Cell viability of SaOs-2 cells for 4 h, 24 h and 3 days. Data are means±SD (n=3; *p<0.05). b) ALP assays on the studied films. Data are means±SD (n=3; *p<0.05).

The results show that, for every time point, all tested samples are non-cytotoxic towards the SaOs-2 cell line, and therefore the materials used to construct the multilayers did not cause toxicity problems neither to the attached cells nor to the cells suspended in culture. Among the various biological functions of osteoblasts, secretion of ALP is an important indicator determining the activity of the cells. The statistical analysis of the data (Figure 8.7b) shows significant differences in SaOs-2 activity adhered to (CHI/ELR-RGD)$_5$ in comparison to (CHI/ELR-RGD)$_4$/CHI coatings, at 4 h, and (CHI/ELR-RDG$^{(-)}$)$_5$ and (CHI/ELR-RGD)$_4$/CHI at 24 h. After 3 days the differences in cell activity become more evident in the surface with ELR-RGD in comparison to films ending in ELR-RDG$^{(-)}$ or CHI.

Differences in the number of cells attached to the different surfaces were also observed, as seen in Figure 8.8.

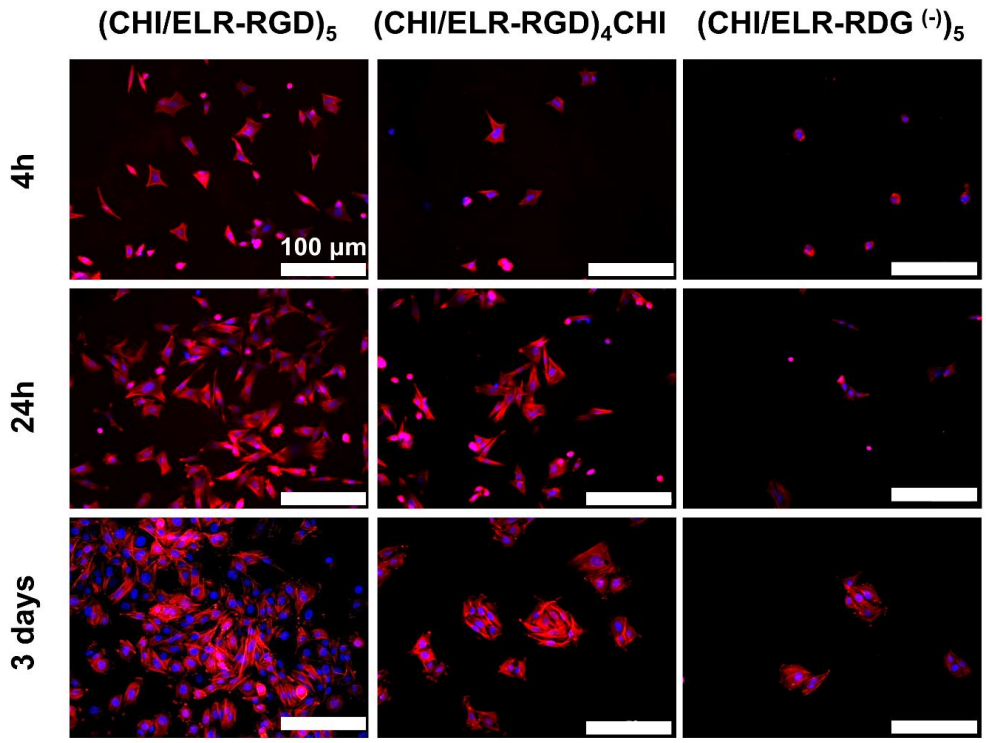


Figure 8.8. DAPI (blue) and phalloidin (red) staining of the studied cells cultured for distinct times on the studied multilayer substrates, ending in CHI, ELR-RGD and ELR-RDG$^{(-)}$. Tests performed at 4 h, 24 h, and 3 days. Scale bar: 100 µm.

Comparing the microscopy images, after 4 h of incubation, ELR-RGD surfaces show a significant attached number of cells, compared with non-modified surfaces or the negative analog RDG. Based on the cell densities of the samples at 24 hours and 3 days, it is possible to verify that (CHI/ELR-RGD)$_5$ coatings demonstrated a very significant cell proliferation in comparison to the coatings ending in CHI and in (RDG)$^{(-)}$. Besides the higher number of cells on the surfaces with RGD, cells seeded on those substrates spread significantly more than the ones on chitosan or the negative control. Thicker and well organized filamentous actin bundles were observed in cells growing on RGD surfaces. From our results, adsorption of ELR-RGD has shown to enhance cell adhesion and activity when compared to the CHI-ending films substrates and the scrambled RDG sequence, showing good *in vitro* performance of the presented films.

8.4 Conclusions

Our results show that ELRs containing biologically relevant peptide sequences can be successfully combined with CHI in a sequential multilayer approach based on electrostatic and hydrophobic interactions. QCM-D results allowed us to study the construction of the polymeric films and its properties, showing the buildup of a film with a linear growth. Although glass was used to assemble such coatings, it is expected in the future that such straightforward surface modification technique will allow us to coat other substrates with more complex geometries, including scaffolds or particles. The stimuli-responsive properties of the films were extensively studied, showing acute and independent cyclic response towards temperature, pH and ionic strength; the values of transition for each stimulus were identified: 50°C, 11, and 1.25 M, respectively. Below each critical transition point, the surfaces were more hydrophobic. Above those, the surface acquired a very hydrophilic character due to the biopolymer chain collapse and subsequent exposure of charged residues to the outer region of the coating. The transition was also evident in the changes in the topography of the surfaces as we increased the pH of the film above the transition values, increasing their roughness due to the aggregation of ELR chains on the top layer.

SaOs-2 osteoblast-like cells were used to test the biological performance of the multilayered system studied *in vitro* of the films. The cells showed increased adhesion and activity with ELR-RGD ending coatings, in comparison to the ones ending with both CHI and the non-bioactive ELR-RDG$^{(-)}$. This work demonstrates the potential to use natural and nature-inspired macromolecules to modify surfaces taking advantage of a simple layer-by-layer technique, which can be further extrapolated to more complex devices. The potential of this technology can further stimulate the development of other similar biomedical products in the near future, such as devices entirely processed through layer-by-layer for the delivery of pharmaceuticals, cell culture or structures for tissue engineering.

8.5 Acknowledgements

We acknowledge the financial support through Fundação para a Ciência e Tecnologia (FCT) from Portugal (PhD grants SFRH/BD/61126/2009 and SFRH/BD/61390/2009), the European regional development fund (ERDF) from EU, from the MICINN (projects MAT 2007-66275-C02-01, MAT 2007-61604, MAT 2009-14195-C03-03 and PSE-300100-2006-1), the JCyL (projects VA034A09 and

VA030A08), the CIBER-BBN (project CB06-01-0003), the JCyL and the Instituto de Salud Carlos III under the "Network Center of Regenerative Medicine and Cellular Therapy of Castilla and León".

8.6 References

[1] Falconnet D., Csucs G., Michelle Grandin H., and Textor M., Surface engineering approaches to micropattern surfaces for cell-based assays, Biomaterials 2006, 27: 3044-3063.

[2] Hook A. L., Voelcker N. H., and Thissen H., Patterned and switchable surfaces for biomolecular manipulation, Acta Biomaterialia 2009, 5: 2350-2370.

[3] Tirrell M., Kokkoli E., and Biesalski M., The role of surface science in bioengineered materials, Surface Science 2002, 500: 61-83.

[4] Alves N. M., Pashkuleva I., Reis R. L., and Mano J. F., Controlling Cell Behavior Through the Design of Polymer Surfaces, Small 2010, 6: 2208-2220.

[5] Levenberg S., and Langer R., Advances in Tissue Engineering, Current Topics in Developmental Biology 2004, 61: 113-134.

[6] Stevens M. M., and George J. H., Exploring and Engineering the Cell Surface Interface, Science 2005, 310: 1135-1138.

[7] Shi J., Alves N., and Mano J., Thermally Responsive Biomineralization on Biodegradable Substrates, Advanced Functional Materials 2007, 17: 3312-3318.

[8] da Silva R. M., López-Pérez P. M., Elvira C., Mano J. F., Román J. S., and Reis R. L., Poly(N-isopropylacrylamide) surface-grafted chitosan membranes as a new substrate for cell sheet engineering and manipulation, Biotechnology and Bioengineering 2008, 101: 1321-1331.

[9] Okano T., Yamada N., Sakai H., and Sakurai Y., A novel recovery system for cultured cells using plasma-treated polystyrene dishes grafted with poly(N-isopropylacrylamide), Journal of Biomedical Materials Research 1993, 27: 1243-1251.

[10] Xia F., Ge H., Hou Y., Sun T., Chen L., Zhang G., and Jiang L., Multiresponsive Surfaces Change Between Superhydrophilicity and Superhydrophobicity, Advanced Materials 2007, 19: 2520-2524.

[11] Delamarche E., Juncker D., and Schmid H., Microfluidics for Processing Surfaces and Miniaturizing Biological Assays, Advanced Materials 2005, 17: 2911-2933.

[12] Schild H. G., Poly(N-isopropylacrylamide): experiment, theory and application, Progress in Polymer Science 1992, 17: 163-249.

[13] Bertrand P., Jonas A., Laschewsky A., and Legras R., Ultrathin polymer coatings by complexation of polyelectrolytes at interfaces: suitable materials, structure and properties, Macromolecular Rapid Communications 2000, 21: 319-348.

[14] Decher G., Fuzzy Nanoassemblies: Toward Layered Polymeric Multicomposites, Science 1997, 277: 1232-1237.

[15] Sher P., Custódio C. A., and Mano J. F., Layer-By-Layer Technique for Producing Porous Nanostructured 3D Constructs Using Moldable Freeform Assembly of Spherical Templates, Small 2010, 6: 2644-2648.

[16] Boudou T., Crouzier T., Ren K., Blin G., and Picart C., Multiple Functionalities of Polyelectrolyte Multilayer Films: New Biomedical Applications, Advanced Materials 2010, 22: 441-467.

[17] Crouzier T., Ren K., Nicolas C., Roy C., and Picart C., Layer-By-Layer Films as a Biomimetic Reservoir for rhBMP-2 Delivery: Controlled Differentiation of Myoblasts to Osteoblasts, Small 2009, 5: 598-608.

[18] Shukla A., Avadhany S. N., Fang J. C., and Hammond P. T., Tunable Vancomycin Releasing Surfaces for Biomedical Applications, Small 2010, 6: 2392-2404.

[19] Tang Z., Wang Y., Podsiadlo P., and Kotov N. A., Biomedical Applications of Layer-by-Layer Assembly: From Biomimetics to Tissue Engineering, Advanced Materials 2006, 18: 3203-3224.

[20] Meyers M. A., Chen P.-Y., Lin A. Y.-M., and Seki Y., Biological materials: Structure and mechanical properties, Progress in Materials Science 2008, 53: 1-206.

[21] Meyer D. E., and Chilkoti A., Genetically Encoded Synthesis of Protein-Based Polymers with Precisely Specified Molecular Weight and Sequence by Recursive Directional Ligation: Examples from the Elastin-like Polypeptide System, Biomacromolecules 2002, 3: 357-367.

[22] Rodríguez-Cabello J. C., Martín L., Alonso M., Arias F. J., and Testera A. M., "Recombinamers" as advanced materials for the post-oil age, Polymer 2009, 50: 5159-5169.

[23] Urry D. W., Molecular Machines: How Motion and Other Functions of Living Organisms Can Result from Reversible Chemical Changes, Angewandte Chemie, International Edition in English 1993, 32: 819-841.

[24] Rodríguez-Cabello J. C., Alonso M., Díez M. I., Caballero M. I., and Herguedas M. M., Structural investigation of the poly(pentapeptide) of elastin, poly(GVGVP), in the solid state, Macromolecular Chemistry and Physics 1999, 200: 1831-1838.

[25] Arias F., Reboto V., Martín S., López I., and Rodríguez-Cabello J., Tailored recombinant elastin-like polymers for advanced biomedical and nano(bio)technological applications, Biotechnology Letters 2006, 28: 687-695.

[26] Nicol A., Channe Gowda D., and Urry D. W., Cell adhesion and growth on synthetic elastomeric matrices containing ARG-GLY–ASP–SER–3, Journal of Biomedical Materials Research 1992, 26: 393-413.

[27] Girotti A., Reguera J., Rodríguez-Cabello J., Arias F., Alonso M., and Testera A., Design and bioproduction of a recombinant multi(bio)functional elastin-like protein polymer containing cell adhesion sequences for tissue engineering purposes, Journal of Materials Science: Materials in Medicine 2004, 15: 479-484.

[28] Swierczewska M., Hajicharalambous C. S., Janorkar A. V., Megeed Z., Yarmush M. L., and Rajagopalan P., Cellular response to nanoscale elastin-like polypeptide polyelectrolyte multilayers, Acta Biomaterialia 2008, 4: 827-837.

[29] Barbosa J., Costa R., Testera A., Alonso M., Rodríguez-Cabello J., and Mano J., Multi-layered films containing a biomimetic stimuli-responsive recombinant protein, Nanoscale Research Letters 2009, 4: 1247-1253.

[30] Costa R. R., Custódio C. A., Testera A. M., Arias F. J., Rodríguez-Cabello J. C., Alves N. M., and Mano J. F., Stimuli-Responsive Thin Coatings Using Elastin-Like Polymers for Biomedical Applications, Advanced Functional Materials 2009, 19: 3210-3218.

[31] Ravi Kumar M. N. V., A review of chitin and chitosan applications, Reactive and Functional Polymers 2000, 46: 1-27.

[32] Alves N. M., and Mano J. F., Chitosan derivatives obtained by chemical modifications for biomedical and environmental applications, International Journal of Biological Macromolecules 2008, 43: 401-414.

[33] Meyer D. E., and Chilkoti A., Purification of recombinant proteins by fusion with thermally-responsive polypeptides, Nat Biotech 1999, 17: 1112-1115.

[34] Girotti A., Reguera J., Arias F. J., Alonso M., Testera A. M., and Rodríguez-Cabello J. C., Influence of the Molecular Weight on the Inverse Temperature Transition of a Model Genetically Engineered Elastin-like pH-Responsive Polymer, Macromolecules 2004, 37: 3396-3400.

[35] Hook F., Kasemo B., Nylander T., Fant C., Sott K., and Elwing H., Variations in Coupled Water, Viscoelastic Properties, and Film Thickness of a Mefp-1 Protein Film during Adsorption and Cross-

Linking: A Quartz Crystal Microbalance with Dissipation Monitoring, Ellipsometry, and Surface Plasmon Resonance Study, Analytical Chemistry 2001, 73: 5796-5804.

[36] Marx K. A., Quartz Crystal Microbalance: A Useful Tool for Studying Thin Polymer Films and Complex Biomolecular Systems at the Solution-Surface Interface, Biomacromolecules 2003, 4: 1099-1120.

[37] Notley S. M., Eriksson M., and Wågberg L., Visco-elastic and adhesive properties of adsorbed polyelectrolyte multilayers determined in situ with QCM-D and AFM measurements, Journal of Colloid and Interface Science 2005, 292: 29-37.

[38] Voinova M. V., Rodahl M., Jonson M., and Kasemo B., Viscoelastic Acoustic Response of Layered Polymer Films at Fluid-Solid Interfaces: Continuum Mechanics Approach, Physica Scripta 1999, 59: 391.

[39] Park E. J., Draper D. D., and Flynn N. T., Adsorption and Thermoresponsive Behavior of Poly(N-isopropylacrylamide-co-N,N'-cystaminebisacrylamide) Thin Films on Gold, Langmuir 2007, 23: 7083-7089.

[40] Cini N., Tulun T., Decher G., and Ball V., Step-by-Step Assembly of Self-Patterning Polyelectrolyte Films Violating (Almost) All Rules of Layer-by-Layer Deposition, Journal of the American Chemical Society 2010, 132: 8264-8265.

[41] Klitzing R. V., Internal structure of polyelectrolyte multilayer assemblies, Physical Chemistry Chemical Physics 2006, 8: 5012-5033.

[42] Picart C., Lavalle P., Hubert P., Cuisinier F. J. G., Decher G., Schaaf P., and Voegel J. C., Buildup Mechanism for Poly(l-lysine)/Hyaluronic Acid Films onto a Solid Surface, Langmuir 2001, 17: 7414-7424.

[43] Fothergill-Gilmore L. A., Peptide Sequence Determination, In Franks F., ed. Protein Biotechnology: Isolation, Characterization, and Stabilization, Totowa NJ, USA: Humana Press; 1993.

[44] Peter M. G., Applications and Environmental Aspects of Chitin and Chitosan, Journal of Macromolecular Science, Part A: Pure and Applied Chemistry 1995, 32: 629 - 640.

[45] Fischer P., Laschewsky A., Wischerhoff E., Arys X., Jonas A., and Legras R., Polyelectrolytes bearing azobenzenes for the functionalization of multilayers, Macromolecular Symposium 1999, 137: 1-24.

[46] Mano J. F., Stimuli-responsive polymeric systems for biomedical applications, Advanced Engineering Materials 2008, 10: 515-527.

[47] Noh H., and Vogler E. A., Volumetric interpretation of protein adsorption: Mass and energy balance for albumin adsorption to particulate adsorbents with incrementally increasing hydrophilicity, Biomaterials 2006, 27: 5801-5812.

[48] Fu J., Ji J., Yuan W., and Shen J., Construction of anti-adhesive and antibacterial multilayer films via layer-by-layer assembly of heparin and chitosan, Biomaterials 2005, 26: 6684-6692.

[49] Yoo D., Shiratori S. S., and Rubner M. F., Controlling Bilayer Composition and Surface Wettability of Sequentially Adsorbed Multilayers of Weak Polyelectrolytes, Macromolecules 1998, 31: 4309-4318.

[50] Azzaroni O., Brown A. A., and Huck W. T. S., UCST Wetting Transitions of Polyzwitterionic Brushes Driven by Self-Association, Angewandte Chemie, International Edition in English 2006, 118: 1802-1806.

[51] Reguera J., Urry D. W., Parker T. M., McPherson D. T., and Rodríguez-Cabello J. C., Effect of NaCl on the Exothermic and Endothermic Components of the Inverse Temperature Transition of a Model Elastin-like Polymer, Biomacromolecules 2007, 8: 354-358.

[52] Urry D. W., Physical Chemistry of Biological Free Energy Transduction As Demonstrated by Elastic Protein-Based Polymers, Journal of Physical Chemistry B 1997, 101: 11007-11028.

[53] Weis-Fogh T., and Andersen S. O., New Molecular Model for the Long-range Elasticity of Elastin, Nature 1970, 227: 718-721.

[54] Wenzel R. N., Resistance of solid surfaces to wetting by water, Industrial and Engineering Chemistry 1936, 28: 988-994.

[55] Berg M. C., Yang S. Y., Hammond P. T., and Rubner M. F., Controlling mammalian cell interactions on patterned polyelectrolyte multilayer surfaces, Langmuir 2004, 20: 1362-1368.

[56] Chua P.-H., Neoh K.-G., Kang E.-T., and Wang W., Surface functionalization of titanium with hyaluronic acid/chitosan polyelectrolyte multilayers and RGD for promoting osteoblast functions and inhibiting bacterial adhesion, Biomaterials 2008, 29: 1412-1421.

[57] Ruoslahti E., RGD and other recognition sequences for integrins, Annual Review of Cell and Developmental Biology 1996, 12: 697-715.

[58] Liu J. C., and Tirrell D. A., Cell response to RGD density in cross-linked artificial extracellular matrix protein films, Biomacromolecules 2008, 9: 2984-2988.

Chapter 9. Nanostructured and thermoresponsive recombinant biopolymer-based microcapsules for the delivery of active molecules[9]

Abstract

Multilayer capsules conceived at the nano- and micro-scales are receiving increasing interest due to their potential role as carriers of biomolecules for drug delivery and tissue engineering. Herein we report the construction of microcapsules by the sequential adsorption of chitosan and a biomimetic elastin-like recombinamer into nanostructured layers on inorganic microparticle templates. The release profile of bovine serum albumin, which was studied at 25 and 37°C, shows higher retention and Fickian diffusion at physiological temperature. The self-assembled multilayers act as a barrier and allowed for sustained release over 14 days. The capsules studied are non-cytotoxic towards L929 cells, thereby suggesting multiple applications in the fields of biotechnology and bioengineering, where high control of the delivery of therapeutics and growth/differentiation factors is required.

[9] This chapter is based on the following publication:

Costa R. R., Custódio C. A., Arias F. J., Rodríguez-Cabello J. C., and Mano J. F., Nanostructured and thermoresponsive recombinant biopolymer-based microcapsules for the delivery of active molecules, Nanomedicine: Nanotechnology, Biology and Medicine 2013, 9 : 895-902, DOI:10.1016/j.nano.2013.01.013.

9.1 Introduction

Recent advances in biomedicine have been driven by the need to develop systems that can effectively encapsulate, protect and deliver an active agent with specific kinetics [1-5]. Such need comes at a time when various classes of biomolecules of interest for the treatment of several diseases and the development of new biomedical devices are becoming widely available. With this increasing availability, the use of smart materials to control the delivery and release of specific agents has followed a similar trend.

Ideally, a biomolecule carrier should act as a compartment in which the permeability of a drug to the exterior can be tuned as this would allow the release rate to be controlled when concerning both therapeutics in traditional drug-delivery applications as well as tissue engineering agents that influence the proliferation and differentiation of cells. The layer-by-layer (LbL) self-assembly of macromolecules – a simple, versatile and inexpensive surface-engineering technique that can be used, under mild conditions, to encapsulate sensitive active agents and biomaterials by either manipulating the architecture of a device or by way of external stimuli – is an approach with the potential to address this issue. These "capsules" could then deliver the encapsulated agents to the target cells by making use of simple release mechanisms into the biological environment [6-9] or by digestion of the cells themselves [10-13]. Although often applied to flat surfaces, LbL can be used to coat surfaces with complex geometries and shapes and can be extrapolated to three dimensions [14-19]. Hollow multilayer capsules are a good example of 3D structures that can act as drug carriers. Inorganic particles are typically used as templates for this purpose as they can be chelated under non-aggressive conditions [20-22]. The use of LbL techniques will therefore ultimately allow control of both the release profile of a specific agent and the permeability of the system by varying the materials and number of layers in the capsule architecture.

The concept of post-construction permeability is of great interest for drug-delivery and tissue-engineering applications as a carrier must be able to retain and preserve the drug but also release it when necessary and in a controlled fashion. An ability to switch the permeability of a multilayer capsule between an "open" and a "closed" state has been demonstrated previously [23-25], but has yet to be fully validated. Temperature, for example, has been suggested to be a possible mechanism for post-loading therapeutic agents using temperatures as high as 50 to 70°C [26-30]. However, such temperatures are not suitable for biological applications. Herein we intend to demonstrate the

entrapping properties of self-assembled coatings with varying numbers of nanolayers combined with the response of a biocompatible system towards an external temperature-based stimulus.

In light of the likely benefits of natural and nature-inspired biomaterials combined with stimuli-responsiveness [31,32], we aimed to construct a new generation of therapeutic containers using a multilayer approach. Chitosan (CHI) and a biomimetic elastin-like recombinamer (ELR) – a recombinant version of elastin-like polymers (ELPs) – were used as constituents for the microcapsule shell. CHI is a well-known natural material with cationic behavior [33]. whereas ELRs are genetically engineered polypeptides that mimic natural elastin and exhibit a primary smart response towards temperature. These recombinant macromolecules are soluble below a specific critical transition temperature (T_t) in an aqueous medium, but undergo a phase separation characterized by the dominant presence of hydrogen bonds and hydrophobic interactions above it [34-38]. They also allow fine control over the peptide structure, thus making it possible to introduce motifs with biological relevance, such as cell-adhesion and mineralization promoters, into their primary valine-proline-glycine-valine-glycine (VPGVG) sequence [14,39,40].

The primary structure of the ELR used herein was designed to present a bioactive behavior by the inclusion of L-arginine-glycine-L-aspartic acid (RGD) residues, while exploiting the negative aspartic acid moieties to enable subsequent self-assembly with chitosan into nanostructured multilayers (schematic structure can be found in Supplemental Figure 9.1). The present work focuses on our ability to construct CHI/ELR microcapsules and to use the temperature-responsive nature of ELRs to control the permeability of engineered multilayer systems. The resulting microcapsules were characterized for their encapsulation efficiency of a model protein, namely bovine serum albumin (BSA). The permeability of the BSA-loaded microcapsules with a varying number of layers was studied at 25 and 37°C, and the biocompatibility of these structures was evaluated *in vitro*.

9.2 Experimental section

9.2.1 Materials for the microcapsule composition

Medium molecular weight chitosan was purchased from Sigma (reference 448877) and purified by a series of filtration and precipitation in water and ethanol steps, followed by freeze-drying. ELR bioproduction was induced using a fermentation process from an *Escherichia coli* strain BLR(DE3) containing the appropriate expression gene. Subsequent to fermentation, the culture was harvested and

lysed by ultrasonic disruption. Insoluble debris was removed by centrifugation and the cleared lysate was subjected to several cycles of cold and warm centrifugations. The polymer in solution was stored at -24°C and then freeze-dried. The detailed methodology has been described previously [35].

9.2.2 ELR aggregate-size measurements

ELR aggregate size was measured using a Nano-ZS from Malvern (United Kingdom) in the temperature range 25–37°C after stabilization for 5 minutes. Samples were prepared at 300 $\mu g \cdot mL^{-1}$ in phosphate buffer solution (PBS, Sigma reference P4417), pH 7.4. A total of 20 runs were performed for each sample to obtain a final average value at constant temperature.

9.2.3 Entrapment of BSA in calcium carbonate particles

BSA entrapment was achieved following the method described by She *et al.* [8]. Thus, to encapsulate 1 mg of BSA, aqueous solutions of anhydrous sodium carbonate (Na_2CO_3 granular, ≥99.5%, Sigma reference 222321) and calcium chloride ($CaCl_2$ anhydrous powder Reag. Ph Eur, VWR reference 1.02378.0500) were prepared at 1 M. Co-precipitation of both solutions was performed by adding 100 µL of Na_2CO_3 followed by 100 µL of $CaCl_2$ to 200 µL of BSA tagged with fluorescein isothiocyanate (FITC) (66 kDa, Sigma reference A9771) at 5 $mg \cdot mL^{-1}$ and stirring rapidly for 30 seconds. Stirring was then stopped and the suspension of newly synthesized calcium carbonate ($CaCO_3$) microparticles left to react and precipitate for 15 min. The supernatant was then removed and the particles washed twice with ultrapure water to remove residual salts and non-entrapped protein. Each supernatant was retained for fluorescence measurements and determination of entrapment losses.

9.2.4 Construction of the multilayer shells and microcapsule formation

The $CaCO_3$ sacrificial templates entrapping FITC-BSA were immersed alternately in chitosan and ELR solutions [300 $\mu g \cdot mL^{-1}$, pH 5.5, 0.15 M of sodium chloride (NaCl, Reag. Ph Eur, Panreac reference 131659] for 10 min each, then washed with 0.15 M NaCl (pH 5.5). Centrifugation was avoided to avoid damage and aggregation of the particles each time the samples were to be retrieved from solution; simple precipitation of the suspension was used instead (3 to 5 min). This process was repeated to increase the number of bilayers until the desired coating had been obtained (1, 3 and 5 bilayers). After construction, the $CaCO_3$ core was removed by chelation with ethylenediamine tetraacetic acid (EDTA

powder, ACS reagent, 99.4–100.6%, Sigma reference E9884; 0.2 M, pH 5.5). Each supernatant and solution was retained for fluorescence measurements and determination of losses during the construction and chelation stages.

9.2.5 Determination of pre-loading encapsulation efficiency

Fluorescence measurements were performed using a Synergie HT microplate ELISA reader (BioTek, USA). Thus, 150 μL of sample was pipetted into a white, opaque 96-well plate in triplicate. Distilled water was used as blank. The excitation (λ_{exc}) and emission (λ_{em}) wavelengths used for the calibration curve and FITC-BSA mass calculations were 485 and 528 nm, respectively. All supernatants collected during entrapment, construction and chelation were measured and quantified. The percentage of fluorescein isothiocyanate (FITC)-BSA mass lost was plotted both for each stage and cumulatively. The encapsulation efficiency was calculated by subtracting the cumulative losses of each architecture from the initial FITC-BSA mass.

9.2.6 In vitro biological performance

A murine fibroblast cell line (L929, European Collection of Cell Cultures) was used for the biological assays. Thus, L929 cells were cultured in Dulbecco's modified Eagle's medium (DMEM, Invitrogen reference 42400-028) with phenol red supplemented with 10% of fetal bovine serum (FBS, Invitrogen, reference 10270-106) and 1% antibiotic/antimicotic (Gibco reference 15240062) in a humidified atmosphere with 5% carbon dioxide (CO_2) at 37°C. For the cell viability test, 2×10^3 cells were seeded on 48-well plates and incubated at 37°C, 5% CO_2. After 24 hours, microcapsules were added to the culture medium in a ratio of 40 microcapsules per cell. After each culturing period, samples were washed twice with phosphate-buffered saline (PBS). A 250 μL aliquot of fetal bovine serum (FBS)-free culture medium and 50 μL of (3-(4,5-dimethylthiazol-2-yl)-5-(3-carboxymethoxyphenyl)-2-(4-sulfophenyl)-2*H*-tetrazolium) (MTS) reagent were added to each well. A cell-free well was used as control. Plates were incubated for 3 h at 37°C, 5% CO_2, protected from light. After incubation, 100 μL of this solution was transferred to a 96-well plate and the plate read using a Synergie HT microplate ELISA reader (BioTek, USA) in 490 nm absorbance mode.

Visualization of the actin cytoskeleton was performed using (tetramethylrhodamine B isothiocyanate)-phalloidin (TRITC-phalloidin, Sigma reference P1951). After each culture period, samples were washed

twice with PBS and fixed with 4% formalin in PBS for 15 min at room temperature. After fixation, cells were incubated with TRITC-phalloidin (10 $\mu g \cdot mL^{-1}$) for 45 min and washed three times with PBS. To stain the nucleus, the cells were incubated with 4',6-diamidino-2-phenylindole (DAPI, Sigma reference D9564) (1 $\mu g \cdot mL^{-1}$) for 5 min then washed with PBS. Cells were observed under an Axioimager Z1M Zeiss fluorescence microscope (Zeiss, Germany).

9.2.7 Quantification of FITC-BSA release

The microcapsules were resuspended in PBS at either 25 or 37°C. The upper limit of five bilayers for the microcapsule architecture was chosen to study the effect of temperature along with small changes in the number of different layers. This study was conducted over 14 days, removing the surrounding PBS from each container every 24 h. An additional sample was taken after 12 h from the start of the study. PBS was fully refreshed at each time point, and 100% BSA was considered to be the total mass remaining in the microcapsules after their construction. The release experiments were performed under mild agitation to improve the diffusion of BSA through the incubating medium. All experiments were performed in triplicate (n=3), with each sample containing the number of capsules resulting from the attempted encapsulation of 1 mg of BSA. To determine the type of release profile for each condition, the release kinetics were determined using the Korsmeyer kinetic model (equation 9.1):

$$M_t / M_\infty = Kt^n \qquad (9.1)$$

where M_t / M_∞ is the fraction of protein released at time t, K is the rate constant for the Korsmeyer model, and n is the exponent that characterizes the release mechanism [41]. The Korsmeyer model is used when the release mechanism from a swellable polymeric device is not well-known or when more than one type of release phenomenon could be involved. The fitting was performed for all architectures and for each temperature.

9.2.8 Microscopy characterization of the $CaCO_3$ microparticles and multilayered microcapsules

A Leica Cambridge S360 scanning electron microscope (United Kingdom) was used to evaluate the morphology of the sacrificial templates. Specimens were pre-coated with a conductive layer of sputtered gold and micrographs recorded at 10 kV. An Olympus FV1000 confocal laser scanning microscope (CLSM, Germany) was used to evaluate the morphology of $(CHI/ELR)_5$ microcapsules loaded with FITC-

BSA. A final layer consisting of a cationic dye (rhodamine B, 10^{-6} M) was further adsorbed. All samples were stabilized at either 25 or 37°C and observed under hydrated conditions.

9.3 Results

In order to evaluate the thermal response of the featured ELR, the size variations of peptide aggregates in aqueous solution were measured as a function of temperature. The results, which are plotted in Figure 9.1, show an increase in aggregate size from around 10 to 3000 nm in aqueous PBS solution. This variation occurs at a T_t of 29°C and is accompanied by an increase in solution turbidity, thus showing that this ELR possesses a T_t in solution above the working room temperature and below the physiological one of 37°C.

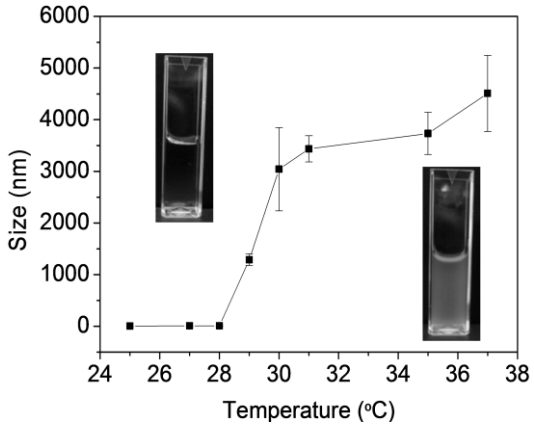


Figure 9.1. Aggregate size profile for a 300 μg·mL^{-1} ELR solution in PBS over the temperature range 25–37°C. Means±standard deviation (SD) are represented. Insets show a transparent solution below 29°C and increased turbidity above it.

$CaCO_3$ particles were prepared by co-precipitation of Na_2CO_3 and $CaCl_2$ solutions under vigorous stirring in a BSA medium and subsequently tagged with FITC. The resulting inorganic particles, with a diameter of around 5-6 μm (Figure 9.2A), were used as BSA-containing sacrificial templates for the alternating incubation with aqueous chitosan and ELR solutions. After construction, the core was chelated with EDTA to form hollow microcapsules, as confirmed by CLSM Figure 9.2B).

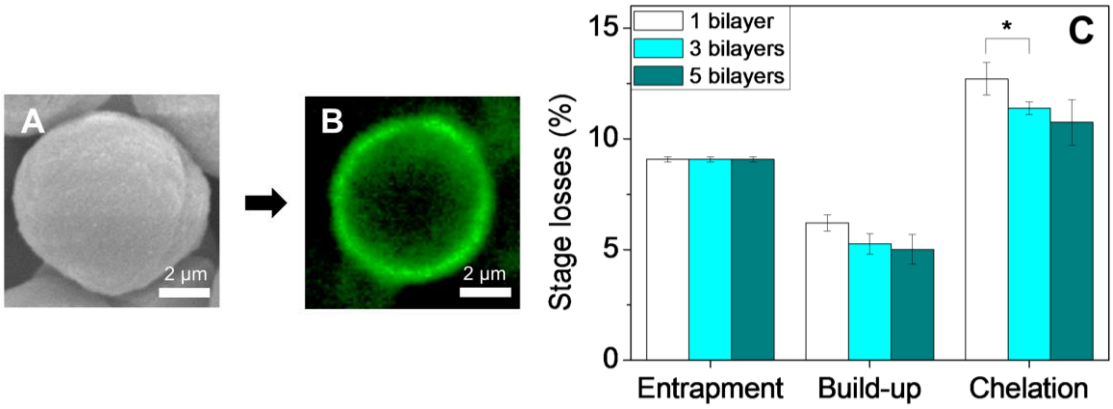


Figure 9.2. (A) SEM image of a $CaCO_3$ microparticle containing entrapped BSA. (B) CLSM image of a microcapsule containing FITC-BSA after chelation. (C) A graphic showing the stage losses measured during construction of the microcapsules. Data represent mean±SD (n=3; *p<0.05).

Structures with one, three and five bilayers, henceforth referred to as $(CHI/ELR)_1$, $(CHI/ELR)_3$ and $(CHI/ELR)_5$, were constructed to study the effects of capsule architecture on the subsequent release of BSA at 25 and 37°C. In order to determine the total encapsulation efficiency, the fluorescence of each supernatant was measured at each stage and the losses calculated with respect to the initial FITC-BSA content in the precipitation medium (1 mg). Although a loss of 9% was registered during the entrapment stage (Figure 9.2C), losses during the construction stage were higher for capsules with fewer layers. The effect of the shell architecture became more evident during the chelation stage, with our observations showing a "burst-release" of 13% for $(CHI/ELR)_1$ and 10% for $(CHI/ELR)_5$.

CLSM images of $(Chi/ELR)_5$ microcapsules at 25 and 37 °C are shown in Figure 3. The capsules are significantly smaller at 37 °C (Figure 9.3B, 3.21±0.63 µm) than at 25 °C (Figure 9.3A, 5.51±0.56 µm), most probably due to a layer rearrangement as a result of the effect of different solvent temperatures on the stimuli-responsive ELR molecules.

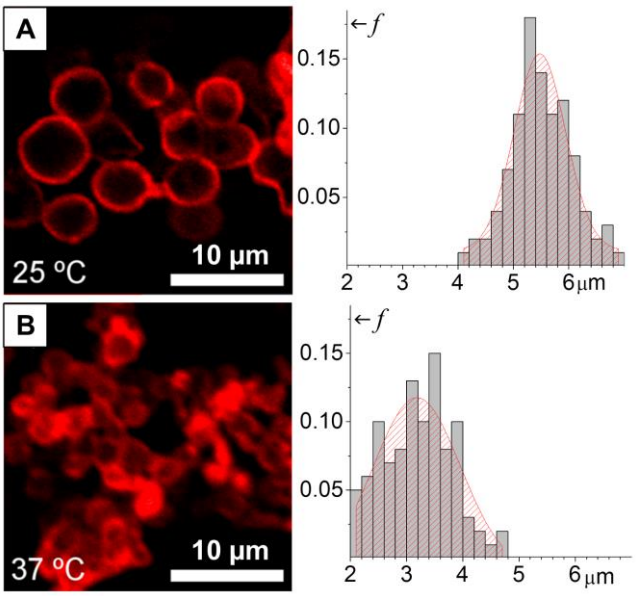


Figure 9.3. Left: CLSM images of pre-loaded $(CHI/ELR)_5$ microcapsules at (A) 25 and (B) 37°C. The final layer was tagged with rhodamine B. Right: size distribution and fractional frequency (f). The normal distribution approximation, which fits a 95% confidence interval, is depicted.

The cytotoxicity of these microcapsules was determined to ascertain whether they could be used in biological systems. Thus, an *in vitro* biological evaluation was carried out using the L929 mouse fibroblast cell line. The cell viability was assessed by MTS after culture in a microcapsule-containing medium (either loaded with BSA or unloaded). The graphic in Figure 9.4A shows a quantitative comparison with the lone L929 control and confirms that the cells cultured in the presence of $(CHI/ELR)_5$ retained their viability at every time-point (24 h, 3 days and 7 days). Furthermore, fluorescence microscopy of cells cultured in the absence (Figure 9.4B) and presence (Figure 9.4C) of BSA-loaded $(CHI/ELR)_5$ microcapsules confirmed that the cell morphology remained unchanged when in contact with the microcapsules. This was the case for both BSA-loaded and -free microcapsules.

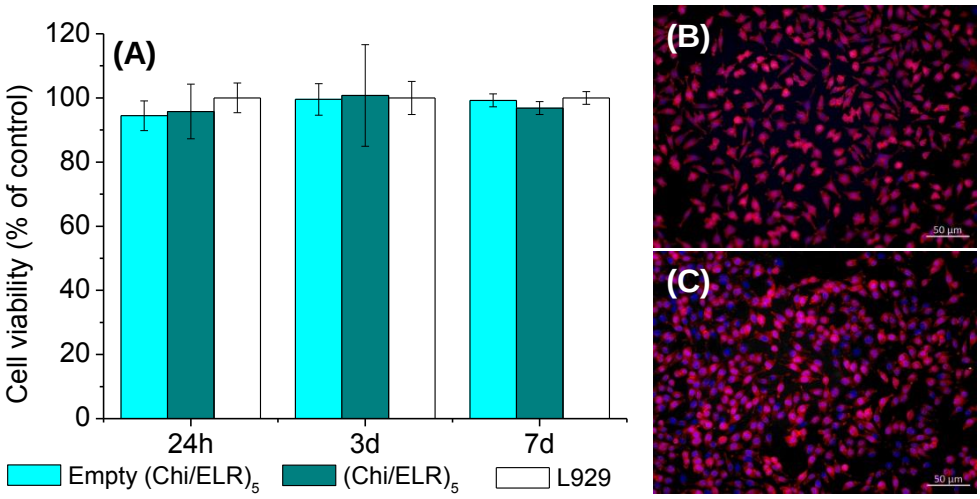


Figure 9.4. (A) Viability of L929 cells after 24 h and 3 and 7 days in the presence of empty and BSA-loaded $(CHI/ELR)_5$ microcapsules. The positive control was L929 cells in the same medium with no microcapsule addition. Data represent mean±SD (n=3; *$p<0.05$). DAPI (blue) and phalloidin (red) staining in fluorescence microscopy of L929 cells after contact with (B) microcapsule-free medium and (C) BSA-loaded $(CHI/ELR)_5$ microcapsules for 24 hours. Scale bar: 50 µm.

The ability to retain an active agent and protect it until delivery is one of the most important features of a drug-delivery system. Our results showed BSA retentions of greater than 70% of the initial 1 mg after construction of the microcapsules, with cumulative losses of 28%, 26% and 25% for $(Chi/ELR)_1$, $(CHI/ELR)_3$ and $(CHI/ELR)_5$, respectively (see Figure 9.2C for stage losses, and Supplemental Figure 9.3 and Supplemental Table 9.1 for detailed cumulative calculations). However, an ability to release this active agent in a controlled manner after encapsulation is equally important. As such, the influence of the total number of layers and temperature on the release profile of BSA from the capsules was investigated. BSA release at different temperatures was studied over a period of 14 days, and the cumulative release profiles for $(CHI/ELR)_1$, $(CHI/ELR)_3$ and $(CHI/ELR)_5$ capsules loaded with BSA at room (25°C) and physiological temperatures (37°C) can be seen in Figure 9.5.

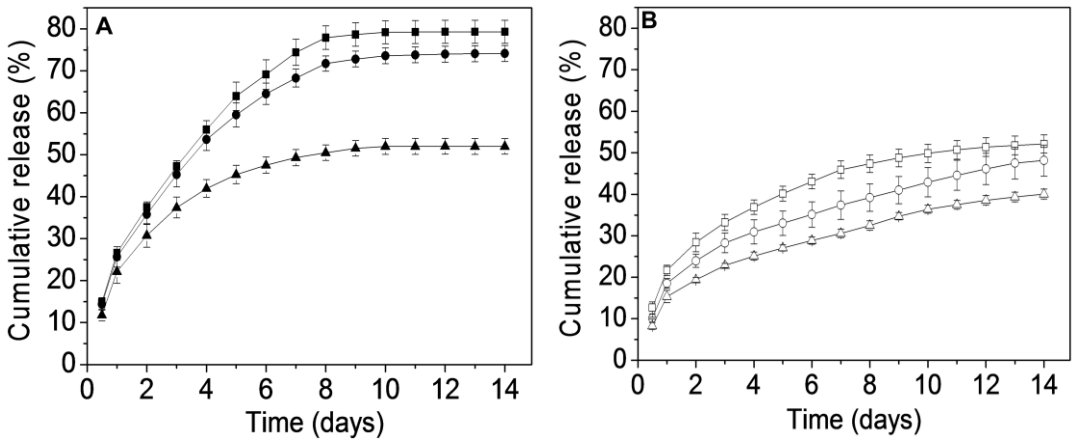


Figure 9.5. Cumulative release of BSA from $(CHI/ELR)_1$, $(CHI/ELR)_3$ and $(CHI/ELR)_5$ microcapsules: ■□, ○●, and ▲Δ, respectively, in PBS (pH 7.4), at (A) 25°C and (B) 37°C.

During this sub-study, 100% of BSA was considered to be the total mass remaining in the microcapsules after their construction. The estimated number of microcapsules in each tested sample was approximately 8×10^8, as calculated by dividing the volume occupied by the precipitated microcapsules (around 70 μL) and the volume occupied by a single microcapsule (diameter of 5.51 μm), disregarding the empty spaces between them. PBS was fully refreshed at each time point, in order to simulate a biological environment in which the delivered therapeutic agent is taken up by the targeted cells. Irrespective of the temperature and number of layers, an initial analysis of the profiles shows that BSA release is sustained over the period studied, with a visible absence of significant burst release at the initial time-points. The release kinetics were markedly influenced by the temperature (see rate constants, *K*, in Table 9.1), with smaller quantities of released FITC-BSA being detected from microcapsules incubated at 37°C. In the case of the more permeable $(CHI/ELR)_1$ capsules, these structures showed a cumulative release of 79% at 25°C after 14 days in PBS, while a value of 52% was obtained at 37°C. The same trend was observed for $(CHI/ELR)_3$ and $(CHI/ELR)_5$.

Release was also dependent on the number of layers in the capsule architecture. Thus, irrespective of the temperature, more layers resulted in greater BSA retention. This finding confirms the shell's ability to act as a tunable barrier against the diffusion of an encapsulated agent. The Fickian or non-Fickian release behavior of BSA was given by the exponent of the Korsmeyer kinetics model, *n*, shown in Table 9.1.

Table 9.1. Exponents of the Korsmeyer kinetics model (n), correlation factors (r^2) and rate constant (K) for each architecture studied.

	25°C			37°C		
Number of bilayers	K	n	r^2	K	n	r^2
1	1.41	0.49	0.95	1.30	0.40	0.96
3	1.39	0.48	0.95	1.22	0.42	0.97
5	1.32	0.41	0.91	1.14	0.43	0.98

Fitting with other models (zero-order, first-order and Higuchi) can be found in the Supplementary Information (Supplemental Figure 9.6 to Supplemental Figure 9.11). The data for capsules incubated at 25°C fit an anomalous (non-Fickian) mode of diffusion ($n > 0.43$), thus suggesting a combination of pure protein diffusion and shell relaxation/swelling mechanisms under these conditions. The $(CHI/ELR)_5$ capsules were an exception to this, with a Fickian mode of diffusion ($n < 0.43$). The capsules also follow a Fickian diffusion model at 37°C. In comparison to the capsules at 25°C, a pure diffusion mechanism occurs under physiological conditions. This effect results from the restructuration of the film which occurs upon deposition of each additional layer [42]. The result is a more densely packed multilayer structure with decreasing polymeric mobility and no anomalous relaxation/swelling mechanism, together with a more compact and stable shell.

9.4 Discussion

The development of drug-delivery systems that can encapsulate, protect and deliver a therapeutic molecule or growth factor in a controlled fashion is of major importance for both current healthcare applications and in the fields of tissue engineering and regenerative medicine. Herein we have exploited temperature and the smart response of ELRs as an actual drug-release mechanism for a pre-encapsulated model protein. Furthermore, our aim was to develop a system that is able to respond at a temperature which will be useful for future applications in human biological studies.

We have conceived and developed biocompatible thermoresponsive microcapsules by taking advantage of the self-assembly properties of chitosan and an ELR using a multilayer approach. The fact that the majority of LbL studies performed to date have involved conventional polyelectrolytes has hindered the extrapolation of this technology to systems exhibiting other capabilities and complexities, including those

that could respond to external stimuli. We have previously demonstrated that, unlike most conventional multilayer combinations, combining these two materials is more favorable when both electrostatic and hydrophobic interactions are exploited, thus allowing for the construction of films as thin as 40 nm (considering a total of five bilayers) [43]. This is feasible if construction is performed under conditions close to the pK_a of the polysaccharide, where both protonated and deprotonated groups can be used. Our results, especially those observed in CLSM (Figure 9.2B and Figure 9.3), demonstrate that it is possible to extrapolate this technology from 2D to 3D and to construct micrometric devices using a non-conventional combination of polymers.

In order to determine the pre-encapsulation efficiency (see Figure 9.2C), all three construction stages were screened for each architecture [$(CHI/ELR)_1$, $(CHI/ELR)_3$ and $(CHI/ELR)_5$]. There was no difference between any of the cases studied during the entrapment stage. Note that at this stage the shell has not yet been assembled, thus meaning that the encapsulation efficiency is solely dependent on the protein/$CaCO_3$ interaction, which at this point in the process is common for all groups. In the following construction stage, and in contrast to our expectations, the losses were higher for thinner capsules. As more adsorption steps and manipulation are involved as construction proceeds, we expected to find higher protein losses for $(CHI/ELR)_5$ microcapsules since BSA should diffuse continuously from the sacrificial core, even if only in insignificant quantities. The explanation for our finding may reside in the fact that the protein lost to the polymer incubation solutions may be retaken up during the addition of subsequent layers to the shell. Indeed, using CLSM we were able to identify a high concentration of FITC-BSA near the capsule shell (see Figure 9.2B). As for the chelation stage, although there is a statistically significant difference between $(CHI/ELR)_1$ and $(CHI/ELR)_3$, the numerical difference is not meaningful (12.7% vs. 11.3%, respectively). Thicker capsules are also able to retain more protein than those with a lower number of bilayers since multilayer shells can act as barriers that hinder the diffusion of molecules from the inner cavity to the surrounding medium [8].

The microcapsules described herein have been shown to undergo temperature-dependent size variations, with two possible shrinkage mechanisms explaining the shrinkage observed upon increasing the temperature. Thus, as discussed previously, the ELR collapses to a more ordered, self-assembled state upon increasing temperature above T_t [35-37], although it is also likely that shrinkage is further amplified by a thermodynamic rearrangement of the layers. Such a rearrangement is driven by the tendency of shells with an even number of layers (1:1 ratio of electrostatic forces) to minimize the

shell/water interface [30]. This is the same mechanism used for post-loading procedures, which have been reported to take place at typical temperatures in the range 50–70°C [27-30].

Despite the fact that such structures have been reported to respond to temperature changes, this has only been applied as a means to post-encapsulate molecules within pre-formed microcapsules. However, other than the exploitation of post-encapsulation procedures, the temperatures required for this are not suitable for biological applications. To the best of our knowledge, this is the first time that such a significant size reduction has been observed at temperatures as low as 37°C. For example, using oppositely charged copolymers of poly(styrene sulfonate) (PSS) and poly(allylamine hydrochloride) (PAH) with poly(*N*-isoproprylacrylamide) (PNIPAAm), Glinel *et al.* [27] have reported a size reduction of only 15% at 60 °C, whereas the present work shows a reduction of 42% at 37°C. Furthermore, these microcapsules retain a temperature response over a relevant temperature range and the changes occur under physiological conditions, similar to what has been demonstrated for the ELR in solution (Figure 9.1). These results allow us to anticipate future applications in the field of biomedicine in areas such as drug delivery, cell/tissue engineering and regenerative medicine.

In order to be used in biomedicine, it was important to assess whether the microcapsules and their content were harmful to cells. The biological performance *in vitro* is presented in Figure 9.4. This study showed that the viability of L929 cells in contact with the capsules (loaded and unloaded) was comparable to those used as positive control. The morphology of lone L929 cells and cells in contact with loaded $(CHI/ELR)_5$ microcapsules was also similar. These results show that these structures are non-cytotoxic towards L929 cells and can therefore be safely used in biomedical applications. Such applications could include the simple release of a biomolecule from a drug release device, with the microcapsules being compacted to form a tablet that can be administered orally. Since these microcapsules are highly retentive at physiological temperatures, they could release specific active agents in quantities within a therapeutic time window. Further possibilities include transcutaneous vaccines for the delivery of biomolecules into the skin, and the local application or injection of microcapsules loaded with growth factors at a defect site in a tissue or organ to facilitate its regeneration. This site could also be a tumor, with low molecular weight anti-cancer drugs being loaded into these reservoirs to kill tumor cells [44]. It should be noted that the temperature at tumor sites is usually slightly higher than 37°C and hyperthermic treatments are used to further increase the temperature locally. For the specific use of these microcapsules in cancer treatments, experiments at slightly higher temperatures (e.g., up to 42°C) using low molecular weight molecules (most

chemotherapeutic drugs have low molecular weights) should be performed in the future. Growth factors, which tend to have a higher molecular weight than chemotherapeutic agents, are also of interest for tissue-engineering applications, where they could be used *in vitro* to control cell metabolism and proliferation and to trigger stem cell differentiation. Vascular endothelial growth factor (VEGF, around 40 kDa), for example, has shown great potential in angiogenesis, one of the most relevant mechanisms in tissue-engineering applications. Similarly, human platelet-derived growth factor (PDGF, around 20-30 kDa) is one of the most active factors in cell migration and differentiation. However, the success of these growth factors in therapeutic applications often requires a spatiotemporal controlled-release system for delivery [45]. This could be achieved by diffusion of the encapsulated load into the medium and by internalization of individual capsules by the cells. The latter case would require the cells concerned to be larger than the individual microcapsules. We did not observe the uptake of capsules by L929 cells in this study, most probably because the size difference between L929 (around 5 to 10 μm) and microcapsules at 37°C (3.21±0.63 μm, Figure 9.3B) is too small for such a phenomenon to occur. In contrast, some stem cells, such as adipose stem cells, may reach 50 μm, thus meaning that applications which envisage their differentiation may be exploited in the future using this kind of micrometric device.

Figure 9.5 shows the BSA-release properties of microcapsules with different numbers of layers at distinct temperatures, together with the Korsmeyer model fitting parameters calculated in Table 9.1. It should be noted that these systems were not designed to operate in an "on/off" basis, such as when exploiting a temperature-dependent post-loading approach, but rather to achieve distinct release profiles that could prove to be useful for the sustained release of molecules in the body or *in vitro*.

The permeability of BSA to the exterior was easily tuned by varying the number of layers. Thus, similarly to the chelation stage during construction, the multilayer shell was able to act as a more effective barrier as the number of layers in it increased, thus allowing for a more sustained release and retentive microcapsule. The results obtained at 25 and 37°C were also interesting as the capsules proved to be more retentive at the latter. These results relate well with the size variations observed in Figure 9.3: the thermoresponsive effect of the CHI/ELR microcapsules results in a reduction in both their size and their permeability, thus making them more retentive. It is notable that, regardless of the test conditions, 100% of the BSA contained in the microcapsules was not released, most likely due to an interaction between the protein and the nanostructured shell. It is possible that a combination with enzymatic

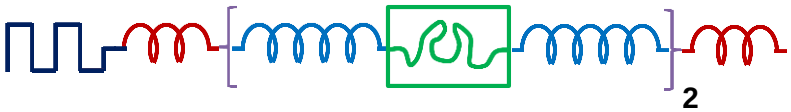
degradation, a mechanism which has been used previously [6,46,47], could lead to total release of the load. However, such a study was outside the scope of this work.

9.5 Conclusion

In summary, size and permeability variations have been achieved by exploiting the temperature response of the ELR, which is amplified by a thermodynamic rearrangement of the multilayer structure at the molecular level. The use of different numbers of layers has allowed the permeability of the shells to be tuned, thus resulting in distinct release profiles for each architecture tested. We envisage the exploitation of these properties at physiological temperature for applications where a long-term release with low initial drug burst is desired. Similarly, the degradation mechanisms of a cellular environment can be simulated to release an active agent completely over the appropriate time period. Due to micrometric size of these capsules, delivering small quantities of growth factors or differentiation agents directly to the cells by digestion is envisaged. The genetically encoded nature of ELRs offers the possibility to engineer molecules containing biologically relevant motifs that could be recognized by specific cells, such as the present case of RGD inclusion. All these possibilities, together with their non-cytotoxic character, make these microcapsules a promising alternative for more highly effective drug delivery and tissue engineering.

9.6 Supplemental information

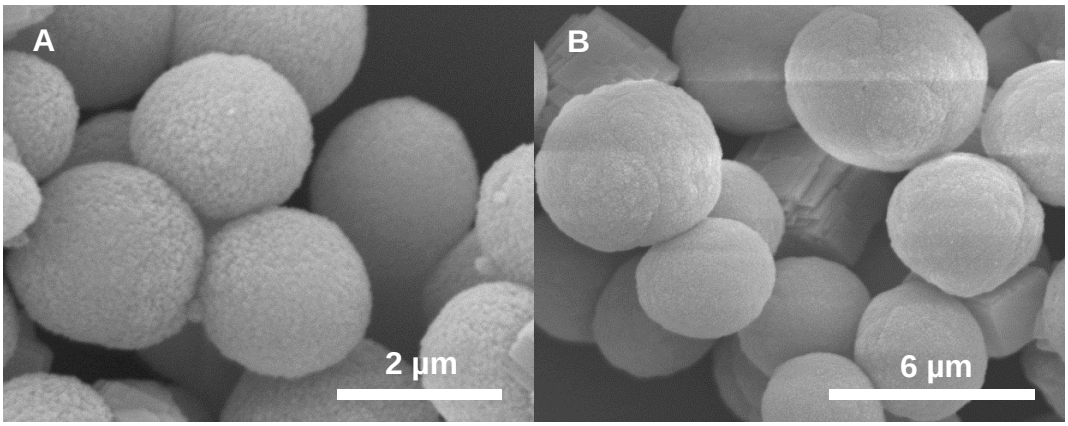
9.6.1 Schematic structure of the ELR



MGKKKP $(VPGVG)_{14}$ {$(VPGIG)_{10}$ (AVTGRGDSPASS) $(VPGIG)_{10}$}$_2$ $(VPGVG)_{14}$ V

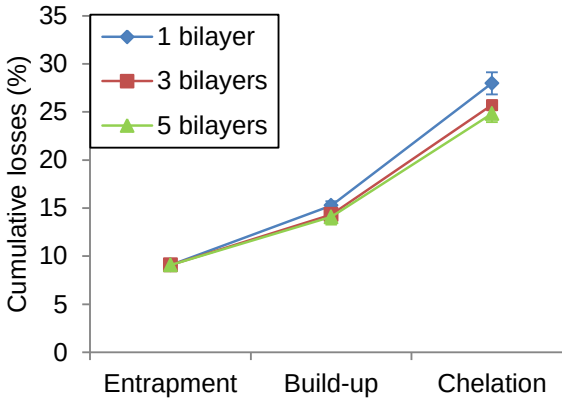
Supplemental Figure 9.1. Schematic of the ELR used. The bioactive sequence containing the negatively charged aspartic acids (RGD) is represented in green.

9.6.2 Morphology of the sacrificial $CaCO_3$ templates:



Supplemental Figure 9.2. Morphology of the sacrificial $CaCO_3$ templates observed by SEM. (A) Calcium carbonate microparticles with no entrapped BSA (≈2 µm) can be compared to (B) their counterparts containing BSA in their interior (≈5-6 µm). In (B) a rhombohedron can be observed in the background.

9.6.3 Cumulative losses and encapsulation efficiency



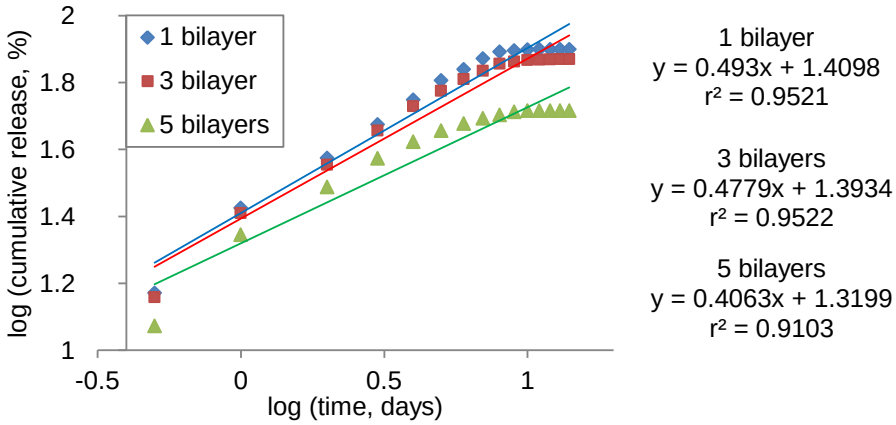
Supplemental Figure 9.3. Cumulative losses during microcapsule construction (from entrapment to chelation). Means±SD are represented.

Supplemental Table 9.1. Calculated encapsulation efficiency, E_e, in %.

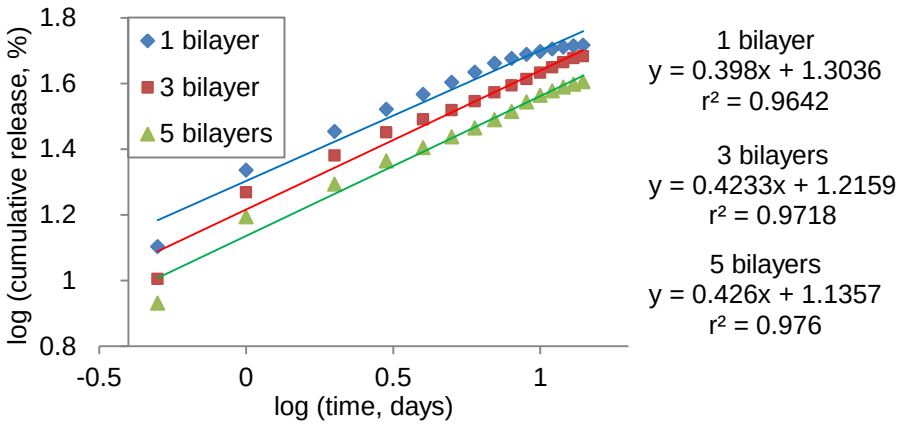
	Stage losses				
Number of bilayers	Entrapment, L_e	Construction, L_b	Chelation, L_c	Total loss	Encapsulation efficiency, E_e
1	9.07	6.20	12.71	27.98	72.02
3	9.07	5.26	11.39	25.72	74.28
5	9.07	5.01	10.75	24.83	75.17

9.6.4 Release kinetics calculation

9.6.4.1 Korsmeyer kinetics



Supplemental Figure 9.4. Release kinetics of the encapsulated BSA at 25°C. Korsmeyer kinetics (log cumulative percent drug released vs. log time), with correlation values (r^2).



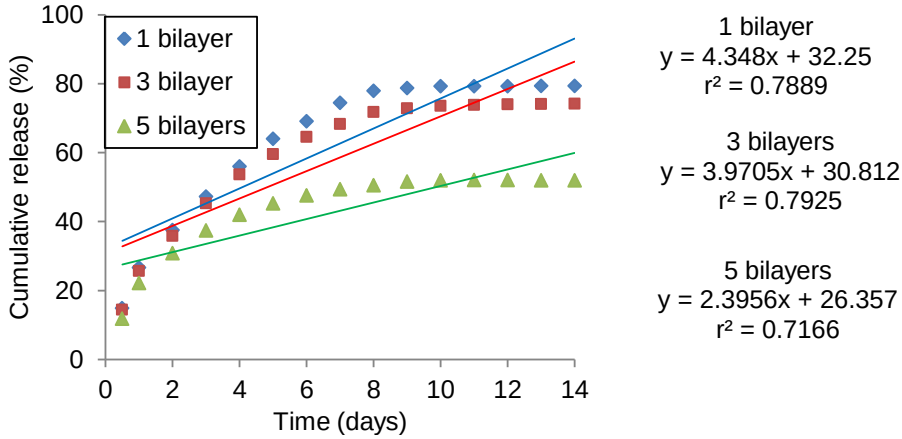
Supplemental Figure 9.5. Release kinetics of the encapsulated BSA at 37 °C. Korsmeyer kinetics (log cumulative percent drug released vs. log time), with correlation values (r^2).

9.6.4.2 Zero-order release

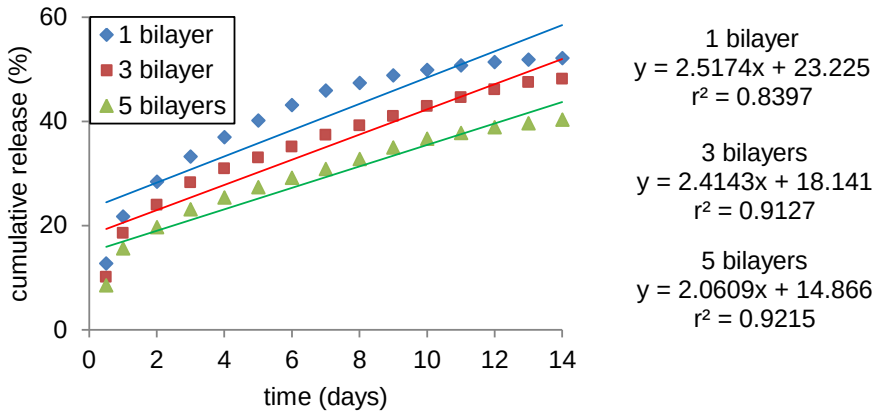
The zero-order release kinetics parameters were determined using the model (equation S1):

$$Q_t = Q_0 + K_0 t \qquad \text{(S1)}$$

where Q_t is the cumulative amount of protein released at time t, Q_0 is the initial amount of protein and K_0 is the rate constant for the zero-order model.



Supplemental Figure 9.6. Release kinetics of the encapsulated BSA at 25°C. Zero-order kinetics (cumulative percent drug released vs. time), with correlation values (r^2).



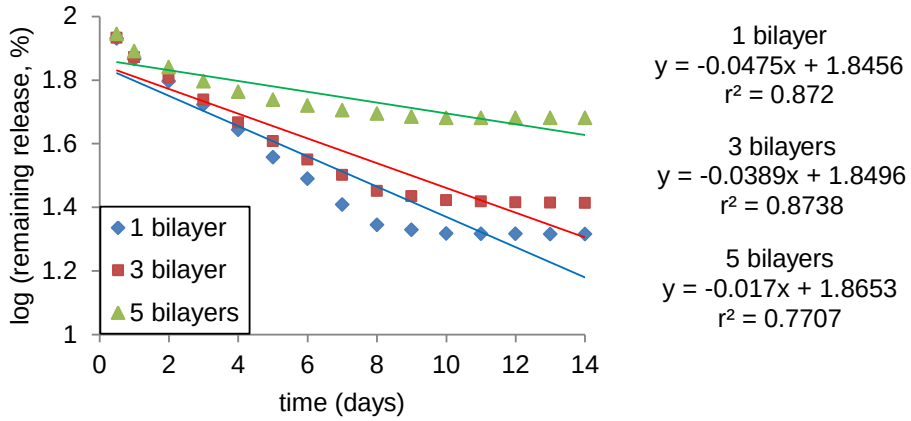
Supplemental Figure 9.7. Release kinetics of the encapsulated BSA at 37°C. Zero-order kinetics (cumulative percent drug released vs. time), with correlation values (r^2).

9.6.4.3 First-order release

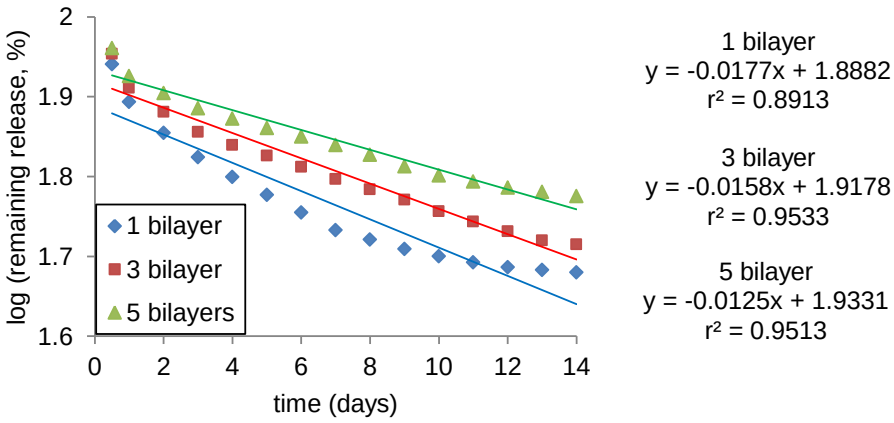
The first-order release kinetics parameters were determined using the model (Equation S2):

$$Log(Q_t) = Log(Q_0) + Kt / 2.303 \qquad \text{(S2)}$$

where Q_t is the cumulative amount of protein released at time t, Q_0 is the initial amount of protein and K is the rate constant for the first-order model.



Supplemental Figure 9.8. Release kinetics of the encapsulated BSA at 25°C. First-order kinetics (log cumulative percent drug remaining vs. time), with correlation values (r^2).



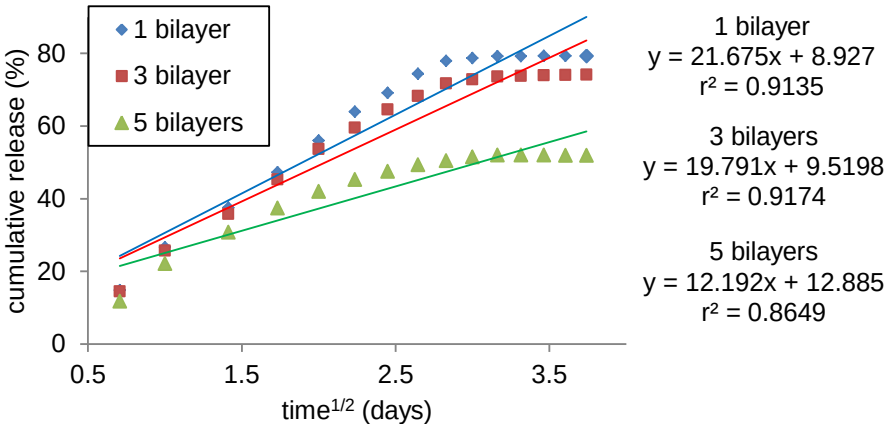
Supplemental Figure 9.9. Release kinetics of the encapsulated BSA at 37°C. First-order kinetics (log cumulative percent drug remaining vs. time), with correlation values (r^2).

9.6.4.4 Higuchi release model

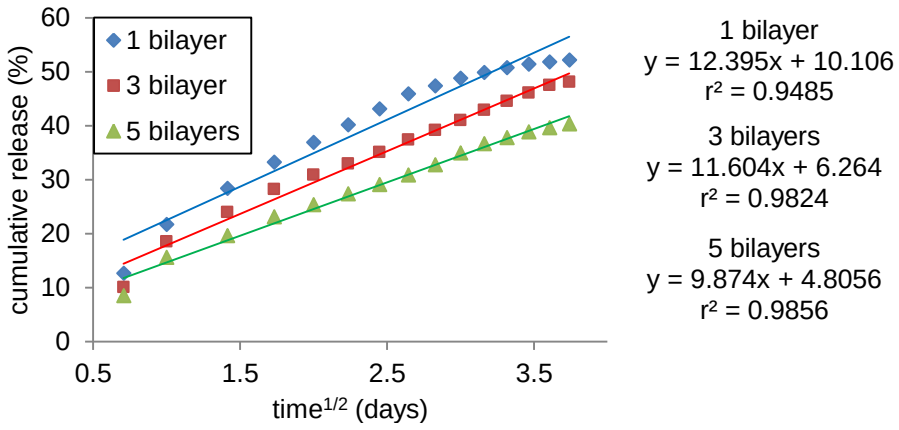
The Higuchi release kinetics parameters were determined using the model (Equation S3):

$$Q = K_H t^{1/2} \quad \text{(S3)}$$

where Q is the cumulative amount of protein released at time t and K_H is the rate constant for the Higuchi model.



Supplemental Figure 9.10. Release kinetics of the encapsulated BSA at 25°C. Higuchi kinetics (cumulative percent drug released vs. square root of time), with correlation values (r^2).



Supplemental Figure 9.11. Release kinetics of the encapsulated BSA at 37°C. Higuchi kinetics (cumulative percent drug released vs. square root of time), with correlation values (r^2).

9.7 Acknowledgements

This work was carried out under the scope of the EU 7th Framework Programme (FP7/2007-2013) under grant agreement no NMP4-SL-2009-229292 (Find&Bind), Fundação para a Ciência e Tecnologia (FCT) from Portugal (PhD grants SFRH/BD/61126/2009 and SFRH/BD/61390/2009), "Fundo Social Europeu" – FSE, "Programa Diferencial de Potencial Humano" – POPH, the MICINN (MAT 2009 14195-C03 03, ACI2009-0890, MAT2010-15310, MAT2010-15982 and PRI-PIBAR-2011-1403), the JCyL (VA049A11, VA152A12 and VA155A12) and "CIBER-BBN. E.C.".

9.8 References

[1] De Cock L. J., De Koker S., De Geest B. G., Grooten J., Vervaet C., Remon J. P., Sukhorukov G. B., and Antipina M. N., Polymeric multilayer capsules in drug delivery, Angewandte Chemie International Edition 2010, 49: 6954-6973.

[2] Langer R., and Tirrell D. A., Designing materials for biology and medicine, Nature 2004, 428: 487-492.

[3] Oliveira M. B., and Mano J. F., Polymer-based microparticles in tissue engineering and regenerative medicine, Biotechnology Progress 2011, 27: 897-912.

[4] Vergaro V., Scarlino F., Bellomo C., Rinaldi R., Vergara D., Maffia M., Baldassarre F., Giannelli G., Zhang X., Lvov Y. M., and Leporatti S., Drug-loaded polyelectrolyte microcapsules for sustained targeting of cancer cells, Advanced Drug Delivery Reviews 2011, 63: 847-864.

[5] Zhao Q., Han B., Wang Z., Gao C., Peng C., and Shen J., Hollow chitosan-alginate multilayer microcapsules as drug delivery vehicle: doxorubicin loading and in vitro and in vivo studies, Nanomedicine: Nanotechnology, Biology and Medicine 2007, 3: 63-74.

[6] Chandrawati R., Odermatt P. D., Chong S.-F., Price A. D., Städler B., and Caruso F., Triggered cargo release by encapsulated enzymatic catalysis in capsosomes, Nano Letters 2011, 11: 4958-4963.

[7] Ochs C. J., Hong T., Such G. K., Cui J., Postma A., and Caruso F., Dopamine-mediated continuous assembly of biodegradable capsules, Chemistry of Materials 2011, 23: 3141-3143.

[8] She Z., Antipina M. N., Li J., and Sukhorukov G. B., Mechanism of Protein Release from Polyelectrolyte Multilayer Microcapsules, Biomacromolecules 2010, 11: 1241-1247.

[9] Su X., Kim B.-S., Kim S. R., Hammond P. T., and Irvine D. J., Layer-by-layer-assembled multilayer films for transcutaneous drug and vaccine delivery, ACS Nano 2009, 3: 3719-3729.

[10] Kreft O., Munoz-Javier A., Sukhorukov G. B., and Parak W. J., Polymer microcapsules as mobile local pH-sensors, Journal of Materials Chemistry 2007, 17: 4471-4476.

[11] Rivera-Gil P., De Koker S., De Geest B. G., and Parak W. J., Intracellular Processing of Proteins Mediated by Biodegradable Polyelectrolyte Capsules, Nano Letters 2009, 9: 4398-4402.

[12] Hosta-Rigau L., Städler B., Yan Y., Nice E. C., Heath J. K., Albericio F., and Caruso F., Capsosomes with Multilayered Subcompartments: Assembly and Loading with Hydrophobic Cargo, Advanced Functional Materials 2010, 20: 59-66.

[13] Poon Z., Chang D., Zhao X., and Hammond P. T., Layer-by-layer nanoparticles with a pH-sheddable layer for in vivo targeting of tumor hypoxia, ACS Nano 2011, 5: 4284-4292.

[14] Costa R. R., Custódio C. A., Testera A. M., Arias F. J., Rodríguez-Cabello J. C., Alves N. M., and Mano J. F., Stimuli-Responsive Thin Coatings Using Elastin-Like Polymers for Biomedical Applications, Advanced Functional Materials 2009, 19: 3210-3218.

[15] Decher G., Fuzzy Nanoassemblies: Toward Layered Polymeric Multicomposites, Science 1997, 277: 1232-1237.

[16] Picart C., Lavalle P., Hubert P., Cuisinier F. J. G., Decher G., Schaaf P., and Voegel J. C., Buildup mechanism for poly(L-lysine)/hyaluronic acid films onto a solid surface, Langmuir 2001, 17: 7414-7424.

[17] Kim B.-S., Park S. W., and Hammond P. T., Hydrogen-bonding layer-by-layer-assembled biodegradable polymeric micelles as drug delivery vehicles from surfaces, ACS Nano 2008, 2: 386-392.

[18] Simchi A., Tamjid E., Pishbin F., and Boccaccini A. R., Recent progress in inorganic and composite coatings with bactericidal capability for orthopaedic applications, Nanomedicine: Nanotechnology, Biology and Medicine 2011, 7: 22-39.

[19] Yang Y., Wimpenny I., and Ahearne M., Portable nanofiber meshes dictate cell orientation throughout three-dimensional hydrogels, Nanomedicine: Nanotechnology, Biology and Medicine 2011, 7: 131-136.

[20] del Mercato L. L., Rivera-Gil P., Abbasi A. Z., Ochs M., Ganas C., Zins I., Sonnichsen C., and Parak W. J., LbL multilayer capsules: recent progress and future outlook for their use in life sciences, Nanoscale 2010, 2: 458-467.

[21] Caruso F., Caruso R. A., and Möhwald H., Nanoengineering of inorganic and hybrid hollow spheres by colloidal templating, Science 1998, 282: 1111-1114.

[22] Petrov A. I., Volodkin D. V., and Sukhorukov G. B., Protein-calcium carbonate coprecipitation: a tool for protein encapsulation, Biotechnology Progress 2005, 21: 918-925.

[23] Gao C., Möhwald H., and Shen J., Enhanced biomacromolecule encapsulation by swelling and shrinking procedures, ChemPhysChem 2004, 5: 116-120.

[24] Mauser T., Dejugnat C., and Sukhorukov G. B., Reversible pH-dependent properties of multilayer microcapsules made of weak polyelectrolytes, Macromolecular Rapid Communications 2004, 25: 1781-1785.

[25] Zhao Q., and Li B., pH-controlled drug loading and release from biodegradable microcapsules, Nanomedicine: Nanotechnology, Biology and Medicine 2008, 4: 302-310.

[26] Bedard M. F., Munoz-Javier A., Mueller R., Del Pino P., Fery A., Parak W. J., Skirtach A. G., and Sukhorukov G. B., On the mechanical stability of polymeric microcontainers functionalized with nanoparticles, Soft Matter 2009, 5: 148-155.

[27] Glinel K., Sukhorukov G. B., Möhwald H., Khrenov V., and Tauer K., Thermosensitive hollow capsules based on thermoresponsive polyelectrolytes, Macromolecular Chemistry and Physics 2003, 204: 1784-1790.

[28] Huang C.-J., and Chang F.-C., Using click chemistry to fabricate ultrathin thermoresponsive microcapsules through direct covalent layer-by-layer assembly, Macromolecules 2009, 42: 5155-5166.

[29] Ibarz G., Dähne L., Donath E., and Möhwald H., Controlled permeability of polyelectrolyte capsules via defined annealing, Chemistry of Materials 2002, 14: 4059-4062.

[30] Köhler K., Möhwald H., and Sukhorukov G. B., Thermal behavior of polyelectrolyte multilayer microcapsules: 2. insight into molecular mechanisms for the PDADMAC/PSS system, The Journal of Physical Chemistry B 2006, 110: 24002-24010.

[31] Mano J. F., Stimuli-responsive polymeric systems for biomedical applications, Advanced Engineering Materials 2008, 10: 515-527.

[32] Mano J. F., Silva G. A., Azevedo H. S., Malafaya P. B., Sousa R. A., Silva S. S., Boesel L. F., Oliveira J. M., Santos T. C., Marques A. P., Neves N. M., and Reis R. L., Natural origin biodegradable systems in tissue engineering and regenerative medicine: present status and some moving trends, Journal of The Royal Society Interface 2007, 4: 999-1030.

[33] Rinaudo M., Chitin and chitosan: Properties and applications, Progress in Polymer Science 2006, 31: 603-632.

[34] Almine J. F., Bax D. V., Mithieux S. M., Nivison-Smith L., Rnjak J., Waterhouse A., Wise S. G., and Weiss A. S., Elastin-based materials, Chemical Society Reviews 2010, 39: 3371-3379.

[35] Girotti A., Reguera J., Rodríguez-Cabello J. C., Arias F. J., Alonso M., and Testera A., Design and bioproduction of a recombinant multi(bio)functional elastin-like protein polymer containing cell adhesion sequences for tissue engineering purposes, Journal of Materials Science: Materials in Medicine 2004, 15: 479-484.

[36] Meyer D. E., and Chilkoti A., Purification of recombinant proteins by fusion with thermally-responsive polypeptides, Nat Biotech 1999, 17: 1112-1115.

[37] Urry D. W., Molecular machines: how motion and other functions of living organisms can result from reversible chemical changes, Angewandte Chemie International Edition in English 1993, 32: 819-841.

[38] Urry D. W., What sustains life? Consilient mechanisms for protein-based machines and materials, New York, U.S.A.: Springer-Verlag, LLC; 2006.

[39] Barbosa J., Costa R., Testera A., Alonso M., Rodríguez-Cabello J., and Mano J., Multi-layered films containing a biomimetic stimuli-responsive recombinant protein, Nanoscale Research Letters 2009, 4: 1247-1253.

[40] Prieto S., Shkilnyy A., Rumplasch C., Ribeiro A., Arias F. J., Rodríguez-Cabello J. C., and Taubert A., Biomimetic calcium phosphate mineralization with multifunctional elastin-like recombinamers, Biomacromolecules 2011, 12: 1480-1486.

[41] Ritger P. L., and Peppas N. A., A simple equation for description of solute release I. Fickian and non-fickian release from non-swellable devices in the form of slabs, spheres, cylinders or discs, Journal of Controlled Release 1987, 5: 23-36.

[42] Porcel C., Lavalle P., Decher G., Senger B., Voegel J. C., and Schaaf P., Influence of the polyelectrolyte molecular weight on exponentially growing multilayer films in the linear regime, Langmuir 2007, 23: 1898-1904.

[43] Costa R. R., Custódio C. A., Arias F. J., Rodríguez-Cabello J. C., and Mano J. F., Layer-by-Layer Assembly of Chitosan and Recombinant Biopolymers into Biomimetic Coatings with Multiple Stimuli-Responsive Properties, Small 2011, 7: 2640-2649.

[44] Zhang L., Guo R., Yang M., Jiang X., and Liu B., Thermo and pH Dual-Responsive Nanoparticles for Anti-Cancer Drug Delivery, Advanced Materials 2007, 19: 2988-2992.

[45] Cao L., and Mooney D. J., Spatiotemporal control over growth factor signaling for therapeutic neovascularization, Advanced Drug Delivery Reviews 2007, 59: 1340-1350.

[46] Price A. D., Zelikin A. N., Wang Y., and Caruso F., Triggered enzymatic degradation of DNA within selectively permeable polymer capsule microreactors, Angewandte Chemie International Edition 2009, 48: 329-332.

[47] Zhao W., Zhang H., He Q., Li Y., Gu J., Li L., Li H., and Shi J., A glucose-responsive controlled release of insulin system based on enzyme multilayers-coated mesoporous silica particles, Chemical Communications 2011, 47: 9459-9461.

Chapter 10. Cellular uptake of multilayered capsules produced with biomimetic and genetically engineered macromolecules[10]

Abstract

Multilayered microcapsules of chitosan and biomimetic elastin-like recombinamers (ELRs) were prepared for intracellular delivery of active agents. Two ELRs containing either the bioactive RGD sequence or a scrambled nonfunctional RDG were used to construct two types of functionalized polymeric microcapsules, both with spherical shape around 4 μm in diameter. Cell viability studies using human mesenchymal stem cells (hMSCs) were performed for microcapsule/cell ratios between 5:1 and 100:1. After 3 and 72 hours of incubation no cytotoxicity was found. Nonetheless, cells incubated with RGD-functionalized microcapsules exhibited higher mean viability values than RDG ones. Internalization efficacy and bioavailability of encapsulated proteins was assessed by monitoring fluorescence changes of DQ-ovalbumin. The data showed that microcapsules' surface functionalization did not influence significantly the internalization by hMSCs, although DQ-ovalbumin was degraded faster from within RGD-functionalized microcapsules. The developed microcapsules let foresee strategies for targeting intracellular drug delivery and to increase drug efficacy.

[10] This chapter is based on the following publication:

Costa R. R., Girotti A., Santos M., Arias F. J., Mano J. F., and Rodríguez-Cabello J. C., Cellular uptake of multilayered capsules produced with biomimetic and genetically engineered macromolecules, submitted (2013).

Chapter 10 – Cellular uptake of multilayered capsules produced with biomimetic and genetically engineered macromolecules

10.1 Introduction

In the field of drug delivery, there has been great interest in the development of nano- and micro-carriers of active agents, such as micelles, liposomes, polymersomes, and polymer capsules [1-3]. Such devices may control the release of encapsulated biomolecules and also their efficacy by delivering them to the location where they are most needed. In particular, the use of nanostructured nano- and micro-capsules made using layer-by-layer (LbL) strategies has been studied as a method to encapsulate and deliver drugs in a controlled manner [4-8]. The principle behind LbL adsorption lies in the existence of intermolecular interactions attracting distinct polymer chains, such as electrostatic contacts, hydrophobic interactions, and hydrogen bonding, which drive the assembly of layers with only a few nanometers onto a surface [9-11]. With this simple and versatile technique, robust coatings can be assembled into bidimensional templates and even complex three-dimensional substrates. For instance, spherical nanostructured microcapsules have been conceived resorting to sacrificial silica (with 500 nm to 5 μm, dissolved in hydrogen fluoride) and porous calcium carbonate particles (with 3 to 5 μm, dissolved in ethylenediamine tetraacetic acid, EDTA) [12]. These structures have already been found to be useful as drug carriers – including of stem cell differentiation promoters – with release kinetics dependent on the number of layers or external stimuli, and as biosensors [13-15].

Multilayer microcapsules may encapsulate and deliver bioactive agents to cells or tissues following conventional release mechanisms to the biological environment [16] or by digestion within the cells themselves [17]. The latter possibility is particularly interesting: by delivering an active agent directly to the cells, where the whole metabolic machinery is found, high drug concentrations could be made available to the targeted tissue using minimal cargo amounts during its encapsulation. Moreover, it could also be possible to circumvent undesirable side effects to circumventing tissues or cells due to premature drug leakage.

Carriers such as dendrimers, micelles and biodegradable nanoparticles have been frequently developed for the intracellular delivery of bioactive agents [18-21]. As carriers, multilayer-coated capsules present several advantages that are not often found together in other conventional fabrication techniques: (i) they can be prepared under mild conditions, what makes it possible for large amounts of sensitive or easily denatured biological molecules [22] and even cells [23] to be encapsulated, (ii) it is possible to encapsulate drugs with low water solubility [5], (iii) they allow controlling better the release kinetics by

varying the number of layers and their composition [24], and (iv) the shell can provide a high degree of functionality by selecting biofunctional constituents that may participate in biological mechanisms [25].

The primary objective of the present work is the design of multilayer microcapsules made of natural and nature-inspired macromolecules exhibiting bioactive sequences for intracellular drug delivery. Namely, chitosan (CHI) and elastin-like recombinamers (ELRs) were used as constituents of the multilayer shells which were assembled onto spherical particles of calcium carbonate. CHI is a well-known polycationic polysaccharide of marine origin which shows biocompatibility, adhesiveness and nontoxicity, as well as bacteriostatic, fungistatic, anti-microbial and hemostatic activities [26]. ELRs, a recombinant type of elastin-like polymers (ELP), are temperature-responsive and biomimetic polypeptides that are soluble in aqueous media below a specific critical transition temperature (T_t) but undergo a phase separation above it [27]. Their recombinant and modular nature is most likely their most attractive property because it allows tuning their physicochemical properties and introducing selected relevant amino acid domains to extend their physiological functionality [28,29]. LbL adsorption can be exploited using ELRs alongside polysaccharides, such as CHI and alginate, by taking advantage of strong electrostatic interactions and the stabilizing effect of weaker hydrophobic interactions [30].

Herein, human mesenchymal stem cells (hMSCs) were incubated with ELR-functionalized microcapsules with the cell adhesion motif arginine-glycine-aspartic acid (RGD). The inclusion of the loop RGD motif of the human structural protein fibronectin in the primary structure of the ELR was expected to add bioactive character to the microcapsules, while exploiting the negatively charged aspartic acids to enable the electrostatic self-assembly mechanism with CHI to occur. It has been reported that the RGD sequence is the minimal sequence required for recognition by the cell adhesion receptor integrins [31]. It is also known that nano/micro-particles modified with RGD show enhanced internalization [32-34]. However, this comparison is often made with unmodified controls, that is, do not undergo any functionalization. Therefore, in addition to RGD, we also constructed microcapsules functionalized with an ELR containing a nonfunctional scrambled RDG sequence. To our knowledge, this is the first time that the internalization efficacy of RGD-functionalized LbL microcapsules is compared with a microcapsule type that substitutes the bioactive group with a nonfunctional analogue, similar in every aspect except for the position of the G and D residues, instead of removing it.

The resulting microcapsules will be characterized in terms of morphology, and cytotoxicity after incubation with hMSCs. The internalization efficacy of the microcapsules will be quantified by flow cytometry in order to identify the existence – or absence – of a receptor-mediated uptake and

consequent influence in the intracellular processing between each microcapsule type. Furthermore, Capsules loaded with DQ-ovalbumin will permit to follow the availability of this protein inside the cells by monitoring the fluorescence changes of the capsules.

10.2 Experimental section

10.2.1 Materials

Medium molecular weight chitosan (ref 448877), sodium carbonate anhydrous (Na_2CO_3, ref 222321) and EDTA (ref E9884) were purchased from Sigma-Aldrich. Chitosan was further submitted to a purification stage consisting in a series of filtration and precipitation in water and ethanol steps, adapted from the method described elsewhere [30], followed by freeze-drying. The final degree of deacetylation was determined to be 82% by ^{1}H-NMR. Calcium chloride ($CaCl_2$) was purchased from VWR (ref 1.02378.0500). Two custom-made ELRs containing either a RGD or RDG sequence – henceforth referred to as ELR-RGD and ELR-RDG$^{(-)}$, respectively – were purchased from Technical Protein Nanobiotechnology (Spain). The characterization of the molecular weight and amino acid composition of the acquired batches were determined by matrix-assisted laser desorption/ionization time-of-flight mass spectroscopy (MALDI-TOF) and amino acid content analysis, respectively, and can be found elsewhere [25]. DQ-ovalbumin (ref D12053) was obtained from Invitrogen.

Paraformaldehyde (ref P6148), Triton X-100 (ref T9284) and Accutase™ (ref A6964) were purchased from Sigma-Aldrich. Human mesenchymal stem cells from human adipose tissue, (hMSCs, ref R7788-115) its basal medium, Dulbecco's modified Eagle's medium (DMEM, ref 31966-021), fetal bovine serum (FBS, ref 16000-044), penicillin streptomycin solution (ref SV30010), trypsin-ethylenediamine tetraacetic acid (EDTA, ref SV30010), Dulbecco's phosphate-buffered saline (DPBS, ref 14190-136), 4-(2-hydroxyethyl)-1-piperazineethanesulfonic acid (HEPES, ref 15630049), Trypan Blue stain 0.4% (ref 15250061), Alexa Fluor 488 phalloidin (ref A12379), LIVE/DEAD® Viability/Cytotoxicity Kit, for mammalian cells (ref L3224), Alamar Blue® (ref DAL1025) and DAPI (ref D21490) were supplied by Invitrogen . All cell culture plastic-ware and consumables were acquired from NUNC.

10.2.2 Measurement of the charges

The ζ-potentials of the ELRs were determined using a Nano-ZS equipment from Malvern (United Kingdom), at 25°C. Aqueous solutions of each ingredient in phosphate-buffered saline (PBS) (pH = 7.4) were used, at a concentration of 300 $\mu g \cdot mL^{-1}$.

10.2.3 Synthesis of calcium carbonate sacrificial templates

Aqueous solutions Na_2CO_3 and $CaCl_2$ were prepared at a concentration of 1 M. Typically, the coprecipitation of both solutions was performed by adding 1 mL of Na_2CO_3 solution followed by 1 mL of $CaCl_2$ to 4 mL of ultrapure water (Milli-Q) under heavy stirring for 30 s. The stirring was then stopped and the suspension of the newly synthesized calcium carbonate ($CaCO_3$) microparticles was left to precipitate and react for 15 min. The supernatant was removed and the particles were washed three times with 0.15 M sodium chloride (NaCl) adjusted to pH 5.5. To produce microcapsules preloaded with a protein cargo, the medium where the precipitation occurs consisted of an aqueous solution of DQ-ovalbumin at a concentration of 160 $\mu g \cdot mL^{-1}$. Unless otherwise stated, all changes of solutions during the template synthesis and construction of microcapsules were performed by leaving the particle suspension precipitating for 10 min, followed by removal of the supernatant and replacement with the next solution – polymeric or for washing.

10.2.4 Construction of the multilayer shells and microcapsule formation

The $CaCO_3$ sacrificial templates were immersed alternately in solutions of CHI and one of the ELRs (300 $\mu g \cdot mL^{-1}$, pH 5.5, 0.15 M NaCl) for 10 min under mild stirring. Each adsorption step was followed by three washing steps with 0.15 M NaCl, pH 5.5: to disaggregate the substrates, the first was accompanied by four sequential ultrasound pulses of 3 seconds each, with the following being just rinsed. This process was repeated until 2 CHI/ELR bilayers were assembled. After the construction of the multilayers, the $CaCO_3$ core was dissolved by EDTA, at 0.2 M, pH 5.5. From this point on, the precipitation of the microcapsules was aided by centrifugation steps (1000 rpm, 25 min) and ultrasound pulses timed as described above. The newly formed hollow microcapsules then followed a washing procedure with EDTA (0.2 M, pH 7.4) and four with ultrapure water. The microcapsules were stored at room temperature until use for a maximum of 24 h in a renewed medium of ultrapure water. In the case of microcapsules intended for cellular assays – loaded with DQ-ovalbumin – DMEM was

used for the washings and storage instead of water. The microcapsule production yield resulting from the mixture of 1 mL of Na_2CO_3 and $CaCl_2$ was estimated to be with a total of 1.1×10^6 microcapsules by microscopy observation.

10.2.5 Characterization of the hybrid microcapsules

The morphology of the produced microcapsules – designated $(CHI/ELR\text{-}RGD)_2$ and $(CHI/ELR\text{-}RDG^{(-)})_2$ – was determined using an environmental scanning electron microscopy (ESEM) (FEI Quanta 200FEG). A number of 2.2×10^4 microcapsules suspended in 200 μL of H_2O was placed on top of a silicon wafer (1 cm^2) and dried overnight at 37°C before the analysis. The samples were placed inside the equipment in a platform with a 20° tilt. Transmission electron microscopy (TEM) images were obtained using a JEOL JEM-1011 HR instrument operating at 80 kV. Prior to the observation, a number of 10^4 microcapsules suspended in 60 μL of H_2O was pipetted onto a TEM grid and left to dry overnight at room temperature. A confocal laser scanning microscope (CLSM, Olympus FV1000, Germany) was used to evaluate the morphology of the microcapsules. For this, a final solution of a cationic dye (rhodamine B, 10^{-6} M) was further adsorbed after the normal construction of the microcapsules. All samples were stabilized at 37°C and observed under hydrated conditions. The fluorescence intensity profiles of 3 distinct microcapsules were plotted using ImageJ software (to assess the formation of spherical hollow structures (provided by NIH, version 1.47v).

10.2.6 Cell culture

hMSCs were cultured in DMEM supplemented with 10% FBS and 100 $U{\cdot}mL^{-1}$ penicillin, 0.1 $mg{\cdot}mL^{-1}$ streptomycin replaced every two day and maintained at 37°C in a 5% carbon dioxide (CO_2) humidified environmental chamber. Near-confluence cells (passages 2–6) were harvested after enzymatically treatment with trypsin/EDTA or Accutase™ and suspended in culture medium, cell counts were evaluated using a standard Trypan Blue exclusion assay and seeded at 3×10^3 $cell{\cdot}cm^{-2}$ on the diverse surfaces utilized and then incubated during 24 hours in standard conditions. Afterwards, the culture medium was refreshed by serum-free medium containing a suspension of CHI/ELR microcapsules. After 3 h of CHI/ELR microcapsules co-incubation, the cultures were maintained for longer times, by supplementing the microcapsule suspension with additional fresh medium to reach the final serum concentration of 2% FBS.

10.2.7 Cell viability assays

Metabolic activity was evaluated by Alamar Blue® and cell viability by LIVE/DEAD® assays. The relative number of hMSCs metabolically active within each experimental condition was evaluated by the Alamar Blue® assay according to the manufacturer guidelines. Briefly, 24 hours after cells seeding, cells culture was washed and then $(CHI/ELR\text{-}RGD)_2$ and $(CHI/ELR\text{-}RDG^{(-)})_2$ microcapsules in serum-free culture medium were added in incremental ratios of 5 to 100 microcapsules per cell. After 3 and 72 h of microcapsules co-incubation, the fluorimetric reduction of 10% Alamar Blue® reagent in culture medium was measured with a microtiter plate reader (SpectraMax M2e Molecular Devices). Non-treated cells were employed as positive control and their fluorescence was considered as the 100% of cells viability.
The viability of cells co-incubated with CHI/ELR was also examined by a LIVE/DEAD® assays. Ten microcapsules per cell of each CHI/ELR microcapsule type were added to the cell culture. The ratio of microcapsules per cell was selected after obtaining the results of the cell viability assays. In this assay, the co-incubation with calcein AM and ethidium homodimer-1 allows distinguishing the cytoplasm of live cells (with esterase cleavage of calcein accompanied by green fluorescence), and dead cells (which compromised membranes enable to stain nucleic acids with red fluorescence). LIVE/DEAD® assays was carried out at different time points (0, 72 and 240 h) according to the manufacturing specifications.

10.2.8 Statistical analysis

Values reported reflect means±standard error (SE) of four samples of four independent cell culture viability experiments at 3 or 72 hours of incubation. The influence of microcapsules/cell ratio on cell viability was analyzed using one-way analysis of variance (ANOVA) and the post test of Bonferroni. All treatment-related effects were considered to be statistically significant at p-value less than 0.05. All data was analyzed using GraphPad Prism 6.0 (GraphPad Software, Inc., La Jolla, CA).

10.2.9 Internalization and intracellular processing experiments

hMSCs were seeded on circular cover glasses (diameter: 10 mm; Thermo Scientific CB00100RA1) deposited in a 48-well plate and incubated during 24 h in standard conditions. $(CHI/ELR\text{-}RGD)_2$ and $(CHI/ELR\text{-}RDG^{(-)})_2$ microcapsules were added to the culture. After 3 or 72 h of incubation, samples were washed with DPBS three times.

Samples for microscopy analysis – confocal, phase-contrast, epifluorescence, and differential interference contrast (DIC) microscopy (Nomarski) – were fixed in 4% paraformaldehyde for 10 min, permeabilized with 0.2% Triton X-100, and stained with DAPI. A confocal microscope (Leica Microsystems, Heidelberg GmbH, microscope confocal Leica SP5) was used for analyzing microcapsules inside the cells. Z-series were performed with a Z-step of 1 μm. The images of each fluorophore and phase contrast were overlaid to obtain a multilayer image using ImageJ software (National Institutes of Health). Bright field and fluorescence microscopy were performed in a NIKON Eclipse Ti fluorescence microscope, equipped with a digital camera system (Digital sight DS-2MBWc), using blue, green and red filters.

10.2.10 Cell analysis by flow cytometry

1.5×10^5 hMSCs were seeded in a 25 cm^2 flasks and cultured as described above. $(CHI/ELR\text{-}RGD)_2$ and $(CHI/ELR\text{-}RDG^{(-)})_2$ microcapsules were added at a microcapsule-to-cell ratio of 10:1 and incubated during 72 h. The cell cultures dissociated by Accutase™ treatment – specially developed for gentle and effective cell dissociation – were washed, counted, suspended in DPBS, 25 mM HEPES 5% FBS and analyzed in a flow cytometer (Beckman Coulter). The assay was repeated three times. All treatment-related effects were considered to be statistically significant at p-value less than 0.05. All data was analyzed using GraphPad Prism 6.0 (GraphPad Software, Inc., La Jolla, CA).

10.3 Results and discussion

First, $CaCO_3$ microparticles were coated with two bilayers of chitosan and the ELRs containing either the motif RGD or RDG. Hollow capsules were produced by their subsequent incubation with EDTA and chelation of the sacrificial core – henceforth referred to as $(CHI/ELR\text{-}RGD)_2$ or $(CHI/ELR\text{-}RDG^{(-)})_2$, respectively. The morphology of the microcapsules was evaluated by CLSM and SEM, and the capsules' wall by TEM (Figure 10.1). TEM (Figure 10.1A), which was used solely to observe the wall delimiting the interior and exterior of the microcapsules, showed a multilayer shell that could be distinguished at the borders of the structure. For the morphological analysis, the samples for microscopy observation were prepared at 37°C.

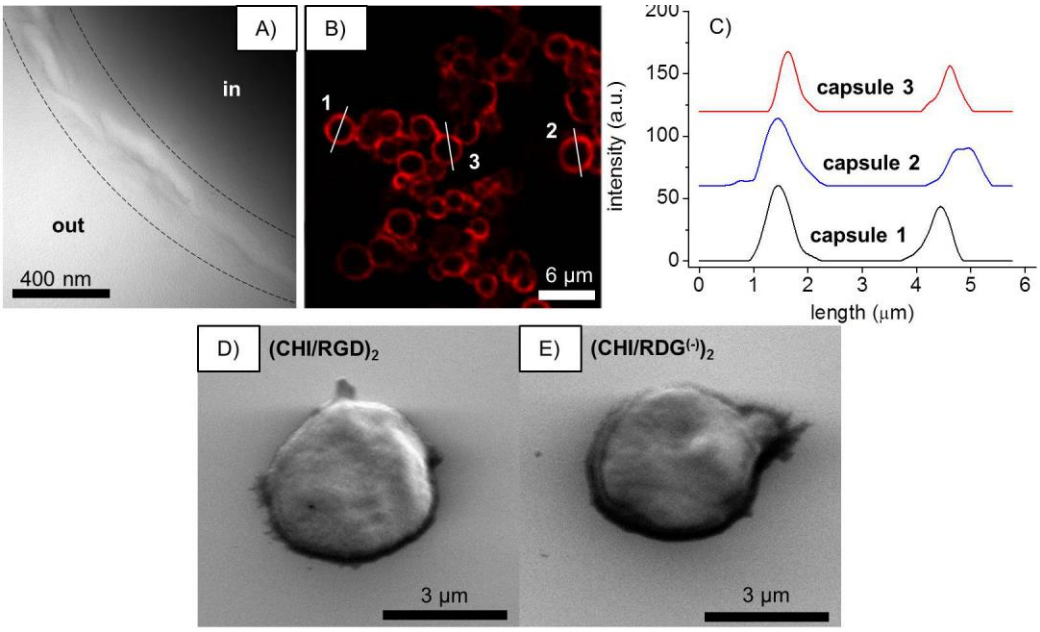


Figure 10.1. (A) Representative TEM image of a microcapsule showing a detail of the multilayer shell delimited by the dashed lines. (B) CLSM micrograph of several microcapsules with the wall tagged with rhodamine. Micrograph is representative of both $(CHI/ELR\text{-}RGD)_2$ and $(CHI/ELR\text{-}RDG^{(-)})_2$ microcapsules. (C) Fluorescence intensity plot profile of three individual microcapsules depicted in (B). The peaks coincide with the capsules' walls, while the plateau in between corresponds to the hollow interior. SEM images of (D) $(CHI/ELR\text{-}RGD)_2$ and (E) $(CHI/ELR\text{-}RDG^{(-)})_2$ microcapsules, with a vertical tilt of 20°.

It is known that this kind of polysaccharide/polypeptide microcapsules experience size variations according to the temperature of the incubation medium. Costa *et al.* [36] demonstrated that this class of microcapsules have a diameter of 5.5 µm at room temperature but shrink when incubated at 37°C, to around 3 µm. Therefore, this temperature was chosen to prepare the samples and assess their morphology under a temperature similar to that of a biological environment.

The preparation of individual polymeric capsules while avoiding aggregation is difficult but necessary for applications that require cellular uptake and survival. Figure 10.1B shows several CHI/ELR microcapsules observed under CLSM. All microcapsules showed diameters of 3–4 µm and had their own individual walls (which served as polymeric reservoirs for the rhodamine dye) and hollow interior (hence not dyed after the 10 minutes treatment). The graphic in Figure 10.1C, where the fluorescence intensity is plotted as a function of the length of the lines drawn, confirms that the interior was empty and thus the dissolution of the $CaCO_3$ core was successful. In Figure 10.1D, the morphological analysis

of $(CHI/ELR\text{-}RGD)_2$ microcapsules shows that the integrity of the wall was maintained through the process of its construction to the moment of their use. This observation indicates that the used operational conditions permitted to obtain individual spherical microstructures. No signs of aggregation were found, what makes the produced microcapsules suitable for the subsequent cellular studies. In Figure 10.1E, microcapsules made of CHI and the $ELR\text{-}RDG^{(-)}$ can be observed. Unlike RGD, RDG is a nonbioactive motif similar to RGD in all aspects, except for the position of the G and D amino acids. As such, the scrambled RDG sequence was previously shown to have significantly less cellular adhesion in respect to its functional RGD counterpart [37,38]. These microcapsules resembled in morphology and size the $(CHI/ELR\text{-}RGD)_2$ microcapsules (Figure 10.1D). With such similarity, it was expectable that differences in the mechanism and efficacy of internalization of these two microcapsule types – if any – would be solely caused by their peptide sequence bioactivity rather than by a morphological discrepancy.

Mesenchymal stem cells (MSCs) are hypoimmunogenic and pluripotent able to differentiate in *in vitro*, *ex vivo* and *in vivo*, into multiple cells types such as osteocytes, adipocytes, chondrocytes, neurocytes, hepatocytes, myocytes, and hematopoietic-supporting stroma. These characteristics have been considered crucial factors when aiming to develop new candidates for clinical use, especially in tissue engineering and regenerative medicine applications, such as transplantation, local implantation, gene therapy, and drug delivery [39,40]. Cellular therapies in particular can be envisaged in order to internalize molecules with the aim to control cellular behavior, such as the induced differentiation of MSCs into osteoblasts [41]. Therefore, the option to use hMSCs in a model of internalization of CHI/ELR microcapsules could open the direct applicability of the methodology described herein.

In order to demonstrate if this kind of hybrid nanostructured microcapsules are suitable for biological applications, we analyzed the *in vitro* viability of hMSCs by means of their metabolic activity in the presence of $(CHI/ELR\text{-}RGD)_2$ and $(CHI/ELR\text{-}RDG^{(-)})_2$. We studied the dose-dependent response effect for two experimental times: 3 h and 72 h. hMSCs were co-incubated with increasing microcapsule/cell ratios within a range of 5 to 100 units per cell. In Figure 2, the cell viability is represented normalized in respect to the positive control, that is, cells cultured without microcapsules. As observed in Figure 10.2A and Figure 10.2B, after 3 h and 72 h of incubation with $(CHI/ELR\text{-}RGD)_2$, the metabolic activity did not vary significantly for the studied ratio range in respect to the positive control.

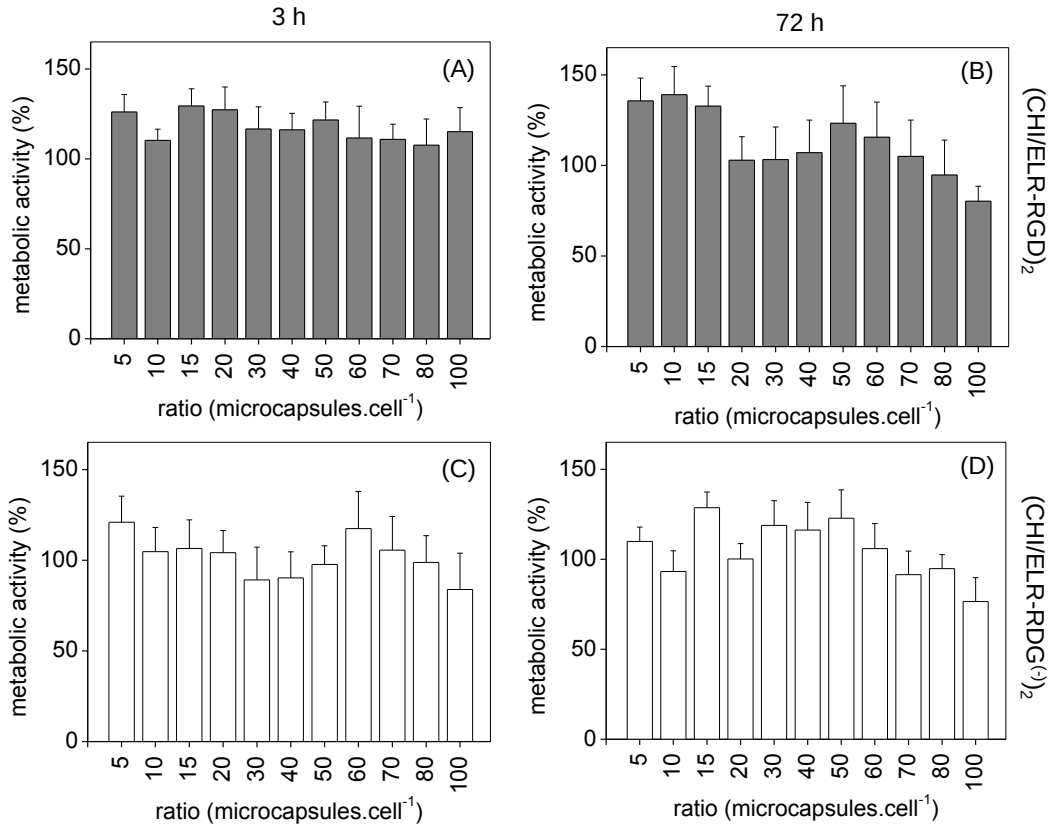


Figure 10.2. Metabolic activity of hMSCs incubated with increasing ratios of (A, B) (CHI/ELR-RGD)$_2$ and (C, D) (CHI/ELR-RDG$^{(-)}$)$_2$ microcapsules for (A, C) 3 h and (B, D) 72 h. Data represent means of four experiments, each performed in quadruplicate, normalized in respect to the positive control. Error bars represent one standard error (mean+SE). No significant statistical differences were found (*p*-value higher than 0.05).

In light of our results, (CHI/ELR-RGD)$_2$ hybrid microcapsules are not only noncytotoxic for hMSCs but can also help maintaining a high cellular metabolic activity over a high ratio of microcapsules in respect to the number of cells. A similar trend was observed for ELR-RDG$^{(-)}$-functionalized microcapsules. For both time-points (Figure 10.2C and Figure 10.2D), there were no apparent metabolic activity differences in respect to the positive control as a function of microcapsule concentrations.

Analyzing the graphics for 72 h of incubation (Figure 10.2B and Figure 10.2D), one can observe that there is a decrease in the mean metabolic activity of cells incubated with either microcapsule type for the highest microcapsule/cell ratios. This decrease can be seen for a ratio higher than 50:1 for (CHI/ELR-RGD)$_2$ and 60:1 for (CHI/ELR-RDG$^{(-)}$)$_2$ microcapsules. When considering cell viability, one could expect that a large quantity of microcapsules will reduce nutrient and gas exchanges between the

internal cellular compartment and the culture medium, eventually leading to cell death [42]. Although the microcapsules presented herein are noncytotoxic towards hMSCs even for the highest studied ratios, it is plausible to affirm that a large number of microcapsules will have negative impact in the metabolic activity of the cells.

Despite the high metabolic activity observed in comparison to the positive control, it was also apparent that cells incubated with (CHI/ELR-RDG$^{(-)}$)$_2$ microcapsules were less viable than their biofunctional analogues. For instance, after incubating 10 microcapsules per cell during 72 h with hMSCs, a viability of 139% (ELR-RGD-based elements) was estimated in comparison to 105% (ELR-RDG$^{(-)}$-based elements), accounting for a reduction of 24%.

In Figure 10.3, the metabolic activity measurements for every microcapsule/cell ratio were coupled together and their mean was calculated to estimate the cellular viability for each microcapsule type.

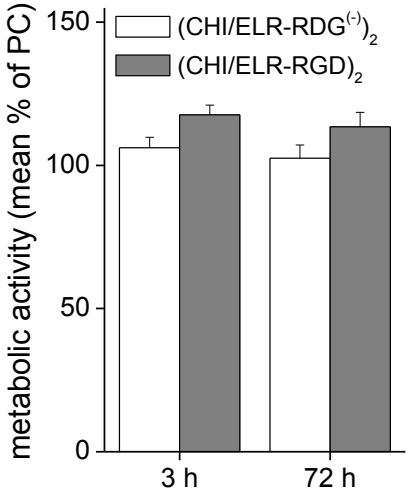


Figure 10.3. Estimated metabolic activity of hMSCs incubated with (CHI/ELR-RGD)$_2$ and (CHI/ELR-RDG$^{(-)}$)$_2$ microcapsules for 3 and 72 h. Data represent means of the viability results performed for microcapsule/cell ratios from 5:1 to 100:1, as compared to the positive control (PC, cells cultured without microcapsules). Error bars represent one standard error (mean+SE). No significant statistical differences were found (*p*-value higher than 0.05).

In the case of the longest incubation time (72 h), hMSCs incubated with RGD-functionalized microcapsules exhibited a mean metabolic activity of 114%, while RDG$^{(-)}$-functionalized ones exhibited 102%. These differences in bioactivity do not account for a significant difference between each

microcapsules type, although the mean bioactivity values of $(CHI/ELR\text{-}RGD)_2$ are higher for all time-points. This small disparity could be the result of RGD-induced integrin activation in the dorsal region of the cells, a non-selective interaction, which is known to be involved in several metabolic pathways, such as those of proliferation and differentiation [43,44].

In light of these results, it seems possible to apply rather large amounts of hybrid microcapsules to hMSCs without severely affecting their viability, even when using the non-functional RDG analogue. The lowest microcapsule/cell ratios also provided the most favorable conditions for hMSCs incubation with both types of functionalized microcapsules. Given these results, we selected a concentration of 10 microcapsules per cell for all subsequent experiments. This way, it would be possible to keep the microcapsule/cell ratio to a minimum while avoiding a massive and systematic microcapsule administration and ensuring a high cellular metabolic activity in respect to the positive control.

Cell viability assays by LIVE/DEAD® were carried out to complement the metabolic activity data for a time-frame of 10 days and can be observed in Figure 10.4.

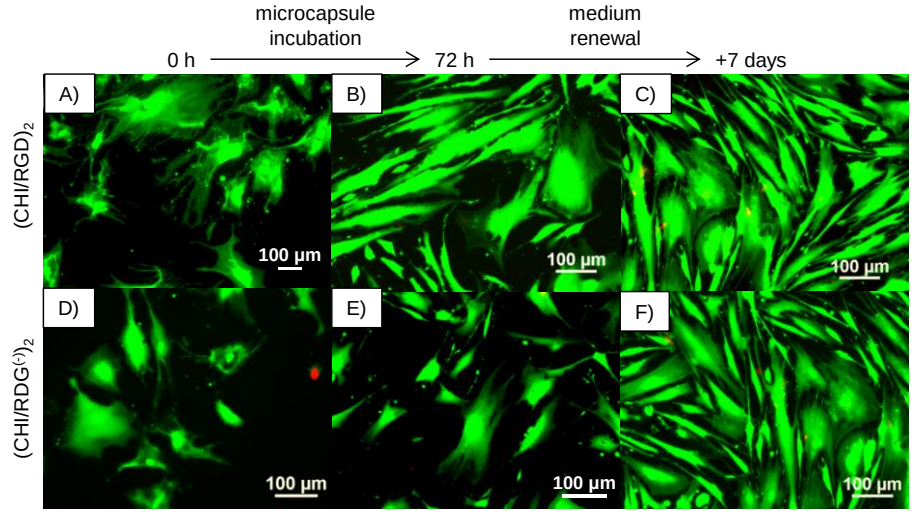


Figure 10.4. Representative microphotographs of LIVE/DEAD® assay of hMSCs incubated with (A, B and C) $(CHI/ELR\text{-}RGD)_2$ and (D, E and F) $(CHI/ELR\text{-}RDG^{(-)})_2$ microcapsules at 0 (A, D) and 72 h (B, E) and 240 h times points. (C, F).

In respect to the $(CHI/ELR\text{-}RGD)_2$ microcapsules effect, after an incubation period of 72 h, the green calcein staining confirmed that the cells were alive and well-spread on the surface (Figure 10.4B). The

same trend is observed for the $(CHI/ELR\text{-}RDG^{(-)})_2$ (Figure 10.4E), with no visible differences between each case. In order to assess if the cells could remain alive after being cultured in the presence of hybrid microcapsules, complete DMEM was added after 72 h to the co-incubation medium. Then this mixture was maintained for another 168 h to a total of 10 days of culture before LIVE/DEAD® assays were performed. As observed in Figure 10.4C and Figure 10.4F, no dead cells were encountered, clearly indicating that hMSCs viability was not affected by the incubation with the foreign microcapsule components – as supported by the metabolic activity assays – even after a longer exposition time.

In order to determine if this class of hybrid microcapsules could be internalized by cells, hMSCs were co-incubated first with $(CHI/ELR\text{-}RGD)_2$ for 72 h. To aid in this microscopy visualization, the microcapsules were loaded with DQ-ovalbumin. This commercially available product is a conjugate of ovalbumin heavily labeled with BODIPY dyes. Due to a characteristic self-quenching mechanism, it exhibits a bright red fluorescence characterized by the close proximity of the fluorescent dyes, but it shifts to a strong green upon proteolysis. This means that it would be possible to follow the internalization of the microcapsules and the intracellular processing of the cargo by fluorescence assays. Confocal microscopy (Figure 10.5) confirmed the presence of internalized RGD-functionalized microcapsules after 72 h of incubation. A yellow color (resulting from the simultaneous fluorescence emission of red and green) could be observed in different planes of the cells, evidencing that the microcapsules containing DQ-ovalbumin were processed by the hMSCs. In Figure 10.5A, the arrows point to bright green dots, indicating the presence of fully degraded microcapsules. To reflect upon the electrostatic interactions between capsules and cellular membrane, the charges of ELR-RGD and $ELR\text{-}RDG^{(-)}$ in aqueous solution were determined by ζ-potential measurements. They were shown to have a charge of -5.7±1.2 mV and -6.3±1.2 mV, respectively, in PBS. One could argue that the negative charge of the ELR outer layer could potentially hinder the internalization by conflicting with the electrostatic nature of the cellular membrane [45]. However, electrostatic interactions alone were previously unable to account for cellular adhesion to surfaces modified with polycations [46] and thus is expected to have little influence in comparison to the bioactive properties of the used macromolecules. Therefore, these results show that cellular uptake of CHI/ELR microcapsules can be achieved and that their intracellular degradation can be followed by the used fluorophore.

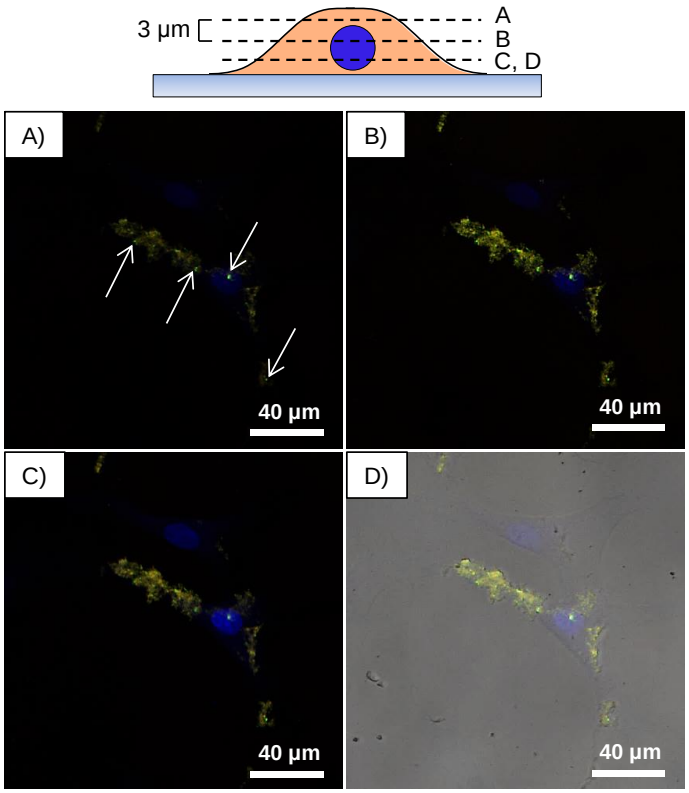


Figure 10.5. Confocal microscopy of hMSCs containing (CHI/ELR-RGD)$_2$ microcapsules within their cytoplasm. The nuclei are stained with DAPI (blue) and the microcapsules loaded with DQ-ovalbumin. The schematics represent the relative position of each plane in the cell (A, B and C). The arrows in (A) point to bright green dots, representing fully processed DQ-ovalbumin. (D) Bright field image was merged with the fluorescence-only image in (C).

After confirming that cellular uptake of this class of microcapsules can be successful, the cells that could effectively internalize microcapsules loaded with DQ-ovalbumin were quantified by flow cytometry. Figure 10.6 shows the results obtained by flow cytometry and the quantification of the internalization efficiency for both microcapsule types. For this analysis, the study of Semmling *et al.* [47], who performed a "flow cytometry"-based assay to analyze the uptake of polyelectrolyte capsules, was taken into consideration. In the case of (CHI/ELR-RGD)$_2$ microcapsules, in Figure 10.6A, viable hMSCs after 72 h of incubation were represented by the area delimited in yellow. Viable cells include cells that were either empty (with low side-scattering intensity, I_{SS}) or internalized microcapsules (with high I_{SS}). Outside these borders, cellular debris, apoptotic cells and microcapsule debris are usually identified here.

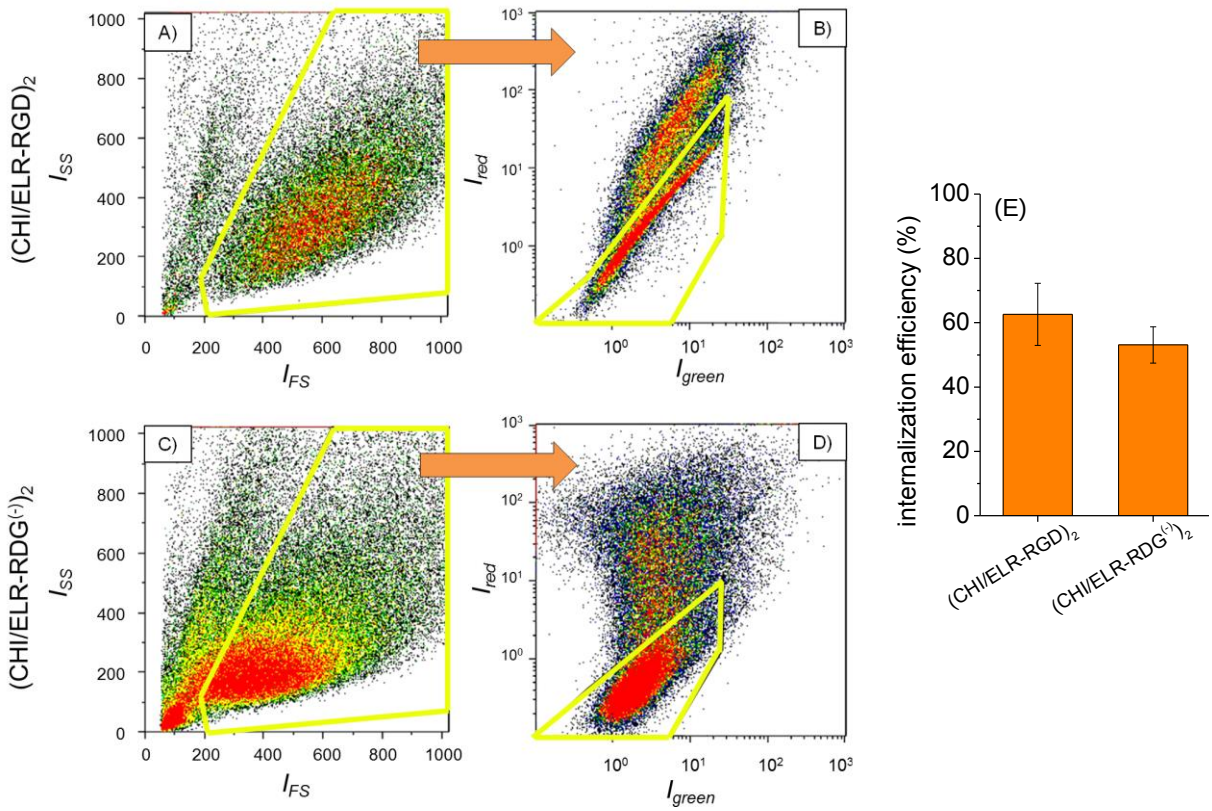


Figure 10.6. Flow cytometry 2D density plots of hMSCs after a 72 h incubation with (A, B) (CHI/ELR-RGD)$_2$ and (C, D) (CHI/ELR-RDG$^{(-)}$)$_2$ microcapsules. The density of the events is color-coded from blue (low frequency) to red (high frequency). (A, C) Side-scattering intensity (I_{SS}) is plotted as a function of forward-scattering intensity (I_{FS}). The area delimited in yellow corresponds to viable cells either empty (low I_{SS}) or with internalized microcapsules (high I_{SS}), and was established based in a control of hMSCs cultured in the absence of microcapsules. (B, D) The events corresponding to viable cells were sorted according to red (I_{red}) and green (I_{green}) fluorescence intensities and events corresponding to empty or cells containing microcapsules were subdivided. (E) Internalization efficiency of each type of capsule for three independent experiments. Data represent means of three independent experiments. Error bars represent two standard errors (mean±SE). No significant statistical differences were found (*p*-value higher than 0.05).

In Figure 10.6B, the identified viable cells were re-plotted according to their red (I_{red}) and green (I_{green}) fluorescence intensities emitted by the DQ-ovalbumin. It should be noted that a cell can bear DQ-ovalbumin-loaded microcapsules in every of these processing stages, that is, DQ-ovalbumin exhibiting red, green, or both. Thus, events with high intensity in either of these spectra corresponded to cells

containing DQ-ovalbumin in distinct stages of intracellular processing: intact, degraded, or in process of degradation. Within the delimited area in Figure 10.6B are found empty cells, verified from a control of cells cultured without microcapsules. The data indicate that 63±17% of the hMSCs have internalized $(CHI/ELR\text{-}RGD)_2$ microcapsules, as depicted in Figure 10.6E.

This same analysis was performed for $(CHI/ELR\text{-}RDG^{(-)})_2$ (see Figure 10.6C and Figure 10.6D), after which an internalization efficiency of 53±10% was determined. No statistical differences were found between both cases, indicating that the exhibition of RGD did not influence the incorporation of the microcapsules by the hMSCs, in respect to microcapsules exhibiting RDG. Nonetheless, the mean internalization efficacy for $(CHI/ELR\text{-}RGD)_2$ was higher than its nonbioactive counterpart, which may indicate a minor contribution of receptor-mediated interactions in the cellular uptake.

Our results indicate that the internalization of LbL microcapsules is not affected significantly when coupled with biofunctional components, contrary to what was demonstrated by other authors.[48,49] For instance, Caruso and coworkers [48] showed that poly(styrene sulfonate)/poly(allylamine hydrochloride) (PSS/PAH) capsules (around 500 nm in diameter) functionalized with humanized A33 monoclonal antibodies could be internalized specifically by LIM1215 colorectal cancer cells. However, in another work, De Koker *et al.* [50] inhibited different endocytic pathways and actin polymerization in bone-marrow-derived dendritic cells. Their results demonstrated that microcapsules with around 3 μm are internalized via macropinocytosis – a nonspecific endocytosis mechanism for foreign materials roughly between 500–2000 nm [51]. Therefore it is likely that macropinocytosis was the major endocytosis mechanism involved in the cellular uptake of carrier devices of this class and size (around 3–4 μm in diameter), to which surface functionalization does not play a determinant role.

Upon internalization of a drug carrier, it is important to ensure that the agent is not only delivered but also available for use by cells. Thanks to the use of DQ-ovalbumin, the consumption of this cargo by cells could be conveniently assessed by fluorescence changes. After quantifying the cellular uptake, the bioavailability of DQ-ovalbumin was evaluated by co-incubating cultured hMSCs with each kind of microcapsules in parallel for 3 and 72 h. In Figure 10.7, representative bright-field and fluorescence microscope images can be observed for $(CHI/ELR\text{-}RGD)_2$ and $(CHI/ELR\text{-}RDG^{(-)})_2$ microcapsules loaded with DQ-ovalbumin. The schematic representation in Figure 10.7A shows the various stages of cellular uptake and intracellular processing of encapsulated protein. Until the cargo reaches a fully degraded state, the intensity of green fluorescence increases and red decreases: their simultaneous emission results in the orange and yellow intermediate colors observable under the fluorescence microscope.

After 3 h of incubation and a rinsing step with DPBS, few microcapsules were detected within the cells, with these few occurrences being mostly red or bright orange.

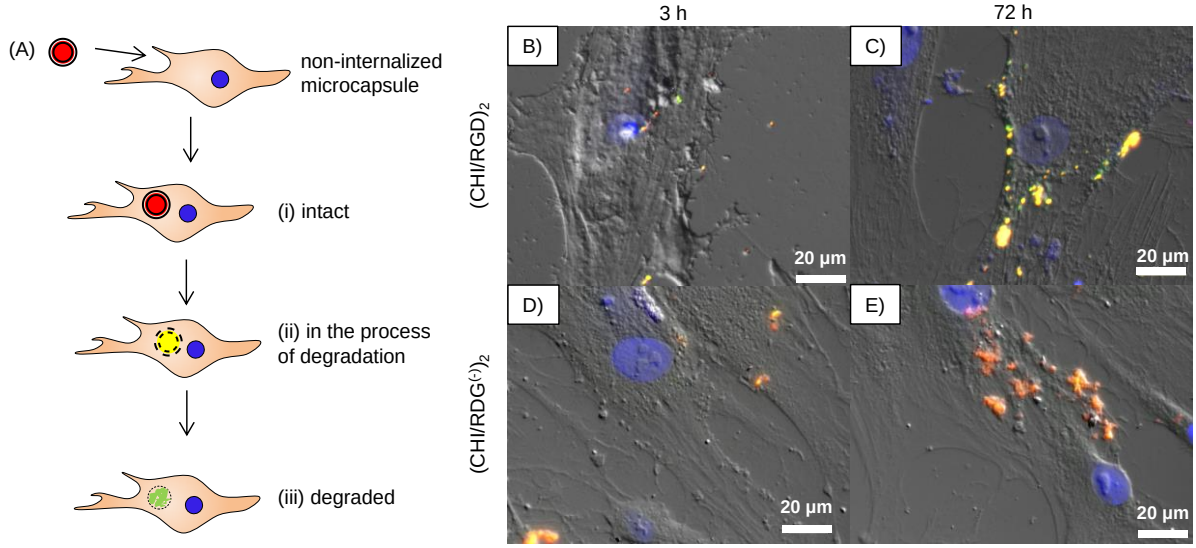


Figure 10.7. The scheme (A) depicts the various degradation stages that DQ-ovalbumin undergoes. Representative microscopy images of $(CHI/ELR\text{-}RGD)_2$ and $(CHI/ELR\text{-}RDG^{(-)})_2$ microcapsules loaded with DQ-ovalbumin incubated with hMSCs after (B, D) 3 or (C, E) 72 h of incubation and DAPI staining (nuclei of the cells stained in blue). A shift from red/orange to green/yellow indicates a transition between fully intact to degraded cargo. Images are of fluorescence and differential interference contrast (DIC) microscopy at 40× magnification.

This observation was common for both $(CHI/ELR\text{-}RGD)_2$ and $(CHI/ELR\text{-}RDG^{(-)})_2$ microcapsules (Figure 10.7B and Figure 10.7D). A closer observation permits to detect some green dots after 3 h of incubation, like in the case of $(CHI/ELR\text{-}RGD)_2$ microcapsules (Figure 10.7B). Such observation is consistent with the work of Rivera-Gil *et al.* [17], in which the same fluorescent protein was used. In their work with nonbiodegradable poly(styrene sulfonate)/poly(allylamine hydrochloride) (PSS/PAH) microcapsules, they concluded that a green fluorescence exhibited in capsules that are not expected to degrade – hence efficiently protecting their cargo – would still be permeable and prone to this fluorescence change. Variables such as the pH and ionic strength influence the permeability of the polyelectrolyte capsules, thus DQ-ovalbumin would still be able to diffuse through the multilayer shell and exposed to proteases and be degraded.

After 72 h of incubation, a higher amount of microcapsules were detected interacting with the cells, in comparison to the shorter time-point, with a predominant presence of yellow capsules found in the case of hMSCs incubated with RGD-functionalized microcapsules and red capsules in the case of cells incubated with the non-functional analogue ones. This observation indicates that, even after 72 h of incubation, distinct stages of microcapsule/cell internalization and intracellular processing could be found. However, judging by the intense yellow and occasional green dots in Figure 10.7C, the bioavailability of DQ-ovalbumin encapsulated within $(CHI/ELR\text{-}RGD)_2$ microcapsules seemed higher.
The microscopy comparison between both types of microcapsules (Figure 10.7) seems to indicate that both $(CHI/ELR\text{-}RGD)_2$ and $(CHI/ELR\text{-}RDG^{(-)})_2$ situations bear little difference in respect to the number of apparent internalized carriers. Nonetheless, a dominant emission fluorescence towards the green spectrum – that of cleaved DQ-ovalbumin – was dominant in the former. This result shows that the cargo of RGD-functionalized microcapsules was processed faster, evidencing a higher bioavailability of DQ-ovalbumin for this carrier type. In this sense, the bioavailability rate of the cargo does not follow the results from the cellular uptake quantification shown in Figure 10.6: the internalization efficacy does not seem much influenced by the surface functionalization, whereas the intracellular processing of their cargo does. The study of the internalization mechanism and intracellular processing has not been much researched. It is true that the role of macropinocytosis was previously demonstrated [50] but it is known that functionalizing an interface can mediate specific integrin interactions [52]. Given that the surface functionalization in this work had little influence in the internalization efficacy, one would expect that the degradation of their cargo would be similar after the studied time of exposure. It could be suggested that the distinct functionality of the adsorbed recombinamers triggers distinct proteolytic pathways, just as RGD may active proliferation- and differentiation-related integrins. However, the study of such mechanism was out of the scope of this work. Such mechanism should be studied in the future in order to properly determine carrier and cargo fates upon cellular uptake, especially for carriers of the same class internalized by similar endocytic mechanisms. With these results, we conclude that CHI/ELR microcapsules can be internalized by hMSCs, regardless of their surface functionalization, and may act as suitable carriers for the intracellular delivery of active agents.

10.4 Conclusion

We presented the fabrication of multilayer microcapsules made of natural and nature-inspired polymers for intracellular delivery of active agents. Thanks to the nature of the constituents, the microcapsules

were noncytotoxic as their degradation does not result in harmful products for the cells. Cellular uptake was demonstrated, showing their potential as carriers for drug delivery directly to the cellular machinery. In the future, this way of delivery may help minimizing drug losses and increasing their delivery control and efficacy. The internalization efficacy demonstrated for hMSCs lets foresee their use in cell/tissue engineering and regenerative medicine where it is important to control the differentiation of stem cells into specific phenotypes. This work confirmed that CHI/ELR microcapsules could interact and be internalized by cells, but experiments with microcapsules loaded with actual active agents are envisaged, such as molecules that trigger the differentiation of cells into specific phenotypes. The mechanism of internalization of the microcapsules at this scale did not depend on the surface functionalization. They were internalized via macropinocytosis although the ELR functionalization suggested a minor role of integrin-mediated mechanisms. In this context, the recombinant nature of ELRs will be of interest to further study the microcapsules' endocytosis mechanism. In particular, it is possible that the production of smaller capsules by using nanotemplates may increase the influence of RGD and facilitate internalization [53]. The inclusion of bioactive motifs other than this generic motif may constitute a strong advantage of using such recombinant technologies, allowing exploring not only specific recognition processes but also degradation pathways for targeted delivery and increased drug efficacy. Therefore, multilayer microcapsules using biomimetic ingredients for intracellular delivery let foresee new strategies to increase the availability of molecules of interest in cells and for targeted biomedical applications.

10.5 Acknowledgements

We acknowledge financial support from Fundação para a Ciência e Tecnologia (grant SFRH/BD/61126/2009), "Fundo Social Europeu", "Programa Diferencial de Potencial Humano", EU 7th Framework Programme (nº REGPOT-CT2012-316331-POLARIS), the EU through the European regional development fund (ERDF), from the MINECO (MAT-2010-15982, MAT2010-15310, PRI-PIBAR-2011-1403 and MAT2012-38043), the JCyL (projects VA049A11, VA152A12 and VA155A12), the CIBER-BBN, and the JCyL and the Instituto de Salud Carlos III under the "Network Center of Regenerative Medicine and Cellular Therapy of Castilla and Leon".

10.6 References

[1] Malam Y., Loizidou M., and Seifalian A. M., Liposomes and nanoparticles: nanosized vehicles for drug delivery in cancer, Trends in Pharmacological Sciences 2009, 30: 592-599.

[2] Meng F., Zhong Z., and Feijen J., Stimuli-Responsive Polymersomes for Programmed Drug Delivery, Biomacromolecules 2009, 10: 197-209.

[3] Szarpak A., Cui D., Dubreuil F., De Geest B. G., De Cock L. J., Picart C., and Auzély-Velty R., Designing hyaluronic acid-based layer-by-layer capsules as a carrier for intracellular drug delivery, Biomacromolecules 2010, 11: 713-720.

[4] Caruso F., Caruso R. A., and Möhwald H., Nanoengineering of inorganic and hybrid hollow spheres by colloidal templating, Science 1998, 282: 1111-1114.

[5] De Cock L. J., De Koker S., De Geest B. G., Grooten J., Vervaet C., Remon J. P., Sukhorukov G. B., and Antipina M. N., Polymeric multilayer capsules in drug delivery, Angewandte Chemie International Edition 2010, 49: 6954-6973.

[6] del Mercato L. L., Rivera-Gil P., Abbasi A. Z., Ochs M., Ganas C., Zins I., Sonnichsen C., and Parak W. J., LbL multilayer capsules: recent progress and future outlook for their use in life sciences, Nanoscale 2010, 2: 458-467.

[7] Petrov A. I., Volodkin D. V., and Sukhorukov G. B., Protein—calcium carbonate coprecipitation: a tool for protein encapsulation, Biotechnology Progress 2005, 21: 918-925.

[8] Tong W., Zhu Y., Wang Z., Gao C., and Möhwald H., Micelles-Encapsulated Microcapsules for Sequential Loading of Hydrophobic and Water-Soluble Drugs, Macromolecular Rapid Communications 2010, 31: 1015-1019.

[9] Gribova V., Auzely-Velty R., and Picart C., Polyelectrolyte multilayer assemblies on materials surfaces: from cell adhesion to tissue engineering, Chemistry of Materials 2011, 24: 854-869.

[10] Shukla A., Avadhany S. N., Fang J. C., and Hammond P. T., Tunable Vancomycin Releasing Surfaces for Biomedical Applications, Small 2010, 6: 2392-2404.

[11] Tang Z., Wang Y., Podsiadlo P., and Kotov N. A., Biomedical Applications of Layer-by-Layer Assembly: From Biomimetics to Tissue Engineering, Advanced Materials 2006, 18: 3203-3224.

[12] Johnston A. P. R., Cortez C., Angelatos A. S., and Caruso F., Layer-by-layer engineered capsules and their applications, Current Opinion in Colloid & Interface Science 2006, 11: 203-209.

[13] Facca S., Cortez C., Mendoza-Palomares C., Messadeq N., Dierich A., Johnston A. P. R., Mainard D., Voegel J.-C., Caruso F., and Benkirane-Jessel N., Active multilayered capsules for in vivo bone formation, Proceedings of the National Academy of Sciences 2010, 107: 3406-3411.

[14] McShane M., and Ritter D., Microcapsules as optical biosensors, Journal of Materials Chemistry 2010, 20: 8189-8193.

[15] Tong W., She S., Xie L., and Gao C., High efficient loading and controlled release of low-molecular-weight drugs by combination of spontaneous deposition and heat-induced shrinkage of multilayer capsules, Soft Matter 2011, 7: 8258-8265.

[16] Su X., Kim B.-S., Kim S. R., Hammond P. T., and Irvine D. J., Layer-by-layer-assembled multilayer films for transcutaneous drug and vaccine delivery, ACS Nano 2009, 3: 3719-3729.

[17] Rivera-Gil P., De Koker S., De Geest B. G., and Parak W. J., Intracellular Processing of Proteins Mediated by Biodegradable Polyelectrolyte Capsules, Nano Letters 2009, 9: 4398-4402.

[18] Nel A. E., Madler L., Velegol D., Xia T., Hoek E. M. V., Somasundaran P., Klaessig F., Castranova V., and Thompson M., Understanding biophysicochemical interactions at the nano-bio interface, Nat Mater 2009, 8: 543-557.

[19] Panyam J., and Labhasetwar V., Biodegradable nanoparticles for drug and gene delivery to cells and tissue, Advanced Drug Delivery Reviews 2003, 55: 329-347.

[20] Patri A. K., Kukowska-Latallo J. F., and Baker Jr J. R., Targeted drug delivery with dendrimers: Comparison of the release kinetics of covalently conjugated drug and non-covalent drug inclusion complex, Advanced Drug Delivery Reviews 2005, 57: 2203-2214.

[21] Wei H., Zhuo R.-X., and Zhang X.-Z., Design and development of polymeric micelles with cleavable links for intracellular drug delivery, Progress in Polymer Science 2013, 38: 503-535.

[22] Volodkin D. V., Larionova N. I., and Sukhorukov G. B., Protein Encapsulation via Porous CaCO3 Microparticles Templating, Biomacromolecules 2004, 5: 1962-1972.

[23] Correia C. R., Reis R. L., and Mano J. F., Multilayered Hierarchical Capsules Providing Cell Adhesion Sites, Biomacromolecules 2013, 14: 743-751.

[24] She Z., Antipina M. N., Li J., and Sukhorukov G. B., Mechanism of Protein Release from Polyelectrolyte Multilayer Microcapsules, Biomacromolecules 2010, 11: 1241-1247.

[25] Angelatos A. S., Katagiri K., and Caruso F., Bioinspired colloidal systems via layer-by-layer assembly, Soft Matter 2006, 2: 18-23.

[26] Rinaudo M., Chitin and chitosan: Properties and applications, Progress in Polymer Science 2006, 31: 603-632.

[27] Urry D. W., What sustains life? A consilient mechanism for protein-based machines and materials, New York: Springer; 2006.

[28] Girotti A., Fernández-Colino A., López I. M., Rodríguez-Cabello J. C., and Arias F. J., Elastin-like recombinamers: Biosynthetic strategies and biotechnological applications, Biotechnology Journal 2011, 6: 1174-1186.

[29] Nettles D. L., Chilkoti A., and Setton L. A., Applications of elastin-like polypeptides in tissue engineering, Advanced Drug Delivery Reviews 2010, 62: 1479-1485.

[30] Costa R. R., Testera A. M., Arias F. J., Rodríguez-Cabello J. C., and Mano J. F., Layer-by-Layer Film Growth Using Polysaccharides and Recombinant Polypeptides: A Combinatorial Approach, The Journal of Physical Chemistry B 2013, 117: 6839-6848.

[31] Hynes R. O., Integrins: Bidirectional, Allosteric Signaling Machines, Cell 2002, 110: 673-687.

[32] Hu Z., Luo F., Pan Y., Hou C., Ren L., Chen J., Wang J., and Zhang Y., Arg-Gly-Asp (RGD) peptide conjugated poly(lactic acid)–poly(ethylene oxide) micelle for targeted drug delivery, Journal of Biomedical Materials Research Part A 2008, 85A: 797-807.

[33] Oba M., Aoyagi K., Miyata K., Matsumoto Y., Itaka K., Nishiyama N., Yamasaki Y., Koyama H., and Kataoka K., Polyplex micelles with cyclic RGD peptide ligands and disulfide cross-Links directing to the enhanced transfection via controlled intracellular trafficking, Molecular Pharmaceutics 2008, 5: 1080-1092.

[34] Xiong X.-B., Mahmud A., Uludağ H., and Lavasanifar A., Multifunctional polymeric micelles for enhanced intracellular delivery of doxorubicin to metastatic cancer cells, Pharmaceutical Research 2008, 25: 2555-2566.

[35] Signini R., and Campana Filho S. P., On the preparation and characterization of chitosan hydrochloride, Polymer Bulletin 1999, 42: 159-166.

[36] Costa R. R., Custódio C. A., Arias F. J., Rodríguez-Cabello J. C., and Mano J. F., Nanostructured and thermoresponsive recombinant biopolymer-based microcapsules for the delivery of active molecules, Nanomedicine: Nanotechnology, Biology and Medicine 2013, 9: 895-902.

[37] Costa R. R., Custódio C. A., Arias F. J., Rodríguez-Cabello J. C., and Mano J. F., Layer-by-Layer Assembly of Chitosan and Recombinant Biopolymers into Biomimetic Coatings with Multiple Stimuli-Responsive Properties, Small 2011, 7: 2640-2649.

[38] Liu J. C., and Tirrell D. A., Cell response to RGD density in cross-linked artificial extracellular matrix protein films, Biomacromolecules 2008, 9: 2984-2988.

[39] Pittenger M. F., Mackay A. M., Beck S. C., Jaiswal R. K., Douglas R., Mosca J. D., Moorman M. A., Simonetti D. W., Craig S., and Marshak D. R., Multilineage potential of adult human mesenchymal stem cells, Science 1999, 284: 143-147.

[40] Uccelli A., Moretta L., and Pistoia V., Mesenchymal stem cells in health and disease, Nature Reviews Immunology 2008, 8: 726-736.

[41] Oliveira J. M., Kotobuki N., Tadokoro M., Hirose M., Mano J. F., Reis R. L., and Ohgushi H., Ex vivo culturing of stromal cells with dexamethasone-loaded carboxymethylchitosan/poly(amidoamine) dendrimer nanoparticles promotes ectopic bone formation, Bone 2010, 46: 1424-1435.

[42] De Koker S., De Geest B. G., Cuvelier C., Ferdinande L., Deckers W., Hennink W. E., De Smedt S. C., and Mertens N., In vivo cellular uptake, degradation, and biocompatibility of polyelectrolyte microcapsules, Advanced Functional Materials 2007, 17: 3754-3763.

[43] Ivaska J., and Heino J., Interplay between cell adhesion and growth factor receptors: from the plasma membrane to the endosomes, Cell and Tissue Research 2010, 339: 111-120.

[44] Johnson M. S., Lu N., Denessiouk K., Heino J., and Gullberg D., Integrins during evolution: Evolutionary trees and model organisms, Biochimica et Biophysica Acta (BBA) - Biomembranes 2009, 1788: 779-789.

[45] Ke J.-H., and Young T.-H., Multilayered polyplexes with the endosomal buffering polycation in the core and the cell uptake-favorable polycation in the outer layer for enhanced gene delivery, Biomaterials 2010, 31: 9366-9372.

[46] Lee H.-S., Eckmann D. M., Lee D., Hickok N. J., and Composto R. J., Symmetric pH-dependent swelling and antibacterial properties of chitosan brushes, Langmuir 2011, 27: 12458-12465.

[47] Semmling M., Kreft O., Muñoz Javier A., Sukhorukov G. B., Käs J., and Parak W. J., A novel flow-cytometry-based assay for cellular uptake studies of polyelectrolyte microcapsules, Small 2008, 4: 1763-1768.

[48] Cortez C., Tomaskovic-Crook E., Johnston A. P. R., Radt B., Cody S. H., Scott A. M., Nice E. C., Heath J. K., and Caruso F., Targeting and Uptake of Multilayered Particles to Colorectal Cancer Cells, Advanced Materials 2006, 18: 1998-2003.

[49] Fischlechner M., Zschörnig O., Hofmann J., and Donath E., Engineering virus functionalities on colloidal polyelectrolyte lipid composites, Angewandte Chemie International Edition 2005, 44: 2892-2895.

[50] De Koker S., De Geest B. G., Singh S. K., De Rycke R., Naessens T., Van Kooyk Y., Demeester J., De Smedt S. C., and Grooten J., Polyelectrolyte microcapsules as antigen delivery vehicles to dendritic cells: uptake, processing, and cross-presentation of encapsulated antigens, Angewandte Chemie International Edition 2009, 48: 8485-8489.

[51] Bishop N. E., An update on non-clathrin-coated endocytosis, Reviews in Medical Virology 1997, 7: 199-209.

[52] Shayakhmetov D. M., Eberly A. M., Li Z.-Y., and Lieber A., Deletion of penton RGD motifs affects the efficiency of both the internalization and the endosome escape of viral particles containing adenovirus serotype 5 or 35 fiber knobs, Journal of Virology 2005, 79: 1053-1061.

[53] Rejman J., Oberle V., Zuhorn I. S., and Hoekstra D., Size-dependent internalization of particles via the pathways of clathrin- and caveolae-mediated endocytosis, Biochemical Journal 2004, 377: 159-169.

Chapter 11. Multifunctional compartmentalized capsules with a hierarchical organization from the nano- to the macro-scales[11]

Abstract

Inspired by the cells' structure, we present compartmentalized capsules with temperature and magnetic-based responsiveness, and hierarchical organization ranging from the nano- to the visible scales. Liquefied alginate macroscopic beads coated with a layer-by-layer (LbL) chitosan/alginate shell served as containers both for model fluorophores and microcapsules, which in their turn encapsulated either another fluorophore or magnetic nanoparticles (MNPs). The microcapsules were coated with a temperature responsive chitosan/elastin-like recombinamer (ELR) nanostructured shell. By varying the temperature from 25°C to 37°C, the two-hour release of rhodamine encapsulated within the microcapsules and its diffusion through the external compartment decreased from 84% and 71%. The devices could withstand handling and centrifugal stress, with 50% remaining intact at a rotation speed of 2000g. MNPs attributed magnetic responsiveness towards external magnetic fields. Such customizable system can be envisaged to transport bioactive agents and cells in tissue engineering applications.

[11] This chapter is based on the following publication:

Costa R. R., Castro-Otero E., Arias F. J., Rodríguez-Cabello J. C., and Mano J. F., Multifunctional compartmentalized capsules with a hierarchical organization from the nano to the macro scales, Biomacromolecules 2013, 14: 2403-2410, DOI:10.1021/bm400527y.

Chapter 11. Multifunctional compartmentalized capsules with a hierarchical organization from the nano- to the macro-scales

11.1 Introduction

Considerable research efforts have been focused on miniaturized compartmental engineering systems with optimized properties over the past decade due to their wealth of potential applications in fields such as catalysis, sensors, drug delivery, disease models, energy storage and microreactors [1-3], which often require complex phenomena to occur simultaneously. Such a multifunctional device that is capable of addressing several reactions at once would, however, be difficult to develop. Perhaps not surprisingly, nature gives us an elegant example of a multifunctional entity in the form of biological cells. Due to their unique hierarchical and compartmentalized organization, they allow numerous compounds to be transported, proteins to be synthesized and enzymatic reactions to be regulated within their cytoplasm. However, building artificial cells is still a technology in its infancy. In an attempt to mimic cells, a great deal of research has focused on hierarchical nano- and microcompartments [4-6]. Multi-shelled organic and inorganic capsules prepared by template-assisted strategies are usually accompanied by harsh processing conditions [7-9]. In contrast, compartmentalized assemblies of polymeric multilayer nano/microcapsules within larger partitions have been achieved by using non-aggressive bottom-up strategies [10-14]. In any case, compartmentalization has allowed combining properties and confine reactions that could not be achieved otherwise with single-component assemblies [4].

The most attractive characteristic of compartmentalized devices does not necessarily involve their potential ability to mimic intracellular reactions, such as confining drugs and enzymatic reactions into partitions [15-17]. Compartmental systems should ideally be customizable by assembling subcompartments which exhibit functions that are not coupled naturally. Moreover, following a proper selection of the constituents, the range of such functions could be widened by exploiting the properties of stimuli-responsive materials [18]. Some examples that would benefit from such approach are the release control of several biomolecules delivered simultaneously for enhanced drug delivery [19], the immobilization of such a device spatially for targeted therapies [20], and the control over a multitude of cellular events that lead to stem cell differentiation [21].

In our goal to construct a hierarchical multifunctional device, we aimed to demonstrate that both molecular compounds and inorganic iron oxide magnetic nanoparticles can be encapsulated in distinct compartments. We report the construction of liquefied microcapsule-containing gel beads manufactured using a hybrid “ionic gelation” strategy of alginate assisted by a layer-by-layer (LbL) approach. LbL is a

simple and versatile technique which allows producing robust coatings, even in substrates with complex geometries. Because it discards the need of organic and harmful solvents, it is an attractive technique for tissue engineering applications [22-24]. In three-dimensional structures, namely spherical capsules, the semi-permeable nature of multilayer coatings can be used to tune the permeability of molecules of interest in or out, or to completely confine them [13,25-27]. Herein, liquefied alginate macrocapsules delimited by multilayer shells of chitosan/alginate (CHI/ALG) were intended to containing microcapsules made of CHI/"elastin-like recombinamer (ELR)" inside. The latter, on their side, contained either magnetic nanoparticles (MNPs) or model molecular compounds, such as the model low molecular weight fluorophores fluorescein isothiocyanate and rhodamine.

CHI and ALG are two well-known polysaccharides of marine origin which show biocompatibility, adhesiveness, non-toxicity, as well as bacteriostatic, fungistatic, anti-microbial and hemostatic activities [28,29]. ELRs, a recombinant type of elastin-like polymer (ELP), are temperature-responsive polypeptides that are soluble in aqueous media below a specific critical transition temperature (T_t) but undergo a phase separation above it [30-32]. Lastly, MNPs are structures susceptible to magnetic fields. They are often used to enhance medical imaging diagnosis of soft tissues (e.g., magnetic resonance imaging, MRI) and temperature-triggered treatments such as hyperthermia and tissue ablation [33-35]. In light of the potential applications of compartmentalized structures, we have studied the properties of each of the structures that can be found at the nano-, micro- and macro-scales, the permeability of the multilayer shells at distinct temperatures (namely the coatings containing the temperature-responsive ELR) and the response to external magnetic fields. We hypothesized that such systems could be fabricated and customized to display smart tunable permeability and spatial mobilization/immobilization.

11.2 Experimental section

11.2.1 Materials

Medium molecular weight chitosan was purchased from Sigma-Aldrich (ref 448877) and purified by a series of filtration and precipitation in water and ethanol steps, adapted from the method described by Signini and Filho [36], followed by freeze-drying. The degree of deacetylation was determined to be 82% (Supplemental Figure 11.1). Alginic acid sodium salt from brown algae was purchased from Sigma-Aldrich (ref 71238) and used as received.

11.2.2 Bioproduction of the elastin-like recombinamers

An ELR containing a L-arginine-glycine-L-aspartic acid (RGD) motif was bioproduced using a fermentation process from an Escherichia coli strain BLR(DE3) containing an appropriate expression gene, obtained using an appropriate protocol for gene design [37]. After fermentation, the culture was harvested and lysed by ultrasonic disruption. Insoluble debris was removed by centrifugation and the cleared lysate was subjected to several cycles of cold (4°C) and warm (40°C) centrifugations, at 10000 rpm for 10 minutes each. Finally, the polymer was dialyzed against ultra-pure Milli-Q water at 4°C in dialysis membranes with a 12 kDa molecular weight cut-off for a minimum of 6 hours, after which the water was changed. After 4 changes of water, the biopolymer was frozen and freeze-dried. Characterization of the bioproduct was done previously [22,38].

11.2.3 Synthesis of magnetic nanoparticles

In a typical synthesis to synthesize spherical iron oxide MNPs, 10 mL of a solution containing 1.2 g of iron(III) chloride hexahydrate ($FeCl_3 \cdot 6H_2O$, Sigma-Aldrich ref. 236489) and 0.6 g of iron(II) chloride tetrahydrate ($FeCl_2 \cdot 4H_2O$, Sigma-Aldrich ref 220299) was added drop-wise to 25 mL of ammonium hydroxide solution (NH_4OH, made of 33% ammonia, NH_3, in H_2O) over 4 h under an inert nitrogen atmosphere. The products of the reaction were collected by magnetic separation and washed three times with ethanol and water. The last washing step was made with ethanol, after which the products were left to dry at room temperature.

11.2.4 Characterization of the MNPs

The shape and morphology of the magnetite nanoparticles were determined using high resolution transmission electronic microscope (TEM, JEOL JEM-1011, operating at 200 kV). Samples were prepared by dropping a dilute aqueous solution (concentration = 1 $mg \cdot mL^{-1}$) of the nanoparticles onto a 200-mesh copper grid and allowing the solvent to evaporate. The magnetization of the MNPs was measured as a function of the applied external magnetic field (maximum value 10 kOe) using a vibrating sample magnetometer (PPMS, Quantum Design) at 300 K.

11.2.5 Temperature-induced aggregate measurements

The aggregate sizes of chitosan, alginate and ELR in solution were measured using the dynamic light scattering (DLS) from a Nano-ZS from Malvern (United Kingdom) for temperatures 25°C/37°C after stabilization for 5 min. The samples of alginate and ELR were prepared at 300 $\mu g \cdot mL^{-1}$ in phosphate-buffered solution (PBS), pH 7.4. In the case of chitosan, the solvent was acetic acid at 1% (w/v) and sodium chloride (NaCl) concentration of 0.15 M, pH 5.5. Measurements were performed first at 25°C, then 37°C and finally back at 25°C. A total of 20 runs were performed for each sample to obtain an average value at stabilized temperature.

11.2.6 Synthesis of the calcium carbonate sacrificial particles, either empty or entrapping fluorophores/MNPs

Aqueous solutions of anhydrous sodium carbonate (Na_2CO_3, Sigma-Aldrich ref 222321) and calcium chloride ($CaCl_2$, VWR ref 1.02378.0500) were prepared at 1 M. In a typical co-precipitation reaction, 100 μg of a desired material was entrapped in a medium of 200 μL of H_2O by adding 100 μL of Na_2CO_3 followed by 100 μL of $CaCl_2$ with rapid stirring for 30 seconds. The H_2O precipitation medium contained the material to be entrapped at a concentration of 500 $\mu g \cdot mL^{-1}$. Three distinct ingredients were added to the H_2O precipitation medium: fluorescein-5(6)-isothiocyanate (FITC, 389 Da, Sigma-Aldrich ref F3651), rhodamine-B isothiocyanate (Rhod, 536 Da, Sigma-Aldrich ref R1755) and MNPs. As a control, empty microcapsules were also fabricated by using solely ultrapure H_2O. Stirring was stopped after 30 s and the suspension of newly synthesized calcium carbonate ($CaCO_3$) microparticles left to react and precipitate for 15 min. The supernatant was then removed and the particles washed twice with ultrapure water to remove residual salts and non-entrapped materials. Unless stated otherwise, all supernatants were retained for fluorescence measurements and quantification of losses until the construction of compartmental capsules was completed.

11.2.7 Construction of the microparticle multilayer coating

The $CaCO_3$ sacrificial templates (empty or entrapping either a fluorophore or MNP) were immersed alternately in CHI and ELR solutions (300 $\mu g \cdot mL^{-1}$, pH 5.5, 0.15 M of NaCl) for 10 min each, then washed with 0.15 M NaCl (pH 5.5 at 0.15 M). Centrifugation was avoided to prevent damage and aggregation of the particles each time the samples were to be retrieved from solution; simple

precipitation of the suspension was used instead (3 to 5 min). This process was repeated until three bilayers had been assembled, $(CHI/ELR)_3$. For the sole purpose of confocal microscopy characterization described below, the $CaCO_3$ cores were chelated at this point by immersion in ethylenediamine tetraacetic acid (EDTA, Sigma-Aldrich ref E9884; 0.2 M, pH 5.5) for 30 min.

11.2.8 Construction of multilayer coated external subcompartment-containing beads

A 1% (w/v) solution of alginic acid sodium salt was prepared. In a typical experiment, the $(CHI/ELR)_3$-coated microparticles were suspended in 1 mL of alginate solution and the resulting suspension extruded through a 25G needle, at a rate of 0.33 $mL \cdot min^{-1}$, into a 0.75% (w/v) solution of $CaCl_2$ under mild stirring. Alginate beads containing coated microparticles were formed by calcium-mediated ionic gelation. The beads were immersed alternately in CHI and ALG solutions (300 $\mu g \cdot mL^{-1}$, pH 5.5, 0.15 M NaCl) for 10 minutes each, then washed with 0.15 M NaCl (pH 5.5 at 0.15 M). This process was repeated until three bilayers had been assembled, $(CHI/ALG)_3$. After the coating had been assembled, the beads were immersed in EDTA. At this point, the $CaCO_3$ sacrificial templates are chelated simultaneously with the liquefied alginate bead.

Liquefied alginate beads coated with $(CHI/ALG)_3$ multilayers loaded with not only empty microcapsules and Rhod in the ALG medium were also constructed. Rhod was suspended alongside the empty microcapsules and encapsulated in the ALG bead compartment instead of in the inner microcapsules. In a typical experiment, Rhod was suspended in ALG at 15 $\mu g \cdot mL^{-1}$. This value was determined by first calculating the construction losses resulting from the Rhod-loaded microcapsules within the external alginate macrocapsule in order to minimize concentration-dependent artifacts (see Supplemental Figure 11.3 for details).

11.2.9 Characterization of the compartmental units

The morphology of the FITC-loaded $(CHI/ELR)_3$ microcapsules was determined using an Olympus FV1000 confocal microscope (Germany). TEM images of both empty and MNP-loaded microcapsules were obtained using a JEOL JEM-1011 HR instrument operating at 80 kV. Prior to the observation, a volume of 60 μL of microcapsule suspension was pipetted onto a transmission electron microscopy (TEM) grid and left to evaporate overnight. An Axioimager Z1M Zeiss microscope (Germany) was used to

observe $(CHI/ALG)_3$-coated liquefied beads using transmitted light and fluorescence microscopy for Rhod-loaded external compartments. The latter also containing FITC-loaded microcapsules were observed to assess the distribution of the subcompartments within the macrocapsules.

11.2.10 Mechanical resistance of the external compartments

A centrifugal rotation test was performed with the samples suspended in PBS to measure the mechanical resistance of the $(CHI/ALG)_3$ macrocapsules. 100 samples were placed in centrifuge tubes and rotated at a starting centrifugal load of 500g. After 5 min, the number of intact beads was counted. Those that remained intact were submitted to incremental centrifugal loads (500g incremental steps) up to a maximum of 5000g. This experiment was performed three times.

11.2.11 Rhodamine release studies

The compartmentalized systems were suspended in PBS at either 25 or 37°C. Prior to this study, Rhod was encapsulated in one of two hierarchical locations: the internal $(CHI/ELR)_3$ microcapsules (with Rhod added during the co-precipitation stage) or the external liquefied alginate $(CHI/ALG)_3$-coated macrocapsules (with Rhod added to the initial alginate solution). The study was conducted for 2 h to assess the early release profile in 3 mL of PBS, with 600 μL of surrounding PBS being removed every 10 min and the container being refilled with the same volume of PBS pre-stabilized at the corresponding temperature. 100% of Rhod was considered to be the total mass remaining in the compartmental systems after taking construction losses into account. The studies were performed three times (n=3).

11.2.12 Magnetic-based responsiveness

Macrocapsules containing MNP-loaded microcapsules were suspended in a PBS-filled square polystyrene Petri dish placed upon a 1×1 cm^2 grid. A 1.3 T permanent neodymium (NdFeB) bar magnet (diameter: 4 mm; length: 2.5 cm) was used to apply the external magnetic field. Ten samples were placed 3 cm away from the magnet, with the latter placed at a height of 1.4 cm from the PBS surface. The movement was recorded on video and the mean normalized distance traversed by the samples plotted as a function of time.

11.3 Results and discussion

The conception of a multifunctional compartmentalized device may involve using several ingredients from distinct classes of materials, depending on the functionalities desired from a system of this kind, and require a huge number of fabrication operations. An illustration of the proposed system is illustrated in Figure 11.1.

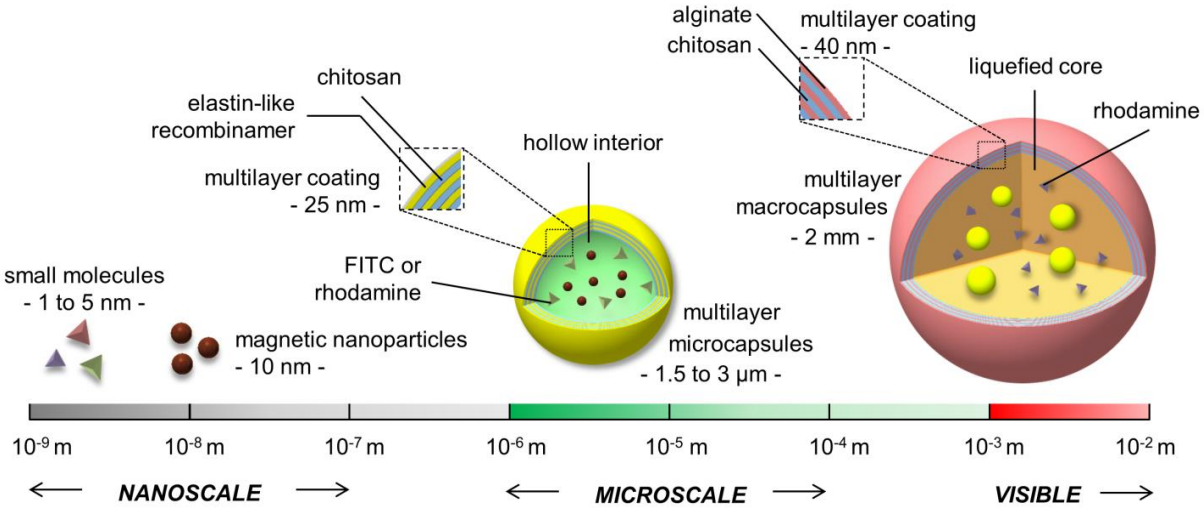


Figure 11.1. Hierarchical organization of the multicompartmental capsules. Liquefied alginate beads, delimited by a $(CHI/ALG)_3$ coating, are visible to the naked eye. Multilayer microcapsules of $(CHI/ELR)_3$ and molecular compounds can be suspended within the aqueous polymer phase. The former can further contain other types of molecular compounds and MNPs.

The borders between compartments consist of multilayer shells with three bilayers for the purpose of proof of concept. Our proposition comprises the fabrication of alginate beads by calcium-promoted ionic gelation separated from the environment by a multilayer coating of three CHI and ALG layers, $(CHI/ALG)_3$, with thickness around 40 nm [39]. Prior to ionic gelation, the microscopic subcompartments are suspended in an ALG solution to form beads containing small spherical structures. These microcapsules are templated in $CaCO_3$ microspheres and delimited by a coating of three CHI and ELR layers, $(CHI/ELR)_3$, with thickness around 25 nm [22]. In the subcompartments we encapsulated further components of smaller scales – fluorophores and MNPs. Since the synthesis of the $CaCO_3$ templates results from the co-precipitation of equimolar solutions of Na_2CO_3 and $CaCl_2$, various substances can be added to the co-precipitation medium and entrapped within it. After the

assembly of all compartments, the inorganic template is removed by treatment with EDTA, which also liquefies the alginate bead to a highly viscous medium. The final product is an external macrocapsule containing internal microcapsules – henceforth referred to as external (EC) and internal compartments (IC), respectively – with each partition being delimited by multilayer membranes.

To ensure that we could assemble structures from different size scales, the hierarchical organization of the proposed system was characterized initially. MNPs, ICs and ECs were observed resorting to distinct microscopy techniques and are shown in Figure 11.2. Note that for every experiment performed, ECs are always loaded with empty ICs, i.e., without any fluorophore encapsulated, unless otherwise specified. Using TEM, the MNPs (Figure 11.2a) were found to have a diameter of about 10 nm which, along with the model molecular compounds, represents the smallest scale present in this system. FITC was encapsulated within $(CHI/ELR)_3$ microcapsules and could be observed by confocal laser scanning microscopy (CLSM) upon removal of the $CaCO_3$ template (Figure 11.2b). We have previously constructed multilayer films made of chitosan and ELRs. Characterization of this ELR – amino acid sequence, matrix-assisted laser desorption/ionization-time of flight (MALDI-TOF), and differential scanning calorimetry (DSC) – which contains a RGD motif, can be found elsewhere.[22,38]

Although used previously to enhance cell adhesion, the primary reason for using this specific ELR herein was to enable LbL construction due to the negative charge provided by the aspartic acids (D), with a pK_a ranging from 3.0–4.7 [40], thus exploiting the biological function of this sequence was not in the scope of this work. The average size of the ICs was 3 μm, what places them at a microscale level. The external compartments act as containers where both ICs and molecular compounds can be entrapped. Encapsulation of the fluorescent molecule Rhod showed that the $(CHI/ALG)_3$ macrocapsules have a diameter of 2 mm (Figure 11.2c) and are therefore representative of the visible scale.

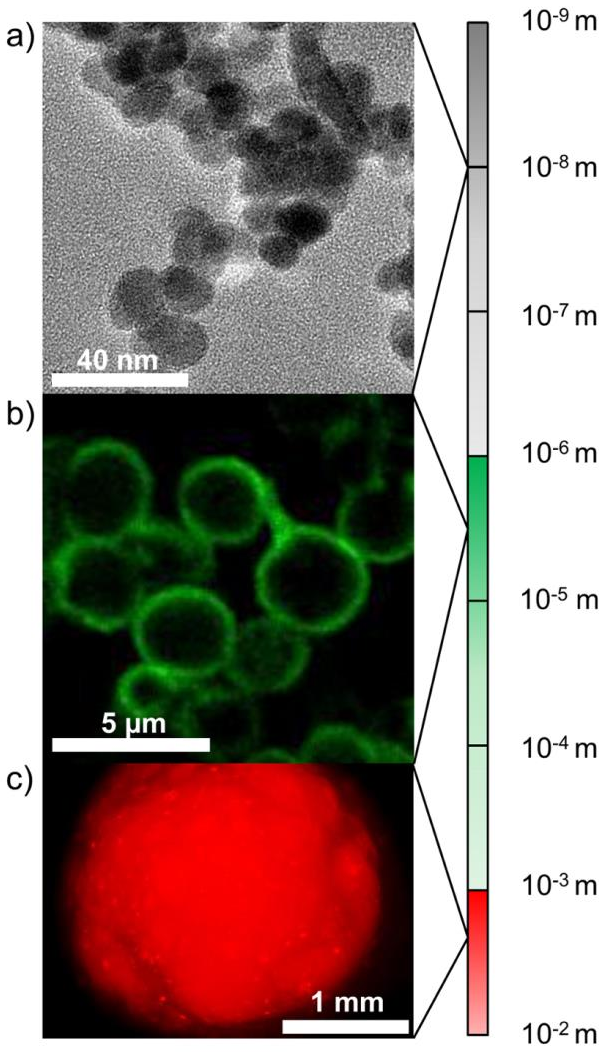


Figure 11.2. Scales of hierarchical components. (a) TEM image of MNPs; (b) CLSM image of FITC-containing $(CHI/ELR)_3$ microcapsules; (c) fluorescence microscopy image of the Rhod-containing liquefied ALG bead coated with $(CHI/ALG)_3$.

The proposed formulation contains ingredients that respond to external stimuli. Namely, the polymeric constituent ELR is known to respond to temperature, while MNPs to magnetic fields. These properties were studied and the results are presented in Figure 11.3. The response to temperature of the polymers used herein – CHI, ALG and ELR – was assessed by means of aggregate size measurements at 25°C and 37°C. In Figure 11.3a, it is shown that the size of ELR aggregates at 25°C is about 200 nm. In contrast to this situation, at 37°C aggregates of around 2000 nm were formed due to the temperature transition of ELRs above their T_t (in Supplemental Figure 11.2, the T_t was determined to be 29°C).

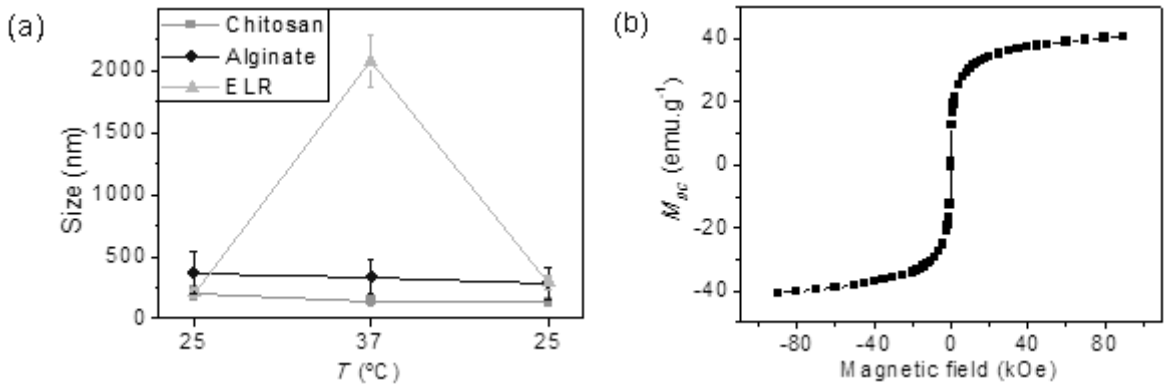


Figure 11.3. Stimuli-responsiveness of the multicompartmental device constituents. (a) aggregate size measurements by DLS of CHI (pH 5.5), ALG and ELR (pH 7.4) at 300 $\mu g \cdot mL^{-1}$ for a temperature cycle of 25–37–25°C; (b) magnetization assay of MNPs.

Upon decreasing the temperature to 25°C once again, it was observed that the aggregate size decreases to around 300 nm, confirming that the polypeptide used herein exhibits a reversible response towards temperature. Thus, the use of ELRs in such multilayer coatings may mean that the permeability of the subcompartments can be tuned simply by switching between room and physiological temperatures. As expected, CHI and ALG were not significantly influenced, since they are not temperature-responsive. For CHI, the working pH was of 5.5, as the pK_a of this polysaccharide is around 6. Nonetheless, CHI is not a temperature responsive biomaterial, therefore pH is not expected to alter its response to this variable. The use of temperature responsive macromolecules could help in controlling the permeability of a carrier coating based on temperature variations, when the release of a specific molecular compound needs to be more sustained or pronounced. At the same time, the use of CHI and ALG allows herein the assembly of a static coating, i.e. that is not stimuli-responsive under the temperature-dependent experimental conditions used further on, used solely for the purpose of encapsulating the rest of the components in its interior.

The other constituent of this system are MNPs. Magnetization measurements with the MNPs are shown in Figure 11.3b. Magnetic particles can be classified as ferromagnetic and paramagnetic/superparamagnetic. Whereas the former exhibit a permanent magnetic dipole moment, with a paramagnetic particle a magnetic dipole moment is induced only when an external magnetic field is applied [41-44]. The MNPs showed a saturation magnetization of 40 $emu \cdot g^{-1}$ and the typical sigmoidal curve of superparamagnetic nanoparticles, thereby confirming their response to magnetic fields and potential use for spatial mobilization/immobilization of a host device. In particular, it is known

that the success in therapeutic applications of growth factors often requires a release system for delivery with spatiotemporal control [45]. Thus the magnetic component may help achieving a better efficacy of the encapsulated agent and reduce losses to surrounding fluids.

Another important characteristic of these systems is their mechanical resistance. The ECs are visible to the naked eye and can therefore easily be handled. However, it is important to determine whether the external LbL coating can withstand handling whilst retaining the liquefied ALG. The integrity of the $(CHI/ALG)_3$ coating was assessed by submitting the macrocapsules to incremental centrifugal stress. Figure 11.4 shows that these macrocapsules can withstand centrifugal stress, with 50% of them remaining intact at a rotation speed of 2000g.

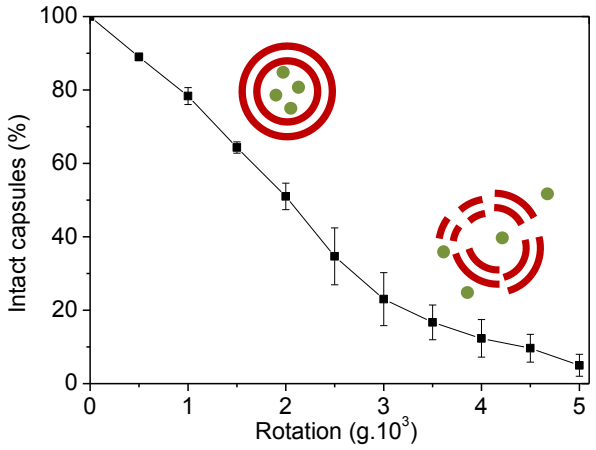


Figure 11.4. Mechanical resistance of $(CHI/ALG)_3$ macrocapsules, ECs, to incremental centrifugal stress, with two standard deviations represented.

At a maximum of 5000g, nearly every macrocapsule was disrupted, with only 5±3% of samples remaining intact. The resistance to handling was also assessed by manipulating them using a Pasteur micropipette. They can be easily and safely manipulated without disrupting the wall integrity, which is an important property when considering not only handling but also transportation or transfer between distinct containers, and biological implantation.

Compartmentalized systems may be useful for entrapping a multitude of molecular compounds with tunable permeability. Figure 11.5a shows the distribution of FITC-loaded ICs within an EC, with the latter encapsulating Rhod.

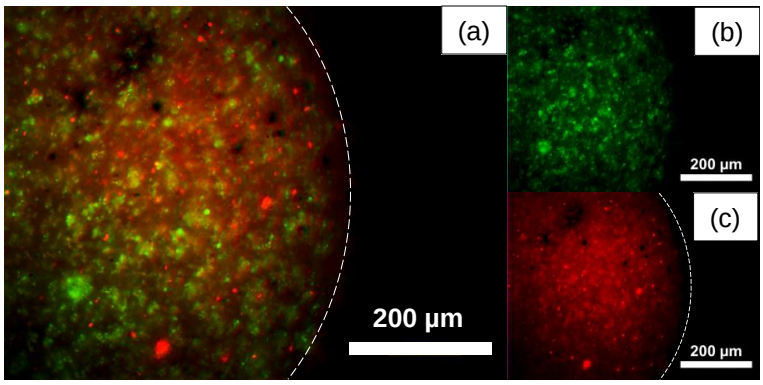


Figure 11.5. Distribution of the $(CHI/ELR)_3$ ICs within $(CHI/ALG)_3$ ECs by fluorescence microscopy. (a) This image was obtained by loading the former with FITC and the latter with Rhod. Separate green (b) and red (c) filters are shown.

The separate fluorescent channels are shown (Figure 11.5b and Figure 11.5c). It is clear that the ICs are homogeneously distributed in the ALG liquefied medium, showing that a compartmentalized structure is definitely conceived.

To further explore the permeability of the compartments, early release studies were performed by loading either the ICs or the ECs with Rhod and plotting the cumulative release of this compound from the $(CHI/ELR)_3$ and $(CHI/ALG)_3$ compartments at 25°C (Figure 11.6a) and 37°C (Figure 11.6b) as a function of time. One important finding from this study was that the release of Rhod encapsulated in the ICs was more sustained at 37°C than at 25°C (84% and 71%, respectively, after 2 h). This phenomenon results from the temperature response of the ELR: at the temperature of 37°C – above T_t – its transition to a more ordered state is triggered and is manifested by the decrease in the shell permeability, an effect previously demonstrated for CHI- and ELR-based microcapsules entrapping bovine serum albumin (BSA) [46]. Such decreased permeability of the microcapsules can therefore be used as a mechanism to control the release of molecular compounds. As such, it could be useful in the field of sustained drug-delivery devices for targeting a therapeutic window, micro-reactors confining chemical reactions, and sensors for the simultaneous detection of macromolecules or gases by diffusion (in or out). It should also be noted that the release of Rhod from the ECs did not change significantly since CHI and ALG are not temperature responsive (90% at 25°C and 92% at 37°C)

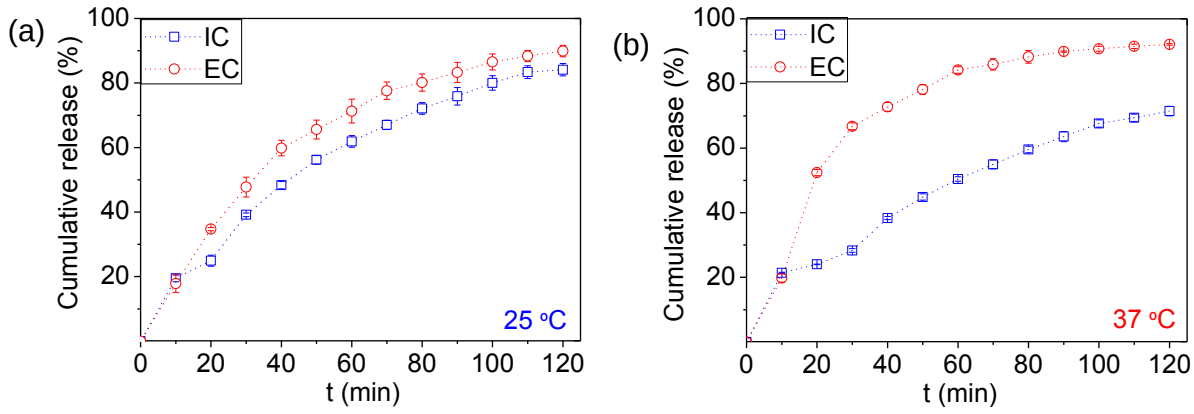


Figure 11.6. Kinetics of Rhod release when encapsulated in the internal $(CHI/ELR)_3$ microcapsules (□) and the external $(CHI/ALG)_3$ compartment (○) at (a) 25°C and (b) 37°C for a time, *t*, of 2 h, with two standard deviations represented. Some standard deviations are too small to be distinguished from the symbol.

Another important finding was that the release of Rhod from the ICs decreased after an initial burst detected at the first time-point. Namely, the Rhod release rate decreased between 10-20 minutes (25°C) and 10–30 minutes (37°C), with this decrease being more pronounced in the latter case. This could be due to the fact that molecules encapsulated within the microcompartmental system have to diffuse through the IC coating to the alginate medium and then through the external coating to the external environment. This would explain the existence of a time-gap that is not present when Rhod is encapsulated within the ECs. Figure 11.7 depicts the proposed mechanism for the initial burst release detected in the IC case.

We hypothesize that this phenomenon results from the release of Rhod by diffusion into the alginate medium during construction of the ECs containing Rhod-loaded ICs, mainly at the chelation stage. At the start of the release studies, this fraction would behave similarly to the EC case at the first time point, with an initial burst similar in magnitude to that of the ECs. The remaining Rhod is released from the ICs at a slower rate. In this regard, in Figure 11.5 we had separated the fluorescence channels of FITC and Rhod. Indeed, immediately after construction of the multicompartmental device, there is a diffusion of FITC throughout the alginate medium, as evidenced by diffuse green zones Figure 11.5b.

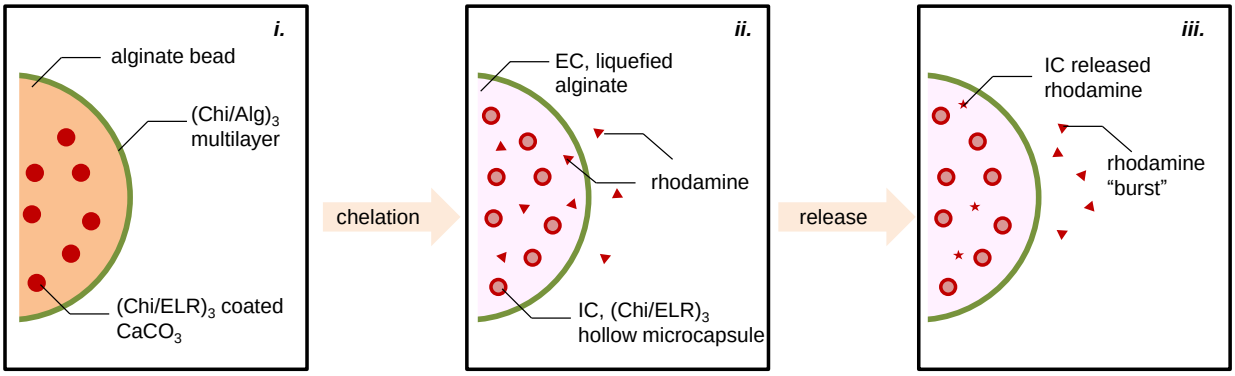


Figure 11.7. Burst mechanism for Rhod loaded within internal microcompartments. (i) At first, Rhod is physically entrapped within $CaCO_3$ templates. (ii) After chelation, a fraction of Rhod is lost and quantified. The samples are rinsed to remove the lost fraction. However, another fraction remains free within the alginate. (iii) At the start of the release studies, the free Rhod diffuses to the exterior and is readily detected. ICs keep releasing Rhod to the alginate medium at a slower rate, and this Rhod is detected later in the experiment.

The existence of two release rate constants is consistent with the "double barrier" effect recently evidenced by Lecommandoux and co-workers for polymersome-in-polymersome systems [47]. In their work, doxorubicin was encapsulated in inner or outer compartments. The fabrication method differed from our LbL mechanism: they were fabricated by nanoprecipitation and an emulsion/centrifugation process, respectively. They observed lower release kinetics when doxorubicin was encapsulated within the internal nanovesicles in comparison to the latter case.

Theoretically, if such initial burst did not occur, a more prolonged time-gap would be visible from the beginning before Rhod from the ICs could be detected. This burst-type release is not necessarily a drawback as some applications may benefit from it. For instance, a higher fraction of antibiotics/anti-inflammatories can be released in the first few minutes after administration when they are most needed, with the rest of the load being released subsequently within a therapeutic window. The release of more than one molecule from a reservoir with independent and tunable rates may be important in drug delivery systems, when the delayed delivery of one active substance with respect to another is desired, or to circumvent premature drug leakage [48]. Moreover, tuning the release rate of a molecular species could be accomplished further by varying the number of layers of the coating: a substance could diffuse through the multilayers with higher release kinetics for thicker coatings, in comparison to a thinner

coating [27,46]. Although the primary interest in compartmental devices has focused on systems for the delivery of therapeutic molecules, other applications have been proposed in fields ranging from actuators to biomaterials for tissue engineering and regenerative medicine [18].

The encapsulation method for $CaCO_3$ entrapment was also used to incorporate MNPs within the ICs. Figure 11.8a shows MNPs observed by TEM homogeneously distributed within these microcapsules.

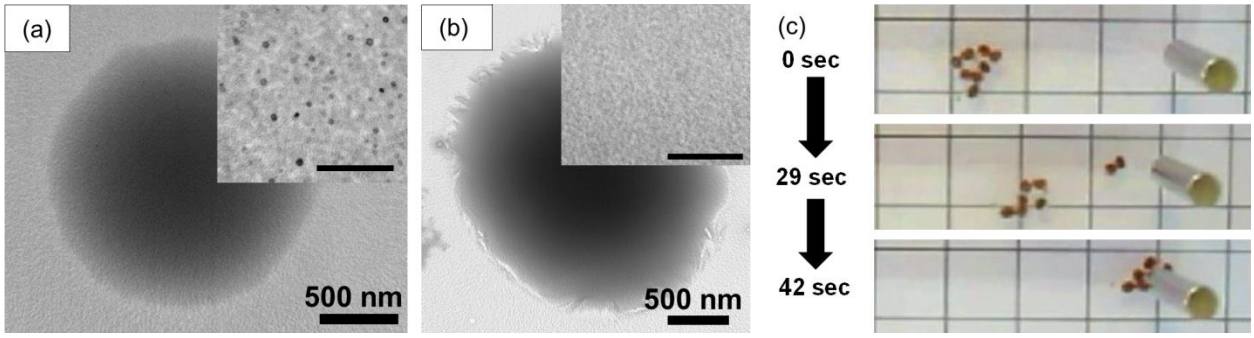


Figure 11.8. Magnetic characteristics of the multicompartmental system. TEM of a $(CHI/ELR)_3$ microcapsule (a) containing MNPs and (b) empty. Insets scale: 50 nm. (c) Attraction of $(CHI/ALG)_3$ ECs containing MNP-loaded $(CHI/ELR)_3$ ICs by a magnet in a PBS medium. The magnet is placed at a height of 1.4 cm on top of a polystyrene cover. The red color is characteristic of the MNPs within the hierarchical structure. Squares are 1×1 cm^2.

Empty microcapsules were used as a control for MNP-loaded ones. In comparison, Figure 11.8b shows empty ICs, where no spherical structure could be detected. As they are empty and the electronic density is lower than MNP-containing ICs, the multilayer shell can be discerned, with creases and folds which are characteristic of collapsed ultrathin walls due to the drying process.

In light of our initial findings, we conducted an experiment where MNP-containing ICs were loaded into ECs and attracted by a magnet placed at a distance of 3 cm (Figure 11.8c). This strategy adds further value to the proposed device in terms of biomimetism. Besides its multicompartmental nature inspired by natural cells and self-assembly mechanism of constituents in which the LbL strategy is based upon, the use of MNPs can be considered to be a biomimetic approach inspired by unique structures with magnetic properties, such as magnetotactic bacteria [49-51]. Magnetic alginate beads have been used previously for applications such as water pollution remediation [52] and magnetic hyperthermia-enhanced doxorubicin release [53], although the magnetic character was not exploited primarily for

spatial mobilization. It took 42 s for all the beads to travel this distance and be completely immobilized. As soon as the magnetic compartmental units were exposed to the external magnetic field, they became attracted to the position at which the maximum magnetic field value was available to them at the surface of the PBS medium. As they got closer to the magnet they were exposed to a stronger magnetic field and the attraction increased. Movement stopped abruptly once they reached the position below where the magnet was placed. The normalized mean distance traveled by MNP-loaded ICs within ECs is represented in Supplemental Figure 11.4. This observation shows how the internal subcompartments can be customized to possess distinct functions, including distinct types of smart responsiveness. Specifically, the entrapment of superparamagnetic nanoparticles within microcapsules could be envisaged for applications that require immobilization, such as localized therapies, and magnetic resonance imaging. The developed devices should also permit the incorporation of living microorganisms and cells inside the EC, as its processing is performed in mild conditions [39].

11.4 Conclusion

In conclusion, we presented a multifunctional system characterized by hierarchical organized spherical compartments. We showed that compartmentalized structures delimited by multilayer coatings can be customized to exhibit properties that are not found coupled in nature. Although the present work was limited to the proof of concept, we envisage that it can be improved in the future. Namely, the multilayer organization makes it possible to tune the permeability of the coatings just by changing the number of layers. Other stimuli could be coupled together: for instance, temperature, pH or light (e.g., from the incorporation of azobenzenes or spiropyrans) could be combined for multifunctional biosensors confining reactions. The genetic nature of ELRs further allows synthesizing biofunctional polypeptides for advanced applications, such as increased cell adhesion or enhanced biomineralization. Cells have been previously encapsulated within alginate beads, but we envision that coupling biological material with functionality such as controlled release of growth factors and provision of adhesion sites may improve cellular sustained survivability over time. Moreover, the addition of magnetic components provides such compartmentalized system potential for biotechnological and biomedical applications where spatial immobilization, high local availability of an active agent or monitoring by magnetic imaging is required.

11.5 Supplemental information

11.5.1 Deacetylation degree of chitosan.

Hydrogen-1 nuclear magnetic resonance (^{1}H-NMR) spectra were recorded using a Varian MR-400 spectrometer to determine the degree of deacetylation (DD) of chitosan. Thus, 10 mg of chitosan was dissolved in 1 mL of deuterated water (D_2O) and 20 μL of deuterated hydrochloric acid (DCl) to form a viscous solution. An aliquot of this solution was placed in a 5 mm NMR tube and the spectrum recorded at 60°C.

The calculation of the DD is presented in Supplemental equation 11.1:

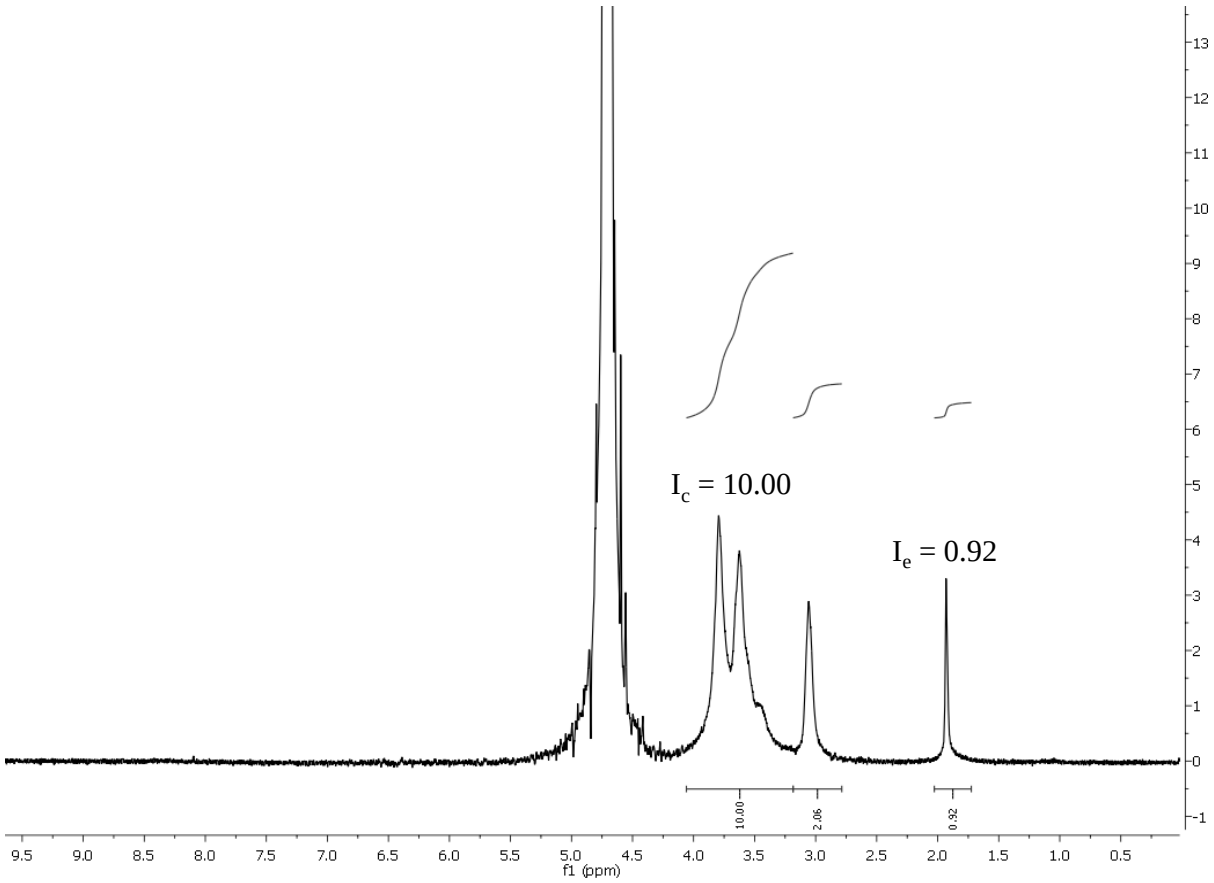
$$DD(\%) = \left[1 - \left(\frac{\frac{1}{3} I_e}{\frac{1}{6} I_c} \right) \right] \times 100 \qquad (11.1)$$

where I_x is the area of each of the peaks (x) identified in Supplemental Figure 11.1. The DD of the purified chitosan used was 81.6%.

11.5.2 ELR transition temperature

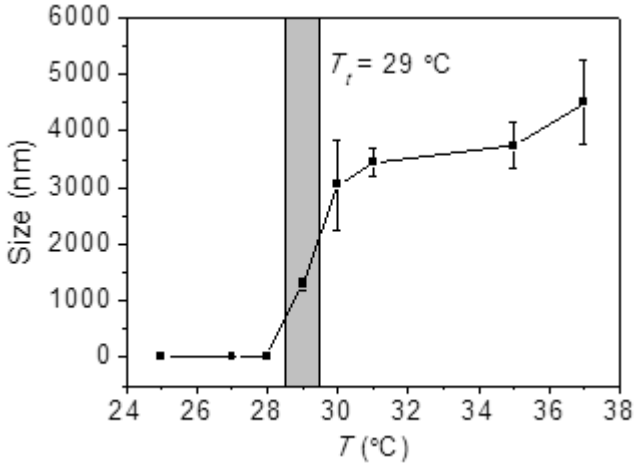
The aggregate sizes of ELR in solution were measured using a Nano-ZS from Malvern (United Kingdom) in the temperature range 25–37°C after stabilization for 5 min. Samples were prepared at 300 μg·mL^{-1} in PBS, pH 7.4. A total of 20 runs were performed for each sample to obtain an average value at stabilized temperature.

In order to evaluate the thermal response of the featured ELR, the size variations of peptide aggregates in aqueous solution were measured as a function of temperature in small increments. It can be seen from Supplemental Figure 11.2 that the ELR forms aggregates of 4.4±2.8 nm at 25°C and 1290±113 nm at 29°C. This abrupt size variation gives a T_t of 29°C for the ELR. ELR self-assembly progresses further with increasing temperature



Supplemental Figure 11.1. ^{1}H-NMR spectrum of the purified chitosan sample, with 10.00 corresponding to I_c peak and 0.92 to I_e peak.

.

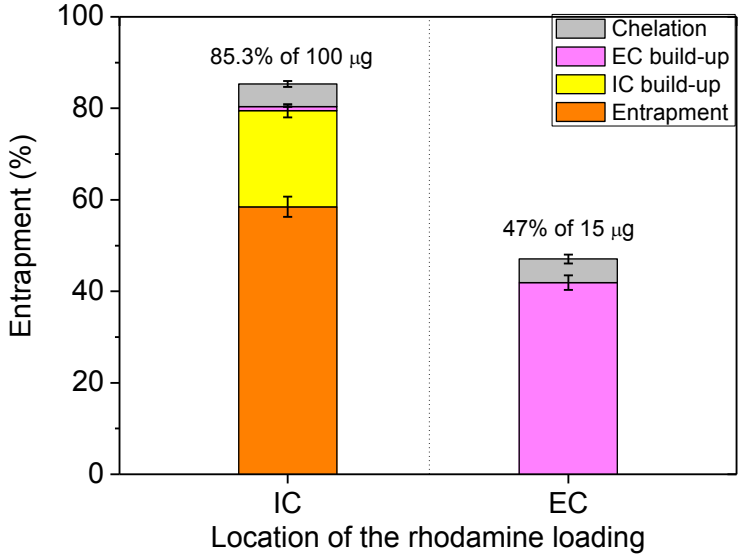


Supplemental Figure 11.2. Aggregate size profile for a 300 μg·mL^{-1} ELR solution in PBS over the temperature range, T, of 25–37°C, with two standard deviations represented.

11.5.3 Rhodamine encapsulation losses

The encapsulation efficiency of Rhod in either the inner or the external compartments was determined by fluorescence measurements of the retrieved supernatants during their construction using a Synergie HT microplate ELISA reader (BioTek, USA). Thus, 150 μL of sample was pipetted into white, opaque 96-well plates in triplicate. Ultrapure water was used as blank. The excitation (λ_{exc}) and emission (λ_{em}) wavelengths used for Rhod mass calculations were 530 and 590 nm, respectively. All supernatants collected during entrapment, construction and chelation stages were measured and quantified. The percentage Rhod loss was plotted for both each stage and cumulatively.

All the supernatants collected during the construction of Rhod-loaded compartments (either internal or external ones) were used to calculate the losses occurred prior to the commencement of the actual release studies. The graphic in Supplemental Figure 11.3 shows the stage and cumulative Rhod losses with respect to the initial encapsulated mass.



Supplemental Figure 11.3. Rhodamine losses during the construction of Rhod-loaded microcapsules (ICs) within macrocapsules (ECs) and empty microcapsules within Rhod-loaded macrocapsules, with two standard deviations represented.

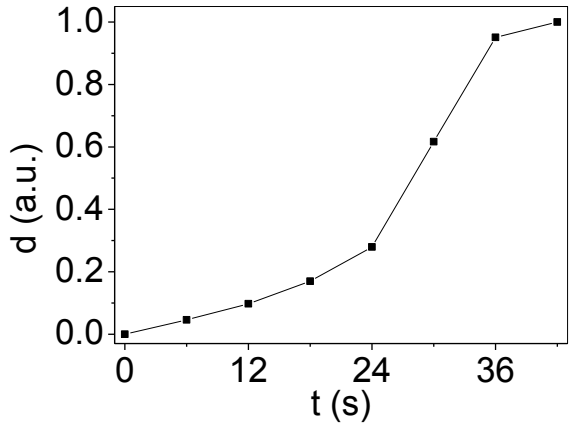
When Rhod was loaded within the inner compartments, the construction process consisted of four stages: (i) entrapment within the $CaCO_3$ particles (orange in the graphic), (ii) buildup of the $(CHI/ELR)_3$ multilayer (yellow), (iii) buildup of the external $(CHI/ALG)_3$ multilayer (purple), and (iv) simultaneous

$CaCO_3$ chelation and alginate bead liquefaction (grey). When Rhod was loaded within the external compartments, losses are only present in stages (iii) and (iv), when Rhod is introduced into the system. The sacrificial template was maintained until the end of stage (iii) to prevent early diffusion during the construction. Thus, Rhod could be protected and physically retained within the sacrificial template until the final stage of chelation.

As mentioned previously, the quantity of Rhod loaded initially differed depending on whether it was encapsulated within the internal or the external compartments. As a result, we first quantified the Rhod losses during the construction of ECs containing Rhod-loaded ICs and found that 85% of Rhod had been lost at the end of the construction, thus meaning that only 15 μg of the initial 100 μg were effectively encapsulated at time-point "0". In an attempt to encapsulate roughly the same mass of fluorophore in the ECs, we loaded them with the equivalent quantity of 15 μg of Rhod during the ionic gelation step of 1 mL of alginate. Note that this value disregards the subsequent loss of 47% that was further quantified following liquefaction of the bead. Furthermore, empty $CaCO_3$-coated particles were loaded at the same time to keep the same subcompartmental structure.

11.5.4 Magnetic responsiveness assay

Figure 11.8c depicted the magnetic responsiveness of the MNP-loaded ICs within ECs. As expected, a group of eight compartmental units were attracted by a magnet placed 3 cm away from their starting point. The normalized distance traveled by each capsule is plotted as a function of time in Supplemental Figure 11.4.



Supplemental Figure 11.4. Normalized mean distance, *d* in arbitrary units, traveled by MNP-loaded ICs within ECs as a function of time, *t*, from their starting point to the point of the highest magnetic field value available.

As soon as the magnetic compartmental units were exposed to the external magnetic field, they became attracted to it. Subsequently they were exposed to an increasingly stronger magnetic field value and the attraction increased. Movement stopped abruptly once they reached the position at which the maximum magnetic field value was available to them.

11.6 Acknowledgements

The authors are grateful for financial support from Fundação para a Ciência e Tecnologia (grant SFRH/BD/61126/2009), "Fundo Social Europeu", "Programa Diferencial de Potencial Humano", EU 7th Framework Programme (nº REGPOT-CT2012-316331-POLARIS), Health and Progress Foundation (Mobility Program for Nanomedicine), Andalusian Initiative for Advanced Therapies (Ministry of Health of the Andalusian Regional Government), EC (FP7-Health-2011 nº 278557 "The Grail", FP7-NMP-2010 nº 263363 "InnovaBone"), MEC of the Spanish Government (MAT2012-38043-C02-01, MAT2010-15310, MAT-2010-15982, PRI-PIBAR-2011-1403, ACI2009-0890), JCyL (VA155A12-2, VA152A12-2, VA049A11-2), Network Center of Regenerative Medicine and Cellular Therapy of Castilla y León funded by the JCyL and the ISCIII, and CIBER-BBN funded by the ISCIII.

11.7 References

[1] Riehemann K., Schneider S. W., Luger T. A., Godin B., Ferrari M., and Fuchs H., Nanomedicine—Challenge and Perspectives, Angewandte Chemie International Edition 2009, 48: 872-897.

[2] Stuart M. A. C., Huck W. T. S., Genzer J., Muller M., Ober C., Stamm M., Sukhorukov G. B., Szleifer I., Tsukruk V. V., Urban M., Winnik F., Zauscher S., Luzinov I., and Minko S., Emerging applications of stimuli-responsive polymer materials, Nat Mater 2010, 9: 101-113.

[3] Zhao Y., and Jiang L., Hollow Micro/Nanomaterials with Multilevel Interior Structures, Advanced Materials 2009, 21: 3621-3638.

[4] Chandrawati R., van Koeverden M. P., Lomas H., and Caruso F., Multicompartment Particle Assemblies for Bioinspired Encapsulated Reactions, The Journal of Physical Chemistry Letters 2011, 2: 2639-2649.

[5] Noireaux V., Maeda Y. T., and Libchaber A., Development of an artificial cell, from self-organization to computation and self-reproduction, Proceedings of the National Academy of Sciences 2011.

[6] Shi J., Zhang L., and Jiang Z., Facile Construction of Multicompartment Multienzyme System through Layer-by-Layer Self-Assembly and Biomimetic Mineralization, ACS Applied Materials & Interfaces 2011, 3: 881-889.

[7] Huang C.-C., Huang W., and Yeh C.-S., Shell-by-shell synthesis of multi-shelled mesoporous silica nanospheres for optical imaging and drug delivery, Biomaterials 2011, 32: 556-564.

[8] Boudou T., Crouzier T., Ren K., Blin G., and Picart C., Multiple Functionalities of Polyelectrolyte Multilayer Films: New Biomedical Applications, Advanced Materials 2010, 22: 441-467.

[9] Xu H., and Wang W., Template Synthesis of Multishelled Cu2O Hollow Spheres with a Single-Crystalline Shell Wall, Angewandte Chemie International Edition 2007, 46: 1489-1492.

[10] De Geest B. G., McShane M. J., Demeester J., De Smedt S. C., and Hennink W. E., Microcapsules Ejecting Nanosized Species into the Environment, Journal of the American Chemical Society 2008, 130: 14480-14482.

[11] Delcea M., Yashchenok A., Videnova K., Kreft O., Möhwald H., and Skirtach A. G., Multicompartmental Micro- and Nanocapsules: Hierarchy and Applications in Biosciences, Macromolecular Bioscience 2010, 10: 465-474.

[12] Hosta-Rigau L., Städler B., Yan Y., Nice E. C., Heath J. K., Albericio F., and Caruso F., Capsosomes with Multilayered Subcompartments: Assembly and Loading with Hydrophobic Cargo, Advanced Functional Materials 2010, 20: 59-66.

[13] Kreft O., Prevot M., Möhwald H., and Sukhorukov G. B., Shell-in-Shell Microcapsules: A Novel Tool for Integrated, Spatially Confined Enzymatic Reactions, Angewandte Chemie International Edition 2007, 46: 5605-5608.

[14] Marguet M., Sandre O., and Lecommandoux S., Polymersomes in “Gelly” Polymersomes: Toward Structural Cell Mimicry, Langmuir 2011, 28: 2035-2043.

[15] Marguet M., Bonduelle C., and Lecommandoux S., Multicompartmentalized polymeric systems: towards biomimetic cellular structure and function, Chemical Society Reviews 2013, 42: 512-529.

[16] Tong W., Song X., and Gao C., Layer-by-layer assembly of microcapsules and their biomedical applications, Chemical Society Reviews 2012, 41: 6103-6124.

[17] Zhang Y., Ruder W. C., and LeDuc P. R., Artificial cells: building bioinspired systems using small-scale biology, Trends in Biotechnology 2008, 26: 14-20.

[18] Mano J. F., Stimuli-Responsive Polymeric Systems for Biomedical Applications, Advanced Engineering Materials 2008, 10: 515-527.

[19] Chen F.-M., Zhang M., and Wu Z.-F., Toward delivery of multiple growth factors in tissue engineering, Biomaterials 2010, 31: 6279-6308.

[20] Sensenig R., Sapir Y., MacDonald C., Cohen S., and Polyak B., Magnetic nanoparticle-based approaches to locally target therapy and enhance tissue regeneration in vivo, Nanomedicine 2012, 7: 1425-1442.

[21] Lutolf M. P., Gilbert P. M., and Blau H. M., Designing materials to direct stem-cell fate, Nature 2009, 462: 433-441.

[22] Costa R. R., Custódio C. A., Arias F. J., Rodríguez-Cabello J. C., and Mano J. F., Layer-by-Layer Assembly of Chitosan and Recombinant Biopolymers into Biomimetic Coatings with Multiple Stimuli-Responsive Properties, Small 2011, 7: 2640-2649.

[23] Gribova V., Auzely-Velty R., and Picart C., Polyelectrolyte Multilayer Assemblies on Materials Surfaces: From Cell Adhesion to Tissue Engineering, Chemistry of Materials 2011, 24: 854-869.

[24] Hammond P. T., Building biomedical materials layer-by-layer, Materials Today 2012, 15: 196-206.

[25] Gao C., Möhwald H., and Shen J. C., Enhanced Biomacromolecule Encapsulation by Swelling and Shrinking Procedures, ChemPhysChem 2004, 5: 116-120.

[26] Mauser T., Déjugnat C., and Sukhorukov G. B., Reversible pH-Dependent Properties of Multilayer Microcapsules Made of Weak Polyelectrolytes, Macromolecular Rapid Communications 2004, 25: 1781-1785.

[27] She Z., Antipina M. N., Li J., and Sukhorukov G. B., Mechanism of Protein Release from Polyelectrolyte Multilayer Microcapsules, Biomacromolecules 2010, 11: 1241-1247.

[28] Mano J. F., Silva G. A., Azevedo H. S., Malafaya P. B., Sousa R. A., Silva S. S., Boesel L. F., Oliveira J. M., Santos T. C., Marques A. P., Neves N. M., and Reis R. L., Natural origin biodegradable systems in tissue engineering and regenerative medicine: present status and some moving trends, Journal of The Royal Society Interface 2007, 4: 999-1030.

[29] Silva T. H., Alves A., Ferreira B. M., Oliveira J. M., Reys L. L., Ferreira R. J. F., Sousa R. A., Silva S. S., Mano J. F., and Reis R. L., Materials of marine origin: a review on polymers and ceramics of biomedical interest, International Materials Reviews 2012, 57: 276-306.

[30] Rodríguez-Cabello J. C., Martín L., Girotti A., García-Arévalo C., Arias F. J., and Alonso M., Emerging applications of multifunctional elastin-like recombinamers, Nanomedicine 2011, 6: 111-122.

[31] Simnick A. J., Lim D. W., Chow D., and Chilkoti A., Biomedical and Biotechnological Applications of Elastin-Like Polypeptides, Polymer Reviews 2007, 47: 121 - 154.

[32] Urry D. W., Molecular Machines: How Motion and Other Functions of Living Organisms Can Result from Reversible Chemical Changes, Angewandte Chemie International Edition in English 1993, 32: 819-841.

[33] Mailänder V., and Landfester K., Interaction of Nanoparticles with Cells, Biomacromolecules 2009, 10: 2379-2400.

[34] Neuberger T., Schöpf B., Hofmann H., Hofmann M., and von Rechenberg B., Superparamagnetic nanoparticles for biomedical applications: Possibilities and limitations of a new drug delivery system, Journal of Magnetism and Magnetic Materials 2005, 293: 483-496.

[35] Oh J. K., and Park J. M., Iron oxide-based superparamagnetic polymeric nanomaterials: Design, preparation, and biomedical application, Progress in Polymer Science 2011, 36: 168-189.

[36] Signini R., and Filho S. P. C., On the preparation and characterization of chitosan hydrochloride, Polymer Bulletin 1999, 42: 159-166.

[37] Rodríguez-Cabello J. C., Girotti A., Ribeiro A., and Arias F. J., Synthesis of Genetically Engineered Protein Polymers (Recombinamers) as an Example of Advanced Self-Assembled Smart Materials, In Navarro M., Planell J. A., eds. Nanotechnology in Regenerative Medicine: Humana Press; 2012.

[38] Pierna M., Santos M., Arias F. J., Alonso M., and Rodriguez-Cabello J. C., Efficient cell and cell-sheet harvesting based on smart surfaces coated with a multifunctional and self-organizing Elastin-Like Recombinamer, Biomacromolecules 2013: DOI: 10.1021/bm400268v.

[39] Correia C. R., Reis R. L., and Mano J. F., Multilayered Hierarchical Capsules Providing Cell Adhesion Sites, Biomacromolecules 2013, 14: 743-751.

[40] Fothergill-Gilmore L. A., Peptide Sequence Determination, In Franks F., ed. Protein Biotechnology: Isolation, Characterization, and Stabilization, Totowa NJ, USA: Humana Press; 1993.

[41] Gennes P. G., and Pincus P. A., Pair correlations in a ferromagnetic colloid, Physik der kondensierten Materie 1970, 11: 189-198.

[42] Mizuki T., Watanabe N., Nagaoka Y., Fukushima T., Morimoto H., Usami R., and Maekawa T., Activity of an enzyme immobilized on superparamagnetic particles in a rotational magnetic field, Biochemical and Biophysical Research Communications 2010, 393: 779-782.

[43] Promislow J. H. E., Gast A. P., and Fermigier M., Aggregation kinetics of paramagnetic colloidal particles, The Journal of Chemical Physics 1995, 102: 5492-5498.

[44] Yang C., Wu J., and Hou Y., Fe3O4 nanostructures: synthesis, growth mechanism, properties and applications, Chemical Communications 2011, 47: 5130-5141.

[45] Cao L., and Mooney D. J., Spatiotemporal control over growth factor signaling for therapeutic neovascularization, Advanced Drug Delivery Reviews 2007, 59: 1340-1350.

[46] Costa R. R., Custódio C. A., Arias F. J., Rodríguez-Cabello J. C., and Mano J. F., Nanostructured and thermoresponsive recombinant biopolymer-based microcapsules for the delivery of active molecules, Nanomedicine: Nanotechnology, Biology and Medicine 2013, 9: 895-902.

[47] Marguet M., Edembe L., and Lecommandoux S., Polymersomes in Polymersomes: Multiple Loading and Permeability Control, Angewandte Chemie International Edition 2012, 51: 1173-1176.

[48] Wong B., Boyer C., Steinbeck C., Peters D., Schmidt J., van Zanten R., Chmelka B., and Zasadzinski J. A., Design and In Situ Characterization of Lipid Containers with Enhanced Drug Retention, Advanced Materials 2011, 23: 2320-2325.

[49] Lu Y., Dong L., Zhang L.-C., Su Y.-D., and Yu S.-H., Biogenic and biomimetic magnetic nanosized assemblies, Nano Today 2012, 7: 297-315.

[50] Xie J., Chen K., and Chen X., Production, modification and bio-applications of magnetic nanoparticles gestated by magnetotactic bacteria, Nano Research 2009, 2: 261-278.

[51] Wang L., Prozorov T., Palo P. E., Liu X., Vaknin D., Prozorov R., Mallapragada S., and Nilsen-Hamilton M., Self-Assembly and Biphasic Iron-Binding Characteristics of Mms6, A Bacterial Protein That Promotes the Formation of Superparamagnetic Magnetite Nanoparticles of Uniform Size and Shape, Biomacromolecules 2011, 13: 98-105.

[52] Rocher V., Siaugue J.-M., Cabuil V., and Bee A., Removal of organic dyes by magnetic alginate beads, Water Research 2008, 42: 1290-1298.

[53] Brulé S., Levy M., Wilhelm C., Letourneur D., Gazeau F., Ménager C., and Le Visage C., Doxorubicin Release Triggered by Alginate Embedded Magnetic Nanoheaters: A Combined Therapy, Advanced Materials 2011, 23: 787-790.

SECTION IV – CONCLUDING REMARKS

Chapter 12. Major conclusion and future perspectives

Chapter 12. Major conclusions and future perspectives

The surface modification technique known as layer-by-layer (LbL) was employed successfully in accordance to the hypothesis of this thesis. Various substrates – both planar and three-dimensional – were coated with natural or biomimetic polymeric constituents distinct in functionality but sharing natural roots. It was then possible to develop multilayer devices intended for a wide range of biomedical applications, namely adhesive films, coatings for biomaterials, drug delivery carriers – for delivery either by drug diffusion or by cellular uptake – and microreactors with customizable properties.

First, it was demonstrated that multilayer films can retain and exhibit the properties of their natural constituents. A phosphonate derivative of levan, a fructose polymer obtained from extremophilic microorganisms, allowed fabricating multilayer films with chitosan (CHI) that exhibited superior adhesive properties in comparison to a multilayer formulation of CHI and alginate (ALG) – two polysaccharides of marine origin widely regarded as good adhesive ingredients. The advantage of using levan was also evident by the superior cell adhesion to films containing this polymer, in comparison to CHI/ALG films. Future developments of levan-functionalized multilayer films may include tests using actual animal tissues to further evaluate their potential as wound healing coatings and tissue sealants for post-surgical procedures.

Elastin-like recombinamers (ELRs) were used as a polypeptide constituent of most multilayer formulations presented herein. Its genetic origin, rooted in natural elastin, allowed using constituents exhibiting a precise amino acid content, sequence, length, and, most importantly, bioactivity. By using an ELR containing the bioactive sequence arginine-glycine-aspartic acid (RGD), substrates with enhanced cell adhesion were made. Given the multiple stimuli-responsive nature of ELRs, it was demonstrated that, like in the case of levan, films containing these polypeptides also retained such responsiveness, namely toward temperature, pH and ionic strength. Raising any of these parameters above an upper threshold triggered the transition of the ELR adsorbed at the surface, leading it to exhibit charged amino acids toward the interface. This phenomenon was translated by an increase of hydrophilicity and surface roughness.

The buildup feasibility of this ELR-RGD with CHI in a multilayer structure was monitored *in situ* using a quartz-crystal microbalance (QCM). Although a construction based on strong electrostatic interactions was first anticipated, there was evidence that weaker hydrophobic interactions could play an important role in this process between polysaccharides and polypeptide-based polymers. Resorting to the QCM

and the mathematical Voigt-based model for viscoelastic films, several distinct ELRs were combined with either CHI or ALG for the construction of hybrid films at distinct values of pH. The estimation of each of the films' thicknesses led to the conclusion that not only electrostatic but also hydrophobic interactions drive the self-assembly of this type of multilayer films, judging by how thicker films could be obtained when using partially neutralized polysaccharides. This result provides a consistent basis to the development of future devices based on this class of coatings by ensuring that the best construction parameters are used in order to achieve thick films across various scales – nano to micro – and stability.

LbL extrapolation to 3D was successful in the form of spherical microcapsules of CHI and ELR for the purpose of drug delivery, envisaging two forms of administration. The first consisted in the pre-encapsulation of a high molecular weight protein, bovine serum albumin (BSA), within the microcapsules and its release by diffusion under distinct temperatures. It was demonstrated that the permeability of the multilayer shell was dependent on the temperature and on the number of layers. Thanks to the incorporation of ELRs in the multilayer formulation, its temperature-triggered phase transition led the microcapsules to be more retentive at physiological than at room temperature, a phenomenon also accompanied by a significant shrinkage of the capsular structures. As expected, a higher number of coating layers also provided a more effective barrier to the diffusion of the encapsulated agent. The reduced release rate verified at physiological temperature may help in the delivery of active agents (e.g., chemotherapeutics) that are necessary locally in small but controlled doses, i.e., within a therapeutic window. Varying the number of layers provided an additional means of control over the release kinetics, what helps further to achieve an appropriate drug release and bioactivity. Future developments may investigate the potential use of these carriers for the delivery of active agents instead of model proteins for a wide spectrum of molecular weights. Ideally, these should be studied under sink conditions, which ensure that the release medium is not saturated by drug so that its release is controlled solely by the delivery system and is not affected by its solubility.

The second mechanism consisted in the delivery of microcapsules directly to the interior of the cells, where the whole cellular machinery is located. Using RGD- and RDG-functionalized microcapsules (with the latter being a nonfunctional analogue of the former) it was possible to determine that the mechanism of internalization of these capsules by human mesenchymal stem cells (hMSCs) was due majorly to a mechanism of macropinocytosis and not due to the surface functionalization. This is an important mechanism of drug delivery since the delivery of drug carriers directly to the cells diminishes potential active agent losses to the extracellular environment by diffusion. Furthermore, drugs may be

delivered to where they are most needed, ensuring a high drug availability and efficacy. However, the intracellular degradation – hence potential drug availability – was faster for RGD-functionalized microcapsules. Future experiments may focus on determining the mechanism behind the distinct intracellular processing rates, which seemed dependent on the surface functionalization of the microcapsules. Furthermore, growth factors and other differentiation agents may be encapsulated to exploit stem cell differentiation mechanisms dependent on controllable dosages and carrier size.

Finally, it was shown that LbL allows achieving higher levels of functionalization, difficult to achieve using the most conventional surface modification strategies. Macrocapsules observable with a naked eye were delimited by CHI/ALG multilayers. This macrodevice exhibited compartmentalization and hierarchical organization from the nano- to the macro-scales. ELR-functionalized microcapsules served as microcompartments suspended within a confined ALG liquefied environment. The microcapsules could be loaded with magnetic nanoparticles, which provided the possibility to guide spatially the whole compartmentalized structure by applying an external magnetic field, which could be useful in applications that require mobilization to and immobilization at a site (e.g., guided therapies). Compartmentalization was exploited to encapsulate rhodamine as a model low molecular weight molecule either in the interior of the microcapsules or in the ALG medium. Release studies at distinct temperatures showed that rhodamine when encapsulated in the microcapsules was released at a lower rate at physiological temperature, thanks to the use of ELRs. When encapsulated in the ALG compartment, the release kinetics was not significantly affected. Incorporating distinct functions in a same system by carefully selecting its constituents lets foresee the construction of customizable microreactors that may exhibit other types of response, for instance, toward temperature, pH or light. Such a device could also be used as a platform for the development of microenvironments that simulate the formation of microtissues or the treatment of diseases at a laboratorial level.

The work developed herein shows how LbL-based strategies have surpassed the simple purpose of modifying a surface. From the results obtained in each of the chapters of this thesis, it is clear that LbL permits to achieve high degrees of functionalization and complexity, both in bioactivity and geometry, for various distinct biomedical applications. Despite the potential of LbL, this technology has been limited to the fabrication of bidimensional devices – some already in medical use. Thus, it is expected that the superior functionalization may result in the development of strategies useful not only for conventional medical applications but also more cutting-edge ones in biomedical engineering, such as tissue engineering.